

Spring 1-1-2011

Performance Modeling and Economic Analysis of Residential Solar Combisystems

John L. Sustar

University of Colorado at Boulder, jlsustar@gmail.com

Follow this and additional works at: https://scholar.colorado.edu/cven_gradetds



Part of the [Civil Engineering Commons](#), [Energy Systems Commons](#), and the [Sustainability Commons](#)

Recommended Citation

Sustar, John L., "Performance Modeling and Economic Analysis of Residential Solar Combisystems" (2011). *Civil Engineering Graduate Theses & Dissertations*. 217.

https://scholar.colorado.edu/cven_gradetds/217

This Thesis is brought to you for free and open access by Civil, Environmental, and Architectural Engineering at CU Scholar. It has been accepted for inclusion in Civil Engineering Graduate Theses & Dissertations by an authorized administrator of CU Scholar. For more information, please contact cuscholaradmin@colorado.edu.

PERFORMANCE MODELING AND ECONOMIC ANALYSIS OF RESIDENTIAL SOLAR

COMBISYSTEMS

BY

JOHN SUSTAR

B.S., UNIVERSITY OF ST. THOMAS, 2006

A thesis submitted to the
Faculty of the Graduate School of the
University of Colorado in partial fulfillment
of the requirements for the degree of
Masters of Science
Department of Civil, Environmental and Architectural Engineering

2011

This thesis entitled:
Performance Modeling and Economic Analysis of Residential Solar Combisystems
written by John Sustar
has been approved for the Department of Civil, Environmental and Architectural Engineering

Moncef Krarti, Ph.D., P.E.

Michael Brandemuehl, Ph.D., P.E.

Jay Burch, Ph.D.

Date _____

The final copy of this thesis has been examined by the signatories, and we find that both the content and the form meet the acceptable presentation standards of scholarly work in the above mentioned discipline.

Sustar, John L. (M.S.: Department of Civil, Environmental and Architectural Engineering)

Performance Modeling and Economic Analysis of Residential Solar Combisystems

Thesis directed by Prof. Moncef Krarti, Ph.D., P.E. and by the National Renewable Energy Laboratory,
Senior Scientist, Jay Burch, Ph.D.

ABSTRACT

In recent years, solar combisystems have received an increasing amount of attention in both the European and U.S. markets due to their ability to increase the energy savings provided by residential active solar water heaters. However, since the extra savings are accompanied by extra installation costs, it is not trivial as to whether or not these systems are a worthy investment, especially when compared to solar water heaters (SWHs). To help answer the question of whether or not these systems are cost-effective, the annual performance of these systems, as a function of location, size and load, was simulated using a TRNSYS model of a typical combisystem. The model was validated using data from a residential combisystem installed in Carbondale, Colorado, which was monitored as part of a Building America research project.

The TRNSYS model was then used to study the annual performance of combisystems for residential applications in six locations within the U.S. The six locations are Phoenix, Atlanta, San Francisco, Denver, Boston, and Chicago. For collector area sizes of 96 ft² or smaller, the performance of these systems is measured by the incremental energy savings it yields in comparison to a SWH of the same system size. Additionally, the combisystems' energy savings are evaluated based on the reduced auxiliary energy required to meet the thermal loads as compared to a reference system without any solar.

This study found that combisystems are able to provide significant energy and cost savings relative to both small SWHs and reference systems. In terms of incremental savings from the combisystem as compared to a SWH of the same size, the largest incremental savings will occur when

DHW loads are small and space heating loads are high. The economic analysis revealed that electric combisystems in the locations of Denver, Boston, and San Francisco yield the highest incremental cost savings and highest incremental breakeven costs relative to a SWH.

Regarding the cost-effectiveness of combisystems relative to a reference system, the analysis reveals that the economics could be favorable for combisystems in the locations of Denver, Boston, and San Francisco, provided that these systems are electric and the thermal loads in these homes are high. However, if evaluating the economics of combisystems in applications for lower space heating loads due to more efficient construction, combisystems—given their current high installation costs— are not a cost-effective option in any locations evaluated.

Acknowledgements

First, I would like to thank all of the staff at the National Renewable Energy Laboratory (NREL) for providing me with the opportunity to work on this project as well as their willingness to fund the project. Specifically, I'd like to thank Jay Burch, Senior Scientist at NREL, for his continuous guidance and his eagerness to assist me and answer all my questions and concerns throughout the project. Also, both Greg Barker and Bob Hendron were extremely helpful in providing me with critical information on the experimental data and clarifying the many questions I had about the experimental process. I'd also like to thank Professor Moncef Krarti and Professor Mike Brandemuehl, as members of my committee, for all their academic guidance and support throughout the duration of the project. Lastly, I would like to thank my family, especially my wife Emily, for all her love, support, and patience.

Table of Contents

Chapter 1	Introduction to Combisystems	1
1.1	Market Overview	2
1.1.1	Market Penetration.....	3
1.2	System Designs	6
1.1.2	European Combisystems.....	7
1.1.3	Building America Systems.....	8
1.3	Thesis Objective.....	11
1.4	Research Overview	12
Chapter 2	Literature Review.....	14
2.1	European Classification Research.....	16
2.2	System Size	17
2.3	Tank Stratification	18
2.4	Load Variation	20
2.5	Previous Modeling Simulations	20
Chapter 3	Experimental Analysis	22
3.1	Experiment Introduction	22
3.2	Uncertainty Analysis.....	32
3.2.1	Thermocouples Differential Bias Error.....	33

3.2.2	Error propagation of calculated values	34
3.2.3	Calculating the total uncertainty	35
3.3	Sky Models	38
3.4	Explanations for Low Measured Collector Efficiency.....	45
3.4.1	Flow Meter Bias.....	45
3.4.2	Fluid Specific Heat.....	48
3.5	Impact of Pipe Losses on Measured Efficiency	49
3.6	Tank Loss Coefficient.....	51
Chapter 4	System Model	55
4.1	Model Description	55
4.1.1	Space Heating Schedule.....	60
4.2	TRNSYS Components	60
4.2.1	Flat Plate Solar Collector with Capacitance: Type 539	60
4.2.2	Storage Tank: Type 534.....	62
4.2.3	Immersed Heat Exchangers within the Tank	63
4.3	Modeling the Collector and Tank	66
4.3.1	Solar Thermal Collector Model	67
4.3.2	Calibration Errors.....	71
4.3.3	Tank Model Calibration.....	72
4.3.4	Calibrated Tank Parameters	82
4.3.5	Analytical Verification of Model	83
4.4	Building Loads.....	85
4.4.1	Space Heating Loads.....	86

4.4.2	Domestic Hot Water Loads.....	92
4.4.3	Parasitic Energy Consumption.....	98
4.5	Collector Orientation and Tilt.....	99
Chapter 5	Results.....	100
5.1	Real-time Operation Results.....	100
5.2	Integrated Hourly Results.....	104
5.3	Monthly Solar and Loads.....	108
5.4	Parametric Study.....	110
5.5	Energy Performance Analysis.....	113
5.5.1	Energy Performance Trends.....	116
5.5.2	Impact of DHW Load.....	127
5.5.3	Impact of House Type.....	132
5.5.4	Impact of Climate.....	137
5.5.5	Impact of Collector Slope.....	149
5.6	Economic Analysis.....	151
5.6.1	Economic Metrics.....	153
5.6.2	System Costs.....	155
5.6.3	Comparing Economics of Combisystem and SWH.....	158
5.6.4	Impact of location on economics.....	166
5.6.5	Sensitivity Analysis.....	169
5.7	System Size Optimization.....	172
Chapter 6	Conclusion and Future Work.....	178
6.1	Combisystems versus SWHs.....	178

6.2	Conclusions for Large Combisystems	181
6.3	Future Work	184
	References	186
	Appendix A: Manufacturer Literature	190
	Appendix B: Building Specifications for Modeling	197
	Appendix C: Tank Heat Exchanger Calibration Tables	203
	Appendix D: TRNSYS Deck File for Calibrated Combisystem Model	207
	Appendix E: Steady State Hand Calculations	245
	Appendix F: Energy and Economic Analysis Results	249

List of Tables

Table 1.1: Classification of solar combisystems as defined by IEA Task 26 (taken from Weiss [7]).....	8
Table 3.1: Combisystem components in the NextGen home in Carbondale, Colorado.....	24
Table 3.2: Components of the data acquisition system on the solar combisystem along with their bias, random, and total errors.	35
Table 3.3: Validation results for diffuse irradiance models that compared the errors of three sky models using measured data in Albany, NY [36].....	39
Table 3.4: Kinematic viscosities of propylene glycol solutions	46
Table 3.5: Impact of glycol/water mixture on the volumetric specific heat of the fluid.....	48
Table 4.1: Solar Thermal Collector with Capacitance Model Parameters.....	68
Table 4.2: Pre-Calibration Tank Parameters.....	73
Table 4.3: Pre Calibration Heat Exchanger Parameters.....	74
Table 4.4: Post Calibration Tank Values	83
Table 4.5: Post Calibration Tank Parameters.....	83
Table 4.6: Steady state calculation assumptions.....	84
Table 4.7: Comparison of steady state results (EES versus TRNSYS)	85
Table 4.8: BEopt and TRNSYS Building Site Energy Consumption for space heating loads	91
Table 4.9: Average daily volumes for the mixed draws (sinks/showers), hot water required the mixed draws, machine draws, and total hot water	96
Table 5.1: Parametric Runs Summary	111
Table 5.2: 2010 State Average Residential Utility Rates (EIA) [62].....	152
Table 5.3: Economics Assumptions for determining the discount rate.....	153

Table 5.4: Optimized collector area and its corresponding NPW for high thermal load, benchmark load, and low thermal load homes in all climates (Low Combisystem Cost).....	175
Table 5.5: Optimized collector area and its corresponding NPW for high thermal load, benchmark load, and low thermal load homes in all climates (High Combisystem Cost)	176
Table B.1: Building Specifications for 1960 Retrofit House.....	197
Table B.2: Building Specifications for IECC 2009 House	198
Table B.3: Building Specifications for Building America 50 percent House	199
Table B.1: TRNSYS Type 56 Inputs for 1960 Retrofit House	200
Table B.1: TRNSYS Type 56 inputs for IECC 2009 House.....	201
Table B.1: TRNSYS Type 56 inputs for Building America 50 percent House	202
Table C.1: Variation of tank UA, heat exchanger length, and number of tank nodes on the lower heat exchanger RSME [kJ/hr].....	203
Table C.2: Variation of tank UA, heat exchanger length, and number of tank nodes on the lower heat exchanger chi-squared values	204
Table C.3: Variation of tank UA, heat exchanger length, and number of tank nodes on the upper heat exchanger RSME [kJ/hr].....	205
Table C.4: Variation of tank UA, heat exchanger length, and number of tank nodes on the upper heat exchanger chi-square values	206

List of Figures

Figure 1.1: Schematic of a simple combisystem.....	1
Figure 1.2: Annual Installed U.S. Capacity for Residential Solar Thermal (2001-2010) [5] [6].....	3
Figure 1.3: Installed capacity of flat plate collectors in operation for both combisystem applications and non-combisystem applications by the end of 2009 [4]	4
Figure 1.4: Flat plate collector capacity installed in 2009 by application (combisystem versus non- combisystem applications) [4]	5
Figure 1.5: Newly installed capacity of glazed water collectors in 2009 [kW_{th} per 1,000 inhabitants] [4]..	6
Figure 1.6. Schematic of the solar combisystem with forced-air distribution found in the Solar Row homes.	9
Figure 1.7. The Discovery House combisystem schematic in Loveland, CO.....	10
Figure 3.1: Schematic of the combisystem along with the data acquisition equipment[1].....	23
Figure 3.2: The tilted pyranometer is located in the upper left corner of the PV array and the horizontal pyranometer is located at the peak of the main roof [1].	26
Figure 3.3: Solar radiation data collected as well as the calculated extraterrestrial horizontal radiation during the two days of one-minute interval data (December 25 th - December 27 th).	27
Figure 3.4: One-minute interval collector loop data collected from 4pm on December 25 th to 4pm on December 27 th	28
Figure 3.5: One-minute interval data showing the upper heat exchanger inlet and outlet temperature and flow rate measurements. The house temperature data shows that the setpoint was roughly 23 °C.	29
Figure 3.6: 30 minute data period of measured temperature and flow rates for the upper heat exchanger shows that heat is both added and extracted from the tank via the upper heat exchanger	30

Figure 3.7: Due to the space heating tempering valve, the flow from the upper heat exchanger to the varies. However, the flow through the radiant floor is constant at 20 liters per minute.	31
Figure 3.8: One-minute interval domestic hot water inlet and outlet temperatures and flow rates.	32
Figure 3.9: Utilizing the Hay and Davies sky model, the tilt radiation was split into beam, sky diffuse, and ground diffuse components.	41
Figure 3.10: Comparing the total measured tilt radiation to the calculated total tilt radiation using the measured horizontal radiation.	42
Figure 3.11: Utilizing the Hay and Davies sky model and the Erbs correlation, the measured horizontal radiation was split into beam, sky diffuse, and ground diffuse components.	42
Figure 3.12: Comparing the calculated solar thermal collector efficiency using the measured tilt radiation, the calculated tilt radiation from the horizontal radiation, and the steady state efficiency using SRCC efficiency parameters.	43
Figure 3.13: Comparing measured data with uncertainty error bars to the expected steady state efficiency	44
Figure 3.14: Viscosity effect on a turbine meter's K-factor [43].....	47
Figure 3.15: The impact of the bias error of the flow meter on the measured efficiency in the collector. .	48
Figure 3.16: The impact of the glycol mixture on the measured efficiency in the collector.	49
Figure 3.17: Comparing the quoted SRCC steady state efficiency to a modified steady state collector efficiency that takes into account the pipe losses which come into play when measuring the collector fluid temperatures in the utility room.	51
Figure 3.18: Hourly Data showing tank temperature data for the duration of one week. The load and collector flows are also shown to indicate when the temperature decays occur in order to calculate the tank loss coefficient.	53
Figure 4.1: A solar combisystem with an electric resistance heater, an indirect solar loop, an indirect space heating loop, and a pressurized tank.	57

Figure 4.2: A solar DHW system with an electric resistance heater, an indirect solar loop, and a pressurized tank. The space heating load is being supplied through an electric tankless boiler connected to a radiant floor loop.	58
Figure 4.3: Schematic of the conventional water heater with a dual element electric water heater and a electric boiler providing heat for the space heating load.	59
Figure 4.4: Comparing the modeled collector efficiency to the modeled collector efficiency measured at the tank.....	69
Figure 4.5: Comparing the measured efficiency to the modeled efficiency measured at the tank using the measured tilt radiation and the calculated tilt radiation inferred from the measured horizontal radiation.	70
Figure 4.6: Comparing the measured collector efficiency to the modeled collector efficiency.	71
Figure 4.7: Impact of lower HX length and number of tank nodes on the RMSE between the model heat transfer and the experimental heat transfer.	75
Figure 4.8: Impact of the upper heat exchanger length and the number of tank nodes on the RMSE of the heat transfer in the upper heat exchanger.....	76
Figure 4.9: Impact of the Tank UA and number of tank nodes on the RMSE of the lower heat exchanger.	77
Figure 4.10: Impact of the tank UA and number of tank nodes on the RMSE of the upper heat exchanger.	78
Figure 4.11: Examining the chi-squared of the three measured heat transfer values in the tank with the upper heat exchanger at 48 ft, lower heat exchanger at 61 ft, and the tank UA at 2.2 W/C.	79
Figure 4.12: Comparing measured delta temperatures and the predicted delta temperatures for the lower heat exchanger on the sunny day.	79
Figure 4.13: Lower Heat Exchanger predicted versus measured heat transfer values.....	80
Figure 4.14: Comparing measured delta temperatures and the predicted delta temperatures for the upper heat exchanger	81

Figure 4.15: Upper heat exchanger predicted versus measured values.....	81
Figure 4.16: Comparing the predicted domestic hot water heat transfer rate to the measured values	82
Figure 4.17. The renderings for the homes that were modeled. The building on the left is slab-on-grade construction, while the home on the right has a basement and was used for the colder climates (Denver, Boston, and Chicago).....	90
Figure 4.18: BEopt and TRNSYS Building Site Energy Consumption for all the home performance levels and climates	92
Figure 4.19: Combined domestic hot water use profile[46]	93
Figure 4.20: In the model, there are two tempering valves which account allow for both hot flow events (125 °F) and mixed flows (105 °F) to occur.	94
Figure 4.21: The one-minute interval draw flow rates over the course of two days shows both the discrete character of the draw profile as well as the differentiation between mixed draws for sinks/showers and hot draws for dish and clothes washers.....	95
Figure 4.22: Daily average hot water draw for the 6 climates and three draw levels.	97
Figure 4.23: Annual water heating energy demand (kWh) for a single-family residence with a constant load profile based on an assumed 60 gal/day draw [55].	98
Figure 5.1: Collector loop operation on June 12 th	101
Figure 5.2: Operation of upper heat exchanger for space heating	102
Figure 5.3: Operation of the DHW flows. The mains water flows through the tempering valve in order to mix with the heated tank water.	103
Figure 5.4: Schematic of energy balance for solar loop.....	105
Figure 5.5: Solar loop energy balance plotted over time	106
Figure 5.6: Schematic of energy balance for storage tank	107
Figure 5.7: Time series energy balance plot in the tank	108
Figure 5.8: Monthly plot of the total load and the solar resource energy for a combisystem in Denver (96 ft ² / 60 gallon draw)	109

Figure 5.9: Monthly plot of the total load and the solar resource energy for a SWH in Denver (96 ft ² / 60 gallon draw)	110
Figure 5.10: Annual energy savings from a SWH with an electric auxiliary water heater [55]	112
Figure 5.11: Average daily horizontal radiation levels for the six locations	113
Figure 5.12: Schematic of Tank Model for Combisystem.....	115
Figure 5.13: Saved Energy for SWHs and Combisystems in Denver Benchmark House	117
Figure 5.14: Solar Fraction for Combisystem in Denver Benchmark House	118
Figure 5.15: Solar Fraction for SWH in Denver	120
Figure 5.16: Solar Fraction for SWH in Phoenix.....	121
Figure 5.17: Space Heating Solar Fraction for Combisystem in Denver Benchmark House	122
Figure 5.18: System efficiency of combisystem versus SWH in Denver Benchmark house	123
Figure 5.19: Collector efficiency in the combisystem and SWH for the three DHW loads	124
Figure 5.20: Average tank temperature of combisystems and SWH systems for the three DHW loads ..	125
Figure 5.21: Annual tank losses of combisystem versus SWH for Denver benchmark house	126
Figure 5.22: Marginal system efficiency of combisystem versus SWH for Denver benchmark house....	127
Figure 5.23: Impact of DHW loads on the annual saved energy of combisystem and SWH for Denver benchmark house	128
Figure 5.24: Impact of DHW load on the relative savings increase of the combisystem relative to the SWH for three collector area sizes (Denver Benchmark House).....	129
Figure 5.25: Impact of DHW loads on the system efficiency of combisystem and SWH for Denver benchmark house	130
Figure 5.26: Impact of DHW loads on the annual saved energy of combisystem and SWH for Phoenix benchmark house	131
Figure 5.27: Impact of DHW loads on the system efficiency of combisystem and SWH for Phoenix benchmark house	132

Figure 5.28: Impact of house type on the annual saved energy of the combisystem and SWH for Denver with 60 gallon per day DHW draws.....	133
Figure 5.29: Impact of house type on the relative savings increase of the combisystem relative to the SWH for three collector area sizes (Denver/60 gallon draw)	134
Figure 5.30: Impact of house type on the system efficiency of the combisystem and SWH for Denver with 60 gallon per day DHW draws.....	135
Figure 5.31: Impact of house type on the annual saved energy of the combisystem and SWH for Phoenix with 60 gallon per day DHW draws.....	136
Figure 5.32: Impact of house type on the system efficiency of the combisystem and SWH for Phoenix with 60 gallon per day DHW draws.....	137
Figure 5.33: Impact of climate on annual saved energy for benchmark house and 60 gallon DHW draw	138
Figure 5.34: Impact of climate on the relative savings increase of the combisystem relative to the SWH for three collector area sizes (Benchmark House/60 gallon draw)	139
Figure 5.35: Impact of climate on system efficiency for benchmark house and 60 gallon DHW draw ...	140
Figure 5.36: Annual specific incident radiation levels on collectors for SWH and Combisystem in all the	141
Figure 5.37: Annual space heat loads for benchmark IECC 2009 house in all the locations	142
Figure 5.38: Monthly Heating Load between San Francisco and Denver	143
Figure 5.39: Monthly incident radiation for combisystem and SWH in San Francisco and Denver	144
Figure 5.40: Monthly incremental savings of combisystem versus SWH for San Francisco and Denver (96 ft ² , 60 gallon draw).....	145
Figure 5.41: Impact of climate on the relative increase in savings from the combisystem as compared to a SWH for a low load house (20 gallon draw/BA 50% House)	146
Figure 5.42: Impact of climate on the relative increase in savings from the combisystem as compared to a SWH for a high load house (100 gallon draw/1960s Retrofit House)	147

Figure 5.43: Impact of climate on the relative increase in savings from a combisystem as compared to a SWH for a house with high space heating and low DHW loads.	148
Figure 5.44: Impact of climate on the relative increase in savings for a house with low space heating loads and high DHW loads.....	149
Figure 5.45: Impact of collector tilt on annual saved energy for both systems and the three DHW loads for Denver benchmark house with 64 ft ² collector area.	150
Figure 5.46: Monthly energy savings for combisystem for three tilt angles in Denver (Benchmark, 60 gallon draw)	151
Figure 5.47: Cost per collector area for SWH using data from the California Solar Initiative solar thermal program.....	156
Figure 5.48: Installed cost regression for the SWH based on actual cost data.	156
Figure 5.49: Cost per collector area for combisystem using data from Weiss [7]	157
Figure 5.50: System costs based on the European system cost data and a \$1,000 incremental cost relative to the SWH cost.	158
Figure 5.51: Lifecycle costs of the SWH and the combisystem as a function of collector area and DHW load (Denver Benchmark House).....	160
Figure 5.52: Net Present Worth of the SWH and the combisystem as a function of collector area and DHW load (Denver Benchmark House)	161
Figure 5.53: Breakeven Cost of the SWH and the combisystem as a function of collector area and DHW load (Denver Benchmark House).....	162
Figure 5.54: Combisystem incremental breakeven installed cost as a function of collector area and DHW load (Denver Benchmark House).....	163
Figure 5.55: Impact of DHW Load and house type on the combisystem incremental breakeven cost relative to the SWH (Denver, 96 ft ² system).....	164
Figure 5.56: LCOE of the SWH and the combisystem as a function of collector area and DHW load (Denver Benchmark House)	165

Figure 5.57: Impact of DHW load and house type on the LCOE (Denver, 96 ft ² system)	166
Figure 5.58: Impact of location on incremental breakeven installed cost for 96 ft ² system. The bars represent the incremental breakeven cost for a benchmark house with a 60 gallon draw. The error bars represent the range of incremental breakeven costs for the combisystem to be cost competitive with SWH, with the range being dependent on the space heating and DHW loads. The dashed lines in the plot show the lower and upper limit incremental costs for combisystems.	167
Figure 5.59: Impact of combisystem installed cost and climate on the LCOE for a 288 ft ² system with an electric auxiliary heater. The error bars show the bounds of LCOEs. The lower bound is for a house with the largest loads (1960s retrofit house with 100 gallon DHW draws) and therefore largest savings and the higher bound is for a house with the smallest loads.	168
Figure 5.60: Impact of combisystem installed cost and climate on the LCOE for a 288 ft ² system with a natural gas auxiliary heater. The error bars show the bounds of LCOEs as described in Figure 5.59.	169
Figure 5.61: Impact of cost of electricity on the NPW of an electric-auxiliary combisystem in Denver (Benchmark, 60 Gallon Draw).....	170
Figure 5.62: Impact of the discount rate and collector area on the net present worth of combisystems (Denver, Benchmark House, 60 Gallon Draw).....	171
Figure 5.63: Impact of Cost of Electricity and relative reduction in the installed cost on the NPW of a 96 ft ² combisystem in Denver (Benchmark House, 60 Gallon Draw).....	172
Figure 5.64: Net Present Worth as a function of collector area for high thermal load, benchmark load, and low thermal load house in Denver (low combisystem cost)	173
Figure 5.65: Net Present Worth as a function of collector area for high thermal load, benchmark load, and low thermal load house in San Francisco (low combisystem cost)	174
Figure 5.66: Net Present Worth and LCOE as a function of collector area for San Francisco with a benchmark load scenario (low combisystem cost)	177

Figure 6.1: Range of incremental site energy savings for 96 ft ² system.....	179
Figure 6.2: Range of incremental annual cost savings for 96 ft ² combisystem	180
Figure 6.3: Range of incremental breakeven costs relative to a SWH for 96 ft ² combisystems. The dashed lines represent the incremental installed costs based on a \$1,000 incremental cost assumption and the incremental costs of European combisystem relative to U.S. SWHs.....	181
Figure 6.4: Annual site energy savings for a 288 ft ² combisystem.....	182
Figure 6.5: Annual cost savings relative to the reference system for a 288 ft ² combisystem.....	183
Figure 6.6: Breakeven costs for 288 ft ² combisystems relative to reference system. The dashed lines represent the installed costs based on the \$1,000 incremental cost assumption and the installed costs of European combisystem for a 288 ft ² system.....	184
Figure A.1: Solar Rating and Certification Corporation Rating for Heliodyne Flat Plate collector	190
Figure F.1: Combisystem and SWH solar fraction for a 1960s Retrofit House(Phoenix).....	250
Figure F.2: Annual saved energy and system efficiency for a 1960s Retrofit House(Phoenix)	251
Figure F.3: LCOE and NPW for electric systems for a 1960s Retrofit House(Phoenix)	252
Figure F.4: Breakeven installed cost and combisystem incremental breakeven cost for electric system for a 1960s Retrofit House(Phoenix).....	253
Figure F.5: LCOE and NPW for gas systems for a 1960s Retrofit House(Phoenix)	254
Figure F.6: Breakeven installed cost and combisystem incremental breakeven cost for gas systems for a 1960s Retrofit House(Phoenix).....	255
Figure F.7: Combisystem and SWH solar fraction for a IECC 2009 House(Phoenix).....	256
Figure F.8: Annual saved energy and system efficiency for a IECC 2009 House(Phoenix)	257
Figure F.9: LCOE and NPW for electric systems for a IECC 2009 House(Phoenix)	258
Figure F.10: Breakeven installed cost and combisystem incremental breakeven cost for electric system for a IECC 2009 House(Phoenix).....	259
Figure F.11: LCOE and NPW for gas systems for a IECC 2009 House(Phoenix).....	260

Figure F.12: Breakeven installed cost and combisystem incremental breakeven cost for gas systems for a IECC 2009 House(Phoenix)	261
Figure F.13: Combisystem and SWH solar fraction for a BA 50% House(Phoenix)	262
Figure F.14: Annual saved energy and system efficiency for a BA 50% House(Phoenix)	263
Figure F.15: LCOE and NPW for electric systems for a BA 50% House(Phoenix).....	264
Figure F.16: Breakeven installed cost and combisystem incremental breakeven cost for electric system for a BA 50% House(Phoenix).....	265
Figure F.17: LCOE and NPW for gas systems for a BA 50% House(Phoenix).....	266
Figure F.18: Breakeven installed cost and combisystem incremental breakeven cost for gas systems for a BA 50% House(Phoenix).....	267
Figure F.19: Combisystem and SWH solar fraction for a 1960s Retrofit House(Atlanta)	268
Figure F.20: Annual saved energy and system efficiency for a 1960s Retrofit House(Atlanta)	269
Figure F.21: LCOE and NPW for electric systems for a 1960s Retrofit House(Atlanta).....	270
Figure F.22: Breakeven installed cost and combisystem incremental breakeven cost for electric system for a 1960s Retrofit House(Atlanta)	271
Figure F.23: LCOE and NPW for gas systems for a 1960s Retrofit House(Atlanta)	272
Figure F.24: Breakeven installed cost and combisystem incremental breakeven cost for gas systems for a 1960s Retrofit House(Atlanta)	273
Figure F.25: Combisystem and SWH solar fraction for a IECC 2009 House(Atlanta)	274
Figure F.26: Annual saved energy and system efficiency for a IECC 2009 House(Atlanta)	275
Figure F.27: LCOE and NPW for electric systems for a IECC 2009 House(Atlanta).....	276
Figure F.28: Breakeven installed cost and combisystem incremental breakeven cost for electric system for a IECC 2009 House(Atlanta)	277
Figure F.29: LCOE and NPW for gas systems for a IECC 2009 House(Atlanta)	278
Figure F.30: Breakeven installed cost and combisystem incremental breakeven cost for gas systems for a IECC 2009 House(Atlanta).....	279

Figure F.31: Combisystem and SWH solar fraction for a BA 50% House(Atlanta)	280
Figure F.32: Annual saved energy and system efficiency for a BA 50% House(Atlanta)	281
Figure F.33: LCOE and NPW for electric systems for a BA 50% House(Atlanta)	282
Figure F.34: Breakeven installed cost and combisystem incremental breakeven cost for electric system for a BA 50% House(Atlanta)	283
Figure F.35: LCOE and NPW for gas systems for a BA 50% House(Atlanta)	284
Figure F.36: Breakeven installed cost and combisystem incremental breakeven cost for gas systems for a BA 50% House(Atlanta)	285
Figure F.37: Combisystem and SWH solar fraction for a 1960s Retrofit House(San Francisco)	286
Figure F.38: Annual saved energy and system efficiency for a 1960s Retrofit House(San Francisco)....	287
Figure F.39: LCOE and NPW for electric systems for a 1960s Retrofit House(San Francisco)	288
Figure F.40: Breakeven installed cost and combisystem incremental breakeven cost for electric system for a 1960s Retrofit House(San Francisco)	289
Figure F.41: LCOE and NPW for gas systems for a 1960s Retrofit House(San Francisco)	290
Figure F.42: Breakeven installed cost and combisystem incremental breakeven cost for gas systems for a 1960s Retrofit House(San Francisco)	291
Figure F.43: Combisystem and SWH solar fraction for a IECC 2009 House(San Francisco)	292
Figure F.44: Annual saved energy and system efficiency for a IECC 2009 House(San Francisco).....	293
Figure F.45: LCOE and NPW for electric systems for a IECC 2009 House(San Francisco).....	294
Figure F.46: Breakeven installed cost and combisystem incremental breakeven cost for electric system for a IECC 2009 House(San Francisco)	295
Figure F.47: LCOE and NPW for gas systems for a IECC 2009 House(San Francisco)	296
Figure F.48: Breakeven installed cost and combisystem incremental breakeven cost for gas systems for a IECC 2009 House(San Francisco)	297
Figure F.49: Combisystem and SWH solar fraction for a BA 50% House(San Francisco).....	298
Figure F.50: Annual saved energy and system efficiency for a BA 50% House(San Francisco).....	299

Figure F.51: LCOE and NPW for electric systems for a BA 50% House(San Francisco)	300
Figure F.52: Breakeven installed cost and combisystem incremental breakeven cost for electric system for a BA 50% House(San Francisco)	301
Figure F.53: LCOE and NPW for gas systems for a BA 50% House(San Francisco).....	302
Figure F.54: Breakeven installed cost and combisystem incremental breakeven cost for gas systems for a BA 50% House(San Francisco)	303
Figure F.55: Combisystem and SWH solar fraction for a 1960s Retrofit House(Denver)	304
Figure F.56: Annual saved energy and system efficiency for a 1960s Retrofit House(Denver)	305
Figure F.57: LCOE and NPW for electric systems for a 1960s Retrofit House(Denver).....	306
Figure F.58: Breakeven installed cost and combisystem incremental breakeven cost for electric system for a 1960s Retrofit House(Denver)	307
Figure F.59: LCOE and NPW for gas systems for a 1960s Retrofit House(Denver)	308
Figure F.60: Breakeven installed cost and combisystem incremental breakeven cost for gas systems for a 1960s Retrofit House(Denver).....	309
Figure F.61: Combisystem and SWH solar fraction for a IECC 2009 House(Denver)	310
Figure F.62: Annual saved energy and system efficiency for a IECC 2009 House(Denver)	311
Figure F.63: LCOE and NPW for electric systems for a IECC 2009 House(Denver).....	312
Figure F.64: Breakeven installed cost and combisystem incremental breakeven cost for electric system for a IECC 2009 House(Denver)	313
Figure F.65: LCOE and NPW for gas systems for a IECC 2009 House(Denver)	314
Figure F.66: Breakeven installed cost and combisystem incremental breakeven cost for gas systems for a IECC 2009 House(Denver).....	315
Figure F.67: Combisystem and SWH solar fraction for a BA 50% House(Denver)	316
Figure F.68: Annual saved energy and system efficiency for a BA 50% House(Denver).....	317
Figure F.69: LCOE and NPW for electric systems for a BA 50% House(Denver).....	318

Figure F.70: Breakeven installed cost and combisystem incremental breakeven cost for electric system for a BA 50% House(Denver)	319
Figure F.71: LCOE and NPW for gas systems for a BA 50% House(Denver)	320
Figure F.72: Breakeven installed cost and combisystem incremental breakeven cost for gas systems for a BA 50% House(Denver)	321
Figure F.73: Combisystem and SWH solar fraction for a 1960s Retrofit House(Boston).....	322
Figure F.74: Annual saved energy and system efficiency for a 1960s Retrofit House(Boston).....	323
Figure F.75: LCOE and NPW for electric systems for a 1960s Retrofit House(Boston)	324
Figure F.76: Breakeven installed cost and combisystem incremental breakeven cost for electric system for a 1960s Retrofit House(Boston).....	325
Figure F.77: LCOE and NPW for gas systems for a 1960s Retrofit House(Boston).....	326
Figure F.78: Breakeven installed cost and combisystem incremental breakeven cost for gas systems for a 1960s Retrofit House(Boston)	327
Figure F.79: Combisystem and SWH solar fraction for a IECC 2009 House(Boston).....	328
Figure F.80: Annual saved energy and system efficiency for a IECC 2009 House(Boston).....	329
Figure F.81: LCOE and NPW for electric systems for a IECC 2009 House(Boston)	330
Figure F.82: Breakeven installed cost and combisystem incremental breakeven cost for electric system for a IECC 2009 House(Boston)	331
Figure F.83: LCOE and NPW for gas systems for a IECC 2009 House(Boston).....	332
Figure F.84: Breakeven installed cost and combisystem incremental breakeven cost for gas systems for a IECC 2009 House(Boston)	333
Figure F.85: Combisystem and SWH solar fraction for a BA 50% House(Boston).....	334
Figure F.86: Annual saved energy and system efficiency for a BA 50% House(Boston)	335
Figure F.87: LCOE and NPW for electric systems for a BA 50% House(Boston)	336
Figure F.88: Breakeven installed cost and combisystem incremental breakeven cost for electric system for a BA 50% House(Boston).....	337

Figure F.89: LCOE and NPW for gas systems for a BA 50% House(Boston).....	338
Figure F.90: Breakeven installed cost and combisystem incremental breakeven cost for gas systems for a BA 50% House(Boston)	339
Figure F.91: Combisystem and SWH solar fraction for a 1960s Retrofit House(Chicago).....	340
Figure F.92: Annual saved energy and system efficiency for a 1960s Retrofit House(Chicago).....	341
Figure F.93: LCOE and NPW for electric systems for a 1960s Retrofit House(Chicago)	342
Figure F.94: Breakeven installed cost and combisystem incremental breakeven cost for electric system for a 1960s Retrofit House(Chicago).....	343
Figure F.95: LCOE and NPW for gas systems for a 1960s Retrofit House(Chicago).....	344
Figure F.96: Breakeven installed cost and combisystem incremental breakeven cost for gas systems for a 1960s Retrofit House(Chicago)	345
Figure F.97: Combisystem and SWH solar fraction for a IECC 2009 House(Chicago).....	346
Figure F.98: Annual saved energy and system efficiency for a IECC 2009 House(Chicago).....	347
Figure F.99: LCOE and NPW for electric systems for a IECC 2009 House(Chicago)	348
Figure F.100: Breakeven installed cost and combisystem incremental breakeven cost for electric system for a IECC 2009 House(Chicago).....	349
Figure F.101: LCOE and NPW for gas systems for a IECC 2009 House(Chicago).....	350
Figure F.102: Breakeven installed cost and combisystem incremental breakeven cost for gas systems for a IECC 2009 House(Chicago)	351
Figure F.103: Combisystem and SWH solar fraction for a BA 50% House(Chicago).....	352
Figure F.104: Annual saved energy and system efficiency for a BA 50% House(Chicago)	353
Figure F.105: LCOE and NPW for electric systems for a BA 50% House(Chicago)	354
Figure F.106: Breakeven installed cost and combisystem incremental breakeven cost for electric system for a BA 50% House(Chicago)	355
Figure F.107: LCOE and NPW for gas systems for a BA 50% House(Chicago).....	356

Figure F.108: Breakeven installed cost and combisystem incremental breakeven cost for gas systems for a
BA 50% House(Chicago) 357

Chapter 1

Introduction to Combisystems

Solar combisystems meet two residential loads: active solar thermal space heating and domestic hot water (DHW). They are typically applied in detached single-family homes, groups of family homes, and multi-family buildings. One key advantage of solar combisystems as compared to conventional solar water heaters (SWHs) is that combisystems increase the solar collector's utilization independent of occupant hot water use because the space heating also utilizes the heat collected by the solar collector [1]. Figure 1.1 shows a schematic of a simple single-tank combisystem that has two immersed heat exchangers and a pressurized tank [1]. In contrast, a SWH system would not include an upper heat exchanger to supplement heat for the space heating.

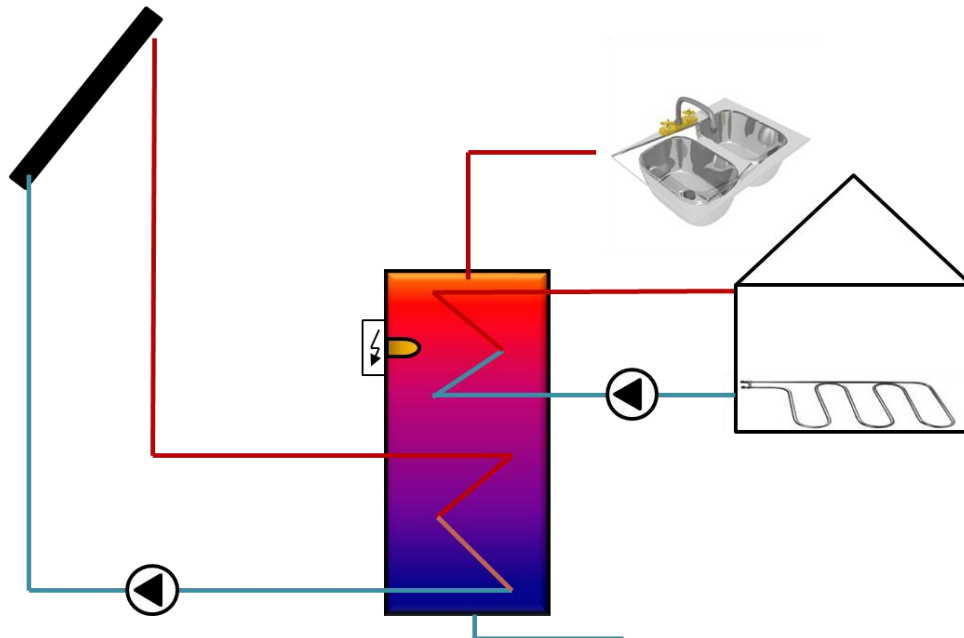


Figure 1.1: Schematic of a simple combisystem.

In terms of disadvantages, as compared to SWHs, combisystems require a relatively large incremental capital investment and the design— including the configuration of the solar collector loop, the storage, and the control system— can be intricate [7]. As trends move towards net zero energy residential designs, some homebuilders are installing solar thermal combisystems to reduce space heating auxiliary energy use, however there has been little research as to how these systems perform as compared to SWHs and how different parameters, such as system sizes, DHW use, and building space loads impact their performance and cost-effectiveness in U.S. climates.

1.1 Market Overview

Solar combisystems originated in the U.S. in the early to mid-20th century in order increase the amount of useful energy harnessed from the solar collectors [9]. The original designs utilized both air and water to transfer energy and their designs were not optimized for low cost and high performance. Years later in the mid-1970s, solar combisystems began to appear more prominently in both the U.S. and Europe, during which time, system designs were still relatively complex [7]. In the U.S., federal tax credits allowed the technology to be cost-effective. In the 1980's, the solar thermal market in the U.S. faded largely due to the expiration of tax credits and the decline of energy prices. Beginning in the 1990s, European installers and solar companies began offering simpler and cheaper systems, but these systems were also often custom-built systems [7]. These designs were also based purely on field experiences with no rigorous research supporting the optimal sizing and selection of system components.

As of 2011, commercialized systems exist in both the U.S. and Europe; however most combisystems are still custom-designed and built, although there are a couple of packaged systems offered by U.S. solar thermal suppliers, including Sunmaxx Solar and Heliodyne [10]. In the last 10 years, the world-wide solar thermal water and space heating annual installed capacity has grown by between 10 to 30 percent every year [2]. In the U.S., the annual installed capacity of solar thermal systems for water heating and space heating has grown by an average of 30 percent since 2001 (see Figure 1.2 [5] [6]).

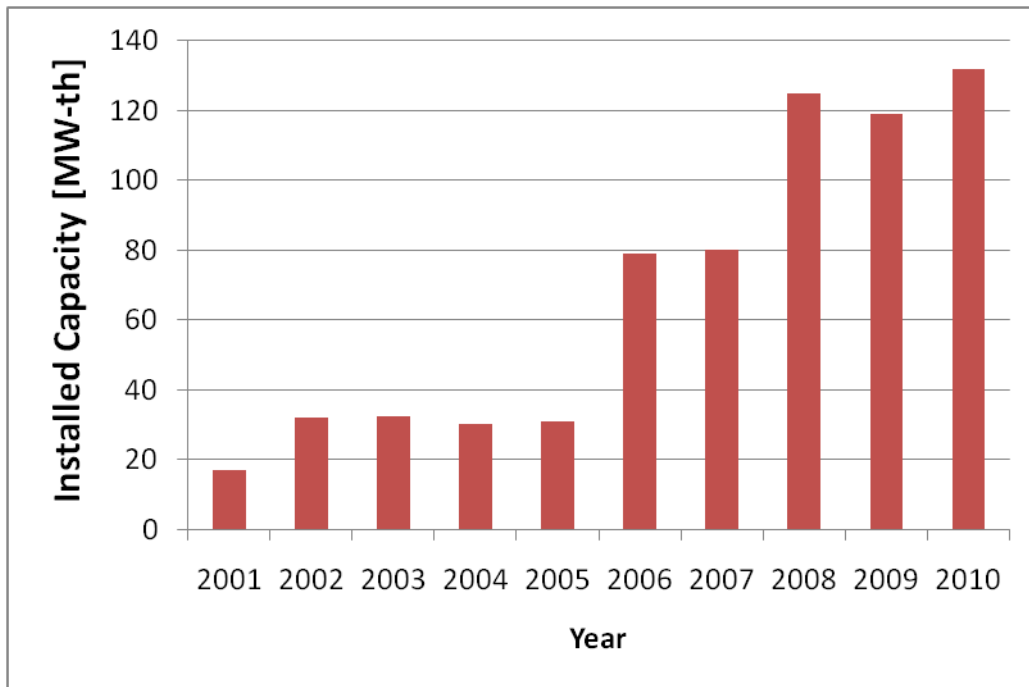


Figure 1.2: Annual Installed U.S. Capacity for Residential Solar Thermal (2001-2010) [5] [6]

1.1.1 Market Penetration

According to International Energy Agency (IEA) data, in the U.S., the penetration of the glazed collector installed capacity used in combisystem applications is currently at 5% (see Figure 1.3) [4]. However, anecdotally, there is evidence that penetration levels are high in a couple of regions within the U.S. For example, according to some U.S. solar supplier representatives, between 60 to 80 percent of the collector area installed in Colorado and more than 50 percent of the collector area installed in the Northeast is for combisystem applications[10] [11]. However, this data was never rigorously verified. In comparison, the total market penetration of combisystem capacity in Germany and Austria is at 30% and 45% respectively (see Figure 1.3).

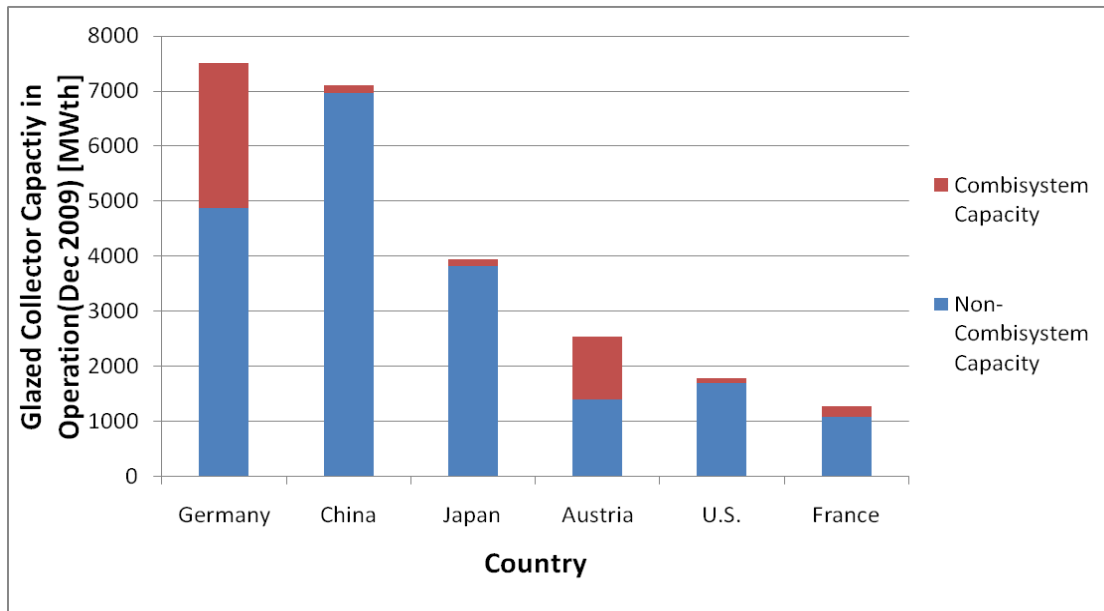


Figure 1.3: Installed capacity of flat plate collectors in operation for both combisystem applications and non-combisystem applications by the end of 2009 [4]

Moreover, in some European markets, the combisystem installation capacity in recent years is growing more rapidly than the solar domestic hot water system capacity [7]. In countries such as Sweden, Switzerland, Denmark, Norway, Germany, and Austria, the newly installed capacity for solar combisystems in 2009 was either equal to or larger than the newly installed capacity for solar domestic hot water systems [4]. In Austria, combisystems now dominate the solar thermal market, with their annual installed capacity market share more than tripling from 20 percent in 2002 to 72 percent in 2009 [8]. In Germany, which is the leader in solar thermal installations in Europe, the newly installed capacity in 2009 for combisystems made up about 65 percent of the total glazed collector installed capacity (see Figure 1.4) [4]. In comparison, the newly installed capacity in the U.S. for combisystem applications accounted for 10% of the total glazed collector capacity market in 2009.

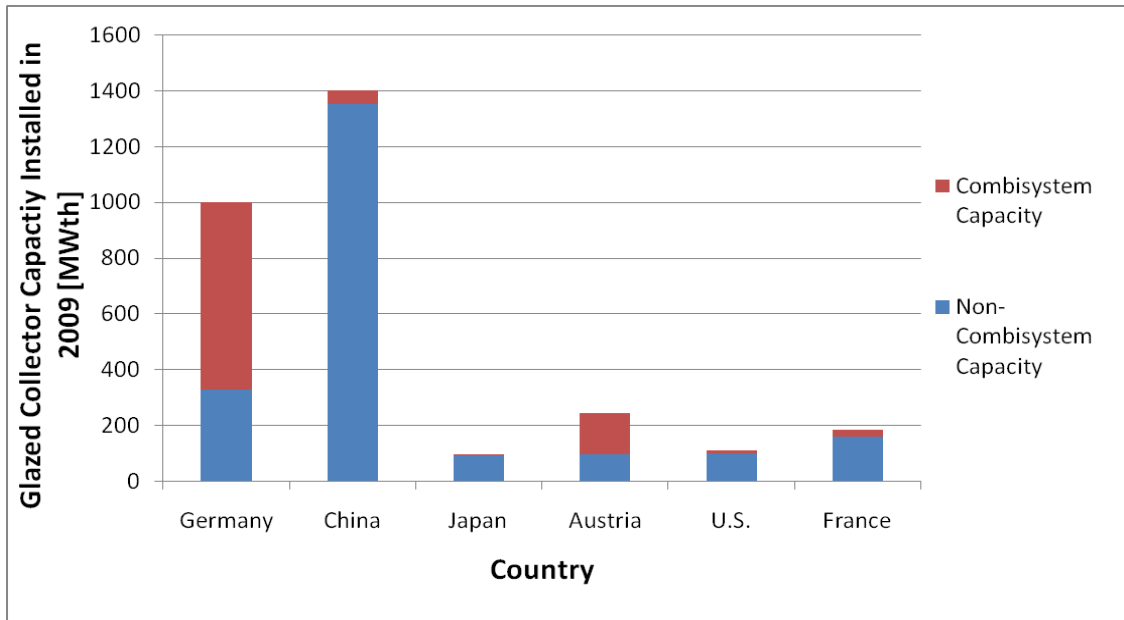


Figure 1.4: Flat plate collector capacity installed in 2009 by application (combisystem versus non-combisystem applications) [4]

Both state and federal incentives and mandates in the U.S. have played a large role in the increase in solar collector installations despite the economic downturn. For example, the Colorado State Residential Renewable Energy Rebate Program offers rebates between \$2,000 and \$3,000 for residential solar thermal systems. Additionally, in 2011, the California Solar Initiative implemented a solar water heating incentive of \$1,875 per installation for homes that use natural gas for water and space heating and \$1,250 per installation for homes that use electricity for water and space heating [5]. Lastly, a 30 percent U.S. federal tax credit is currently available, which when combined with aggressive local and state rebates, can significantly reduce the system installed cost and improve the economics of systems. Despite these generous tax credits in the U.S., the sales of solar thermal systems in the U.S. are quite low per capita, as compared to other countries (see Figure 1.5 [4]).

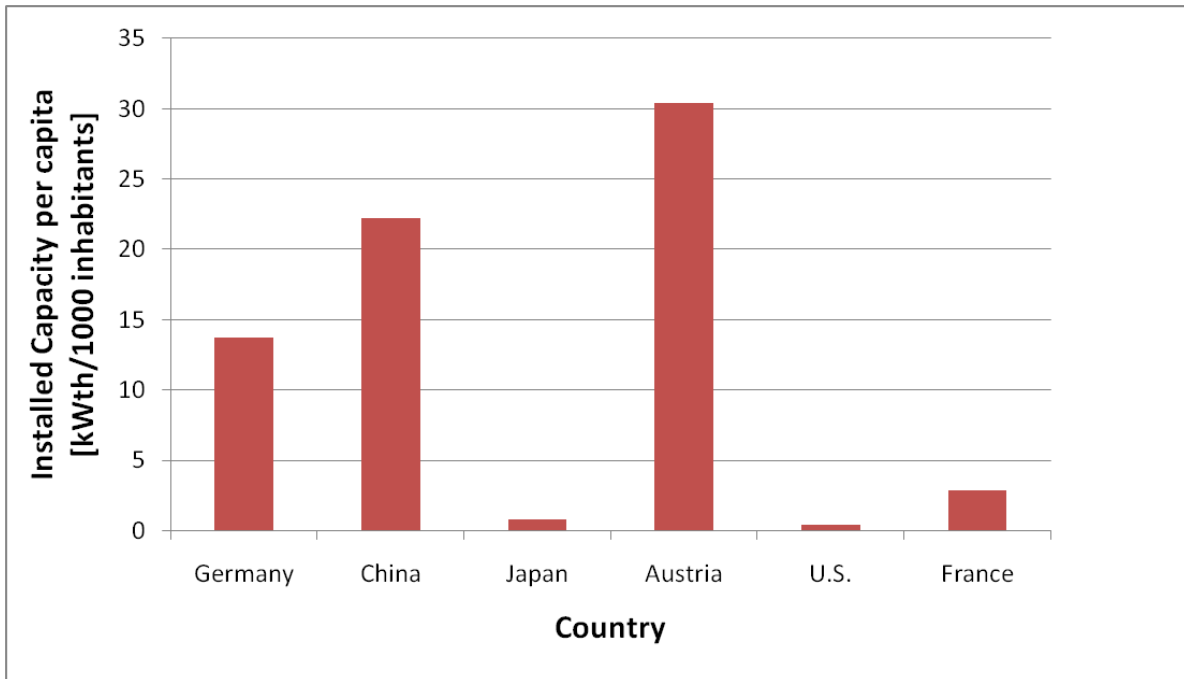


Figure 1.5: Newly installed capacity of glazed water collectors in 2009 [kW_{th} per 1,000 inhabitants] [4]

1.2 System Designs

Solar combisystems consist of the following five subsystems: a solar collector loop, a storage tank, a control system, an auxiliary heater, and a heat distribution system. System sizes vary but in general, combisystems typically use a stratified sensible heat storage tank ranging from 100 to 1000 gallons and are coupled to up to 400 ft² of solar collectors. Some European combisystems utilize seasonal storage tanks, which have a capacity of more than 20,000 gallons, in order to store the excess heat produced in the summer months for use in the winter time [7]. These large seasonal storage systems are technically feasible to implement, but are much less cost-effective than smaller combisystems due to high storage and installation costs.

The heat distribution system typically incorporates a hydronic heating loop— tied to either radiant floors, baseboard heaters, or air handler heating coils— which are either directly or indirectly heated by the storage tank. As a reference, the Building America projects have integrated combisystems

with both forced-air and radiant floor heating systems, however in general, radiant floor heating systems tend to be more common in new construction projects since they offer increased thermal comfort and they allow for lower supply temperatures[10]. Additionally, a concrete slab can increase the performance of a system due to its ability to store additional thermal energy in the floor. In terms of auxiliary heat sources, combisystems typically use either internal electric resistance elements or external fuel-based boilers.

1.1.2 European Combisystems

The most widespread solar combisystem design and performance research originated from a late-1990s initiative from the IEA Solar Heating & Cooling Programme (SHC). As part of the European initiative, researchers evaluated the performance and classification of existing European combisystem designs in order to better understand how to categorize and compare the different system designs installed in the field [7]. The European survey (known as IEA Task 26 Solar Combisystem) revealed that 21 unique combisystem designs exist in Europe. The systems can be divided into the following two main classification groups: heat storage strategies and auxiliary heat management (see Table 1.1). The heat storage strategy classification describes how the heat is stored to supply space heat to the house and how tank stratification is maintained [7]. The auxiliary heat management classification describes how the heat generated by the auxiliary heater is stored and distributed.

Table 1.1. Classification of solar combisystems as defined by IEA Task 26 (taken from Weiss [7])

Heat storage categories	Auxiliary heat management categories
A. No controlled storage device for space heating	(M) Mixing mode: The space heating loop is supplied by a store charged by both solar and aux
B. Heat management and stratification enhancement using multiple tanks and/or multiple inlet/outlet pipes and/or three/four way valves to control inlet/outlet pipes	(P) Parallel mode: The space heating loop is fed by either the aux or solar
C. Heat management using natural convection in storage tanks and/or between them to maintain stratification to a certain extent (no built-in stratifiers)	(S) Serial mode: The space heating loop may be fed by the aux heater or by both the solar and aux connected in series on the return line of the space heating loops
D. Heat management using natural convection in storage tanks and stratifiers	
B/D: Heat management using natural convection in storage tanks and built-in stratifiers as well as multiple tanks	

1.1.3 Building America Systems

Combisystems have been installed in several of Building America projects, including a few located in Colorado. In fact, the system that was used to validate the model is a system that was built for a Carbondale, Colorado house. The Carbondale combisystem is described in Section 3.1.

In terms of other Building America systems, in 2008, the Wonderland Hill Development Company, a Boulder Colorado based housing developer, partnered with Building America to construct a community of energy-efficient homes called Solar Row. Located in Boulder, Colorado, the housing community consists of 9 housing units (one 5-plex and two duplexes) — all of which have solar combisystems installed. All the units are equipped with similar combisystem equipment, however the two duplexes have force-air heating systems while the 5-plex has hydronic radiant floor heating. In the Solar Row homes, the designers utilized the IEA Task 26 C/S design with two tanks— a preheat tank that is heated by the solar loop and an auxiliary tank. Heat management for space heating utilizes natural convection (IEA Task 26 heat storage classification “C”) in the two storage tanks and between the two storage tanks to maintain temperature stratification. Additionally, the Solar Row system operates in serial mode (IEA Task 26 auxiliary classification “S”) meaning that the space heating loop may be fed by the

auxiliary heater or by both the solar and auxiliary connected in series on the return line of the space heating loop (see Figure 1.6). This system utilizes 96 ft² of flat plate solar collectors, a preheat 180 gallon storage tank, and a 40 gallon electric element auxiliary tank.

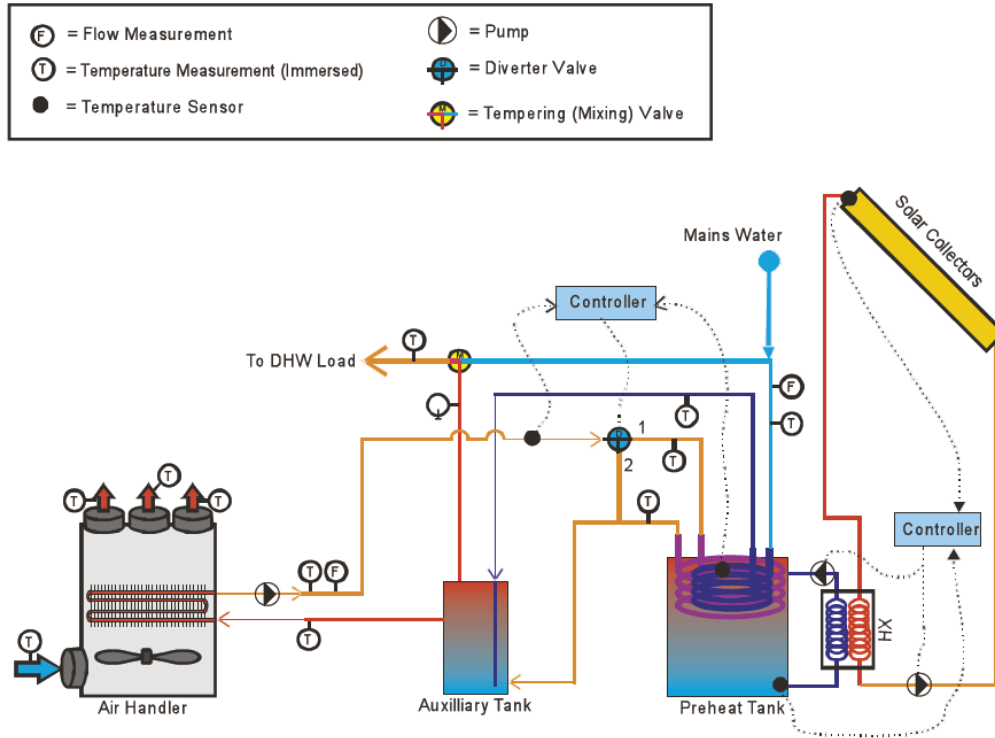


Figure 1.6. Schematic of the solar combisystem with forced-air distribution found in the Solar Row homes.

As part of another Building America partnership, McStain Neighborhoods, a Colorado-based homebuilder, built the Discovery House in Loveland, Colorado. Completed in 2005, the house offers an assortment of energy saving features, which include a solar combisystem. The solar combisystem consists of a drainback solar hot water system with three 32 ft² collectors (a total 96 ft² of flat-plate solar collectors). The solar combisystem utilizes two storage tanks— a 180 gallon solar storage tank and a 34 gallon auxiliary gas-fired boiler. The house utilizes both hydronic floor and forced-air heating, which are supplemented by the solar storage tank.

Figure 1.7 shows the schematic of the solar combisystem implemented in the Discovery House. A thermostat on the solar storage tank controls whether or not the return water from the hydronic floor and heating coil bypasses the solar storage immersed heat exchanger. The thermostat controls solenoid valves labeled 'S1' and 'S2' which are placed in parallel. If the solar storage water is above 110 °F, the valve labeled 'S1' opens and the space heating return water flows through the immersed heat exchanger in the solar storage tank. If the solar storage is below 110 °F, the return water bypasses the solar storage tank and the water is heated directly by the auxiliary boiler. The reason for the 110 °F threshold is due to the minimum heating coil supply water temperature requirement of 110 °F in order to meet the space heating load.

For the domestic hot water system, the mains water always flows through the immersed heat exchanger in the solar storage and the boiler in series. In this system, the domestic hot water mixes with the space heating loop water, which is potential health concern since potable water is flowing through the air handler heating coils and the hydronic floor PEX (cross-linked polyethylene) tubing.

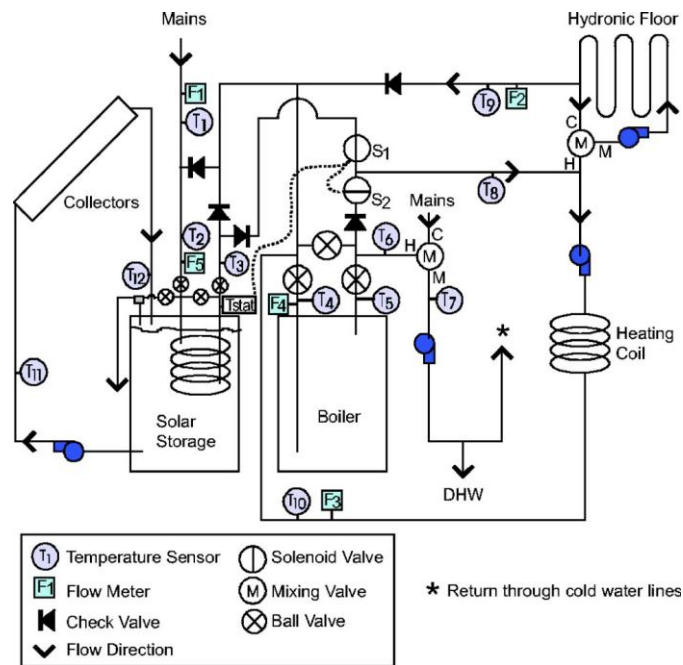


Figure 1.7. The Discovery House combisystem schematic in Loveland, CO.

1.3 Thesis Objective

The research topic originated in light of a Building America project evaluation which revealed that an installed solar domestic hot water system was not providing the anticipated energy savings due to the occupant's low domestic hot water usage [12]. Additionally, it was determined that the low domestic hot water usage both decreased system and collector efficiency substantially due to higher tank temperatures and therefore higher collector inlet temperatures. To overcome low system performance due to low domestic hot water usage, one thought was to add a heat exchanger to the system and dump the otherwise unused solar heat into the house during the heating season to help cover some of the space heating load and increase the solar utilization of the system.

The thesis research project evaluates the performance and cost-effectiveness of a selected combisystem and compares its performance to a selected solar domestic hot water system to determine whether the increased energy savings can be justified given the incremental cost to install a combisystem. To determine the energy savings provided by the solar collectors, the selected systems are compared to conventional system with a standard water heater tank and space heating boiler. As part of this thesis project, the following two questions will be addressed:

- How does the energy performance of combisystems compare to the energy performance of SWHs as a function of system size and loads (both DHW and space heating)?
- Are combisystems a good option (from an economic standpoint) in any location in the U.S.?

Addressing these questions will help evaluate whether the enhanced cost savings of combisystems make up for the incremental installed cost of combisystems as compared to SWHs. The results will be useful to determine whether it is cost-effective for the U.S. solar thermal market to take a similar path as the European solar thermal market path—where combisystems make up a significantly larger share of the residential solar thermal market.

1.4 Research Overview

The thesis report is organized into several chapters, which describe the steps taken in order to analyze experimental data, develop the combisystem and SWH model, and simulate the annual performance of the systems with various sizes. The research process began by reviewing the existing research literature on solar thermal combisystem designs and the various parameters that impact the overall performance of the system. Next, the combisystem, which was monitored as part of a Building America project in Carbondale, Colorado, is described and its performance is analyzed. This combisystem consists of two flat-plate collectors, a single-tank with two immersed heat exchangers, and an external boiler. The experimental analysis chapter consists of the testing methodology, the data monitoring description, the experimental results, and an uncertainty analysis of the measured results.

Thereafter, a model was created in order to simulate the performance of the Carbondale single-tank system. To develop the models, existing components within the Transient System Simulations (TRNSYS) software standard library and the Thermal Energy System Specialists (TESS) library were used. To verify the accuracy of the model, the model outputs were compared to the experimental data from the Building America Carbondale combisystem using inputs from the experimental data. A full description of the model developed is found in Chapter 4.

Using the TRNSYS model, a number of parametric simulations were conducted to test the performance of the combisystem and the SWH under varying conditions. The parametric studies completed were:

- The impact of solar collector area with constant storage volume to collector area ratio (i.e. 1.5 gallon/ft²) on system performance;
- The impact of daily DHW draw volumes on system performance;

- And the impact of space heating loads by modeling low-performance (1960s Retrofit), mid-performance (IECC 2009), and high-performance homes (50% reference relative to Building American Benchmark) on combisystem performance.

These parametric studies were performed to study the model's sensitivity and the impact of variations in system size and system loads on the performance of the systems. The parametric simulations were performed using Typical Meteorological Year 3 (TMY3) data sets from six U.S. cities, which were Chicago, Boston, Denver, San Francisco, Atlanta, and Phoenix.

Based on the results of the parametric runs, the performance of the combisystems and SWHs were evaluated by developing plots that show annual solar fractions, auxiliary savings relative to a conventional water heater/space heating system, and collector efficiencies between all the individual configurations. When evaluating the effect of increasing solar collector area on the performance of the system, the impact of the collector area size on the marginal system efficiencies was evaluated. Annual marginal system efficiency is defined as the change in total savings in hot water and space heating divided by the change in total solar incidence, where the changes are due to increasing the collector area.

After analyzing the energy performance between the systems, an economic analysis was performed— where the system's cost-effectiveness was compared. The economic analysis was completed using assumptions regarding installed costs, operations and maintenance (O&M) costs, system life spans, energy costs, and discount rates. The economic analysis looked into the impact of system parameters on the life cycle cost, the net present worth as compared to a conventional system, breakeven costs as compared to both a SWH and reference system, and the levelized cost of energy for both combisystems and SWH systems. After calculating the economic metrics for all the systems, the combisystem's and SWH's cost-effectiveness was evaluated and compared to the reference system.

Chapter 2

Literature Review

With the increased popularity of active solar heating systems during the 1970s, much attention in the research community focused on the performance of generic combisystem designs. One of the initial studies to examine the impact of system design and dimensions on the annual performance of combisystems was conducted by Klein et al.[13]. Using TRNSYS to interconnect mathematical models to simulate the annual system performance, the study computed the system performance as a function of the collector area and storage capacity [13].

Due to increased demand for designers to easily model the annual performance of these systems, the F-Chart tool was developed by Klein and Beckman in the late 1970s [13]. Using the F-Chart tool, the performance of both generic liquid-based and air-based solar combisystems can be analyzed instantaneously [13]. To perform its calculations, the tool utilizes correlation coefficients, which were derived as a result of several hundred thermal performance numerical simulations, to describe the system's solar fraction as a function of two dimensionless parameters. The two parameters describe the ratio of collector losses to heating loads and the ratio of absorbed solar radiation to heating loads. The tool allows for the variation in collector area, collector type, storage capacity, and thermal loads when determining the fraction of the load supplied by solar energy.

A study by Brandemuehl and Beckman describes an economic evaluation method for optimally sizing combisystems with the utilization of the F-Chart tool [15]. The study explains the development of a simplified procedure for sizing economically optimal solar combisystems and evaluating the economics of combisystems in comparison to conventional systems without solar. The economic optimization method utilizes a set of derived economic equations to determine the optimal collector area for a

particular climate. The method bases the lifecycle economics of the combisystem on two economic variables, the annual fuel cost savings and the system installed cost [15]. As part of the study, parametric simulations using F-Chart were conducted in various climates to develop energy performance correlations for estimating optimal collector area and evaluating their economic feasibility.

In the development of F-Chart, a number of assumptions about systems and loads are made, which allows for the simplification of performance calculations. For example, in terms of the system model design, the storage tanks are assumed to be isothermal, which leads to conservative energy savings due to the overestimation of the collector inlet temperature [13]. In terms of the thermal loads in the house, F-Chart makes some simplifications. For example, the DHW loads were estimated by assuming a constant DHW delivery temperature, annual average mains water temperature, and constant daily draw. Additionally, the space heating loads are estimated using the degree day method for a residence with a certain building load coefficient [15]. The development of the F-Chart method served as the springboard for the development of several other mathematical correlation methods that were used to determine the annual system performance of solar heating systems. For example, Lameiro et al. derived curve-fits called the GFL Method to determine location-dependent annual performance of solar combisystems [16].

Due to the number of assumptions made to develop F-Chart, such as the assumption regarding the isothermal tank, Duffie et al. [17] studied the accuracy of the F-Chart method in predicting the annual performance of systems that are reasonably close in design to the generic combisystem configuration used in F-Chart. The study compared F-chart predictions and experimental performance results for 20 installed combisystems. The results showed that the agreement between the F-Chart results and actual performance of the installed systems was within 15% [17]. Other studies have also shown good agreement between the measured and F-chart predicted annual performance of solar combisystems [18]. In general, studies have concluded that F-Chart is valid for the predicting the energy savings of systems that are close in design to the F-Chart system configuration and within the ranges of F-Chart model parameters.

2.1 European Classification Research

Over the last 15 years, an increasing amount of research has been performed on the impact of solar combisystem designs. In Europe, most of the solar combisystem design and performance research originated from the IEA Solar Heating & Cooling Programme (SHC). Since then, several European researchers have studied various combisystem design parameters that have an impact on the performance of solar combisystems. Much of the previous research on solar combisystems in Europe has focused on optimization and design of combisystems. The Europeans have evaluated the performance of a variety of combisystem designs and have also evaluated the effect of sizing, storage geometry, collector efficiency and draw profiles on performance of combisystems.

As part of the European IEA initiative, researchers evaluated the performance and classification of existing European combisystem designs in order to better understand how to categorize and compare the different system designs installed in the field [7]. The IEA researchers studied the various combisystem designs and identified 21 unique European designs. The solar combisystem designs identified by the researchers utilize significantly larger solar collector areas as compared to SWHs—typically 2 to 10 times larger— as they need to capture more energy in order to achieve higher solar fractions given the additional space heating load. Also, the researchers found that the domestic hot water solar fraction in these combisystems varied based on the system configuration, but the solar-supplied energy typically accounted for about 10 to 50 percent of the total demand [7]. To ensure that the system can supply hot water and space heat even during days with low solar irradiation, systems utilize an auxiliary heat source that is typically in the form of either an electric element or side-arm fuel-based boiler.

As part of the IEA-SHC Task 26 project, the researchers identified several key design considerations that will increase both the system efficiency and energy savings [7]. The research identified a couple important tank loss guidelines to improve the performance of solar combisystems.

First, in terms of the auxiliary-heated water, both the volume and temperature setpoint of the auxiliary volume in the storage tank should be minimized, but the system should still be designed to meet the load [26]. Studies found that increasing the volume of the auxiliary storage both increases tank losses— due to larger surface areas— and reduces the storage volume available for solar energy charging, thus reducing the system’s solar fraction [21]. The second guideline in the study, which is more obvious, is that tank heat losses should be reduced by adding tank insulation. Of course, there are diminishing returns to add insulation onto a tank, so after certain insulation thickness, it’s no longer cost-effective to add more. A 2004 report examined a variety of parameters on the performance of 12 solar combisystem designs investigated in IEA-SHC Task 26 and found that storage insulation thicknesses above 15 cm do not increase the thermal performances and top insulation is less significant than side insulation because the top area is smaller [26].

2.2 System Size

As part of the IEA-SHC research, the researchers investigated the influence of collector size and storage volume on the energy savings in various European designs [7]. One of the key observations from the study was that larger storage tanks do not necessarily increase the performance of the system and the system performance can even decrease because tank losses are larger in larger storage tanks. The research found that energy savings decrease as specific volume increases above 150 liters/m² for all system designs. The study concluded that a good rule of thumb for storage size is between 50 liters and 100 liters for every square meter of collector.

In one of the early studies, Braun et al. studied the impact of storage volume to collector area on the system performance using TRNSYS annual simulations [19]. The simulations were conducted using Madison meteorological data. The study showed that the solar fraction increases significantly as storage increases up until 50 liters/m². Between 50 liters/m² and 1500 liters/m², the system’s solar fraction is

fairly constant. Above 1500 liters/m², a storage capacity that large enough to provide a couple days of solar storage, the solar fraction of the system increases gradually.

In terms of seasonal storage, the performance of a solar combisystem with seasonal storage (~10,000 gallons of storage) was evaluated for a typical one-story house in Montreal Canada in 2010 [24]. The study concludes that a seasonal storage system is able to fully cover both the space heating and DHW loads using the solar energy exclusively by the second year of operation, when the tank becomes fully charged. However, the simple payback of the system is quite long—ranging from 26 to 55 years depending of the collector efficiency chosen. The results also showed that the seasonal storage combisystem with flat-plate collectors offer better economics as compared to evacuated tube collectors. TRNSYS was used to model the seasonal-storage solar combisystem with radiant floors.

Additionally, a 2010 study by Lundh examined that effect of storage size and storage geometry on the performance of solar combisystems [21]. The main issue with increasing the size of the storage is the increased complication of installation. The height to diameter ratio of commercial tanks is typically 2 to 2.5. To get around installation constraints, installers must use multiple small tanks with conventional dimensions, however the multiple tank setup increases the cost per volume of storage, tank losses and space required in the house. In terms of the geometry of tanks, the study found that a well-insulated storage tank is rather insensitive to the geometry although maximum energy savings are found in systems with height to diameter ratios of 2 to 4 for the storage. The research also found that for a combisystem with 30 m² of collectors and a volume larger than 4 m³ (~1000 gallons) is not cost-effective. Lastly, the study found that systems with internal auxiliary storage increase savings by up to 2.5% as compared to external auxiliary tanks due to increased tank losses associated with external tanks.

2.3 Tank Stratification

Several studies have looked at the impact of stratification on system performance. They have found that in order to operate at maximum efficiency, the solar storage tank should maintain

stratification—cooler temperatures on the bottom and warmer temperatures at the top. Stratification allows the optimal use of the tank with minimal heat tank losses and allows the collector inlet temperature to be as low as possible, thus increasing the efficiency of the solar collector. A study in 1979 showed that increased stratification in the tank will improve the efficiency of solar collectors by 5 to 15 percent [22].

Stratification can be created in tanks by adding heat (charging) to the top of the tank and removing heat (discharging) from the bottom. Charging and discharging occurs through the use of inlets/outlets as well as immersed heat exchangers. Immersed heat exchangers tend to create thermal temperature zones above the heat exchanger when charging the tank and below the heat exchanger when discharging the tank. Creating thermal zones above or below the heat exchanger mixes the water, which limits the amount of stratification created by heat exchangers. On the other hand, charging and discharging the tank using direct inlets/outlets are better at creating stratification than immersed heat exchangers but the inlets/outlets must be positioned correctly to do so. One method for improving stratification in Europe has been to introduce a stratifying tube within the tank. A stratifying tube is an immersed tube with several outlets where the incoming hot water is directed into the tank at the level where the temperature is the same as the incoming water [7]. This stratification strategy is not widely implemented in the U.S. most likely due to the more complex and expensive design of the storage tank.

In 2007, Andersen and Furbo compared three solar combisystem designs in three different houses with different space heating systems [23]. The reference case solar combisystem was equipped with a solar-side immersed heat exchanger and a direct inlet for the space heating loop. The researchers demonstrated the impact of inlet stratification pipes on the thermal performance of the system. Based on the model simulations, they found that the thermal performance of combisystems increases by 7 to 14 percent by using stratifiers for the solar collector loop and space heating loop rather than immersed heat exchangers. Additionally, the study found because loads vary so much throughout the year with combisystems, stratifiers are much better choice as compared to internal heat exchangers and direct inlets because stratifiers are less sensitive to varying operating temperatures.

2.4 Load Variation

A couple of studies have examined the impact of loads on the performance of combisystems. In 2005, Lund investigated the sizing of solar thermal combisystems with short-term heat storage in buildings with different heat loads [25]. The study found that oversizing a solar thermal system to provide some space heating proved to be advantageous for less efficient buildings, where there was a space heating demand in some of the warmer months. However for newer, more efficient buildings, this oversizing strategy leads to a negative economic outcome. The study concluded that sizing the solar thermal system to supply some space heating is not economically advantageous in all residential buildings.

Previous research in Europe has found that more realistic water draw profiles using TRNSYS modeling software will impact the resulting annual solar fraction. A study in 2000 looked at the influence of DHW load profiles with a constant heat demand, since DHW draws can have a severe impact on the temperature stratification in the tank [27]. The study found that the fractional energy savings between models with simplified profiles and models with more realistic profiles (1 minute timescale draws) can differ by up to about 3 percent. The study used TRNSYS and modeled an unpressurized tank with external heat exchangers on the solar supply and DHW load side, and direct heating to the space heating.

2.5 Previous Modeling Simulations

Much of the previous research that has been discussed in this chapter has been conducted with the utilization of simulation software. Historically, the most popular tool for simulating system performance for solar combisystems has been TRNSYS (Transient System Simulations). TRNSYS software is a component-based tool where the users integrates individual components (such as collectors, pipes, tanks, auxiliary heaters) using component inputs and outputs in order to build system models.

In each TRNSYS component, there are component parameters, which are fixed values set by the user, and component inputs, which can either be constant or be passed into the component by another

component's output. In the case of iterative calculations within TRNSYS, the user can specify the convergence tolerance limit which ensures that calculations are accurate within the user's specifications. The specified convergence tolerance will have an impact on the balancing of the energy equations within the system and subsystems.

As part of IEA-SHC Task 26, the researchers simulating the annual performance of combisystems developed a single modeling methodology. This ensured that the simulation results were consistent from system to system for comparative reasons. As part of the methodology, there were several modeling assumptions and simplifications. One of the major assumptions was that the heat losses from the tank and the auxiliary were not considered as heat input to the building [7]. This is an important assumption because heat losses vary depending on the storage temperature, size of storage, storage heat loss coefficient value, the auxiliary efficiency, as well as the location of the system and ventilation of the location. This modeling simplification implies the heat losses do not decrease the space heating load in the winter or increase the space cooling load in the summer. Other assumptions included in the modeling methodology were that the systems were modeled using the hourly weather data, the hot water load time step was 6 minutes, and the collector is treated independently from the building and has no impact on solar gains on the roof.

In the models developed for Task 26, the solar combisystems utilized a large number of TRNSYS components that are standard components that are used for simulating solar water heater systems, such as multi-node storage tanks, immersed heat exchangers, and solar collectors with capacitance effects [27]. These models were all validated against measured data. Additionally, the models developed for the IEA-SHC research utilized a multi-zone building model, however only one zone was used in the building model due to constraints on the simulation duration [7].

Chapter 3

Experimental Analysis

In partnership with Building Science Consortium (BSC), the Community Office for Resource Efficiency (CORE) and Fenton Construction built a high performance home, dubbed a Next Generation (NextGen) home in Carbondale, Colorado that included a solar thermal combisystem. Constructed in 2004, the NextGen home is a 1250 ft², 1-story, 3 bedroom single family residence with a crawl space. From late 2004 to early 2007, the National Renewable Energy Laboratory (NREL) residential buildings researchers performed field testing and long-term monitoring in order to track the performance of key building systems under occupied conditions.

3.1 Experiment Introduction

The solar combisystem components consist of two flat plate solar collectors, a tankless condensing boiler, and a pressurized solar storage tank with two immersed heat exchangers (see Figure 3.1).

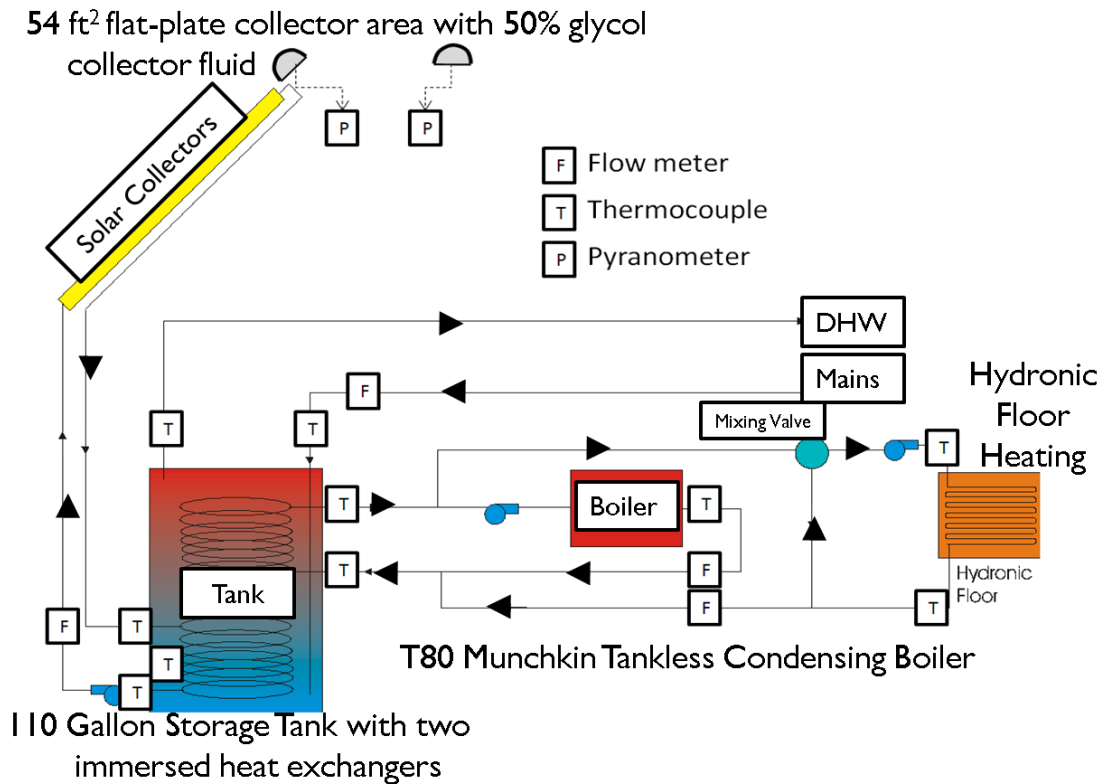


Figure 3.1: Schematic of the combisystem along with the data acquisition equipment[1].

As seen in Figure 3.1, the storage tank is indirectly connected with the solar collectors and the boiler/space heating through coiled immersed heat exchangers within the tank. The solar collector loop utilizes a glycol/water mixture and it transfers heat to the tank through the lower immersed heat exchanger. The boiler/space heating utilizes the upper heat exchanger to transfer heat to and from the tank. The tank is pressurized and the domestic hot water is directly heated by the tank. Table 3.1 describes the primary system components.

Table 3.1: Combisystem components in the NextGen home in Carbondale, Colorado.

System Component	Manufacturer/Model	Size/Capacity	Other Notes
Flat Plate Solar Collectors	Heliodyne Gobi 3366 with glycol/water heat transfer fluid	53.6 ft ²	1.1 gallon fluid capacity; 26 lb copper absorber; Intercept efficiency: 0.701; 1 st order coefficient: 3.732 W/m ² -C; 2 nd order coefficient: 0.0107 W/ W/m ² -C ² ; Linear Fit IAM coefficient: -0.26
Tankless condensing boiler	Munchkin T80	80 kBtu/hr capacity	92% AFUE; Efficiency varies with return water temperature and partial load conditions
Pressurized Storage Tank	Steibel Eltron 2 coil SBB 400 K SOL	110 gallons	Two immersed heat exchangers (copper), Upper HX length- 55.12 ft; Lower HX length- 40.2 ft; Tank PU Foam insulation: 2.95 in. thick

The NREL researchers installed several sensors and a data acquisition equipment to monitor the system. Thermocouples and flow meters were attached to individual flow loops within the system (the collector loop, the DHW, and the space heating loop) and data was sampled at a one minute interval and stored once per hour. All the data was collected using a Campbell Scientific CR10 data acquisition system, which was connected to a standard telephone line for remote communications. The data logger was located in the utility closet because the tank and boiler, as well as the sensors measuring the performance of the combisystem were located in the utility closet. Figure 3.1 shows the location of the thermocouples, flow meters, and pyranometers used to measure the performance of the combisystem [1].

Four water flow meters and ten thermocouples were installed to facilitate measurement of the solar and auxiliary energy to the DHW and space heating loads [1]. To determine the energy delivered to the DHW load, a flowmeter measured the volume flowrate of the cold water entering the pressurized tank. The inlet and outlet fluid temperatures were measured by surface-mounting thermocouples on the pipes, which were covered with R-5 pipe insulation. To determine the energy delivered to and from tank through the upper heat exchanger, flow meters measured the volume flowrate through the boiler as well as through the hydronic floor. Thermocouples were used to measure the inlet and outlet water temperature of the upper heat exchanger. To measure the useful energy from the solar collectors, a flow meter measured

the flow rate in the solar collector glycol loop. The temperature difference across the lower exchanger was measured using thermocouples, which were attached to the collector loop pipes in the utility closet [1]. The tank temperature was measured using a thermocouple placed in the lower dry well of the tank, which was located in between the inlet and outlet ports of the lower heat exchanger (see Figure 3.1). Lastly, to measure the indoor environment temperature, thermocouples were installed in four locations within the house, including the utility closet. The indoor air temperature thermocouples were located inside shields mounted 5 feet above the floor on interior walls [1].

The pipes leading to and from the solar collector from the tank are estimated by researchers as being 20 feet in length for each direction— with 5 feet of the pipe being located in outdoor ambient conditions and 15 feet in conditioned space[65]. The pipes have an inside diameter of 0.75 inches and are covered with R-2.5 insulation.

Figure 3.2 shows the southwest elevation view of the Carbondale house with the solar combisystem installed. The photovoltaic array is located on the sloped roof on the left and the two flat plate solar collectors are mounted on the window overhang on the right side of the house. To measure the solar radiation, two pyranometers were installed on the house. The tilted pyranometer was mounted on the upper left corner of the PV array at a 45 degree angle, which is on the same plane as the flat plate collectors. The horizontally-mounted pyranometer was located at the peak of the main roof (Figure 3.2).

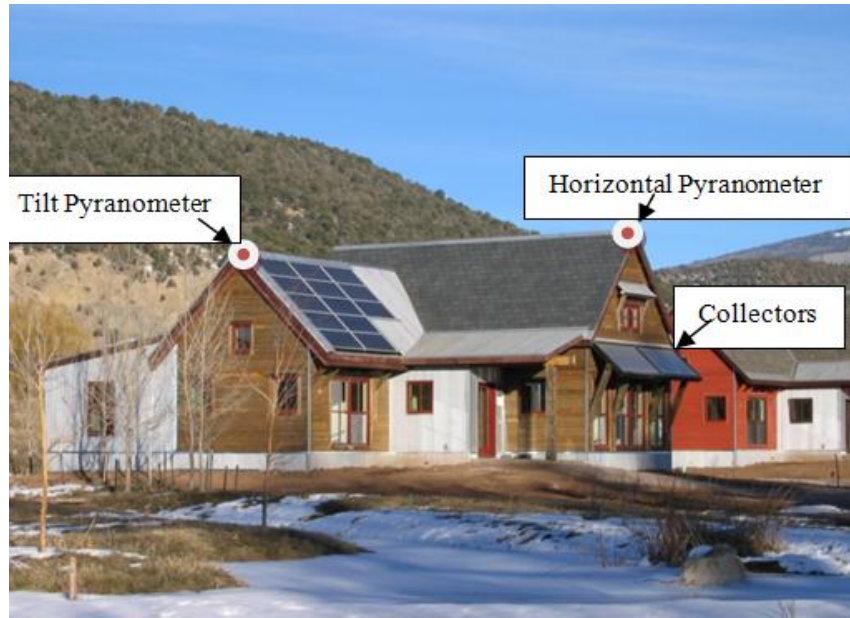


Figure 3.2: The tilted pyranometer is located in the upper left corner of the PV array and the horizontal pyranometer is located at the peak of the main roof [1].

The data acquisition system stored the data every hour for two years; however there were a couple of days where the researchers stored the one-minute interval data. Data stored in late December 2004 provided two full days to examine the near real-time performance of the system. During these two days, the weather was sunny and cold, which meant that the solar collector pump, the boiler pump, and the hydronic floor pump were all delivering energy to and from the tank. The two days of one-minute interval data collection occurred between the afternoon of December 25th and the afternoon of December 27th. Figure 3.3 shows the tilted and horizontal solar radiation during those 48 hours of one-minute interval measurements. The pyranometer readings show the site received high amounts of solar radiation on both days, with the second day of the data collection being partly cloudy.

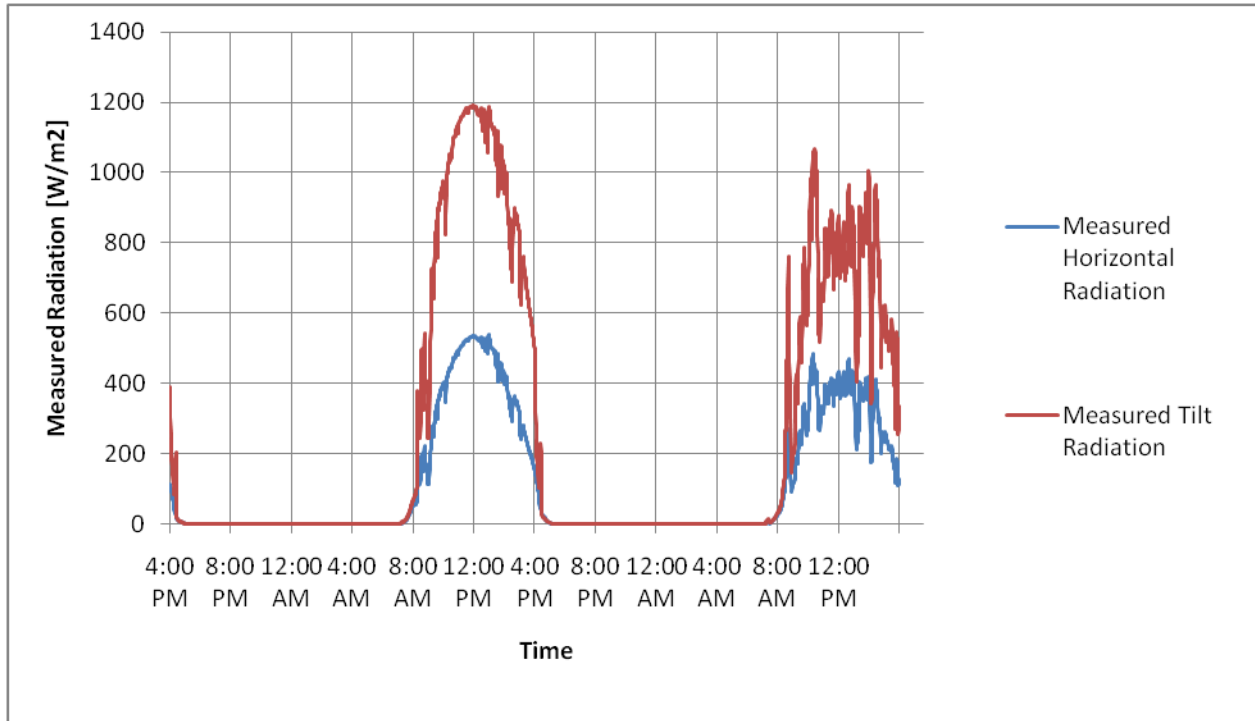


Figure 3.3: Solar radiation data collected as well as the calculated extraterrestrial horizontal radiation during the two days of one-minute interval data (December 25th- December 27th).

Figure 3.4 shows the collector loop temperature and flow rate outputs during the two days of one-minute interval data. This data shows that over the 48 hours of data collection, the ambient outdoor temperature ranged from -15 degrees Celsius to 3 degrees Celsius. By observing the collector loop flow rate and the collector inlet and outlet temperatures during the first night, one will notice what appears to be reverse thermo-siphoning during the first night of data collection. The one-way check valve, which was installed on the collector loop to prevent flow in the reverse direction, was evidently not functioning correctly [1]. The reason the flow meter data shows the flow measurements in the forward direction is because the flow meter pulse counter cannot distinguish between forward and reverse flow.

Due to the malfunctioning check valve, thermal energy was being extracted from the tank more quickly during the first night, as observed by the bottom tank temperature measurement (see Figure 3.4). The figure shows that the heat loss rate from the tank as shown with the tank temperature sensor is

roughly 10 times larger during first night of data collection as compared to the second night, where no reverse thermo-siphoning occurs. On the sunny day (December 26th), the temperature difference between the collector inlet and outlet averaged to be 1.9 °C and the flow rate through the collector was 11.35 liters per minute, which is equivalent to 3 gallons per minute. As seen in Figure 3.4, the collector flow meter has a resolution limit of 1 pulse per gallon (equivalent to 1 pulse per 3.78 liters), which presents some error limitations when validating the system performance. In order to overcome these limitations, a moving average for the flow rate was calculated in order to smooth out the flow rate variation caused by the resolution limits.

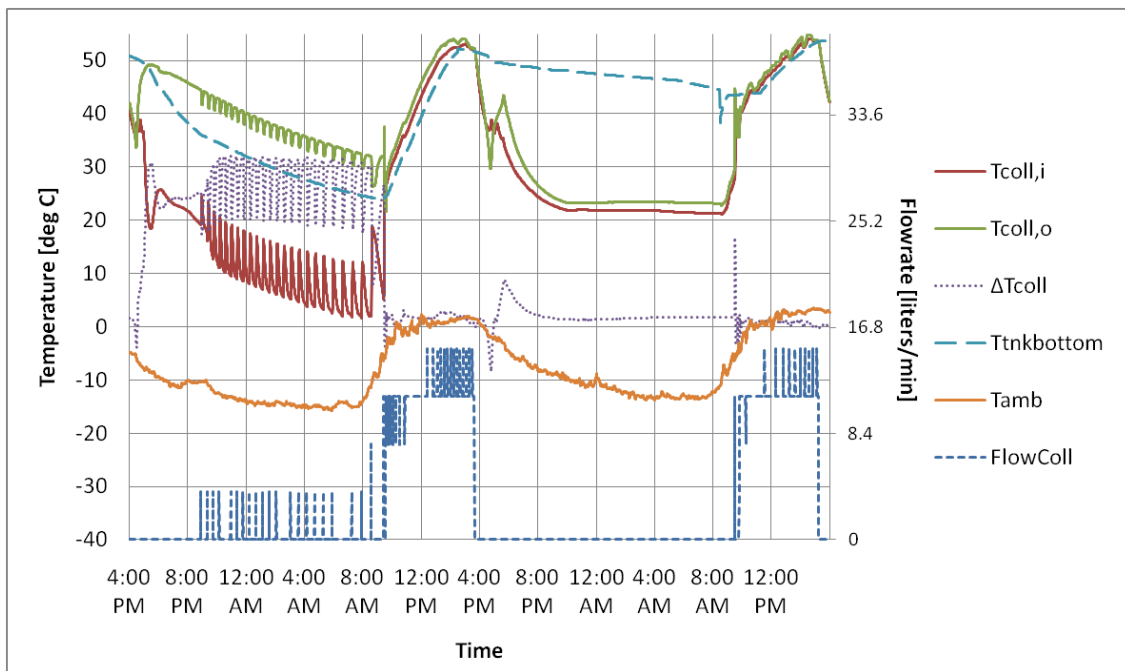


Figure 3.4: One-minute interval collector loop data collected from 4pm on December 25th to 4pm on December 27th

The flow through the upper heat exchanger, which serves as the heat exchanger to transfer heat into the tank from the boiler and transfer heat out of the tank to provide heat to the hydronic floor, ranged from 0 to 35 liters per minute over the course of the two days of one-minute interval data collection. During the monitoring period, there were times when both the boiler pump and hydronic floor pump were

both operating, periods when only either the boiler pump or heating pump were operating, and periods when there was no flow through the upper heat exchanger. Figure 3.5 shows that the hydronic floor pump and the boiler pump were operating during the nighttime in order to maintain the house setpoint and they both turned off during the day when the house was heated passively.

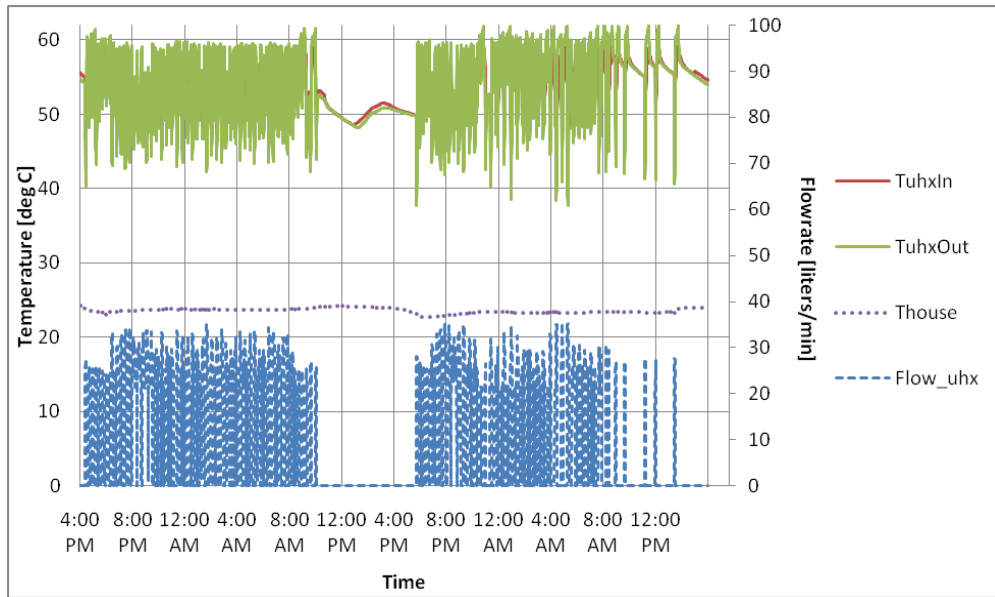


Figure 3.5: One-minute interval data showing the upper heat exchanger inlet and outlet temperature and flow rate measurements. The house temperature data shows that the setpoint was roughly 23 °C.

A closer look at the temperature and flow rate data for the upper heat exchanger reveals that heat can either be extracted from or added to the tank via the upper heat exchanger depending on the temperature of fluid entering the tank. Figure 3.6 shows that when inlet fluid temperatures are high, the boiler is on and heat will be added to the tank, whereas when inlet fluid temperatures are low, heat will be extracted from the tank.

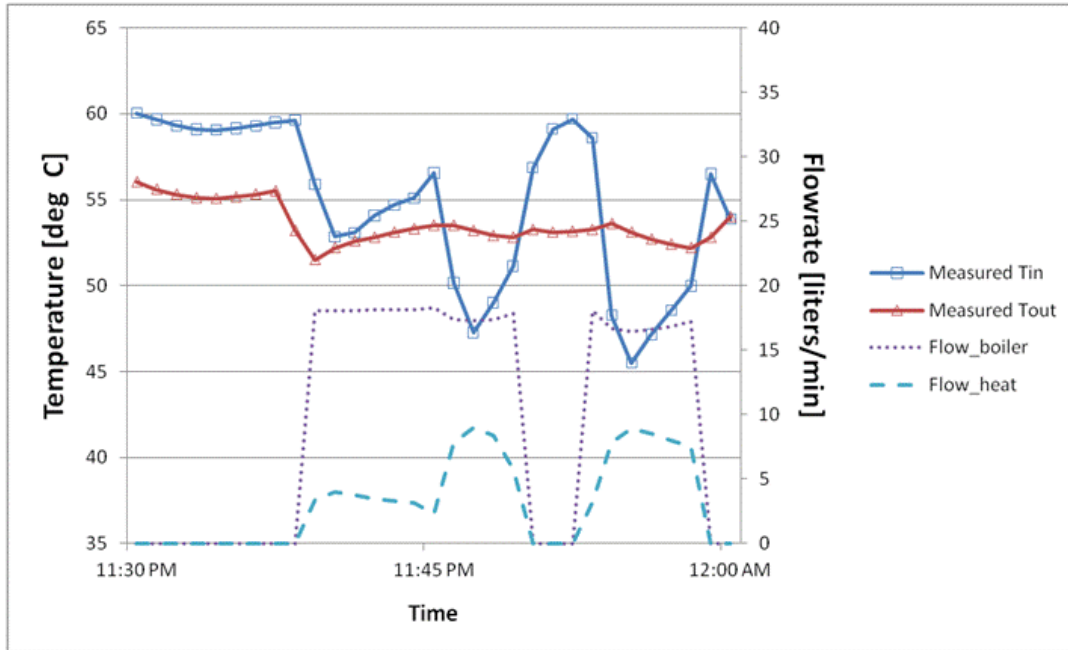


Figure 3.6: 30 minute data period of measured temperature and flow rates for the upper heat exchanger shows that heat is both added and extracted from the tank via the upper heat exchanger

In Figure 3.6, the flow from the tank to the radiant floor system varies. This variation in flow is due to the tempering valve, which controls the flow from the tank to the tempering valve depending on the temperature of that fluid and the temperature of the return fluid from radiant floor system. As seen in Figure 3.7, the tempering valve maintains a constant supply temperature of about 37 °C. Additionally, the flow through the radiant floor is constant at 20 liters per minute.

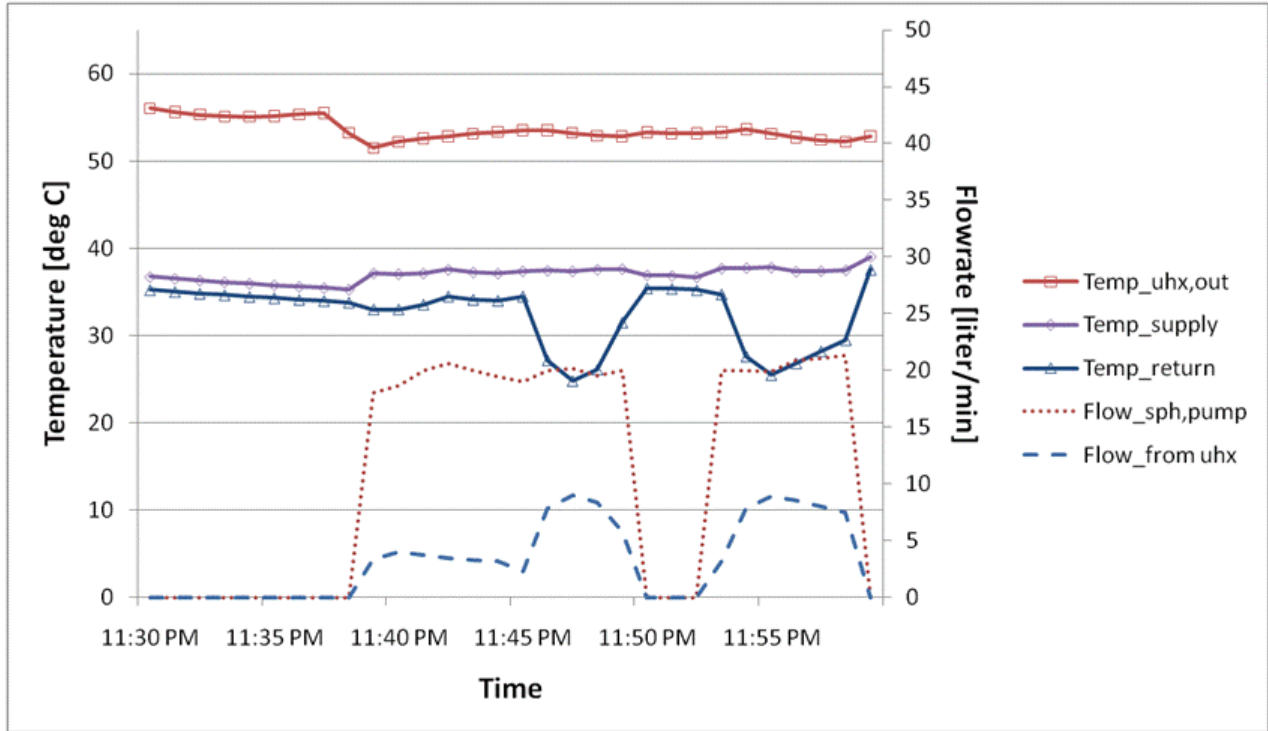


Figure 3.7: Due to the space heating tempering valve, the flow from the upper heat exchanger to the varies. However, the flow through the radiant floor is constant at 20 liters per minute.

The domestic hot water data shows that, during the two days of one-minute interval data collection, there were less than a dozen discrete hot water draw events. Two of these draws had flow rates greater than 5 liters per minute and most of the draws had flows that were less than 2 liters per minutes (see Figure 3.8).

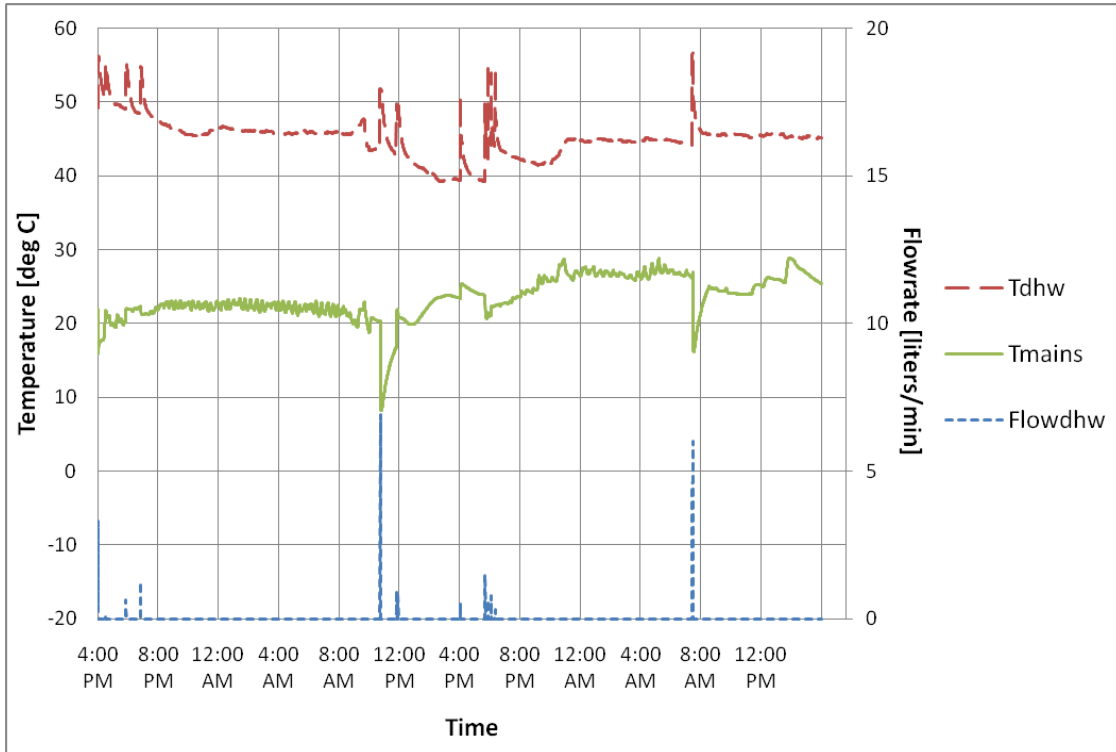


Figure 3.8: One-minute interval domestic hot water inlet and outlet temperatures and flow rates.

3.2 Uncertainty Analysis

An uncertainty analysis quantifies the accuracy and the precision in the experimental data measurements. The uncertainty of a measurement has two error components, which can be combined in order to quantify a measurement's total error [44]. The bias error (σ_{bias}) and the random error (σ_{rand}) are combined to determine the total error by taking the square root of the sum of the squares of the individual errors as shown in equation 3.1.

$$\sigma_{\text{total}} = \sqrt{\sigma_{\text{bias}}^2 + \sigma_{\text{random}}^2}$$

3.1

First, the bias error (also referred to as the systematic error) can be thought of as the accuracy of the measurement. Bias errors will generally occur in experimental data when a sensor or its data acquisition systems is not calibrated correctly. For example, if a thermocouple consistently reads 0.5°C as the temperature of ice water when the value to be measured is 0°C, the measurement has a bias error of 0.5°C. For this experimental analysis, the bias error used to quantify the uncertainty is taken directly from the quoted uncertainty by the manufacturer's specifications.

The random error, which is also known as the measurement precision, can be caused by unknown and unpredictable noise during the monitoring. The random error can occur within the measurement equipment (such as high frequency noise in electronic circuits) or in the environmental conditions (such as sudden changes in ambient air temperature due to pockets of warm air). Random errors are thought of as having a Gaussian normal distribution and can typically be determined by calculating the standard deviation (Equation 3.2):

$$\sigma_y = \sqrt{\frac{1}{N-1} \sum_{i=1}^N (y_i - y_m)^2} \quad 3.2$$

Where N is the sample size, y_i is the observed values of the sample measurements and y_m is the mean value of the measurements. However, determining the random error based on the standard deviation requires that the measurement be repeated identically over the sample. Since measurements were not repeated identically during the monitoring period, the random error was taken as zero.

3.2.1 Thermocouples Differential Bias Error

The Omega Type-T thermocouples used to monitor the system had a quoted tolerance of ± 0.5 °C or $\pm 0.4\%$ at temperatures greater than 125 °C [42]. The manufacturer does not specify the confidence limit of the ± 0.5 °C tolerance, so it is assumed in this analysis that the thermocouples have a 2 standard deviation (95%) measurement confidence level [46], which means that a standard deviation of ± 0.25 °C

will be assumed. Additionally, the Campbell Scientific CR10 data logger, which was used to measure the voltage created by the thermocouples, have a quoted tolerance for the reference junction temperature of ± 0.2 °C [43]. Additionally, the thermocouples will present a bias in temperature readings due to their placement on the surface of the pipes (covered by about R-5 insulation) rather than within the fluid. The bias error as a result of the surface mounting will vary depending on the ambient and fluid temperature, but a simple thermal resistance network calculation reveals that the bias error will be about 0.1 °C at nominal operating conditions. By taking the square root of the sum of the squares of the individual bias error, the thermocouple will have a total bias uncertainty of about ± 0.3 °C.

However, since the difference in thermocouple temperature measurements was used to calculate heat rate values, it can be assumed in the analysis that a number of bias errors in the thermocouple measurements will cancel out. For example, it could be assumed that wires used in the thermocouples came from the same location on the spool of wire (which reduces the variation in material property errors when calculating ΔT). Additionally, the two thermocouples are using the same calibration circuitry in the data logger, which cancels out most of the error in measuring the reference temperature. Lastly, since both thermocouples are surface mounted and covered with the same insulation material, the bias will also mostly cancel when calculating the temperature difference. Therefore, for this analysis, when a temperature is used when differenced with another thermocouple, it is assumed that the ΔT measurements will have a total bias error of ± 0.2 °C.

3.2.2 Error propagation of calculated values

The error propagation of the calculated values using several pieces of experimental data was determined based on the Kline-McClintock method of uncertainty analysis [33]. With the goal of determining the effects of each potential measurement error, the Kline-McClintock method examines the impact of individual uncertainties and is referred to as the propagation of uncertainty. The total uncertainty, σ_y , in a function $y=f(x_1, x_2, \dots, x_n)$, can be estimated as follows using the uncertainties of each independent measured variable, $\sigma_{x,i}$:

$$\sigma_y = \sqrt{\sum_{i=1}^n \left(\frac{\partial y}{\partial x_i} \sigma_{x_i} \right)^2}$$

In Equation 3.3, $\sigma_{x,i}$ is the total error in each of the individual measured values (x_1, x_2, \dots, x_n) and $\frac{\partial y}{\partial x_i}$ is the partial derivative of the calculated value with respect to each individual measured value.

3.2.3 Calculating the total uncertainty

As discussed above, the bias errors were derived from the manufacturer's quoted tolerance values and the random errors were set to zero. Based on these assumptions, the errors are summarized in Table 3.2. Since the solar radiation and fluid flow bias errors are stated in percentages and these measurements vary, the total error is stated at a nominal measurement value.

Table 3.2: Components of the data acquisition system on the solar combisystem along with their bias, random, and total errors.

Measurement	Component	Make/Model	σ_{bias}	σ_{random}	$\sigma_{\text{total (nominal)}}$
Solar Radiation [W/m ²]	Pyranometer	Li-Cor, Inc LI-200SZ	±5%	-	±40 W/m ² (at 800 W/m ²)
Fluid Flow [liters/min]	Water Meter	Omega FTB-6107-A-PS	±1.5%	-	±0.17 liters/min (at 11.35 l/m)
Temperature Differential [°C]	Type T Thermocouples	Omega FF-T-20S-TWSH	±0.2 °C	-	±0.2 °C

Using the thermocouple, flow rate, and pyranometer data, the instantaneous collector efficiency, η , was calculated by taking the ratio of useful energy gain by the collector over the total incidence radiation on the collector (see Equation 3.4).

$$\eta = \frac{\dot{V} \rho c_p \Delta T}{A_{coll} G_T} \quad 3.4$$

Where \dot{V} is the volumetric flow rate, ρ is the fluid density, c_p is the fluid specific heat, A_{coll} is the SRCC-reported collector gross area and G_T is the total incidence radiation. The collector fluid was stated to be nominally 50% glycol and 50% water [65], which means that the density is 1041 kg/m³ and the specific heat is 3.55 kJ/kg-°C. The flow meter calibration was based upon water as the work fluid, rather than the glycol mixture.

The partial derivatives were then derived based on Equation 3.4 for calculating the uncertainty for the efficiency at each time step. The first partial derivative shows the uncertainty of the efficiency with respect to the delta temperature measurements.

$$\frac{\partial \eta}{\partial \Delta T} = \frac{\dot{V} \rho c_p}{A_{coll} G_T} \quad 3.5$$

The next partial derivative shows the uncertainty of the efficiency with respect to tilt radiation measurement:

$$\frac{\partial \eta}{\partial G_T} = -\frac{\dot{V} \rho c_p \Delta T}{A_{coll} G_T^2} \quad 3.6$$

Lastly, the partial derivative with respect to volume flow rate is shown below:

$$\frac{\partial \eta}{\partial \dot{V}} = \frac{\rho c_p \Delta T}{A_{coll} G_T} \quad 3.7$$

The total uncertainty for the experimental collector efficiency from the measured values is:

$$\sigma_\eta = \sqrt{\left(\frac{\partial \eta}{\partial \dot{V}} \sigma_{\dot{V}}\right)^2 + \left(\frac{\partial \eta}{\partial G_T} \sigma_{G_T}\right)^2 + \left(\frac{\partial \eta}{\partial \Delta T} \sigma_{\Delta T}\right)^2} \quad 3.8$$

At nominal operating conditions, volume flow rate uncertainty component, $\frac{\partial \eta}{\partial \dot{V}} \sigma_{\dot{V}}$, is 0.5%, the temperature uncertainty component, $\frac{\partial \eta}{\partial \Delta T} \sigma_{\Delta T}$, is 4%, and the radiation uncertainty component, $\frac{\partial \eta}{\partial G_T} \sigma_{G_T}$, is 1.9%. The total uncertainty at nominal operating conditions is 4.4%.

Next, the uncertainty of the heat transfer for the flows going into the tank was determined. First, using the thermocouple and flow rate data, the instantaneous heat transfer rate, \dot{Q} , was calculated by multiplying the volume flow rate, density, specific heat, and temperature delta values.

$$\dot{Q} = \dot{V} \rho c_p \Delta T \quad 3.9$$

The partial derivatives with respect to the two measurements were derived as follows:

$$\frac{\partial \dot{Q}}{\partial \dot{V}} = \rho c_p \Delta T \quad 3.10$$

$$\frac{\partial \dot{Q}}{\partial \Delta T} = \dot{V} \rho c_p \quad 3.11$$

The total uncertainty for the experimental tank heat transfer from the measured values is:

$$\sigma_{\dot{Q}} = \sqrt{\left(\frac{\partial \dot{Q}}{\partial \dot{V}} \sigma_{\dot{V}}\right)^2 + \left(\frac{\partial \dot{Q}}{\partial \Delta T} \sigma_{\Delta T}\right)^2} \quad 3.12$$

3.3 Sky Models

Since the solar radiation data was collected by pyranometers, instruments that measure the total solar radiation, sky models were required to split the total radiation into beam, sky diffuse, and ground diffuse components. The split of the total radiation into beam, sky diffuse, and ground diffuse radiation components is required when modeling the solar collector performance because each of these components has a unique effective incidence angle. The unique effective incidence angle of each radiation component impacts the total absorbed solar radiation of the flat-plate collector because the transmittance-absorptance product ($\tau\alpha$) of the collector is angular dependent for each radiation component [29].

There are a couple of methods for splitting the total radiation into beam, sky diffuse, and ground diffuse components. In this validation study, both the isotropic model and the Hay and Davies model were considered. Both are relatively simple models in comparison to a complex model such as the Perez model, which uses empirical formulas and tables [29]. Studies examining the accuracy of these models have found that the isotropic model is poor at estimating tilt radiation as compared to anisotropic models, such as the Hay and Davies model and Perez model [34] [36] (see Table 3.3).

Table 3.3: Validation results for diffuse irradiance models that compared the errors of three sky models using measured data in Albany, NY [36]

	Root Mean Square Error [kJ/hr-m ²]	Mean Bias Error [kJ/hr-m ²]
Isotropic	125.5	46.2
Hay	87.2	23.3
Perez	49.1	11.8

The sky model method ultimately chosen for this validation study was the Hay and Davies model, since it required simple calculations and provided relatively accurate results as shown in Table 3.3 [36]. In the Hay-Davies model, the diffuse radiation component takes into account both the isotropic component and the circumsolar diffuse component [29]. In comparison, the isotropic model only takes into account the isotropic component for calculating the sky diffuse component, which results in a lower diffuse radiation component for south-facing surfaces. To account for the circumsolar diffuse radiation, the Hay and Davies model uses an anisotropy sky index, A_i , which is calculated as:

$$A_i = \frac{I_b}{I_o} \quad 3.13$$

And is a function of the beam radiation, I_b , and the extraterrestrial radiation, I_o .

Utilizing the anisotropy sky index, the Hay and Davies tilted surface diffuse radiation is calculated as:

$$I_{d,T} = I_d \left[(1 - A_i) \left(\frac{1 + \cos \beta}{2} \right) + A_i R_b \right] \quad 3.14$$

where R_b is the tilt benefit geometry factor, and β is the slope of the collector. Within the brackets of equation 3.14, the first term represents the isotropic sky diffuse radiation and the second part represents the circumsolar diffuse radiation. The amount of circumsolar and beam radiation on a tilted surface is

estimated by using the geometric factor, R_b , which is the ratio of beam radiation on the tilted surface to radiation on a horizontal surface. The geometry factor is expressed as:

$$R_b = \frac{\cos \theta}{\cos \theta_z} \quad 3.15$$

where θ_z , the zenith angle, represents the position of the sun in the sky relative to a horizontal surface and θ , the incidence angle, represents the position of the sun relative to the sloped surface. To correlate I_d/I , the fraction of radiation on a horizontal plane which is diffuse, with the clearness index (k_T), the Erbs correlation was used [35]. In the Erbs correlation, smaller k_T values results in a higher fraction of diffuse radiation. The clearness index is calculated using the horizontal irradiance (I) and extraterrestrial irradiance (I_o).

$$k_T = \frac{I}{I_o} \quad 3.16$$

Lastly, the total radiation on a tilted surface using the Hay and Davies model is calculated as:

$$I_T = I_b R_b + I_d \left[(1 - A_i) \left(\frac{1 + \cos \beta}{2} \right) + A_i R_b \right] + I \rho_g \left(\frac{1 - \cos \beta}{2} \right) \quad 3.17$$

Where ρ_g is the ground reflectance, which is assumed to be 0.2, I is the total horizontal radiation, and I_d is the diffuse radiation on the horizontal plane. Within equation 3.17, the first term is the beam component, the second term is the sky diffuse component, and the last term is the ground diffuse component.

To solve for these three components using measured tilt radiation data, an iterative approach is required to solve for horizontal total radiation (I), horizontal beam (I_b), and horizontal diffuse radiation (I_d), while taking into account that the horizontal total radiation is equal to the sum of the horizontal beam and horizontal diffuse radiation. For the iteration process, first the horizontal total radiation (I) is assumed to be some value, then the horizontal diffuse radiation (I_d) and horizontal beam radiation (I_b) are

determined using the Erbs correlation, and lastly the total tilt radiation is calculated using equation 3.17. If the calculated total tilt radiation is either too small or large than the measured total radiation, the horizontal total radiation is either increased or decreased. When the measured and the calculated total radiation are within $1 \times 10^{-6} \text{ W/m}^2$ of each other, the iteration process is terminated.

Based on the Hay and Davies sky model and the Erbs correlation, the total measured tilt radiation was split into beam, sky diffuse, and ground diffuse components (see Figure 3.9). The model calculations show that about one-third of the radiation on the mostly sunny day is diffuse radiation and the rest is beam radiation.

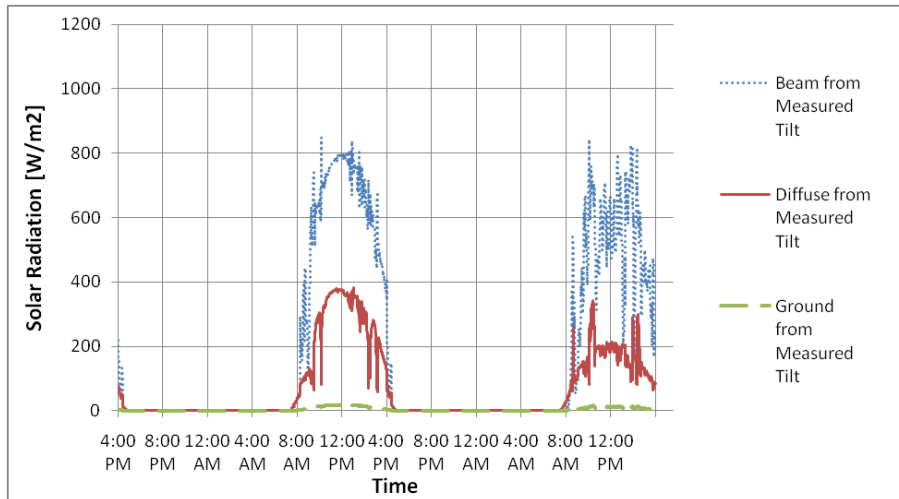


Figure 3.9: Utilizing the Hay and Davies sky model, the tilt radiation was split into beam, sky diffuse, and ground diffuse components.

Next, Figure 3.10 shows the measured tilt radiation as compared to the calculated tilt radiation from the horizontal radiation using the anisotropic sky model. The figure shows that the calculated tilt radiation from the horizontal radiation data is up to 10% lower than the measured tilt radiation.

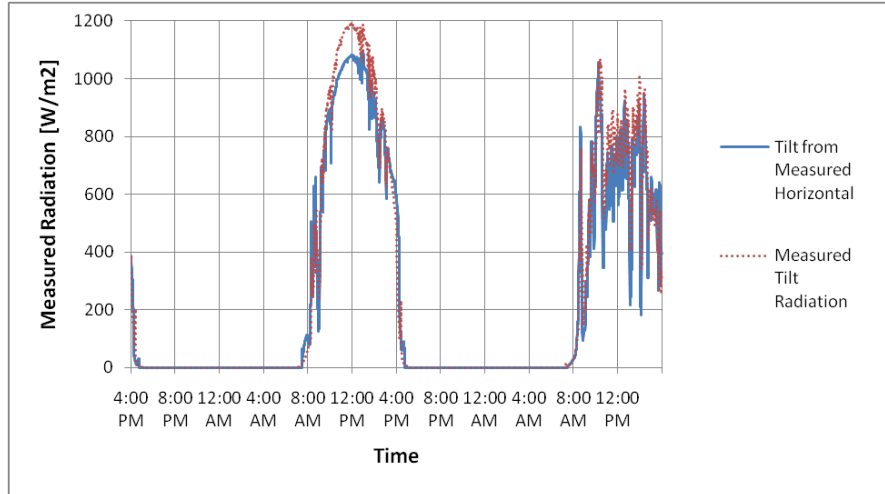


Figure 3.10: Comparing the total measured tilt radiation to the calculated total tilt radiation using the measured horizontal radiation.

Additionally, Figure 3.11 shows the horizontal radiation data split between the beam, diffuse and ground diffuse components using the Hay-Davies model.

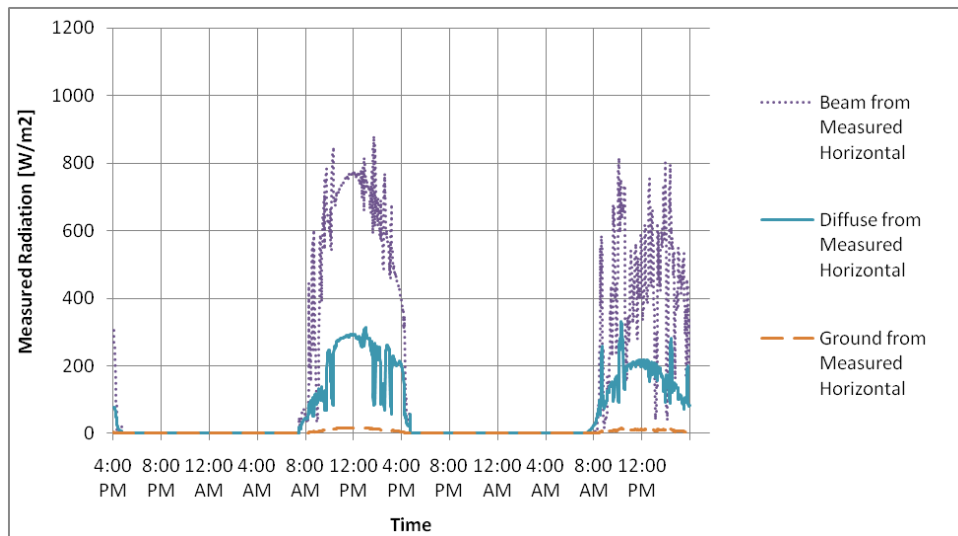


Figure 3.11: Utilizing the Hay and Davies sky model and the Erbs correlation, the measured horizontal radiation was split into beam, sky diffuse, and ground diffuse components.

Next, the two radiation values, the measured tilt radiation and the calculated tilt radiation based on the horizontal radiation, were used to determine the measured efficiency of the collector. Figure 3.2

shows that the measured efficiency is significantly lower than the expected steady state efficiency of the collector. The expected steady state efficiency is derived using the collector's SRCC rating values (see Appendix A). The figure also shows that using the calculated tilt radiation from the horizontal radiation measurements yields a slightly higher measured collector efficiency as compared to calculating the measured efficiency using the measured tilt radiation values.

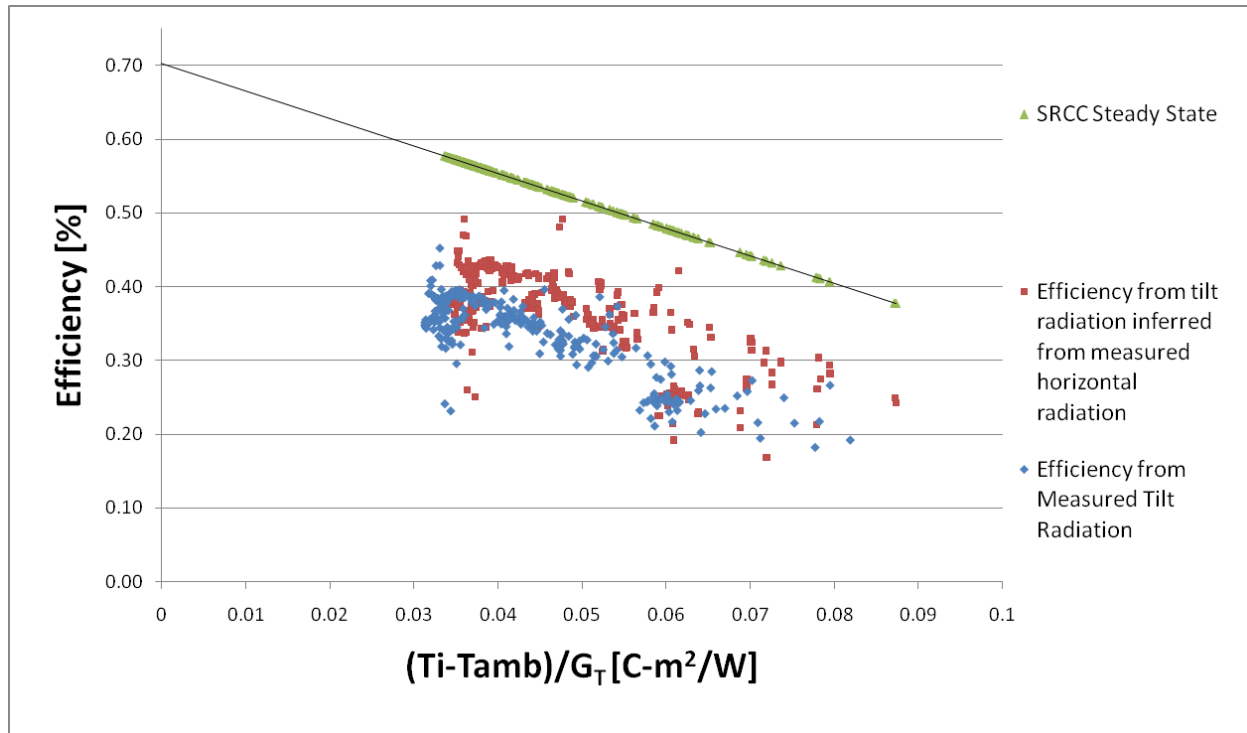


Figure 3.12: Comparing the calculated solar thermal collector efficiency using the measured tilt radiation, the calculated tilt radiation from the horizontal radiation, and the steady state efficiency using SRCC efficiency parameters.

Because the horizontal radiation measured data yielded collector efficiency results that showed a better correlation to the expected collector efficiency as compared to the tilt radiation measured data, the tilt radiation data was considered suspect. Additionally, during the monitoring process, the researchers compared the collector plane pyranometer's measurement to a measurement in the same plane using an instrument-grade thermopile pyranometer, and confirmed that the original tilt pyranometer was providing readings that were about 10 percent to high [65]. Additionally, the tilted pyranometer is situated on the

roof where reflections from the metal roof coverings and the PV array contribute to the incident radiation measurement. This extra radiation would have resulted in an unrealistically large irradiance when calculating the collector efficiency. Based on this information, it was decided to utilize the horizontal radiation data rather than the tilt radiation data to evaluate the measured efficiency of the collector.

Next, with the derived uncertainty of the measured collector efficiency, the measured efficiency using the inferred tilt radiation values from the horizontal radiation data, is compared against the SRCC steady state efficiency (see Figure 3.13). The figure shows that steady state efficiency lies outside the bounds of the measured collector efficiency uncertainty. The bias error of the measured efficiency as compared to the steady state efficiency is 18%. However, it should be noted that the measured data shows an efficiency trend that matches the expected steady state efficiency trend as a function of $\Delta T/G_T$.

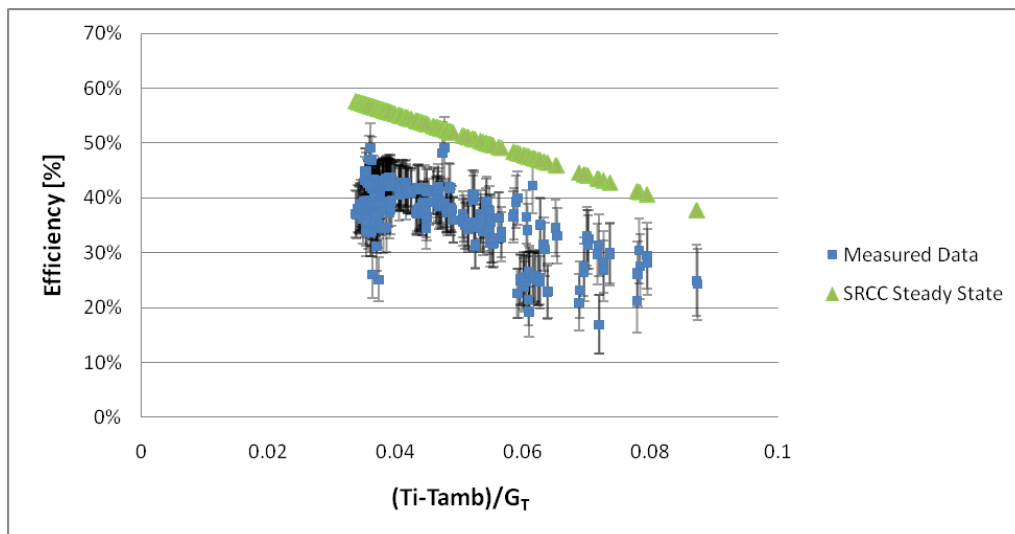


Figure 3.13: Comparing measured data with uncertainty error bars to the expected steady state efficiency

3.4 Explanations for Low Measured Collector Efficiency

It is evident that measured efficiency has a significant bias error. There could be a number of reasons for the poor performance of the solar collectors. In terms of explaining why the measured efficiency for the solar collectors is much lower than expected, it is possible that number of factors came into play.

For one, it could be that the horizontal pyranometer was not calibrated correctly. However, even after calculating the tilt radiation using the Hay-Davies sky model with the horizontal radiation measurements while assuming a low ground reflectance coefficient of 0.2, which is a conservative reflectance coefficient that assumes no snow cover, the measured efficiency was still significantly lower than expected. Utilizing a higher ground reflectance coefficient, such as 0.8 (which would mean that there was snow cover), to calculate the tilt radiation would have resulted in measured collector efficiencies with an even larger bias as compared to the expected collector efficiency.

Also, it is possible that collectors were just poor performing collectors. For example, the collectors may have had manufacturer defects and there is the possibility that the collectors were soiled, which could significantly impact the transmittance-absorbance efficiency of the collector. Poor performance could also be explained by a low quality absorber coating, or a glazing that differs from the specified glazing. Another possibility is that one or more risers in the collectors may be blocked with debris, reducing the effective collector area and degrading performance.

3.4.1 Flow Meter Bias

Another factor that could lead to significant bias error in the collector's measured efficiency is the inaccuracy of the flow rate measurement, which is somewhat in question because the flow meter calibration is stated for pure water, which has a kinematic viscosity of 1 centistoke (mm^2/s), as opposed to glycol mixtures, which have larger kinematic viscosities. According to the flow meter manufacturer,

turbine flow meters are highly sensitive to viscosity variations and should be calibrated for measuring fluids that have a higher viscosity than water [45].

Kinematic viscosity is the fluid property that quantifies its resistance to flow and it can have a significant impact on the rotational speed of the rotor within the flow meter. Therefore utilizing a turbine meter for measuring the flow rate of a fluid with a viscosity that differs from what the meter was calibrated for will create a bias error in the flow rate measurements. The bias error will result in measured flow rates are the lower than the actual flow rates, which consequentially results in measured collector efficiencies that are lower than the actual collector efficiency.

Table 3.4 shows the kinematic viscosities of various glycol/water solutions at 20°C ranging from 0% to 50% glycol by weight [29]. If it is assumed that the percent glycol in the collector fluid is 50%, the fluid has a viscosity that is six times larger than the viscosity of pure water, which is significant enough to result in bias errors in the flow rate measurements when using a turbine flow meter.

Table 3.4: Kinematic viscosities of propylene glycol solutions

Percent Glycol in glycol/water mixture	Kinematic Viscosity [centistokes]
50%	6.2
40%	4.3
30%	2.9
20%	2.0
10%	1.5
0%	1.0

Figure 3.14 shows the impact of viscosity variations from 1 to 100 centistokes on various sized flow meters ($\frac{1}{2}$ " to 3") as published by the flow meter manufacturer [45]. The turbine flow meter used to measure the collector fluid flow rate is a $\frac{3}{4}$ " meter and was measuring flow rates that were 15% of its maximum flow rate measurement. In Figure 3.14, the normalized K-factor represents the number of pulses the flow meter generates per unit of volume of fluid. A K-factor that is less than 1.0 presents a bias

error in the flow measurements. The figure shows that smaller flow meters are more sensitive to higher viscosities. Additionally, the figure shows that the lower portion of the flow meter's measurement range is more sensitive to viscosity variations than the higher portion of the flow meter's measurement range.

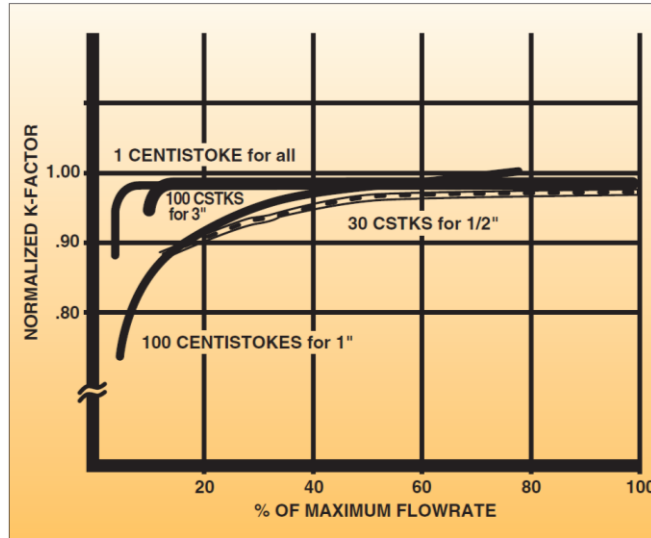


Figure 3.14: Viscosity effect on a turbine meter's K-factor [45]

Based on the information presented in Figure 3.14 and assuming the viscosity of the glycol/water mixture is 6 centistokes, it is difficult to determine a precise bias error for the flow meter. However, after conversing with the manufacturer's flow meter representatives [46], a normalized K-factor was estimated to be as large as 0.95, which translates into a 5% bias error flow measurement. An assumed 5% bias error in the flow rate will result in calculated measured efficiencies that are 2.5% lower than the actual measured collector efficiency, assuming that the collector efficiency is 50%. The bias in the flow measurement has an impact on the calculated measured efficiency, however as shown in Figure 3.15, the flow rate bias error by itself does not seem to completely explain the lower than expected collector efficiency.

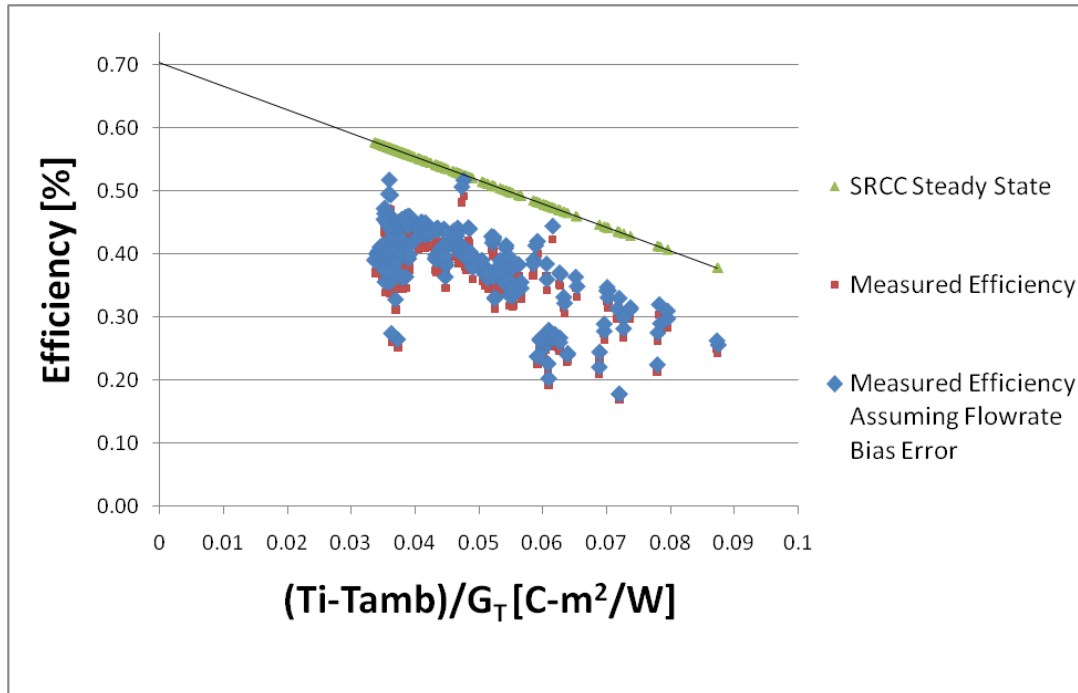


Figure 3.15: The impact of the bias error of the flow meter on the measured efficiency in the collector.

3.4.2 Fluid Specific Heat

Lastly, there may be a gross error in the assumed glycol/water mixture. For this analysis, based on the experimental information received [65], it was assumed that the percent glycol was 50%, which meant that the specific heat by volume was 3699 kJ/m³-C. If the percent glycol was really 20% as opposed to 50%, the specific heat by volume increases to 4081 kJ/m³-C, which leads to a 13% increase in the calculated useful energy gain by the collector. Table 3.5 shows the impact of the glycol/water mixture on the volumetric specific heat of the fluid.

Table 3.5: Impact of glycol/water mixture on the volumetric specific heat of the fluid.

Percent Glycol in glycol/water mixture	Specific Heat (by mass) [kJ/kg-°C]	Density [kg/m ³]	Specific Heat (by volume) [kJ/m ³ -°C]
50%	3.55	1040	3692
40%	3.74	1034	3868
30%	3.91	1026	4010
20%	4.01	1017	4081
0%	4.18	1000	4180

Figure 3.16 shows the impact of the glycol properties on the measured efficiency of the collector. For the assumed 50% glycol mixture, the measured efficiency has a bias error of 18% relative to the collector steady state efficiency, whereas with a 20% glycol mixture, the measured efficiency has a bias error of 10% relative to the collector steady state efficiency.

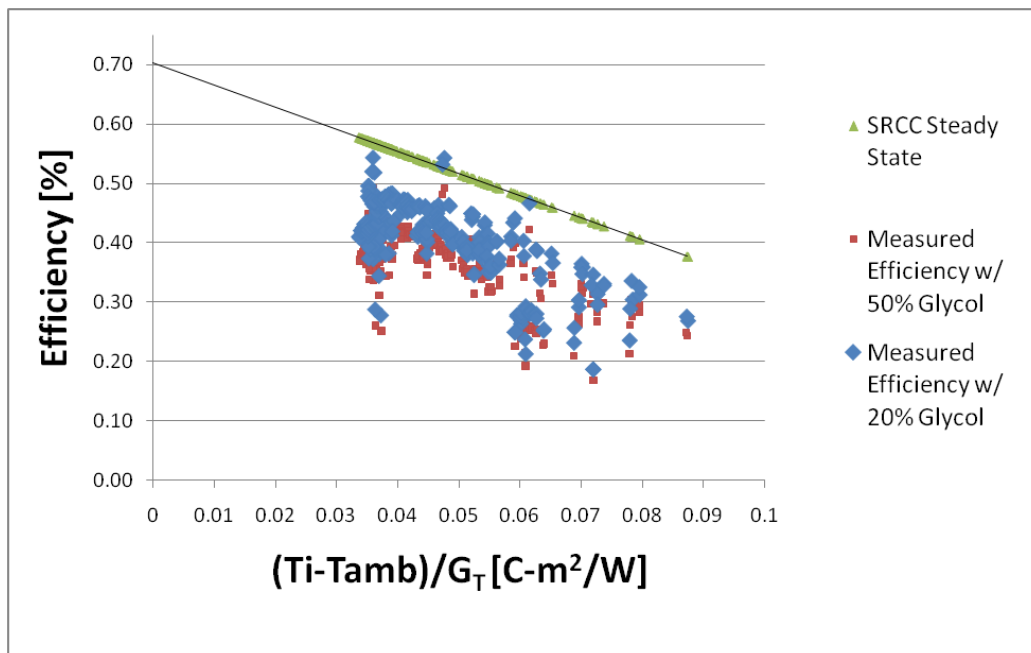


Figure 3.16: The impact of the glycol mixture on the measured efficiency in the collector.

3.5 Impact of Pipe Losses on Measured Efficiency

In the experiment, the thermocouples measuring the collector fluid temperatures were located inside of the utility closet, which meant that the standalone collector efficiency was not being measured due to extra energy losses in the pipes leading to and returning from the collector. By measuring collector fluid temperatures inside the house, one can think of the combination of the pipes leading to and returning from the collector and the solar collector itself as having a thermal performance similar to the standalone collector, but with modified values for the loss coefficient, $F_R U_L$ and the transmittance-absorbance

efficiency $F_R(\tau\alpha)$ [29]. These two collector parameters, U_L and $(\tau\alpha)$ help describe the steady-state instantaneous efficiency of collector using the definition:

$$\eta = \frac{Q_u}{A G_T} = F_R(\tau\alpha) - \frac{F_R U_L (T_i - T_a)}{G_T} \quad 3.18$$

Where T_i is the collector inlet temperature and T_a is the ambient temperature. The modified efficiency equation that includes pipe losses will be similar to equation 3.18, but will have modified transmittance-absorbance and loss coefficient values denoted as $(\tau\alpha)'$ and U_L' respectively [29]. Using Duffie and Beckman as a reference [29], the modified transmittance-absorbance value is derived as:

$$\frac{(\tau\alpha)'}{(\tau\alpha)} = \frac{1}{1 + \frac{U_d A_o}{(\dot{m} C_p)_c}} \quad 3.19$$

And the modified loss coefficient is derived as:

$$\frac{U_L'}{U_L} = \frac{1 - \frac{U_d A_i}{(\dot{m} C_p)_c} + \frac{U_d (A_i + A_o)}{A_c F_R U_L}}{1 + \frac{U_d A_o}{(\dot{m} C_p)_c}} \quad 3.20$$

Where A_i and A_o are the areas for the heat loss of the inlet and outlet pipes, U_d is the loss coefficient from the pipes, which takes into account the insulation thickness and conductivity surrounding the pipes. Using these equations derived from Beckman [29] as well as the pipe dimensions as described in the beginning of this chapter, the modified transmittance-absorbance efficiency coefficient is calculated as 0.7005, which is less than 0.1% lower than the collector's quoted $F_R(\tau\alpha)$, and the modified loss coefficient is 3.925, which is 5% larger than the collector's quoted $F_R U_L$. It turns out that the modified coefficient only makes a minor impact on the steady state efficiency as seen in Figure 3.1. Even though

the pipe loss has a minor impact on the collector efficiency; the impact of the pipe losses was still included when modeling the system in TRNSYS.

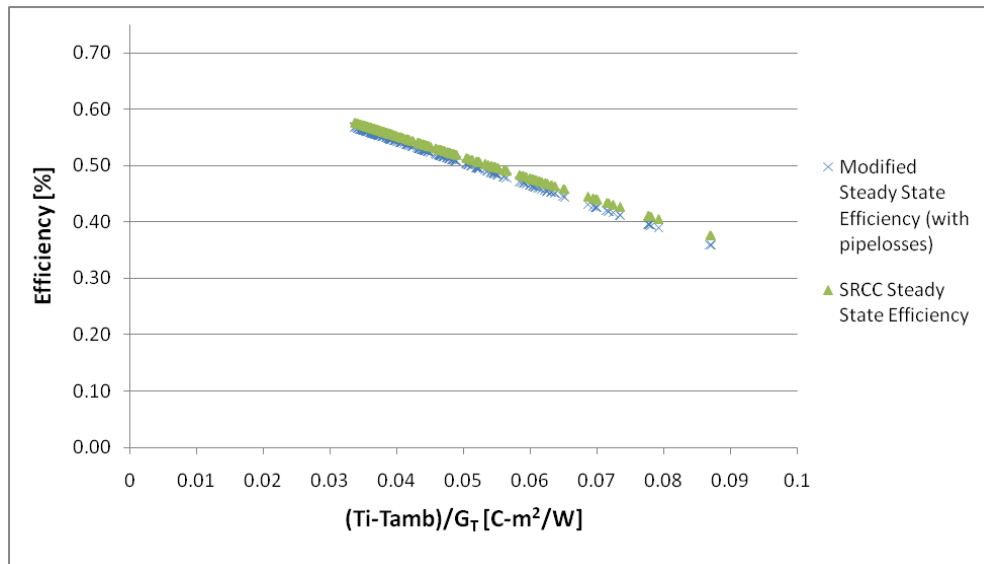


Figure 3.17: Comparing the quoted SRCC steady state efficiency to a modified steady state collector efficiency that takes into account the pipe losses which come into play when measuring the collector fluid temperatures in the utility room.

3.6 Tank Loss Coefficient

The decay method is used to determine the overall loss coefficient of the tank. The tank loss coefficient, also known as UA_{tank} , is determined by the decaying tank temperatures during the nighttime hours in the summer, when there were no solar gains and no DHW and space heating loads. To calculate the loss coefficient, the temperature data from the single tank temperature sensor was used. Ideally, the average tank temperature is used to calculate the total loss coefficient of the tank since the temperature decay rates at the bottom of the tank can differ from temperature decay rates at the top of the tank [32]. There are a number of causes for differing temperature decay rates throughout the tank including thermal shorts at different locations within the tank. For example, ground thermal shorts at the bottom supports of the tank could cause the temperature at the bottom of the tank to decay more quickly than the temperature

at the top of the tank. However, given that only one tank temperature sensor was used during the monitoring of the Carbondale combisystem, that single temperature node was used to calculate the tank loss coefficient. The sensor was located in the solar temperature sensor well, which is located in the mid-section the lower heat exchanger.

Although, no information on the tank's stratification is known in this case, it is expected that when the solar loop is operating during the day, the tank is well-mixed and when no energy is added during the nighttime, the tank becomes stratified due to the natural convection currents that form within the tank. The natural convection currents are caused by heat loss through the side walls of the tank. The heat loss through the walls results in the fluid near the side walls of the tank to have a lower temperature than the temperature at the center of the tank. The relatively cooler fluid on the sides of the tank then flows downward, thus causing a convection current off the tank side walls. This convection current loop that occurs during stratification may result in the tank temperature at the bottom of the tank to decay more rapidly than the temperature at the top of the tank [32].

Figure 3.18 shows the temperatures in the tank over the course of a week during the summer. During this time period, there are no flow rates through the upper heat exchanger, however there are some nighttime DHW draws, which results in increased temperature decays in the tank during the night. To determine the approximated loss coefficient of the tank, the temperature decay data during the nights without DHW draws was used.

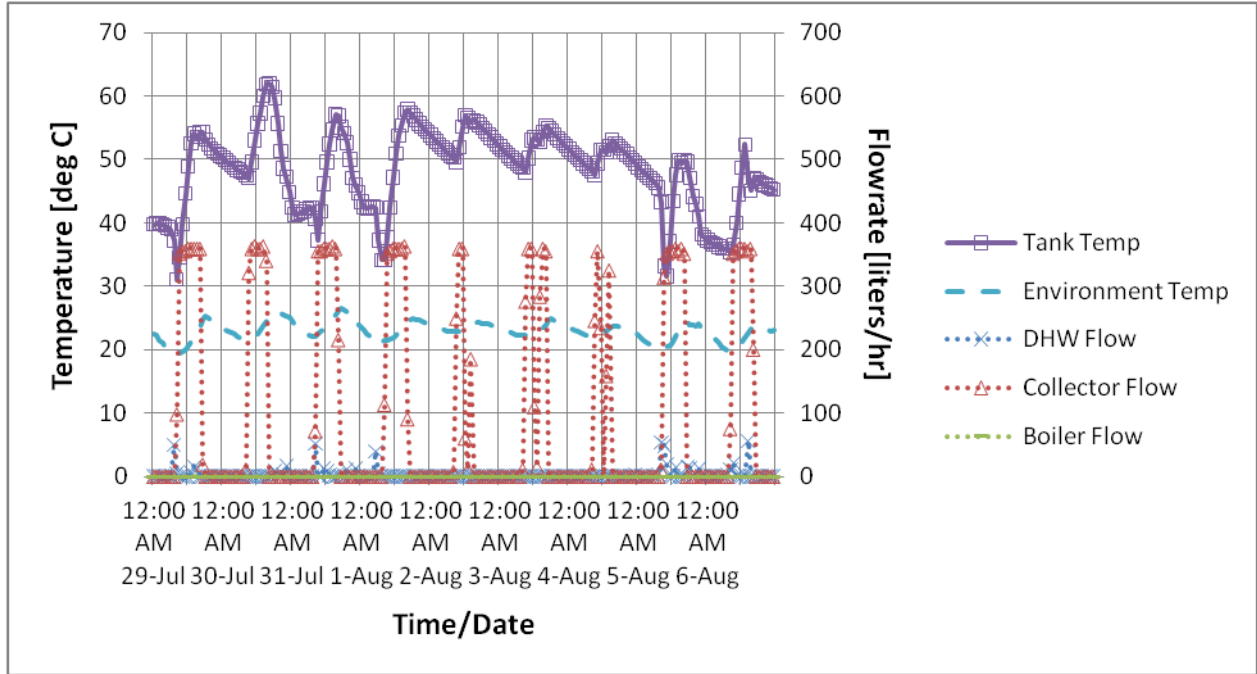


Figure 3.18: Hourly Data showing tank temperature data for the duration of one week. The load and collector flows are also shown to indicate when the temperature decays occur in order to calculate the tank loss coefficient.

With a known tank capacitance, $(mC_p)_{\text{tank}}$, and known environment temperatures surrounding the tank, the rate of energy lost from the storage tank, $\frac{dQ}{dt}$, can be determined by measuring the rate of temperature decay, $\frac{dT_{\text{tank}}}{dt}$. The tank loss coefficient is calculated from the expression:

$$UA_{\text{tank}} = C_{\text{tank}} \frac{\ln \left(\frac{T(t_{\text{beg}}) - T_{\text{env}}}{T(t_{\text{end}}) - T_{\text{env}}} \right)}{t_{\text{end}} - t_{\text{beg}}} \quad 3.21$$

where C_{tank} is the capacitance of the tank, $T(t_{\text{beg}})$ and $T(t_{\text{end}})$ are tank temperatures at the beginning and ending times of the decay, T_{env} is the ambient temperature for the tank.

Based on a selection of nighttime temperature decay time periods during the summer with no DHW or space heating load draws, the average loss coefficient of the tank for each of these decay time periods was calculated to be 2.3 ± 0.6 W/C, which is equivalent to an R-value of about $7.6 \text{ hr-F-ft}^2/\text{Btu}$. By comparison, the tank has 2.95 inches of polyurethane foam insulation, which would have an R-value of $17.7 \text{ hr-F-ft}^2/\text{Btu}$, assuming that polyurethane foam has a thermal conductivity of 0.022 W/m-K [49] . The reason for the reduced overall R-value of the tank is most likely due to the uninsulated “thermal shorts” caused by the copper pipes attached to the tank and immersed heat exchangers as well as the tank supports. The heat loss coefficient results mirrors the rule of thumb used by SRCC to calculate the effective tank UA values that include all thermal shorts, which is to halve the R-Value of the insulation [12].

Chapter 4

System Model

One of the main goals of this project is to determine whether it is cost-effective to add extra components, such as an extra heat exchanger and more complex controls, onto a standard solar domestic hot water system in order to supplement the space heating load with solar energy. In order to evaluate the impact that adding a space heating component has on the increased performance of a solar water heater, it is desirable that both the SWH and the combisystem models be similar systems utilizing the same collector area, storage size, and solar-side heat exchanger.

It is expected that a small combisystem that is setup to be used for DHW and space heating will offset most DHW loads year round (except during the winter) and will only contribute minimally to the space heating during the shoulder months in the Spring and Fall when there is still heating loads and the solar collectors are operating at higher efficiencies as compared to the winter months. As collector area and storage volume increase, the amount of solar energy utilized is expected to increase in a solar combisystem configuration. However, the amount that the system will offset auxiliary space heating loads will depend on several factors, such as the loads and vacation periods. For example, if the homeowner takes a vacation in the middle of winter, the solar thermal energy that would otherwise be wasted in a SWH can be used to heat the home.

4.1 Model Description

There were several important design considerations that played a large role in creating the combisystem model. First, the model was never intended to be enhanced by altering the storage design in order to study the optimal combisystem design. The model was based solely on the Carbondale system,

which used a single tank to serve as both the solar storage and the auxiliary storage. Second, based on previous research which showed that combisystems operate more efficiently when paired with radiant floor heating systems, since radiation floor heating systems require lower supply temperatures as opposed to baseboard convectors, the model utilized a radiation floor heating system to give the combisystem as much of an advantage as possible. Additionally, it was decided to substantially oversize the auxiliary heater in the system, so that there would be minimal issues with the system not being able to meet both the space heating and domestic hot water loads. Lastly, the auxiliary heating element was placed within the upper portion of the tank between the upper and lower inlets of the upper load-side heat exchanger. This placement allowed the upper heat exchanger to utilize both solar storage (below the auxiliary heater) and auxiliary storage (above the auxiliary heater) to meet the space heating load.

Figure 4.1 shows the combisystem schematic as it was modeled in TRNSYS. Similar to the Carbondale system, the modeled system is a single tank system with a solar-side lower heat exchanger and a space heating load-side upper heat exchanger. The domestic hot water ports are directly connected to the tank.

In terms of controls, the tank has a set point of 51.67 °C (125 °F) with a 2 °C (3.6 °F) deadband that is centered on the setpoint. The solar loop control system utilizes a differential controller with an upper deadband of 10 °C (18 °F) and a lower deadband of 2°C (3.6 °F), which means that the solar pump starts operating when collector outlet fluid temperature is 10°C above the temperature at the bottom of the tank and the pump is turned off when the collector inlet fluid temperature falls to only 2°C above the temperature at the bottom of the tank. Additionally, if the lower thermostat on the tank reaches 88°C (190 °F), the solar controller shuts down the solar pump in order to prevent tank overheating.

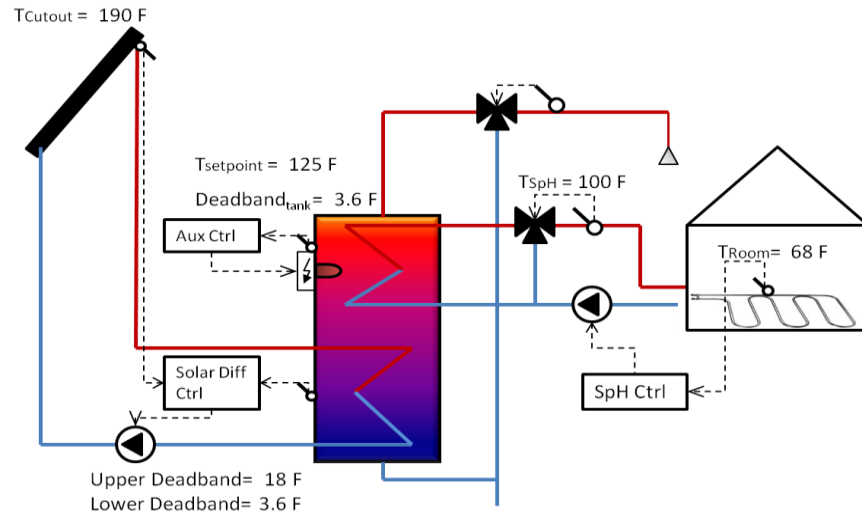


Figure 4.1: A solar combisystem with an electric resistance heater, an indirect solar loop, an indirect space heating loop, and a pressurized tank.

The upper element in the combisystem tank is located approximately 6 inches from the bottom of the upper heat exchanger. This was designed so that the upper heat exchanger, which supplies the space heating load, can utilize energy that is collected from the solar collectors whenever the tank temperature at the level of the bottom of the upper heat exchanger is higher than the return water temperature from the radiant floor space heating. The portion of the heat exchanger that is above the tank heating element is being supplied energy from the auxiliary heat source. The capacity of the auxiliary heater in the tank for the combisystem is oversized at 30 kW, which is a theoretical capacity, in order for the tank to be able to meet both the space heating and DHW loads.

The SWH is similar to the combisystem, however rather than having an upper heat exchanger, the space heating load is being met with a separate auxiliary heat source that is connected to the radiant floor space heating loop (see Figure 4.2). The control scheme for the solar loop and the auxiliary heating element are the same as the control scheme for the combisystem solar loop and auxiliary heating element. The capacity of the auxiliary heater in the SWH is set to 4.5 kW which is a typical capacity for electric elements in a SWH.

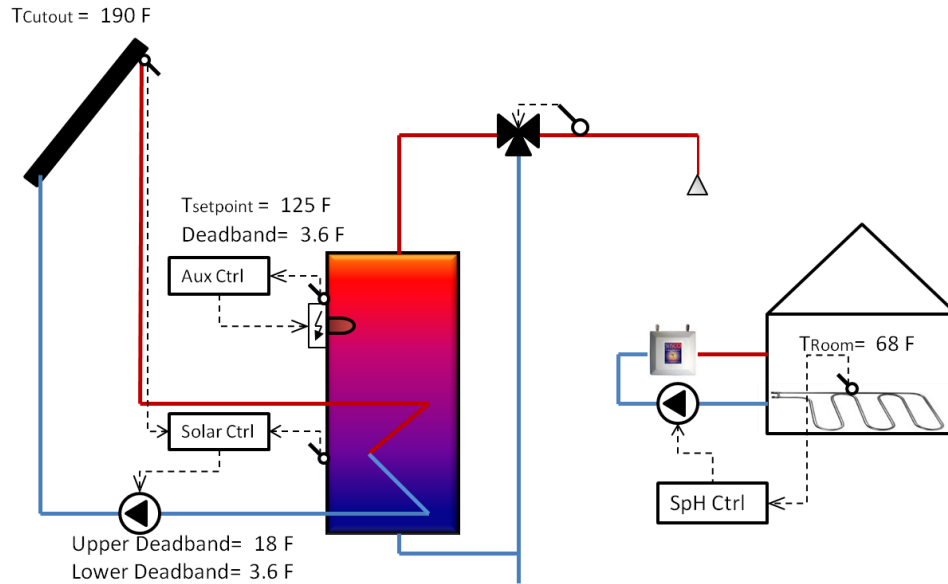


Figure 4.2: A solar DHW system with an electric resistance heater, an indirect solar loop, and a pressurized tank. The space heating load is being supplied through an electric tankless boiler connected to a radiant floor loop.

The study compares the auxiliary energy use of the solar thermal systems to a conventional 36 gallon electric hot water tank. In the conventional water heater setup, two 4.5 kW electric resistance elements provide power to heat the tank. The controller for the elements utilize master/slave control scheme, so that only one element is on at a time. In a master/slave control system for the electric resistance water heater, the top element is the master and the bottom element is the slave in the control scheme. The bottom element only turns on if the upper thermostat setpoint is satisfied— meaning that the upper element is off— and the bottom thermostat temperature is below the lower deadband. In this model, both the upper element and the bottom element have a thermostat with the same setpoint of 125°F, but the upper thermostat controlling the upper element has a deadband of 2 °C (3.6 °F) and the lower thermostat controlling the lower element has a deadband 5°C (9 °F).

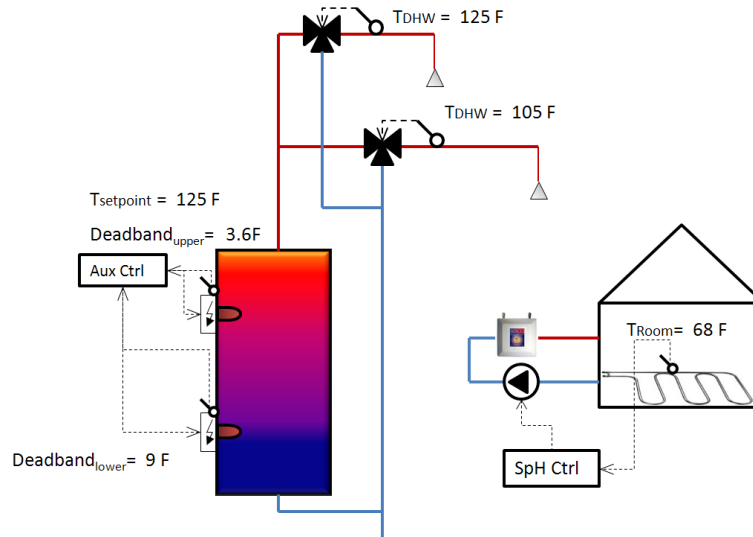


Figure 4.3: Schematic of the conventional water heater with a dual element electric water heater and a electric boiler providing heat for the space heating load.

A couple of important modeling assumptions were made when developing the model. First, it was assumed that the heat losses from the tank did not interact with the home's thermal zone. This modeling assumption implies the heat losses do not decrease the space heating load in the winter or increase the space cooling load in the summer. For a 144 gallon tank, which is the storage size for a 96 ft² collector area system, the annual tank losses were on the order of 3 GJ. For a Denver benchmark house, the tank losses during the heating season are equivalent to roughly 5% of the space heating load. So, if the tank losses were assumed to interact with the home's thermal zones, they would reduce heating auxiliary energy usage by roughly 5%, which is a significant reduction in auxiliary energy usage. However, if the tank losses interacted with the building's thermal zone during the cooling season, the air conditioner loads would increase significantly especially because the tank is operating at higher temperatures, which increases the tank losses.

Other assumptions included in the modeling were that the model operated on a 1-minute time step, the collector is treated independently from the building and has no impact on solar gains in the attic, and the inlet piping from the mains was placed outside the house.

4.1.1 Space Heating Schedule

For all the simulations, the space heating set point was set year round at 20 °C (68 °F) which is 1.67 °C lower than the Building America benchmark heating setpoint. The set point is lower than the Building America benchmark set point because it is assumed that the thermal comfort is improved by adding the radiant floor heating due to the floor surface temperature being higher with a radiant floor system in comparison to a conventional forced air heating system. The deadband for the space heating thermostat in the model is set at 0.5 °C.

4.2 TRNSYS Components

Several standard components from the TRNSYS 17 library such as the data reader, radiation processor, plotters/printers and integrators were used to develop the combisystem models. Simulations were run at 1-minute time step intervals to match the data collection intervals during the Carbondale house validation study, which represents a good compromise between representing realistic draws and simulation duration. The following TRNSYS components were used to simulate the systems.

4.2.1 Flat Plate Solar Collector with Capacitance: Type 539

A flat plate solar collector with capacitance effects was used to model the flat plate collector in TRNSYS (Type 539) [67]. Type 539 models a solar thermal collector that considers the effects of the collector mass, which includes the collector fluid, tubes, and absorber plate, on the performance of the system. Capacitance is important to model in thermal collectors since the capacitance impacts the instantaneous efficiency of the system. The model utilizes system parameters such as the transmittance-absorbance efficiency ($F_R(\tau\alpha)$), the loss coefficient ($F_R U_L$), the second order loss coefficient, the test flow

conditions, and the incidence angle modifier (IAM), which are all values that are published as part of the Solar Rating Certification Corporation (SRCC) certification[39].

The absorber model is divided into a user-specified number of nodes in the flow direction in an effort to describe the temperature of the fluid as it flows through the absorber. In each node, the solar gains, thermal losses and the effects of capacitance are calculated [67]. The general differential equation for the calculating fluid temperature for each isothermal node j in a solar thermal collector with capacitance effects is expressed as:

$$C_j \frac{dT_j}{dt} = F' (S_j - A_j U_L (T_j - T_{amb})) - \dot{m} C_p (T_j - T_{inlet,j}) \quad 4.1$$

where C_j is the absorber mass including the heat transfer fluid divided by the number of nodes, F' is the collector efficiency factor, S_j is the total absorbed solar radiation (a function of the incidence angle modifiers for beam and diffuse terms) divided by the number of nodes, A_j is the total collector area divided by the number of nodes, T_j is the collector fluid temperature of the node, $T_{inlet,j}$ is the fluid temperature entering the node, and U_L is the overall thermal loss coefficient. The total absorbed radiation, S , is expressed as:

$$S = (\tau\alpha) * IAM * A_{coll} * G_T \quad 4.2$$

Where $(\tau\alpha)$ describes how the collector absorbs solar energy, IAM is derived using the incidence angle and user-specified IAM coefficients, G_T is the total radiation incident on the tilted solar collector.

Lastly, the collector efficiency factor, F' , represents the ratio of the actual useful energy gain to the useful energy gain if the collector absorber temperature was the temperature of the fluid and is derived using the user-specified test condition and collector performance parameters:

$$F' = -\frac{\dot{m}_{test} C_{p,test}}{A U_L} \ln \left(1 - \frac{F_R U_L A_C}{\dot{m} C_p} \right) \quad 4.3$$

To solve these equations, the model uses an approach where it sets a collector removal factor (F_R) to a typical value, calculates the collector characteristics F' , U_L , and $(\tau\alpha)$, and then solves the nodal differential equation for each collector node [67]. It turns out that collector removal factor (F_R) is arbitrary due to the nature of the variables in the equations, so therefore F_R can be set to any typical value without hindering the calculation of the collector characteristic variables.

4.2.2 Storage Tank: Type 534

The stratified tank is modeled using the vertically cylindrical fluid-filled, constant volume storage tank with immersed heat exchangers model, Type 534 [66]. This model is a TESS storage tank library component that allows the user to divide the tank into isothermal temperature nodes to model stratification created in storage tank. In this model, the tank is divided into a user-specified number of nodes and energy balances are calculated for each section of the tank and temperatures of the each node are calculated for each time step. The nodes interact thermally with nodes above and below through fluid conduction and fluid movement. The fluid in the storage tank also interacts thermally with the fluid in the immersed heat exchangers, the surrounding ambient temperature, and directly through inlet and outlet ports.

In simple terms, the model can be described using energy balance equations which calculate each node's temperature and the temperature of the heat exchanger at each time step,

$$\frac{dT_{Tankj}}{dt} = \frac{(Q_{inj} - Q_{out,j})}{C_{Tankj}} \quad 4.4$$

where $Q_{in,j}$ and $Q_{out,j}$ are tank node energy functions that are dependent on ambient temperature, inlet fluid conditions, flow rates, and heat exchanger temperature, and the temperature of the heat exchanger at each time step,

$$\frac{dT_{HX}}{dt} = \frac{(Q_{in,HX} - Q_{out,HX})}{C_{HX}} \quad 4.5$$

where $Q_{in,HX}$ and $Q_{out,HX}$ depend on the inlet fluid temperature and flow rate to the heat exchanger and the tank temperature [66].

4.2.3 Immersed Heat Exchangers within the Tank

Within the Type 534 model, two immersed heat exchangers exist. The bottom heat exchanger is modeled as a coiled tube heat exchanger and is connected to the solar collector loop to transfer heat from the solar collector outlet to the storage tank. The top heat exchanger is also modeled as a coiled tube heat exchanger and transfers heat to the space heating load and from the boiler. An inlet port at bottom node and outlet port at the top node of the tank are used to model the domestic hot water flows.

Both solar side heat exchanger and load/auxiliary side heat exchanger validation studies were performed using the one-minute interval test data. From this data, the tank and heat exchanger models were calibrated so that the model outputs matched the experimental data to within the experimental uncertainty. The model was forced to the experimental heat exchanger inlet temperature, flow rates, environment temperatures. In the model, the heat transfer coefficient of the heat exchanger in the tank for each isothermal heat exchanger node is calculated as [66]:

$$\frac{1}{UA} = \frac{1}{h_o A_o} + R_w + \frac{1}{h_i A_i} \quad 4.6$$

Where h_o and h_i are the outer and inner surface heat transfer coefficients, A_o and A_i are the outer and inner surface areas for the heat exchanger node, R_w is the heat exchanger tube resistance.

The outer surface heat transfer coefficient is calculated as:

$$h_o = N_{ud} * \frac{k}{d_o} \quad 4.7$$

Where N_{ud} is the Nusselt number, k is the water thermal conductivity, and d_o is the outer diameter of the heat exchanger. Initially in the model calibration process which is describe below, the calibration of both heat exchangers was conducted by varying the coefficient for natural convection, C , to calculate the Nusselt number, which is expressed as [66]:

$$N_{ud} = C * (Ra)^n \quad 4.8$$

Where Ra is the Rayleigh number and C and n are constants, which are dependent on the geometry of the heat exchanger surface and the flow regime. The value of n is typically 0.25 for laminar flow and 0.333 for turbulent flows and the value of C is typically less than 1 [37]. The Rayleigh number, Ra is calculated using:

$$Ra = \frac{g\beta\Delta TD_c^3}{\nu\alpha} \quad 4.9$$

Rayleigh number hand calculations show that for the lower heat-exchanger, Ra is in the range of 7.5×10^7 to 3×10^8 , depending on the temperature of the heat transfer fluid and the nodal tank temperature.

To determine the inner surface heat transfer coefficient, the flow is assumed to be fully developed and the Reynolds number is calculated as [66]:

$$Re_{hx} = \frac{4 * \dot{m}}{(\pi * d_i * \mu)} \quad 4.10$$

and Prandtl number is calculated as:

$$Pr_{hx} = \frac{C_p * \mu}{k} \quad 4.11$$

Where \dot{m} is the mass flow rate through the heat exchanger, μ is the fluid viscosity, k is the fluid thermal conductivity, and C_p is the fluid specific heat. Depending on the flow rate within the heat exchangers, the Reynolds number is calculated to be in the range of 400 to 1000 and the Prandtl number is calculated to be 0.94.

For coiled tube heat exchangers, the critical Reynolds number for transition from laminar flow to turbulence flow is calculated as:

$$Re_{crit} = 20000 * \left(\frac{d_i}{d_{coil}} \right)^{0.32} \quad 4.12$$

With d_{coil} as the diameter of the coiled tube heat exchanger and d_i is the inside diameter of the heat exchanger tubing. The calculated Re_{crit} for the tank's heat exchangers is 8100, which is higher by an order of magnitude than the calculated Reynolds number, implying the flow inside the heat exchanger is laminar. Using this calculation, the exponent to calculate the Nusselt number (see Equation 4.8) should be set to 0.25.

The heat transfer coefficients in coiled tube heat exchangers is larger than the heat transfer in straight horizontal heat exchangers due to the irregular flows that are created in the curved tubes, which amount to higher fluid velocities at the outer tube wall and low velocities at the inner tube wall. The Manlapanz and Churchill's empirical formula [38] is used to calculate the Nusselt number for laminar flow in coiled tube heat exchangers [66].

$$Nu_{hx} = \left[\left(4.364 + \frac{4.636}{1 + \left(\frac{1342}{Pr_{hx}} \right)^2} + 1.816 * \left(\frac{DE}{1 + \frac{1.15}{Pr_{hx}}} \right)^{2/3} \right)^3 \right]^{1/3} \quad 4.13$$

Where the Dean number, DE, which accounts for the irregular flow in the helical tube, is calculated using:

$$DE = Re_{hx} \frac{\left(\frac{d_i}{d_{coil}} \right)^{0.5}}{1 + \left(\frac{Pitch_{coil}}{\pi * d_i} \right)^2} \quad 4.14$$

The inside heat transfer coefficient is then calculated as:

$$h_i = Nu_{hx} * \frac{k}{d_i} \quad 4.15$$

4.3 Modeling the Collector and Tank

In the model, only one component, Type 534 (Stratified Storage Tank), was calibrated. For Type 534, both the storage tank along with the immersed heat exchangers inside the storage tank, were calibrated based on the experimental results. For Type 539, since there was a large discrepancy between the measured collector efficiency and the expected steady state efficiency, the flat-plate collector model was analytically verified based on the steady state efficiency [29].

For the flat-plate collector, the initial parameters were acquired from the Solar Rating and Certification Corporation published literature [39], which had information on the net aperture area, fluid capacity, collector materials, and the transmittance-absorbance efficiency, loss coefficient, and incident angle modifier. For the storage tank, the initial parameters, such as the storage size and dimensions, tank materials, heat exchanger dimensions, and heat exchanger properties, were derived from the manufacturer's cut sheets (see Appendix A) [52].

During the calibration process of the storage tank, the model parameters were altered using a parametric analysis in order to minimize the error between the model outputs and the experimental results. The root mean square error (RMSE) was derived based on the one-minute time step experimental results. The parametric study of the parameters was performed in order to minimize the error over the two-days of one-minute interval data collection. Additionally, the chi-square test was performed to show the validity of the model

4.3.1 Solar Thermal Collector Model

In modeling the solar thermal collector with capacitance, many of the parameters were taken from the Solar Rating & Certification Corporation rating sheet for the Heliodyne flat-plate collector (see Appendix A for the rating sheet). The thermal capacitance, C_{th} , of the collector was derived using the collector fluid capacity and the mass of the absorber in the collector:

$$C_{th} = (m_{fluid} * c_{p,fluid}) + (m_{absorber} * c_{p,absorber}) \quad 4.16$$

where m_{fluid} is the mass of fluid in the collector, $c_{p,fluid}$ is the specific heat of the glycol, $m_{absorber}$ is the mass of the collector absorber, and $c_{p,absorber}$ is the specific heat of the absorber. In this case, m_{fluid} for both collectors is 8.6 kg, $m_{absorber}$ for both collectors is 19.7 kg[40], and $c_{p,absorber}$ is 0.39 kJ/kg-K[41].

Table 4.1 shows the solar thermal collector parameters for the model.

Table 4.1: Solar Thermal Collector with Capacitance Model Parameters

Parameters	Value
Collector Area (2 collectors)	4.97 m ²
Fluid Specific Heat	3.55 kJ/kg-K
Intercept Efficiency (a ₀)	0.702
1st Order Efficiency Coefficient (a ₁)	13.44 kJ/hr-m ² -K
2nd Order Efficiency Coefficient (a ₂)	0.04 kJ/hr-m ² -K ²
Tested Flow Rate per Unit Area	74.88 kg/hr
Fluid Specific Heat at Test Conditions	4.18 kJ/kg-K
1st-order IAM Coefficient	-0.26
Capacitance of Collectors	38.2 kJ/K
Number of Collector Nodes	50
Collector Tilt	45 deg
Collector Azimuth	0 deg (South)

Since the thermocouples were located on the pipes by the tank inside the utility room as opposed to near the inlet and outlet to the solar collector, the model created in TRNSYS takes into account the pipe losses going to and from the solar collector. The pipe losses affect the actual collector efficiency by decreasing the transmittance-absorbance efficiency, $F_R(\tau\alpha)$, and increasing the loss coefficient, $F_R U_L$ (see Section 3.5 for a full description of the impact of the pipe losses on the measured efficiency).

Figure 4.4 shows that the modeled efficiency taking into account the pipe losses impacts the collector efficiency by reducing the transmittance-absorbance efficiency by about 3%. Additionally the plot shows that the modeled efficiency correlates closely with the expected steady-state efficiency. The impact of the capacitance in the collector in the model can clearly be seen when comparing the the modeled efficiency to the steady-state efficiency.

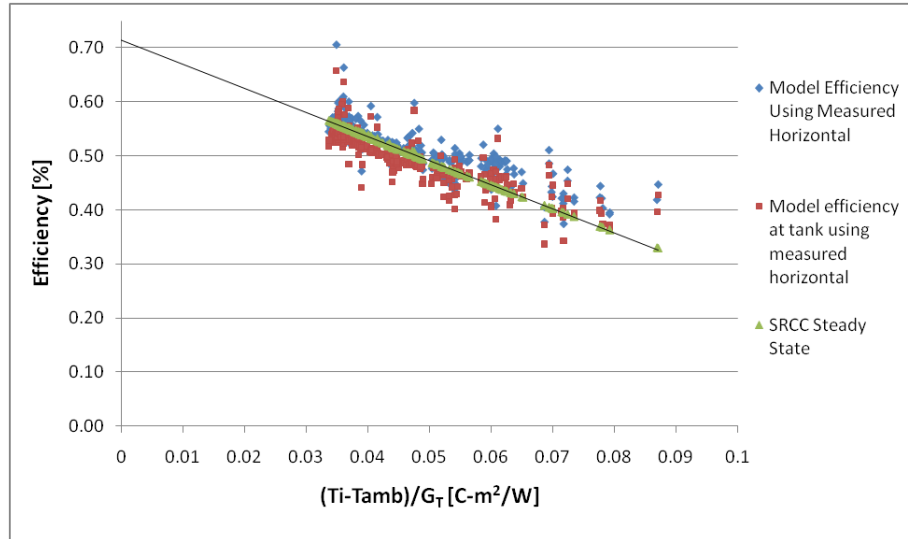


Figure 4.4: Comparing the modeled collector efficiency to the modeled collector efficiency measured at the tank.

Next, the modeled efficiency at the tank is compared against the measured efficiency using the calculated tilt radiation from the measured horizontal radiation data. As expected, the measured efficiency shows a significant bias error (see Figure 4.5). Additionally, the figure shows occasional measured uncertainty error bars, which accounts for the quoted uncertainties of the experimental measurements as well as the assumed 5% bias error in the flow measurements as a result of the uncalibrated flow meter. Figure 4.5 reveals that the majority of the predicted efficiency values fall outside the bounds of the error of the measured values, but clearly, the bias uncertainty as a result of an uncalibrated flow meter helps explain some of the bias error between the measured and predicted values.

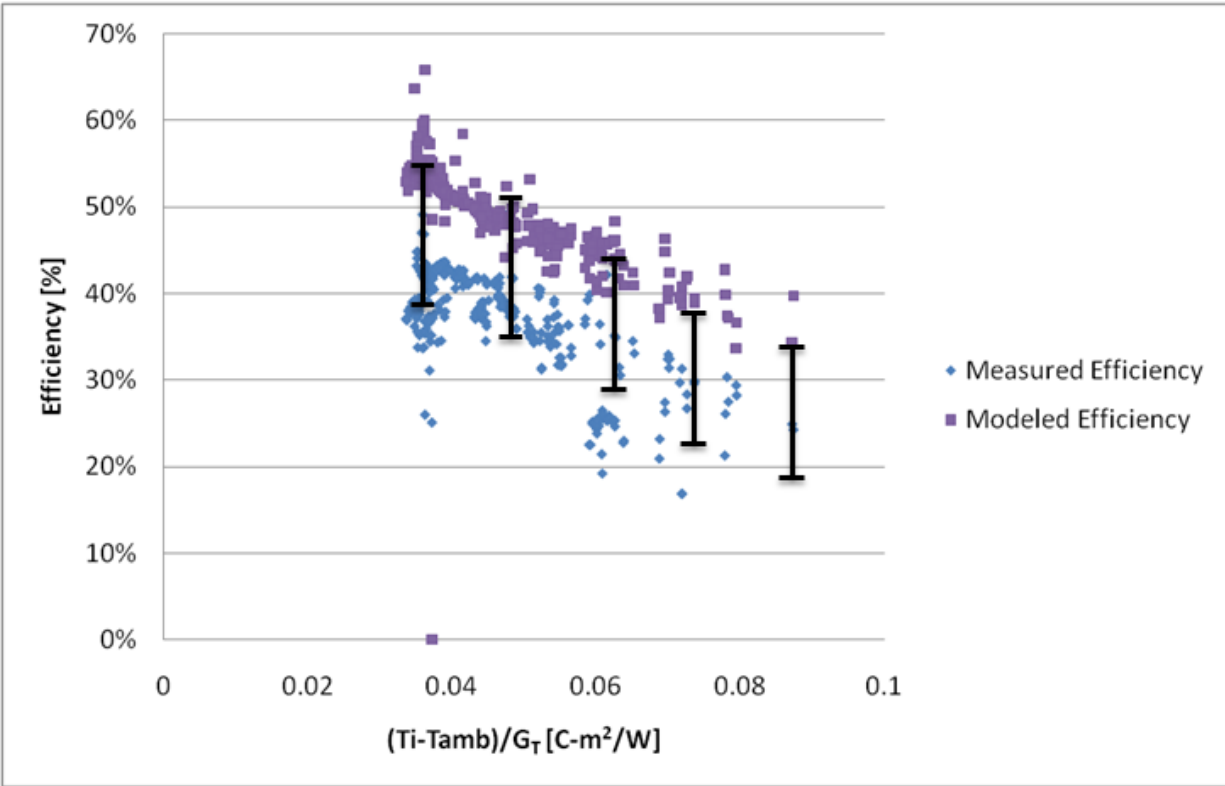


Figure 4.5: Comparing the measured efficiency to the modeled efficiency measured at the tank using the measured tilt radiation and the calculated tilt radiation inferred from the measured horizontal radiation.

Figure 4.6 once again shows that many of the modeled efficiency points falls outside the bounds of the uncertainty of the measured efficiency, however there are predicted efficiency values that lie within the uncertainty of the measured values. The mean bias error between the measured efficiency using the tilt radiation inferred from the horizontal radiation and the predicted efficiency is 12.5%.

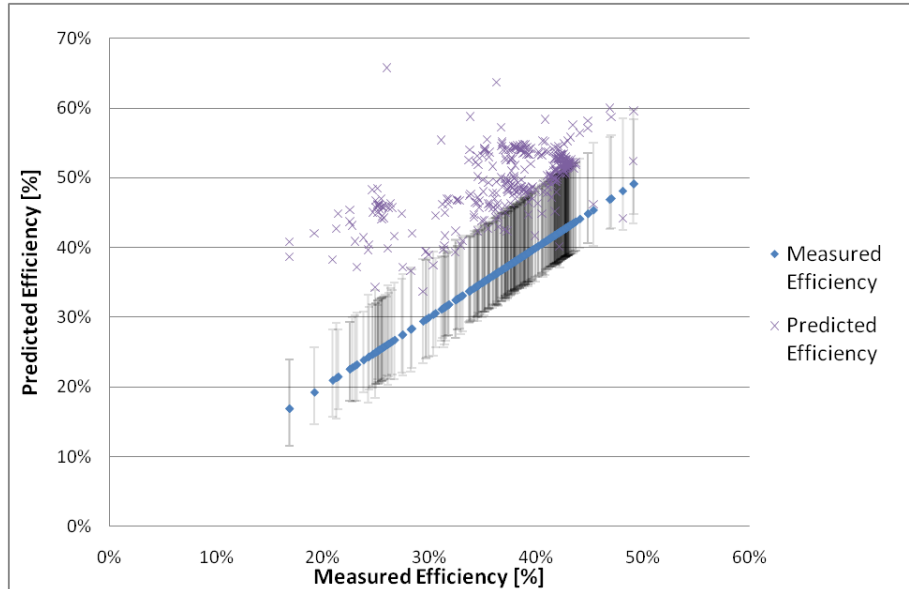


Figure 4.6: Comparing the measured collector efficiency to the modeled collector efficiency.

After coming to the conclusion that measured efficiency is well below the expected collector efficiency due to reasons that still remain unknown, but could be partially explained by an uncalibrated flow meter, the collector as modeled was used because the measured efficiency values followed the modeled output efficiency trends as a function of $\Delta T/G_T$.

4.3.2 Calibration Errors

The root mean square error (RMSE) was determined to measure the difference between the values predicted by the model and the values actually observed in the experimental data. In the case of the tank model calibration, the RMSE examined the error between the experimental heat transfer (for both heat exchangers and the domestic hot water draws) and the modeled heat transfer (for both heat exchangers and the domestic hot water draws). Although errors between the experimental results and the model vary at each time step, the RMSE serves to aggregate all the errors into a single average error. The RMSE is calculated as:

$$RMSE = \sqrt{\frac{1}{n} \sum_{i=1}^n (X_{n,meas} - X_{n,pred})^2} \quad 4.17$$

Using the experimental uncertainty analysis to derive an experimental total uncertainty (σ), a chi-squared metric was used to determine the validity of the models. The chi-squared χ^2 is determined using:

$$\chi^2 = \frac{1}{N} \sum_{i=1}^N \frac{(X_{n,model} - X_{n,experiment})^2}{\sigma_{experiment}^2} \quad 4.18$$

In calculating the chi-squared values, only the experimental uncertainty was considered and the uncertainty of the model was neglected. Sometimes the model uncertainty is considered in the validation; but here the uncertainty of the models was assumed to be zero.

The chi-square test is used to determine the validity of the heat transfer rates within each heat exchanger in the model. A chi-squared value that is about 1 means that the error between the experimental results and the model results is comparable to the uncertainty of the experimental results, which means that the model is calibrated to within the uncertainty of the experimental data.

4.3.3 Tank Model Calibration

The tank model, Type 534, was calibrated to the experiment results using the 2 days of 1-minute interval data. For the calibration of this component, the initial parameters, such as the tank dimensions, heat exchanger properties, lengths and coil heat exchangers dimensions, and the locations of the inlet/outlet ports and heat exchanger inlets and outlets were acquired from the manufacturer's literature. The tank UA was set to the calculated UA value of 2.2 W/C using the temperature decay method (see Section 3.6).

The inlet temperatures and flow rates for the heat exchangers and the domestic hot water flow as well as the ambient temperature from the experiment were used as inputs to the model. Each heat exchanger was then calibrated by altering the UA of the heat exchanger and the level stratification in the tank by altering the length of the heat exchangers and the number of tank nodes. The root mean square error between the model and the experimental results were recorded during the duration of the simulation for the heat transfer in the lower heat exchanger, upper heat exchanger, and domestic hot water load. The parametric study of the heat exchanger lengths and tank nodes was performed until the RMSE was minimized. Additionally, the chi-square values were derived to determine the validity of the model. Table 4.2 and Table 4.3 show the pre calibrated model tank and heat exchanger parameters. Initially, the storage tank was set to 12 nodes and the heat exchanger lengths were set to 16.8 meters for the lower heat exchanger and 12.2 meters for the upper heat exchanger.

Table 4.2: Pre-Calibration Tank Parameters

Storage Tank Volume	0.341 m ³
Storage Tank Height	1.524 m
Storage Tank R-Value	0.373 hr-m ² -C/kJ
Storage Tank U-Value	2.679 kJ/hr-m ² -C
Additional Thermal Conductivity	180 kJ/hr-m-C
Storage Tank Number of Nodes	12

Table 4.3: Pre Calibration Heat Exchanger Parameters

Heat Exchanger Inside Diameter	0.025 m
Heat Exchanger Outside Diameter	0.029 m
Solar (lower) Heat Exchanger Tubing Length	16.764 m
Height of Solar-side (lower) Heat Exchanger Inlet	0.760 m
Height of Solar-side (lower) Heat Exchanger Outlet	0.183 m
Diameter of Coil, Lower HX	0.475 m
Coil Pitch, Lower HX	0.087 m
Node number of lower HX inlet	7
Node number of lower HX outlet	11
Number of HX nodes (lower)	10
Load/Boiler (upper) Heat Exchanger Tubing Length	12.192 m
Height of Load/Boiler (upper) Heat Exchanger Inlet	0.899 m
Height of Load/Boiler (upper) Heat Exchanger Outlet	1.271 m
Diameter of Coil, Upper HX	0.475 m
Coil Pitch, Upper HX	0.062 m
Node number of upper HX inlet	5
Node number of upper HX outlet	2
Number of HX Nodes (upper)	10
Multiplier for natural convection (HX)	1
Exponent for natural convection (HX)	0.25

Since the modeling of the upper heat exchanger depended on the heat added to the tank by the lower heat exchanger during the day when the solar loop was in operation and was stratifying the tank, the first step in the calibration process was to vary the lower heat exchanger length and the number of tank nodes with a constant tank UA value, which was derived using the temperature decay method. Figure 4.7 shows the RMSE results of the lower heat exchanger calibration, which was conducted by varying the lower heat exchanger from 15.8 meters to 19.5 meters and by varying the tank number of nodes from 10 nodes to 20 nodes. The RMSE results show that the minimum RMSE occurs with a 18.5 meter length and 18 node tank model.

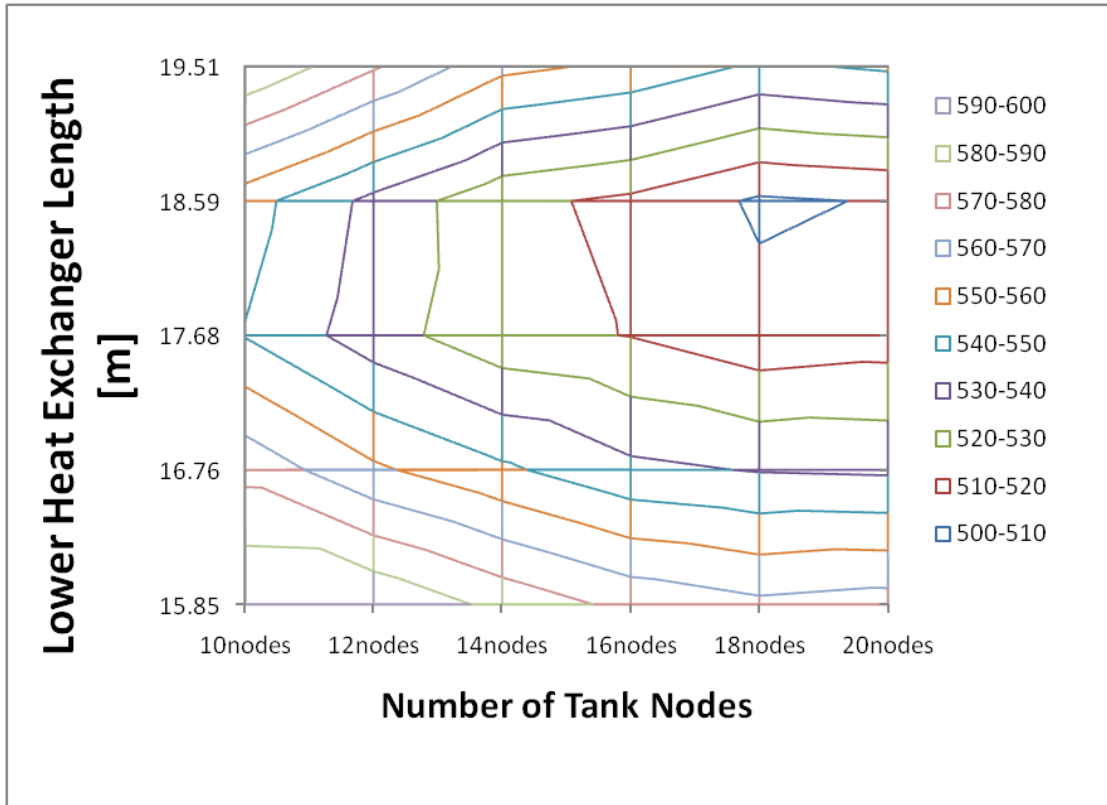


Figure 4.7: Impact of lower HX length and number of tank nodes on the RMSE between the model heat transfer and the experimental heat transfer.

Based on the results of the lower heat exchanger calibration, the lower heat exchanger length was set at 18.5 meters, and the next step was to vary the upper heat exchanger length and the number of tank nodes to determine the optimum calibration upper heat exchanger length. Figure 4.8 shows the impact of the upper heat exchanger length and number of tank nodes on the RMSE of the heat transfer for the upper heat exchanger. The results show that upper heat exchanger length that offers the lowest error is 14.6 meters with either an 18 or 20 node tank model.

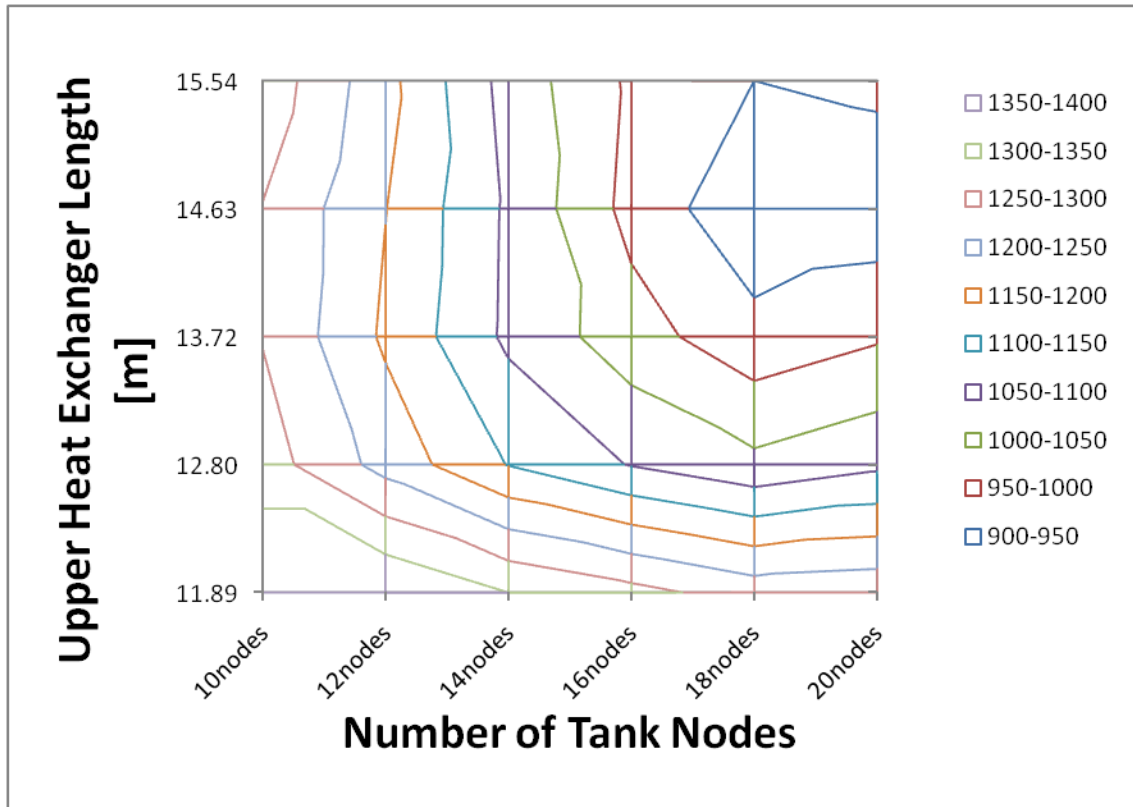


Figure 4.8: Impact of the upper heat exchanger length and the number of tank nodes on the RMSE of the heat transfer in the upper heat exchanger

Next, with both the upper and the lower heat exchanger lengths set based on the lowest RMSE of the heat transfer through the heat exchangers, the tank UA was varied to examine if there is any significant impact on the RMSE of the heat exchanger heat transfer values. Figure 4.9 shows that the minimum RSME values will occur with the overall tank UA set to 2.2 or 2.3 W/C.

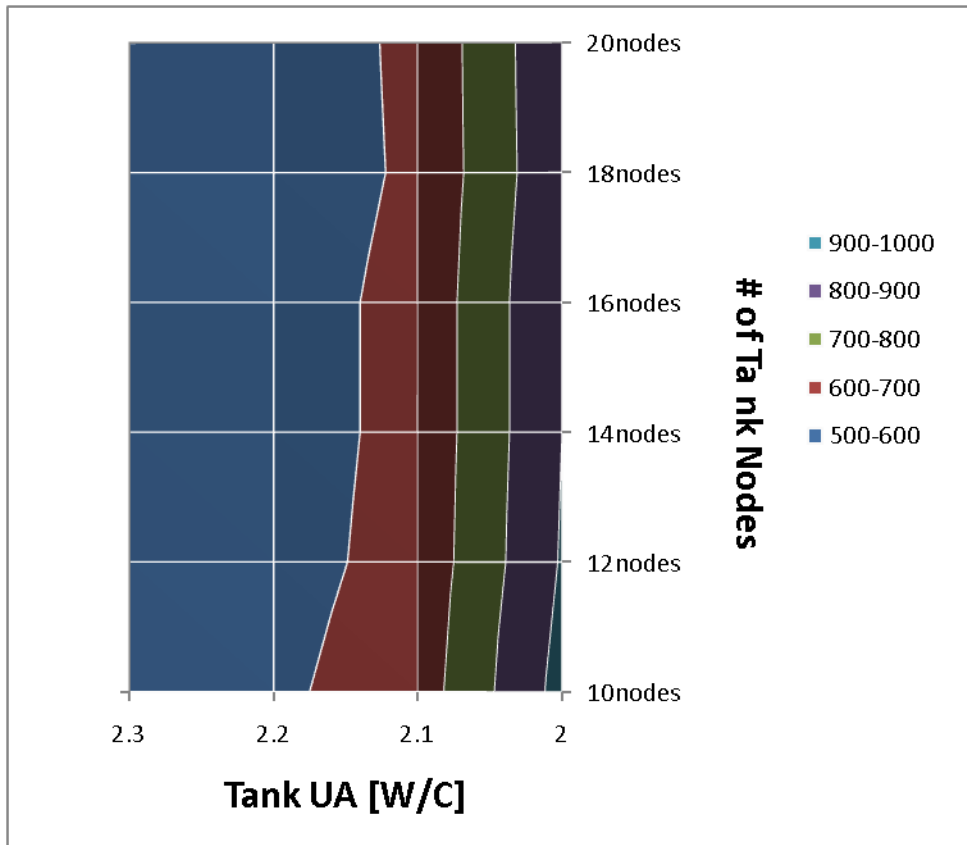


Figure 4.9: Impact of the Tank UA and number of tank nodes on the RMSE of the lower heat exchanger.

Figure 4.10 shows the impact of varying the tank UA on the upper heat exchanger heat transfer RMSE. The figure shows that the lowest RMSE values will occur when the tank UA is set to 2.2 W/C and the number of tank nodes is above 14 nodes.

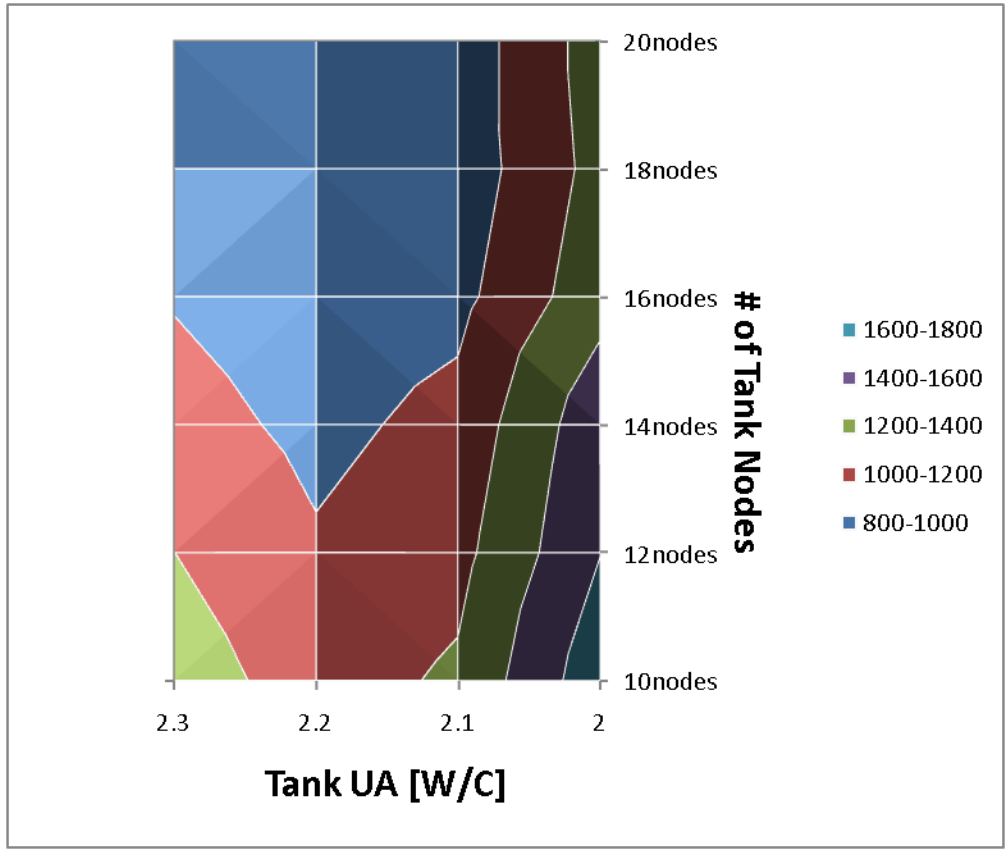


Figure 4.10: Impact of the tank UA and number of tank nodes on the RMSE of the upper heat exchanger.

The last step was to examine chi-squared for lower heat exchanger, upper heat exchanger and domestic hot water heat transfer results by varying tank nodes. For this step, the lower heat exchanger was set at 18.5 meters, the upper heat exchanger was set at 14.6 meters, and the tank UA was set at 2.2 W/C. The chi-square values of the three heat transfer calculations were compared and it was determined that an 18 tank node model yielded a tank model that best matched the experimental values (see Figure 4.11).

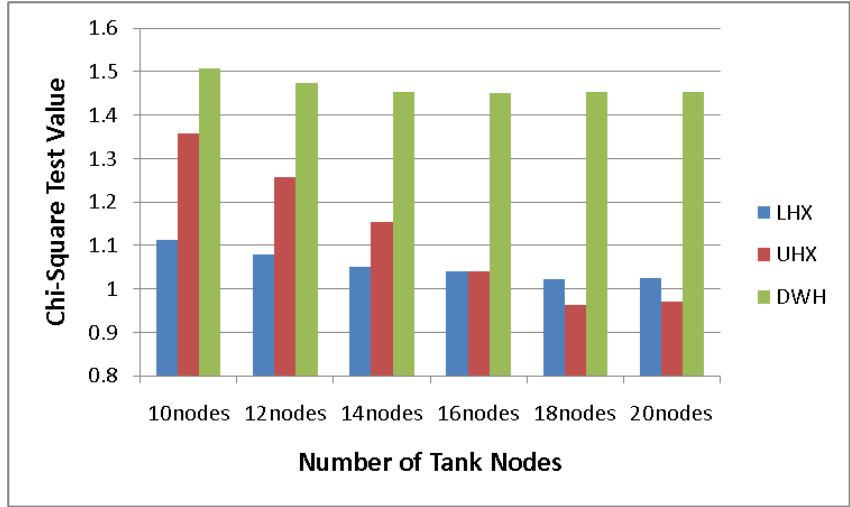


Figure 4.11: Examining the chi-squared of the three measured heat transfer values in the tank with the upper heat exchanger at 48 ft, lower heat exchanger at 61 ft, and the tank UA at 2.2 W/C.

With the calibrated tank model set based on the RMSE of the one-minute interval data, the measured and the predicted results were compared to see the difference between the experimental results and the model results. A comparison plot of the calibration model temperature values and the experiment temperature values for the first day of one-minute interval data is shown in Figure 4.12. The plot shows occasional experimental error bars for the measured temperature differential.

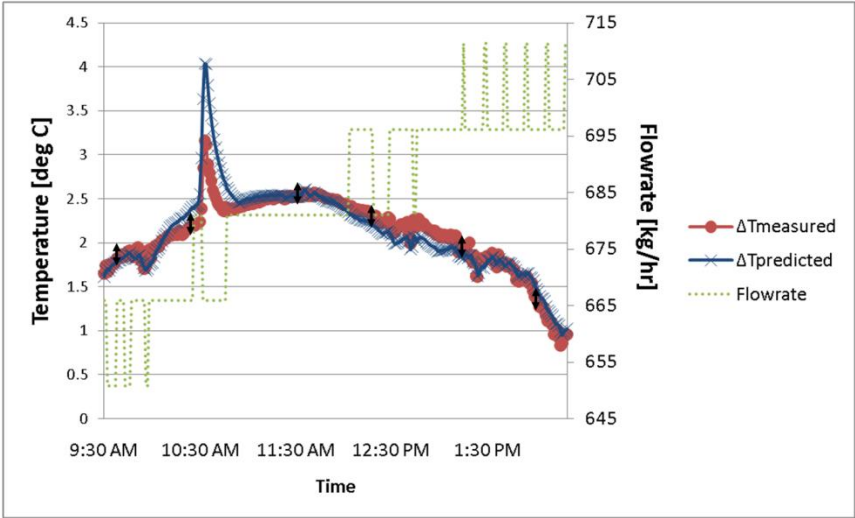


Figure 4.12: Comparing measured delta temperatures and the predicted delta temperatures for the lower heat exchanger on the sunny day.

Figure 4.13 shows the lower heat exchanger predicted versus measured heat transfer values for the two days of measured data. The plot shows that most of the predicted values are within the experimental uncertainty with a few of the predicted values falling out of uncertainty range. It could be that the predicted values are falling outside the uncertainty of the experimental results because of the resolution or calibration of the solar loop flow rate. As discussed in Chapter 3, the flow rate for the solar loop was recorded with poor resolution, so in an effort to correct the issue, the moving average of the flow rate was calculated and used as an input for the model.

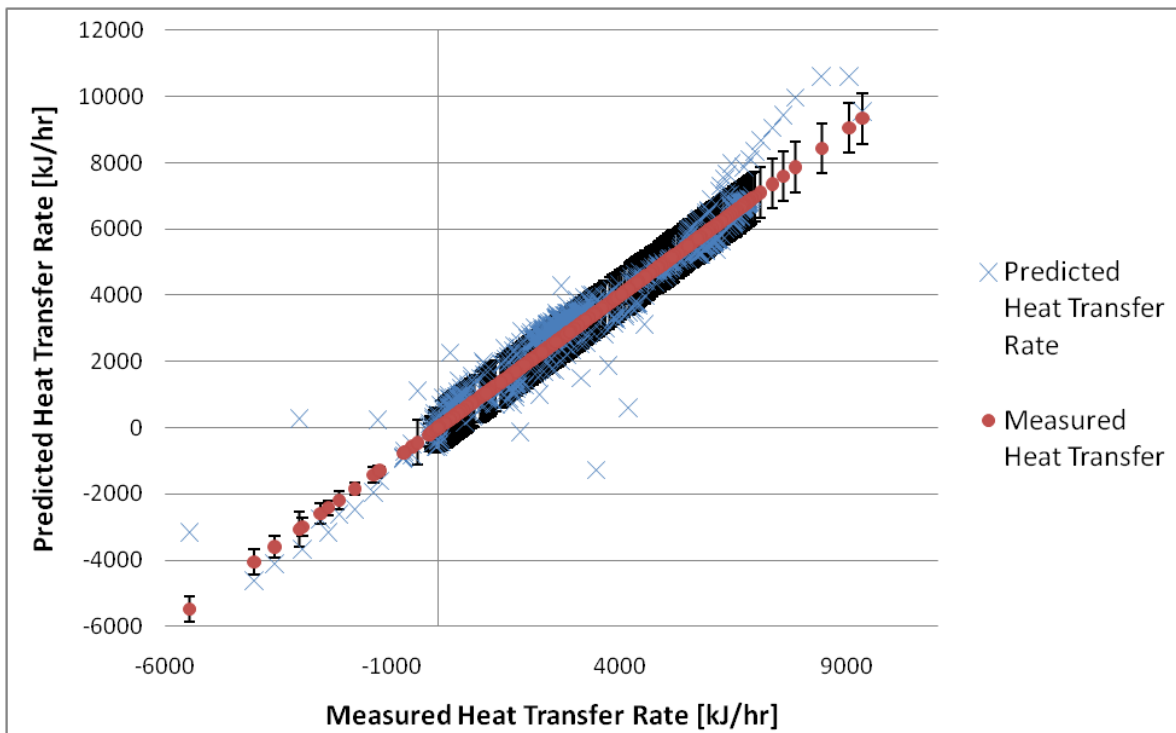


Figure 4.13: Lower Heat Exchanger predicted versus measured heat transfer values

Next, the upper heat exchanger measured delta temperatures were compared the model delta temperatures. Figure 4.14 shows a comparison plot of the calibration model temperature values and the experiment temperature values for the 30 minutes of one-minute data. The plot shows occasional experimental error bars for the measured temperature differential.

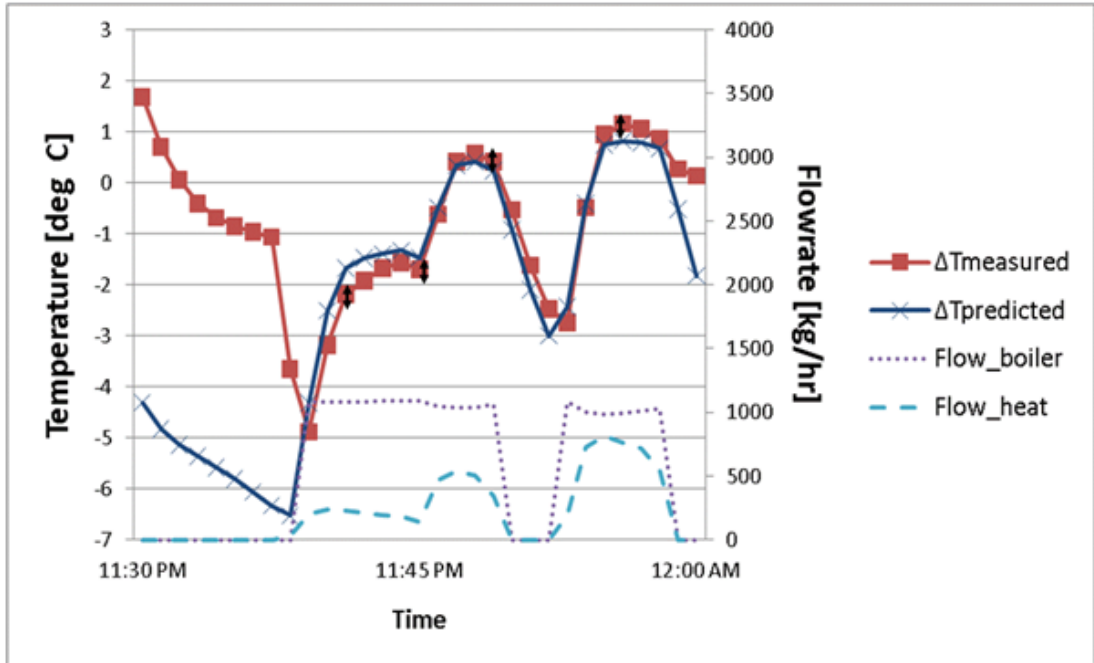


Figure 4.14: Comparing measured delta temperatures and the predicted delta temperatures for the upper heat exchanger

Figure 4.15 shows the upper heat exchanger predicted versus measured heat transfer values for the one-minute data. The plot shows that most of the predicted values are within the experimental uncertainty with a few exceptions when the predicted values reside outside of uncertainty range.

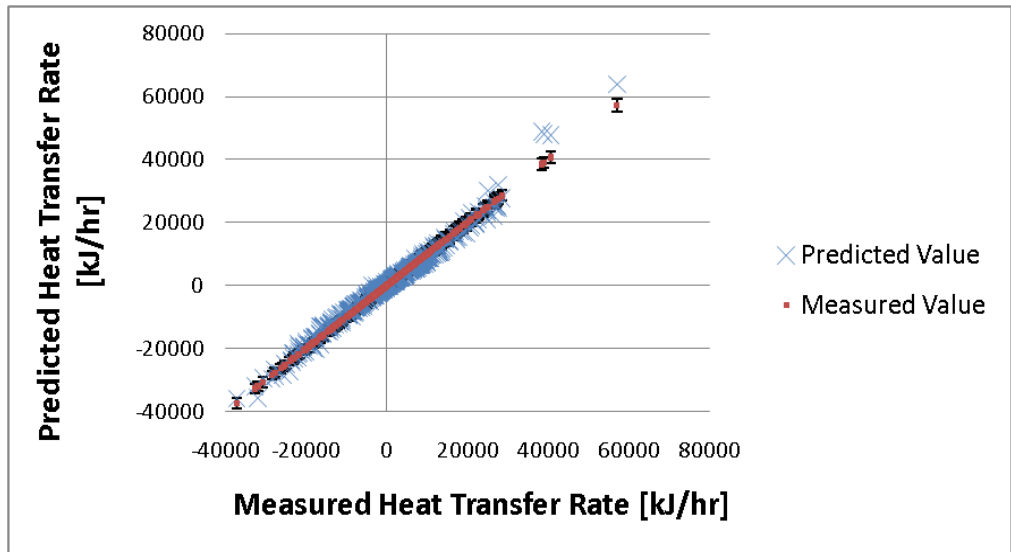


Figure 4.15: Upper heat exchanger predicted versus measured values

Lastly, Figure 4.16 shows the comparison of the measured domestic hot water heat transfer rate to the predicted heat transfer rate. The plot shows that several of the predicted values are larger than the measured values, however the chi-squared for the domestic hot water predicted heat transfer error was less than 2, so it was determined that the model was calibrated sufficiently.

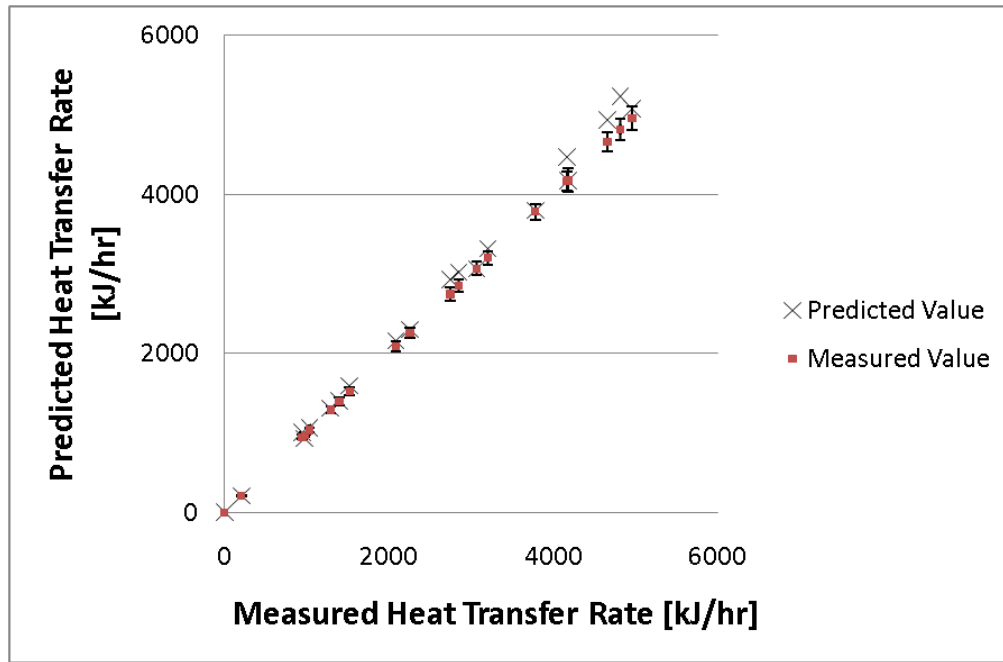


Figure 4.16: Comparing the predicted domestic hot water heat transfer rate to the measured values

4.3.4 Calibrated Tank Parameters

Based on the calibration process, the tank and heat exchanger values were altered and this model was used for the annual simulations (see Table 4.4 and Table 4.5). As compared to the pre calibration model, the upper heat exchanger area was increased by 11%, the lower heat exchanger area was increased by 14% and the number of tank nodes increased from 12 to 18 nodes. Additionally, the tank UA was reduced by 4% as compared to the calculated temperature decay derived tank UA.

Table 4.4: Post Calibration Tank Values

Storage Tank Volume	0.341	m ³
Storage Tank Height	1.524	m
Storage Tank R-Value	0.409	hr-m ² -C/kJ
Storage Tank U-Value	2.446	kJ/hr-m ² -C
Additional Thermal Conductivity	180	kJ/hr-m-C
Storage Tank Number of Nodes	18	

Table 4.5: Post Calibration Tank Parameters

Heat Exchanger Inside Diameter	0.025	m
Heat Exchanger Outside Diameter	0.029	m
Solar (lower) Heat Exchanger Tubing Length	18.5928	m
Height of Solar-side (lower) Heat Exchanger Inlet	0.170	m
Height of Solar-side (lower) Heat Exchanger Outlet	0.041	m
Diameter of Coil, Lower HX	0.475	m
Coil Pitch, Lower HX	0.017	m
Node number of lower HX inlet	10	
Node number of lower HX outlet	16	
Number of HX nodes (lower)	10	
Load/Boiler (upper) Heat Exchanger Tubing Length	14.6304	m
Height of Load/Boiler (upper) Heat Exchanger Inlet	0.201	m
Height of Load/Boiler (upper) Heat Exchanger Outlet	0.284	m
Diameter of Coil, Upper HX	0.475	m
Coil Pitch, Upper HX	0.012	m
Node number of upper HX inlet	8	
Node number of upper HX outlet	3	
Number of HX Nodes (upper)	10	
Multiplier for natural convection (HX)	1	
Exponent for natural convection (HX)	0.25	

4.3.5 Analytical Verification of Model

To verify the accuracy of the solar combisystem TRNSYS model, a steady state model was simulated and those results were compared to the results of steady state energy balance hand calculations.

The hand calculations verify that the TRNSYS model is accurately modeling the system as it was designed. The results from the hand calculations closely match the results from the TRNSYS model results, which helps verify that the TRNSYS model is accurately determining the performance of the system.

To create a steady state model, a number of parameters were set as constants in the TRNSYS model. First, the insolation was set to a constant value with a normal incident angle with regards to the flat-plate solar collector, so that the useful energy gain by the solar collectors could be calculated without using incident angle modifier coefficients. Second, the domestic hot water draw was set to constant in order to easily calculate energy taken out of the tank. Third, the space heating load and water flow was set to a constant in order to calculate steady state supply and return temperatures. Table 4.6 shows the steady state calculation assumptions.

Table 4.6: Steady state calculation assumptions

Parameter	Value
FR($\tau\alpha$)	0.702 -
FRUL	13.44 kJ/hr-m ² -C ²
Incident Radiation	3600 kJ/hr-m ²
A _{coll}	2.97 m ²
Pipe U _L	8.18 kJ/hr.m ² .K
Tank U _L	2.40 kJ/hr.m ² .K
Tank SA	3.28 m ²
cp _{water}	4.18 kJ/kg-C
cp _{glycol}	3.55 kJ/kg-C
Mains Temperature	15 C
Outdoor Temperature	10 C
Indoor Temperature	20 C
Collector Flow	708 kg/hr
DHW Flow	22.71 kg/hr
SpH Flow	22.71 kg/hr

The hand calculations included calculating energy transfer from the solar collector, solar immersed heat exchanger, domestic hot water, space heating, and tank losses (see Appendix E for hand calculations). These energy balance equations were solved iteratively using Engineering Equations Solver (EES), an equation solving program. Using the assumptions found in Table 4.6, EES solved the useful solar energy gain, return and supply temperatures from the solar collector, the efficiency of the collector, and the average tank temperature to within 2% of the TRNSYS steady state results. Table 4.7 shows a summary of the calculated useful solar gain, domestic hot water energy, tank loss energy, and space heating energy versus the TRNSYS results.

Table 4.7: Comparison of steady state results (EES versus TRNSYS)

	EES Results	TRNSYS Results	Percent Difference
Q_{sol} [kJ/hr]	5333	5261	1.4%
Q_{DHW} [kJ/hr]	-4037	-3960	1.9%
$Q_{tankloss}$ [kJ/hr]	-296	-301	-1.7%
Q_{SpH} [kJ/hr]	-1000	-1000	0.0%

4.4 Building Loads

Part of the project was to determine the impact of solar combisystem performance in different climates with different building heating loads. Based on geographic climate consideration, six different locations were chosen: Denver, Phoenix, Chicago, Boston, Atlanta, and San Francisco. These locations represent the majority of climates in the US, including cold, mixed-dry, marine, hot-dry, and mixed-humid.

To simulate the building loads, TMY3 (Typical Meteorological Year) data files were read from the TRNSYS library component Type 15, which is a weather data processor that combines data reading, radiation processing and sky temperature[51]. The component reads an energy plus weather format of a TMY3 file to output all the weather conditions and radiation levels for multiple surfaces, which are inputs

for other model components. To estimate the radiative sky temperature from the TMY3 weather data, it utilizes the Martin and Berdahl sky temperature correlation [53]. The mains water temperature is approximated within the TRNSYS component using an algorithm that determines the daily mains water temperature based on the location and time of year. The equation is based on analysis by Christensen and Bruch of the National Renewable Energy Laboratory (NREL) using mains water temperature data for multiple locations from several studies [54].

4.4.1 Space Heating Loads

The radiant floor heat distribution system is modeled using the radiant slab with embedded pipes and ground storage effects model. The reason that radiant floor heating was chosen for this model was because radiant floor systems require lower supply water temperatures (100 °F) as compared convectional forced air heating coils and baseboard radiators, which require between 140 °F and 180 °F to meet the heating load. The lower supply temperatures means that the tank setpoint can be lower, which is optimal for solar combisystems because tank losses are smaller and system efficiencies are higher when tank temperatures are lower.

The radiant floor slab is a Thermal Energy System Specialists (TESS) ground coupling library component (Type 653). This component models a simple radiant slab floor heating system that operates under a couple of assumptions. First, the slab is assumed to be single isothermal concrete mass, which means that there are no temperature gradients within the slab as it heats up and cools down. Second, heat transfer rate from the fluid to the slab is modeled using a heat exchanger effectiveness approach. The effectiveness approach takes into account parameters set by the user, such as the slab mass, specific heat, and heat capacity of the slab.

All the residences analyzed in this thesis are two-story, 2,500 ft² finished floor homes. The buildings are modeled using the TRNSYS Type 56 multi-zone building component. This component utilizes the program TRNBuild. The multi-zone building model is quite complex and capable of modeling

several thermal zones within a building, however for simplicity reasons, only a single conditioned zone was assumed when creating the model. Separate unconditioned zones were created for the attic and the basement. By creating a building model using Type 56, the model was able to calculate radiation heat transfer through the building envelope and windows, infiltration losses, humidity and capacitance effects, heat transfer from a radiant floor model, and internal sensible and latent heat gains from lighting, appliances, and people. The model calculates the air temperature in the building based on the climate and radiation data, the schedule of internal gains, infiltration, gains from the ground coupling model, and the hydronic radiant floor gains.

In an attempt to model several building performance types for each climate zone, the buildings are modeled according to a low-performance building type (a 1960s retrofit house), a benchmark performance building type (IECC 2009), and high-performance building type (50% reference relative to Building America Benchmark). The site heating load of the TRNSYS buildings are compared to BEopt simulations to ensure the TRNSYS heating loads are reasonable. The BEopt simulations were developed by selecting the corresponding building specification parameters for each location and building type (see Appendix B for the building specification).

Each building is modeled with a 12.8 m x 9.2 m (118 m²) footprint. In the cold climates, which included Denver, Boston, and Chicago, the buildings were modeled with an unconditioned basement. In the warmer climates of Atlanta, San Francisco, and Phoenix, the model simulations assume a slab-on-grade construction. Slab and basement ground coupling are modeled using the simplified ASHRAE model from Type 714 and 715, respectively. Both these models are Thermal Energy System Specialists (TESS) ground coupling library components that use algebraic formulations to estimate heat transfer through slabs and basements.

In terms of infiltration, the following equation was used to determine the ELA (effective leakage area (m²)), which is defined as the amount of open area that would result in the same total air exchange as the actual leakage area of a house at 4 Pa:

$$ELA = SLA * CFA \quad 4.19$$

where SLA is the specific leakage area as defined by the building specifications and CFA is the conditioned floor area (m²) [50]. For example, the SLA for a Building America house is 0.00036. To determine the infiltration air changes, Type 960 from the TESS library was used. This model is based on the Sherman and Grimsrud (1980) model to calculate the building infiltration rate. Using the ELA, the airflow rate from infiltration is calculated using:

$$\dot{V} = ELA(f_s * \Delta T + f_w * v_w^2)^{1/2} \quad 4.20$$

Where ΔT is the difference between the indoor and outdoor temperatures in degrees C and v_w is the period-average wind speed in m/s, and f_s and f_w are the stack and wind coefficients. As a two-story building that is moderately shielded, the stack coefficient in SI Units is 0.000290 and the wind coefficient is 0.000231 [62]. The air change rate per hour (ACH) is determined by:

$$ACH = \frac{\dot{V} * 3600 \frac{s}{hr} * 0.001 \frac{m^3}{L}}{V_{home}} \quad 4.21$$

The internal mass of furniture and contents is assumed to be equal to 8 lb/ft² of the conditioned floor space as defined by the Building America Research Benchmark [50]. A specific heat capacitance of 0.7 kJ/kg-K was also assumed based on the assumed properties of common building materials (wood, steel, and glass) and all the buildings contents [63]. Therefore, the thermal capacitance for main zones of the Type 56 TRNSYS buildings is 6350 kJ/K. For the attic and basement zones, an internal mass is assumed to be 1 lb/ft² and the specific heat capacitance is assumed to be 0.7 kJ/kg-K, so the thermal capacitance of these two zones is calculated as 396 kJ/K.

The internal gains applied to Type 56 were taken directly from the Building America House Simulation Protocols [50]. To model the internal occupant gains, the occupant gains for a 3 bedroom house were used [50]. The sensible and latent loads are 10805 Btu/day and 8075 Btu/day, respectively. The sensible load is assumed to 70% radiative and 30% convective. For the Benchmark lighting, 66 percent of the lamps are incandescent, 21 percent are CFL, and 13 percent are T-8 lamps. The lighting gains for a 2,500ft² house are taken from the Building America Research Benchmark to be 1689 kWh annually [50]. Additionally, the benchmark applies monthly multipliers for the lighting to account for the seasonality impact of the lighting load. The load is assumed to 70% radiative and 30% convective. The miscellaneous gains are taken from the Building America Research Benchmark and include everything except lighting and occupants loads. The miscellaneous sensible and latent loads are 40695 Btu/day and 6474 Btu/day, respectively. The sensible load is assumed to 70% radiative and 30% convective. The annual internal sensible and latent internal gains are 24.5 MMBtu and 5.3 MMBtu respectively.

As stated above, the impact of space heating loads was evaluated by modeling low-performance (1960 retrofit house), benchmark performance (IECC 2009), and high-performance homes (50% reference relative to Building America Benchmark) in TRNSYS. To determine the low-performance and high-performance building design specifications, NREL used BEOpt, a building energy optimization software tool to determine the optimal residential energy efficiency packages for a 1960s-era home and a 50% source energy savings home relative the Building America Benchmark house for various U.S. cities in all the International Conservation Code (IECC) climate regions[58] [59].

For the 1960s-era home, the researchers analyzed the benefits of retrofit packages on a 1,280 ft² house in eight U.S. cities. The research was intended to provide general guidelines and recommendations for a package of individual upgrade measures specific to a typical era-specific pre-retrofit construction house[58]. In terms of developing the high-performance home models, Building America residential researchers evaluated the potential energy reduction impacts for a range of efficiency upgrades to determine whole-house technology packages for high-performance homes that achieve 50% in source

energy savings relative to the Building America Benchmark. The researchers published the specifications for the technology packages for cities within each major climate region [59].

The modeled buildings were developed for a two-story, three bedroom, 2500-ft² west facing house with an 15% window-to-floor ratio. Based on the six climates and three building performance levels, 20 models were created using TRNBuild (see Appendix B for the building envelop specifications).



Figure 4.17. The renderings for the homes that were modeled. The building on the left is slab-on-grade construction, while the home on the right has a basement and was used for the colder climates (Denver, Boston, and Chicago).

To verify the building models created in TRNSYS, BEopt software was used for comparison. Table 4.8 shows the site energy comparison of each building performance level for the 6 climates that were used in the parametric analysis. These heating loads are based on all the assumptions listed above. All of the TRNSYS annual heating loads are accurate to within 30 percent of the BEopt heating loads. The RMSE between the BEopt and TRNSYS annual space heating loads is 7 GJ, with the average of the absolute value of the percent error being 10%.

Table 4.8: BEopt and TRNSYS Building Site Energy Consumption for space heating loads

Building Type	City	BEOpt [GJ]	TRNSYS [GJ]	Percent Difference Between BeOpt and TRNSYS
1960 Retrofit	Phoenix	21.2	19.7	7.1%
	SF	76.4	59.9	21.6%
	Atlanta	71.3	74.7	-4.8%
	Denver	119.1	138	-15.9%
	Boston	155.5	153	1.6%
	Chicago	160.2	159	0.7%
2009 IECC	Phoenix	10.8	10.4	3.5%
	SF	39.3	34.5	12.1%
	Atlanta	38.8	35.7	8.1%
	Denver	48.9	53.2	-8.7%
	Boston	64.6	60.6	6.2%
	Chicago	68.3	67	1.9%
50% Home	Phoenix	5.4	6.19	-15.3%
	SF	31.3	30.6	2.1%
	Atlanta	32.2	26.8	16.8%
	Denver	30.7	38.3	-24.6%
	Boston	38.3	42.8	-11.8%
	Chicago	40.9	48.6	-18.7%

Figure 4.18 shows the annual space heating load for each building type for the 6 climates using both Type 56 in TRNSYS and BEOpt. The figure shows that the space heating loads calculated between the two modeling software were relatively close in most cases. The figure also shows that the annual space heating load in the 1960 retrofit house is 2 to 3 times larger than the annual space heating load for the modeled 2009 IECC. In general, the Building America 50% house annual space heating load is between 30% and 50% lower than the annual space heating load of the 2009 IECC house.

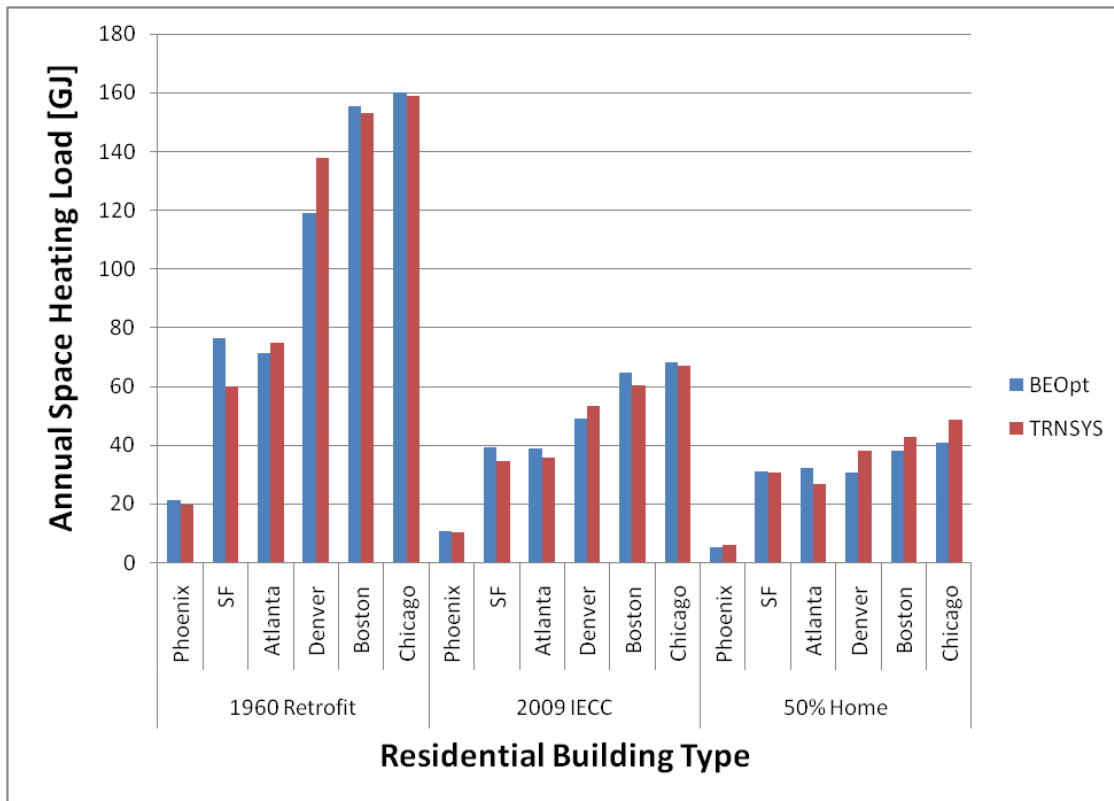


Figure 4.18: BEOpt and TRNSYS Building Site Energy Consumption for all the home performance levels and climates

4.4.2 Domestic Hot Water Loads

The energy savings from solar water heaters depends significantly on the domestic hot water usage profile. It is widely accepted that domestic hot water usage varies significantly on a daily, hourly, and minute timescale basis. Until recently, the Building America Benchmark used a simplistic, non-variable approach to defining hot water use. A fixed daily volume of hot water was used year round, with minor adjustments to the hot water use to reflect seasonal variations in mains temperature. For example, colder mains temperatures during the winter results in higher hot water use in order to maintain a proper hot water supply temperature. The hourly profile is also based on a continuous normalized double-hump domestic hot water use profile as seen in Figure 4.19 — with peak usage occurring during the morning

and evening— rather than using discrete hot water draws to more accurately reflect the time distribution of the load [48].

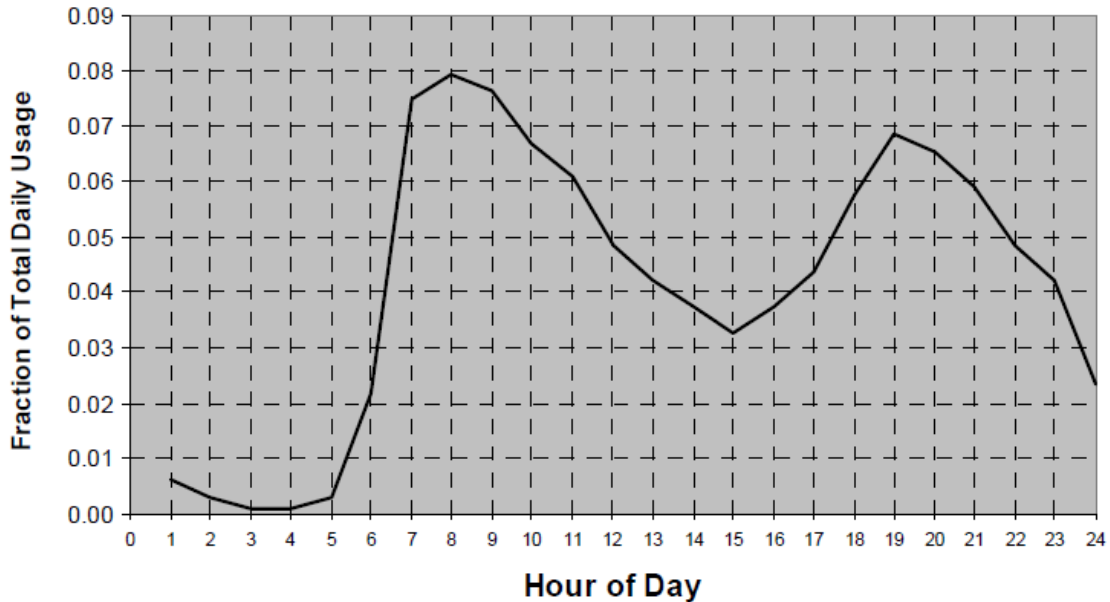


Figure 4.19: Combined domestic hot water use profile[48]

Since the variability in occupant use patterns can greatly impact water heater performance, discrete domestic hot water load profiles were generated using the Building America DHW Event Generator [48]. The Building America Event Generator is a spreadsheet-based tool that generates random domestic hot water profiles based on probability functions that describe the overall daily average usage, event duration, event flow rate, and clustering of draws. The probability distributions were developed using monitored data from residential hot water use studies. The tool also accounts for vacation periods, weekend versus weekday usage variation, and the impact of seasonality on tempered loads (sinks, shower, bath) [48]. The tool was used to develop a hot water profile for a 20 gallon per day household, 60 gallon per day household, and 100 gallon per day household. In each of the three discrete DHW profiles generated, there is a total of 2 weeks of vacation during the year (7 days in May, 3 days in August, and 4 days in December) [48].

When the event generator tool outputs the DHW end-use profile, it separates mixed end-use water draws from hot end-use water draws. The mixed water draws, which are representing draws that use both hot and cold water, will mix the tank hot water with mains water to achieve a desired tempering value temperature for sink, bath, and shower events (105 °F). The hot water draws, which are representing draws that use high water temperatures (such as for dishwasher and clothes washer events), will only use the tank hot water unless the water temperatures leaving the tank should exceed the load set point of 125 °F. This occurs during the summer when tank temperature rises above the tank set point due to higher solar gains. Figure 4.20 shows how the two tempering valves are utilized in the model to meet both the hot loads for dishwasher/clothes washers and the mixed loads for showers/sinks/baths.

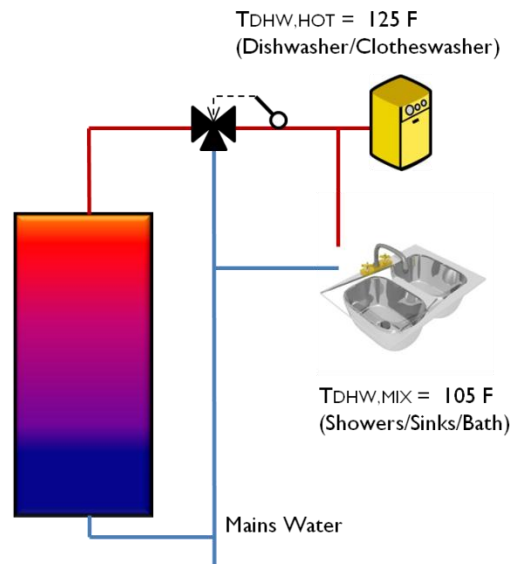


Figure 4.20: In the model, there are two tempering valves which account allow for both hot flow events (125 °F) and mixed flows (105 °F) to occur.

Figure 4.21 shows two days of a one-minute interval discrete draw profile with both mixed draws and hot draws, for the case of 100 gallon daily draw.

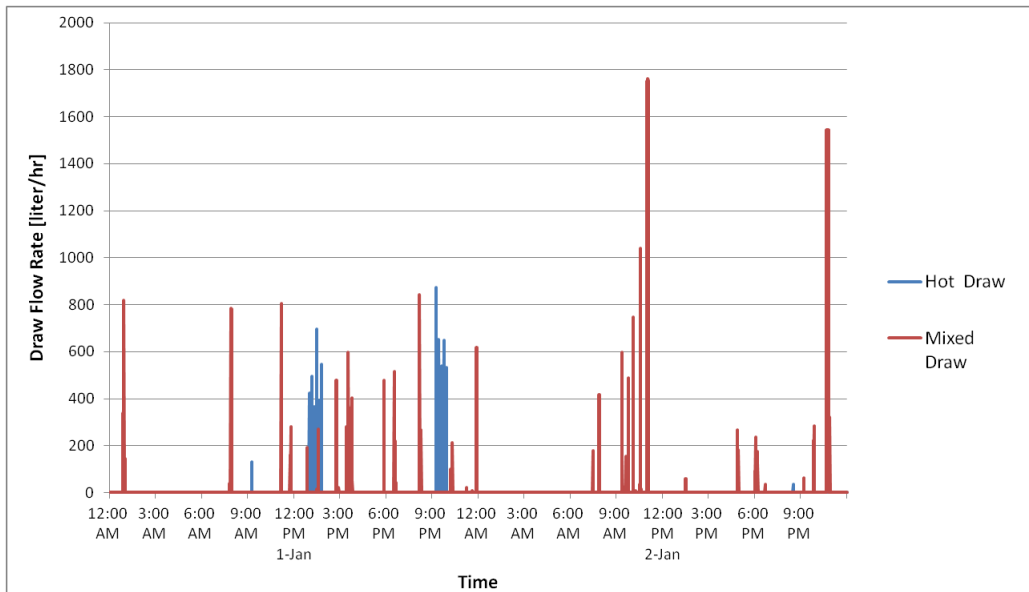


Figure 4.21: The one-minute interval draw flow rates over the course of two days shows both the discrete character of the draw profile as well as the differentiation between mixed draws for sinks/showers and hot draws for dish and clothes washers.

In this model, it is assumed that each house in every climate will use the same volume of water for the sinks/showers and machines. However, the volume of hot water from the tank will vary depending on the climate due to influence of mains water temperatures on the DHW load. Table 4.9 shows how the volume of hot water required to meet these loads, $V_{DHW,Mix}$ and $V_{DHW,Tot}$, varies depending on the climate. Also, as seen in the table, the volume of mixed draws, V_{mix} , the volume of machine draws, $V_{machine}$, do not vary from climate to climate.

Table 4.9: Average daily volumes for the mixed draws (sinks/showers), hot water required the mixed draws, machine draws, and total hot water

		V_{mix}	$V_{DHW,Mix}$	$V_{machine}$	$V_{DHW,Tot}$
Phoenix	Low	23.32	13.86	3.62	17.48
	Mid	69.92	40.94	10.70	51.64
	High	113.82	68.19	17.57	85.76
Atlanta	Low	23.32	16.07	3.62	19.69
	Mid	69.92	48.29	10.70	58.99
	High	113.82	80.84	17.57	98.41
San Fran	Low	23.32	16.65	3.62	20.26
	Mid	69.92	50.36	10.70	61.06
	High	113.82	84.24	17.57	101.81
Denver	Low	23.32	17.23	3.62	20.84
	Mid	69.92	52.23	10.70	62.93
	High	113.82	86.97	17.57	104.55
Boston	Low	23.32	17.18	3.62	20.79
	Mid	69.92	52.11	10.70	62.81
	High	113.82	86.81	17.57	104.38
Chicago	Low	23.32	17.25	3.62	20.86
	Mid	69.92	52.37	10.70	63.07
	High	113.82	87.14	17.57	104.72

As stated above, for the parametric study, discrete event profiles were created with 3 levels of domestic hot water usage levels (approximately 75.8 lit/day (20 gal/day) for low loads, 227.3 lit/day (60 gal/day) for medium loads, and 378.8 lit/day (100 gal/day) for high loads). Figure 4.22 shows the daily average hot water draws for each climate and each draw profile (low, mid, and high). The standard deviation for the low, mid, and high draws are 1.34 gal/day, 4.42 gal/day, and 7.36 gal/day respectively.

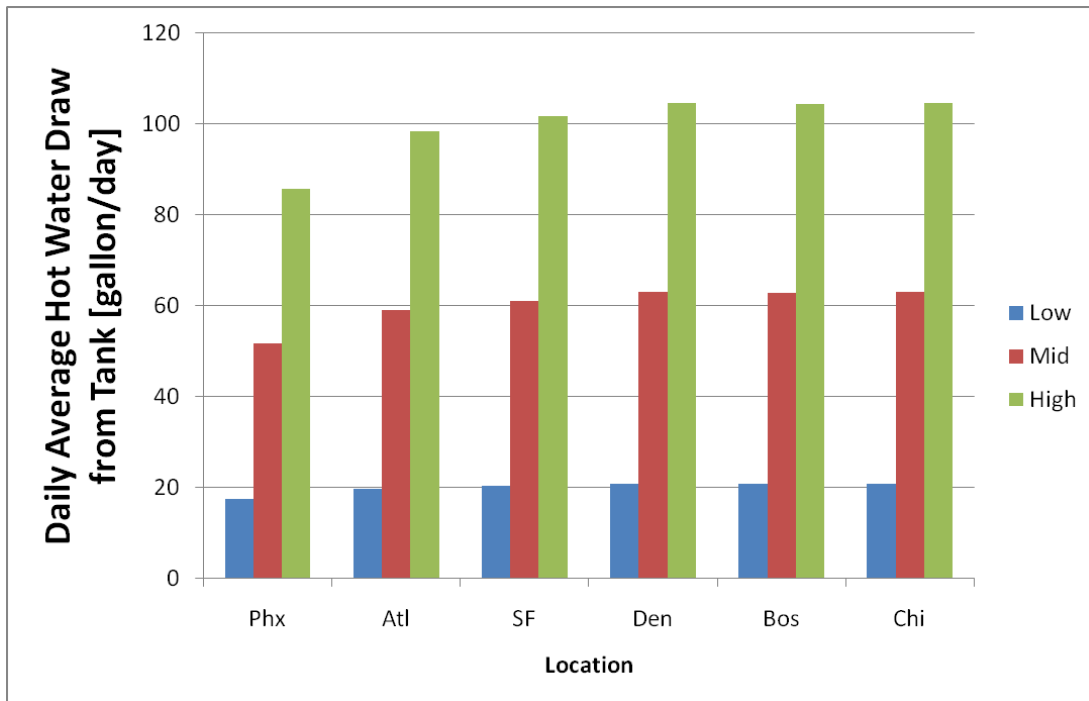


Figure 4.22: Daily average hot water draw for the 6 climates and three draw levels.

Additionally, DHW energy demand in various part of the U.S. was also studied in a 2011 NREL report which examined the economics of residential solar water heaters in the U.S. [57]. Figure 4.23 is a figure taken from that report which shows that the energy required to heat DHW in warmer climates is significantly smaller as compared to colder climates. Of the six climates selected for the parametric study, Phoenix has the lowest annual DHW loads, while Denver, Chicago, and Boston have the highest annual DHW loads.

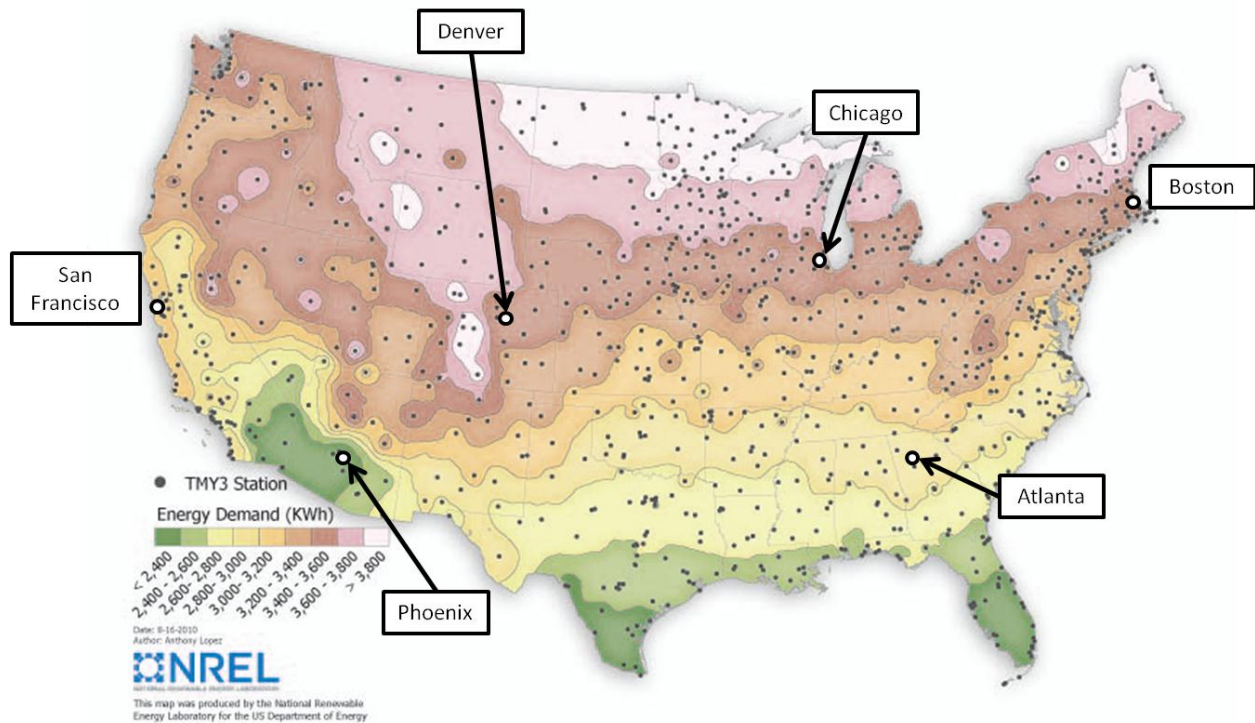


Figure 4.23: Annual water heating energy demand (kWh) for a single-family residence with a constant load profile based on an assumed 60 gal/day draw [57].

4.4.3 Parasitic Energy Consumption

In both the combisystem and the solar water heater systems, single-speed pumps are placed in the heat distribution system to provide distribute fluid in order to meet the space heat load and in the collector loop to supply the tank with solar energy. The annual energy consumption of the pumps is calculated by multiplying the power consumption of all the pumps and the annual operation time. In the model, it is assumed that none of the pump power is converted to fluid thermal energy, since the pump is not located within the stream of the fluid.

The pump power for the collector loop was estimated at 15 watts per gallons per minute (gpm) [55]. The pump flow rate for the collector loop was estimated at 1 gpm per collector with a 32 ft² area.

These values were taken as rule of thumb values from the NREL System Advisor Model (SAM) [55]. The pump power for the space heating radiant floor was set at 93 Watts with a constant flow rate of 5.3 gpm. These values were taken directly from the Carbondale radiant floor system specification [1].

4.5 Collector Orientation and Tilt

For the purposes of this study, the mounting of the solar collectors in the model was held constant year round. For all the climates and systems, the mounted collector azimuth angle was set to 0° which is due south. The tilt angles of the SWH and the combisystems were set based on design guidelines presented by Ramlow [56]. For the SWH that is used year-round for DHW loads, the tilt angle is set at the site's latitude, which varies depending on the site. For the combisystem which is used for both space heating and DHW loads, the mounting tilt of the collectors is set at the latitude plus 15 degrees. The increased mounting tilt for the combisystem is implemented in the model in order to maximize incident radiation in the winter months when the sun is lower in the sky in order to provide more solar energy to the space heating load. The comparison of performance at other tilt angles is found in section 5.5.5.

Chapter 5

Results

This chapter presents the results from the annual simulations for both the solar combisystem and the SWHs. As part of analyzing the results, the one-minute time step, hourly, monthly, and annual results were investigated.

5.1 Real-time Operation Results

One-minute time interval output data from the model shows the standard operation of the system. To fully understand the real-time operation of the system, the system as a whole was split into three subsystems, which include the solar loop, the space heating loop, and the domestic hot water. Plotting the temperature and the flow rates for each of these subsystems reveals how the controls operate to regulate the flow rates based on input temperatures to deliver energy to and from the tank.

Figure 5.1 shows the operation of the collector loop for a period of 12 hours in Denver, CO on a sunny June 12th day for a system with a 96 ft² collector area and 144 gallon storage volume. The green dotted line shows the collector flow rate, the purple dashed line shows the tank fluid temperature at tank node 14, which represents the node on the tank for the solar temperature probe, and the blue and red solid lines show the collector inlet and output temperatures, respectively.

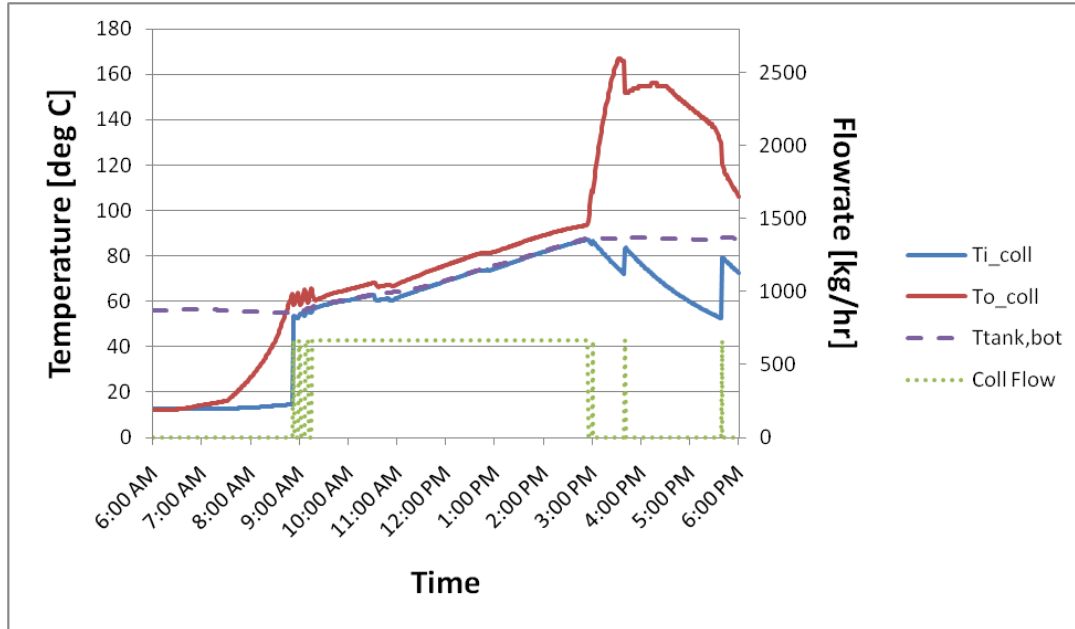


Figure 5.1: Collector loop operation on June 12th

The plot shows that in the morning when the collector outlet temperature is warming up, the differential controller turns on the collector loop pump when the collector outlet temperature reaches 10°C above the tank temperature and turns off the collector loop pump when the collector outlet temperature falls below 2°C above the tank temperature. This control scheme causes the collector loop pump to switch on and off at startup because the radiation on the collector is not large enough in the morning to maintain collector outlet temperature at least 2°C above the tank temperature. However, once the collector outlet temperature maintains at least a 2°C differential temperature at 9:30 AM, the collector loop delivers a constant flow rate to the tank until 3 PM. At 3 PM, the differential controller shuts off the solar pump because the tank reached the high limit cutout temperature, which is 88°C. The high limit cutout temperature is an overheating protection control mechanism to protect the tank from exceedingly high fluid temperatures. The controller remains off until the monitored tank temperature falls below the high limit cut-out temperature, which occurs a couple of times in the late afternoon.

Next, Figure 5.2 shows the operation of the upper heat exchanger when the space heating thermostat calls for heat to be delivered to the house during the nighttime in March for a Denver benchmark house. The blue dotted line represents the flow rate through the upper heat exchanger, the blue solid line represents the upper heat exchanger inlet temperature (at tank node 8), the red solid line shows the temperature of the heat exchanger fluid at node 7, the green solid line represents to the heat exchanger outlet temperature at node 3, and purple dashed line represents the tank temperature at the top of the tank.

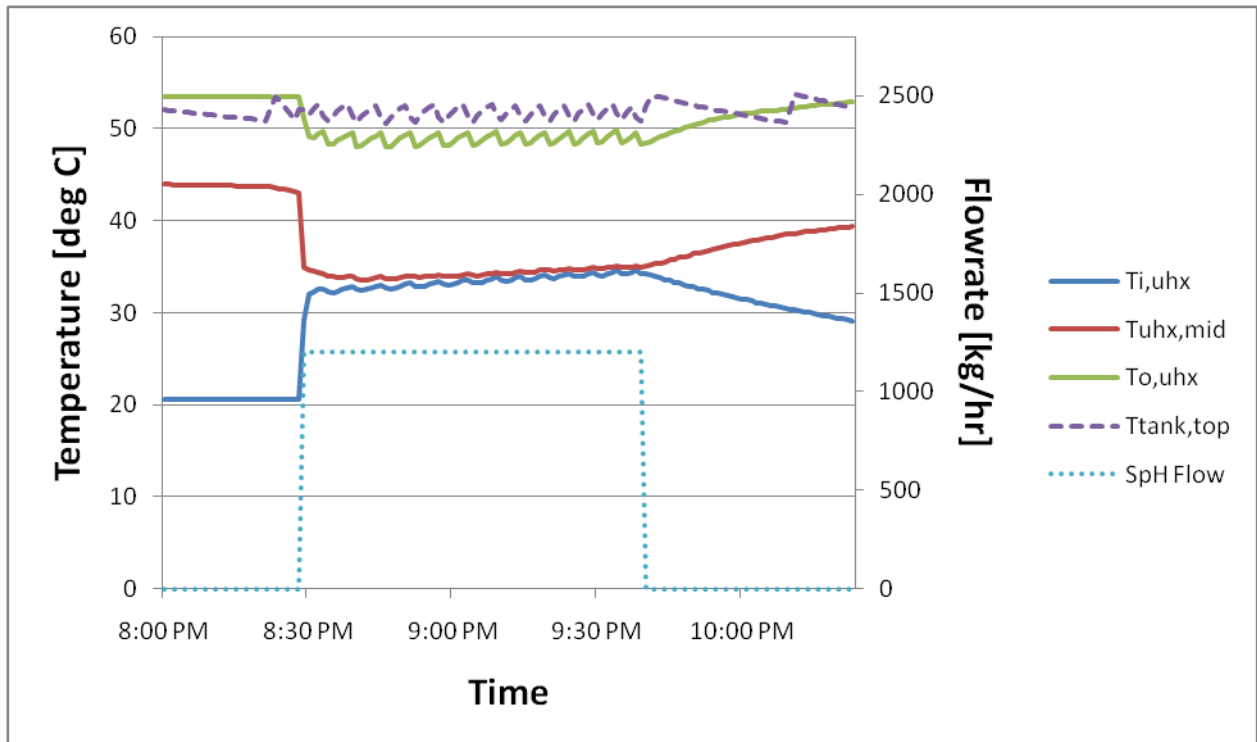


Figure 5.2: Operation of upper heat exchanger for space heating

During this time period, Figure 5.2 shows that the upper heat exchanger is extracting a small amount of heat from the portion of the tank that is below the auxiliary heater node as evident by the red line representing the heat exchanger fluid temperature at node 7 being higher than the heat exchanger inlet temperature at node 8. Since this lower portion of the heat exchanger is below the auxiliary tank heater, the fluid in the bottom part of the upper heat exchanger is utilizing heat from the bottom of the tank, which is energy supplied by the solar resource. In contrast, the upper portion of the upper heat exchanger

is supplied by the auxiliary heater. During this time period, the majority of the temperature rise in the heat exchanger fluid is supplied by the auxiliary heater. The rise and fall of the tank temperature at the top of the tank is due to the temperature 2°C dead band for the auxiliary heater switching off and on.

Figure 5.3 shows the real-time operation of the tempering valves for the DHW flows. The dotted purple line is the mains water temperature, the orange dotted line is the tank temperature at the top of the tank, purple solid line is the flow rate for mixed water events for sinks/showers (40.5 °C), the green solid line is the flow rate for hot water events for dish/clothes washers (51.7 °C), and the red and blue dashed lines represent the hot tank water flow and mains water flow rate, respectively, for each event.

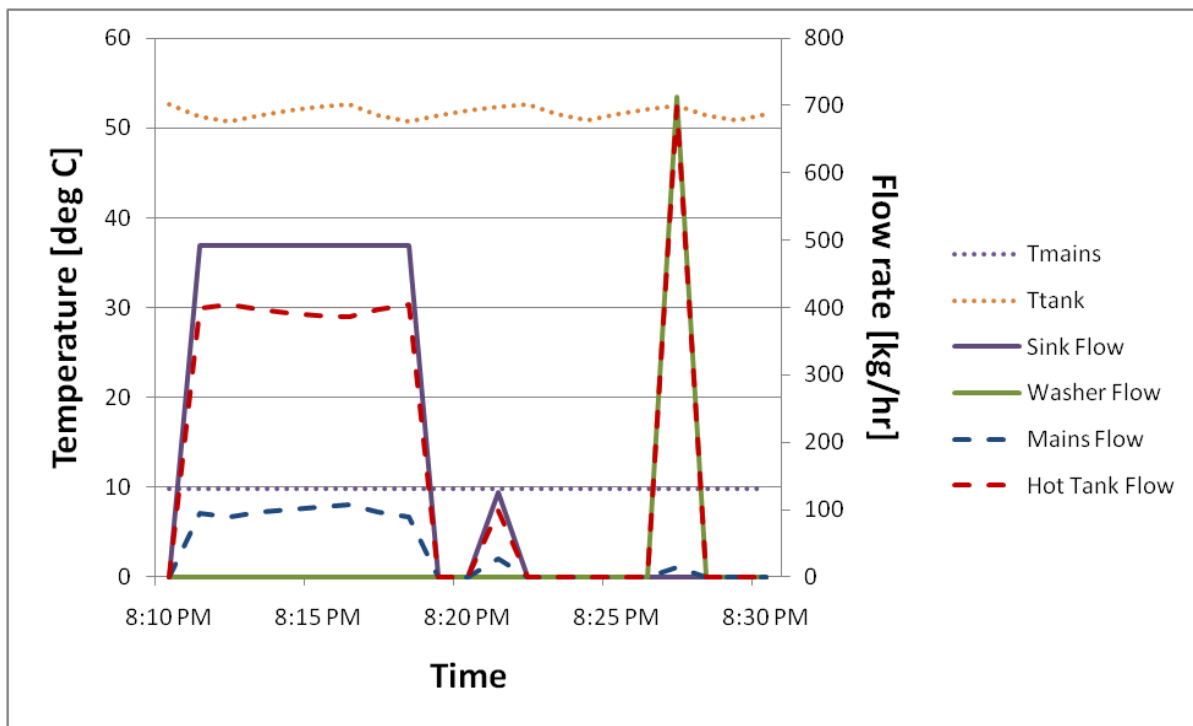


Figure 5.3: Operation of the DHW flows. The mains water flows through the tempering valve in order to mix with the heated tank water.

As stated before, there are two types of DHW flows in the model: mixed flows for sinks and showers and hot flows for dishwashers and clothes washers. In the model, each of these flow events has its own tempering valve which regulates the amount of tank hot water being extracted from the tank based on the specified desired temperature for the DHW event. The flow rates of the tank hot water and the

mains water is determined by the temperatures of those two fluids. To illustrate the operation of the two tempering valve, Figure 5.3 shows that for mixed flow events, significant amounts of mains water is mixed with the hot tank water to achieve a 40.5 °C mixed temperature. Additionally, Figure 5.3 shows that for hot water events, if the tank water temperature is above 51.7 °C, either due to the auxiliary dead band or the solar resource heating up the tank above the tank setpoint, the hot water tempering valve will mix mains water with the tank hot water to achieve the desired 51.7 °C temperature.

5.2 Integrated Hourly Results

As part of the process for evaluating and verifying the results of the model simulations, energy rates in the model were integrated over hour periods and energy balances were calculated to ensure that all of the model energy inputs were equivalent to the model energy outputs to within a reasonable error. The energy balances were calculated for the both the solar loop and the tank system.

An energy balance equation takes into account all the input energy, output energy, and energy stored within the system. In theory, the stored energy in a system should equal the difference of the input energy and output energy in the model. The solar loop energy balance is calculated as follows:

$$Q_{storage} = Q_{solar,useful} - (Q_{pipeloss} + Q_{sol,hx}) \quad 5.1$$

where $Q_{storage}$ is the stored energy in the solar loop, $Q_{solar,useful}$ is the useful energy input from the solar collector, $Q_{pipeloss}$ are the pipe losses between the collector and the tank, and $Q_{solar,hx}$ is the energy delivered to the tank from the lower heat exchanger. The energy balance error is calculated as the difference between the energy input, the energy output, and the energy storage divided by the energy input.

$$\% Error = \frac{Q_{input} - Q_{output} - Q_{storage}}{Q_{input}} \quad 5.2$$

To illustrate the energy balance in the solar loop, each of the energy variables in equation 5.1 is depicted in Figure 5.4.

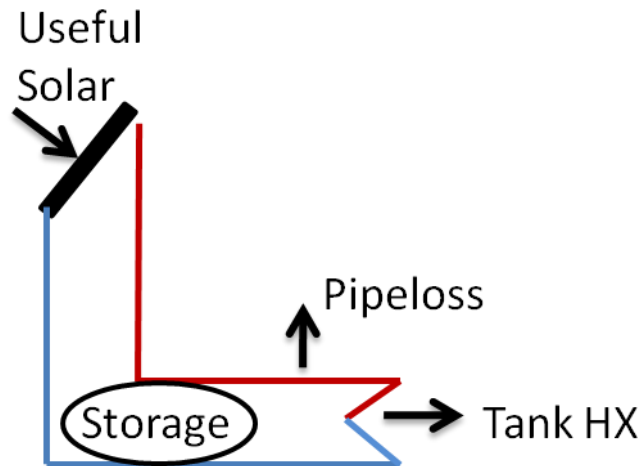


Figure 5.4: Schematic of energy balance for solar loop

To determine the energy balance, all of the energy calculations were integrated over a period of an hour and plotted in a time series to verify that the model was accurately modeling the system. Figure 5.5 shows the solar loop hourly energy values plotted over three days in March for a 96 ft² collector area system in Denver. The plot shows that the majority of the energy transfer in the solar loop is the input useful solar energy and the energy transfer into the tank through the heat exchanger, while pipe losses and energy storage in the pipes have smaller energy values. The energy balance error for the solar loop as calculated using equation 5.2 averaged to be 0.26 +/- 0.04% with a maximum of 0.62% over the course of the annual simulation.

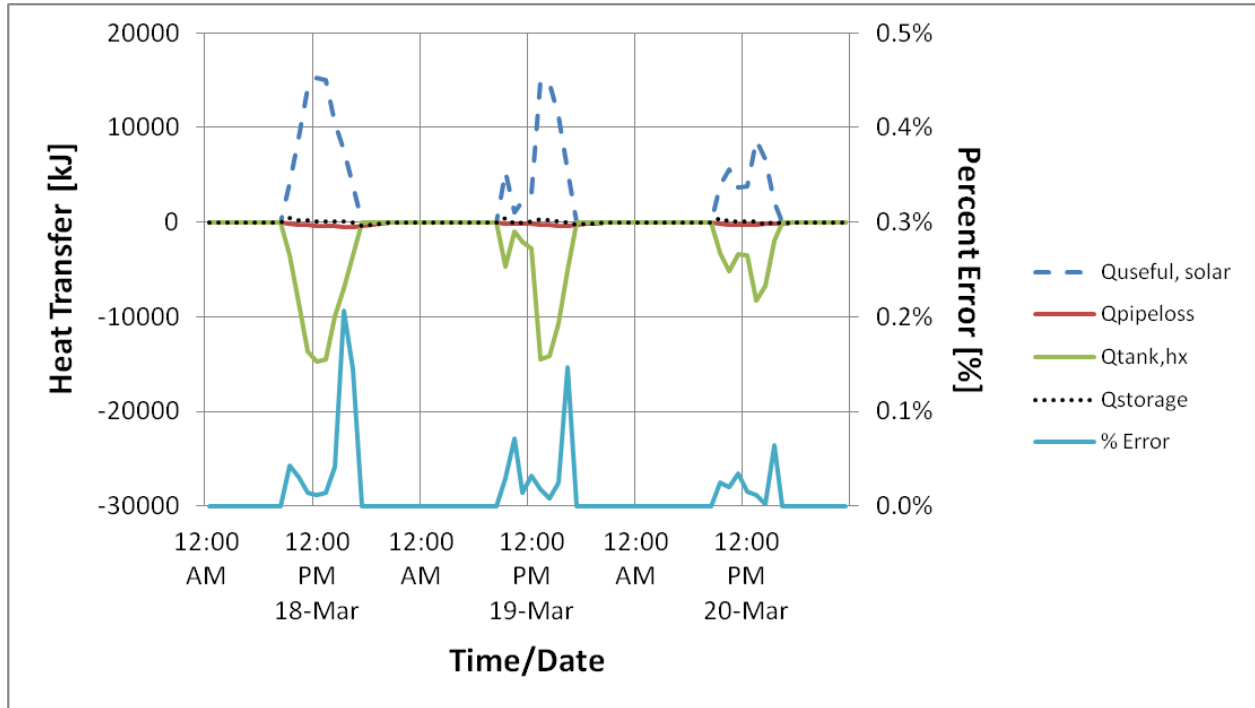


Figure 5.5: Solar loop energy balance plotted over time

The same process to find the error in the energy balance in the solar loop was used to determine the energy balance error in the tank. Drawing an energy balance around the tank, the tank energy balance can be written as:

$$Q_{storage} = (Q_{aux} + Q_{sol,hx}) - (Q_{tankloss} + Q_{dhw} + Q_{hx,sph}) \quad 5.3$$

where $Q_{storage}$ is the stored energy in the tank fluid and the heat exchanger fluid, Q_{aux} is the input auxiliary tank energy, $Q_{solar,hx}$ is the energy added by the solar heat exchanger, $Q_{tankloss}$ is the tank loss, Q_{dhw} is the energy delivered to the DHW load, and $Q_{hx,sph}$ is the energy delivered to the space heating load from the upper heat exchanger. To illustrate the energy balance in the solar loop, each of the energy variables in equation 5.3 is depicted in Figure 5.6.

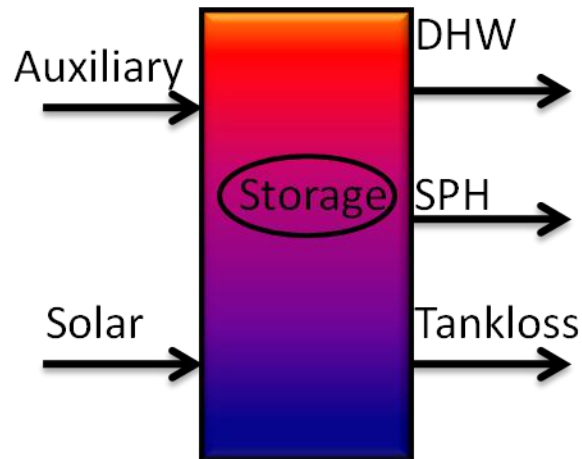


Figure 5.6: Schematic of energy balance for storage tank

Figure 5.7 shows the time series of energy balance calculations for the tank during the winter. The plot shows that energy is added to the tank by the auxiliary heater in the night to supply energy to the upper heat exchanger. During this time, little energy storage in the tank occurs. In contrast, during the daytime, energy is being delivered to the tank by the lower heat exchanger and that energy is being stored in the tank. During this time period, the tank losses and the domestic hot water loads are small relative to the solar, auxiliary, and space heating energy values. The energy balance error for the tank as calculated using equation 5.2 averaged to be 0.54 +/- 0.1% with a maximum of 0.92% over the course of the annual simulation.

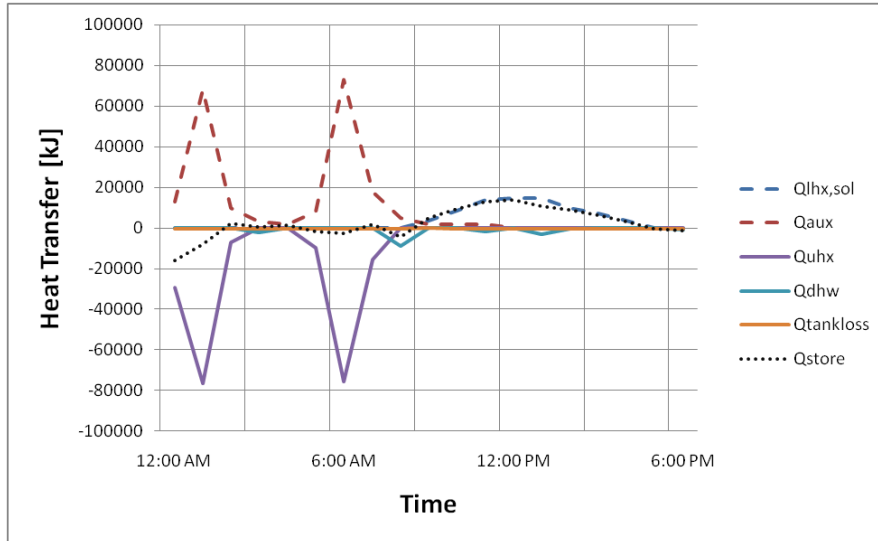


Figure 5.7: Time series energy balance plot in the tank

5.3 Monthly Solar and Loads

The monthly solar energy and the load results for both the combisystems and the SWHs were analyzed to verify that the model output energy values are reasonable. Figure 5.8 shows the monthly total load and the collected useful solar energy for a combisystem in Denver benchmark house with 96 ft² collector area and a 60 gallon per day DHW draw. The plot is divided into three zones, which are labeled by numbers in the plot. Zone 1, which is the zone that covers the largest portion of the plot, is the total load in the building that exceeds the amount of useful solar energy. In a combisystem, where the system is serving both the space heating and DHW load, the time period when the load exceeds the solar resource will be during the winter months, when the load is large. During this time, the auxiliary heater is required to meet the building load. Zone 2, which is portion of the plot where the useful solar energy section overlaps the total load section, represents is the building's load that can be met by the solar energy. Zone 3 is the solar energy that exceeds the load. In a combisystem, solar energy will likely only exceed the load in the summer months, when the load is at its minimum.

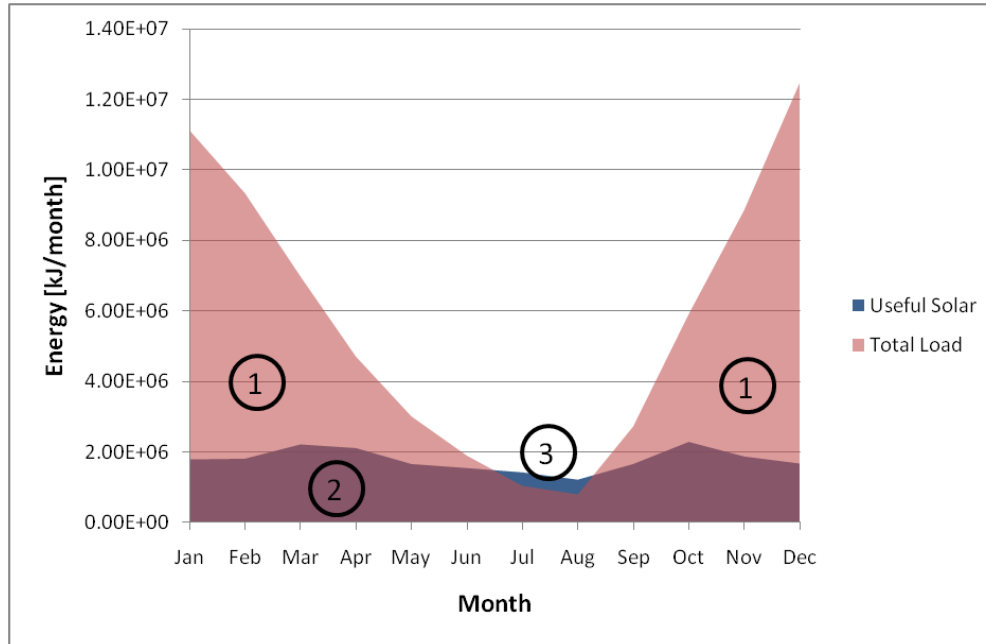


Figure 5.8: Monthly plot of the total load and the solar resource energy for a combisystem in Denver (96 ft²/ 60 gallon draw)

Figure 5.9 shows the monthly total load and the collected useful solar energy for a SWH in Denver with 96 ft² collector area and a 60 gallon per day DHW draw. In contrast to Figure 5.8, which shows that zone 1 occupies the majority of the plot, the SWH plot shows that zone 2 occupies the majority of the plot. Zone 2, which represents is the building's load that can be met by the solar energy, means that the 96 ft² collector area SWH in Denver will yield high solar fractions. Additionally, the large SWH also means that in the majority of the months, the useful solar energy exceeds the DHW load.

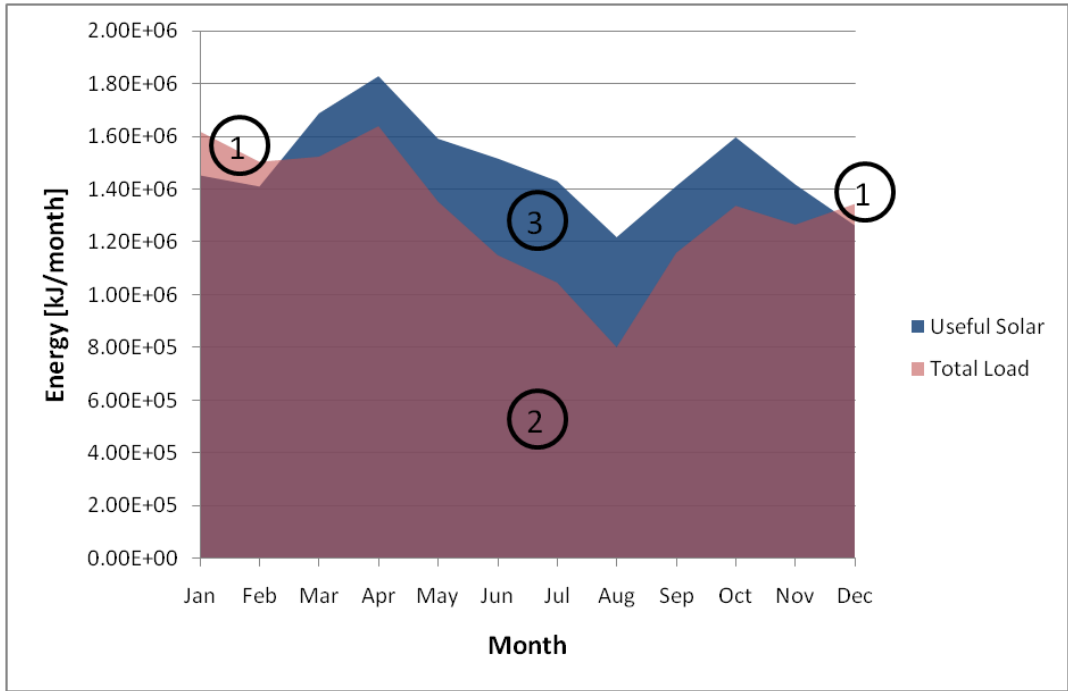


Figure 5.9: Monthly plot of the total load and the solar resource energy for a SWH in Denver (96 ft²/ 60 gallon draw)

5.4 Parametric Study

A parametric study was performed to determine the impact of model parameters on the performance of systems. The varied parameters included the location, the system collector area, the DHW load, and the house type. The location and the house type both have an impact the space heating load. Both the combisystem model and the SWH model were simulated using every combination of these four parameters. Table 5.1 shows a summary of the system parameters and their corresponding parametric variations.

Table 5.1: Parametric Runs Summary

System Parameter	Parametric Runs
Locations [City]	Phoenix, Atlanta, San Francisco, Denver, Boston, Chicago
System Size (collector area [ft ²])	SWH- 32, 64, 96; Combisystem- 32, 64, 96, 160, 224, 288
Average DHW Load per day	20 gallons (low), 60 gallons (mid), 100 gallons (high)
House Type	1960s Retrofit, 2009 IECC, 50% BA

Each of the locations studied present some unique climate-specific parameters, which will impact the energy savings of the combisystem and the SWH. For example, the amount of energy savings from a SWH can be impacted largely by climate parameters such as cloud cover, solar resource, and mains water temperature, which impacts the DHW load. As part of the NREL study that examined the break-even costs of residential solar water heaters in the U.S. [57], a map was created that showed the annual energy savings by a SWH as compared to a conventional electric storage tank for all the TMY3 locations in the U.S. (see Figure 5.10). The study used the Solar Advisor Model (SAM) to simulate a two-tank glycol active SWH with an auxiliary electric heater and storage tank with a collector area of 40 ft² and a 60 gallon storage volume. The figure shows that San Francisco and Denver yield the highest annual energy savings (greater than 2,200 kWh annually), while the remainder of the locations studied in the thesis (as shown on the map) yield annual energy savings of less than 2,050 kWh annually.

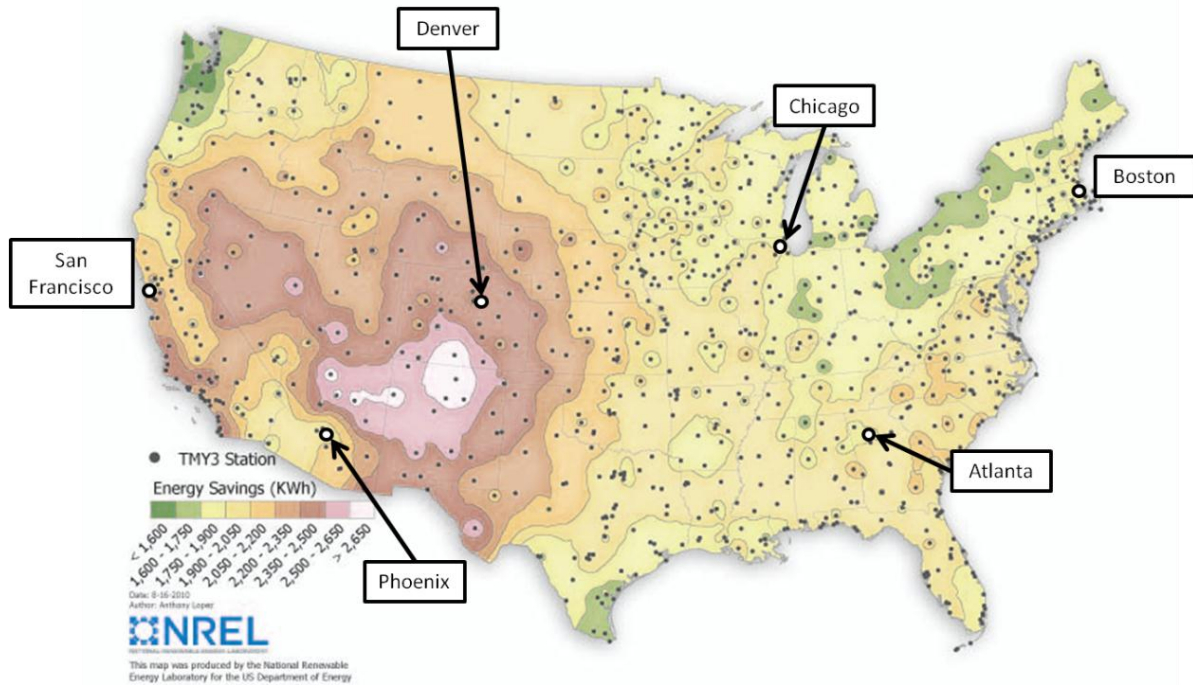


Figure 5.10: Annual energy savings from a SWH with an electric auxiliary water heater [57]

It may sound counter-intuitive that San Francisco presents a good solar resource for SWHs, however the TMY3 data taken from the San Francisco Airport, shows that, despite highly variable and microclimatic weather conditions in San Francisco, on an annual basis, the solar radiation resource is relatively high and stable. Based on the TMY3 weather data, the average horizontal solar radiation in San Francisco is $5.12 \text{ kWh/m}^2/\text{day}$ over the period of data collection. In comparison, the average horizontal solar radiation in Denver is slightly lower at $5.06 \text{ kWh/m}^2/\text{day}$. Figure 5.11 shows the average daily horizontal radiation levels for the six cities studied in the thesis.

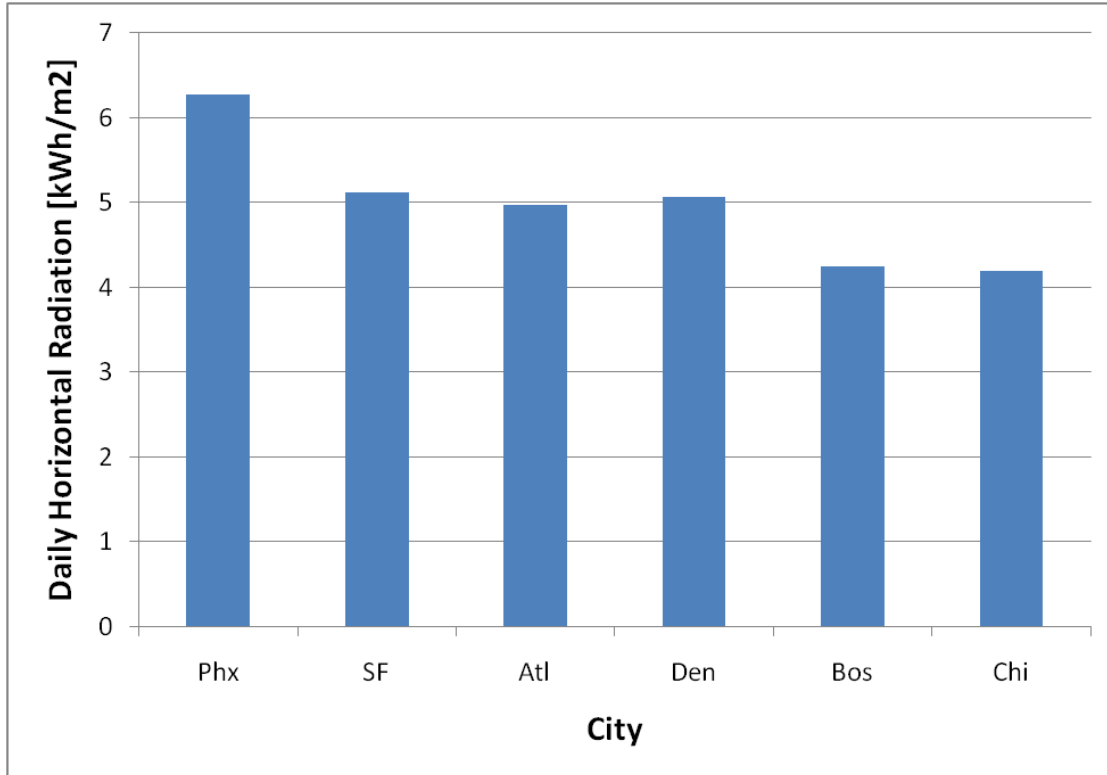


Figure 5.11: Average daily horizontal radiation levels for the six locations

5.5 Energy Performance Analysis

One of the goals of this thesis is to compare the energy performance of a combisystem versus a solar water heater. To accurately determine the performance of solar combisystem and solar water heater and to adequately compare the performances between the two with detailed simulation models, the system's auxiliary energy usage was compared to the auxiliary energy usage of a reference system without solar collectors.

For each parametric run, the annual saved energy is calculated as:

$$Q_{saved} = (Q_{aux,no-sol} + \delta Q_{load,no-sol}) - (Q_{aux,sol} + \delta Q_{load,sol}) \quad 5.4$$

Where δQ_{load} is a penalty value used to normalize the auxiliary energy usage, which is equal to the amount of load that the system was not able to meet over the course of the year. One can think of it as the additional energy required, which would be supplied by a 100 percent efficient and infinite capacity water heater, in order for the system to meet 100 percent of the water heating and space heating load. This penalty factor was applied to the saved energy equation because there are periods during the year where the water heater element capacity was not large enough to keep up with the demand of the system's water heating and space heating load. In equation 5.4, the first parenthesis term is the auxiliary energy usage for a conventional system without solar and the second parenthesis term is the auxiliary energy usage for the system with solar collectors.

Based on the calculated saved energy in equation 5.4, the system efficiency is determined as:

$$\eta_{system} = \frac{Q_{saved,annual}}{I_{T,annual} * A_{coll}} \quad 5.5$$

The system efficiency differs from the collector efficiency in that collector efficiency looks at the ratio of the collector's total energy input to the useful energy output. The system efficiency looks at the ratio of the system's saved energy as compared to a conventional system to the collector's energy input from radiation, which means that the system efficiency takes into account the energy losses from the tank and the pipes in the solar collector loop. As compared to the collector efficiency, the system efficiency will typically be about 5 to 10 percentage points lower than the solar collector's efficiency due to the fact that system efficiency takes into account the extra energy losses in the solar system. Additionally, the marginal system efficiency was determined by the ratio of the change in energy savings to the change in total solar incidence as a function of increasing the collector area.

$$\eta_{marginal,system} = \frac{\Delta Q_{saved,annual}}{(I_{T,annual} \Delta A_{coll})} \quad 5.6$$

The annual solar fraction is defined as the ratio of the annual saved energy from the solar thermal system to the auxiliary energy required to meet the load in a conventional system. In mathematical terms, the solar fraction is determined as:

$$f_{solar} = \frac{Q_{saved,annual}}{Q_{fuel,no-solar,annual}} \quad 5.7$$

Additionally, the fraction of the space heating load that was covered by the solar energy was estimated by splitting the upper heat exchanger into two separate heat exchangers: the solar-assisted heat exchanger and the auxiliary-assisted heat exchanger. Figure 5.12 shows a schematic of the combisystem tank with the split between the solar space heat and the auxiliary space heat. The auxiliary heating element is located at node 6, the solar-assisted upper heat exchanger is located in nodes 7 and 8 and the auxiliary-assisted upper heat exchanger is located in nodes 3 through 6. Because the tank storage volume varied during the parametric study, the volume of the tank occupied by the solar space heat exchanger and the auxiliary space heat exchanger varied as well. For example, for a 96 ft² collector area and 144 gallon tank system, the volume of the tank occupied by the solar-assisted heat exchanger is 8 gallons and the volume of the tank occupied by the auxiliary-assisted heat exchanger is 16 gallons. Additionally, Figure 5.12 shows that the solar loop heat exchanger occupies the tank in nodes 10 through 16.

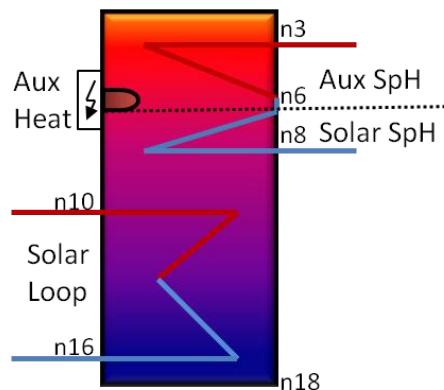


Figure 5.12: Schematic of Tank Model for Combisystem

To determine the estimated space heating solar fraction, the energy delivered by the solar-assisted upper heat exchanger was divided by the total space heating load.

$$f_{solar,sph} = \frac{Q_{sol,uhx}}{Q_{sph,no-sol}} \quad 5.8$$

5.5.1 Energy Performance Trends

The energy performance of the combisystem and the SWH was analyzed by calculating the energy performance metrics as described in the previous section for each parametric run. These energy performance metrics include saved energy, solar fraction, space heating solar fraction, efficiency, and marginal efficiency. With these energy performance metrics plotted on the y-axis and the collector area on the x-axis, the performance of the two systems can easily be compared. Within this plot, the impact of DHW load is also shown by displaying the system performance for each DHW draw level.

Of course, this one plot with energy performance and collector area on the two axes cannot show the impact of all the varying parameters, so additional plots were created to display the impact of system loads and climate on the energy performance of the two systems. The impact of all the parameters are analyzed in later in Chapter 5.

First, the system's saved energy as compared to the conventional system without solar is plotted with respect to collector area. Figure 5.13 shows the saved energy for both a SWH system and combisystem for three DHW loads in a benchmark house in Denver, CO. The saved energy for the combisystems are depicted with a solid line and open shape and the saved energy for the SWH systems are depicted with the dashed line and a filled shape. Additionally, the plot shows the performance of the systems with the three DHW loads. The low DHW load (20 gallons/day) is represented by the diamond shape, the mid DHW load (60 gallons/day) is represented by the square shape, and the high DHW load (100 gallons/day) is represented by the triangle shape. Lastly, the saved energy plot shows the DHW total

loads and the Space Heater loads, which are independent of collector area and represent the theoretical maximum energy savings that a system could yield. For a SWH system, the theoretical maximum energy savings is its corresponding DHW load (the horizontal load line can be thought of as the energy saving curve's asymptote). In contrast, the combisystems theoretical maximum energy savings is their corresponding DHW load plus the space heating load.

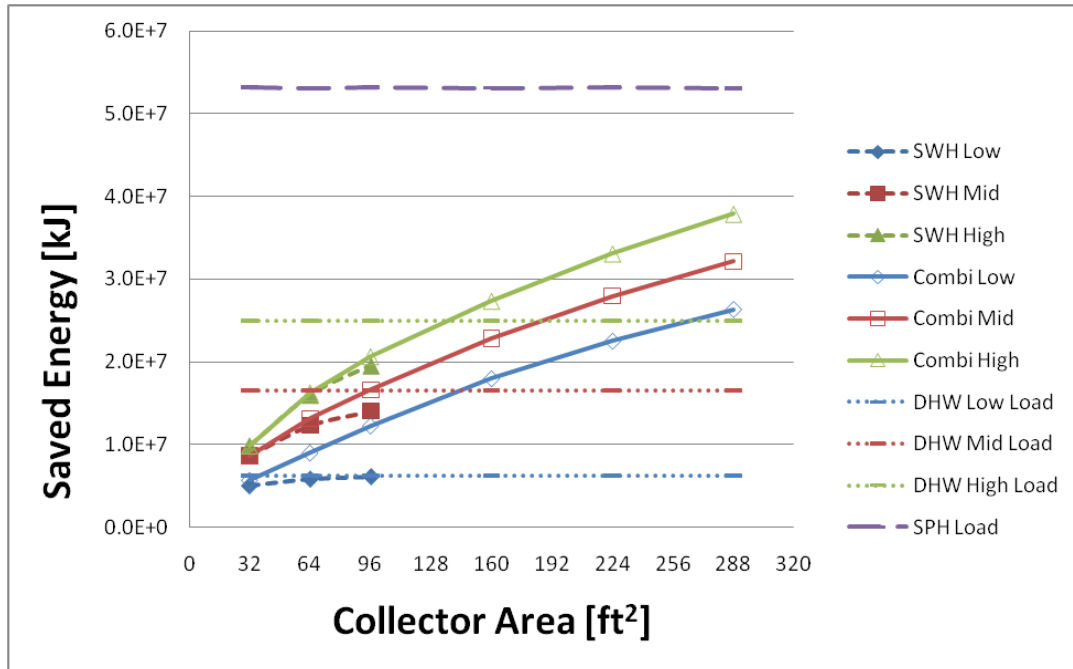


Figure 5.13: Saved Energy for SWHs and Combisystems in Denver Benchmark House

Figure 5.13 shows several key performance trends with regards to the saved energy between the combisystem and the SWH. First, as collector area increases, the saved energy in both systems also increases, although the rate of increased savings diminishes as collector area increases. Second, as collector area increases, the saved energy difference between the combisystem and the SWH system grows. This is because the SWH system energy savings is limited greatly by a smaller load, especially when the collector area is large and the DHW load is low. Combisystems on the other hand serve a larger load which means that its absolute energy savings keep increasing with collector size even in systems

with large collector areas. The third trend is that with systems with 32 ft² collector area, the combisystems offer little savings as compared to SWH systems even with small DHW loads. Additionally, even with a 64 ft² collector area system, a combisystem will offer little additional energy savings as compared to a SWH if the DHW loads are high.

Next, Figure 5.14 and Figure 5.15 show the solar fraction for the combisystem and the SWH system respectively. As a reminder, the solar fraction is the ratio of the savings to the auxiliary energy required to meet the load without solar. Given this definition, it's not unexpected that for both systems, the solar fraction increases with collector area, since savings increase with larger systems. However, for the combisystem, the solar fraction will be much lower than in a SWH system because the load (space heating and DHW) and the auxiliary energy required to meet the load in the combisystem is much larger than energy required to meet just the DHW load in the SWH system.

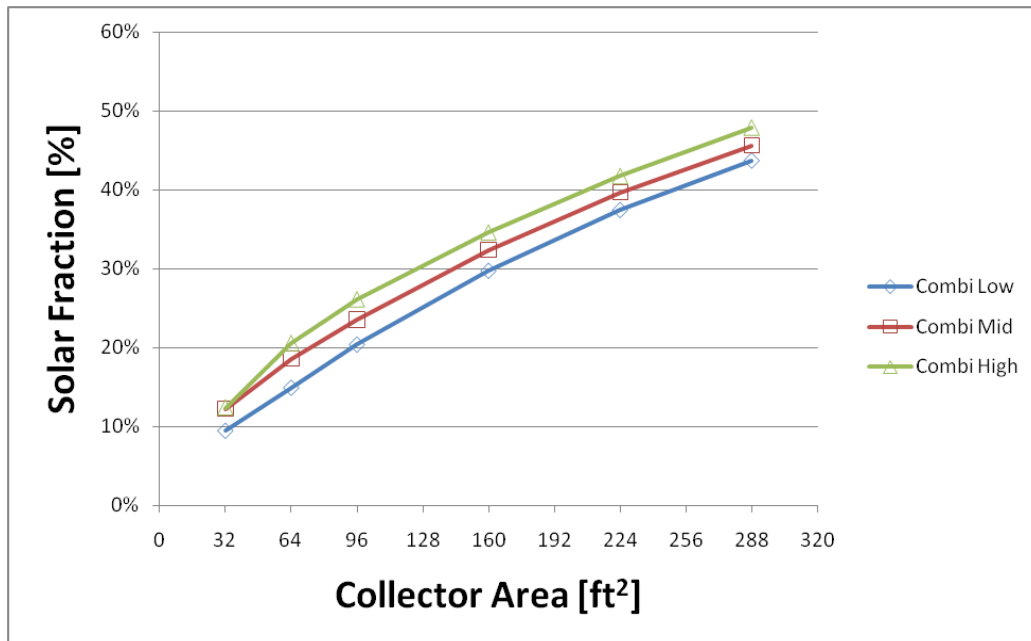


Figure 5.14: Solar Fraction for Combisystem in Denver Benchmark House

There are a couple of key observations when evaluating the solar fraction of these two systems. First, in the combisystem with 32 ft² collector area, the solar fraction for the mid and high DHW loads are the essentially the same, which means that the relative increased savings from increasing the DHW load from 60 to 100 gallons per day is equal to the relative increase in auxiliary energy required to meet the increased load, which consists of both the space heating and the DHW load for the combisystem. For all other cases with the combisystem, for a given collector area size, the relative increased savings from increasing the DHW load are larger than the relative increase in auxiliary energy required to the meet the load, which explains why higher DHW loads results in higher system solar fractions for a given collector area. In contrast, for a SWH system, the systems with lower DHW loads result in higher solar fractions than a system with higher DHW loads. This means that the relative increased savings from increasing the DHW load is smaller than the relative increase in auxiliary energy required to meet the larger DHW load.

The impact of the three levels of loads on the order to the solar fractions for both the SWH and the combisystem is almost entirely dictated by the relative increase in the energy required to meet the next level of load (for example, moving from a low DHW load to a medium DHW load). In the SWH case, the relative increase in energy to meet a higher DHW load is much greater than the relative increase in energy to meet a higher DHW plus space heating load in the combisystem case.

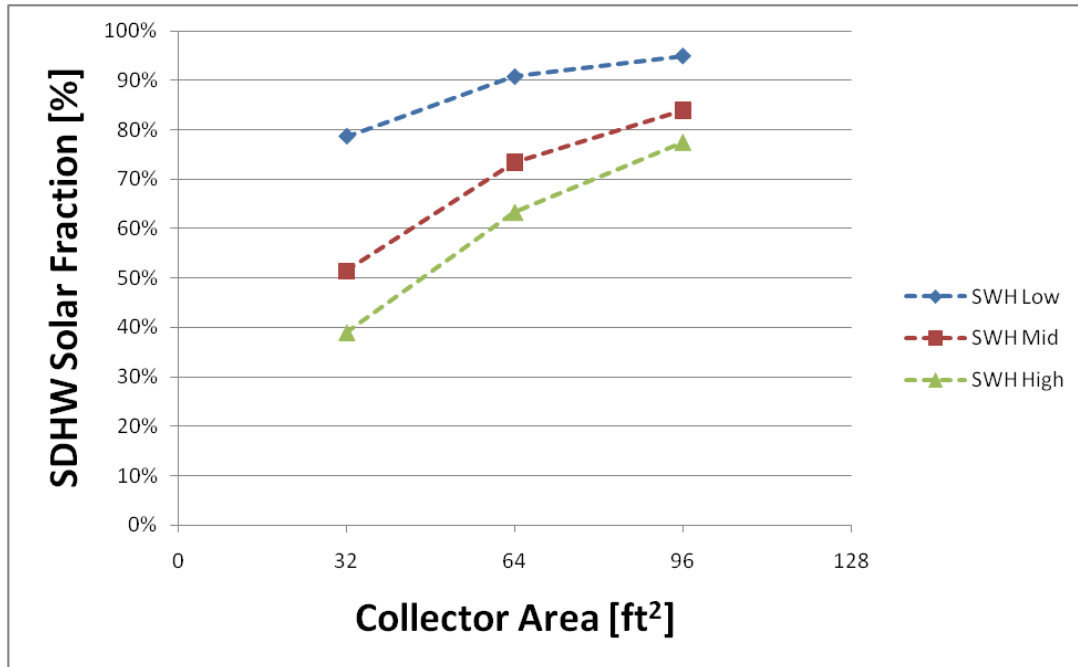


Figure 5.15: Solar Fraction for SWH in Denver

Additionally, in Figure 5.15, the solar fractions for the three DHW loads begin to converge as collector area increases. This is due to the larger systems reaching a system saturation limit with solar supplying almost all of the energy required to meet the DHW load in large systems. For example, in the Denver climate, a 32 ft² collector area system will have a solar fraction between 40% and 80% depending on the DHW load. Meanwhile, a 96 ft² collector area SWH system will have solar fraction ranging from 78% to 95% depending on the DHW load. This convergence effect as collector area increases is even more apparent in climates with smaller DHW loads, such as Phoenix, where a 96 ft² collector system will be able to supply a 95% solar fraction regardless of the magnitude of the DHW load (see Figure 5.16).

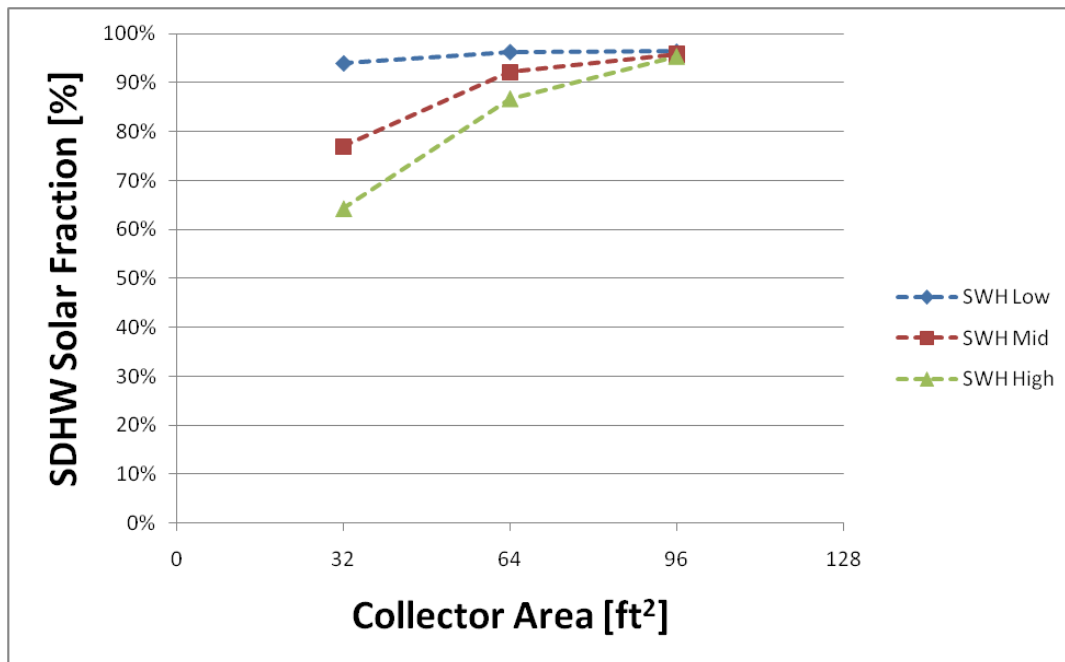


Figure 5.16: Solar Fraction for SWH in Phoenix

Next, in Figure 5.17, the space heating solar fraction is plotted for the combisystem as a function of DHW load and collector area. The space heating solar fraction for a Denver benchmark house can reach as high as 37% for a 288 ft² collector area system with a low DHW draw. The order of the space heating solar fraction for the three DHW loads for a given collector area is the same as the order of the solar fraction for the three DHW load in the SWH system case. However, in this space heating solar fraction case, the order to the solar fractions as a function of DHW load can be thought as the increased DHW load being detrimental to the system's ability to utilize solar energy for space heating. For example, for a 32 ft² collector area system size, the high DHW load results in none of the solar resource being utilized for the space heating load, whereas a low DHW load means that a small portion of the space heating is satisfied with the solar resource.

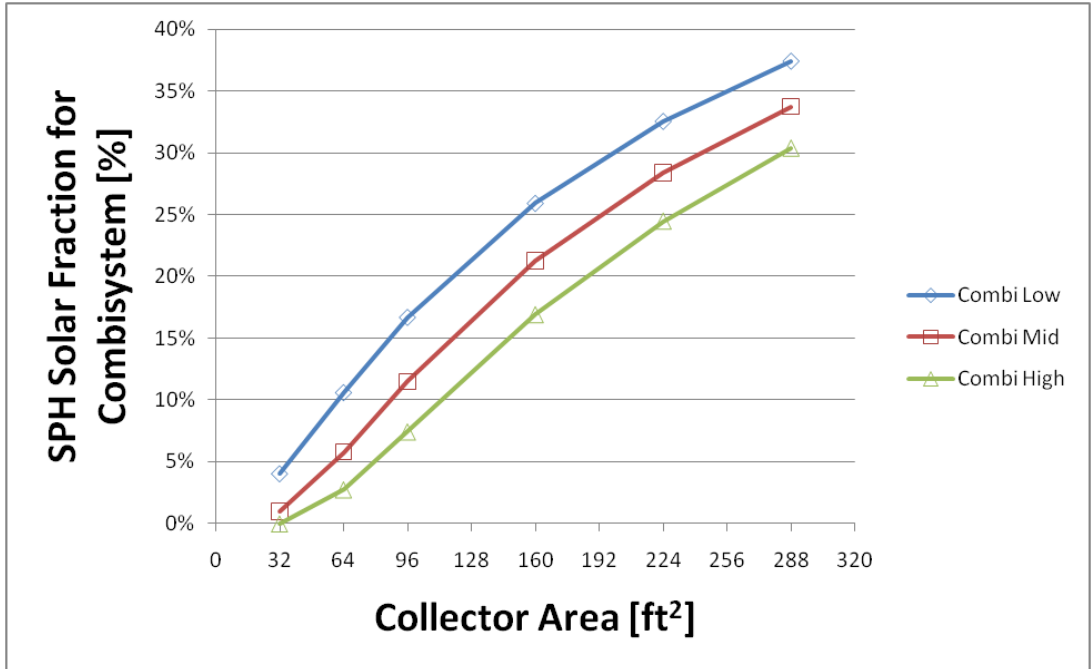


Figure 5.17: Space Heating Solar Fraction for Combi system in Denver Benchmark House

Figure 5.18 shows that the system efficiency of both the combi system and the SWH system decreases as collector area increases, with the SWH system efficiency decreasing more quickly than the combi system system efficiency as a function of collector area.

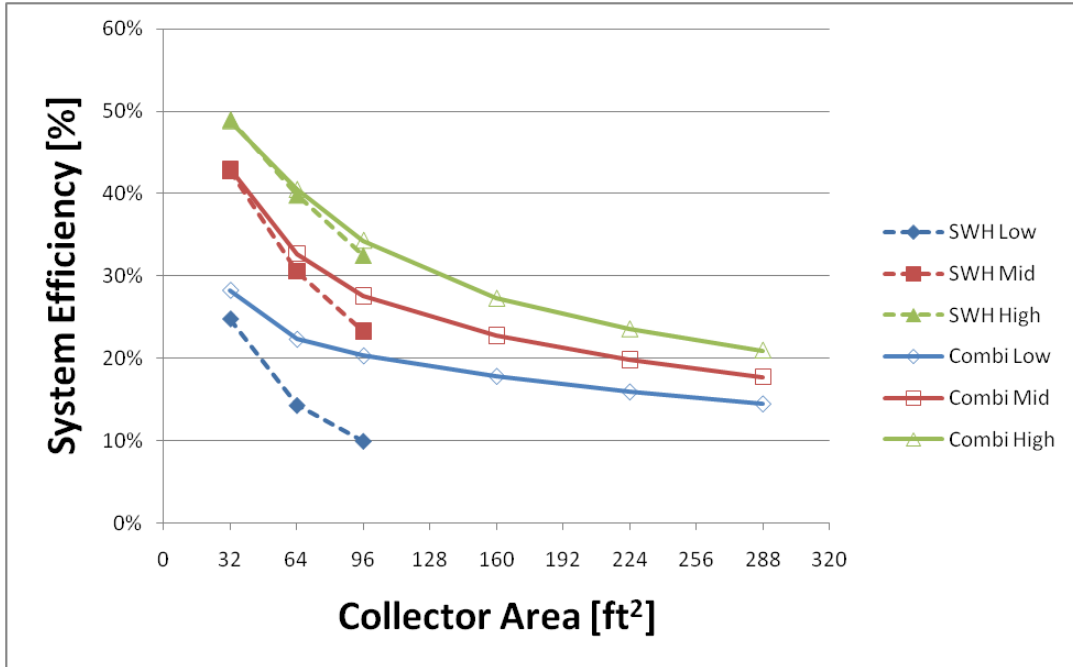


Figure 5.18: System efficiency of combisystem versus SWH in Denver Benchmark house

There are a couple of important factors that go into determining the system efficiency. First, the collector efficiency plays a large role in the system's efficiency. Figure 5.19 shows that the collector efficiency in the combisystem and SWH system follows the same trend as the system efficiency as collector area increases.

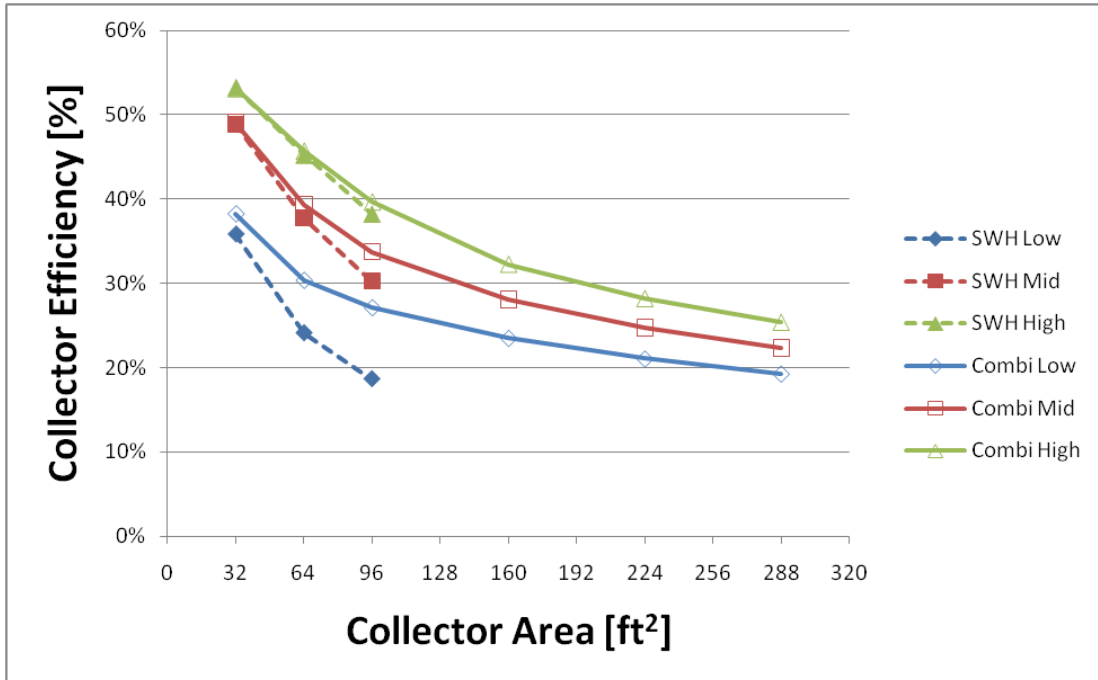


Figure 5.19: Collector efficiency in the combisystem and SWH for the three DHW loads

Since collector efficiency decreases with increasing inlet fluid temperature, it's expected that the collector efficiency will decrease as collector area increases. This effect is due to the fact that the higher temperature inlet fluid has a lower capacity to be heated. The reason why the smaller collector area systems have a lower inlet fluid temperature is because the tanks in small systems run cooler than the tanks in larger systems. The temperature of the tank also impacts the amount of heat that the solar loop can dump into the immersed heat exchanger and directly impacts the temperature of the collection inlet fluid. Figure 5.20 shows the average tank temperature for the two systems with respect to the collector area and the DHW load. The plot shows that tank temperatures are lowest in small systems with high DHW loads, which means that collector inlet fluid temperatures are lowest and collector efficiencies are highest in small systems with high DHW loads. Additionally, Figure 5.20 shows that combisystems will have a lower average tank temperature as compared to SWH. This is due to the fact that combisystems have higher loads to dump heat into as compared to SWH systems.

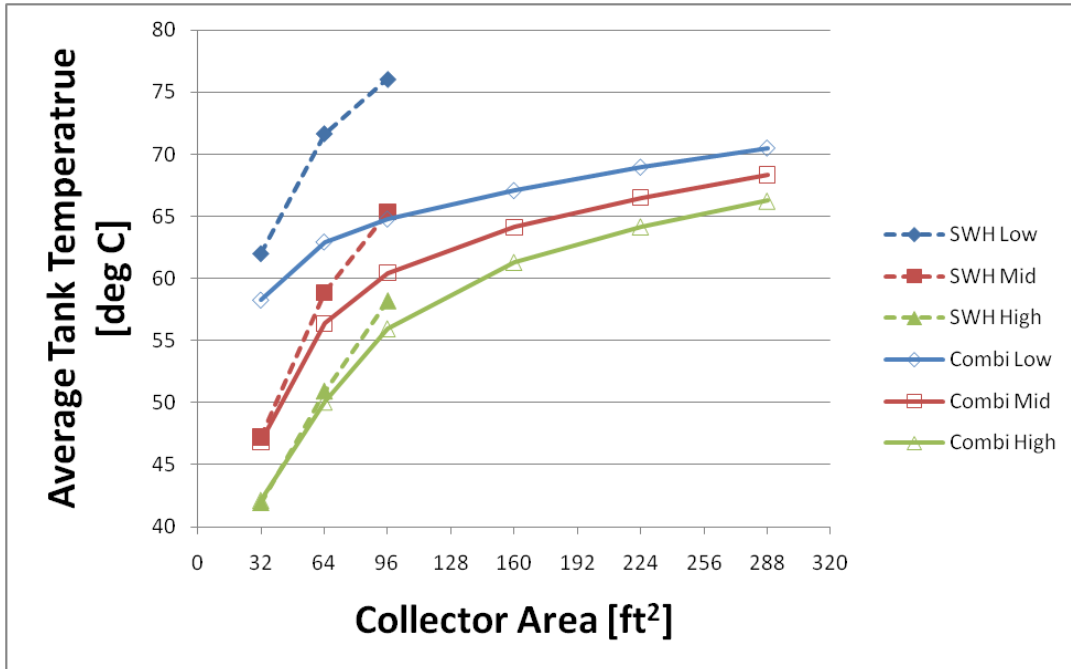


Figure 5.20: Average tank temperature of combisystems and SWH systems for the three DHW loads

Additionally, the average tank temperature will have an impact on the tank losses and also the system efficiency. Figure 5.21 shows that larger systems will have larger tank losses because the average tank temperatures are higher. Also, SWH systems will have larger tank losses than combisystems because the tank temperatures are higher in SWH systems.

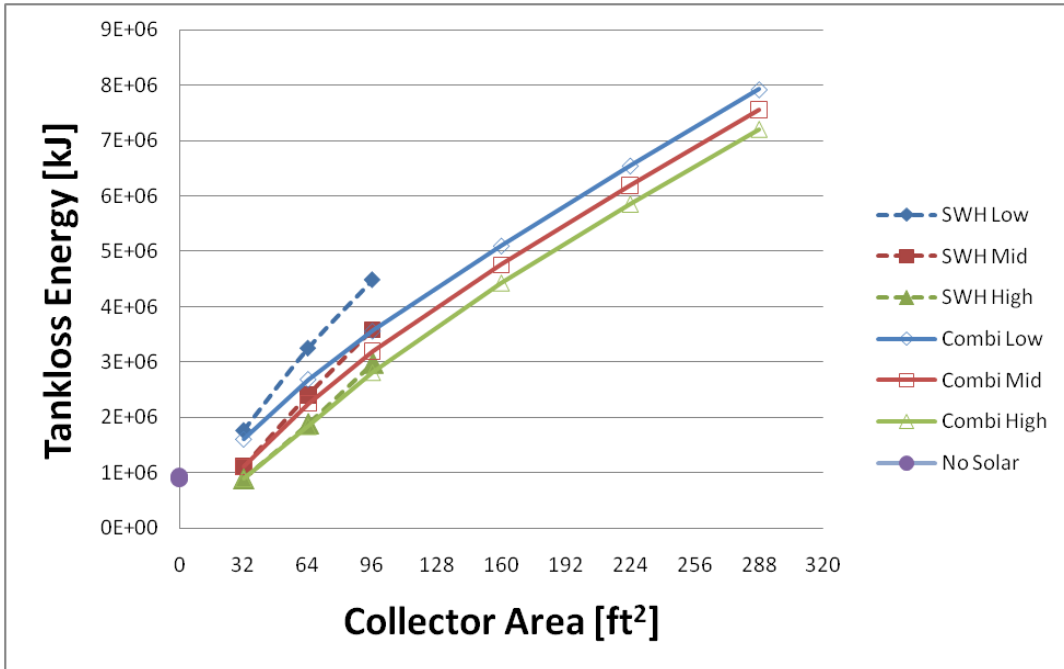


Figure 5.21: Annual tank losses of combisystem versus SWH for Denver benchmark house

Next, Figure 5.22 shows the marginal system efficiency plotted with respect to collector area and DHW loads. The marginal system efficiency is defined as the ratio of the change in savings to the change in solar incidence, where the changes are due to increasing the area of the collector. As seen in the figure, the marginal system efficiency for the SWH decreases more rapidly than the marginal system efficiency for the combisystem. This is due to the fact that SWH systems have higher tank losses and higher collector inlet fluid temperatures as compared to combisystems.

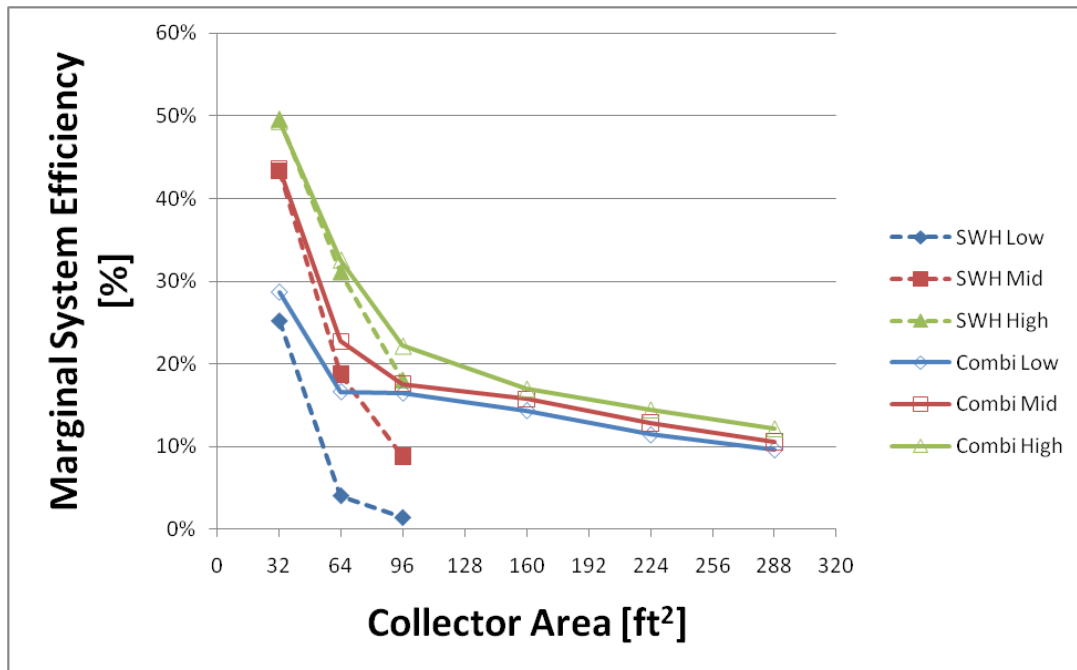


Figure 5.22: Marginal system efficiency of combisystem versus SWH for Denver benchmark house

5.5.2 Impact of DHW Load

For a single climate and house type, the following plots show the performance of the combisystem as compared to the SWHs for the three different DHW loads and two system sizes. Figure 5.23 shows the impact the DHW loads on the annual saved energy for the two systems for the collector areas of 32 ft² and 96 ft² in a Denver benchmark house. As expected, the figure shows that for systems with low DHW consumption, the difference between the saved energy for combisystems and SWHs will be much greater than in systems with high DHW consumption. Additionally, the figure shows that the incremental savings of the combisystem are much greater for the larger collector area than with the small system. In fact, a 96 ft² combisystem with low DHW consumption can increase the energy savings by 100% as compared to a SWH. In contrast, with a 32 ft² collector area system, the combisystem will provide no additional savings as compared to the SWH with a high DHW load.

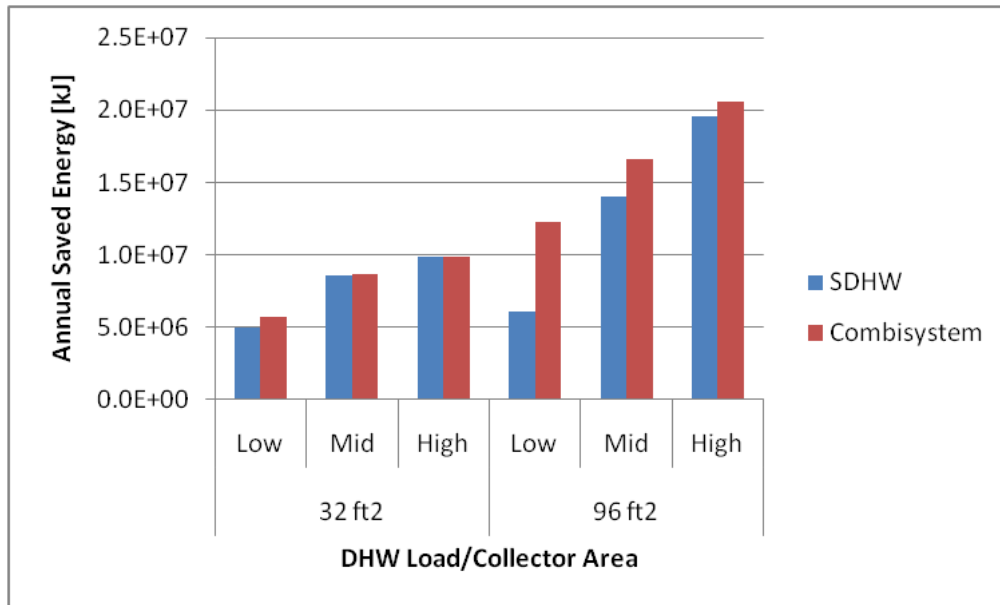


Figure 5.23: Impact of DHW loads on the annual saved energy of combisystem and SWH for Denver benchmark house

Figure 5.24 shows that the incremental savings of the combisystem relative to a SWH are much greater for the larger collector areas than with the small system. In fact, a 96 ft² combisystem with low DHW consumption can increase the energy savings by a factor of 2. In contrast, with a 32 ft² collector area system, the combisystem will only provide 5% savings as compared to the SWH with a low DHW load. With high DHW loads, the savings increase with the combisystem relative to the SWH is minimal, regardless of the system size. From this figure, it can be concluded that DHW loads will have a fairly large impact on the incremental relative savings that a combisystem will yield in comparison to a SWH, especially with larger systems.

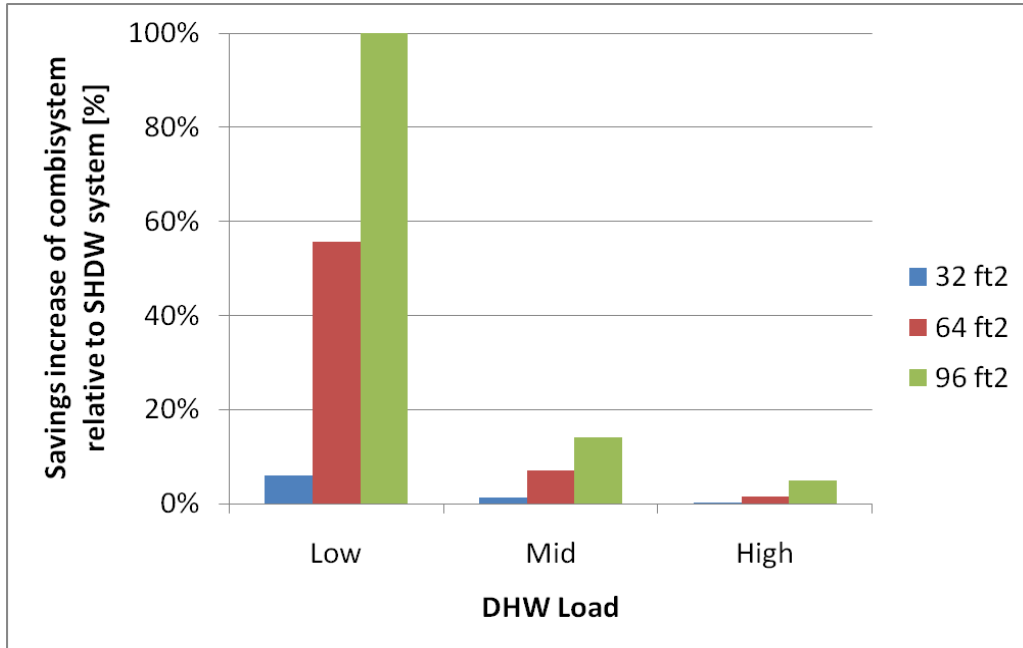


Figure 5.24: Impact of DHW load on the relative savings increase of the combisystem relative to the SWH for three collector area sizes (Denver Benchmark House)

Next, the impact of the DHW loads on the system efficiency is shown in Figure 5.25. The figure shows that the incremental increased system efficiency for the combisystem as compared to the SWH will be much greater when the DHW load is low. In high DHW load situations, the combisystem will provide little additional efficiency benefits because the high DHW load is utilizing most of the solar resource already. In fact, in small systems when the DHW load is high, the combisystem will operate at the same system efficiency as the SWH. On the other hand, with low DHW loads, the presence of the upper heat exchanger in the combisystem to extract more energy from the tank, will reduce the overall average tank temperature, and increase the collector efficiency will allow the system to operate at a much higher efficiency as compared to the SWH. In fact, with a 96 ft² system, the combisystem with a low DHW load will operate twice as efficiently as a SWH with a low DHW load.

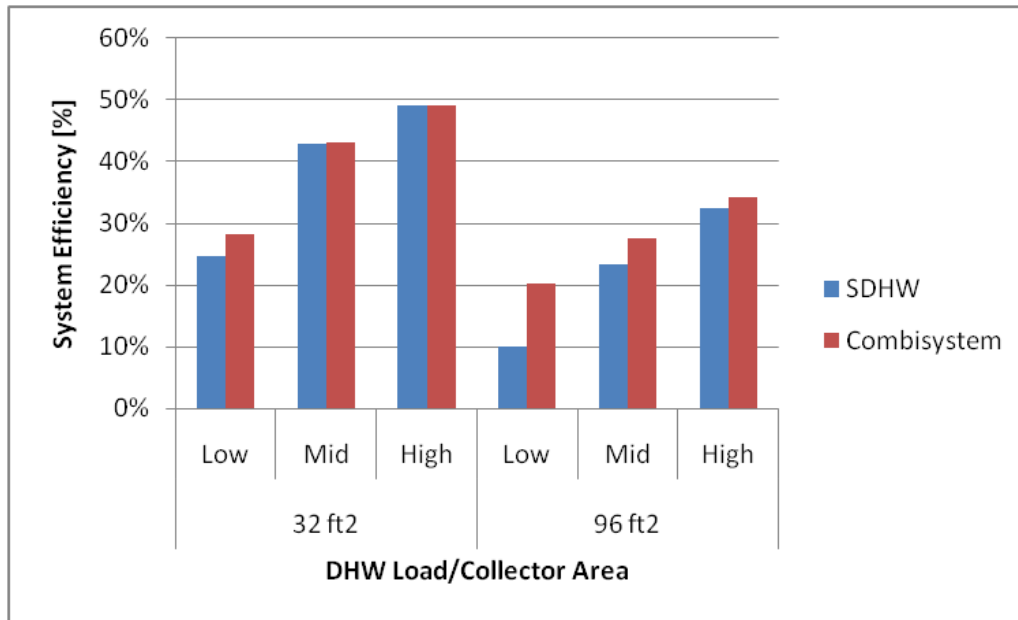


Figure 5.25: Impact of DHW loads on the system efficiency of combisystem and SWH for Denver benchmark house

The impact of the DHW load on the two system’s energy performance is also evaluated with a benchmark house in Phoenix, a sunny climate with a small heating load. Figure 5.26 shows the annual saved energy for both the 32 ft² and 96 ft² system with low, medium, and high DHW loads. As with the Denver benchmark house case, the figure shows that for systems with low DHW loads, the difference between the saved energy between combisystems and SWHs will be much greater as compared to incremental savings between the two systems with high DHW loads (see Figure 5.26).

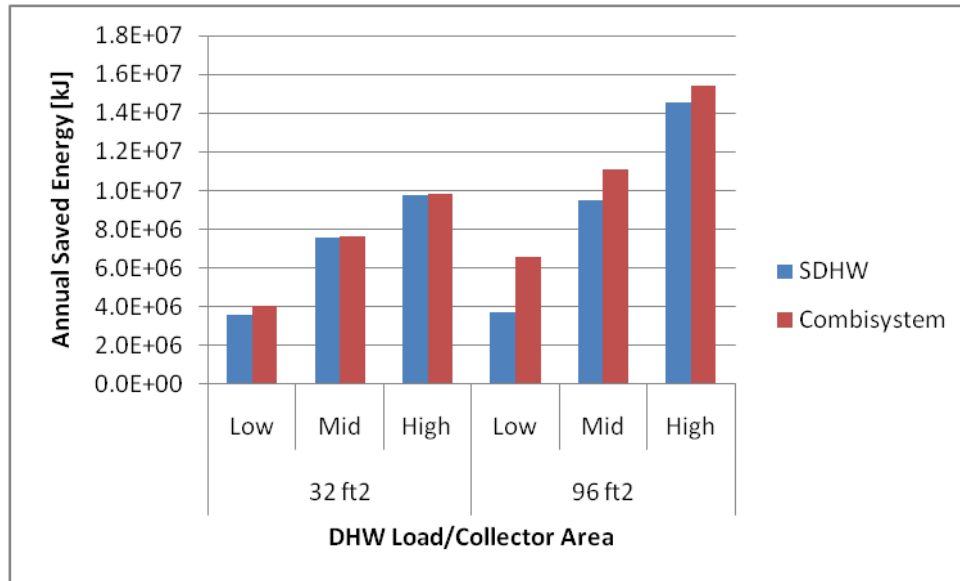


Figure 5.26: Impact of DHW loads on the annual saved energy of combisystem and SWH for Phoenix benchmark house

Figure 5.27 shows the impact of DHW loads on the system efficiency of the combisystem and SWH for Phoenix benchmark house. Once again, the incremental efficiency gains from going from a SWH to combisystem will be much more pronounced in low DHW loads than with high DHW loads.

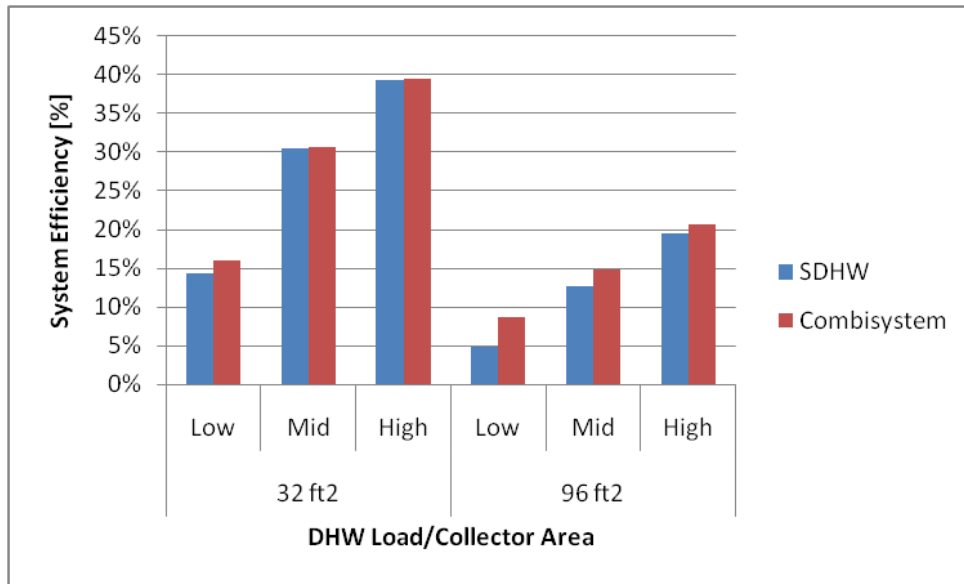


Figure 5.27: Impact of DHW loads on the system efficiency of combisystem and SWH for Phoenix benchmark house

5.5.3 Impact of House Type

Next, the impact of the house type on the energy performance of the system is analyzed for a couple of collector area sizes. The house type will have an impact on the energy performance of the system since the lower performance 1960 retrofit house will have a much higher heating load as compared to the IECC 2009 benchmark and Building America 50% house.

Figure 5.28 shows the impact of the house type on the absolute energy savings for both a combisystem and a SWH for the Denver climate with a 60 gallon per day DHW draw. As expected, the figure shows that the incremental savings from going from a SWH to a combisystem are more significant in the 1960 retrofit house than in the BA 50% house. Additionally, the incremental savings is more prominent in the 96 ft² than the 32 ft² system, since the larger system is collecting more solar energy, which the house can use to satisfy the space heating load.

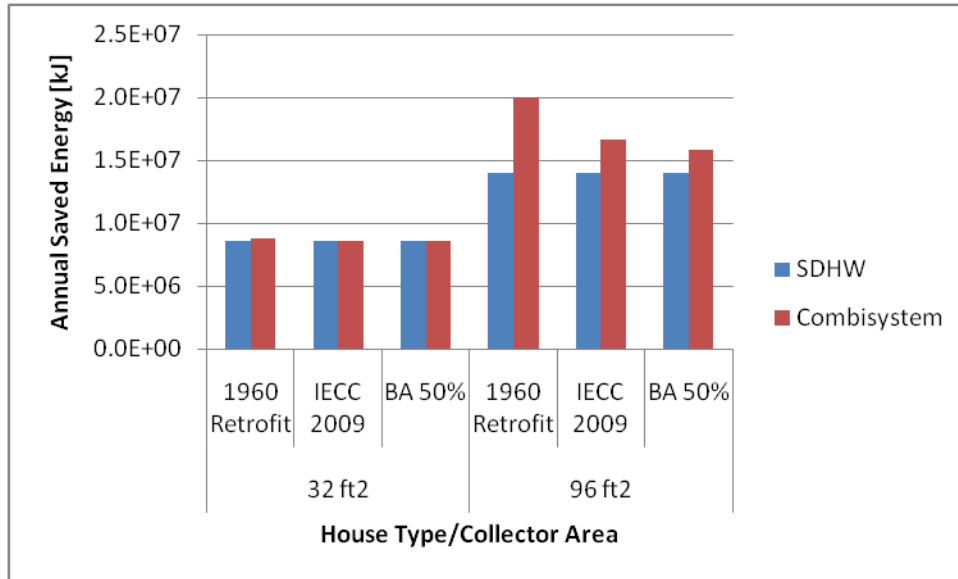


Figure 5.28: Impact of house type on the annual saved energy of the combisystem and SWH for Denver with 60 gallon per day DHW draws

Figure 5.29 shows the impact of the house type on the relative savings increase of the combisystem as compared to the SWH. As seen in the figure, for a 96 ft² system serving the space heating loads of a 1960 retrofit house, the combisystem will provide a 43% increase in energy savings as compared to the SWH. In comparison, the same sized combisystem will only provide 14% increased savings as compared to a SWH if installed on a Building America 50% house. In the 32 ft² sized systems, the collector area is too small to provide any significant incremental savings for the combisystem application as compared to the SWH because the 60 gallon DHW draw is utilizing most of the solar energy.

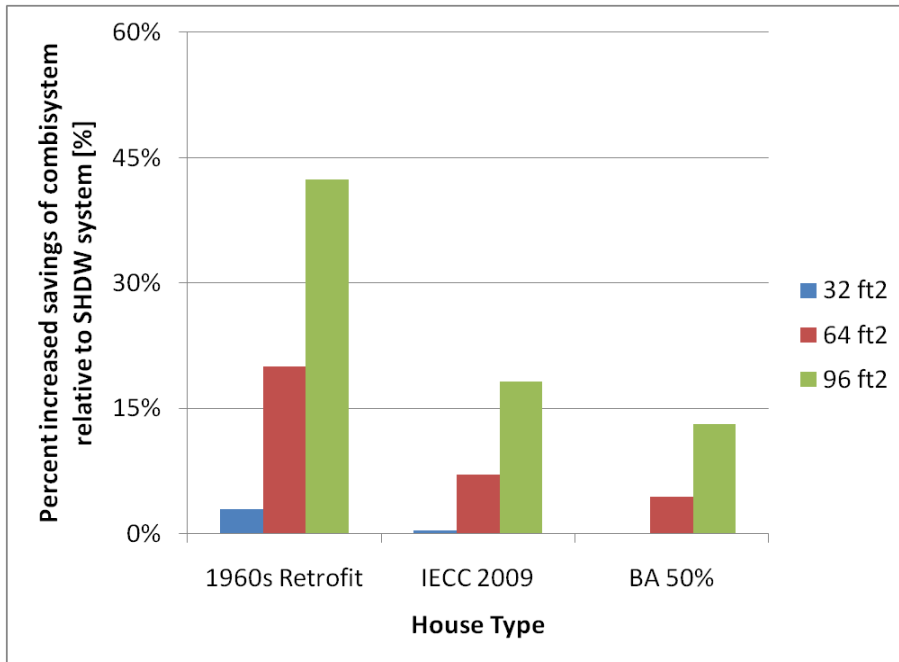


Figure 5.29: Impact of house type on the relative savings increase of the combisystem relative to the SWH for three collector area sizes (Denver/60 gallon draw)

The house type will also have a significant impact on the system efficiency between the two systems. Figure 5.30 shows that the impact of the house type on system efficiency will be much more prominent in the 96 ft² system than in the 32 ft² system. In the smaller systems, the combisystem paired with the 1960 retrofit house will boost the system efficiency by less than 2 percent as compared to the SWH, whereas the combisystem paired with a 50% house will provide no incremental system efficiency gain as compared to the SWH. In the larger collector areas, the combisystem will increase the system efficiency by 10 percent in the 1960 retrofit house and by 4 percent in the Building America 50% house as compared to the SWH.

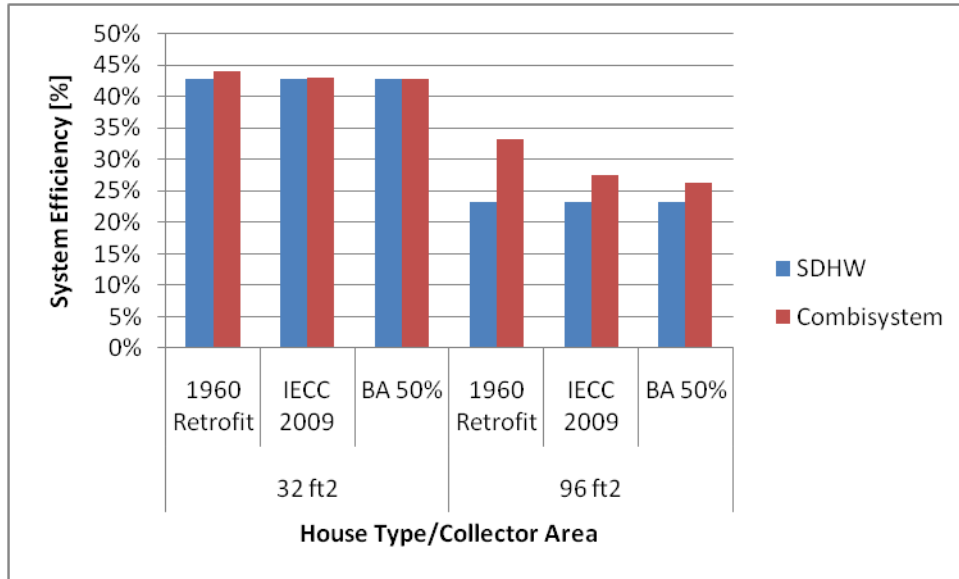


Figure 5.30: Impact of house type on the system efficiency of the combisystem and SWH for Denver with 60 gallon per day DHW draws

The impact of the house type is also examined in a Phoenix climate with a 60 gallon per day DHW load. Figure 5.31 reveals that the combisystem will provide only minimal incremental savings as compared the SWH for the 32 ft² systems regardless of the house type. For the 96 ft² system, the combisystem paired with the 1960 retrofit house will increase saving by 20% as compared to the SWH. When paired with a Building America 50% house, the combisystem will increase savings by only 9% as compared to the SWH.

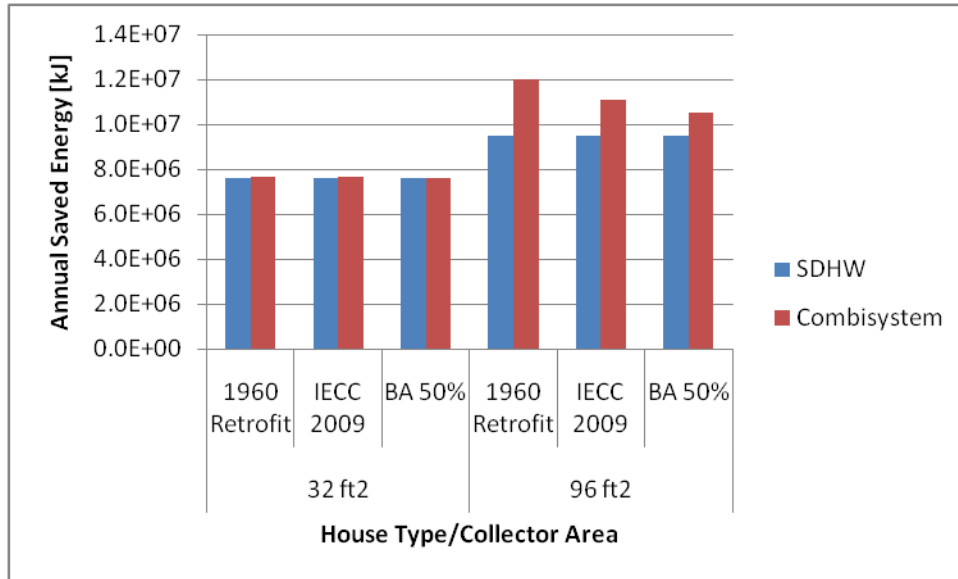


Figure 5.31: Impact of house type on the annual saved energy of the combisystem and SWH for Phoenix with 60 gallon per day DHW draws

Figure 5.32 shows the impact of the house type on the system efficiency for the Phoenix climate. Similarly to the Denver case, the impact of the house type on the system efficiency will be more prominent in the 96 ft² systems than in the 32 ft² systems. For the 32 ft² systems, the combisystem will provide less than 0.5% increased system efficiencies for all house types as compared to the SWH. For the 96 ft² systems, the combisystem paired with the 1960 retrofit house will provide an incremental increased system efficiency of 7% and when paired with a 50 percent house, the system will provide a 2% incremental increased system efficiency.

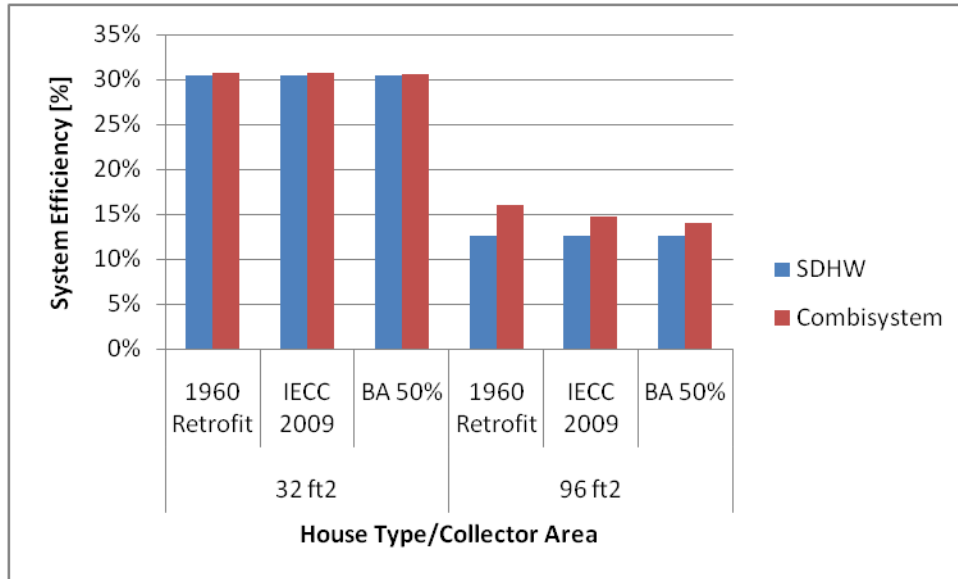


Figure 5.32: Impact of house type on the system efficiency of the combisystem and SWH for Phoenix with 60 gallon per day DHW draws

5.5.4 Impact of Climate

The impact of climate on the energy performance is examined to determine which climates provide the greatest additional energy saving benefit from the combisystem as compared to the SWH. To examine the impact of location, the house type and the DHW load were held constant and the energy saving were compared for all climates for the 32 ft² and 96 ft² system sizes.

Figure 5.33 shows the impact of climate for benchmark house types with 60 gallon per day DHW draws. As expected, for the 32 ft² size systems, the combisystem will provide little to no additional energy savings in all climates. This is due to the fact that the small collector size can only provide enough solar energy to supplement the 60 gallon per day DHW load. In contrast, for the 96 ft² size systems, the combisystem will provide additional savings in all climates, with the largest absolute incremental savings being in San Francisco and Denver.

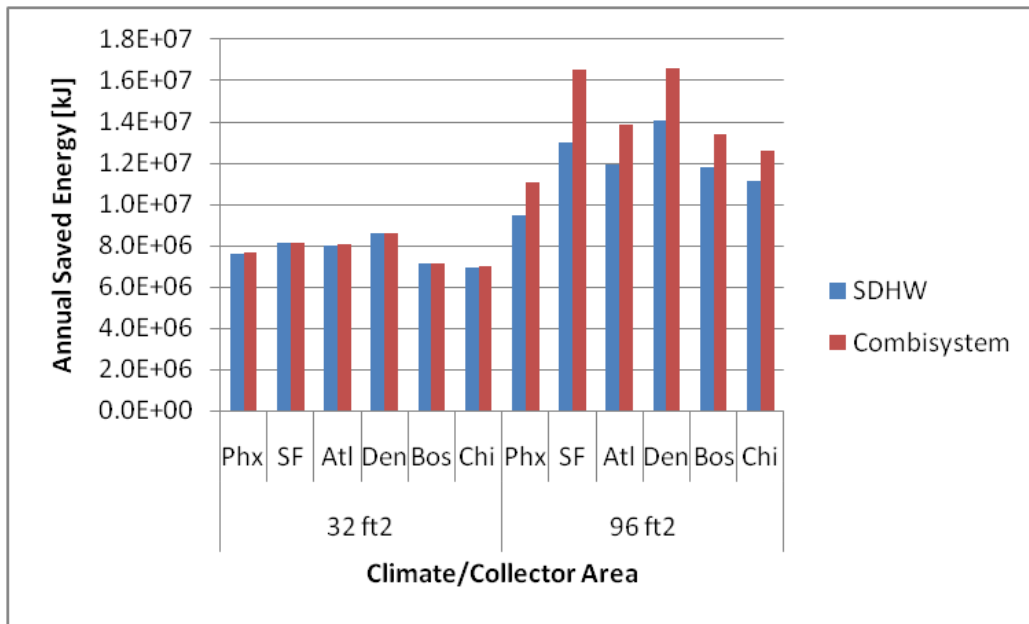


Figure 5.33: Impact of climate on annual saved energy for benchmark house and 60 gallon DHW draw

Figure 5.34 shows the impact of the location on the percent increased saving of the combisystem as compared to the SWH. At small collector sizes, the relative increased savings will be minimal in all climates, but in the 96ft² system size, the relative increase in savings will be significant in all climates, especially In San Francisco, where the combisystem yields an additional savings of 27% as compared to the SWH and in Denver, where the combisystem provides 18% increased savings as compared to the SWH. In the climates with worst solar resource, Boston and Chicago, the increased relative savings from the combisystem will be less than 15%.



Figure 5.34: Impact of climate on the relative savings increase of the combisystem relative to the SHW for three collector area sizes (Benchmark House/60 gallon draw)

Additionally, the impact of location on system efficiency is examined for all the climates in Figure 5.35. The figure shows that in 32 ft² systems, the combisystem will only provide marginal efficiency gains as compared to the SWH. The highest system efficiency for both a combisystem and a SWH in the 32 ft² system size category occurs in Denver. For the 96 ft² system sizes, the combisystems will provide significant increased incremental system efficiencies in all the climates, with the largest incremental increased efficiency occurring in San Francisco and Denver. The figure shows that systems in Phoenix will operate at the lowest system efficiency, which is due to the smaller loads which results in higher collector inlet temperatures and lower collector efficiencies.

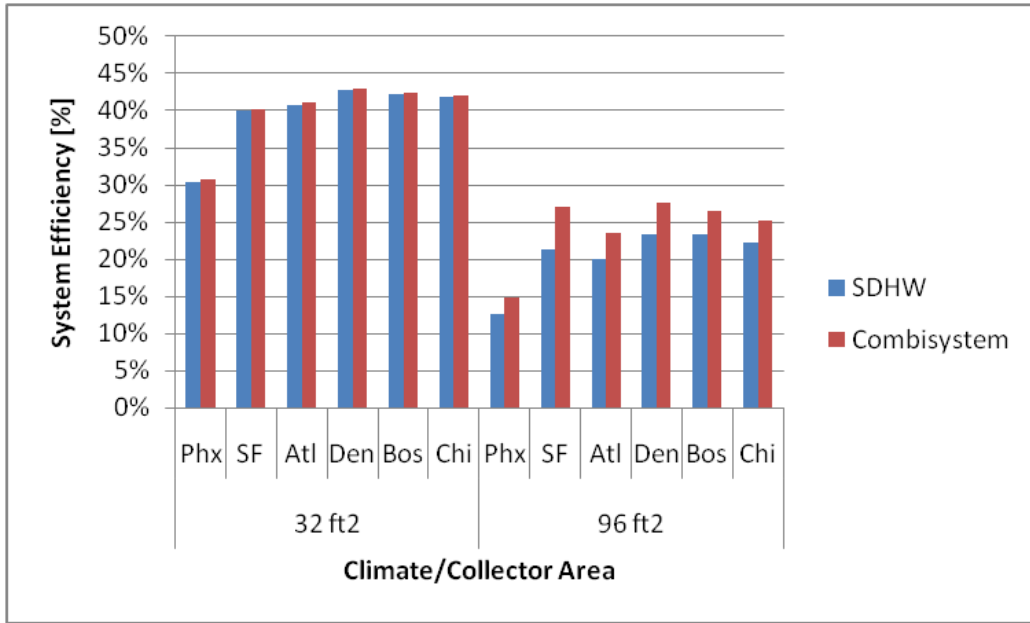


Figure 5.35: Impact of climate on system efficiency for benchmark house and 60 gallon DHW draw

In analyzing the impact that climate has on the performance of the combisystem as compared to a SWH, the annual incident radiation levels on the collectors for both the SWHs and combisystems were compared across all locations (see Figure 5.36). In this figure, annual incident radiation values are 4% to 7% higher for the SWH as compared to the combisystem because the SWH collectors are tilted at latitude, which is optimal in terms of annual incident radiation, whereas the combisystem collectors are tilted at latitude plus 15° in order to capture more solar radiation during the winter months.



Figure 5.36: Annual specific incident radiation levels on collectors for SWH and Combi system in all the

Figure 5.36 shows that the incident radiation levels in Phoenix are 18 to 38 percent higher than the incident radiation levels in the other cities. However, even with the high incident radiation levels, the relative savings from the combisystem in Phoenix are lower than other cities with lower incident radiation levels. This is due to the relatively low space heating loads in Phoenix in comparison to the other locations (see Figure 5.37 for a comparison of space heating loads in the Benchmark in all locations). Also, as seen in Figure 5.36, the locations with the lowest annual incident radiation levels are Boston and Chicago. Incidentally, these cities also have the highest space heating loads, which might suggest that incremental savings from the combisystem could be relatively large in comparison to locations with lower space heating loads. However, the lower annual incident radiation levels results in the savings in these locations being smaller than other cities with higher annual solar radiation levels. In San Francisco and Denver, both of which have comparable annual incident solar radiation, the combination of their significant space heating loads with moderately high solar radiation results in higher relative increased savings from the combisystem.

Figure 5.37 shows the annual space heating loads for the IECC 2009 benchmark house for all the locations. Phoenix has relatively low annual space heating loads and both Boston and Chicago have relatively high space heating loads.

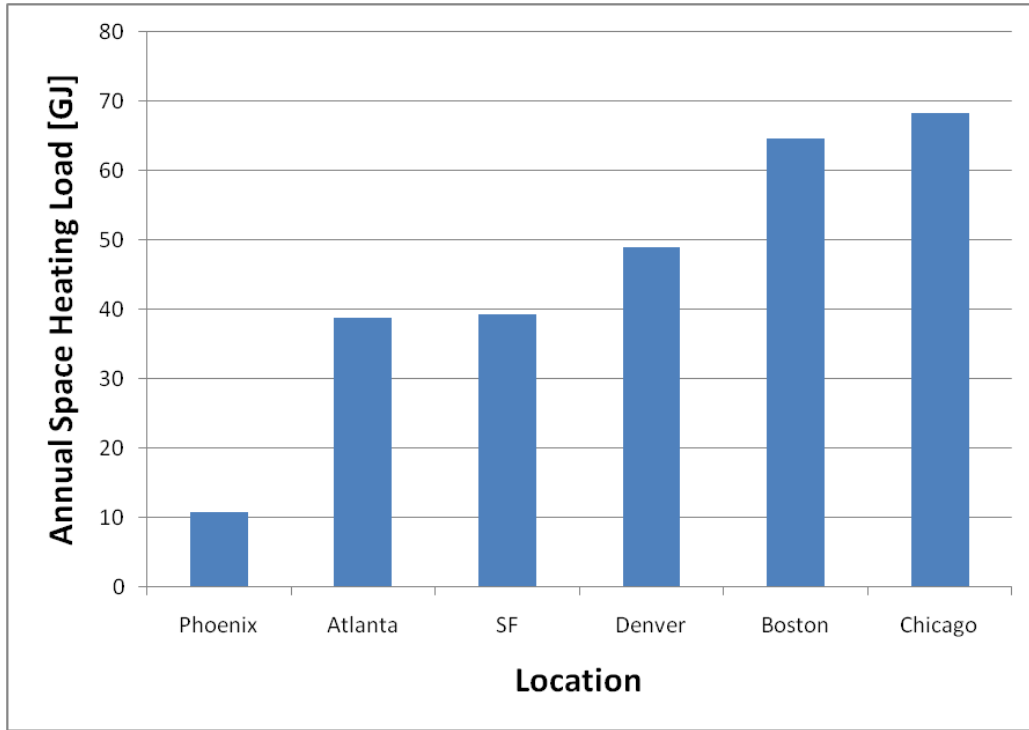


Figure 5.37: Annual space heat loads for benchmark IECC 2009 house in all the locations

When analyzing the impact that location has on the performance of the combisystem relative to the SWH, it was revealed a combisystem in San Francisco will provide larger relative incremental savings (reference Figure 5.34) as well as larger absolute incremental savings (reference Figure 5.33) as compared to Denver. At first glance, since Denver and San Francisco have comparable annual incident radiation levels and Denver has larger space heating loads, a combisystem in Denver would be expected to provide larger incremental savings than a combisystem in San Francisco. However, a combisystem in San Francisco yielded larger absolute savings and relative savings for 64 ft² and 96ft² systems as compared to a combisystem in Denver.

In examining this phenomenon, the monthly incremental savings, space heating loads, and incident radiation levels were compared between San Francisco and Denver. First, monthly heating loads are examined for both San Francisco and Denver for a benchmark house (see Figure 5.38). The comparison of monthly heat loads reveals that although Denver has larger heating loads during the winter months, San Francisco has heating loads year round and in particular, during the late Spring and Summer, which provides more opportunity year round for the combisystem to supplement the space heating loads with solar energy.

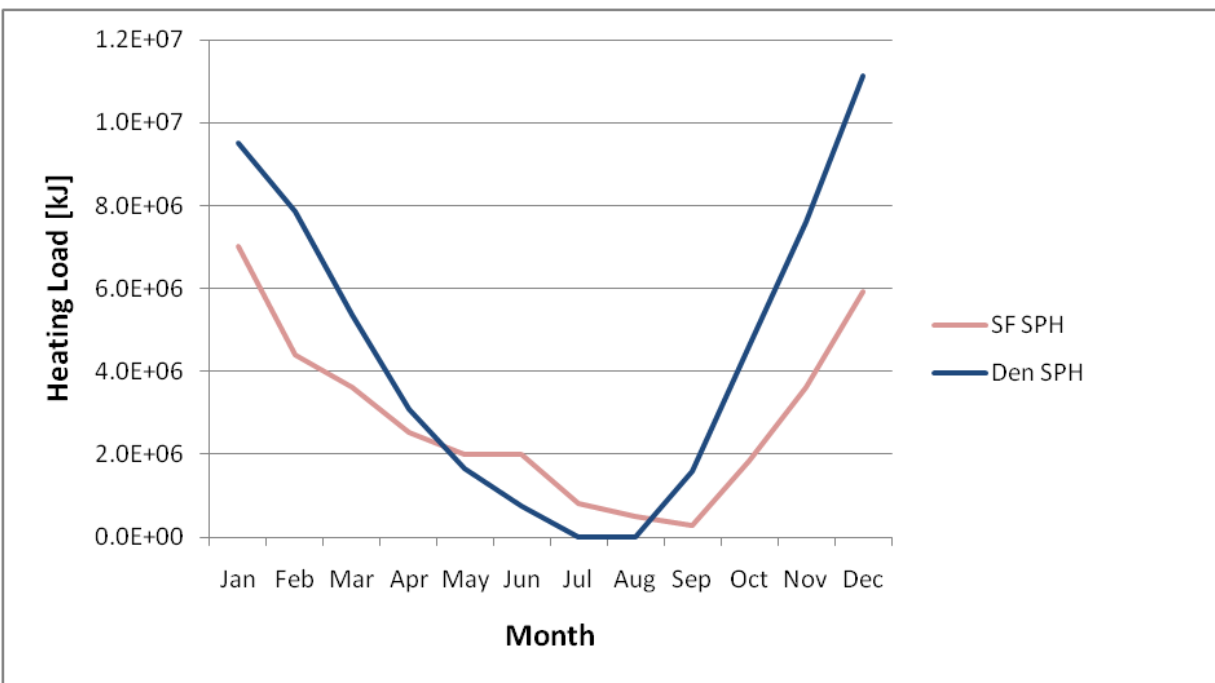


Figure 5.38: Monthly Heating Load between San Francisco and Denver

Next, the monthly incident radiation levels for both the SWH and combisystem were plotted for both Denver and San Francisco (see Figure 5.39). The figure shows that Denver has about 20% higher incident radiation levels during the winter months, but San Francisco has higher incident radiation levels during the period between late Spring and early Fall. In fact, during the late Spring to early Fall period,

when San Francisco still has some space heating loads, the monthly incident radiation is up to 13% higher in San Francisco as compared to Denver.

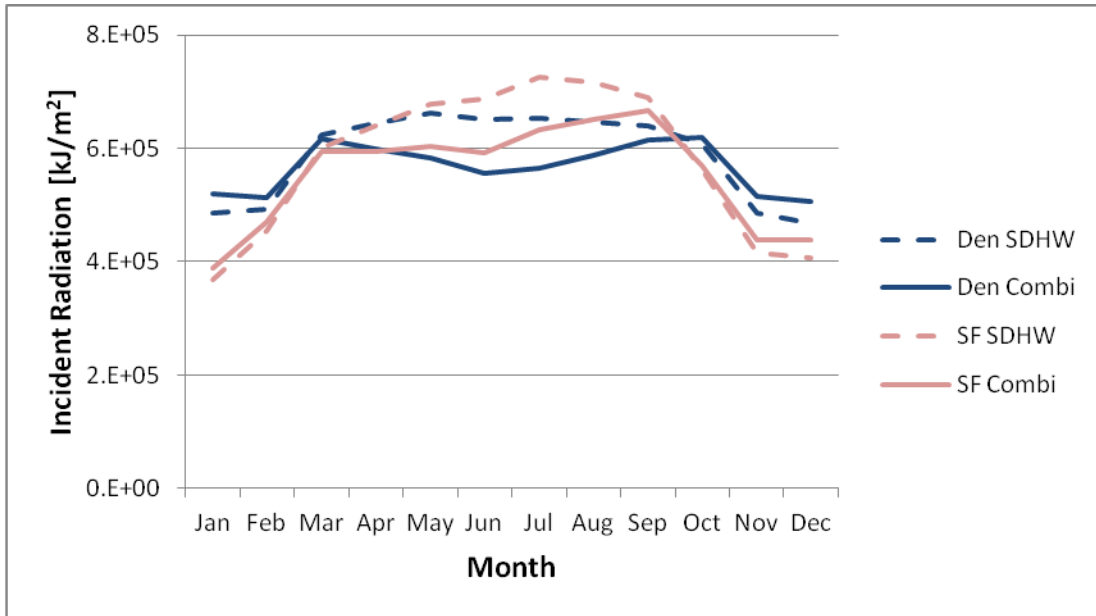


Figure 5.39: Monthly incident radiation for combisystem and SWH in San Francisco and Denver

Lastly, the monthly incremental savings provided by the combisystem relative to the SWH for Denver and San Francisco are compared in Figure 5.40. The monthly incremental savings figure shows that San Francisco has much larger incremental savings in April through August as compared to Denver. This is due to the higher space heating loads and the higher incident radiation during these months. Additionally, the incremental savings are more constant throughout the year in San Francisco as compared to Denver, which has significantly larger incremental savings in Spring and Fall as compared to the Winter.

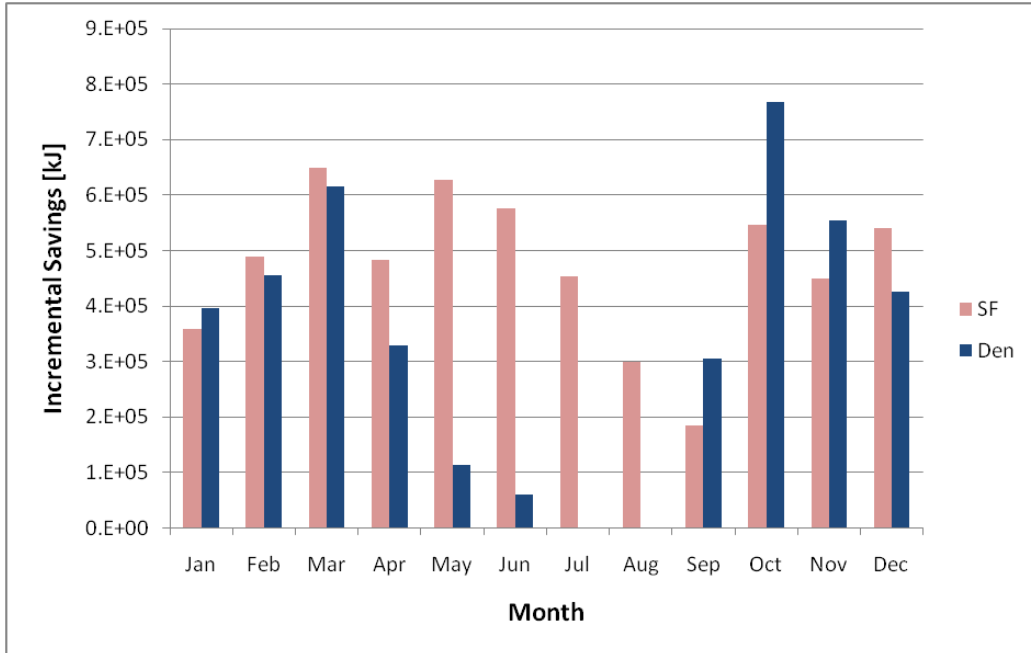


Figure 5.40: Monthly incremental savings of combisystem versus SWH for San Francisco and Denver (96 ft², 60 gallon draw)

Next, the incremental savings are evaluated in both low load and high load homes. For the low load home evaluation, the DHW draw is set at 20 gallons per day and the house type is a BA 50% house. The relative increase in savings, as shown in Figure 5.41, shows that the incremental savings will be largest in San Francisco and Denver and lowest in Phoenix, Boston, and Chicago. This analysis shows that even with a high performance house, a low DHW load will yield significant savings in locations with moderately high space heating loads and a relatively good solar resource.



Figure 5.41: Impact of climate on the relative increase in savings from the combisystem as compared to a SHDW for a low load house (20 gallon draw/BA 50% House)

For the high load home evaluation, the DHW draw is set at 100 gallon per day and the house type is the 1960s retrofit house (see Figure 5.42). This figure reveals that the largest incremental savings occur in Denver and unlike previous figures that show the impact of climate on the increase in savings, the relative savings in Boston and Chicago are larger than the relative savings in San Francisco for the 96 ft² system.

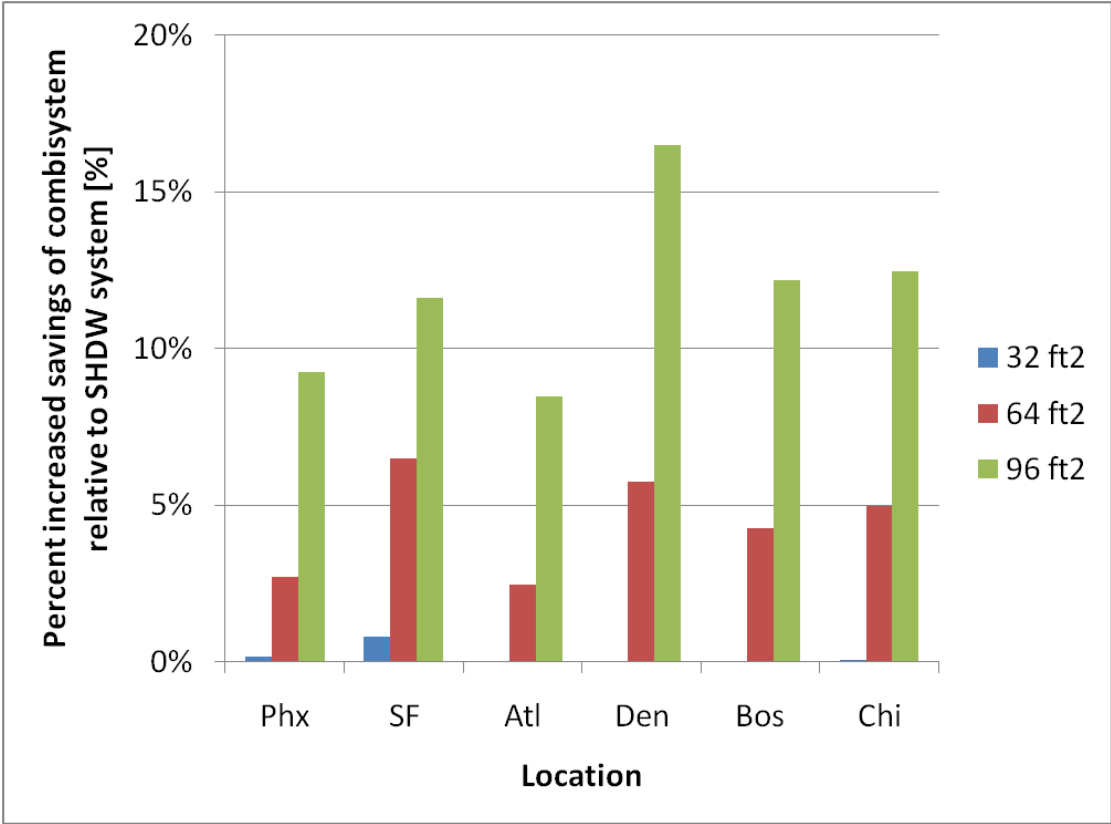


Figure 5.42: Impact of climate on the relative increase in savings from the combisystem as compared to a SWH for a high load house (100 gallon draw/1960s Retrofit House)

Additionally, since the analysis of the impact of the DHW load and the house type revealed that low DHW loads and high space heating loads result in the largest incremental savings from the combisystem, the increase in savings was compared across all locations for a load scenario with a 20 gallon draw and a 1960s retrofit house. Figure 5.43 shows that incremental savings will be fairly significant in all climates in all three system sizes. In particular, in San Francisco and Denver, the combisystem will provide twice the savings for a 64 ft² system and three times the savings for a 96 ft², relative to a SWH.

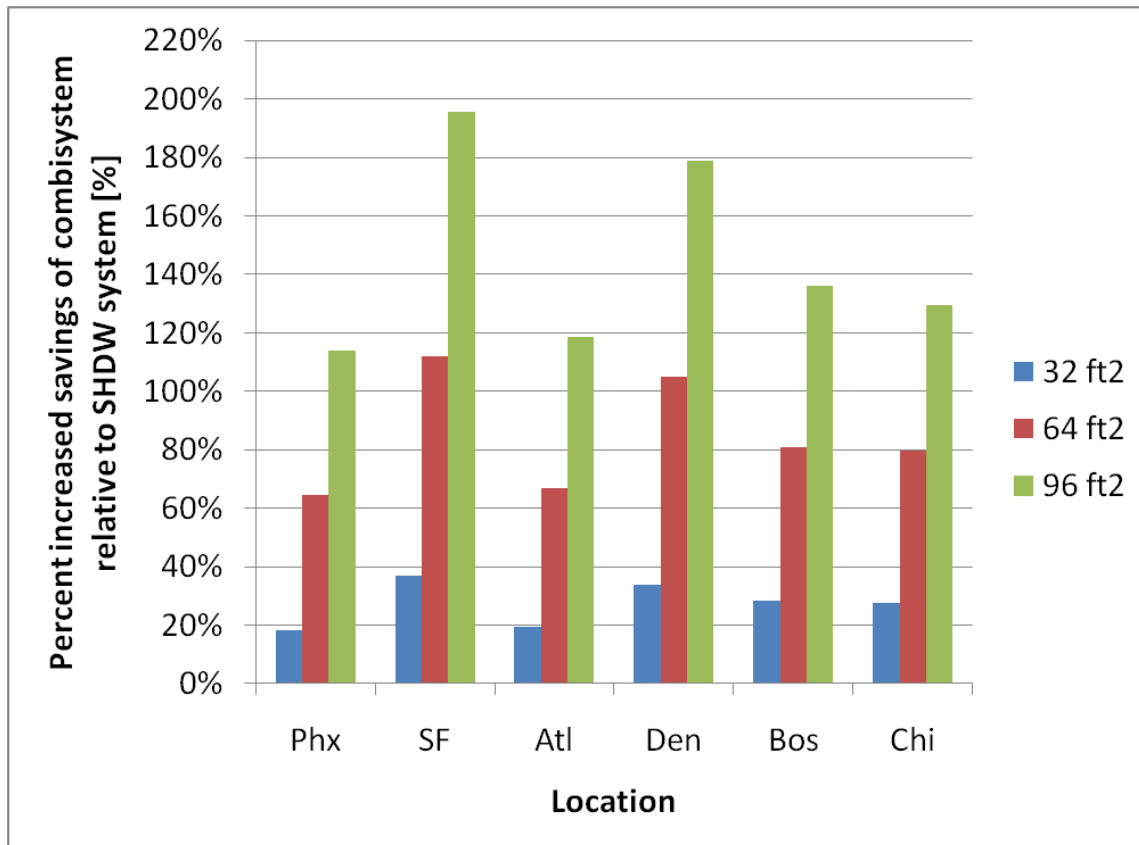


Figure 5.43: Impact of climate on the relative increase in savings from a combisystem as compared to a SHDW for a house with high space heating and low DHW loads.

Next, in order to bound the analysis in terms of best case scenarios and worst case scenarios for incremental savings from combisystems, the increased savings was evaluated for a house with low space heating loads and high DHW loads. Figure 5.44 shows that the incremental savings will be minor in all climates for all system sizes.

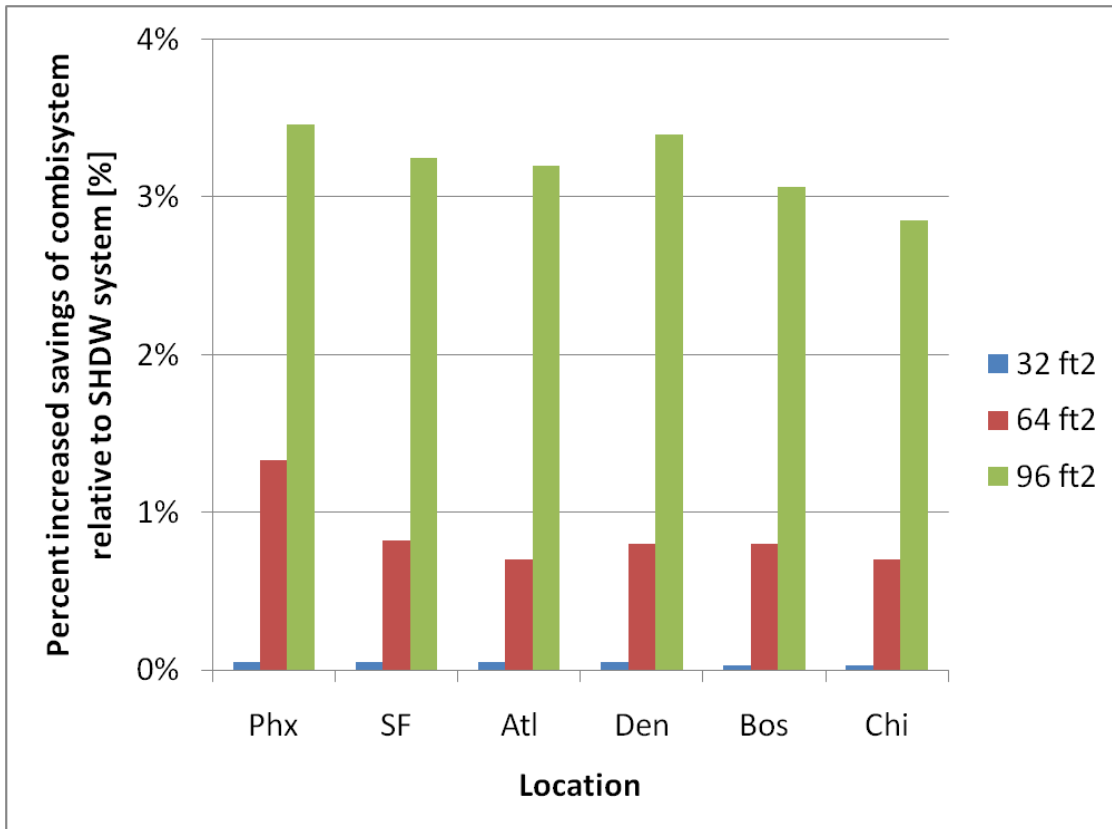


Figure 5.44: Impact of climate on the relative increase in savings for a house with low space heating loads and high DHW loads

5.5.5 Impact of Collector Slope

The dependency of the annual energy savings on the collector tilt angle is shown in Figure 5.45. In all of the previous simulation results, in an effort to maximize savings from the system, the collector tilt was set at the location’s respective latitude for the SWH, which is optimal for systems with relatively flat loads year round, and at the location’s respective latitude plus 15° for the combisystem, which is thought of as optimal for systems that serve higher loads during the winter months [56].

To show the effects of collector tilt on the annual performance on these systems, Figure 5.45 shows the impact of 5 collector tilt angles on the annual energy saving for both systems with all three DHW loads for a Denver benchmark house with a 64 ft² sized system. For Denver, since the latitude is

40°, the tilt angle in increments of 15° with tilts between 25° and 85° were studied. This parametric study confirms that the optimal collector tilt angle for maximum energy savings for a SWH is latitude (independent of DHW load) , and the optimal collector tilt angle for maximum energy savings for the combisystem is latitude plus 15° (independent of DHW load). Additionally, this parametric study shows that for tilt angles between 25° and 70°, the impact on the annual energy savings for both systems will be 6% or less in comparison to the maximum energy savings. For tilt angles of 85°, a tilt angle that is not at all practical in residential roof applications because it's essentially perpendicular to the ground, the savings in comparison to the maximum savings drops by 20% or more for both systems and all three DHW loads.

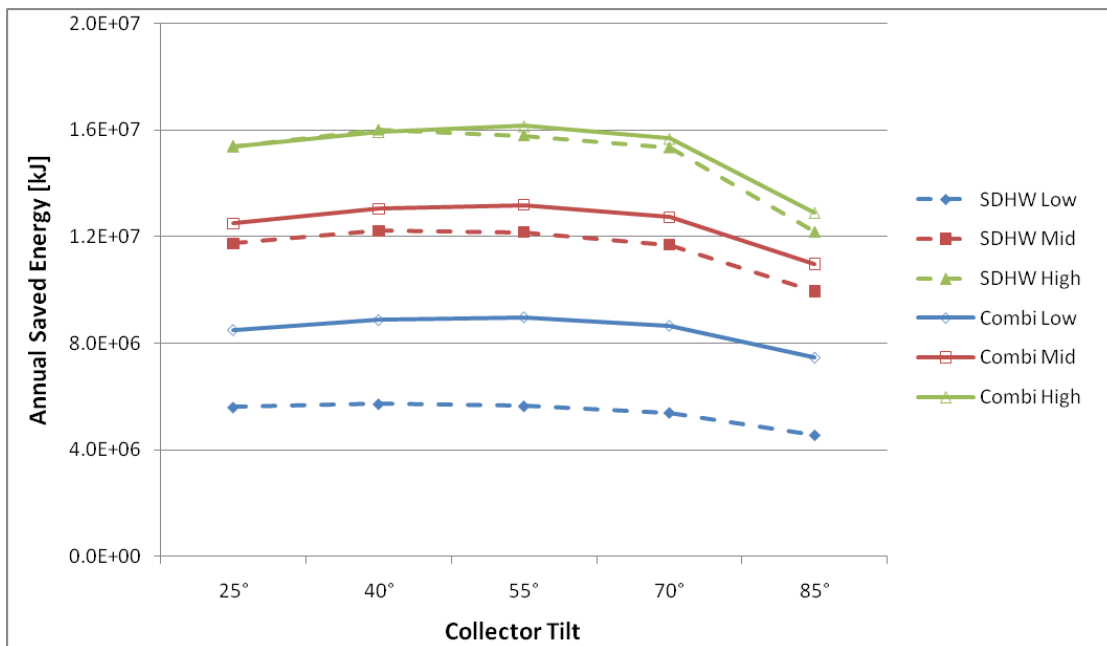


Figure 5.45: Impact of collector tilt on annual saved energy for both systems and the three DHW loads for Denver benchmark house with 64 ft² collector area.

Next, the monthly energy savings are analyzed for three collector tilts for a combisystem in a Denver benchmark house application with a 60 gallon draw (see Figure 5.46). The figure clearly shows that both the 25° and 55° tilt angle, the overall annual savings will be fairly similar, although savings in

the winter with the 55° tilt angle will be slightly higher. For the 85° tilt angle, the savings will be high the in winter, but significantly lower in the summer months.

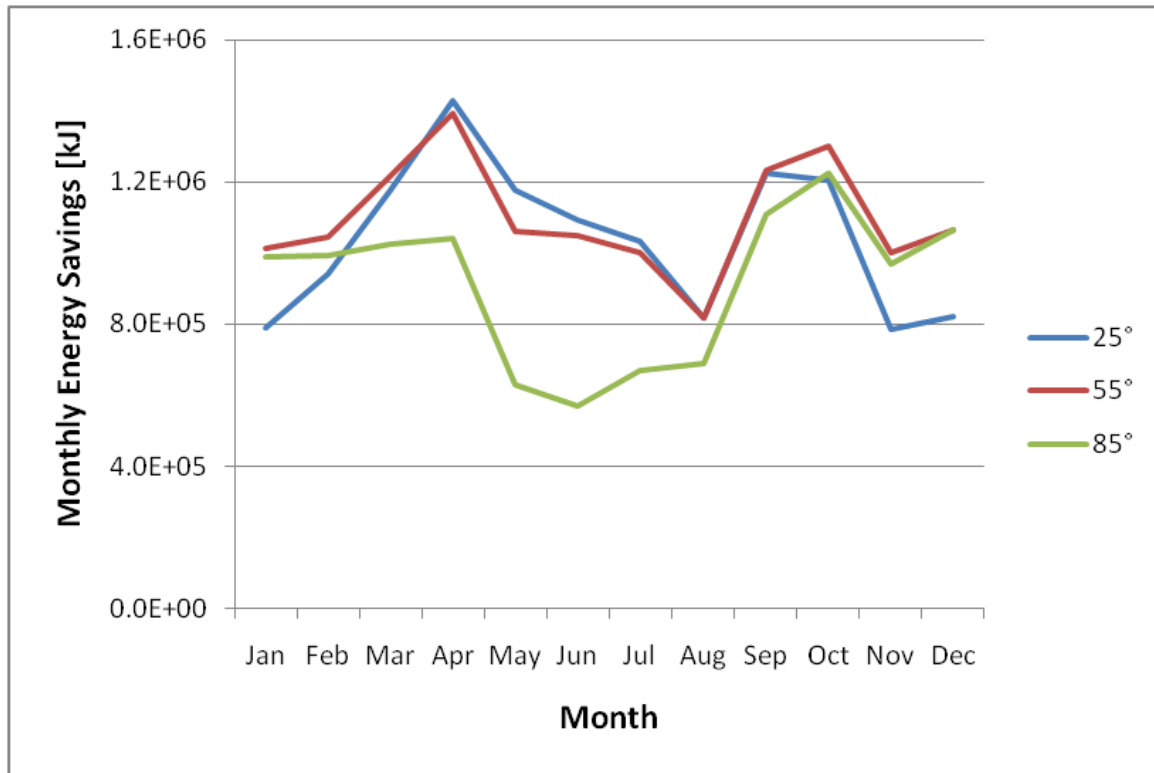


Figure 5.46: Monthly energy savings for combisystem for three tilt angles in Denver (Benchmark, 60 gallon draw)

5.6 Economic Analysis

An economic analysis was conducted to determine the cost-effectiveness of a combisystem relative to the cost-effectiveness of a SWH. In each climate, the economic calculations are performed as a function of system size, the DHW and space heating loads, and type of fuel (electric versus natural gas). For the natural gas system, an efficiency of 82% is applied to determine the auxiliary energy consumed by a constant efficiency natural gas boiler.

Additionally, the economics of the two systems are compared to the economics of a system without any solar thermal. For the reference non-solar system, it is assumed that the electric system costs

\$400 for the water heater and \$2,000 for the electric tankless boiler in the radiant floor space heating system. For the natural gas reference system, it is assumed that the water heater costs \$800 and the natural boiler costs \$3000. For the solar thermal system costs, in addition to the cost of the solar thermal system, which includes the cost of the collectors, tank, controls, and installation, it is assumed that the same reference system costs apply due to the fact that the solar thermal system is not able to provide enough heat to meet all the heating loads throughout the year.

For calculating the life-cycle costs and net present worth values for the systems, the 2010 Energy Information Administration (EIA) state average rates for this analysis were used as shown in Table 5.2 [64].

Table 5.2: 2010 State Average Residential Utility Rates (EIA) [64]

Location	Electricity (\$/kWh)	Natural Gas (\$/therm)
Phoenix, AZ	\$0.097	\$1.54
San Francisco, CA	\$0.152	\$0.92
Atlanta, GA	\$0.093	\$1.77
Denver, CO	\$0.104	\$0.79
Boston, MA	\$0.153	\$1.45
Chicago, IL	\$0.102	\$0.91

For determining the economic metrics, a discount rate is applied, which discounts the saved energy and auxiliary energy usage based on an assumed system lifespan, inflation rate, and interest rate. The uniform series present worth (USPW) represents the number of years that the uniform annual energy savings will occur (see Table 5.3 for the economic assumptions)

Table 5.3: Economics Assumptions for determining the discount rate

Life (N)	30 years
Inflation Rate (λ)	3 %
Interest Rate (i)	5.5 %
Discount Rate (r_d)	2.4 %
USPW	21.1 years

In Table 5.3, the discount rate, r_d , is calculated as:

$$r_d = \frac{i - \lambda}{1 + \lambda} \quad 5.9$$

The USPW, which takes into account the calculated discount rate is determined as:

$$USPW(d, N) = \frac{1 - (1 + r_d)^{-N}}{r_d} \quad 5.10$$

Where N equals the lifespan of the system. For this study, the lifespan of the system is assumed to be 30 years.

5.6.1 Economic Metrics

Three primary economic metrics were calculated as part of this study. The first metric calculated is the lifecycle cost. The lifecycle cost takes into account the present day cost, which includes the installed cost, the annual operations and maintenance costs, the annual auxiliary energy usage, the cost of energy, and the USPW. This metric was used to compare the lifecycle cost of the solar thermal systems to the lifecycle cost of the reference system. The life cycle cost is calculated as:

$$LCC = IC + \left[\left(O\&M_{annual} + (Q_{aux,annual} * COE) \right) * USPW \right] \quad 5.11$$

Where IC represents the initial capital cost of the system $O\&M_{annual}$ represents the annual operation and maintenance cost, and COE is the cost of energy.

Next the net present worth was calculated using the installed cost, the annual operation and maintenance costs, annual saved energy relative to the reference system, the cost of energy, and the $USPW$. A net present worth can also be determined by taking the difference of the reference system's lifecycle cost and the solar thermal system's lifecycle cost. A positive NPW values represents a system that is cost-effective in comparison to the reference system. The net present worth is calculated as:

$$NPW = -IC + [(-O\&M_{annual} + (Q_{saved} * COE)) * USPW] \quad 5.12$$

As an add-on to the NPW calculation, the breakeven cost is calculated by iteratively changing the initial cost of the solar system until the net present worth equals zero. The breakeven cost is equivalent to the system's present day installed cost where the energy saving costs with the solar thermal system is equivalent to the energy costs of the reference system over the system's lifespan. Breakeven costs can be used to find the installed system cost (\$/system) required, for a given price of fuel (cents/kWh) and a given $O\&M$ cost, in order for a system to become cost-effective using discounted energy cost savings. A system that is cost-effective using the breakeven cost method is when its installed cost is below the breakeven installed cost.

Additionally, incremental breakeven costs for the combisystem relative to the SWH breakeven cost was determined by taking the difference of the combisystem's breakeven cost and the SWH 's breakeven cost. This metric was used to determine the maximum incremental cost of the combisystem, relative to the SWH cost, for the combisystem to be cost competitive with the SWH . Since the energy performance and economics for the SWH were only evaluated for the 32 ft² through 96 ft² collector area

range, the incremental breakeven costs for the combisystem were only determined for the 32 ft² through 96 ft² sizes.

Lastly, the levelized cost of energy (LCOE) represents the cost of generating energy for a particular system. In this study, the LCOE is represented as cost per kWh for the electric systems and is represented as cost per therm for the system with a natural gas boiler. The LCOE is also equivalent to the utility cost of energy required for a system to have a net present worth of zero. To determine the cost-effectiveness of the solar thermal system relative to the reference system, the LCOE can be compared to the utility cost of auxiliary energy. If the LCOE is lower than the utility cost of energy, then the system yields a positive net present worth over its lifetime. The LCOE is calculated as:

$$LCOE = \frac{(IC + O\&M_{lifespan})}{Q_{saved} * USPW} \quad 5.13$$

Where the energy savings are converted to kilowatt-hours when determining the LCOE for electric systems and are converted to therms when determining the LCOE for natural gas systems.

5.6.2 System Costs

For determining the net present worth and lifecycle costs of these systems, installed costs of both the SWH and combisystem were estimated based on acquired installed cost data. These installed system costs were converted to cost per collector area and a best-fit 2nd order polynomial regression was created based on the cost per square foot data based on the best possible R² value.

The cost per square foot of collector area for the SWH is based on the cost data collected as part of the California Solar Initiative residential solar water heater installations [61]. This data provided installed system costs for collector areas that ranged from 27 ft² to 82 ft². Based on this data, the linear regression was created which provided an R² value of 0.72 (see Figure 5.47).

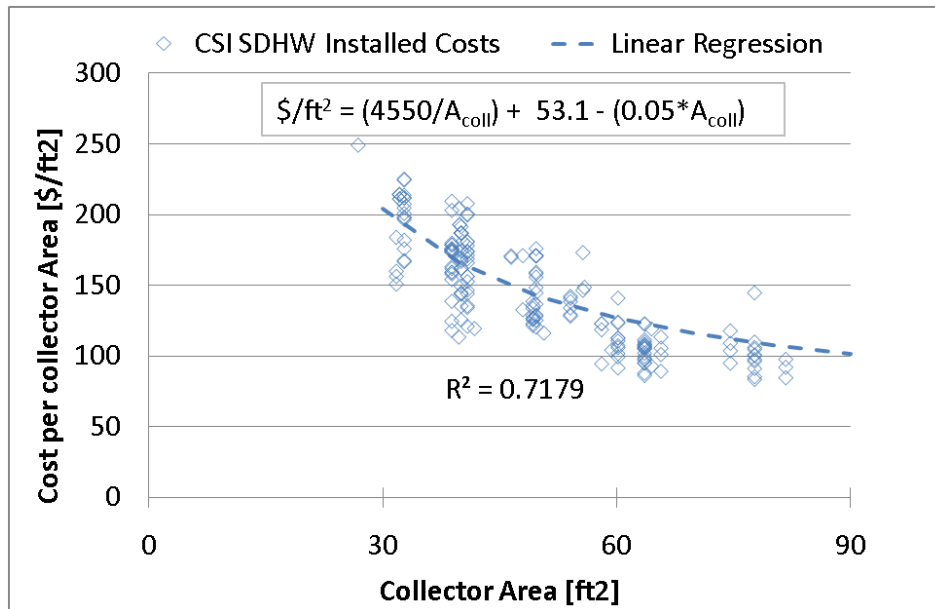


Figure 5.47: Cost per collector area for SWH using data from the California Solar Initiative solar thermal program

Figure 5.48 shows the installed costs regression used for the economics of the SWHs in the 32 ft² through 96 ft². Since the installed costs data only provided system costs for systems up to 82 ft², the regression was extrapolated for systems sizes up to 96 ft².

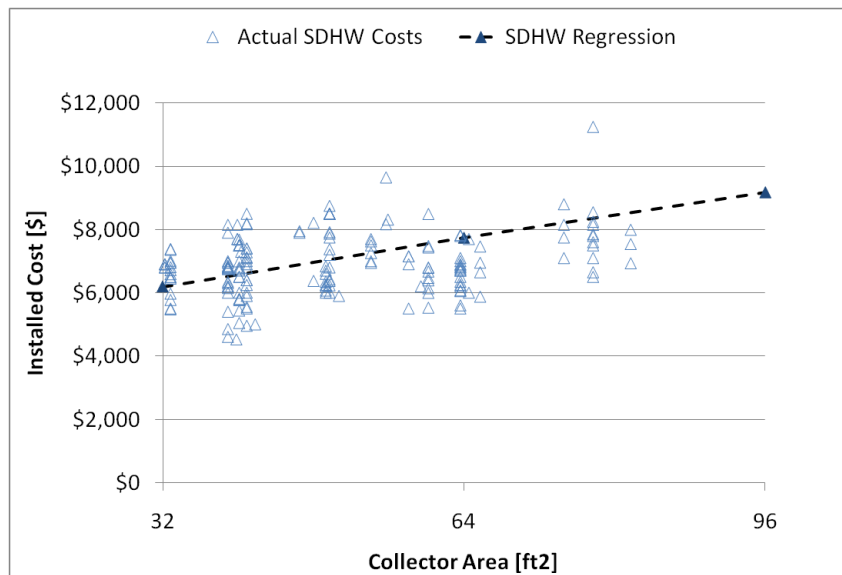


Figure 5.48: Installed cost regression for the SWH based on actual cost data.

For the combisystem estimated installed costs, the 2nd order polynomial best-fit regression was created based on European system costs as provided by the IEA research [7]. These system costs were converted from Euros to U.S. Dollars (USD) based on the exchange rate of 1.43 USD per 1 Euro. Based on this data, the linear regression was created which provided an R² value of 0.67 (see Figure 5.49).

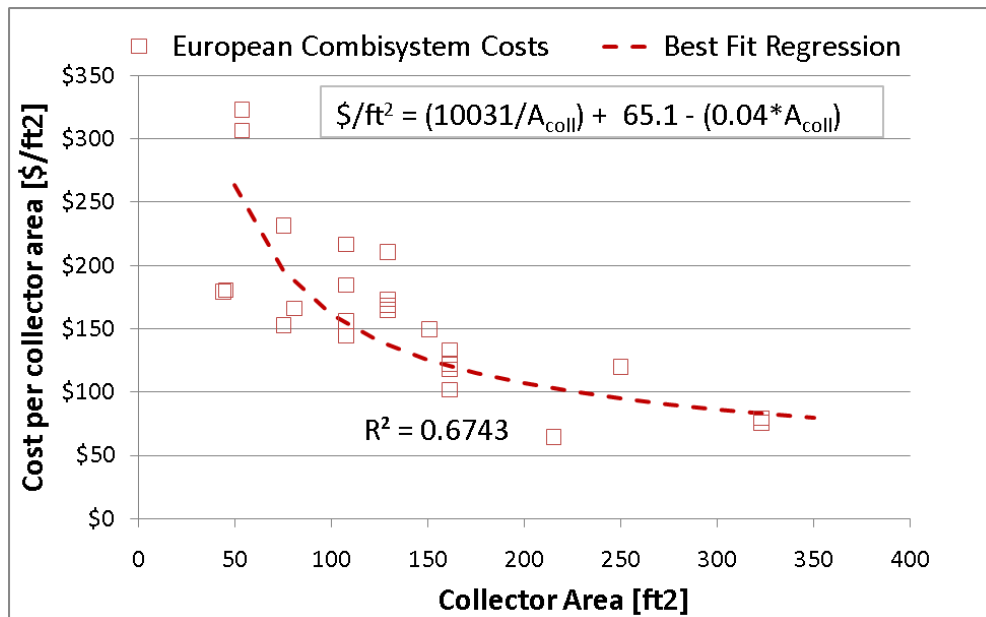


Figure 5.49: Cost per collector area for combisystem using data from Weiss [7]

Along with the European cost best-fit regression, which shows that systems will cost \$25,000 as the system size approaches 300 ft² (see Figure 5.50), another combisystem cost regression was developed, which is based on the SWH data. This other regression assumes the combisystem cost regression has the same slope as the SWH cost regression, but the combisystem will have a fixed incremental cost relative to the SWH cost, which accounts for the extra costs that go into the combisystem design and implementation. For this cost regression, it is estimated that the incremental cost will be \$1,000 (\$300 for the extra heat exchanger, \$100 for the combisystem controller, \$600 for the extra installation and design).

Additionally, since system sizes go up to 288 ft² in this study, it is assumed that the SWH cost data can be extrapolated for these larger system sizes. As seen in Figure 5.50, the estimated system cost for a 300 ft² system using the fixed incremental cost regression is about one-third the cost as based on the European data. In this study, since no U.S. combisystem cost data was acquired, both the European best fit regression and the fixed incremental cost regression were used in order to create low and high bounds on the installed cost.

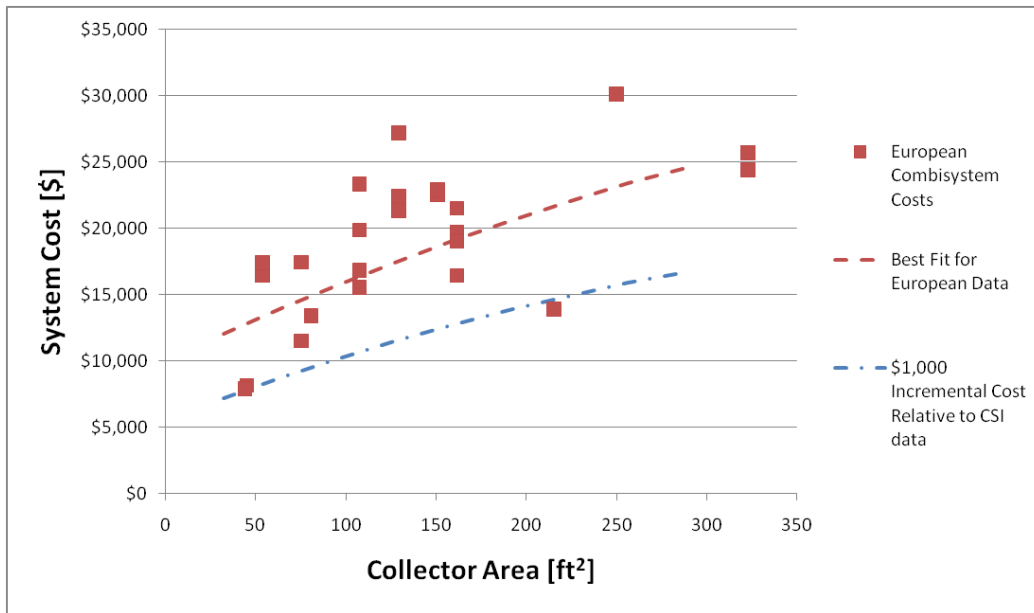


Figure 5.50: System costs based on the European system cost data and a \$1,000 incremental cost relative to the SWH cost.

5.6.3 Comparing Economics of Combisystem and SWH

Using the metrics described in section 5.6.1, the economics of the combisystem and SWH are compared. The following figures in this section show the economics of the combisystem and SWH with varying system sizes for a Denver Benchmark House with electric auxiliary heaters. In these cases, the \$1,000 incremental cost regression for the combisystem is used based on the premise that if the

combisystems are not cost-effective using the fixed incremental cost regression, then they certainly will not be cost-competitive using the European cost regression.

Figure 5.51 shows the lifecycle costs of both the SWH and Combisystem as a function of collector area system size and DHW load (low, mid, and high). In general, for a low DHW load, a smaller system will be more cost effective than a larger system because increased marginal system cost with respect to collector area does not justify the marginal additional savings. For high DHW loads, since there is more opportunity to save energy, the additional marginal savings with respect to increased collector area do justify the increased cost of the system, and therefore lifecycle costs decrease as a function of system size.

For the SWHs, the 32 ft² system with low and medium DHW loads will provide the lowest lifecycle cost. For the high DHW load scenario, the 64 ft² system will provide the lowest lifecycle cost. For the combisystem with low DHW loads, the 32 ft² system will yield the lowest lifecycle cost, but for high DHW loads, the largest combisystem will yield the lowest lifecycle cost. For the combisystem with the medium DHW load, the lifecycle cost appears to be independent of the system size. This is due to the marginal cost savings and marginal system cost being equal as a function of increased collector area.

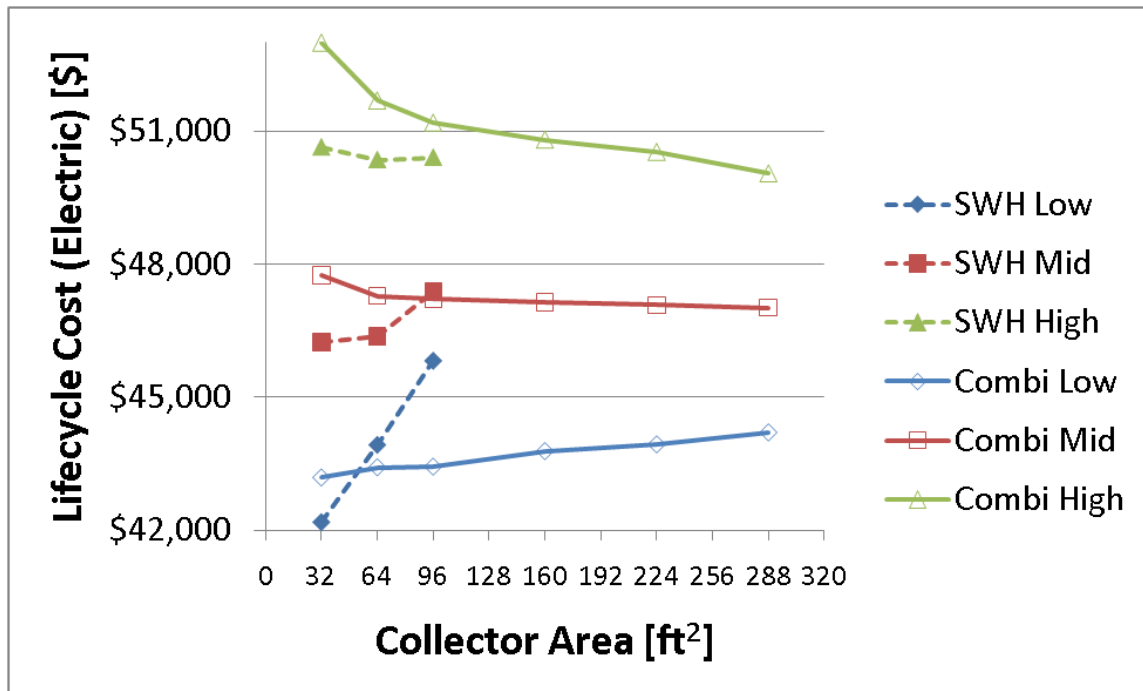


Figure 5.51: Lifecycle costs of the SWH and the combisystem as a function of collector area and DHW load (Denver Benchmark House)

Next, the net present worth of both the SWH and combisystem as a function of collector area system size and DHW load are compared (see Figure 5.52). The figure shows that all the systems yield a negative net present worth, which means that the lifecycle cost for the reference system is lower than the lifecycle cost of the solar thermal systems. In general, the higher DHW load will yield a higher net present worth, since there is more opportunity for savings with higher DHW loads. Additionally, for low DHW loads, the smallest system will yield best economics. In comparing the economics of combisystems and SWH, low DHW loads will allow combisystems to be more cost-effective than SWHs in 64 ft² and 96 ft² system size range.

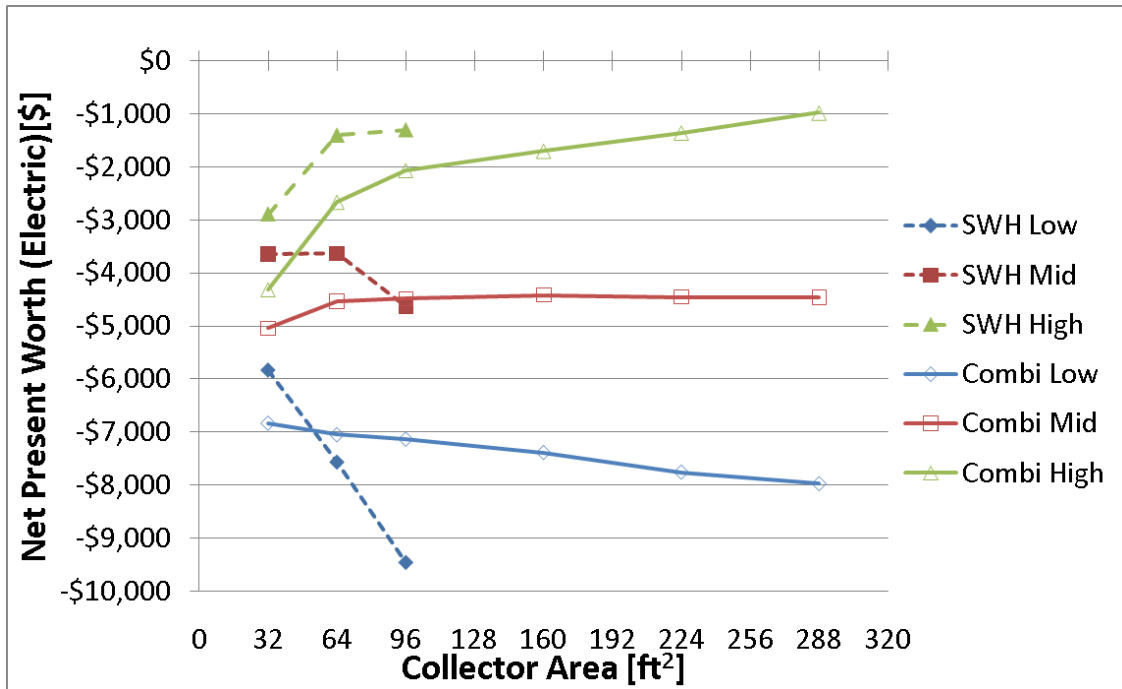


Figure 5.52: Net Present Worth of the SWH and the combisystem as a function of collector area and DHW load (Denver Benchmark House)

Figure 5.53 shows the breakeven costs for the SWH and combisystems as a function of collector area and DHW load. As a reminder, the breakeven cost is the installed costs required for the system to be cost-competitive with the reference system. For comparative reasons, the figure also shows the installed costs used to determine the lifecycle cost and net present worth of these systems. The figure shows that all the breakeven costs fall below the installed costs for all system sizes, which means that none of these systems are cost-effective relative to the reference system. Additionally, the figure shows that high DHW loads increase the breakeven cost for both the combisystem and SWH because the system savings are larger with high DHW loads as compared to low DHW loads. In comparing the breakeven cost between the combisystem and SWH for high DHW loads, the incremental breakeven cost for the combisystem relative to the SWH is small, which means that the incremental cost of the combisystem will need to be minor if it is to be cost-competitive with the SWH.

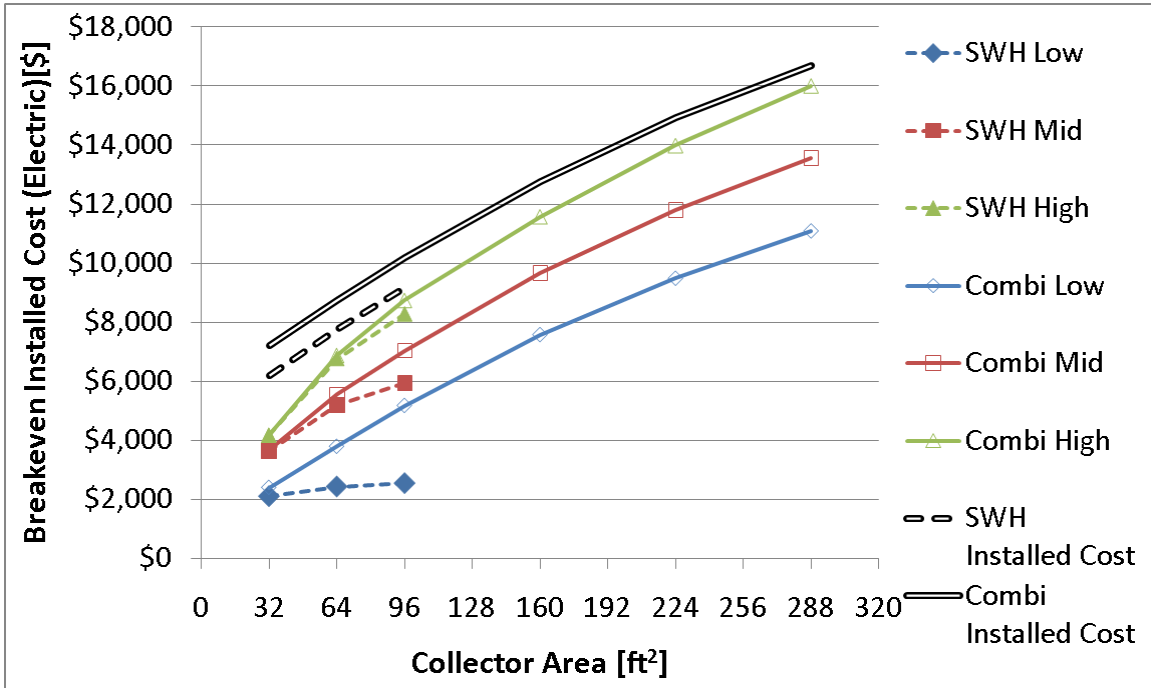


Figure 5.53: Breakeven Cost of the SWH and the combisystem as a function of collector area and DHW load (Denver Benchmark House)

Based on Figure 5.53, Figure 5.54 shows the combisystem incremental breakeven cost relative to the SWH breakeven cost for the combisystem to be as cost-effective as the SWH. This figure provides insight into the maximum incremental cost that a combisystem can have in order for it to be as cost-effective as a SWH. For example, for a 32 ft² system, since the combisystem does not provide significant incremental savings relative to the SWH, the combisystem can have an incremental cost of less than \$300 in order for the system to breakeven with the SWH. For the 96 ft² system, the incremental cost can range from \$500 to \$2,600 depending on the DHW load. Lower DHW loads will allow the incremental breakeven cost to be higher because the incremental savings potential is higher with lower DHW loads.

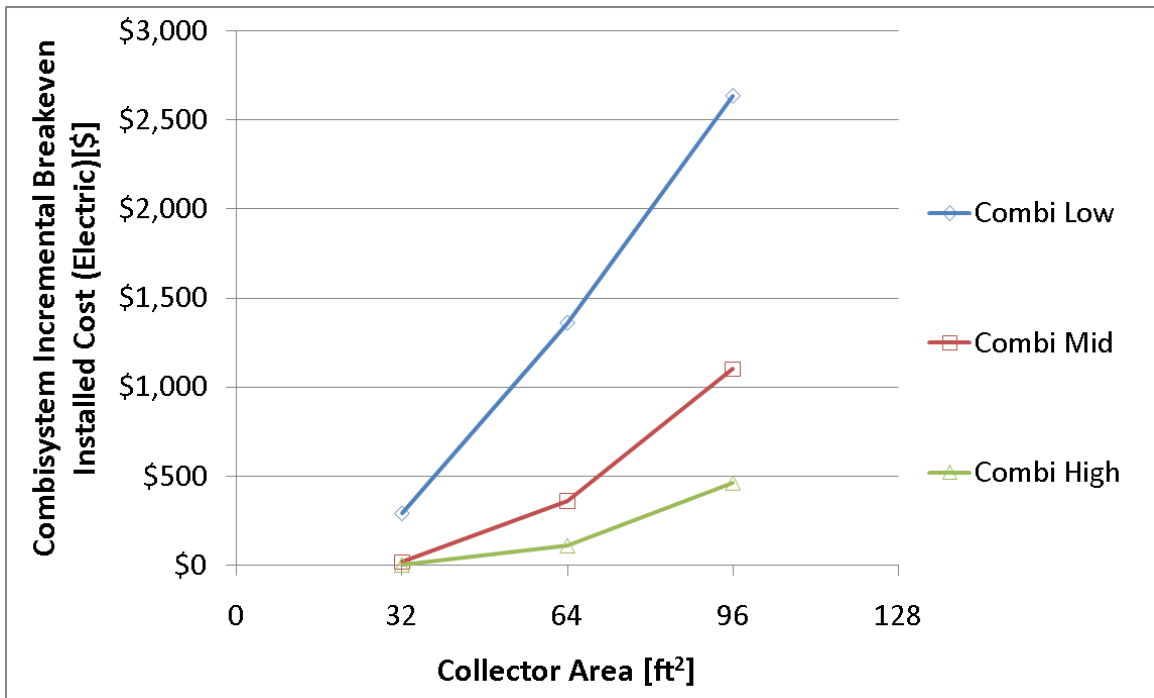


Figure 5.54: Combi system incremental breakeven installed cost as a function of collector area and DHW load (Denver Benchmark House)

In general, a combisystem serving a house with high space heating loads and low DHW loads will yield the largest incremental savings and therefore yield the highest incremental breakeven cost relative to a SWH (see Figure 5.55). In contrast, a combisystem serving a high performance house and high DHW loads will yield the lowest incremental breakeven costs. Therefore, when determining the upper and lower bounds for incremental breakeven costs for a particular system size and location, a 1960s retrofit house paired with low DHW loads will provide the upper bound and a Building American 50% house paired with high DHW loads will provide the lower bound.

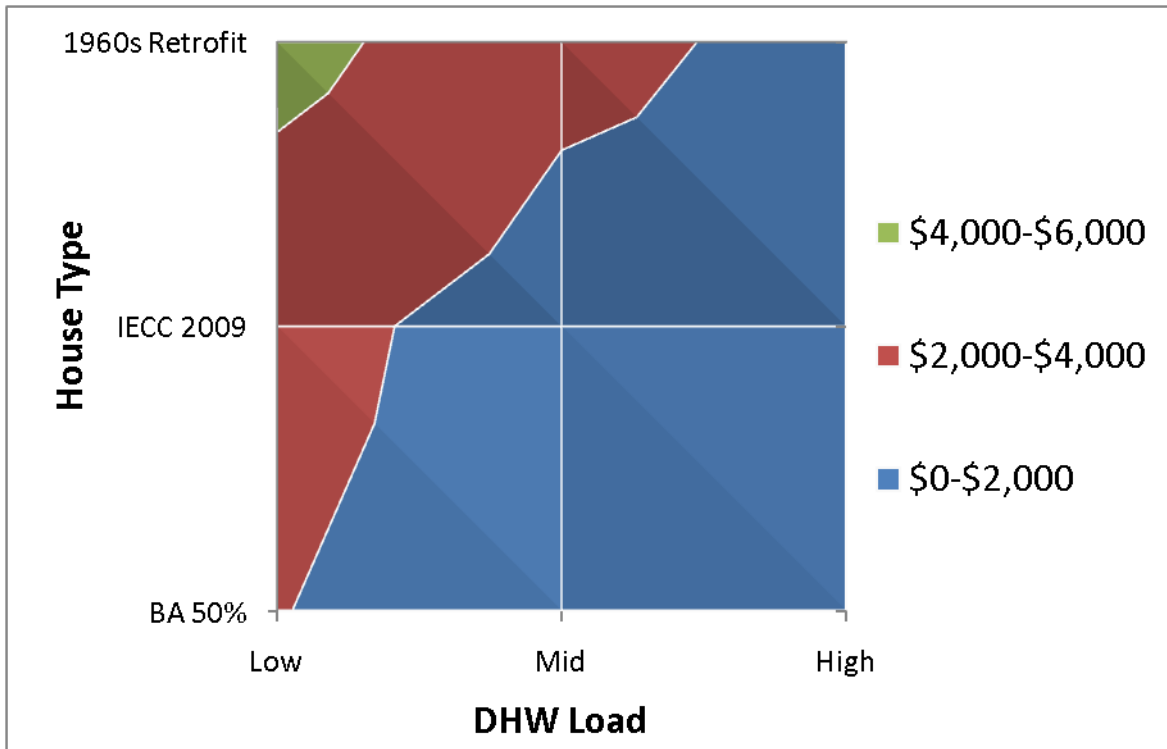


Figure 5.55: Impact of DHW Load and house type on the combisystem incremental breakeven cost relative to the SWH (Denver, 96 ft² system)

Figure 5.56 shows the LCOE is the SWH and combisystem as a function of collector area and DHW load as well as the cost of electricity used for the Denver cost analysis. In general, the combisystem LCOE will decrease as collector increases because marginal increased savings as a function of system size is still significant even with low DHW loads and large combisystems in Denver.

For SWHs, the LCOE is highly dependent on the DHW load. For example, for low DHW loads, the LCOE will increase as collector area increases because incremental saving with larger collector areas are small. In contrast, for high DHW loads, since system savings will significantly increase as a function of collector area, the LCOE will decrease as a function of increasing collector area.

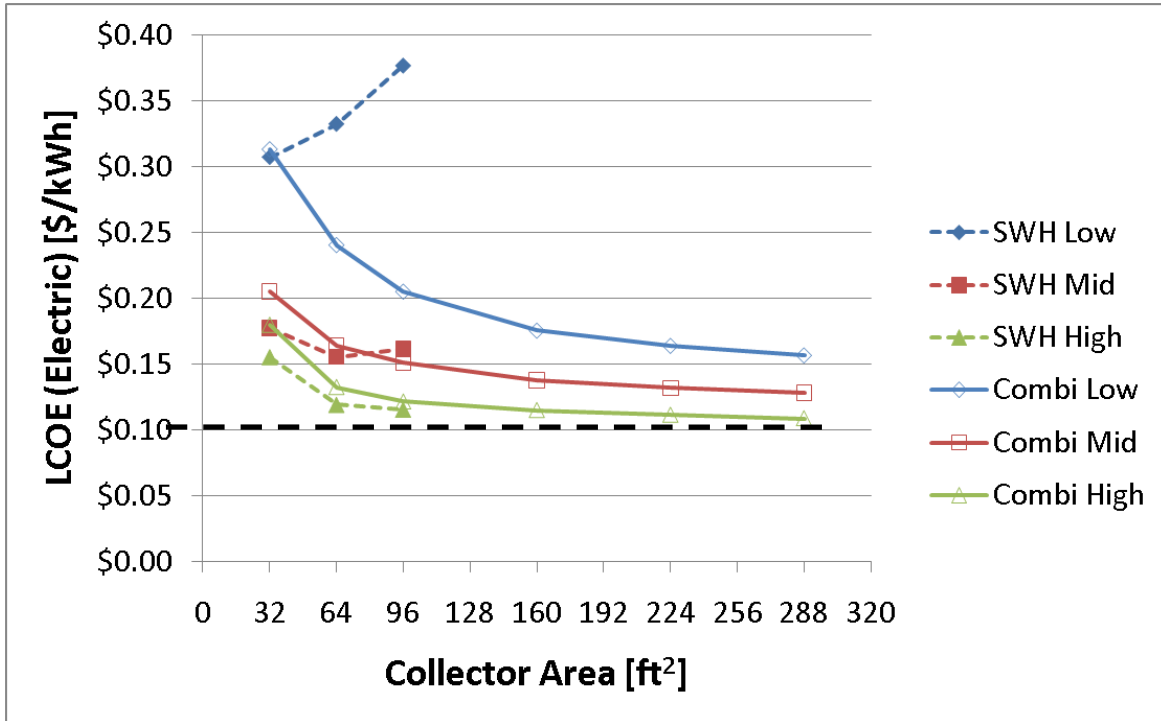


Figure 5.56: LCOE of the SWH and the combisystem as a function of collector area and DHW load (Denver Benchmark House)

Figure 5.57 shows that buildings with low energy consumption will yield a higher LCOE due to lower savings potential and buildings with high energy consumption will yield a low LCOE due to increased energy savings. Therefore, the upper and lower bounds in terms of the most cost-effective load scenario for a combisystem relative to a reference system is a 1960s retrofit house paired with high DHW load. The least cost-effective load scenario for combisystems relative to a reference system is a Building America house paired with low DHW loads.

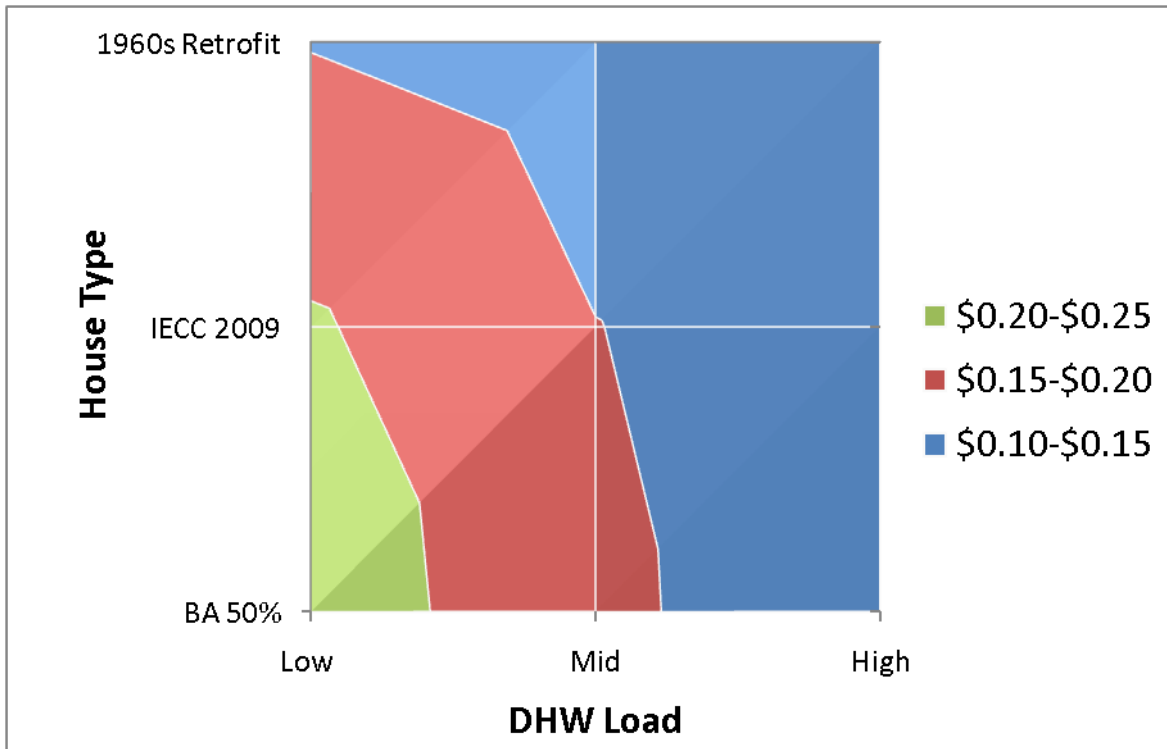


Figure 5.57: Impact of DHW load and house type on the LCOE (Denver, 96 ft² system)

5.6.4 Impact of location on economics

The location's cost of energy and its solar resource both play a large role in the economics of solar water heaters. In terms of the impact of fuel type on economics, since the cost of electricity is much higher per unit of energy as compared to the cost of natural gas, electric systems provide more favorable economics for solar thermal systems as compared to natural gas systems because the value of the saved energy is more significant for electric systems.

Figure 5.58 shows the incremental breakeven installed cost for both electric and natural gas systems for a 96 ft² collector area on a Benchmark house with a 60 gallon DHW draw. The error bars represent the range of incremental breakeven costs for the combisystem to be cost competitive with SWH, with the range being dependent on the space heating and DHW loads. The upper limit is the incremental breakeven cost for a 1960s retrofit house with a 20 gallon DHW draw. This combination of loads yields

the largest incremental savings for combisystems relative to SWH. The lower limit is the incremental breakeven cost for a 50 % house with a 100 gallon DHW draw. The dashed lines in the plot show the lower and upper limit incremental costs for combisystems based on the \$1,000 incremental cost assumption (lower bound cost) and the European cost data (upper bound cost). Figure 5.58 shows that for most locations, if space heating loads are high and DHW loads are low, the incremental breakeven cost of the combisystem is above the \$1,000 incremental cost limit. However, for a benchmark house with a 60 gallon draw, only San Francisco and Denver yield incremental costs for electric systems that are above the \$1,000 incremental cost threshold.

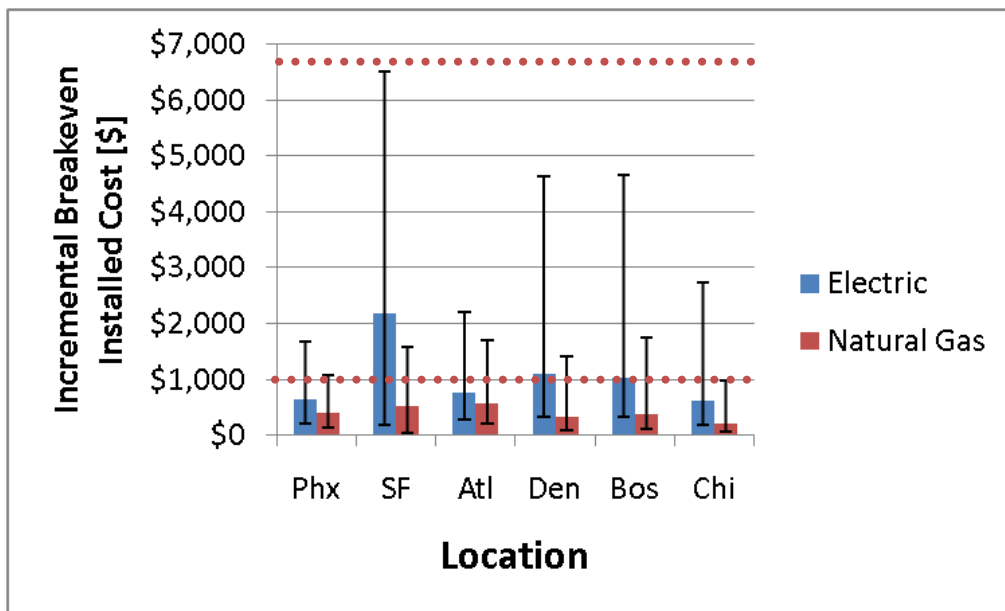


Figure 5.58: Impact of location on incremental breakeven installed cost for 96 ft² system. The bars represent the incremental breakeven cost for a benchmark house with a 60 gallon draw. The error bars represent the range of incremental breakeven costs for the combisystem to be cost competitive with SWH, with the range being dependent on the space heating and DHW loads. The dashed lines in the plot show the lower and upper limit incremental costs for combisystems.

In terms of evaluating the economics of large combisystems, Figure 5.59 shows the impact of combisystem installed cost and climate on the LCOE for a 288 ft² system with an electric auxiliary heater. The figure shows the upper and lower bounds for LCOE, where the lower bound LCOE is a high energy

consumption house and the upper bound LCOE is a lower energy consumption house. As seen in the figure, the high European system cost will prevent most systems from being cost-effective, assuming a \$0.12/kWh cost of energy. While when using the \$1,000 incremental cost estimate and assuming a \$0.12/kWh cost of energy, the systems will begin to become cost-effective in all climates for the high energy consumption house with the exception of Phoenix

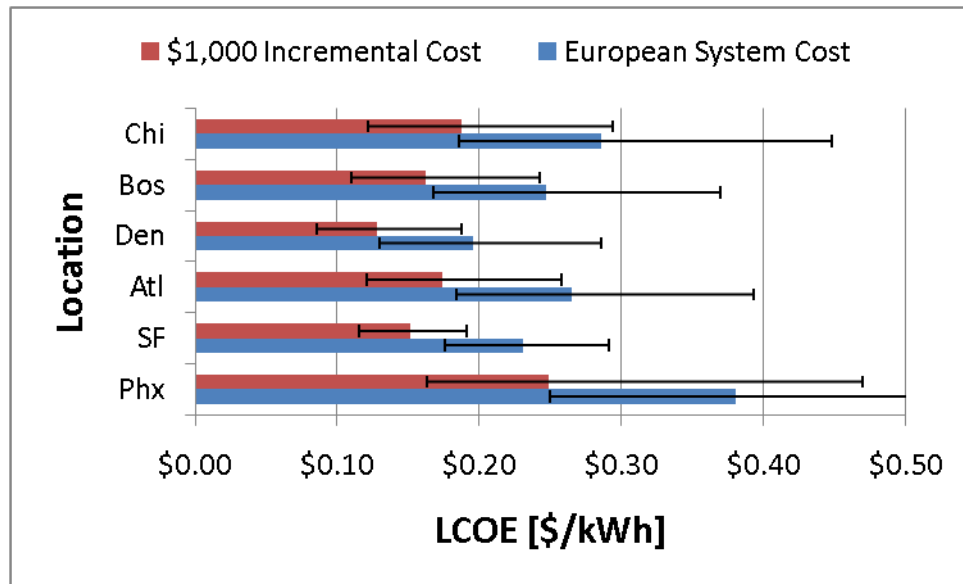


Figure 5.59: Impact of combisystem installed cost and climate on the LCOE for a 288 ft² system with an electric auxiliary heater. The error bars show the bounds of LCOEs. The lower bound is for a house with the largest loads (1960s retrofit house with 100 gallon DHW draws) and therefore largest savings and the higher bound is for a house with the smallest loads.

For a natural gas system, Figure 5.60 shows that no location will yield a cost-effective system for 288 ft² system size, assuming a \$1.50 per therm cost of natural gas. As in the electric LCOE figure, Denver yields the lowest LCOE followed by San Francisco.

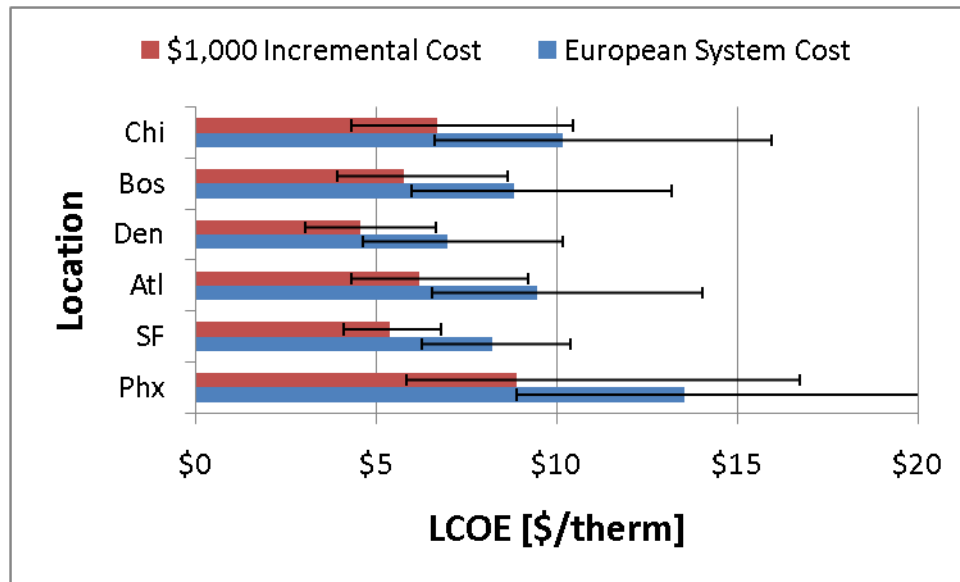


Figure 5.60: Impact of combisystem installed cost and climate on the LCOE for a 288 ft² system with a natural gas auxiliary heater. The error bars show the bounds of LCOEs as described in Figure 5.59.

5.6.5 Sensitivity Analysis

Additionally, a sensitivity analysis was conducted to determine how the installed costs, cost of energy, and discount rates impact the economics of these systems. All the sensitivity plots show the economics of an electric-auxiliary system in Denver Benchmark house with a 60 gallon DHW draw.

Figure 5.61 shows the impact of the cost of electricity and collector area on the net present worth of combisystems. The figure reveals that a large system paired with a low cost of energy results in the worst-case economics, where as a large system paired with a high cost of energy results in the best-case economics. Based on this fact, this plot shows that economics of large systems is more sensitive to the cost of energy than smaller systems. This is due to the high installation costs of large combisystems, which are difficult to recover the costs for when energy costs are low. However, when energy costs are high, the increased savings of larger system will allow the system to recover costs over its lifetime. For

small systems, if the cost of energy increases, the cost-effectiveness also improves, however not as drastically since the small systems are yielding lower energy savings.

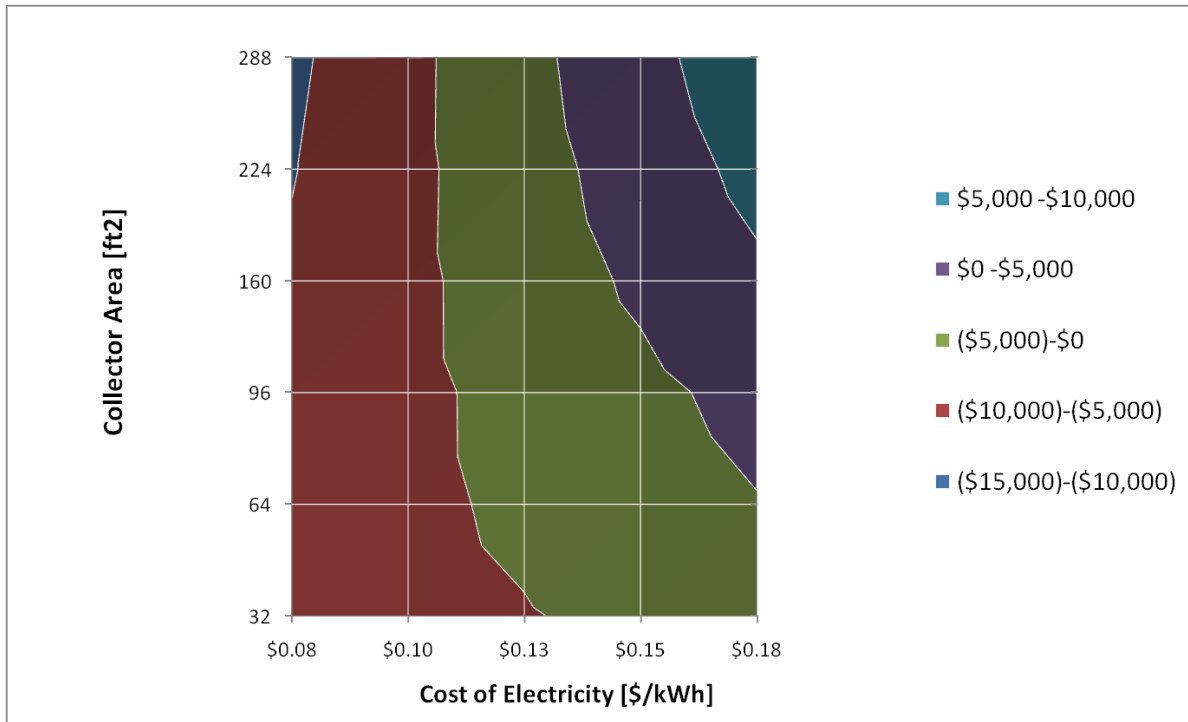


Figure 5.61: Impact of cost of electricity on the NPW of an electric-auxiliary combisystem in Denver (Benchmark, 60 Gallon Draw)

Figure 5.62 shows the impact of discount rate and collector area on the net present worth of a combisystem. A low discount rate will result in larger lifetime savings and therefore better economics for combisystems. However, larger systems are much more sensitive to the discount rate. Similarly to the impact of cost of energy on the net present worth, it is difficult for the larger system to recover their high installation costs when value of energy cost saving are low, which is the case with high discount rates. However, when discount rates are low, the value of the energy savings increase significantly for a large combisystem, thus allowing the system to become cost-effective.

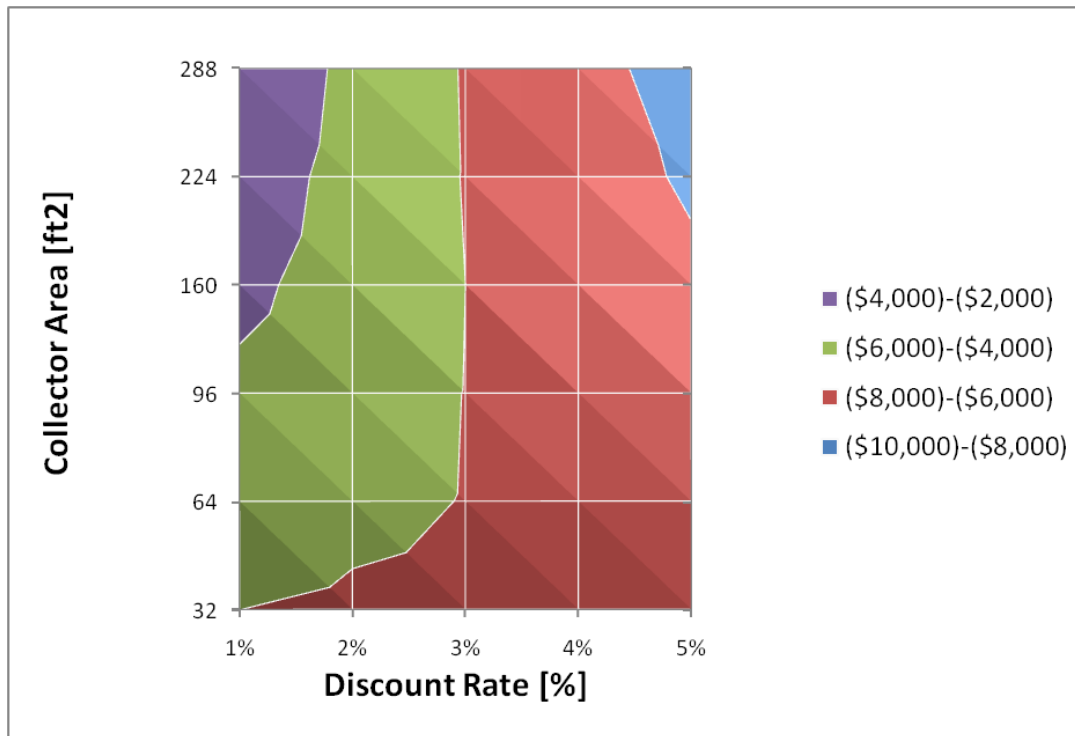


Figure 5.62: Impact of the discount rate and collector area on the net present worth of combisystems (Denver, Benchmark House, 60 Gallon Draw)

Figure 5.63 shows the impact of the cost of electricity and reduction in installed cost on the NPW of a 96 ft² combisystem in Denver. The figure shows that as the cost of electricity increases and the installed cost decreases, the system becomes cost-effective. For this particular system, if the cost of electricity increases to \$0.165 or if the system installed cost decreases by 50%, the system becomes cost-effective. Additionally, a combination of a 30% increase in the cost of electricity and a 30% reduction in the cost of the system will also yield a cost-effective combisystem.

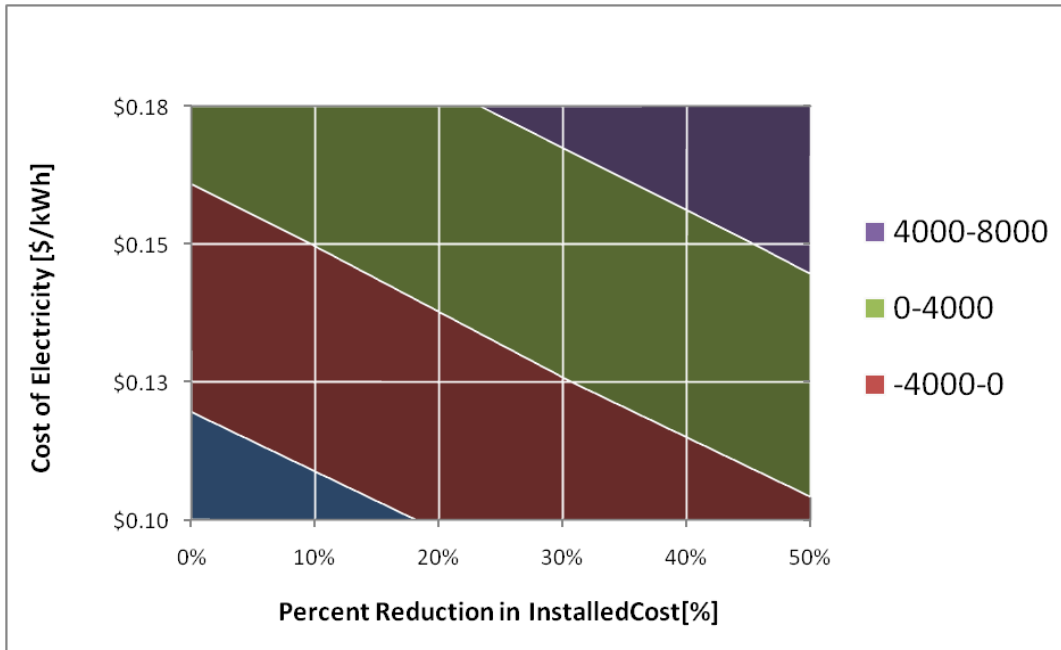


Figure 5.63: Impact of Cost of Electricity and relative reduction in the installed cost on the NPW of a 96 ft² combisystem in Denver (Benchmark House, 60 Gallon Draw)

5.7 System Size Optimization

The economic optimization as a function of system size for a combisystem design is based on both the system performance parameters and all the economic assumptions. For this analysis, the net present worth was analyzed as a function of collector area for all the heating load scenarios and climates to determine the optimum collector area size for the combisystem design. The optimum collector area, for a given heat load, location, and economic assumption, will yield the maximum net present worth.

An example of the the impact of collector area on the net present worth is presented in Figure 5.64. The figure shows the net present worth as a function of collector area for low thermal load, benchmark load, and high thermal load scenarios in Denver using the low combisystem installed costs. The low thermal load curve corresponds to a scenario in which the system cannot compete with the reference system. Additionally, since the smallest system yields the highest net present worth, it means that the optimum system size is zero collector area. The benchmark load curve corresponds to a scenario

where the system will have a non-zero collector area optimum, but will still not be competitive with the reference system. In this case, the optimum system size is 160 ft², although system sizes ranging from 64 ft² to 288 ft² will yield essentially the same economics. Lastly, the high thermal load curve corresponds to a scenario where the optimum collector area size is 288 ft² or larger and the system is cost-effective in comparison to a reference system. For this study, the largest system size analyzed was 288 ft² so therefore the optimum size is unknown when the optimum is shown to be 288 ft².

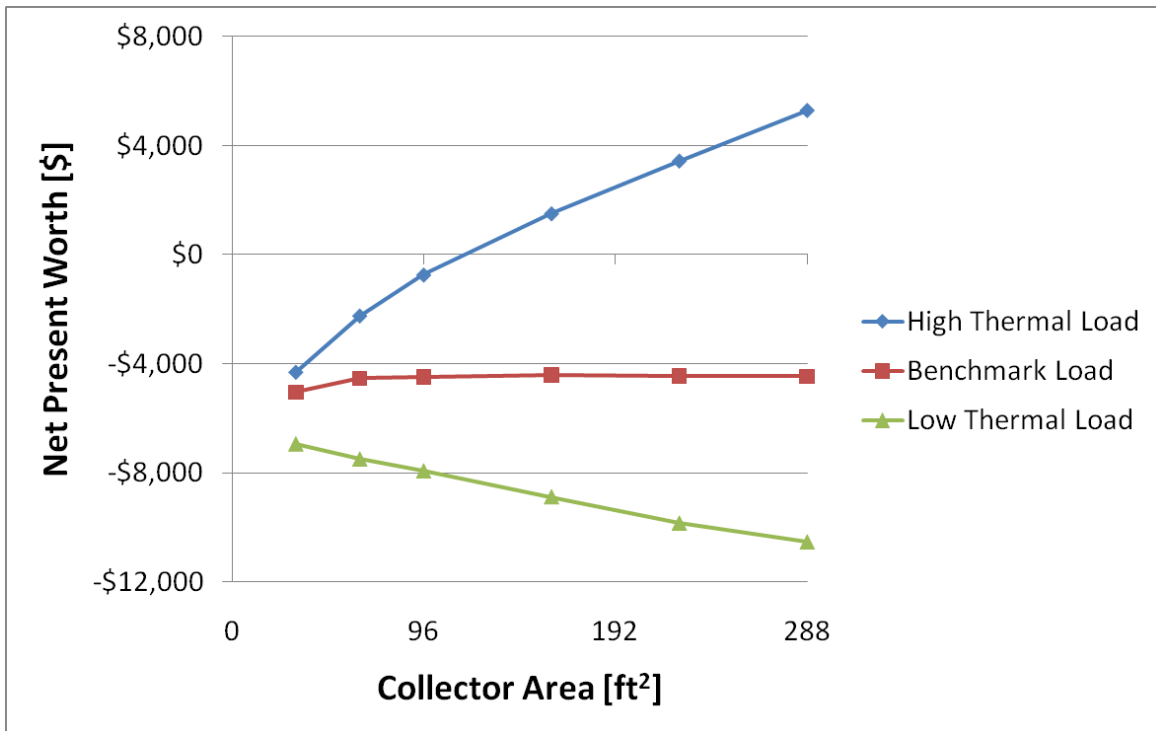


Figure 5.64: Net Present Worth as a function of collector area for high thermal load, benchmark load, and low thermal load house in Denver (low combisystem cost)

Figure 5.65 shows the net present worth as a function of collector area for low thermal load, benchmark load, and high thermal load scenarios in San Francisco using the low combisystem installed costs. In this case, all the load scenarios present a non-zero collector area optimum. For both the low thermal load and benchmark thermal load scenarios, the optimum collector area occurs at 160 ft², however the benchmark load scenario is cost-effective relative to a reference system, while the low

thermal load scenario is not cost-effective. Once again, the high thermal load curve corresponds to a scenario where the optimum collector area size is 288 ft² or larger.

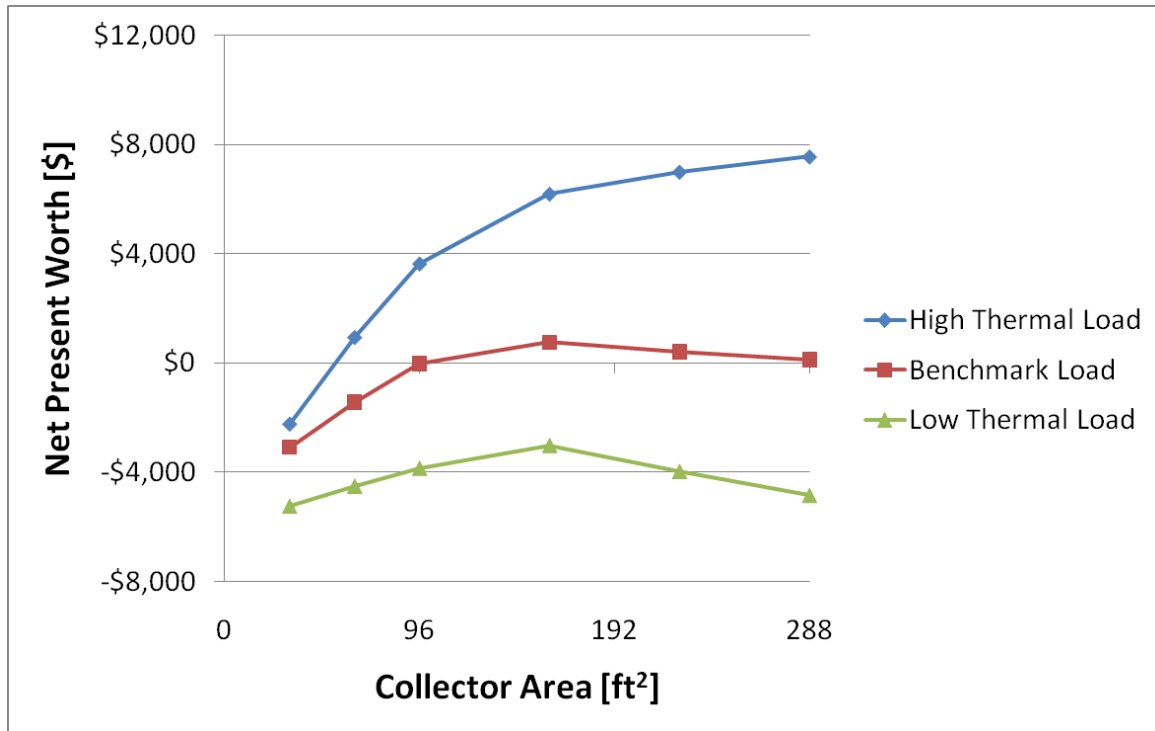


Figure 5.65: Net Present Worth as a function of collector area for high thermal load, benchmark load, and low thermal load house in San Francisco (low combisystem cost)

Table 5.4 shows the optimized collector area size and its corresponding net present worth using the low combisystem installed costs for high thermal load, benchmark load, and low thermal load scenarios in all climates. The table shows three different optimization scenarios that can occur with regards to the optimum system size. The first scenario, which is denoted by “N/A” in the table, indicates that system has a zero collector area optimum. The second scenario, which occurs when the NPW is negative, indicates that there is a non-zero collector area optimal system; however the system is not cost-effective as compared to the conventional system. The last scenario occurs when there is an optimum size and the NPW is positive, indicating that the system is cost-effective. Additionally, the table shows that in

a number of scenarios where the optimum collector area is 288+ ft², which means that optimum system size is 288 ft² or larger.

Table 5.4 shows that the optimum system sizes for the high thermal load scenarios generally occur at 288+ ft². The exception occurs in Atlanta, where the optimum collector area is 64 ft². For the low thermal load scenario, only San Francisco yields an optimum system size.

Table 5.4: Optimized collector area and its corresponding NPW for high thermal load, benchmark load, and low thermal load homes in all climates (Low Combisystem Cost)

	High Thermal Load		Benchmark Load		Low Thermal Load	
	Size [ft ²]	NPW [\$]	Size [ft ²]	NPW [\$]	Size [ft ²]	NPW [\$]
Phoenix	N/A	N/A	N/A	N/A	N/A	N/A
Atlanta	64	(\$4,355)	N/A	N/A	N/A	N/A
San Francisco	288+	\$7,500	160	\$750	160	(\$3,016)
Denver	288+	\$5,296	160	(\$4,418)	N/A	N/A
Boston	288+	\$9,156	288+	(\$1,381)	N/A	N/A
Chicago	288+	(\$3,790)	N/A	N/A	N/A	N/A

Table 5.5 presents similar information as in Table 5.4, however the economic analysis was conducted using the high combisystem installed costs rather than the low combisystem installed costs. As compared to Table 5.4, Table 5.5 shows that the optimum collector areas are generally smaller as a result of the higher combisystem installed costs. For example, with the benchmark load scenario, the optimum collector areas in San Francisco, Denver, and Boston all decrease as a result of the higher installed costs. Additionally, the economic assumption of higher installed costs yields optimum system sizes which will not be competitive with the reference system.

Table 5.5: Optimized collector area and its corresponding NPW for high thermal load, benchmark load, and low thermal load homes in all climates (High Combisystem Cost)

	High Thermal Load		Benchmark Load		Low Thermal Load	
	Size [ft ²]	NPW [\$]	Size [ft ²]	NPW [\$]	Size [ft ²]	NPW [\$]
Phoenix	N/A	N/A	N/A	N/A	N/A	N/A
Atlanta	64	(\$11,881)	N/A	N/A	N/A	N/A
San Francisco	160	(\$3,276)	96	(\$8,170)	96	(\$11,997)
Denver	288+	(\$7,176)	64	(\$12,012)	N/A	N/A
Boston	288+	(\$3,316)	64	(\$10,498)	N/A	N/A
Chicago	64	(\$12,000)	N/A	N/A	N/A	N/A

Lastly, Figure 5.66 shows the correlation between the two economic metrics, LCOE and the NPW, and the optimum system size when the LCOE is falls below the location’s cost of energy. In this case, Figure 5.66 shows the impact of collector on the two economic metrics for San Francisco with a benchmark load scenario and low combisystem installed cost. At optimum system size, which occurs at 160 ft², the LCOE is below the \$0.15/kWh cost of electricity, as indicated by the dotted line. As seen in Figure 5.66, the minimum LCOE, which falls below the location’s cost of electricity, corresponds to a maximum net present worth at 160 ft².

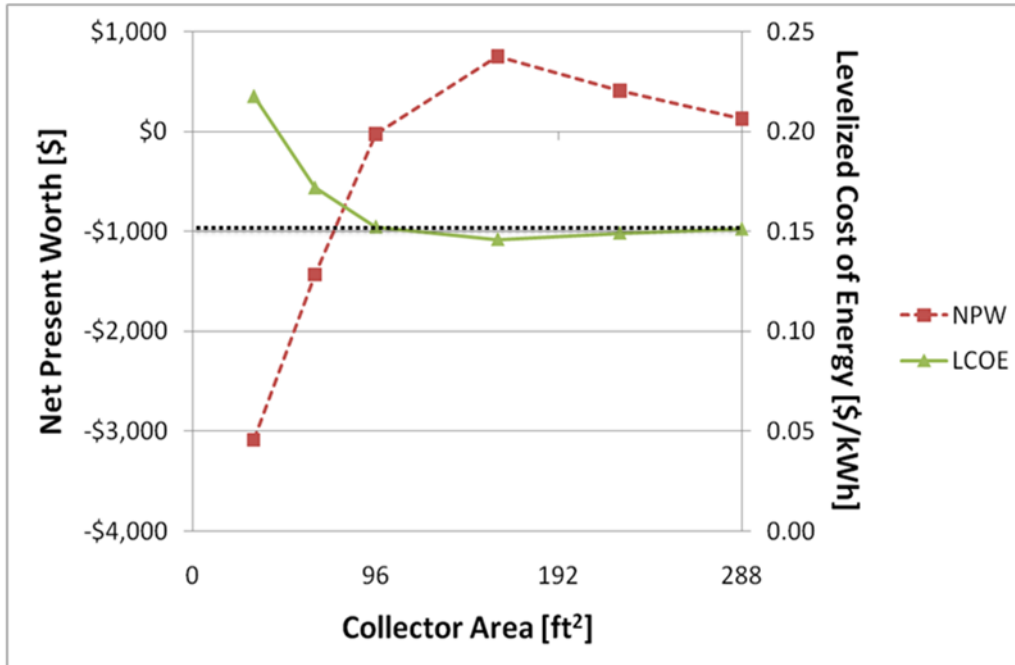


Figure 5.66: Net Present Worth and LCOE as a function of collector area for San Francisco with a benchmark load scenario (low combisystem cost)

Chapter 6

Conclusion and Future Work

6.1 Combisystems versus SWHs

It is clear that combisystems will provide incremental energy and cost savings in comparison to a standard SWH, however the magnitude of these incremental savings is highly dependent on the system size, the loads, and the climate. As found in Chapter 5, the largest incremental savings from a combisystem relative to a SWH will occur when DHW loads are small and space heating loads are high. In contrast, the smallest incremental savings from a combisystem relative to a SWH will occur when DHW loads are high and space heating loads are low. Based on these two bounds, the incremental site energy savings from combisystems can be evaluated across all the locations (see Figure 6.1). Since the 96 ft² system provides the largest incremental savings in all climates with all building types, the results from a 96 ft² system are shown in the figure below.

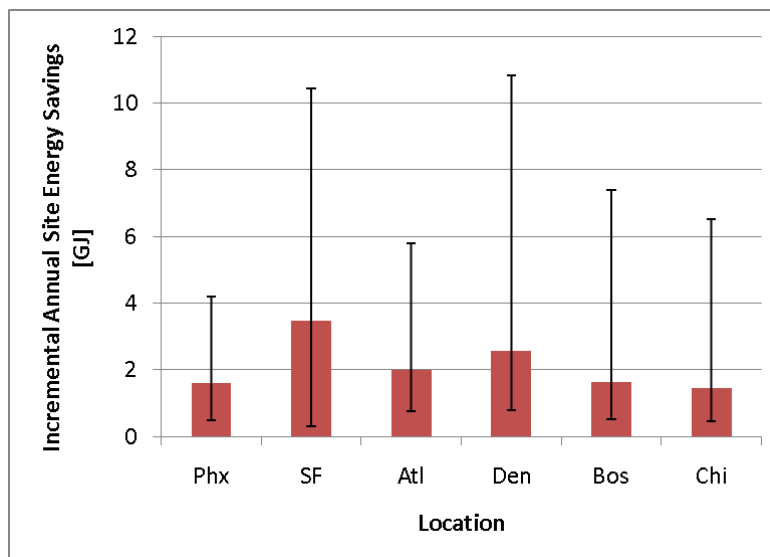


Figure 6.1: Range of incremental site energy savings for 96 ft² system.

The solid bars in Figure 6.1 represent the site energy savings for a benchmark house and 60 gallon daily draw and the error bars represent the lower and upper bounds of the incremental savings. Based on this figure, it is evident that the incremental savings from a 96 ft² can vary drastically depending on the load scenario. Additionally, the figure shows climate plays a large role in the magnitude of the incremental savings, however it is clear that the locations of Denver and San Francisco yield the highest incremental savings, largely due to their relatively significant space heating loads and relatively high incident solar radiation. In the case of San Francisco, the space heating loads and high incident solar radiation in the late Spring play a large role in the combisystem yielding high incremental site energy savings in comparison to the SWH.

In evaluating the economics between SWH and combisystems, both the incremental energy savings and the cost of energy will play a significant role in the incremental annual cost savings between the combisystem and the SWH. Figure 6.2 shows the range of incremental annual cost savings for both electric and gas system. As in Figure 6.1, the solid bars represent the load scenario for a benchmark house and 60 gallon daily DHW draw and the error bars represent the lower and upper bounds of the incremental cost savings. For the electric case, San Francisco will yield the largest incremental cost savings due to its high cost of electricity (\$0.15/kWh). For the natural gas case, all climates will yield less than \$80 annual incremental cost savings even with high space heating loads and low DHW loads.

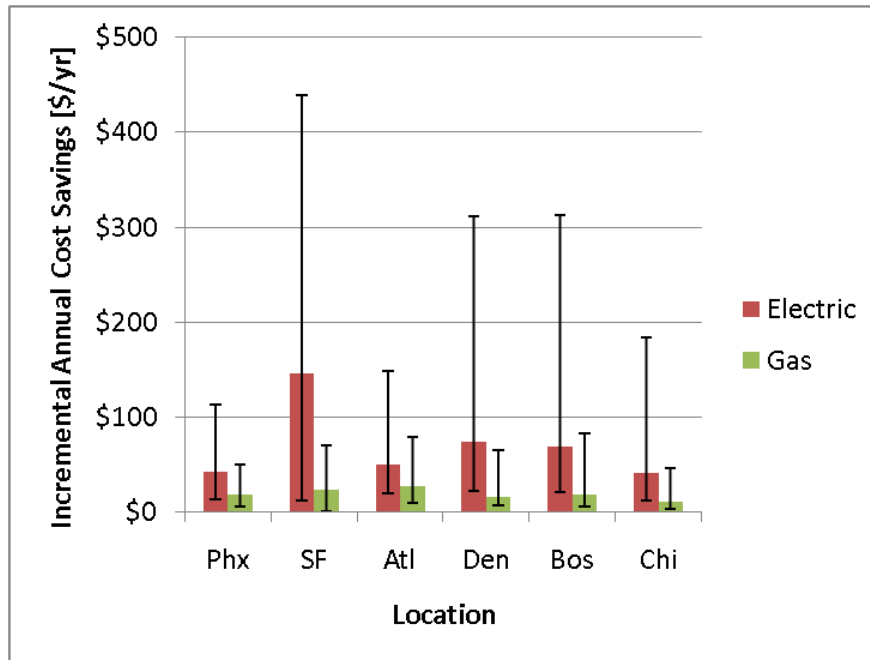


Figure 6.2: Range of incremental annual cost savings for 96 ft² combisystem

In examining the incremental breakeven costs for combisystems to be as cost-effective as SWHs, this value will also vary considerably depending the loads and climate. Figure 6.3 shows the range of incremental breakeven costs for combisystems along with dashed lines which represent the incremental installed costs of combisystems based on a \$1,000 incremental cost assumption and the incremental costs of European combisystem relative to U.S. SWHs for a 96 ft² system. This figure reveals that, if it's assumed that the incremental cost of combisystems lies somewhere in between the \$1,000 incremental cost assumption and the European incremental costs, electric combisystems can compete economically with SWHs all location given high space heating loads and low DHW loads. In terms gas systems, combisystems will be able to compete with SWH in all locations with the exception of Phoenix and Chicago.

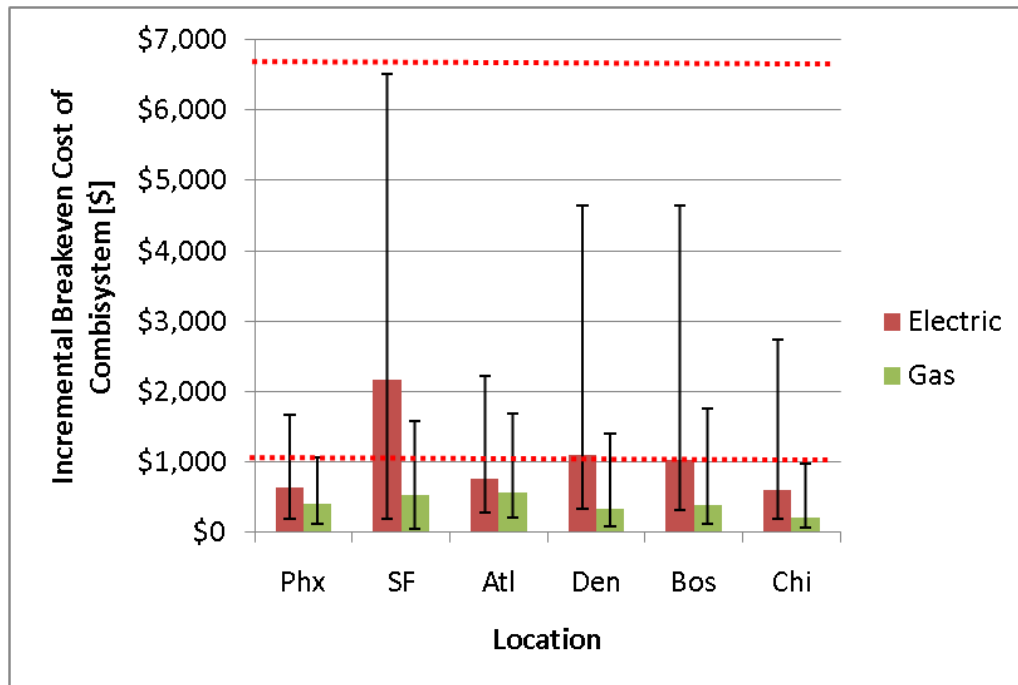


Figure 6.3: Range of incremental breakeven costs relative to a SWH for 96 ft² combisystems. The dashed lines represent the incremental installed costs based on a \$1,000 incremental cost assumption and the incremental costs of European combisystem relative to U.S. SWHs.

6.2 Conclusions for Large Combisystems

In terms of large combisystems with collector areas in the range of 288 ft² and storage tanks with a capacity 432 gallons, it is evident, based on the annual simulations, that these systems can yield high site energy savings especially in Denver, where the space heating loads are significant and the solar radiation, especially during the winter, is large enough to yield high space heating solar fractions.

Figure 6.4 shows the annual savings relative to a reference system for a 288 ft² combisystem that serves a benchmark house with 60 gallon daily average DHW draws. The error bars represent the upper and lower bounds for site energy savings. As revealed in Chapter 5, the largest savings relative to a reference system will occur when building thermal loads are high (high DHW load and large space heating load) and the lowest savings relative to a reference system will occur when building thermal loads

are low (low DHW load and low space heating load). In terms of comparing the performance among locations, Denver will yield the highest annual energy savings, followed by San Francisco and Boston. In Phoenix, large combisystems will yield much lower site energy savings due to low space heating loads.

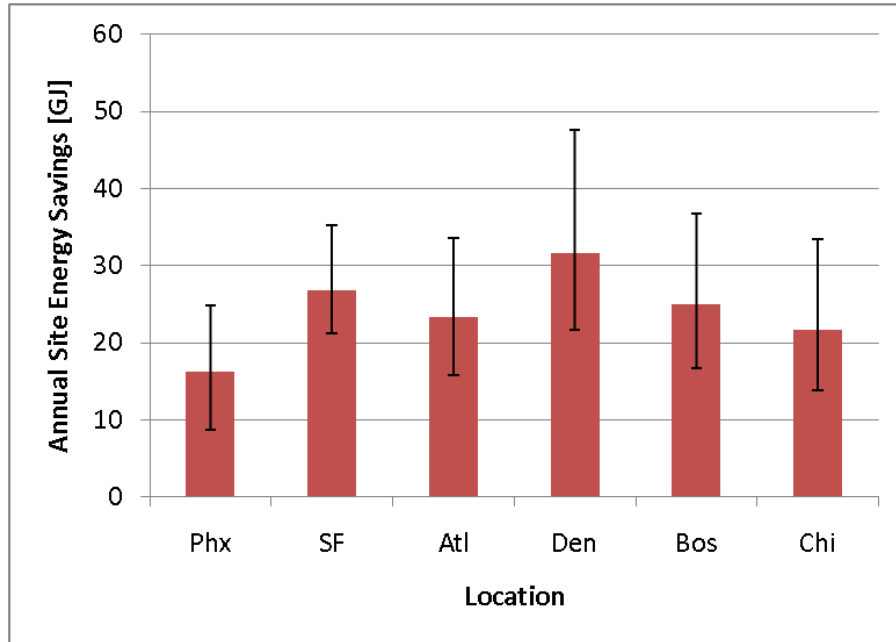


Figure 6.4: Annual site energy savings for a 288 ft² combisystem

In terms of cost savings relative to a reference system between all locations, the annual cost savings for an electric system will be largest in San Francisco and Boston due to high electricity costs (\$0.15 per kWh). Annual electricity cost savings will be as high as almost \$1,600 in Boston for a house with high thermal loads. In terms of gas systems, due to the extremely high cost of natural gas in Georgia (\$1.77 per therm), systems in Atlanta will yield the largest annual energy cost savings.

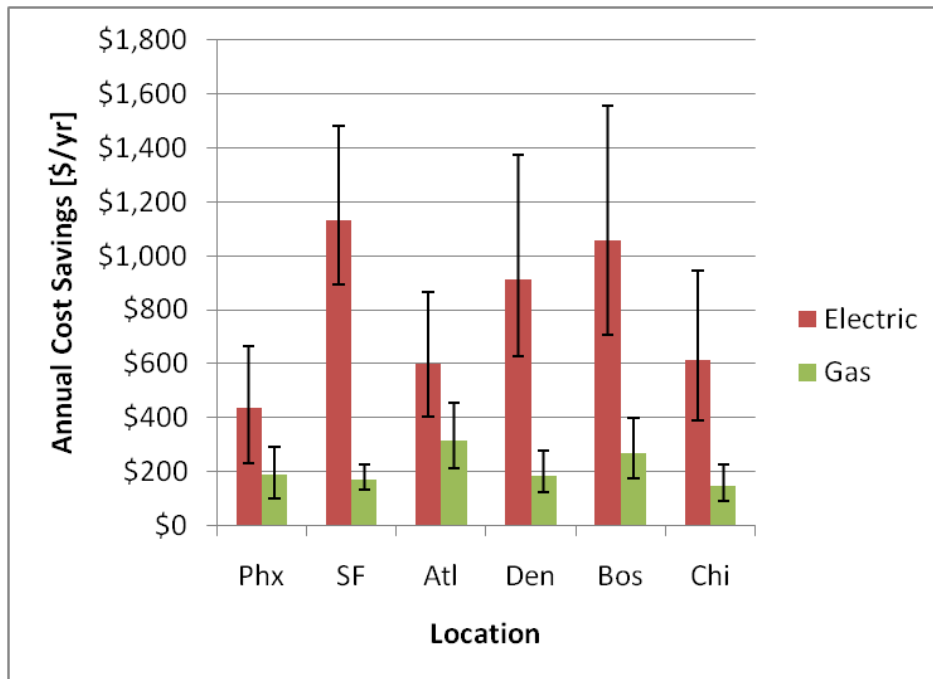


Figure 6.5: Annual cost savings relative to the reference system for a 288 ft² combisystem

Once again, while making the assumption that the installed costs of combisystem lies somewhere between the \$1,000 incremental cost relative to SWH costs and the European combisystem costs, it was determined that large combisystems in only a few locations will be able to breakeven economically relative to a reference system. Providing that homes have larger than average thermal loads, electric systems will be cost-effective in San Francisco, Denver, and Boston (see Figure 6.6). Although not entirely accurate, an average thermal load home in this case is assumed to be 2009 IECC construction with 60 gallon DHW draw. The combisystem breakeven costs for an average thermal load home is depicted by the solid bars in Figure 6.6. As seen in Figure 6.6, natural gas systems will not be cost-effective in any climate, regardless of the building thermal loads.

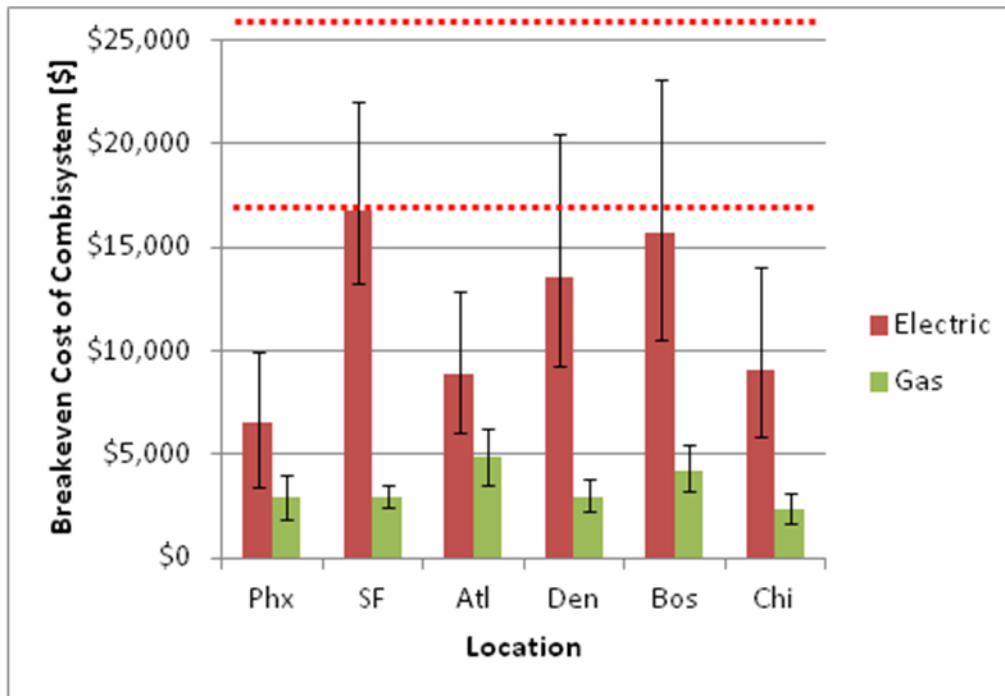


Figure 6.6: Breakeven costs for 288 ft² combisystems relative to reference system. The dashed lines represent the installed costs based on the \$1,000 incremental cost assumption and the installed costs of European combisystem for a 288 ft² system.

6.3 Future Work

This study found that combisystems are able to provide significant energy and cost savings relative to both small SWHs and reference systems. However, these saving metrics were developed based on a combisystem design that was by no means an optimized system. For example, the studies conducted in Europe have looked into the optimal sizing of systems and the optimal use of the solar storage tank and have found the savings can increase significantly by varying these parameters in the system design.

For example, the extensive research in Europe has revealed that optimal storage sizing for solar is between 1.3 gallon and 2.6 gallons per ft² of collector area [7]. Although the storage size in this study was 1.5 gallons per ft² of collector area, the top one-third of the tank was occupied by auxiliary storage, so in reality, the solar storage was more like 1 gallon per ft² of collector area. Based on the previous research that has examined the impact of storage sizing on the system performance, additional work could be

performed to examine how the storage volume to collector area ratio can impact the annual performance of the modeled system in U.S. climates.

Additionally, European research has found that the thermal performance of combisystems increases by 7 to 14 percent by using stratifiers for the solar collector loop and space heating loop rather than immersed heat exchangers [23]. Although solar system suppliers in the U.S. are not yet marketing solar storage tanks with stratifiers, a study that examines how replacing the solar-side heat exchanger with an inlet stratifier impacts the performance and economics of the combisystem could provide some incentive for U.S. suppliers to start marketing tanks with built-in inlet stratifiers.

Another avenue of research that could be worth exploring is the impact of heating system type on the performance of combisystem. This study examined the performance of combisystems paired with radiant floor heating systems, which occupy a small share of the market in comparison to forced-air system within the U.S. housing sector. The small market share of radiant floor heating systems in the U.S. is likely due to their incremental costs as compared to forced-air systems. However, a study that examines the performance between a combisystem paired with a radiant floor heating system and a combisystem paired with a forced-air heating system could provide insight as to if the increased savings from a combisystem paired with a radiant floor heating system justifies the incremental cost of radiant floor heating system.

Lastly, it could be worth investigating whether evacuated-tube collectors provide any increased savings in climates such as Boston and Chicago. Since evacuated-tube collectors perform better than flat-plate collectors in cloudy and cold conditions, it may be worth the additional simulation work to replace the flat-plate collector model with an evacuated-tube model in order to see the impact that evacuated-tube collector have on the annual performance of combisystems, especially in locations that receive less radiation and have significant space heating loads in the winter.

References


- [1] Hendron, Bob, et al. *Building America Field Test and Analysis Report: CORE H1 and H2 Houses--Carbondale, CO*. Golden, CO: Building America, July 21, 2005.
- [2] Greentech Knowledge Solutions, *Solar Water Heaters in India: Market Assessment Studies and Survey for Different Sectors and Demand Segments*, New Delhi, India, January 20, 2010.
- [3] Solar Energy Industries Association, *US Solar Industry Year in Review 2009*, April 15, 2010.
- [4] Werner Weiss and Franz Mauthner, *Solar Heat Worldwide: Markets and Contributions to the Energy Supply 2009*, IEA-SHC 2011 Edition (May 2011).
- [5] Solar Energy Industries Association, *U.S. Solar Market Insight: 1st Quarter 2011: Executive Summary*, 2011.
- [6] Sherwood, Larry, *U.S. Solar Market Trends: 2009*, Interstate Renewable Energy Council, July 2010. http://irecusa.org/wp-content/uploads/2010/07/IREC-Solar-Market-Trends-Report-2010_7-27-10_web1.pdf
- [7] Weiss, Werner, *Solar Heating Systems for Houses: A Design Handbook for Solar Combisystems*. UK: James & James (Science Publishers) Ltd., 2003.
- [8] Epp, Baerbel, *Long-term Trend in Austria: Combi Systems in Retrofitted Houses*. Global Solar Thermal Energy Council. Retrieved May 27, 2011 from: <http://www.solarthermalworld.org/node/2919>
- [9] Engebretson, C.D. *The Use of Solar Energy for Space Heating—M.I.T.: Solar House IV*. Proceeding of the UN Conference on New Sources of Energy (1964).
- [10] Adam Lee, Sales Representative, SunMaxx Solar, Denver, CO. Personal Communication June 28, 2011.
- [11] Hubbart, Rick, Solar Design and Sales Manager, Ferguson Enterprises, Denver, CO. Personal Communications: June 29, 2011.
- [12] Burch, Jay, Senior Scientist, National Renewable Energy Laboratory (NREL), Golden, CO. Personal Communications.
- [13] Klein S.A., W. A. Beckman and J. A. Duffie. *A Design Procedure for Solar Heating Systems*. Solar Energy 18, 113-123 (1976).
- [14] Klein S.A., W. A. Beckman and J. A. Duffie. *A Design Procedure for Solar Air Heating Systems*. Solar Energy 19, 509 (1976).
- [15] Brandemuehl, M. J. and W. A. Beckman. *Economic Evaluation and Optimization of Solar Heating Systems*. Solar Energy 23, 1-10 (1979)

- [16] Lameiro, G. and P. Bendt, *The GFL Method for Sizing Solar Energy Space and Water Heating Systems*. Solar Energy Research Institute (1978)
- [17] Duffie, J.A. and J.W. Mitchell. *F-Chart: Predictions and Measurements*, ASME Journal of Solar Energy Engineering, pp. 105 (1983).
- [18] Kelly, C. J. *Comparison of field measured performance with F-Chart Predictions*. ASME Solar Energy Division 4th Annual Meeting., pp 47-58 (1982)
- [19] Braun, J.E., S.A. Klein, and J.W. Mitchell. *Seasonal Storage of Energy in Solar Heating*. Solar Energy 26. pp.403-411 (1981)
- [20] Van Koppen, C., J. P. S. Thomas, and W. B. Veltkamp. *The Actual Benefits of Thermally Stratified Storage in Small and Medium Sized Solar Systems*. ISES Biennial Meeting (1979).
- [21] Lundh, Magdalena, et al. *Influence of store dimensions and auxiliary volume configuration on the performance of medium-sized solar combisystems*. Solar Energy (July 2010): 1095-1102.
- [22] Sharp, M.L. *Stratified Thermal Storage in Residential Solar Energy Applications*. Journal of Energy, 106-113 (1979).
- [23] Andersen, E. and S. Furbo. *Theoretical Comparison of Solar Water/Space-Heating Combi Systems and Stratifications Design Options*. ASME. Journal of Solar Energy Engineering (2007): 438
- [24] Radu Zmeureanu and H. Rivard. *Solar Combi-system with Season Thermal Storage*. Journal of Building Performance Simulation (May 2010)
- [25] Lund, P.D. *Sizing and Applicability Considerations of Solar Combi-systems*. Solar Energy (January 2005): 59-71.
- [26] Streicher, W. and R. Heimrath. *Analysis of System Reports of Task 26 for Sensitivity of Parameters*. Technical Report for Subtask C. 2004.
- [27] Jordan, Ulrike and Klaus Vajen. *Influence of the DHW Load Profile on the Fractional Energy Savings: A Case Study of a Solar Combi-system with TRNSYS Simulations*. Solar Energy (2000)
- [28] Holman, J.P. *Experimental Methods for Engineers*. s.l. : McGraw-Hill, 1994. Sixth Edition.
- [29] Duffie, J.A. and Beckman, W.A. *Solar Engineering of Thermal Processes*. Hoboken, NJ : Wiley, 2006. 3rd Edition.
- [30] Krarti, Moncef. Personal Communication. *University of Colorado*. January 2011.
- [31] D'Antonio, Peter C. *Maximizing Small-Boiler Efficiency*. s.l. : PCD Engineering Services Inc., August 2006.
- [32] Burch, Jay, et al. *Diagnosis of Solar Water Heaters Using Solar Storage Tank Surface Temperature Data*. Conference Paper, NREL/CP-550-45465, April 2009.
- [33] Kline, S.J., and F.A. McClintock, *Describing Uncertainties in Single-Sample Experiments*, Mechanical Engineering, Vol. 75, No. 1, January 1953: 3-8.

- [34] Cucumo, M., et al. *Experimental testing of models for the estimation of hourly solar radiation on vertical surfaces at Arcavacata di Rende*, Solar Energy 81 (2007) p. 692-695.
- [35] Erbs, D.G., Klein, S.A., Duffie, J.A., *Estimation of the diffuse radiation fraction for hourly, daily, and monthly average global radiation*. Solar Energy 28, 293-302 (1982)
- [36] Hay, John E., *Calculating Solar Radiation For Inclined Surfaces: Practical Approaches*. Renewable energy Vol. 3 No. 4/5 pp. 373-380 (1993)
- [37] Cengel, Yunus A., et al. *Fundamentals of Thermal-Fluid Sciences: Third Edition in SI Units*. McGraw-Hill Companies (2008)
- [38] Kakac, Sadik et al, *Handbook of Single-Phase Convective Heat Transfer*. Wiley-Interscience (1987)
- [39] Solar Rating and Certification Corporation for Heliodyne Flat Plate collector, <http://www.solar-rating.org>.
- [40] SunEarth, Standard Absorber Plate Specifications, <http://sunearthinc.com/collectors/sunburst/>
- [41] Engineering ToolBox, Metals-Specific Heats of Common Metals, http://www.engineeringtoolbox.com/specific-heat-metals-d_152.html
- [42] Omega Engineering Inc., ANSI and IEC Color Codes for Thermocouples, Wire and Connectors, http://www.omega.com/toc_asp/frameset.html?book=Temperature&file=TC_GEN_SPECS_REF
- [43] Campbell Scientific, CR10XTCR Thermocouple Reference Instruction Manual, <http://www.campbellsci.com/documents/manuals/cr10xtcr.pdf>
- [44] Exell, R.H.B. *Practical Mathematics: Error Analysis*, University of Technology Thonburi, <http://www.jgsee.kmutt.ac.th/exell/PracMath/ErrorAn.htm> (2001).
- [45] Omega Engineering Inc. *Turbine and Paddlewheel Flowmeters Flow Reference Section*, http://www.omega.com/green/pdf/turbine_paddle_ref.pdf.
- [46] Palmer, Gary, Segment Director, Omega Engineering Inc., gpalmer@omega.com.
- [47] National Institute of Standards and Technology (NIST), *Engineering Statistics Handbook*, <http://itl.nist.gov/div898/handbook/>, Updated 6/23/2010.
- [48] Hendron, R., Burch, J. *Tool for Generating Realistic Residential Hot Water Event Schedules*, Conference Paper, NREL/CP-550-47685, August 2010.
- [49] The Engineering Toolbox, Thermal Conductivity of Common Materials and Gases, http://www.engineeringtoolbox.com/thermal-conductivity-d_429.html
- [50] Hendron, R., Engebrecht, C., *Building America House Simulation Protocols*, National Renewable Energy Laboratory Building Technologies Program (Revised October 2010).
- [51] Thermal Energy System Specialists, *The TESS Component Libraries*, <http://www.tess-inc.com>.

- [52] Stiebel Eltron Dual Heat Exchanger Tanks, http://www.stiebel-eltron-usa.com/techdata_sbb.html (retrieved March 2011).
- [53] M. Martin, P. Berdahl, *Characteristics of Infrared Sky Radiation in the United States*, Lawrence Berkeley Laboratory, University of California - Berkeley, Solar Energy Vol. 33, No. 3/4, pp. 321-336, 1984.
- [54] Robert Hendron, *Building America Research Benchmark Definition, Updated December 20, 2007*, Technical Report. NREL/TP-550-42662 (January 2008).
- [55] Aron Dobos, Personal Communication, National Renewable Energy Laboratory, aron.dobos@nrel.gov. (April 20, 2011).
- [56] Bob Ramlow, *Solar Water Heating: A Comprehensive Guide to Solar Water and Space Heating Systems*, New Society Publishers, October 2009.
- [57] Hannah Cassard, *Break-even Cost for Residential Solar Water Heating in the United States: Key Drivers and Sensitivities*, NREL/TP-6A20-48986 (Feb 2011).
- [58] B. Polly, M. Gestwick, et al. *A Method for Determining Optimal Residential Energy Efficiency Retrofit Packages*, National Renewable Energy Laboratory Building Technologies Program (April 2011)
- [59] R. Anderson and D. Roberts, *Maximizing Residential Energy Savings: Net Zero Energy Home Technology Pathways*, Technical Report NREL/TP-550-44547 (November 2008)
- [60] Holman, J.P. *Experimental Methods for Engineers*. s.l. : McGraw-Hill, 1994. Sixth Edition.
- [61] California Center for Sustainable Energy, Data from California Solar Initiative Residential Solar Water Heater Program. Acquired by NREL: System Advisor Model (SAM) (November 2010).
- [62] Krarti, Moncef, *Energy Audit of Building Systems: An Engineering Approach*, CRC Press LLC (2000).
- [63] Haglund, Bruce, *Thermal Mass in Passive Solar and Energy-Conserving Buildings*, http://arch.ced.berkeley.edu/vitalsigns/res/downloads/rp/thermal_mass/mass-sml.pdf (1995).
- [64] Energy Information Administration, 2010. Electric power monthly – average retail Price of electricity to ultimate customers by end-use sector, by state. Retrieved May 11, 2011 from: http://www.eia.doe.gov/cneaf/electricity/epm/table5_6_b.html
- [65] Greg Barker, Personal Communications, Mountain Energy Partnership (February 2011).
- [66] Thermal Energy System Specialists (TESS). Type 534: Cylindrical Stratified Storage Tank with Immersed Heat Exchangers. TESS, Madison, Wisconsin, 2007.
- [67] Thermal Energy System Specialists (TESS). Type 539: Flat Plate Collector with Capacitance and Flow Modulation. TESS, Madison, Wisconsin, 2006.

Appendix A : Manufacturer Literature

<p>SOLAR COLLECTOR CERTIFICATION AND RATING</p>  <p>SRCC OG-100</p>	<p>CERTIFIED SOLAR COLLECTOR</p> <p>SUPPLIER: Heliodyne, Inc. 4910 Seaport Avenue Richmond, CA 94804 USA</p> <p>MODEL: 336 013</p> <p>COLLECTOR TYPE: Gobi Glazed Flat-Plate</p> <p>CERTIFICATION#: 2007026A</p>
--	--

COLLECTOR THERMAL PERFORMANCE RATING							
Megajoules Per Panel Per Day				Thousands of BTU Per Panel Per Day			
CATEGORY (Ti-Ta)	CLEAR DAY	MILDLY CLOUDY	CLOUDY DAY	CATEGORY (Ti-Ta)	CLEAR DAY	MILDLY CLOUDY	CLOUDY DAY
A (-5 °C)	36.8	27.8	18.9	A (-9 °F)	34.9	26.4	17.9
B (5 °C)	33.1	24.1	15.2	B (9 °F)	31.4	22.9	14.4
C (20 °C)	27.6	18.8	10.1	C (36 °F)	26.2	17.8	9.6
D (50 °C)	17.3	9.3	2.1	D (90 °F)	16.4	8.8	2.0
E (80 °C)	7.8	1.7	0.0	E (144 °F)	7.4	1.6	0.0

A- Pool Heating (Warm Climate) B- Pool Heating (Cool Climate) C- Water Heating (Warm Climate) D- Water Heating (Cool Climate) E- Air Conditioning

Original Certification Date: 17-OCT-07

COLLECTOR SPECIFICATIONS

Gross Area:	2.487 m ²	26.77 ft ²	Net Aperture Area:	2.29 m ²	24.64 ft ²
Dry Weight:	48.8 kg	108. lb	Fluid Capacity:	4.1 liter	1.1 gal
Test Pressure:	1103. kPa	160. psig			

COLLECTOR MATERIALS

Frame:	Aluminum Extrusion
Cover (Outer):	Low Iron Tempered Glass
Cover (Inner):	None

Pressure Drop

Flow		ΔP	
ml/s	gpm	Pa	in H ₂ O

Absorber Material:	Tube - Copper / Plate - Copper
Absorber Coating:	Black Chrome

Insulation Side:	Isocyanurate Foam
Insulation Back:	Isocyanurate Foam & Fiberglass

TECHNICAL INFORMATION

Efficiency Equation [NOTE: Based on gross area and (P)=Ti-Ta]	Y INTERCEPT	SLOPE
S I UNITS: $\eta = 0.701 - 3.73220 (P)/I - 0.01070 (P)^2/I$	0.703	-4.544 W/m²·°C
I P UNITS: $\eta = 0.701 - 0.65743 (P)/I - 0.00105 (P)^2/I$	0.703	-0.800 Btu/hr·ft²·°F

Incident Angle Modifier [(S)-1/cosθ - 1, 0°≤θ≤60°]	Model Tested:	Gobi 336 013
Ks & tau_{ext} = 1 0.040 (S) -0.291 (S) ²	Test Fluid:	Water
Ks & tau_{ext} = 1 -0.25 (S) Linear Fit	Test Flow Rate:	200 ml/s·m ² 0.0295 gpm/ft ²

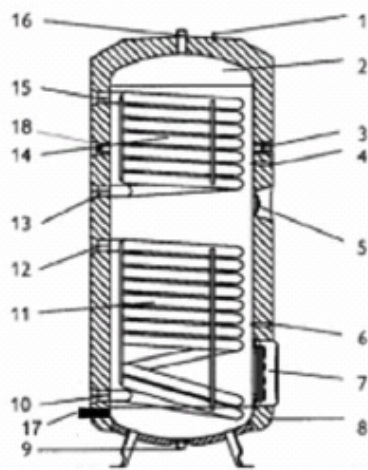
REMARKS:

December, 2010
 Certification must be renewed annually. For current status contact:
 SOLAR RATING & CERTIFICATION CORPORATION
 c/o FSEC • 1579 Clearlake Road • Cocoa, FL 32922 • (321) 638-1537 • Fax (321) 638-1010

Figure A.1: Solar Rating and Certification Corporation Rating for Heliodyne Flat Plate collector

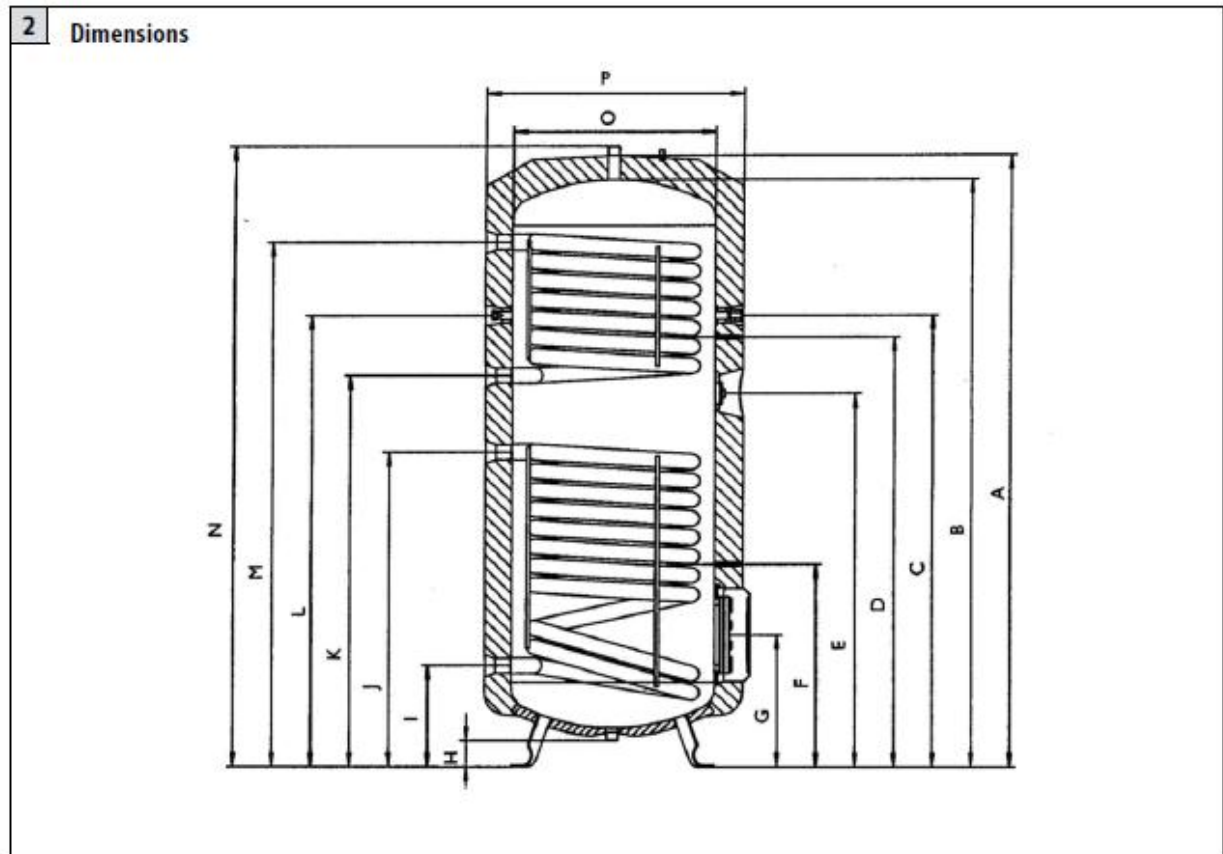
Dual Heat Exchanger Storage Tank (Stiebel Eltron SBB 400 Plus)

1 Components of the SBB S / SBB Plus



1. Sacrificial anode indicator
2. Glass lined steel tank
3. Thermometer well
4. Immersion sleeve for boiler temperature probe
5. Spare port
6. Immersion sleeve for solar temperature probe
7. Inspection port
8. Expanded polystyrene-thermal insulation
9. Cold water inlet (SBB 300 & 400 S/Plus)
10. Solar/main inlet
11. Solar/main heat exchanger
12. Solar/main return
13. Heat exchanger from boiler feed (SBB 300, 400, 600 Plus)
14. Upper heat exchanger (SBB 300, 400, 600 Plus)
15. Heat exchanger to boiler return (SBB 300, 400, 600 Plus)
16. Warm water outlet / T&P relief valve location
17. Cold water inlet (SBB 600 Plus)
18. Circulation port

Model Item no.		SBB 300 PLUS 187873	SBB 400 PLUS 187874	SBB 600 PLUS 187875
Contents				
Storage capacity	Gal / l	80.6 / 305	108.6 / 411	162.9 / 617
Volume of heat exchanger, top	Gal / l	1.9 / 7.3	2.2 / 8.2	2.5 / 9.6
Volume of heat exchanger, bottom	Gal / l	2.7 / 10.1	2.9 / 11.3	3.5 / 13.2
Pressure				
Working pressure	PSI / bar	150 / 10	150 / 10	150 / 10
Tested to pressure	PSI / bar	217 / 15	217 / 15	217 / 15
Max. pressure of boiler loop	PSI / bar	150 / 10	150 / 10	150 / 10
Temperature				
Max. temperature lower loop	°F / °C	203 / 95	203 / 95	203 / 95
Max. temperature of upper loop	°F / °C	203 / 95	203 / 95	203 / 95
Heat exchanger				
Surface area heat exchanger top	sq in / m ²	1705 / 1.1	2,015 / 1.3	2945 / 1.9
Surface area heat exchanger bottom	sq in / m ²	2325 / 1.5	2,635 / 1.7	3875 / 2.5
Weights				
Tank weight empty	lb. / kg	339 / 154	412 / 187	544 / 247
Tank weight full	lb. / kg	988 / 448	1,362 / 618	1,955 / 887
Other				
Standby losses in 24 hours	BTU / kWh	6,500 / 1.9	7500 / 2.2	10,000 / 2.9
Cold/hot water connection		for 1" copper pipe with adapters, provided with unit		



Type		SBB 300 s / Plus	SBB 400 s / Plus	SBB 600 Plus
A	Height of unit w/insulation	in/mm 66.1/1679	72.7/1848	68.3/1735
B	Height of unit without insulation	in/mm 63.3/1609	70.1/1781	65.7/1670
C	Height of well for temp. sensor	in/mm 46.4/1179	48.7/1238	46.9/1192
D	Height thermometer	in/mm 41.1/1045	43.0/1093	41.5/1055
E	Height spare port	in/mm 40.3/1025	42.4/1078	40.9/1040
F	Height of well for temp. sensor	in/mm 21.9/557	22.0/560	23.4/595
G	Height inspection flange	in/mm 14.4/365	14.4/367	15.9/405
H	Height cold water feed	in/mm 2.9/73	2.6/65	2.0/50
I	Height solar cold feed	in/mm 11.0/280	11.1/282	10.9/277
J	Height solar hot return	in/mm 34.0/865	34.1/867	33.9/862
K	Height heater hot boiler return	in/mm 38.4/975	44.5/1130	42.9/1089
L	Height circulation port	in/mm 52.7/1339	63.0/1600	57.2/1453
M	Height cold boiler feed	in/mm 52.7/1339	63.0/1600	57.2/1453
N	Overall height	in/mm 67.08/1704	73.74/1873	69.29/1760
O	Width without thermal insulation	in/mm 21.65/550	23.62/600	29.52/750
P	Width with thermal insulation	in/mm 27.55/700	29.52/750	36.22/920

Omega Turbine Flow Meter (FTB6107-A)

All models shown smaller than actual size.



MOST POPULAR MODELS HIGHLIGHTED!

To Order (Specify Model Number)										
Model No.	Price	MNPT Port Size (in)	Normal Operating Range	Min. Test Flow* (GPM)	Length of Body mm (in)	Diameter mm (in)	Overall Height mm (in)	Weight kg (lb)	"-PS" pulse/gal	Maximum Pressure Drop (psid)
Bronze Body (Horizontal Mounting Suggested)										
FTB6105-A	\$73	1/2"	1 to 20 GPM	0.125	191 (7.5)	102 (4.0)	133 (5.5)	1.9 (4.25)	230.0	8.5
FTB6107-A	73	1/2"	1 to 20 GPM	0.125	191 (7.5)	102 (4.0)	133 (5.5)	1.9 (4.25)	230.0	8.5
FTB6107A	113	3/4"	0.5 to 30 GPM	0.25	229 (9.0)	121 (4.75)	140 (5.5)	4.0 (8.75)	133.2	13.0
FTB6110	169	1.0"	0.75 to 50 GPM	0.5	273 (10.75)	179 (7.06)	176 (6.94)	6.0 (13.25)	60.0	11.5
FTB6115	475	1.5"	5 to 100 GPM	1.5	321 (12.63)	191 (7.5)	216 (8.5)	9.8 (21.6)	22.6	11.5
FTB6120	570	2.0"	8 to 160 GPM	2.0	387 (15.25)	222 (8.75)	260 (10.25)	17.6 (38.8)	16.28	12.75
Polymer Body (Horizontal Mounting Suggested)										
FTB6205	\$63	1/2"	0.25 to 20 GPM	0.13	191 (7.5)	121 (4.75)	137 (5.38)	1.4 (3.0)	200.0	11.5
FTB6207	63	3/4"	0.25 to 25 GPM	0.13	191 (7.5)	121 (4.75)	137 (5.38)	1.4 (3.0)	200.0	13.0
FTB6207X	88	3/4"	0.5 to 30 GPM	0.25	229 (9.0)	127 (5.0)	152 (5.97)	1.8 (4.0)	133.2	13.0
FTB6208	138	1	2 to 30 GPM	0.5	229 (9.0)	127 (5.0)	152 (5.97)	1.8 (4.0)	133.2	13.0

* Minimum measurable with 5% of reading accuracy. † Male NPT. †† Female NPT with adaptor flanges. Add suffix "-PT" for total only or "-PS" for rate and total for pulse output on FTB6000 Series. Add \$59 for "-PT"; add \$108 for "-PS". Register is hermetically sealed or weathertight with pulse output. Pulse option adds 3/8" to height. With "PT" pulse output option: 1 pulse/gal for 1" and smaller; 1 pulse/10 gal for 1 1/2" and 2". PT pulser is a contact closure rated at 3 A @ 125 Vac. Not compatible with FTB7000 Series. PS pulser is a solid state device that requires a 6 to 24 Vdc external source 3 wire with pull-up resistor.

FTB7000 Series (Must be mounted horizontally with register facing up)

Model No.	Price	FNPT Port Size (in)	Flow Range (GPM)	Cont. Duty (GPM)	Overall Length	"B" Dim. mm (in)	Width mm (in)	Ship Wt kg (lb)	Max Pressure Drop (psid)
Bronze Body									
FTB7115	\$652	1.5	3 to 200	160	254 (10)	80 (3.16)	187 (7.37)	10.9 (24.0)	9.0
FTB7120	723	2.0	3 to 200	160	254 (10)	80 (3.16)	187 (7.37)	13.2 (29.0)	9.0
FTB7130	1134	3.0	4 to 750	600	305 (12)	106 (4.16)	187 (7.37)	16.4 (36.0)	8.0
FTB7140	1795	4.0	7 to 1250	1000	356 (14)	127 (5.0)	217 (8.56)	27.3 (60.0)	9.0
FTB7160	3099	6.0	15 to 2500	2000	457 (18)	148 (5.84)	279 (11.00)	50.5 (111.0)	4.5

Add suffix "-LPR" or "-HPR" for pulse output for FTB7000. Add \$255 to list price for either. LPR is a 4-watt reed switch, rated 50 Vac/Vdc @ 50 mA. Pulse rate = 1 pulse/gal for 1 1/2" and 2"; 1 pulse/10 gal all larger sizes. HPR is a solid state optical pickup, 6 to 15 Vdc power input. 10 pulse/gal for 1 1/2" and 2"; 1 pulse/gal all larger sizes. Pulse option adds 0.34 kg (4 lb) to weight and 32 mm (1 1/4") to height.

Combination Meters (Must be mounted horizontally with register facing up)

Model No.	Price	FNPT Port Size (in)	Flow Range (GPM)	Cont. Duty (GPM)	Overall Length mm (in)	Width mm (in)	Ship Wt kg (lb)	
FTB6720	\$1591	2	0.25 to 160	100	432 (17.0)	319 (12.56)	15.5 (34.0)	
FTB6730	2268	3	0.25 to 650	325	432 (17.0)	337 (13.25)	25.1 (55.25)	
FTB6740	2951	4	0.25 to 1150	575	508 (20.0)	359 (14.12)	30.5 (67.12)	
FTB6760	5669	6	0.75 to 2500	1560	502 (19.75)	446 (17.56)	78.2 (172.0)	
ME-1868	100	Reference Book: Turbulent Flow						

Comes with complete operator's manual.

Ordering Example: FTB7160-LPR, 6" bronze body long-life water meter with 15 to 2500 gpm range and pulser, \$3099 + 255 = \$3354.

F

CR10XTCR Thermocouple Reference

1. General

The Model CR10XTCR Probe contains a thermistor for measuring temperature and is used as a reference temperature for thermocouples measured with the CR10X. It is installed between the two terminal stripes in the wiring panel. After all the thermocouples are wired, the wiring panel cover is installed to minimize temperature gradients on the terminal strip.

1.1 Specifications

Temperature Measurement Range: -35° to +50°C

Thermistor Interchangeability Error: Typically $<\pm 0.2^{\circ}\text{C}$ over 0°C to 60°C ± 0.4 @ -35°C .

Polynomial Linearization Error: $<\pm 0.5^{\circ}\text{C}$ over -35°C to $+50^{\circ}\text{C}$.

2. Accuracy — Temperature Sensor

The overall probe accuracy is a combination of the thermistor's interchangeability specification, the precision of the bridge resistors, and the polynomial error. In a "worst case" all errors add to an accuracy of $\pm 0.4^{\circ}\text{C}$ over the range of -24° to 48°C and $\pm 0.9^{\circ}\text{C}$ over the range of -38°C to 53°C . The major error component is the interchangeability specification of the thermistor, tabulated in Table 1. For the range of 0° to 50°C the interchangeability error is predominantly offset. The bridge resistors are 0.1% tolerance with a 10 ppm temperature coefficient. Polynomial errors are tabulated in Table 2 and plotted in Figure 1.

TABLE 1. Thermistor Interchangeability Specification

Temperature (°C)	Temperature Tolerance ($\pm^{\circ}\text{C}$)
-40	0.40
-30	0.40
-20	0.32
-10	0.25
0 to +50	0.20

TABLE 2. Polynomial Error	
-40 to +56	$<\pm 1.0^{\circ}\text{C}$
-38 to +53	$<\pm 0.5^{\circ}\text{C}$
-24 to +48	$<\pm 0.1^{\circ}\text{C}$

Appendix B : Building Specifications for Modeling

Table B.1: Building Specifications for 1960 Retrofit House

	San Fran	Phoenix	Denver	Chicago	Atlanta	Boston
Ceiling R-Value [hr-ft ² -F/Btu]	38	38	49	49	38	49
Wood Frame Wall R-Value [hr-ft ² -F/Btu]	13	13	13	13	13	13
Floor insulation [hr-ft ² -F/Btu]	13	11	19	19	13	19
Basement Wall [hr-ft ² -F/Btu]	0	0	6	6	0	6
Slab, 2ft depth [hr-ft ² -F/Btu]	0	0	0	0	0	0
Fenestration U-Factor [Btu/hr-ft ² ·°F]	0.87	0.87	0.87	0.87	0.87	0.87
Window SHGC	0.62	0.62	0.62	0.62	0.62	0.62
Specific Leakage Area	0.0009	0.0009	0.0009	0.0009	0.0009	0.0009

Table B.2: Building Specifications for IECC 2009 House

	San Fran	Phoenix	Denver	Chicago	Atlanta	Boston
Ceiling R-Value [hr-ft ² -F/Btu]	30	30	38	38	30	38
Wood Frame Wall R-Value [hr-ft ² -F/Btu]	13	13	18	18	13	18
Floor insulation [hr-ft ² -F/Btu]	19	13	30	30	19	30
Basement Wall [hr-ft ² -F/Btu]	0	0	10	10	0	10
Slab, 2ft depth [hr-ft ² -F/Btu]	4	0	0	0	0	0
Fenestration U-Factor [Btu/hr-ft ² ·°F]	0.35	0.4	0.35	0.35	0.4	0.35
Window SHGC	0.35	0.3	0.35	0.35	0.35	0.3
Specific Leakage Area	0.00036	0.00036	0.00036	0.00036	0.00036	0.00036

Table B.3: Building Specifications for Building America 50 percent House

	San Fran	Phoenix	Denver	Chicago	Atlanta	Boston
Ceiling R-Value [hr-ft ² -F/Btu]	50	30	50	50	50	50
Wood Frame Wall R-Value [hr-ft ² -F/Btu]	27	19	25	25	21	25
Floor insulation [hr-ft ² -F/Btu]	19	13	30	30	19	30
Basement Wall [hr-ft ² -F/Btu]	0	0	13	13	0	13
Slab, 2ft depth [hr-ft ² -F/Btu]	4	0	0	0	0	0
Fenestration U-Factor [Btu/hr-ft ² ·°F]	0.29	0.3	0.25	0.25	0.3	0.25
Window SHGC	0.3	0.26	0.35	0.35	0.26	0.35
Specific Leakage Area	0.0003	0.0003	0.00015	0.00015	0.0003	0.00015

Table B.1: TRNSYS Type 56 Inputs for 1960 Retrofit House

	San Fran	Phoenix	Denver	Chicago	Atlanta	Boston
Ceiling U-Value [W/m ² -K]	0.149	0.149	0.116	0.116	0.149	0.116
Wall U-Value [W/m ² -K]	0.437	0.437	0.437	0.437	0.437	0.437
Floor insulation U-Value [W/m ² -K]	0.437	0.516	0.299	0.299	0.437	0.299
Basement Wall U-Value [W/m ² -K]	N/A	N/A	0.946	0.946	N/A	0.946
Slab, 2ft depth [W/m ² -K]	N/A	N/A	N/A	N/A	N/A	N/A
Fenestration U-Factor [W/m ² -K]	3.200	2.540	2.540	2.540	5.160	2.540
Window SHGC	0.698	0.440	0.440	0.440	0.682	0.440
Window Selected in TRNSYS	Insulating, 2.8	FLOAT_19	Luxguard SINGUARD CLEAR Argon	CLEAR Argon	FLOAT_19	CLEAR Argon

Table B.1: TRNSYS Type 56 inputs for IECC 2009 House

	San Fran	Phoenix	Denver	Chicago	Atlanta	Boston
Ceiling U-Value [W/m2-K]	0.189	0.189	0.149	0.149	0.189	0.149
Wall U-Value [W/m2-K]	0.437	0.437	0.315	0.315	0.437	0.315
Floor insulation U-Value [W/m2-K]	0.299	0.437	0.189	0.189	0.299	0.189
Basement Wall U-Value [W/m2-K]	N/A	N/A	0.568	0.568	N/A	0.568
Slab, 2ft depth [W/m2-K]	1.420	N/A	N/A	N/A	N/A	N/A
Fenestration U-Factor [W/m2-K]	2.540	2.830	1.430	1.430	2.540	1.430
Window SHGC	0.440	0.755	0.605	0.605	0.440	0.605
Window Selected in TRNSYS	Clear Argon	Insulating, 2.8	Clear Plus Argon	Clear Plus Argon	Insulating, 2.8	Clear Plus Argon

Table B.1: TRNSYS Type 56 inputs for Building America 50 percent House

	San Franc	Phoenix	Denver	Chicago	Atlanta	Boston
Ceiling U-Value [W/m ² -K]	0.114	0.189	0.114	0.114	0.114	0.114
Wall U-Value [W/m ² -K]	0.210	0.299	0.227	0.227	0.270	0.227
Floor insulation U-Value [W/m ² -K]	0.299	0.437	0.189	0.189	0.299	0.189
Basement Wall U-Value [W/m ² -K]	N/A	N/A	0.437	0.437	N/A	0.437
Slab, 2ft depth [W/m ² -K]	1.420	N/A	N/A	N/A	N/A	N/A
Fenestration U-Factor [W/m ² -K]	2.3	1.3	1.29	1.29	2.3	1.29
Window SHGC	0.295	0.298	0.330	0.330	0.295	0.330
Window Selected in TRNSYS	LowE Argon Silver	LowE Argon	LowE Ar	LowE Ar	LowEArgon	LowE Ar

Appendix C : Tank Heat Exchanger Calibration Tables

Table C.1: Variation of tank UA, heat exchanger length, and number of tank nodes on the lower heat exchanger RSME [kJ/hr]

UA [W/C]	Heat Exchanger Length [m]	Number of Nodes					
		10node s	12node s	14node s	16node s	18node s	20node s
2.3	15.85	614.13	599.23	587.08	577.08	572.09	574.34
	16.76	577.08	561.79	551.82	542.32	539.37	538.52
	17.68	549.55	534.49	522.99	519.67	513.14	515.26
	18.59	554.15	537.25	522.53	517.83	508.54	510.66
	19.51	603.24	581.29	562.78	557.73	548.22	551.49
2.2	15.85	626.66	611.46	599.06	588.86	583.76	586.06
	16.76	607.45	591.36	580.86	570.86	567.76	566.86
	17.68	597.33	580.96	568.46	564.86	557.76	560.06
	18.59	602.33	583.96	567.96	562.86	552.76	555.06
	19.51	609.33	587.16	568.46	563.36	553.76	557.06
2.1	15.85	939.99	917.19	898.59	883.29	875.64	879.09
	16.76	728.94	709.63	697.03	685.03	681.31	680.23
	17.68	686.93	668.11	653.73	649.59	641.43	644.07
	18.59	668.59	648.20	630.44	624.78	613.57	616.12
	19.51	731.20	704.59	682.15	676.03	664.51	668.47
2	15.85	1597.99	1559.23	1527.61	1501.60	1488.59	1494.46
	16.76	1122.57	1092.84	1073.43	1054.95	1049.22	1047.56
	17.68	989.18	962.07	941.37	935.41	923.65	927.46
	18.59	962.77	933.41	907.83	899.68	883.54	887.21
	19.51	1169.92	1127.35	1091.45	1081.66	1063.22	1069.56

Table C.2: Variation of tank UA, heat exchanger length, and number of tank nodes on the lower heat exchanger chi-squared values

UA [W/C]	Heat Exchanger Length [m]	Number of Nodes					
		10node s	12node s	14node s	16node s	18node s	20node s
2.3	15.85	1.14	1.11	1.09	1.07	1.06	1.06
	16.76	1.07	1.04	1.02	1.00	1.00	1.00
	17.68	1.02	0.99	0.97	0.96	0.95	0.95
	18.59	1.03	0.99	0.97	0.96	0.94	0.95
	19.51	1.12	1.08	1.04	1.03	1.02	1.02
2.2	15.85	1.16	1.13	1.11	1.09	1.08	1.09
	16.76	1.12	1.10	1.08	1.06	1.05	1.05
	17.68	1.11	1.08	1.05	1.05	1.03	1.04
	18.59	1.12	1.08	1.05	1.04	1.02	1.03
	19.51	1.13	1.09	1.05	1.04	1.03	1.03
2.1	15.85	1.74	1.70	1.66	1.64	1.62	1.63
	16.76	1.35	1.31	1.29	1.27	1.26	1.26
	17.68	1.27	1.24	1.21	1.20	1.19	1.19
	18.59	1.24	1.20	1.17	1.16	1.14	1.14
	19.51	1.35	1.30	1.26	1.25	1.23	1.24
2	15.85	2.96	2.89	2.83	2.78	2.76	2.77
	16.76	2.08	2.02	1.99	1.95	1.94	1.94
	17.68	1.83	1.78	1.74	1.73	1.71	1.72
	18.59	1.78	1.73	1.68	1.67	1.64	1.64
	19.51	2.17	2.09	2.02	2.00	1.97	1.98

Table C.3: Variation of tank UA, heat exchanger length, and number of tank nodes on the upper heat exchanger RSME [kJ/hr]

UA [W/C]	Heat Exchanger Length [m]	Number of Nodes					
		10node s	12node s	14node s	16node s	18node s	20node s
2.3	11.89	1520.52	1442.95	1349.97	1316.00	1277.78	1286.27
	12.80	1323.56	1231.96	1147.73	1097.17	1061.89	1089.33
	13.72	1297.57	1191.76	1090.06	1021.06	967.10	994.08
	14.63	1298.27	1201.16	1091.85	984.13	910.77	918.49
	15.54	1332.97	1216.15	1080.84	991.57	919.07	926.70
2.2	11.89	1169.63	1109.97	1059.63	1032.97	1002.97	1009.63
	12.80	1102.97	1026.63	975.97	932.97	902.97	926.30
	13.72	1099.63	1009.97	942.63	882.97	836.30	859.63
	14.63	1109.63	1026.63	942.63	849.63	786.30	792.97
	15.54	1129.63	1030.63	944.30	866.30	802.97	809.63
2.1	11.89	1754.45	1664.95	1589.45	1549.45	1504.45	1514.45
	12.80	1323.56	1231.96	1171.16	1119.56	1083.56	1111.56
	13.72	1264.58	1161.46	1084.03	1015.41	961.74	988.58
	14.63	1231.69	1139.56	1065.17	943.09	880.65	880.19
	15.54	1355.56	1236.76	1133.16	1039.56	963.56	971.56
2	11.89	2982.56	2830.41	2702.06	2634.06	2557.56	2574.56
	12.80	2038.28	1897.22	1803.58	1724.12	1668.68	1711.80
	13.72	1820.99	1672.50	1561.00	1462.19	1384.91	1423.55
	14.63	1731.02	1595.39	1533.85	1329.76	1268.14	1293.88
	15.54	2168.89	1978.81	1813.05	1663.29	1541.69	1554.49

Table C.4: Variation of tank UA, heat exchanger length, and number of tank nodes on the upper heat exchanger chi-square values

UA [W/C]	Heat Exchanger Length [m]	Number of Nodes					
		10nodes	12nodes	14nodes	16nodes	18nodes	20nodes
2.3	11.89	1.90	1.80	1.69	1.64	1.60	1.61
	12.80	1.65	1.54	1.43	1.37	1.33	1.36
	13.72	1.62	1.49	1.36	1.28	1.21	1.24
	14.63	1.62	1.50	1.36	1.23	1.14	1.15
	15.54	1.67	1.52	1.35	1.24	1.15	1.16
2.2	11.89	1.46	1.39	1.32	1.29	1.25	1.26
	12.80	1.38	1.28	1.22	1.17	1.13	1.16
	13.72	1.37	1.26	1.18	1.10	1.05	1.07
	14.63	1.39	1.28	1.18	1.06	0.98	0.99
	15.54	1.41	1.29	1.18	1.08	1.00	1.01
2.1	11.89	2.19	2.08	1.99	1.94	1.88	1.89
	12.80	1.65	1.54	1.46	1.40	1.35	1.39
	13.72	1.58	1.45	1.36	1.27	1.20	1.24
	14.63	1.54	1.42	1.33	1.18	1.10	1.10
	15.54	1.69	1.55	1.42	1.30	1.20	1.21
2	11.89	3.73	3.54	3.38	3.29	3.20	3.22
	12.80	2.55	2.37	2.25	2.16	2.09	2.14
	13.72	2.28	2.09	1.95	1.83	1.73	1.78
	14.63	2.16	1.99	1.92	1.66	1.59	1.62
	15.54	2.71	2.47	2.27	2.08	1.93	1.94

Appendix D : TRNSYS Deck File for Calibrated Combisystem

Model

```
VERSION 17
*****
**
*** TRNSYS input file (deck) generated by TrnsysStudio
*** on Monday, June 06, 2011 at 18:44
*** from TrnsysStudio project: C:\Documents and Settings\jsustar\My
Documents\ParaStudy\CE\D\A\CEDA.tpf
***
*** If you edit this file, use the File/Import TRNSYS Input File function in
*** TrnsysStudio to update the project.
***
*** If you have problems, questions or suggestions please contact your local
*** TRNSYS distributor or mailto:software@cstb.fr
***
*****
**

*****
**
*** Units
*****
**

*****
**
*** Control cards
*****
**
* START, STOP and STEP
CONSTANTS 5
START=0
STOP=8760
STEP=0.016666666
CArea = 32! ft2
High = 0.6
* User defined CONSTANTS

SIMULATION   START      STOP  STEP ! Start time      End time      Time step
TOLERANCES  0.001  0.0001      ! Integration      Convergence
LIMITS 1000 1000 1001      ! Max iterations  Max warnings
          Trace limit

DFQ 1          ! TRNSYS numerical integration solver method
WIDTH 80      ! TRNSYS output file width, number of
characters
NOLIST          ! NOLIST statement
```

```

                                ! MAP statement
SOLVER 0 1 1                    ! Solver statement           Minimum
relaxation factor Maximum relaxation factor
NAN_CHECK 0                     ! Nan DEBUG statement
OVERWRITE_CHECK 0              ! Overwrite DEBUG statement
TIME_REPORT 0                  ! disable time report
EQSOLVER 0                     ! EQUATION SOLVER statement

* Model "controller" (Type 2)
*

UNIT 3 TYPE 2      controller
*$UNIT_NAME controller
*$MODEL .\Controllers\Differential Controller w_ Hysteresis\for
Temperatures\Solver 0 (Successive Substitution) Control Strategy\Type2b.tmf
*$POSITION 355 205
*$LAYER Main #
*$# NOTE: This control strategy can only be used with solver 0 (Successive
substitution)
*$#
PARAMETERS 2
5          ! 1 No. of oscillations
CutOutTemp      ! 2 High limit cut-out
INPUTS 6
13,1          ! Coll:Outlet temperature ->Upper input temperature Th
26,28         ! Type534-Coiled:Tank nodal temperature-14 ->Lower input
temperature Tl
26,1          ! Type534-Coiled:Temperature at outlet ->Monitoring temperature
Tin
3,1           ! controller:Output control function ->Input control function
0,0           ! [unconnected] Upper dead band dT
0,0           ! [unconnected] Lower dead band dT
*** INITIAL INPUT VALUES
20.0 20 200 0 10.0 2.0
*-----
--

* Model "Sim Int" (Type 24)
*

UNIT 5 TYPE 24      Sim Int
*$UNIT_NAME Sim Int
*$MODEL .\Utility\Integrators\Quantity Integrator\TYPE24.tmf
*$POSITION 282 549
*$LAYER Main #
PARAMETERS 2
STOP          ! 1 Integration period
0             ! 2 Relative or absolute start time
INPUTS 15
Solar         ! Losses:Solar ->Qsol-1
26,10         ! Type534-Coiled:Auxiliary heating rate ->Qauxtank-2
0,0           ! [unconnected] Qauxsph-3
19,3          ! SolPmp:Power consumption ->Qpumpsol-4
51,3          ! SpHPmp:Power consumption ->Qpumpsph-5
Tanklosstotal ! Losses:Tanklosstotal ->Qtankloss-6
26,5          ! Type534-Coiled:Energy delivered to flow ->Qdhw-7
26,42         ! Type534-Coiled:Energy delivered to HX-1 ->Qsphaux-8

```

```

12,24          ! Weather:Total tilted surface radiation for surface-1 -
>Qinc-9
13,3          ! Coll:Useful energy gain ->Quseful-10
26,2          ! Type534-Coiled:Flow rate at outlet ->DHWconsump-11
26,46         ! Type534-Coiled:Energy delivered to HX-2 ->Qsphsol-12
26,1          ! Type534-Coiled:Temperature at outlet ->Thot-13
26,3          ! Type534-Coiled:Average tank temperature ->Ttank-14
32,1          ! Type56: 1- TAIR_MAIN ->Thouse-15
*** INITIAL INPUT VALUES
0.0 0.0 0.0 0.0 0.0 0.0 0.0 0.0 0.0 0.0 0.0 0.0 0.0 0.0 0.0

```

--

* Model "Daily Integration" (Type 24)

*

```

UNIT 6 TYPE 24      Daily Integration
*$UNIT_NAME Daily Integration
*$MODEL  .\Utility\Integrators\Quantity Integrator\TYPE24.tmf
*$POSITION 279 401
*$LAYER Outputs #
PARAMETERS 2
24          ! 1 Integration period
0           ! 2 Relative or absolute start time
INPUTS 12
Solar       ! Losses:Solar ->Qsol-1
26,10      ! Type534-Coiled:Auxiliary heating rate ->Qauxtank-2
0,0        ! [unconnected] Qauxaph-3
19,3       ! SolPmp:Power consumption ->Qpumpsol-4
51,3       ! SpHPmp:Power consumption ->Qpumpsph-5
Tanklosstotal ! Losses:Tanklosstotal ->Qtankloss-6
26,5       ! Type534-Coiled:Energy delivered to flow ->Qdhw-7
26,42      ! Type534-Coiled:Energy delivered to HX-1 ->Qsphaux-8
12,24      ! Weather:Total tilted surface radiation for surface-1 -
>Qinc-9
13,3       ! Coll:Useful energy gain ->Quseful-10
26,2       ! Type534-Coiled:Flow rate at outlet ->DHWConsump-11
26,46      ! Type534-Coiled:Energy delivered to HX-2 ->Qsphsol-12
*** INITIAL INPUT VALUES
0.0 0.0 0.0 0.0 0.0 0.0 0.0 0.0 0.0 0.0 0.0 0.0

```

--

* Model "Daily Results" (Type 25)

*

```

UNIT 9 TYPE 25      Daily Results
*$UNIT_NAME Daily Results
*$MODEL  .\Output\Printer\Unformatted\No Units\Type25c.tmf
*$POSITION 607 399
*$LAYER Main #
PARAMETERS 10
24          ! 1 Printing interval
START       ! 2 Start time
STOP        ! 3 Stop time
45          ! 4 Logical unit
0           ! 5 Units printing mode

```

```

0          ! 6 Relative or absolute start time
-1         ! 7 Overwrite or Append
-1         ! 8 Print header
0          ! 9 Delimiter
1          ! 10 Print labels
INPUTS 14
6,1       ! Daily Integration:Qsol-1 ->Input to be printed-1
6,2       ! Daily Integration:Qauxtank-2 ->Input to be printed-2
6,3       ! Daily Integration:Qauxsph-3 ->Input to be printed-3
6,4       ! Daily Integration:Qpumpsol-4 ->Input to be printed-4
6,5       ! Daily Integration:Qpumpsph-5 ->Input to be printed-5
6,6       ! Daily Integration:Qtankloss-6 ->Input to be printed-6
6,7       ! Daily Integration:Qdhw-7 ->Input to be printed-7
6,8       ! Daily Integration:Qsphaux-8 ->Input to be printed-8
6,9       ! Daily Integration:Qinc-9 ->Input to be printed-9
6,10      ! Daily Integration:Quseful-10 ->Input to be printed-10
6,11      ! Daily Integration:DHWconsump-11 ->Input to be printed-11
FSol_d     ! Efficiencies:FSol_d ->Input to be printed-12
EtaColl_d  ! Efficiencies:EtaColl_d ->Input to be printed-13
6,12      ! Daily Integration:Qsphsol-12 ->Input to be printed-14
*** INITIAL INPUT VALUES
Qsol Qauxtank Qauxsph Qpumpsol Qpumpsph Qtankloss Qdhw Qsph_aux Qinc
Quseful DHWConsump FSol etacoll Qsph_sol
*** External files
ASSIGN "ComE_d.txt" 45
*|? Output file for printed results |1000
*-----
--

* EQUATIONS "Efficiencies"
*
EQUATIONS 6
EtaColl_d = [6,10] / (CollectorArea*[6,9]+1e-6)
FSol_d = 1 - ( [6,2] / ([6,7] + [6,8] + [6,12]+1e-6) )
EtaColl = ([5,10] / (CollectorArea*[5,9]+1e-6))*100
FSol = (1 - ( [5,2] / ([5,7] + [5,8] + [5,12]+1e-6) ))*100
EtaColl_m = [61,10] / (CollectorArea*[61,9]+1e-6)
FSol_m = 1 - ( [61,2] / ([61,7] + [61,8] + [61,12] + 1e-6) )
*$UNIT_NAME Efficiencies
*$LAYER Main
*$POSITION 425 445

*-----
--

* Model "Totals" (Type 25)
*
UNIT 11 TYPE 25      Totals
*$UNIT_NAME Totals
*$MODEL .\Output\Printer\Unformatted\No Units\Type25c.tmf
*$POSITION 585 465
*$LAYER Weather - Data Files #
PARAMETERS 10
STOP          ! 1 Printing interval
STOP          ! 2 Start time

```

```

STOP          ! 3 Stop time
46           ! 4 Logical unit
0            ! 5 Units printing mode
0            ! 6 Relative or absolute start time
-1           ! 7 Overwrite or Append
-1           ! 8 Print header
0            ! 9 Delimiter
1            ! 10 Print labels
INPUTS 14
5,1          ! Sim Int:Qsol-1 ->Input to be printed-1
5,2          ! Sim Int:Qauxtank-2 ->Input to be printed-2
5,3          ! Sim Int:Qauxsph-3 ->Input to be printed-3
5,4          ! Sim Int:Qpumpsol-4 ->Input to be printed-4
5,5          ! Sim Int:Qpumpsph-5 ->Input to be printed-5
5,6          ! Sim Int:Qtankloss-6 ->Input to be printed-6
5,7          ! Sim Int:Qdhw-7 ->Input to be printed-7
5,8          ! Sim Int:Qsphaux-8 ->Input to be printed-8
5,9          ! Sim Int:Qinc-9 ->Input to be printed-9
5,10         ! Sim Int:Quseful-10 ->Input to be printed-10
5,11         ! Sim Int:DhwConsump-11 ->Input to be printed-11
FSol         ! Efficiencies:FSol ->Input to be printed-12
EtaColl      ! Efficiencies:EtaColl ->Input to be printed-13
5,12         ! Sim Int:Qsphsol-12 ->Input to be printed-14
*** INITIAL INPUT VALUES
Qsol Qauxtank Qauxsph Qpumpsol Qpumpsph Qtankloss Qdhw Qsph_aux Qinc
Quseful DHWconsump FSol etacoll Qsph_sol
*** External files
ASSIGN "ComE_t.txt" 46
*|? Output file for printed results |1000
-----
--
* Model "Weather" (Type 15)
*
UNIT 12 TYPE 15      Weather
*$UNIT_NAME Weather
*$MODEL .\Weather Data Reading and Processing\Standard Format\Energy+ Weather
Files (EPW)\Type15-3.tmf
*$POSITION 136 172
*$LAYER Main #
PARAMETERS 27
3            ! 1 File Type
47           ! 2 Logical unit
3            ! 3 Tilted Surface Radiation Mode
0.2         ! 4 Ground reflectance - no snow
0.7         ! 5 Ground reflectance - snow cover
7           ! 6 Number of surfaces
1           ! 7 Tracking mode-1
Cslope      ! 8 Slope of surface-1
CAzim       ! 9 Azimuth of surface-1
1           ! 10 Tracking mode-2
NSlope      ! 11 Slope of surface-2
NAzim       ! 12 Azimuth of surface-2
1           ! 13 Tracking mode-3
SSlope      ! 14 Slope of surface-3
SAzim       ! 15 Azimuth of surface-3

```

```

1          ! 16 Tracking mode-4
ESlope     ! 17 Slope of surface-4
EAzim      ! 18 Azimuth of surface-4
1          ! 19 Tracking mode-5
WSlope     ! 20 Slope of surface-5
WAzim      ! 21 Azimuth of surface-5
1          ! 22 Tracking mode-6
NRSlope    ! 23 Slope of surface-6
NRAzim     ! 24 Azimuth of surface-6
1          ! 25 Tracking mode-7
SRSlope    ! 26 Slope of surface-7
SRAzim     ! 27 Azimuth of surface-7
*** External files
ASSIGN "C:\Documents and Settings\jsustar\My
Documents\ParaStudy\Weather\USA_CO_Boulder-Broomfield-
Jefferson.County.AP_TMY3.epw" 47
*|? Which file contains the Energy+ weather data? |1000
*-----
--

* Model "Coll" (Type 539)
*

UNIT 13 TYPE 539 Coll
*$UNIT_NAME Coll
*$MODEL .\Solar Library (TESS)\Flat Plate Solar Collector\Type539.tmf
*$POSITION 373 98
*$LAYER Main #
*$# This component sets the flow rate for all connected flow loop components
if the variable speed option is enabled.
PARAMETERS 16
1          ! 1 Number in series
CollectorArea ! 2 Collector area
CpColl       ! 3 Fluid specific heat
1          ! 4 Collector test mode
FRta        ! 5 Intercept efficiency (a0)
FRUL        ! 6 1st order efficiency coefficient (a1)
FRUL2       ! 7 2nd order efficiency coefficient (a2)
TestFlow    ! 8 Tested flow rate per unit area
4.18       ! 9 Fluid specific heat at test conditions
B0          ! 10 1st-order IAM coefficient
0.0        ! 11 2nd-order IAM coefficient
0.0        ! 12 Minimum flowrate
10000.0     ! 13 Maximum flowrate
CollCapac   ! 14 Capacitance of Collector
50         ! 15 Number of Nodes
30.5       ! 16 Initial Temperature
INPUTS 10
19,1       ! SolPmp:Outlet fluid temperature ->Inlet temperature
19,2       ! SolPmp:Outlet flow rate ->Inlet flowrate
12,1       ! Weather:Dry bulb temperature ->Ambient temperature
12,31      ! Weather:Beam radiation for surface-1 ->Beam radiation on
the tilted surface
12,38      ! Weather:Sky diffuse radiation for surface-1 ->Sky diffuse
radiation on tilted surface
12,45      ! Weather:Ground reflected diffuse radiation for surface-1
->Ground-reflected diffuse radiation on tilted surface

```

```

12,59          ! Weather:Angle of incidence for surface-1 ->Incidence
angle
12,66          ! Weather:Slope of surface-1 ->Collector slope
0,0           ! [unconnected] Pump Control Specification
0,0           ! [unconnected] Outlet Temperature Setpoint
*** INITIAL INPUT VALUES
20.0 100.0 10.0 0.0 0.0 0.0 45.0 45 0 40
*-----
--

```

```

* Model "IPipe-2" (Type 31)
*

```

```

UNIT 14 TYPE 31    IPipe-2
*$UNIT_NAME IPipe-2
*$MODEL .\Hydronics\Pipe_Duct\Type31.tmf
*$POSITION 342 251
*$LAYER Outputs #
TRACE START STOP
PARAMETERS 6
PipeID          ! 1 Inside diameter
PipeL_ITC       ! 2 Pipe length
PipeUvalue      ! 3 Loss coefficient
DensColl        ! 4 Fluid density
CpColl          ! 5 Fluid specific heat
Tglycol_initial ! 6 Initial fluid temperature
INPUTS 3
26,37           ! Type534-Coiled:Temperature at HX Outlet-3 ->Inlet
temperature
26,38           ! Type534-Coiled:HX flow rate-3 ->Inlet flow rate
32,1            ! Type56: 1- TAIR_MAIN ->Environment temperature
*** INITIAL INPUT VALUES
10.0 100.0 20
*-----
--

```

```

* Model "OPipe-2" (Type 31)
*

```

```

UNIT 15 TYPE 31    OPipe-2
*$UNIT_NAME OPipe-2
*$MODEL .\Hydronics\Pipe_Duct\Type31.tmf
*$POSITION 265 251
*$LAYER Main #
TRACE START STOP
PARAMETERS 6
PipeID          ! 1 Inside diameter
PipeL_OTC       ! 2 Pipe length
PipeUvalue      ! 3 Loss coefficient
DensColl        ! 4 Fluid density
CpColl          ! 5 Fluid specific heat
Tglycol_initial ! 6 Initial fluid temperature
INPUTS 3
14,1            ! IPipe-2:Outlet temperature ->Inlet temperature
14,2            ! IPipe-2:Outlet flow rate ->Inlet flow rate
12,1            ! Weather:Dry bulb temperature ->Environment temperature
*** INITIAL INPUT VALUES

```



```

10.0 100.0 10.0
*-----
--

* Model "Opipe" (Type 31)
*

UNIT 16 TYPE 31    Opipe
*$UNIT_NAME Opipe
*$MODEL .\Hydronics\Pipe_Duct\Type31.tmf
*$POSITION 460 116
*$LAYER Main #
TRACE START STOP
PARAMETERS 6
PipeID           ! 1 Inside diameter
PipeL_OTC        ! 2 Pipe length
PipeUvalue       ! 3 Loss coefficient
DensColl         ! 4 Fluid density
CpColl           ! 5 Fluid specific heat
20               ! 6 Initial fluid temperature
INPUTS 3
13,1             ! Coll:Outlet temperature ->Inlet temperature
13,2             ! Coll:Outlet flow rate ->Inlet flow rate
12,1             ! Weather:Dry bulb temperature ->Environment temperature
*** INITIAL INPUT VALUES
10.0 100.0 10.0
*-----
--

* Model "IPipe" (Type 31)
*

UNIT 17 TYPE 31    IPipe
*$UNIT_NAME IPipe
*$MODEL .\Hydronics\Pipe_Duct\Type31.tmf
*$POSITION 540 116
*$LAYER Outputs #
TRACE START STOP
PARAMETERS 6
PipeID           ! 1 Inside diameter
PipeL_ITC        ! 2 Pipe length
PipeUvalue       ! 3 Loss coefficient
DensColl         ! 4 Fluid density
CpColl           ! 5 Fluid specific heat
Tglycol_initial  ! 6 Initial fluid temperature
INPUTS 3
16,1             ! Opipe:Outlet temperature ->Inlet temperature
16,2             ! Opipe:Outlet flow rate ->Inlet flow rate
32,1             ! Type56: 1- TAIR_MAIN ->Environment temperature
*** INITIAL INPUT VALUES
10.0 100.0 20
*-----
--

* EQUATIONS "Collector"
*
EQUATIONS 20

```

```

CollSlope = 39+15!Tilt for combi
CollAz = 0.0
CollectorArea = CArea/10.7639!m2
NumCollSer = 1
FRta = 0.701
FRUL = 3.7322*3.6!kJ/hr-m2-C = 0.577
FRUL2 = 0.0107*3.6!kJ/hr-m2-C2
B0 = -0.26
TestFlow = 20*3.6*1.04!convert ml/s to kg/hr for 50%glycol
PipeID = 0.75 /39.3701!pipe inside diameter
PipeL_ITC = 25.0 /3.2808!to collector indoor length
PipeL_OTC = 5.0 /3.2808!to collector outdoor length
PipeL_IFC = 25.0 /3.2808!from collector inside length
PipeL_OFC = 5.0 /3.2808!from collector outdoor length
PipeRvalue = 2.5/5.678/3.6!R 2.5 insulation for piping
PipeUvalue = 1/PipeRvalue
CollCapac = (CArea/26.77)*((4.1*3.55*1.04)+(11.8*0.386))
Tglycol_initial = 30
CutOutTemp = 87.778!C; 190F
Qinc = [12,24]*CollectorArea
*$UNIT_NAME Collector
*$LAYER Main
*$POSITION 66 32

*-----
--

* Model "SolPmp" (Type 3)
*

UNIT 19 TYPE 3      SolPmp
*$UNIT_NAME SolPmp
*$MODEL .\Hydronics\Pumps\Single Speed\Type3b.tmf
*$POSITION 249 148
*$LAYER Outputs #
TRACE START STOP
PARAMETERS 9
Flw_ColPmp          ! 1 Maximum flow rate
CpColl              ! 2 Fluid specific heat
Pwr_ColPmp          ! 3 Maximum power
ConvCoeff           ! 4 Conversion coefficient
1                   ! 5 Power coefficient-1
0                   ! 6 Power coefficient-2
0                   ! 7 Power coefficient-3
0                   ! 8 Power coefficient-4
0                   ! 9 Power coefficient-5

INPUTS 3
15,1                ! OPipe-2:Outlet temperature ->Inlet fluid temperature
15,2                ! OPipe-2:Outlet flow rate ->Inlet mass flow rate
3,1                 ! controller:Output control function ->Control signal
*** INITIAL INPUT VALUES
20.0 100.0 1.0
*-----
--

* EQUATIONS "Fluid"

```

```

*
EQUATIONS 4
CpColl = 3.55!50% Glycol
CpLoad = 4.19!Water
DensColl = 1040!50% Glycol
DensLoad = 1000!Water
*$UNIT_NAME Fluid
*$LAYER Main
*$POSITION 68 523

*-----
--

* EQUATIONS "Pump"
*
EQUATIONS 6
Flw_ColPmp = 20*(3600/1000)*1.04*CollectorArea!kg/hr, 20ml/s-m2, 32 ft2 ~1
gpm
Flw_HFPmp = 1200!kg/hr--> 5.3 gpm
Pwr_ColPmp = 15*Flw_ColPmp*(0.264/60) *3.6
Pwr_HFPmp = 92 *3.6
Qpump = [19,3]+[51,3]
ConvCoeff = 0.5!fraction of pump power that is converted to fluid thermal
energy
*$UNIT_NAME Pump
*$LAYER Main
*$POSITION 53 160

*-----
--

* EQUATIONS "Tank Parameters"
*
EQUATIONS 10
StrTnkVol = CollectorArea*1.5*(0.0037854/0.0929)!1.5 gal/ft2 for storage
StrTnkHgt = 5 * 0.3048 !5
StrTnkRval = 17* 0.04895 / 2!17.7 originally
StrTnkEnvT = 20
StrTnkUval = 1/StrTnkRval
StrNodes = 18
TankSetpoint = 51.667!125 F
k_tank = 3.6*50!Mild Steel conductivity 50 W/m-K -> kJ/hr-m-K
Qaux2 = 3*16200*[29,2]!4.5 kW
Qaux1 = 3*16200*[29,1]!4.5 kW
*$UNIT_NAME Tank Parameters
*$LAYER Main
*$POSITION 651 31

*-----
--

* EQUATIONS "HX Constants"
*
EQUATIONS 28

```

```

HXid = 0.995 /39.3701!HX inside diameter
HXod = 1.125 /39.3701!HX outside diameter
HXLlength = 60 *0.3048!18.29m
HXLinHgt = StrTnkHgt*0.499
HXLoutHgt = StrTnkHgt*0.120
HXLcoilDia = 0.475
HXLcoilPch = 0.585*StrTnkHgt*3.1416*HXLcoilDia/(HXLlength-3.1416*HXLcoilDia)
HXUlength = 48*0.3048!14.63m
HXUinHgt = StrTnkHgt*0.68
HXUoutHgt = StrTnkHgt*0.84
HXUcoilDia = 0.475
HXUcoilPch = 0.415*StrTnkHgt*3.1416*HXUcoilDia/(HXUlength-3.1416*HXUcoilDia)
NodNumHXLi = MAX(StrNodes-INT(HXLinHgt*StrNodes/StrTnkHgt),1)
NodNumHXLo = MAX(StrNodes-INT(HXLoutHgt*StrNodes/StrTnkHgt),1)
NodNumHXUi = MAX(StrNodes-INT(HXUinHgt*StrNodes/StrTnkHgt),1)
NodNumHXUo = MAX(StrNodes-INT(HXUoutHgt*StrNodes/StrTnkHgt),1)
k_hx = 1389.6 !conductivity of copper
NodesHXU = 7
NodesHXL = 7
FracHXU = 1/NodesHXU
FracHXL = 1/NodesHXL
NodesHXUsol = 7
FracHXUsol = 1/NodesHXUsol
HXUsol_length = 16*0.3048!14.63m
HXUsol_inHgt = 0.6
HXUsol_outHgt = 0.68
NodNumHXUsoli = MAX(StrNodes-INT(HXUsol_inHgt*StrNodes/StrTnkHgt),1)
NodNumHXUsolo = MAX(StrNodes-INT(HXUsol_outHgt*StrNodes/StrTnkHgt),1)
*$UNIT_NAME HX Constants
*$LAYER Outputs
*$POSITION 773 31

```

```

*-----
--

```

```

* EQUATIONS "Coll slope/azim"
*
EQUATIONS 2
CSlope = CollSlope
CAzim = CollAz
*$UNIT_NAME Coll slope/azim
*$LAYER Main
*$POSITION 71 286

```

```

*-----
--

```

```

* EQUATIONS "SpH House"
*
EQUATIONS 17
TSETPOINT = 20
NSlope = 90
NAzim = 180
SSlope = 90
SAzim = 0

```

```

ESlope = 90
EAzim = -90
WSlope = 90
WAzim = 90
NRSlope = 45
NRAzim = 180
SRSlope = 45
SRAzim = 0
Slablength = 12
Slabwidth = 9.68
Slabdepth = 0.2
PEXLength = 40
*$UNIT_NAME SpH House
*$LAYER Main
*$POSITION 59 427

```

```

*-----
--

```

```

* Model "Type534-Coiled" (Type 534)
*

```

```

UNIT 26 TYPE 534   Type534-Coiled
*$UNIT_NAME Type534-Coiled
*$MODEL .\Storage Tank Library (TESS)\Cylindrical Storage Tank\Vertical
Cylinder\Version without Plug-In\Coiled Tube HXs\Type534-Coiled.tmf
*$POSITION 473 236
*$LAYER Main #
*$# CYLINDRICAL STORAGE TANK
PARAMETERS 157
-1          ! 1 LU for data file
18          ! 2 Number of tank nodes
1           ! 3 Number of ports
3           ! 4 Number of immersed heat exchangers
0           ! 5 Number of miscellaneous heat flows
StrTnkVol   ! 6 Tank volume
StrTnkHgt   ! 7 Tank height
0           ! 8 Tank fluid
CpLoad      ! 9 Fluid specific heat
DensLoad    ! 10 Fluid density
2.14        ! 11 Fluid thermal conductivity
3.21        ! 12 Fluid viscosity
0.00026     ! 13 Fluid thermal expansion coefficient
StrTnkUval  ! 14 Top loss coefficient
StrTnkUval  ! 15 Edge loss coefficient for node-1
StrTnkUval  ! 16 Edge loss coefficient for node-2
StrTnkUval  ! 17 Edge loss coefficient for node-3
StrTnkUval  ! 18 Edge loss coefficient for node-4
StrTnkUval  ! 19 Edge loss coefficient for node-5
StrTnkUval  ! 20 Edge loss coefficient for node-6
StrTnkUval  ! 21 Edge loss coefficient for node-7
StrTnkUval  ! 22 Edge loss coefficient for node-8
StrTnkUval  ! 23 Edge loss coefficient for node-9
StrTnkUval  ! 24 Edge loss coefficient for node-10
StrTnkUval  ! 25 Edge loss coefficient for node-11
StrTnkUval  ! 26 Edge loss coefficient for node-12

```

```

StrTnkUval      ! 27 Edge loss coefficient for node-13
StrTnkUval      ! 28 Edge loss coefficient for node-14
StrTnkUval      ! 29 Edge loss coefficient for node-15
StrTnkUval      ! 30 Edge loss coefficient for node-16
StrTnkUval      ! 31 Edge loss coefficient for node-17
StrTnkUval      ! 32 Edge loss coefficient for node-18
StrTnkUval      ! 33 Bottom loss coefficient
k_tank          ! 34 Additional thermal conductivity
1              ! 35 Inlet flow mode
StrNodes        ! 36 Entry node
1              ! 37 Exit node
0              ! 38 Flue loss coefficient for node-1
0              ! 39 Flue loss coefficient for node-2
0              ! 40 Flue loss coefficient for node-3
0              ! 41 Flue loss coefficient for node-4
0              ! 42 Flue loss coefficient for node-5
0              ! 43 Flue loss coefficient for node-6
0              ! 44 Flue loss coefficient for node-7
0              ! 45 Flue loss coefficient for node-8
0              ! 46 Flue loss coefficient for node-9
0              ! 47 Flue loss coefficient for node-10
0              ! 48 Flue loss coefficient for node-11
0              ! 49 Flue loss coefficient for node-12
0              ! 50 Flue loss coefficient for node-13
0              ! 51 Flue loss coefficient for node-14
0              ! 52 Flue loss coefficient for node-15
0              ! 53 Flue loss coefficient for node-16
0              ! 54 Flue loss coefficient for node-17
0              ! 55 Flue loss coefficient for node-18
3              ! 56 Type of HX-1
7              ! 57 Number of HX nodes-1
0              ! 58 HX fluid-1
CpLoad          ! 59 HX fluid specific heat-1
DensLoad        ! 60 HX fluid density-1
2.14           ! 61 HX fluid thermal conductivity-1
3.21           ! 62 HX fluid viscosity-1
0.6            ! 63 Multiplier for natural convection-1
0.6            ! 64 Exponent for natural convection-1
1.0            ! 65 Geometry factor for natural convection-1
1.0            ! 66 Geometry exponent for natural convection-1
HXid           ! 67 Inner tube diameter-1
HXod           ! 68 Outer tube diameter-1
k_hx           ! 69 HX wall thermal conductivity-1
HXUlength      ! 70 Length of coiled tubes-1
1              ! 71 Number of tubes-1
0.             ! 72 HX header volume-1
0.0006        ! 73 HX cross sectional area-1
HXUcoilDia     ! 74 Coil diameter-1
HXUcoilPch     ! 75 Coil pitch-1
5              ! 76 Tank node for HX node-1-1
FracHXU        ! 77 Fraction of HX length-1-1
4              ! 78 Tank node for HX node-1-2
FracHXU        ! 79 Fraction of HX length-1-2
4              ! 80 Tank node for HX node-1-3
FracHXU        ! 81 Fraction of HX length-1-3
3              ! 82 Tank node for HX node-1-4
FracHXU        ! 83 Fraction of HX length-1-4

```

```

3          ! 84 Tank node for HX node-1-5
FracHXU    ! 85 Fraction of HX length-1-5
2          ! 86 Tank node for HX node-1-6
FracHXU    ! 87 Fraction of HX length-1-6
2          ! 88 Tank node for HX node-1-7
FracHXU    ! 89 Fraction of HX length-1-7
3          ! 90 Type of HX-2
7          ! 91 Number of HX nodes-2
0          ! 92 HX fluid-2
CpLoad     ! 93 HX fluid specific heat-2
DensLoad   ! 94 HX fluid density-2
2.14      ! 95 HX fluid thermal conductivity-2
3.21      ! 96 HX fluid viscosity-2
0.6       ! 97 Multiplier for natural convection-2
0.6       ! 98 Exponent for natural convection-2
1.0       ! 99 Geometry factor for natural convection-2
1.0       ! 100 Geometry exponent for natural convection-2
HXid      ! 101 Inner tube diameter-2
HXod      ! 102 Outer tube diameter-2
k_hx      ! 103 HX wall thermal conductivity-2
HXUsol_length ! 104 Length of coiled tubes-2
1         ! 105 Number of tubes-2
0         ! 106 HX header volume-2
0.006     ! 107 HX cross sectional area-2
HXUcoilDia ! 108 Coil diameter-2
HXUcoilPch ! 109 Coil pitch-2
10        ! 110 Tank node for HX node-2-1
FracHXUsol ! 111 Fraction of HX length-2-1
10        ! 112 Tank node for HX node-2-2
FracHXUsol ! 113 Fraction of HX length-2-2
10        ! 114 Tank node for HX node-2-3
FracHXUsol ! 115 Fraction of HX length-2-3
10        ! 116 Tank node for HX node-2-4
FracHXUsol ! 117 Fraction of HX length-2-4
9         ! 118 Tank node for HX node-2-5
FracHXUsol ! 119 Fraction of HX length-2-5
9         ! 120 Tank node for HX node-2-6
FracHXUsol ! 121 Fraction of HX length-2-6
9         ! 122 Tank node for HX node-2-7
FracHXUsol ! 123 Fraction of HX length-2-7
3         ! 124 Type of HX-3
7         ! 125 Number of HX nodes-3
0         ! 126 HX fluid-3
CpColl    ! 127 HX fluid specific heat-3
DensColl  ! 128 HX fluid density-3
2.14     ! 129 HX fluid thermal conductivity-3
3.21     ! 130 HX fluid viscosity-3
0.6      ! 131 Multiplier for natural convection-3
0.6      ! 132 Exponent for natural convection-3
1.0      ! 133 Geometry factor for natural convection-3
1.0      ! 134 Geometry exponent for natural convection-3
HXid     ! 135 Inner tube diameter-3
HXod     ! 136 Outer tube diameter-3
k_hx     ! 137 HX wall thermal conductivity-3
HXLlength ! 138 Length of coiled tubes-3
1        ! 139 Number of tubes-3
0.       ! 140 HX header volume-3

```

```

0.0006          ! 141 HX cross sectional area-3
HXLcoilDia      ! 142 Coil diameter-3
HXLcoilPch      ! 143 Coil pitch-3
13             ! 144 Tank node for HX node-3-1
FracHXL        ! 145 Fraction of HX length-3-1
14             ! 146 Tank node for HX node-3-2
FracHXL        ! 147 Fraction of HX length-3-2
14             ! 148 Tank node for HX node-3-3
FracHXL        ! 149 Fraction of HX length-3-3
15             ! 150 Tank node for HX node-3-4
FracHXL        ! 151 Fraction of HX length-3-4
15             ! 152 Tank node for HX node-3-5
FracHXL        ! 153 Fraction of HX length-3-5
16             ! 154 Tank node for HX node-3-6
FracHXL        ! 155 Fraction of HX length-3-6
16             ! 156 Tank node for HX node-3-7
FracHXL        ! 157 Fraction of HX length-3-7
INPUTS 48
60,1           ! Tee-2_hot:Outlet temperature ->Inlet temperature for port
60,2           ! Tee-2_hot:Outlet flow rate ->Inlet flow rate for port
26,35          ! Type534-Coiled:Temperature at HX Outlet-2 ->Inlet
temperature for HX-1
26,36          ! Type534-Coiled:HX flow rate-2 ->Inlet flow rate for HX-1
50,1           ! Type653:Outlet fluid temperature ->Inlet temperature for HX-2
50,2           ! Type653:Outlet fluid flow rate ->Inlet flow rate for HX-2
17,1           ! IPipe:Outlet temperature ->Inlet temperature for HX-3
17,2           ! IPipe:Outlet flow rate ->Inlet flow rate for HX-3
32,1           ! Type56: 1- TAIR_MAIN ->Top loss temperature
32,1           ! Type56: 1- TAIR_MAIN ->Edge loss temperature for node-1
32,1           ! Type56: 1- TAIR_MAIN ->Edge loss temperature for node-2
32,1           ! Type56: 1- TAIR_MAIN ->Edge loss temperature for node-3
32,1           ! Type56: 1- TAIR_MAIN ->Edge loss temperature for node-4
32,1           ! Type56: 1- TAIR_MAIN ->Edge loss temperature for node-5
32,1           ! Type56: 1- TAIR_MAIN ->Edge loss temperature for node-6
32,1           ! Type56: 1- TAIR_MAIN ->Edge loss temperature for node-7
32,1           ! Type56: 1- TAIR_MAIN ->Edge loss temperature for node-8
32,1           ! Type56: 1- TAIR_MAIN ->Edge loss temperature for node-9
32,1           ! Type56: 1- TAIR_MAIN ->Edge loss temperature for node-10
32,1           ! Type56: 1- TAIR_MAIN ->Edge loss temperature for node-11
32,1           ! Type56: 1- TAIR_MAIN ->Edge loss temperature for node-12
32,1           ! Type56: 1- TAIR_MAIN ->Edge loss temperature for node-13
32,1           ! Type56: 1- TAIR_MAIN ->Edge loss temperature for node-14
32,1           ! Type56: 1- TAIR_MAIN ->Edge loss temperature for node-15
32,1           ! Type56: 1- TAIR_MAIN ->Edge loss temperature for node-16
32,1           ! Type56: 1- TAIR_MAIN ->Edge loss temperature for node-17
32,1           ! Type56: 1- TAIR_MAIN ->Edge loss temperature for node-18
32,1           ! Type56: 1- TAIR_MAIN ->Bottom loss temperature
0,0            ! [unconnected] Gas flue temperature
0,0            ! [unconnected] Inversion mixing flow rate
0,0            ! [unconnected] Auxiliary heat input for node-1
0,0            ! [unconnected] Auxiliary heat input for node-2
0,0            ! [unconnected] Auxiliary heat input for node-3
Qaux2          ! Tank Parameters:Qaux2 ->Auxiliary heat input for node-4
Qaux1          ! Tank Parameters:Qaux1 ->Auxiliary heat input for node-5
0,0            ! [unconnected] Auxiliary heat input for node-6
0,0            ! [unconnected] Auxiliary heat input for node-7
0,0            ! [unconnected] Auxiliary heat input for node-8

```



```

0,0      ! [unconnected] Auxiliary heat input for node-9
0,0      ! [unconnected] Auxiliary heat input for node-10
0,0      ! [unconnected] Auxiliary heat input for node-11
0,0      ! [unconnected] Auxiliary heat input for node-12
0,0      ! [unconnected] Auxiliary heat input for node-13
0,0      ! [unconnected] Auxiliary heat input for node-14
0,0      ! [unconnected] Auxiliary heat input for node-15
0,0      ! [unconnected] Auxiliary heat input for node-16
0,0      ! [unconnected] Auxiliary heat input for node-17
0,0      ! [unconnected] Auxiliary heat input for node-18
*** INITIAL INPUT VALUES
20.0 0.0 20.0 0.0 20.0 0.0 20.0 0.0 20.0 20.0 20.0 20.0 20.0 20.0 20.0 20.0 20.0
20.0 20.0 20.0 20.0 20.0 20.0 20.0 20.0 20.0 20.0 20.0 20.0 20.0 20.0 20.0 -100 0.0 0.0
0.0 0.0 0.0 0.0 0.0 0.0 0.0 0.0 0.0 0.0 0.0 0.0 0.0 0.0 0.0 0.0 0.0
DERIVATIVES 18
58      ! 1 Initial Tank Temperature-1
56      ! 2 Initial Tank Temperature-2
30      ! 3 Initial Tank Temperature-3
30      ! 4 Initial Tank Temperature-4
29      ! 5 Initial Tank Temperature-5
28.5    ! 6 Initial Tank Temperature-6
58      ! 7 Initial Tank Temperature-7
58      ! 8 Initial Tank Temperature-8
58      ! 9 Initial Tank Temperature-9
58      ! 10 Initial Tank Temperature-10
58      ! 11 Initial Tank Temperature-11
58      ! 12 Initial Tank Temperature-12
58      ! 13 Initial Tank Temperature-13
58      ! 14 Initial Tank Temperature-14
58      ! 15 Initial Tank Temperature-15
58      ! 16 Initial Tank Temperature-16
58      ! 17 Initial Tank Temperature-17
58      ! 18 Initial Tank Temperature-18
*-----
--

* Model "Type1502" (Type 1502)
*
UNIT 29 TYPE 1502 Type1502
*$UNIT_NAME Type1502
*$MODEL .\Controllers Library (TESS)\Aquastats\Heating Mode\Type1502.tmf
*$POSITION 702 129
*$LAYER Outputs #
PARAMETERS 4
2      ! 1 Number of heating stages
5      ! 2 # oscillations permitted
2      ! 3 Temperature dead band
0      ! 4 Number of stage exceptions
INPUTS 4
26,15      ! Type534-Coiled:Tank nodal temperature-1 ->Fluid
temperature
0,0      ! [unconnected] Lockout signal
0,0      ! [unconnected] Setpoint temperature for stage-1
0,0      ! [unconnected] Setpoint temperature for stage-2
*** INITIAL INPUT VALUES
20.0 0 51.667 50.6

```

```

*-----
--

* Model "Type56" (Type 56)
*

UNIT 32 TYPE 56      Type56
*$UNIT_NAME Type56
*$MODEL .\Loads and Structures\Multi-Zone Building\Type56.tmf
*$POSITION 963 618
*$LAYER Main #
*$#

PARAMETERS 3
50      ! 1 Logical unit for building description file (.bui)
0       ! 2 Star network calculation switch
0.50    ! 3 Weighting factor for operative temperature

INPUTS 51
12,1    ! Weather:Dry bulb temperature -> 1- TAMB
12,7    ! Weather:Percent relative humidity -> 2- RELHUMAMB
12,4    ! Weather:Effective sky temperature -> 3- TSKY
12,1    ! Weather:Dry bulb temperature -> 4- TSGRD
12,16   ! Weather:Solar zenith angle -> 5- AZEN
12,17   ! Weather:Solar azimuth angle -> 6- AAZM
12,25   ! Weather:Total tilted surface radiation for surface-2 ->
7- IT_NORTH
12,26   ! Weather:Total tilted surface radiation for surface-3 ->
8- IT_SOUTH
12,27   ! Weather:Total tilted surface radiation for surface-4 ->
9- IT_EAST
12,28   ! Weather:Total tilted surface radiation for surface-5 ->
10- IT_WEST
12,29   ! Weather:Total tilted surface radiation for surface-6 ->
11- IT_NROOF
12,30   ! Weather:Total tilted surface radiation for surface-7 ->
12- IT_SROOF
12,32   ! Weather:Beam radiation for surface-2 -> 13- IB_NORTH
12,33   ! Weather:Beam radiation for surface-3 -> 14- IB_SOUTH
12,34   ! Weather:Beam radiation for surface-4 -> 15- IB_EAST
12,35   ! Weather:Beam radiation for surface-5 -> 16- IB_WEST
12,36   ! Weather:Beam radiation for surface-6 -> 17- IB_NROOF
12,37   ! Weather:Beam radiation for surface-7 -> 18- IB_SROOF
12,60   ! Weather:Angle of incidence for surface-2 -> 19- AI_NORTH
12,61   ! Weather:Angle of incidence for surface-3 -> 20- AI_SOUTH
12,62   ! Weather:Angle of incidence for surface-4 -> 21- AI_EAST
12,63   ! Weather:Angle of incidence for surface-5 -> 22- AI_WEST
12,64   ! Weather:Angle of incidence for surface-6 -> 23- AI_NROOF
12,65   ! Weather:Angle of incidence for surface-7 -> 24- AI_SROOF
12,107  ! Weather:Ground reflectance -> 25- GRDREF
hOutside ! hOutside:hOutside -> 26- HOUTSIDE
0,0     ! [unconnected] 27- TVNT_AUX
0,0     ! [unconnected] 28- MVNT_AUX
0,0     ! [unconnected] 29- RHVNT_AUX
0,0     ! [unconnected] 30- MVNT_SOLAR
0,0     ! [unconnected] 31- TVNT_SOLAR
0,0     ! [unconnected] 32- RHVNT_SOLAR
0,0     ! [unconnected] 33- QSLAB
Occ_hr_Sens ! InternalGains:Occ_hr_Sens -> 34- OCC_SENS

```



```

Basement = 1
slabArea = 117
slabPerim = 44
slabRvalue = 0.1389+2/5.678/3.6
avgIndoor = 20
avgBasement = 15
avgAmb = 22.22
AmpSurf = 12.00
DayMinTemp = 31
SiteSoil_k = 4.356 !kJ/hr.m.K
SiteSoil_rho = 3200 !kg/m3
SiteSoil_cp = 0.84 !kJ/kg.K
InsRvalue = 0.32
InsEdgeLength = 0.6096!2m
BasementRvalue = 13/5.678/3.6!R-13
*$UNIT_NAME SoG
*$LAYER Water Loop
*$POSITION 670 680

```

```

*-----
--

```

```

* Model "Type715" (Type 715)
*

```

```

UNIT 39 TYPE 715 Type715
*$UNIT_NAME Type715
*$MODEL .\Ground Coupling Library (TESS)\Simplified ASHRAE
Approach\Basements\Type715.tmf
*$POSITION 764 689
*$LAYER CollectorLoop #
PARAMETERS 12
12.8      ! 1 Length of basement
9.15      ! 2 Width of basement
3.0       ! 3 Depth of basement
slabRvalue      ! 4 R-value of slab and walls
0          ! 5 R-value of insulation
avgBasement      ! 6 Average annual indoor temperature
avgAmb          ! 7 Average annual outdoor temperature
ampSurf         ! 8 Amplitude of ambient temperature
DayMinTemp      ! 9 Day of maximum heat transfer
SiteSoil_k      ! 10 Soil thermal conductivity
SiteSoil_rho    ! 11 Soil density
SiteSoil_cp     ! 12 Soil specific heat

```

```

*-----
--

```

```

* EQUATIONS "Qslab"
*

```

```

EQUATIONS 2
Slabloss = ([37,1]*PrtIns) ! kJ/hr
BasementsLoss = [39,1]*Basement
*$UNIT_NAME Qslab
*$LAYER Main
*$POSITION 862 646

```

*-----
--

* EQUATIONS "InternalGains"

*

EQUATIONS 10

Occ_Day_Sens = 10805*1.055 ! Btu/day --> kJ/Day

Occ_hr_Sens = Occ_Day_Sens*[44,1]

Occ_Day_Lat = 8075*1.055 ! Btu/day --> kJ/day

Occ_hr_Lat = Occ_Day_Lat*[44,1]/2454

Lgt_Day_Sens = 7.44*3600 ! kWh/day --> kJ/day

Lgt_hr_Sens = Lgt_Day_Sens*[43,1]

Eqp_Day_Sens = 40695*1.055 ! Btu/day --> kJ/day

Eqp_hr_Sens = Eqp_Day_Sens*[42,1]

Eqp_Day_Lat = 6474*1.055 ! Btu/day --> kJ/day

Eqp_hr_Lat = Eqp_Day_Lat*[45,1]/2454

*\$UNIT_NAME InternalGains

*\$LAYER Water Loop

*\$POSITION 899 776

*-----
--

* Model "Type14c" (Type 14)

*

UNIT 42 TYPE 14 Type14c

*\$UNIT_NAME Type14c

*\$MODEL .\Utility\Forcing Functions\Internal Gains\Type14c.tmf

*\$POSITION 699 895

*\$LAYER CollectorLoop #

PARAMETERS 48

0 ! 1 Initial value of time
0.028 ! 2 Initial value of gains
1 ! 3 Time at point-1
0.026 ! 4 Internal gains at point -1
2 ! 5 Time at point-2
0.024 ! 6 Internal gains at point -2
3 ! 7 Time at point-3
0.024 ! 8 Internal gains at point -3
4 ! 9 Time at point-4
0.024 ! 10 Internal gains at point -4
5 ! 11 Time at point-5
0.03 ! 12 Internal gains at point -5
6 ! 13 Time at point-6
0.044 ! 14 Internal gains at point -6
7 ! 15 Time at point-7
0.049 ! 16 Internal gains at point -7
8 ! 17 Time at point-8
0.047 ! 18 Internal gains at point -8
9 ! 19 Time at point-9
0.044 ! 20 Internal gains at point -9
10 ! 21 Time at point-10
0.042 ! 22 Internal gains at point -10
11 ! 23 Time at point-11

```

0.041      ! 24 Internal gains at point -11
12         ! 25 Time at point-12
0.039      ! 26 Internal gains at point -12
13         ! 27 Time at point-13
0.038      ! 28 Internal gains at point -13
14         ! 29 Time at point-14
0.037      ! 30 Internal gains at point -14
15         ! 31 Time at point-15
0.04       ! 32 Internal gains at point -15
16         ! 33 Time at point-16
0.048      ! 34 Internal gains at point -16
17         ! 35 Time at point-17
0.061      ! 36 Internal gains at point -17
18         ! 37 Time at point-18
0.064      ! 38 Internal gains at point -18
19         ! 39 Time at point-19
0.06       ! 40 Internal gains at point -19
20         ! 41 Time at point-20
0.057      ! 42 Internal gains at point -20
21         ! 43 Time at point-21
0.052      ! 44 Internal gains at point -21
22         ! 45 Time at point-22
0.045      ! 46 Internal gains at point -22
23         ! 47 Time at point-23
0.036      ! 48 Internal gains at point -23

```

```

*-----
--

```

```

* Model "Type14d" (Type 14)
*

```

```

UNIT 43 TYPE 14      Type14d
*$UNIT_NAME Type14d
*$MODEL .\Utility\Forcing Functions\Lighting\Type14d.tmf
*$POSITION 711 829
*$LAYER Main #
PARAMETERS 48
0          ! 1 Initial value of time
0.008     ! 2 Initial value of lighting
1         ! 3 Time at point-1
0.008     ! 4 Lighting at point -1
2         ! 5 Time at point-2
0.008     ! 6 Lighting at point -2
3         ! 7 Time at point-3
0.008     ! 8 Lighting at point -3
4         ! 9 Time at point-4
0.024     ! 10 Lighting at point -4
5         ! 11 Time at point-5
0.05      ! 12 Lighting at point -5
6         ! 13 Time at point-6
0.056     ! 14 Lighting at point -6
7         ! 15 Time at point-7
0.05      ! 16 Lighting at point -7
8         ! 17 Time at point-8
0.022     ! 18 Lighting at point -8
9         ! 19 Time at point-9
0.015     ! 20 Lighting at point -9

```

```

10          ! 21 Time at point-10
0.015      ! 22 Lighting at point -10
11          ! 23 Time at point-11
0.015      ! 24 Lighting at point -11
12          ! 25 Time at point-12
0.015      ! 26 Lighting at point -12
13          ! 27 Time at point-13
0.015      ! 28 Lighting at point -13
14          ! 29 Time at point-14
0.015      ! 30 Lighting at point -14
15          ! 31 Time at point-15
0.026      ! 32 Lighting at point -15
16          ! 33 Time at point-16
0.056      ! 34 Lighting at point -16
17          ! 35 Time at point-17
0.078      ! 36 Lighting at point -17
18          ! 37 Time at point-18
0.105      ! 38 Lighting at point -18
19          ! 39 Time at point-19
0.126      ! 40 Lighting at point -19
20          ! 41 Time at point-20
0.128      ! 42 Lighting at point -20
21          ! 43 Time at point-21
0.088      ! 44 Lighting at point -21
22          ! 45 Time at point-22
0.049      ! 46 Lighting at point -22
23          ! 47 Time at point-23
0.02       ! 48 Lighting at point -23

```

--

```

* Model "Type14a" (Type 14)
*

```

```

UNIT 44 TYPE 14      Type14a
*$UNIT_NAME Type14a
*$MODEL .\Utility\Forcing Functions\Occupancy\Type14a.tmf
*$POSITION 710 765
*$LAYER Water Loop #
PARAMETERS 48
0          ! 1 Initial value of time
0.061     ! 2 Initial number of people
1         ! 3 Time at point-1
0.061     ! 4 Occupancy at point -1
2         ! 5 Time at point-2
0.061     ! 6 Occupancy at point -2
3         ! 7 Time at point-3
0.061     ! 8 Occupancy at point -3
4         ! 9 Time at point-4
0.061     ! 10 Occupancy at point -4
5         ! 11 Time at point-5
0.061     ! 12 Occupancy at point -5
6         ! 13 Time at point-6
0.061     ! 14 Occupancy at point -6
7         ! 15 Time at point-7
0.052     ! 16 Occupancy at point -7
8         ! 17 Time at point-8

```

```

0.024      ! 18 Occupancy at point -8
9          ! 19 Time at point-9
0.015      ! 20 Occupancy at point -9
10         ! 21 Time at point-10
0.015      ! 22 Occupancy at point -10
11         ! 23 Time at point-11
0.015      ! 24 Occupancy at point -11
12         ! 25 Time at point-12
0.015      ! 26 Occupancy at point -12
13         ! 27 Time at point-13
0.015      ! 28 Occupancy at point -13
14         ! 29 Time at point-14
0.015      ! 30 Occupancy at point -14
15         ! 31 Time at point-15
0.015      ! 32 Occupancy at point -15
16         ! 33 Time at point-16
0.018      ! 34 Occupancy at point -16
17         ! 35 Time at point-17
0.032      ! 36 Occupancy at point -17
18         ! 37 Time at point-18
0.053      ! 38 Occupancy at point -18
19         ! 39 Time at point-19
0.053      ! 40 Occupancy at point -19
20         ! 41 Time at point-20
0.053      ! 42 Occupancy at point -20
21         ! 43 Time at point-21
0.061      ! 44 Occupancy at point -21
22         ! 45 Time at point-22
0.061      ! 46 Occupancy at point -22
23         ! 47 Time at point-23
0.061      ! 48 Occupancy at point -23

```

```

*-----
--

```

```

* Model "Type14f" (Type 14)
*

```

```

UNIT 45 TYPE 14      Type14f
*$UNIT_NAME Type14f
*$MODEL .\Utility\Forcing Functions\Relative Humidity\Type14f.tmf
*$POSITION 688 959
*$LAYER CollectorLoop #
PARAMETERS 48
0          ! 1 Initial value of time
0.017     ! 2 Initial value of relative humidity
1         ! 3 Time at point-1
0.014     ! 4 Relative humidity at point -1
2         ! 5 Time at point-2
0.012     ! 6 Relative humidity at point -2
3         ! 7 Time at point-3
0.012     ! 8 Relative humidity at point -3
4         ! 9 Time at point-4
0.015     ! 10 Relative humidity at point -4
5         ! 11 Time at point-5
0.026     ! 12 Relative humidity at point -5
6         ! 13 Time at point-6
0.049     ! 14 Relative humidity at point -6

```



```

7          ! 15 Time at point-7
0.058     ! 16 Relative humidity at point -7
8          ! 17 Time at point-8
0.055     ! 18 Relative humidity at point -8
9          ! 19 Time at point-9
0.052     ! 20 Relative humidity at point -9
10         ! 21 Time at point-10
0.047     ! 22 Relative humidity at point -10
11         ! 23 Time at point-11
0.046     ! 24 Relative humidity at point -11
12         ! 25 Time at point-12
0.045     ! 26 Relative humidity at point -12
13         ! 27 Time at point-13
0.04      ! 28 Relative humidity at point -13
14         ! 29 Time at point-14
0.038     ! 30 Relative humidity at point -14
15         ! 31 Time at point-15
0.043     ! 32 Relative humidity at point -15
16         ! 33 Time at point-16
0.059     ! 34 Relative humidity at point -16
17         ! 35 Time at point-17
0.086     ! 36 Relative humidity at point -17
18         ! 37 Time at point-18
0.078     ! 38 Relative humidity at point -18
19         ! 39 Time at point-19
0.058     ! 40 Relative humidity at point -19
20         ! 41 Time at point-20
0.048     ! 42 Relative humidity at point -20
21         ! 43 Time at point-21
0.042     ! 44 Relative humidity at point -21
22         ! 45 Time at point-22
0.032     ! 46 Relative humidity at point -22
23         ! 47 Time at point-23
0.025     ! 48 Relative humidity at point -23

```

```

*-----
--

```

```

* Model "Type960" (Type 960)
*

```

```

UNIT 47 TYPE 960   Type960
*$UNIT_NAME Type960
*$MODEL .\Utility Library (TESS)\Infiltration Models\LBL
Infiltration\Type960.tmf
*$POSITION 859 490
*$LAYER Main #
PARAMETERS 14
2          ! 1 Humidity Mode
10         ! 2 Windspeed Height
0.25      ! 3 WS Terrain Coef 1
0.67      ! 4 WS Terrain Coef 2
0.25      ! 5 Terrain Coef 1
0.67      ! 6 Terrain Coef 2
9.81      ! 7 Acceleration of Gravity
571.17    ! 8 Conditioned space volume
3         ! 9 Zone Height
0.24      ! 10 Shielding Factor

```

```

ELAinf          ! 11 Zone leakage area
0.5            ! 12 Ceiling Fraction of Leakage
0.5            ! 13 Floor Fraction of Leakage
5              ! 14 Zone Wind Height
INPUTS 9
12,1          ! Weather:Dry bulb temperature ->Ambient temperature
12,6          ! Weather:Humidity ratio ->Ambient humidity ratio
12,7          ! Weather:Percent relative humidity ->Ambient relative humidity
(not used)
12,10         ! Weather:Atmospheric pressure ->Ambient pressure
12,8          ! Weather:Wind velocity ->Wind speed
32,1          ! Type56: 1- TAIR_MAIN ->Zone temperature
32,4          ! Type56: 4- ABSHUM_MAIN ->Zone humidity ratio
0,0           ! [unconnected] Zone RH (not used)
0,0           ! [unconnected] Zone pressure
*** INITIAL INPUT VALUES
20 0.001 50 1 2 20 0.001 50 1
*-----
--

* EQUATIONS "Infil"
*
EQUATIONS 13
TdeltaINF = abs([12,1]-[32,1])
fs = 0.000290!Two stories
fw = 0.000231!Shielding class 3
SLAinf = 0.00015 !Set the SLA
CFAinf = 232.26 !m2
ELAinf = SLAinf*CFAinf
Vdotinf = ELA*((fs*TdeltaINF+fw*([12,8])^2)^(1/2))
Vhouse = 571.17 !m3
INFACH = (Vdotinf*60*60*0.001)/Vhouse
Terrain1 = 0.25! Urban terrain
Terrain2 = 0.67!Urban
Shield = 0.24!Moderate Shielding
ELA = ELAinf*100^2
*$UNIT_NAME Infil
*$LAYER Water Loop
*$POSITION 745 520

*-----
--

* Model "Type653" (Type 653)
*
UNIT 50 TYPE 653 Type653
*$UNIT_NAME Type653
*$MODEL .\Ground Coupling Library (TESS)\Simplified Radiant Floor\Type653.tmf
*$POSITION 880 343
*$LAYER Water Loop #
*$# Simplified Radiant Floor
PARAMETERS 25
Slablength     ! 1 Length of slab
Slabwidth      ! 2 Width of slab
Slabdepth      ! 3 Thickness of slab

```

```

2300      ! 4 Slab density
0.1       ! 5 Slab specific heat
20        ! 6 Initial slab temperature
0.0001    ! 7 R-value for top surface
50        ! 8 R-value for edge surfaces
50        ! 9 R-value for bottom surface
0.9       ! 10 Emissivity of the top surface
0         ! 11 Emissivity of the edges
0         ! 12 Emissivity of the bottom surface
0.4       ! 13 Absorptance of the top surface
0         ! 14 Absorptance of the edge surfaces
0         ! 15 Absorptance of the bottom surface
PEXLength ! 16 Total pipe length
0.016     ! 17 Pipe inside diameter
0.02      ! 18 Pipe outside diameter
1         ! 19 Number of identical circuits
4.190     ! 20 Fluid specific heat
1000.0    ! 21 Fluid density
10        ! 22 Nodes along the pipe
1         ! 23 Top surface mode
1         ! 24 Edge surface mode
1         ! 25 Bottom surface mode
INPUTS 18
51,1      ! SpHPmp:Outlet fluid temperature ->Inlet fluid temperature
51,2      ! SpHPmp:Outlet flow rate ->Inlet fluid flow rate
32,1      ! Type56: 1- TAIR_MAIN ->Top convective loss temperature
0,0       ! [unconnected] Edge convective loss temperature
0,0       ! [unconnected] Bottom convective loss temperature
0,0       ! [unconnected] Top surface convection coefficient
0,0       ! [unconnected] Edge surface convection coefficient
0,0       ! [unconnected] Bottom surface convection coefficient
0,0       ! [unconnected] Top radiative loss temperature
0,0       ! [unconnected] Edge radiative loss temperature
0,0       ! [unconnected] Bottom radiative loss temperature
0,0       ! [unconnected] Incident radiation upon top surface
0,0       ! [unconnected] Incident radiation upon edge surfaces
0,0       ! [unconnected] Incident radiation upon bottom surface
32,5      ! Type56: 5- QCOMO_S22 ->Top surface heat transfer from Type 56
building
0,0       ! [unconnected] Edge surface heat transfer from Type 56 building
0,0       ! [unconnected] Bottom surface heat transfer from Type 56
building
0,0       ! [unconnected] HX Effectiveness
*** INITIAL INPUT VALUES
20.0 0 20.0 20.0 20.0 35. 35. 35. 20.0 20.0 20.0 0 0 0 0 0 0 0.6
*-----
--

* Model "SpHPmp" (Type 3)
*
UNIT 51 TYPE 3      SpHPmp
*$UNIT_NAME SpHPmp
*$MODEL .\Hydronics\Pumps\Single Speed\Type3b.tmf
*$POSITION 772 372
*$LAYER Main #
TRACE START STOP

```

```

PARAMETERS 5
Flw_HFPmp      ! 1 Maximum flow rate
CpLoad         ! 2 Fluid specific heat
Pwr_HFPmp      ! 3 Maximum power
ConvCoeff      ! 4 Conversion coefficient
1              ! 5 Power coefficient
INPUTS 3
26,33          ! Type534-Coiled:Temperature at HX Outlet-1 ->Inlet fluid
temperature
26,34          ! Type534-Coiled:HX flow rate-1 ->Inlet mass flow rate
54,1           ! Type1502-2:Control signal for stage heating ->Control signal
*** INITIAL INPUT VALUES
20.0 100.0 1.0
*-----
--

* Model "Type1502-2" (Type 1502)
*

UNIT 54 TYPE 1502 Type1502-2
*$UNIT_NAME Type1502-2
*$MODEL .\Controllers Library (TESS)\Simple Thermostat\Simple Heating
Thermostat\Type1502.tmf
*$POSITION 1046 451
*$LAYER Main #
PARAMETERS 4
1              ! 1 Number of heating stages
5              ! 2 # oscillations permitted
0.5           ! 3 Temperature dead band
0             ! 4 Number of stage exceptions
INPUTS 3
32,1          ! Type56: 1- TAIR_MAIN ->Fluid temperature
0,0           ! [unconnected] Lockout signal
0,0           ! [unconnected] Setpoint temperature for stage
*** INITIAL INPUT VALUES
20.0 0 20
*-----
--

* EQUATIONS "Losses"
*
EQUATIONS 4
Tanklosstotal = [26,6]+[26,8]+[26,7]
Solar = -1*[26,50]
Pipelosstotal = [14,3]+[15,3]+[16,3]+[17,3]
PipeCapacitance = [14,7]+[15,7]+[16,7]+[17,7]
*$UNIT_NAME Losses
*$LAYER Main
*$POSITION 74 628
*-----
--

* EQUATIONS "DHW-2"
*
EQUATIONS 8

```

```

HotWaterDraw = DHWMult*(([57,1]+[57,3]+[57,5]+[57,7]+[57,9]+[57,11]))+1E-2
HotDraw =
DHWMult*( (LT([57,2],2.5)*[57,1])+(LT([57,4],2.5)*[57,3])+(LT([57,6],2.5)*[57,
5])+(LT([57,8],2.5)*[57,7])+(LT([57,10],2.5)*[57,9])+(LT([57,12],2.5)*[57,11]
))
MixedDraw =
DHWMult*( (GT([57,2],2.5)*[57,1])+(GT([57,4],2.5)*[57,3])+(GT([57,6],2.5)*[57,
5])+(GT([57,8],2.5)*[57,7])+(GT([57,10],2.5)*[57,9])+(GT([57,12],2.5)*[57,11]
))
DHWMult = 0.65*Low+1.3*Mid+1.6*High
Low = 0
Mid = 0

```

```

Thot = 51.667 !125F
Tmix = 43.333!110F
*$UNIT_NAME DHW-2
*$LAYER Main
*$POSITION 177 793

```

```

*-----
--

```

```

* Model "DHWProf-2" (Type 9)
*

```

```

UNIT 57 TYPE 9      DHWProf-2
*$UNIT_NAME DHWProf-2
*$MODEL .\Utility\Data Readers\Generic Data Files\First Line is Simulation
Start\Free Format\Type9a.tmf
*$POSITION 55 784
*$LAYER Main #
PARAMETERS 54
2          ! 1 Mode
0          ! 2 Header Lines to Skip
12         ! 3 No. of values to read
0.016667  ! 4 Time interval of data
-1         ! 5 Interpolate or not?-1
1.0       ! 6 Multiplication factor-1
0         ! 7 Addition factor-1
1         ! 8 Average or instantaneous value-1
-1        ! 9 Interpolate or not?-2
1.0       ! 10 Multiplication factor-2
0         ! 11 Addition factor-2
1         ! 12 Average or instantaneous value-2
-1        ! 13 Interpolate or not?-3
1.0       ! 14 Multiplication factor-3
0         ! 15 Addition factor-3
1         ! 16 Average or instantaneous value-3
-1        ! 17 Interpolate or not?-4
1.0       ! 18 Multiplication factor-4
0         ! 19 Addition factor-4
1         ! 20 Average or instantaneous value-4
-1        ! 21 Interpolate or not?-5
1.0       ! 22 Multiplication factor-5
0         ! 23 Addition factor-5
1         ! 24 Average or instantaneous value-5

```

```

-1          ! 25 Interpolate or not?-6
1.0        ! 26 Multiplication factor-6
0          ! 27 Addition factor-6
1          ! 28 Average or instantaneous value-6
-1         ! 29 Interpolate or not?-7
1.0       ! 30 Multiplication factor-7
0         ! 31 Addition factor-7
1         ! 32 Average or instantaneous value-7
-1        ! 33 Interpolate or not?-8
1.0      ! 34 Multiplication factor-8
0        ! 35 Addition factor-8
1        ! 36 Average or instantaneous value-8
-1       ! 37 Interpolate or not?-9
1.0     ! 38 Multiplication factor-9
0       ! 39 Addition factor-9
1       ! 40 Average or instantaneous value-9
-1      ! 41 Interpolate or not?-10
1.0    ! 42 Multiplication factor-10
0      ! 43 Addition factor-10
1      ! 44 Average or instantaneous value-10
-1     ! 45 Interpolate or not?-11
1.0   ! 46 Multiplication factor-11
0     ! 47 Addition factor-11
1     ! 48 Average or instantaneous value-11
-1    ! 49 Interpolate or not?-12
1.0  ! 50 Multiplication factor-12
0    ! 51 Addition factor-12
1    ! 52 Average or instantaneous value-12
57   ! 53 Logical unit for input file
-1   ! 54 Free format mode

```

*** External files

```

ASSIGN "C:\Documents and Settings\jsustar\My Documents\ParaStudy\DHW Event
Generator\HighUse_60s_Mixed.txt" 57

```

```

*|? Input file name |1000

```

```

*-----
--

```

```

* Model "Diverter-Hot" (Type 11)
*

```

```

UNIT 58 TYPE 11      Diverter-Hot

```

```

*$UNIT_NAME Diverter-Hot

```

```

*$MODEL .\Hydronics\Tempering Valve\Other Fluids\Type11b.tmf

```

```

*$POSITION 297 797

```

```

*$LAYER Main #

```

```

PARAMETERS 2

```

```

4          ! 1 Tempering valve mode

```

```

7          ! 2 Nb. of oscillations allowed

```

```

INPUTS 4

```

```

12,5      ! Weather:Mains water temperature ->Inlet temperature

```

```

HotDraw   ! DHW-2:HotDraw ->Inlet flow rate

```

```

26,1     ! Type534-Coiled:Temperature at outlet ->Heat source temperature

```

```

Thot     ! DHW-2:Thot ->Set point temperature

```

```

*** INITIAL INPUT VALUES

```

```

20.0 100.0 55.0 54.444

```

```

*-----
--

```

* Model "Diverter-2-Mixed" (Type 11)
*

UNIT 59 TYPE 11 Diverter-2-Mixed
*\$UNIT_NAME Diverter-2-Mixed
*\$MODEL .\Hydronics\Tempering Valve\Other Fluids\Typellb.tmf
*\$POSITION 340 872
*\$LAYER Main #
PARAMETERS 2
4 ! 1 Tempering valve mode
7 ! 2 Nb. of oscillations allowed
INPUTS 4
12,5 ! Weather:Mains water temperature ->Inlet temperature
MixedDraw ! DHW-2:MixedDraw ->Inlet flow rate
26,1 ! Type534-Coiled:Temperature at outlet ->Heat source temperature
Tmix ! DHW-2:Tmix ->Set point temperature
*** INITIAL INPUT VALUES
20.0 100.0 55.0 43.333

--

* Model "Tee-2_hot" (Type 11)
*

UNIT 60 TYPE 11 Tee-2_hot
*\$UNIT_NAME Tee-2_hot
*\$MODEL .\Hydronics\Tee-Piece\Other Fluids\Typellh.tmf
*\$POSITION 452 808
*\$LAYER Main #
PARAMETERS 1
1 ! 1 Tee piece mode
INPUTS 4
59,1 ! Diverter-2-Mixed:Temperature at outlet 1 ->Temperature at inlet 1
59,2 ! Diverter-2-Mixed:Flowrate at outlet 1 ->Flow rate at inlet 1
58,1 ! Diverter-Hot:Temperature at outlet 1 ->Temperature at inlet 2
58,2 ! Diverter-Hot:Flowrate at outlet 1 ->Flow rate at inlet 2
*** INITIAL INPUT VALUES
20.0 100.0 20.0 100.0

--

* Model "Monthly Integration-2" (Type 24)
*

UNIT 61 TYPE 24 Monthly Integration-2
*\$UNIT_NAME Monthly Integration-2
*\$MODEL .\Utility\Integrators\Quantity Integrator\TYPE24.tmf
*\$POSITION 283 666
*\$LAYER Main #
PARAMETERS 2
-1 ! 1 Integration period
0 ! 2 Relative or absolute start time
INPUTS 12
Solar ! Losses:Solar ->Qsol-1
26,10 ! Type534-Coiled:Auxiliary heating rate ->Qauxtank-2

```

0,0          ! [unconnected] Qauxsph-3
19,3         ! SolPmp:Power consumption ->Qpumpsol-4
51,3         ! SpHPmp:Power consumption ->Qpumpsph-5
Tanklosstotal      ! Losses:Tanklosstotal ->Qtankloss-6
26,5         ! Type534-Coiled:Energy delivered to flow ->Qdhw-7
26,42        ! Type534-Coiled:Energy delivered to HX-1 ->Qsphaux-8
12,24        ! Weather:Total tilted surface radiation for surface-1 -
>Qinc-9
13,3         ! Coll:Useful energy gain ->Quseful-10
26,2         ! Type534-Coiled:Flow rate at outlet ->DHWConsump-11
26,46        ! Type534-Coiled:Energy delivered to HX-2 ->Qsphsol-12
*** INITIAL INPUT VALUES
0.0 0.0 0.0 0.0 0.0 0.0 0.0 0.0 0.0 0.0 0.0
*-----
--

* Model "Monthly Results" (Type 25)
*

UNIT 62 TYPE 25      Monthly Results
*$UNIT_NAME Monthly Results
*$MODEL .\Output\Printer\Unformatted\No Units\Type25c.tmf
*$POSITION 439 680
*$LAYER Main #
PARAMETERS 10
-1          ! 1 Printing interval
START       ! 2 Start time
STOP       ! 3 Stop time
58         ! 4 Logical unit
0          ! 5 Units printing mode
0          ! 6 Relative or absolute start time
-1         ! 7 Overwrite or Append
-1         ! 8 Print header
0          ! 9 Delimiter
1          ! 10 Print labels
INPUTS 17
61,1       ! Monthly Integration-2:Qsol-1 ->Input to be printed-1
61,2       ! Monthly Integration-2:Qauxtank-2 ->Input to be printed-2
61,3       ! Monthly Integration-2:Qauxsph-3 ->Input to be printed-3
61,4       ! Monthly Integration-2:Qpumpsol-4 ->Input to be printed-4
61,5       ! Monthly Integration-2:Qpumpsph-5 ->Input to be printed-5
61,6       ! Monthly Integration-2:Qtankloss-6 ->Input to be printed-6
61,7       ! Monthly Integration-2:Qdhw-7 ->Input to be printed-7
61,8       ! Monthly Integration-2:Qsphaux-8 ->Input to be printed-8
61,9       ! Monthly Integration-2:Qinc-9 ->Input to be printed-9
61,10      ! Monthly Integration-2:Quseful-10 ->Input to be printed-10
61,11      ! Monthly Integration-2:DHWConsump-11 ->Input to be
printed-11
FSol_m     ! Efficiencies:FSol_m ->Input to be printed-12
EtaColl_m  ! Efficiencies:EtaColl_m ->Input to be printed-13
61,12     ! Monthly Integration-2:Qsphsol-12 ->Input to be printed-14
5,13      ! Sim Int:Thot-13 ->Input to be printed-15
5,14      ! Sim Int:Ttank-14 ->Input to be printed-16
5,15      ! Sim Int:Thouse-15 ->Input to be printed-17
*** INITIAL INPUT VALUES
Qsol Qauxtank Qauxsph Qpumpsol Qpumpsph Qtankloss Qdhw Qsph_aux Qinc
Quseful DHWConsump FSol etacoll Qsph_sol Thot Ttank Thouse

```



```

*** External files
ASSIGN "****.txt" 58
*|? Output file for printed results |1000
*-----
--

* EQUATIONS "hOutside"
*
EQUATIONS 1
hOutside = MAX(0.001, (8.23+4.00*[12,8]-0.057*[12,8]*2)*3.6)
*$UNIT_NAME hOutside
*$LAYER Main
*$POSITION 589 798

*-----
--

* Model "Sim Int-2" (Type 24)
*

UNIT 56 TYPE 24      Sim Int-2
*$UNIT_NAME Sim Int-2
*$MODEL .\Utility\Integrators\Quantity Integrator\TYPE24.tmf
*$POSITION 1061 335
*$LAYER Main #
PARAMETERS 2
STOP                ! 1 Integration period
0                   ! 2 Relative or absolute start time
INPUTS 7
50,4                ! Type653:Fluid heat transfer ->Input to be integrated-1
50,5                ! Type653:Top surface heat transfer ->Input to be integrated-2
50,6                ! Type653:Bottom heat transfer ->Input to be integrated-3
50,7                ! Type653:Edge heat transfer ->Input to be integrated-4
50,8                ! Type653:HX heat transfer ->Input to be integrated-5
50,9                ! Type653:Storage heat transfer ->Input to be integrated-6
32,2                ! Type56: 2- QHEAT_MAIN ->Input to be integrated-7
*** INITIAL INPUT VALUES
0.0 0.0 0.0 0.0 0.0 0.0 0.0
*-----
--

* Model "HourInteg" (Type 24)
*

UNIT 65 TYPE 24      HourInteg
*$UNIT_NAME HourInteg
*$MODEL .\Utility\Integrators\Quantity Integrator\TYPE24.tmf
*$POSITION 951 43
*$LAYER Main #
PARAMETERS 2
1                   ! 1 Integration period
0                   ! 2 Relative or absolute start time
INPUTS 24
Qinc                ! Collector:Qinc ->Qinc-1
13,3                ! Coll:Useful energy gain ->Quseful-2
Pipelosstotal      ! Losses:Pipelosstotal ->Qpipeloss-3

```

```

19,3      ! SolPmp:Power consumption ->Qpumpcoll-4
26,50     ! Type534-Coiled:Energy delivered to HX-3 ->Qlhx_sol-5
26,42     ! Type534-Coiled:Energy delivered to HX-1 ->Quhx-sph-6
26,5      ! Type534-Coiled:Energy delivered to flow ->Qdhw-7
TanklossTotal      ! Losses:TanklossTotal ->Qtankloss-8
26,10     ! Type534-Coiled:Auxiliary heating rate ->Qaux_tank-9
50,8      ! Type653:HX heat transfer ->Qsph-10
0,0       ! [unconnected] Qsphaux-11
51,3      ! SpHPmp:Power consumption ->Qpumpsph-12
BasementsLoss     ! Qslab:BasementsLoss ->Qbasement-13
0,0       ! [unconnected] Qinf-14
26,12     ! Type534-Coiled:Tank energy storage rate ->Qstore-15
26,51     ! Type534-Coiled:HX energy storage rate-3 ->QLHXStore-16
26,43     ! Type534-Coiled:HX energy storage rate-1 ->QUHXStore-17
PipeCapacitance   ! Losses:PipeCapacitance ->Qpipestore-18
50,9      ! Type653:Storage heat transfer ->Qsphstore-19
26,14     ! Type534-Coiled:Tank energy balance error -
>TankEnergyBalance-20
26,46     ! Type534-Coiled:Energy delivered to HX-2 ->Quhxsol-21
26,47     ! Type534-Coiled:HX energy storage rate-2 ->Quhxsolstore-22
ErrorCalc_lhx     ! Equa:ErrorCalc_lhx ->LHXError[kJ]-23
ErrorCalc_uhx     ! Equa:ErrorCalc_uhx ->UHXError[kJ]-24

```

*** INITIAL INPUT VALUES

```

0.0 0.0 0.0 0.0 0.0 0.0 0.0 0.0 0.0 0.0 0.0 0.0 0.0 0.0 0.0 0.0 0.0 0.0 0.0
0.0
0.0 0.0 0.0 0.0

```

```

*-----
--

```

```

* Model "Hour Results" (Type 25)
*

```

UNIT 66 TYPE 25 Hour Results

*\$UNIT_NAME Hour Results

*\$MODEL .\Output\Printer\Unformatted\No Units\Type25c.tmf

*\$POSITION 1102 53

*\$LAYER Main #

PARAMETERS 10

```

1      ! 1 Printing interval
START  ! 2 Start time
STOP   ! 3 Stop time
59     ! 4 Logical unit
0      ! 5 Units printing mode
0      ! 6 Relative or absolute start time
-1     ! 7 Overwrite or Append
-1     ! 8 Print header
0      ! 9 Delimiter
1      ! 10 Print labels

```

INPUTS 57

```

65,1   ! HourInteg:Qinc-1 ->Input to be printed-1
65,2   ! HourInteg:Quse-2 ->Input to be printed-2
65,3   ! HourInteg:Qpipeloss-3 ->Input to be printed-3
65,4   ! HourInteg:Qpumpcoll-4 ->Input to be printed-4
67,1   ! HourAverage:Ti_coll-1 ->Input to be printed-5
67,2   ! HourAverage:To_coll-2 ->Input to be printed-6
67,3   ! HourAverage:md_coll-3 ->Input to be printed-7
65,5   ! HourInteg:Qlhx_sol-5 ->Input to be printed-8

```

```

65,6      ! HourInteg:Quhx_sph-6 ->Input to be printed-9
65,7      ! HourInteg:Qdhw-7 ->Input to be printed-10
65,8      ! HourInteg:Qtankloss-8 ->Input to be printed-11
65,9      ! HourInteg:Qaux_tank-9 ->Input to be printed-12
67,4      ! HourAverage:Ti_lhx-4 ->Input to be printed-13
67,5      ! HourAverage:To_lhx-5 ->Input to be printed-14
67,6      ! HourAverage:Ti_uhx-6 ->Input to be printed-15
67,7      ! HourAverage:To_uhx-7 ->Input to be printed-16
67,8      ! HourAverage:md_sph-8 ->Input to be printed-17
67,9      ! HourAverage:md_dhwmix-9 ->Input to be printed-18
67,10     ! HourAverage:md_dhwhot-10 ->Input to be printed-19
67,11     ! HourAverage:md_dhwcold-11 ->Input to be printed-20
67,12     ! HourAverage:Tdhw-12 ->Input to be printed-21
67,13     ! HourAverage:Tdhw-13 ->Input to be printed-22
67,14     ! HourAverage:Tdhw-14 ->Input to be printed-23
65,10     ! HourInteg:Qsph-10 ->Input to be printed-24
65,11     ! HourInteg:Qsphaux-11 ->Input to be printed-25
65,12     ! HourInteg:Qpumpsph-12 ->Input to be printed-26
67,15     ! HourAverage:Tisph-15 ->Input to be printed-27
67,16     ! HourAverage:Thouse-16 ->Input to be printed-28
65,13     ! HourInteg:Qbasement-13 ->Input to be printed-29
65,14     ! HourInteg:Qinf-14 ->Input to be printed-30
SolarBalance      ! HourCalc:SolarBalance ->Input to be printed-31
TankBalance      ! HourCalc:TankBalance ->Input to be printed-32
SPHBalance      ! HourCalc:SPHBalance ->Input to be printed-33
FSol_h          ! HourCalc:FSol_h ->Input to be printed-34
EtaColl_h       ! HourCalc:EtaColl_h ->Input to be printed-35
65,15          ! HourInteg:Qstore-15 ->Input to be printed-36
65,16          ! HourInteg:Qlhxstore-16 ->Input to be printed-37
65,17          ! HourInteg:Quhxstore-17 ->Input to be printed-38
65,18          ! HourInteg:Qpipestore-18 ->Input to be printed-39
65,19          ! HourInteg:Qsphstore-19 ->Input to be printed-40
67,17          ! HourAverage:T1-17 ->Input to be printed-41
67,18          ! HourAverage:T3-18 ->Input to be printed-42
67,19          ! HourAverage:T5-19 ->Input to be printed-43
67,20          ! HourAverage:T7-20 ->Input to be printed-44
67,21          ! HourAverage:T9-21 ->Input to be printed-45
67,22          ! HourAverage:T11-22 ->Input to be printed-46
67,23          ! HourAverage:T13-23 ->Input to be printed-47
67,24          ! HourAverage:T15-24 ->Input to be printed-48
67,25          ! HourAverage:T17-25 ->Input to be printed-49
HXUEff         ! HourCalc:HXUEff ->Input to be printed-50
HXLEff         ! HourCalc:HXLEff ->Input to be printed-51
65,24          ! HourInteg:UHXError-24 ->Input to be printed-52
65,23          ! HourInteg:LHXError-23 ->Input to be printed-53
Qauxtot        ! HourCalc:Qauxtot ->Input to be printed-54
65,20          ! HourInteg:TankEnergyBalance-20 ->Input to be printed-55
65,21          ! HourInteg:Quhxsol-21 ->Input to be printed-56
65,22          ! HourInteg:Quhxsolstore-22 ->Input to be printed-57
*** INITIAL INPUT VALUES
Qinc Quseful Qpipeloss Qpumpcol Ti_coll To_coll md_coll Qlhx_sol Quhx_sph
Qdhw Qtankloss Qaux_tank Ti_lhx To_lhx Ti_uhx To_uhx md_sph md_dhwmix
md_dhwhot md_dhwcold Tmains Tdhw Tdhw Tdhw Qsph Qauxsph Qpumpsph Ti_sph
Thouse Qbasement Qinf SolBal TankBal SPHBal fsol etacoll Qstore Qlhxstore
Quhxstore Qpipestore Qsphstore T1 T3 T5 T7 T9 T11 T13 T15 T17 HXUEff HXLEff
HXUError[kJ] HXLError[kJ] Qauxtot TankEnergyBalance Quhxsol Quhxstore

```



```

TankBalance = [65,9]-([65,8]+[65,7]+[65,6]+[65,21])-[65,5]-[65,15]-[65,16]-
[65,17]-[65,22]
SPHBalance = [65,21]+[65,6]+([65,12]/2)-Qsptot_h-[65,19]
Qsptot_h = [65,10]
HXUEff = MIN(([67,6]-[67,7])/([67,6]-(([67,17]+[67,18]+[67,19])/3)+1E-6),1)
HXLEff = MIN(([67,4]-[67,5])/([67,4]-(([67,25]+[67,24])/2)+1E-6),1)
Qauxtot = [65,9]
*$UNIT_NAME HourCalc
*$LAYER Main
*$POSITION 1086 138

*-----
--

* Model "Tee_cold" (Type 11)
*

UNIT 69 TYPE 11 Tee_cold
*$UNIT_NAME Tee_cold
*$MODEL .\Hydronics\Tee-Piece\Other Fluids\Typellh.tmf
*$POSITION 463 886
*$LAYER Main #
PARAMETERS 1
1 ! 1 Tee piece mode
INPUTS 4
59,3 ! Diverter-2-Mixed:Temperature at outlet 2 ->Temperature at inlet
1
59,4 ! Diverter-2-Mixed:Flow rate at outlet 2 ->Flow rate at inlet 1
58,3 ! Diverter-Hot:Temperature at outlet 2 ->Temperature at inlet 2
58,4 ! Diverter-Hot:Flow rate at outlet 2 ->Flow rate at inlet 2
*** INITIAL INPUT VALUES
20.0 100.0 20.0 100.0
*-----
--

* Model "Tee_mixed-2" (Type 11)
*

UNIT 70 TYPE 11 Tee_mixed-2
*$UNIT_NAME Tee_mixed-2
*$MODEL .\Hydronics\Tee-Piece\Other Fluids\Typellh.tmf
*$POSITION 545 850
*$LAYER Main #
PARAMETERS 1
1 ! 1 Tee piece mode
INPUTS 4
26,1 ! Type534-Coiled:Temperature at outlet ->Temperature at inlet 1
26,2 ! Type534-Coiled:Flow rate at outlet ->Flow rate at inlet 1
69,1 ! Tee_cold:Outlet temperature ->Temperature at inlet 2
69,2 ! Tee_cold:Outlet flow rate ->Flow rate at inlet 2
*** INITIAL INPUT VALUES
20.0 100.0 20.0 100.0
*-----
--

* EQUATIONS "RadFlr"

```

```

*
EQUATIONS 1
Topslab = [50,4]-[50,9]
*$UNIT_NAME RadFlr
*$LAYER Main
*$POSITION 1130 407

*-----
--

* EQUATIONS "Equa"
*
EQUATIONS 2
ErrorCalc_lhx = [26,50]-([26,52]-[26,51])
ErrorCalc_uhx = [26,42]-([26,44]-[26,43])
*$UNIT_NAME Equa
*$LAYER Main
*$POSITION 1012 706

*-----
--

* Model "Type65d" (Type 65)
*
UNIT 63 TYPE 65      Type65d
*$UNIT_NAME Type65d
*$MODEL .\Output\Online Plotter\Online Plotter Without File\Type65d.tmf
*$POSITION 1074 226
*$LAYER Main #
PARAMETERS 12
3          ! 1 Nb. of left-axis variables
4          ! 2 Nb. of right-axis variables
15         ! 3 Left axis minimum
75         ! 4 Left axis maximum
0.0        ! 5 Right axis minimum
40         ! 6 Right axis maximum
1          ! 7 Number of plots per simulation
12         ! 8 X-axis gridpoints
0          ! 9 Shut off Online w/o removing
-1         ! 10 Logical unit for output file
0          ! 11 Output file units
0          ! 12 Output file delimiter
INPUTS 7
26,1       ! Type534-Coiled:Temperature at outlet ->Left axis variable-1
26,3       ! Type534-Coiled:Average tank temperature ->Left axis variable-2
32,1       ! Type56: 1- TAIR_MAIN ->Left axis variable-3
65,7       ! HourInteg:Qdhw-7 ->Right axis variable-1
65,10      ! HourInteg:Qsph-10 ->Right axis variable-2
Qaux1      ! [equation] Right axis variable-3
Qaux2      ! Tank Parameters:Qaux2 ->Right axis variable-4
*** INITIAL INPUT VALUES
Tout AverageTank Thouse Qdhw Qsph Qaux1 Qaux2
LABELS 3
"Temperatures"

```

"Heat transfer rates"

"Graph 1"

*-----

--

END

Appendix E : Steady State Hand Calculations

Verification of Solar Collector Model

Constant Weather (Solar radiation, incident angle, Mains temp)

Constant DHW flow

Collector Parameters

$$T_{\text{amb}} = 10 \text{ [C]}$$

$$\dot{V}_{\text{coll}} = 3 \cdot \left| 0.2271 \cdot \frac{\text{m}^3/\text{hr}}{\text{gal}/\text{min}} \right|$$

$$\rho_{\text{glycol}} = 1040 \text{ [kg/m}^3\text{]}$$

$$c_{p,\text{glycol}} = 3.55 \text{ [kJ/kg-C]}$$

$$FR_{\tau,\alpha} = 0.702$$

$$FR_{UL} = 3.73 \cdot \left| 3.6 \cdot \frac{\text{kJ}/(\text{hr}\cdot\text{m}^2\text{-C})}{\text{W}/(\text{m}^2\text{-C})} \right|$$

$$A_{\text{coll}} = 32 \cdot \left| 0.09290304 \cdot \frac{\text{m}^2}{\text{ft}^2} \right|$$

$$I_T = 1000 \cdot \left| 3.6 \cdot \frac{\text{kJ}/\text{hr}\cdot\text{m}^2}{\text{W}/\text{m}^2} \right|$$

$$\eta_{\text{coll}} = FR_{\tau,\alpha} - FR_{UL} \cdot \left[\frac{T_{\text{to,coll}} - T_{\text{amb}}}{I_T} \right]$$

$$\eta_{\text{coll}} = \frac{Q_{\text{useful}}}{A_{\text{coll}} \cdot I_T}$$

$$Q_{\text{useful}} = \dot{V}_{\text{coll}} \cdot \rho_{\text{glycol}} \cdot c_{p,\text{glycol}} \cdot (T_{\text{from,coll}} - T_{\text{to,coll}})$$

Solar immersed HX

$$\varepsilon_{\text{hx}} = 0.23$$

$$\varepsilon_{\text{hx}} = \frac{T_{\text{from,coll}} - T_{\text{to,coll}}}{T_{\text{from,coll}} - T_{\text{tank}}}$$

$$\dot{Q}_{\text{hx}} = \dot{V}_{\text{coll}} \cdot \rho_{\text{glycol}} \cdot c_{p,\text{glycol}} \cdot (T_{\text{from,coll}} - T_{\text{to,coll}})$$

Tank Parameters (tankloss)

$$V_{\text{tank}} = 105 \cdot \left| 0.003785412 \cdot \frac{\text{m}^3}{\text{gal}} \right|$$

$$H_{\text{tank}} = 5 \cdot \left| 0.3048 \cdot \frac{\text{m}}{\text{ft}} \right|$$

$$\text{Tank}_{U,\text{value}} = \frac{1}{8.5} \cdot \left| 20.44 \cdot \frac{\text{kJ}/\text{hr}\cdot\text{C}\cdot\text{m}^2}{\text{Btu}/\text{hr}\cdot\text{F}\cdot\text{ft}^2} \right|$$

$$T_{\text{room}} = 20 \text{ [C]}$$

$$V_{\text{tank}} = H_{\text{tank}} \cdot \pi \cdot r_{\text{tank}}^2$$

$$SA_{\text{tank}} = 2 \cdot \pi \cdot r_{\text{tank}}^2 + H_{\text{tank}} \cdot 2 \cdot \pi \cdot r_{\text{tank}}$$

$$\dot{Q}_{\text{tankloss}} = \text{Tank}_{U,\text{value}} \cdot SA_{\text{tank}} \cdot (T_{\text{tank}} - T_{\text{room}})$$

DHW Parameters

$$\dot{V}_{\text{dhw}} = 0.1 \cdot \left| 0.2271 \cdot \frac{\text{m}^3/\text{hr}}{\text{gal}/\text{min}} \right|$$

$$\rho_{\text{water}} = 1000 \text{ [kg/m}^3\text{]}$$

$$c_{p,\text{water}} = 4.18 \text{ [kJ/kg-C]}$$

$$T_{\text{mains}} = 15 \text{ [C]}$$

$$\dot{Q}_{\text{dhw}} = \dot{V}_{\text{dhw}} \cdot \rho_{\text{water}} \cdot c_{p,\text{water}} \cdot (T_{\text{tank}} - T_{\text{mains}})$$

SpH Parameters

$$\dot{V}_{\text{SpH}} = 0.1 \cdot \left| 0.2271 \cdot \frac{\text{m}^3/\text{hr}}{\text{gal}/\text{min}} \right|$$

$$\dot{Q}_{\text{SpH}} = 1000 \text{ [kJ/hr]}$$

$$T_{\text{from,SpH}} = T_{\text{tank}} - \frac{\dot{Q}_{\text{SpH}}}{\dot{V}_{\text{SpH}} \cdot \rho_{\text{water}} \cdot c_{p,\text{water}}}$$

Energy Balance

$$\text{Balance} = \dot{Q}_{\text{tankloss}} + \dot{Q}_{\text{dhw}} + \dot{Q}_{\text{SpH}} - \dot{Q}_{\text{hx}}$$

$$\dot{Q}_{\text{hx}} = \dot{Q}_{\text{tankloss}} + \dot{Q}_{\text{dhw}} + \dot{Q}_{\text{SpH}}$$

Resistance Network

$$\frac{1}{U \cdot SA} = \frac{1}{h_o \cdot SA} + \frac{D - D_i}{k_{cu}} + \frac{1}{h_i \cdot SA}$$

$$U_{k,j,h} = U \cdot \left| 3.6 \cdot \frac{\text{kJ/hr-K}}{\text{W/K}} \right|$$

$$Q_{\text{hx}} = U_{k,j,h} \cdot (T_s - T_{\text{inf}})$$

External Convection Heat Transfer Coefficient

Call **External**_{Flow,Cylinder} (Fluid\$, T_{inf}, T_s, P, u_{inf}, D : F_{dL}, h, C_d, Nusselt, Re)

$$D_{\text{coil}} = 0.475$$

$$Re_{\text{crit}} = 20000 \cdot \left[\frac{D}{D_{\text{coil}}} \right]^{0.32}$$

$$\mu = \mathbf{Visc} ('Water', T=T_s, P=P)$$

$$k = \mathbf{k} ('Water', T=T_s, P=P)$$

$$k_{\text{kJ}} = k \cdot \left[0.001 \cdot \frac{\text{kJ/s}}{\text{W}} \right]$$

$$cp = \mathbf{Cp} ('Water', T=T_s, P=P)$$

$$Pr_{\text{hx}} = cp \cdot \frac{\mu}{k_{\text{kJ}}}$$

$$Re_{\text{hx}} = 4 \cdot \frac{\dot{m}}{\pi \cdot D \cdot \mu}$$

$$Pr = \mathbf{Pr} ('Water', T=T_s, P=P)$$

$$\text{pitch}_{\text{coil}} = 0.07184 \text{ [m]}$$

$$HE = \frac{Re_{\text{hx}} \cdot \left[\frac{D}{D_{\text{coil}}} \right]^{0.5}}{1 + \left[\frac{\text{pitch}_{\text{coil}}}{\pi \cdot D} \right]^2}$$

$$Nusselt_{\text{hx}} = \left[\left(\frac{48}{11} + \frac{\frac{51}{11}}{\left[1 + \frac{1342}{Pr_{\text{hx}} \cdot HE^2} \right]^2} \right)^3 + 1.816 \cdot \left(\frac{HE}{1 + \frac{1.15}{Pr_{\text{hx}}}} \right)^{1.5} \right]^{(1/3)}$$

$$h_o = Nusselt_{\text{hx}} \cdot \frac{k}{D}$$

Internal Convection Heat Transfer

Call **FC**_{horizontal,cylinder} (Fluid\$, T_s, T_∞, P, D : h, Nusselt, Ra)

$$k_{\text{water}} = \mathbf{k} ('Water', T=T_s, P=P)$$

$$h_{\text{internal}} = Nusselt \cdot \frac{k_{\text{water}}}{D}$$

Appendix F : Energy and Economic Analysis Results

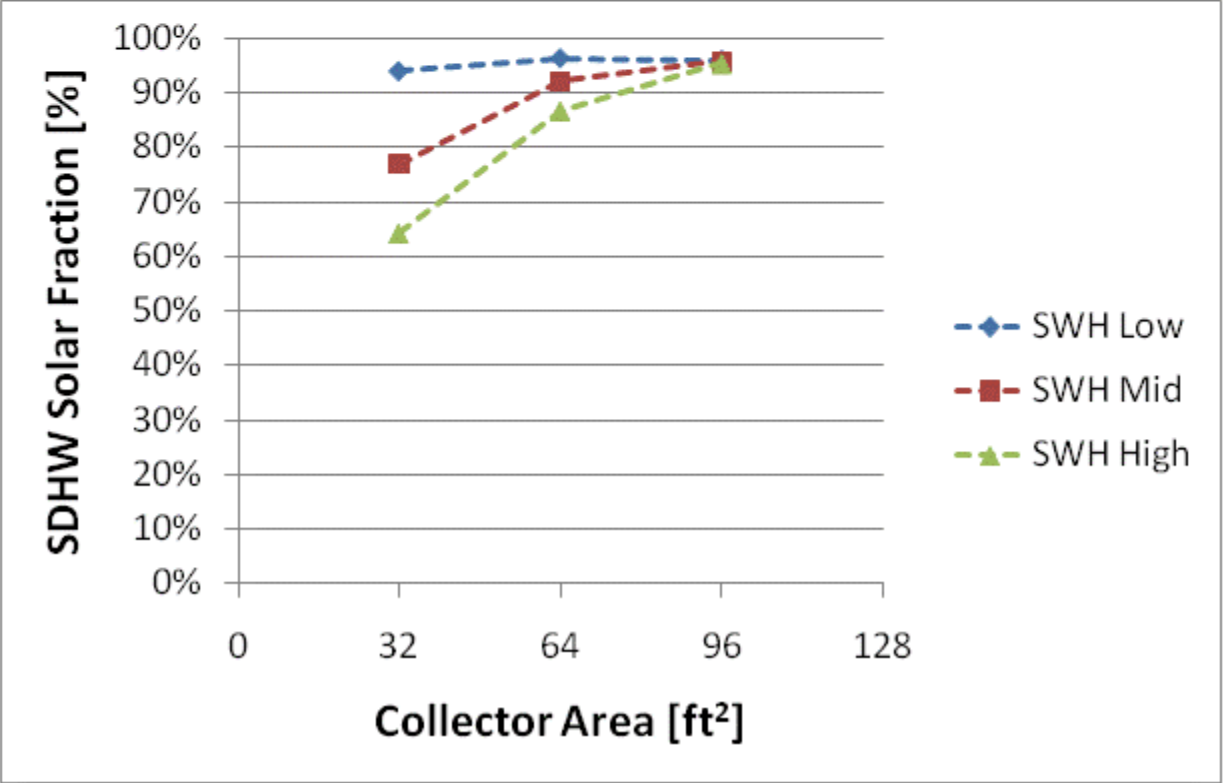
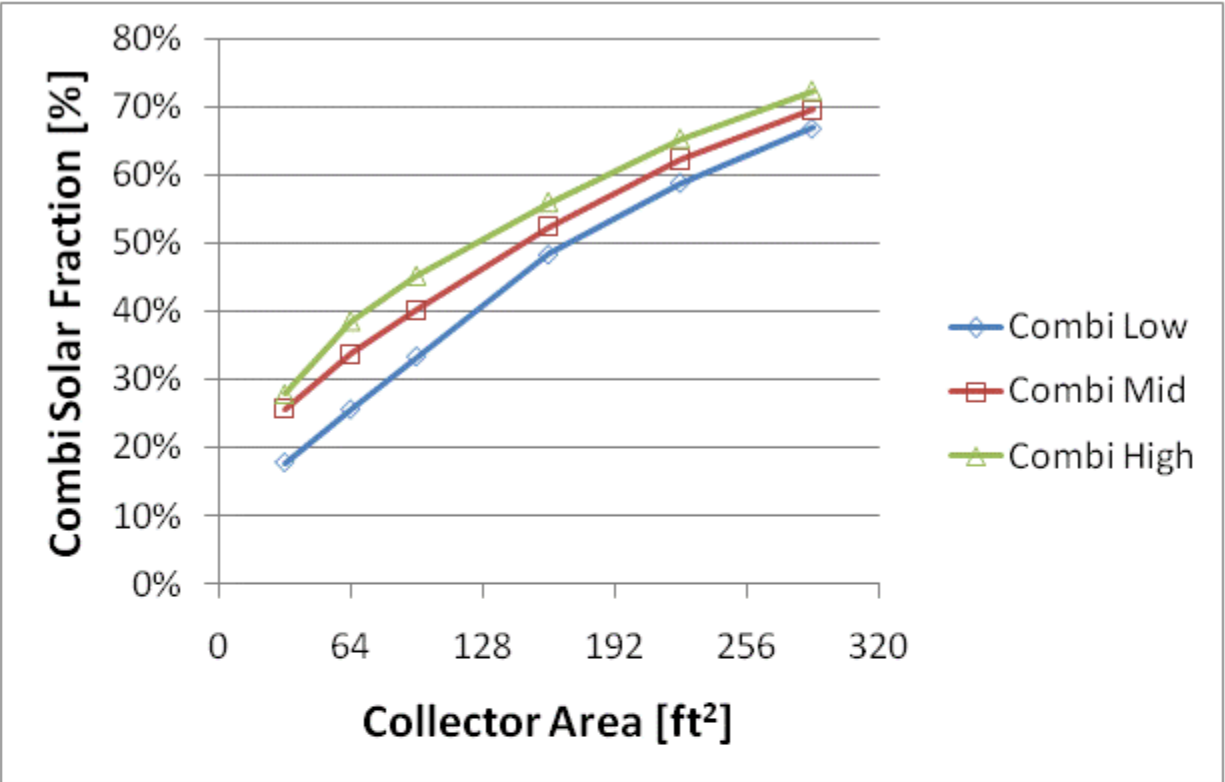


Figure F.1: Combisystem and SWH solar fraction for a 1960s Retrofit House(Phoenix)

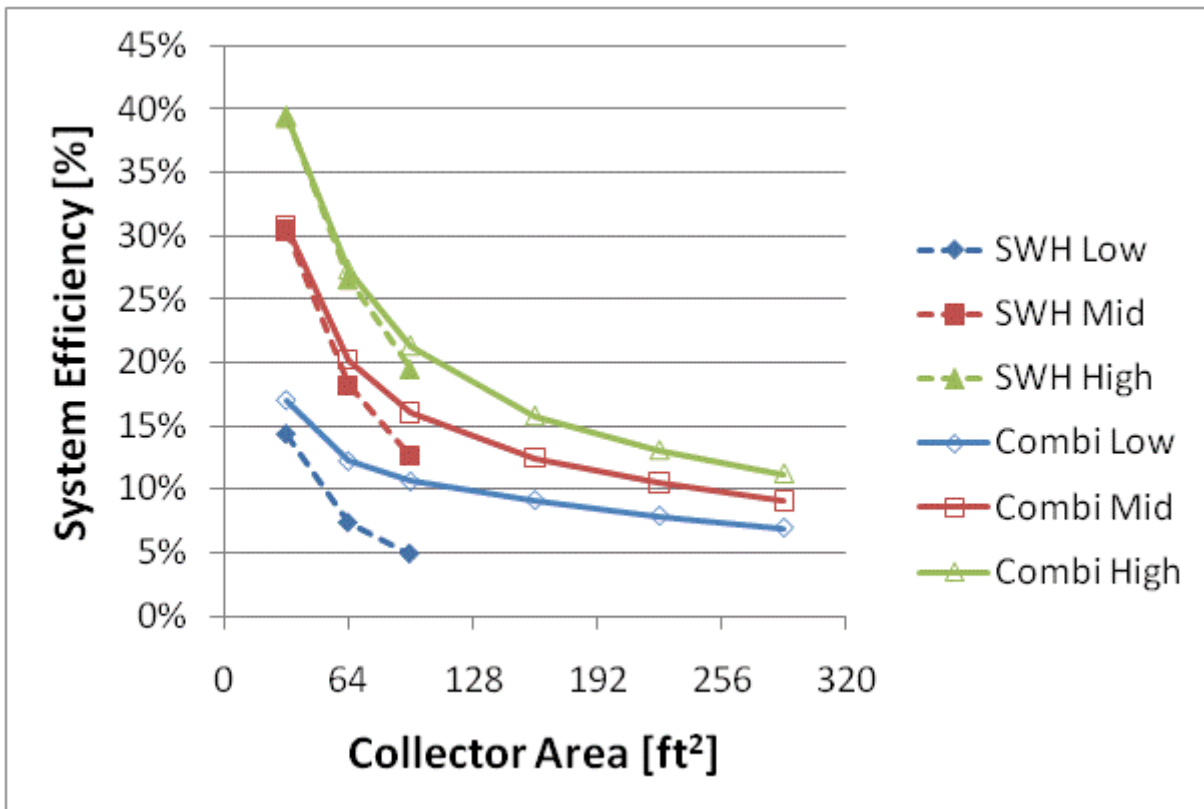
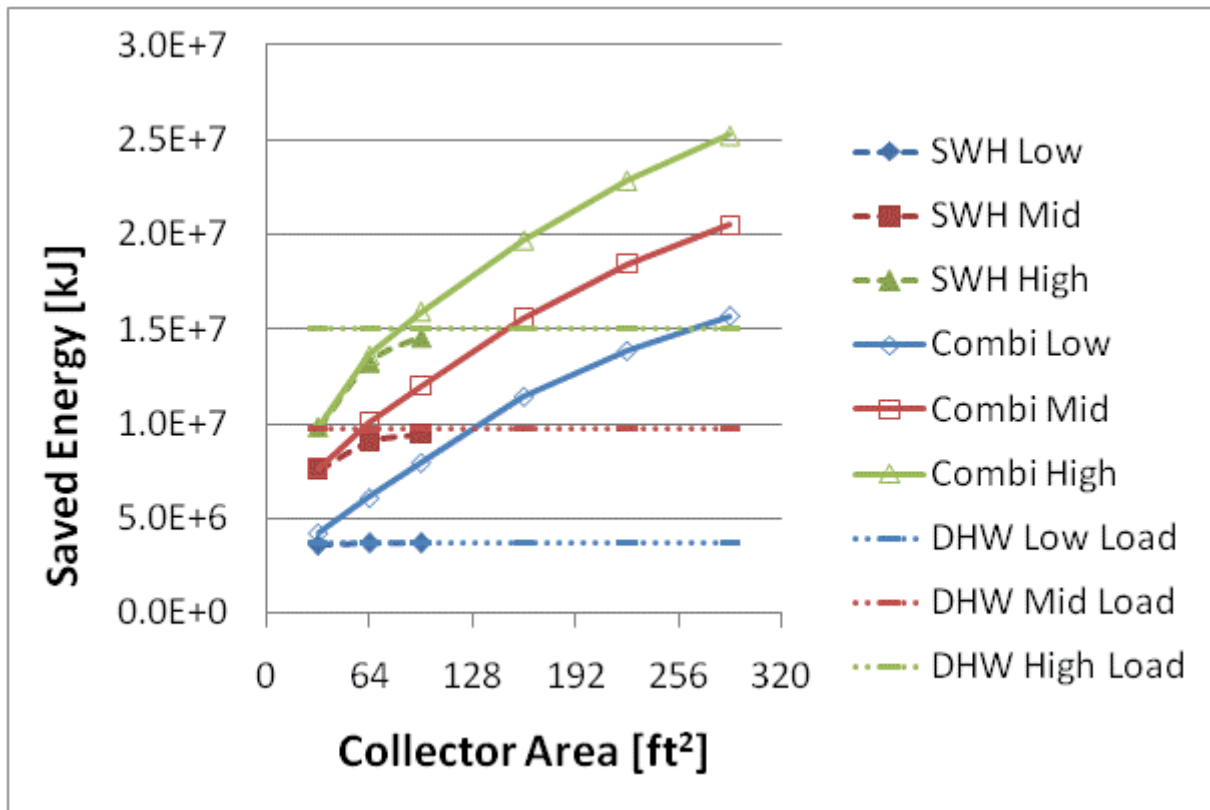


Figure F.2: Annual saved energy and system efficiency for a 1960s Retrofit House(Phoenix)

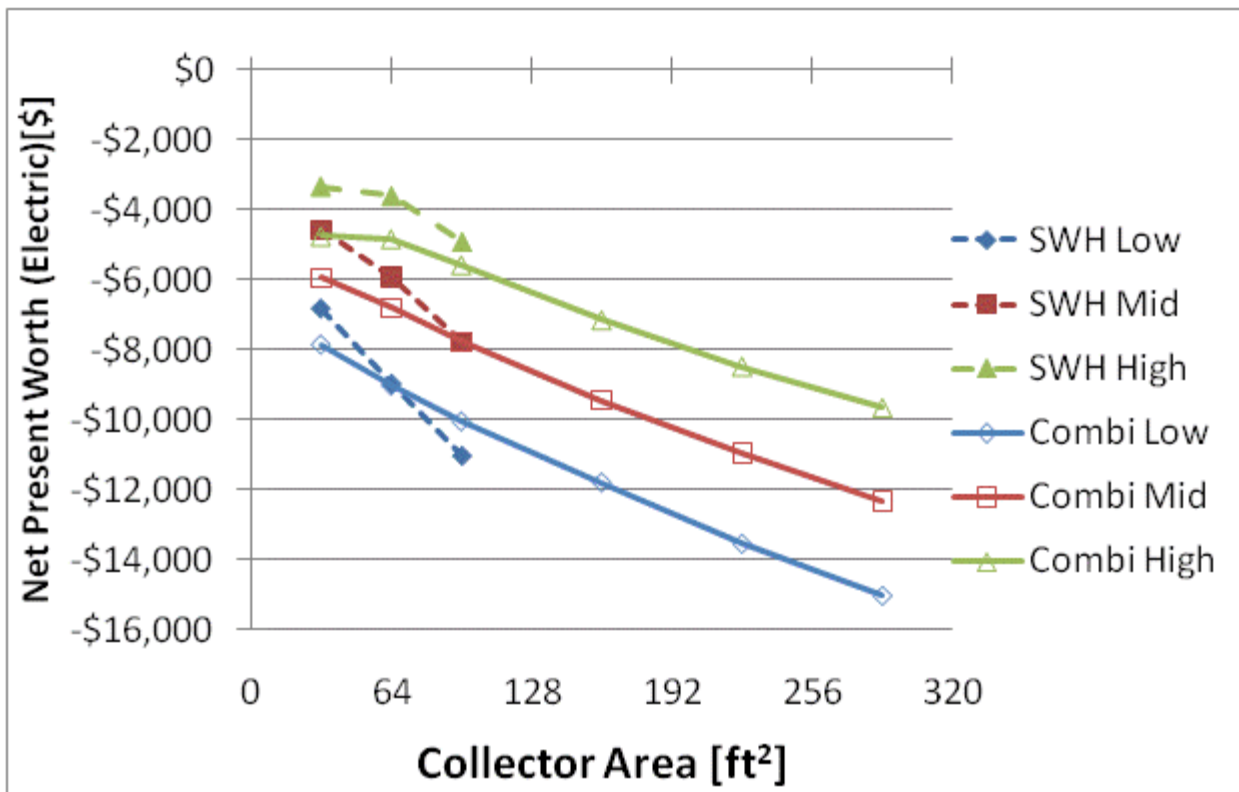
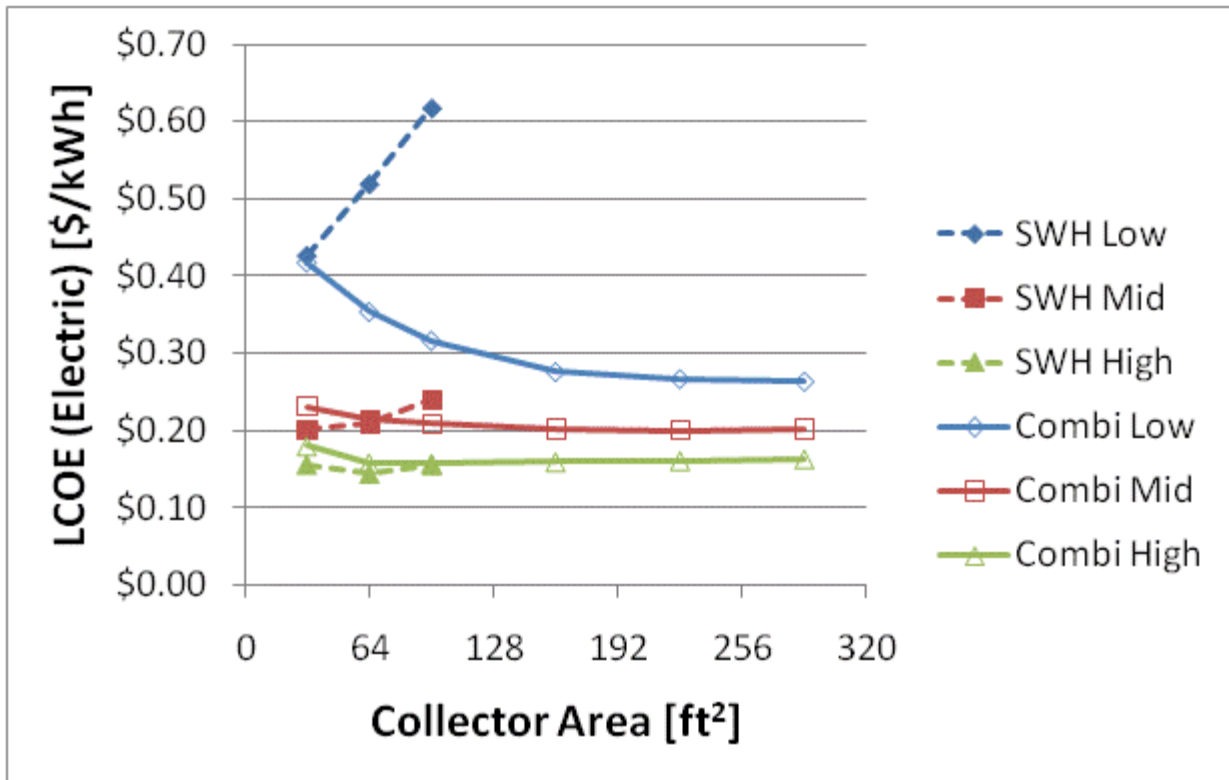


Figure F.3: LCOE and NPW for electric systems for a 1960s Retrofit House(Phoenix)

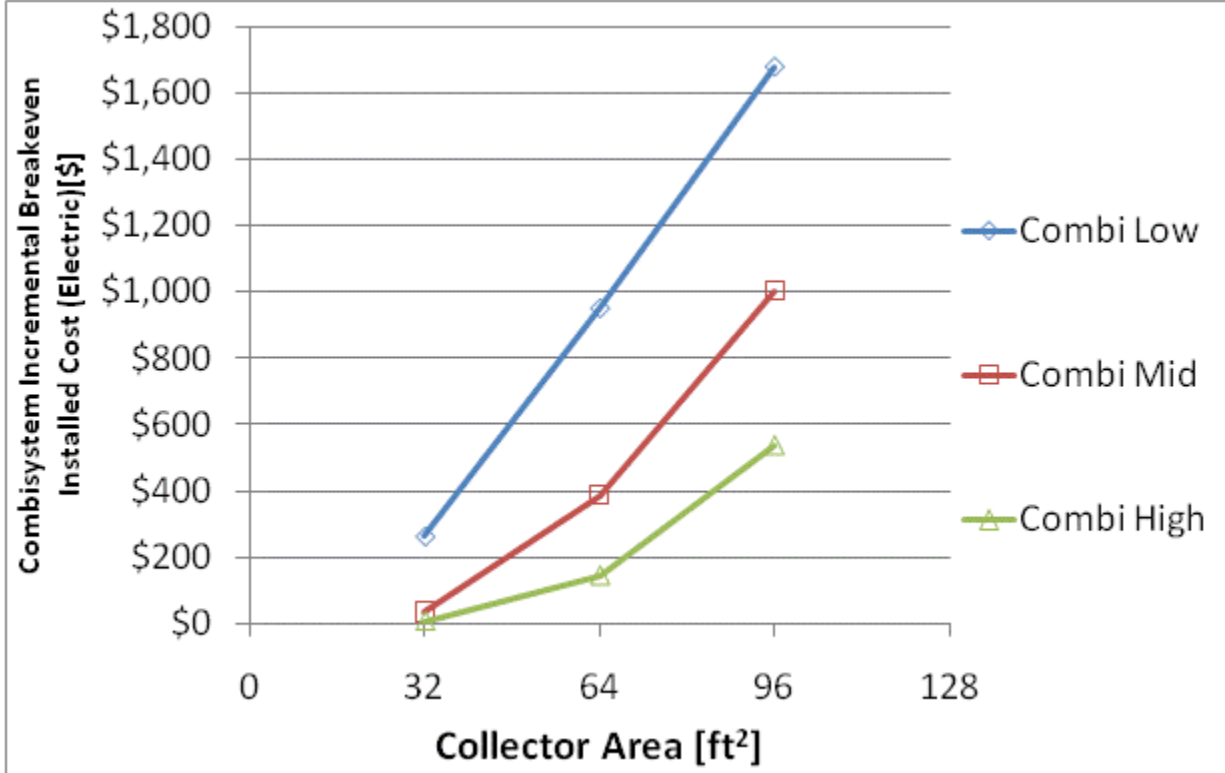
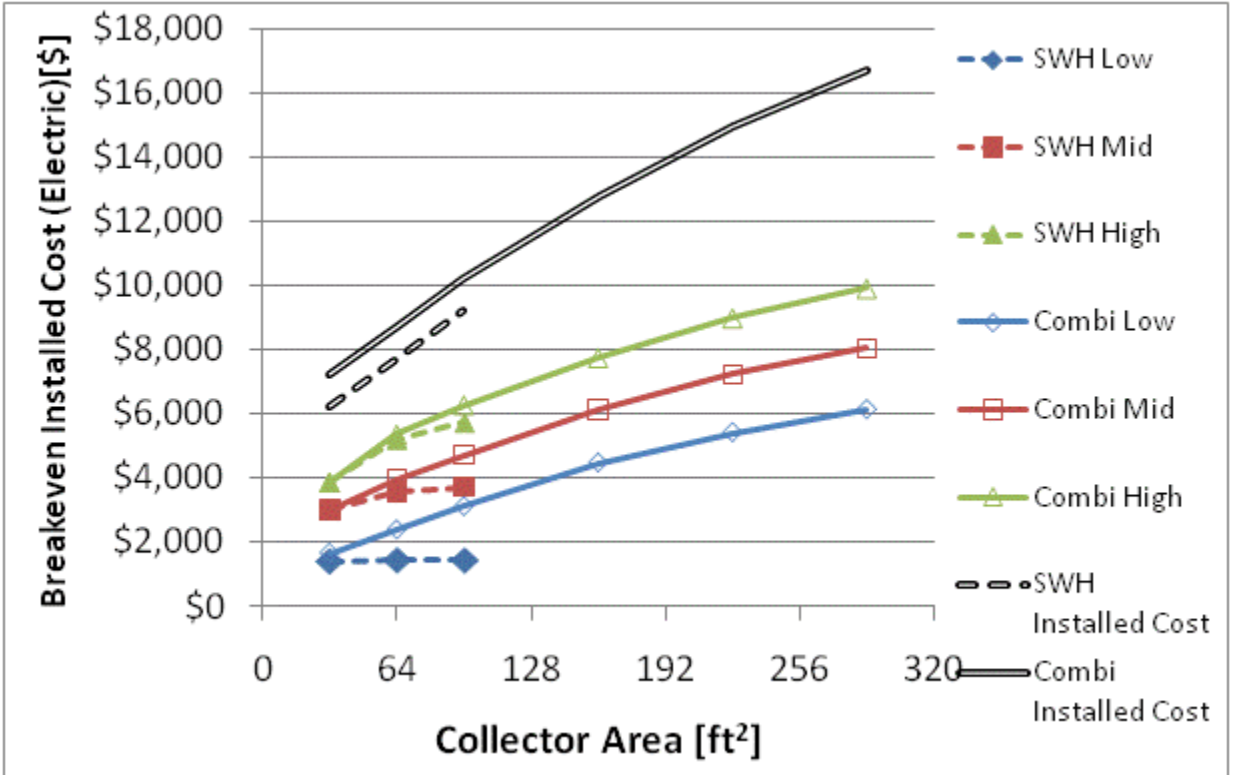


Figure F.4: Breakeven installed cost and combisystem incremental breakeven cost for electric system for a 1960s Retrofit House(Phoenix)

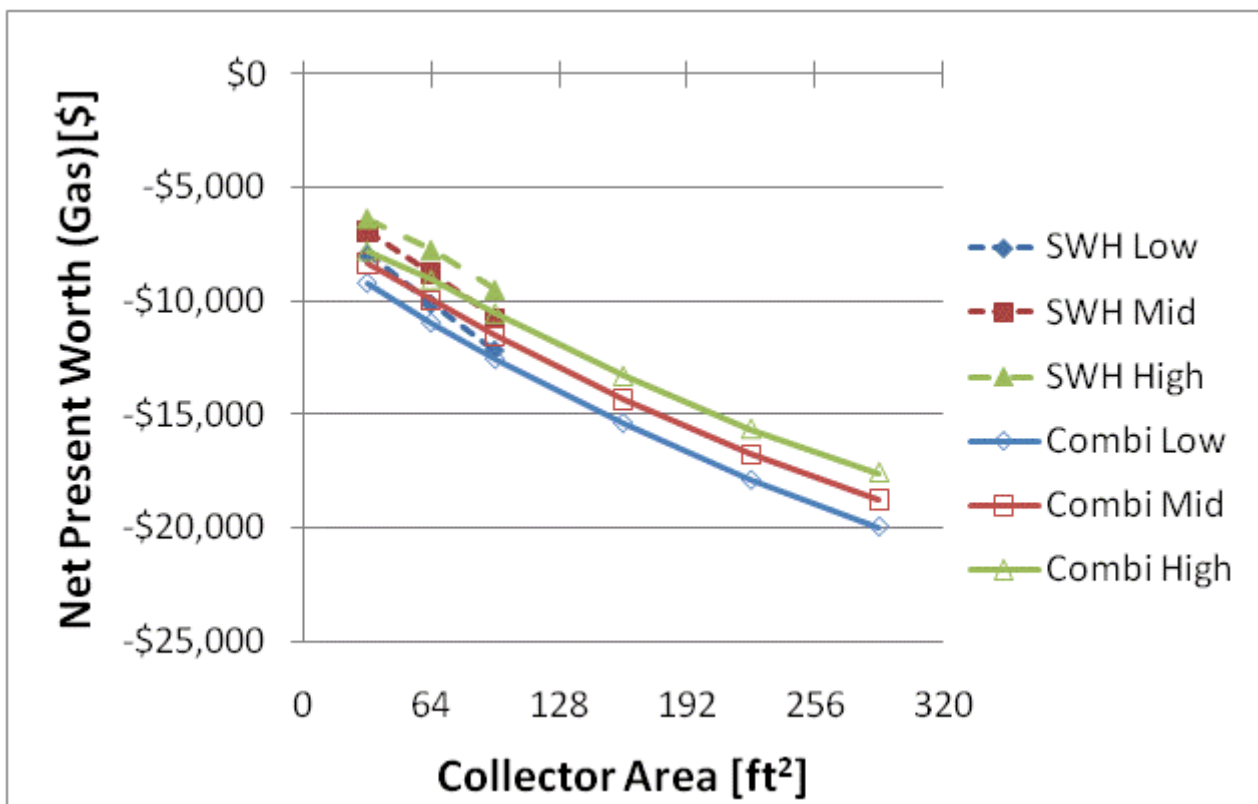
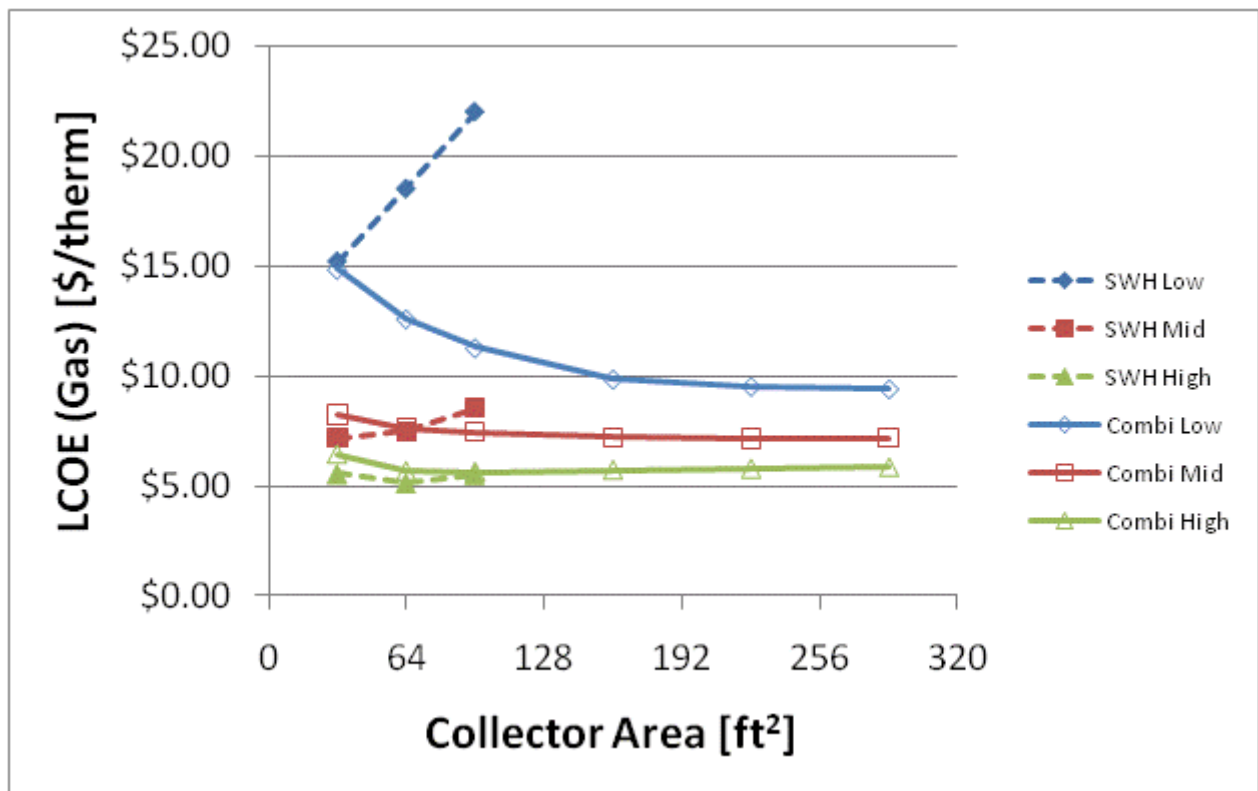


Figure F.5: LCOE and NPW for gas systems for a 1960s Retrofit House(Phoenix)

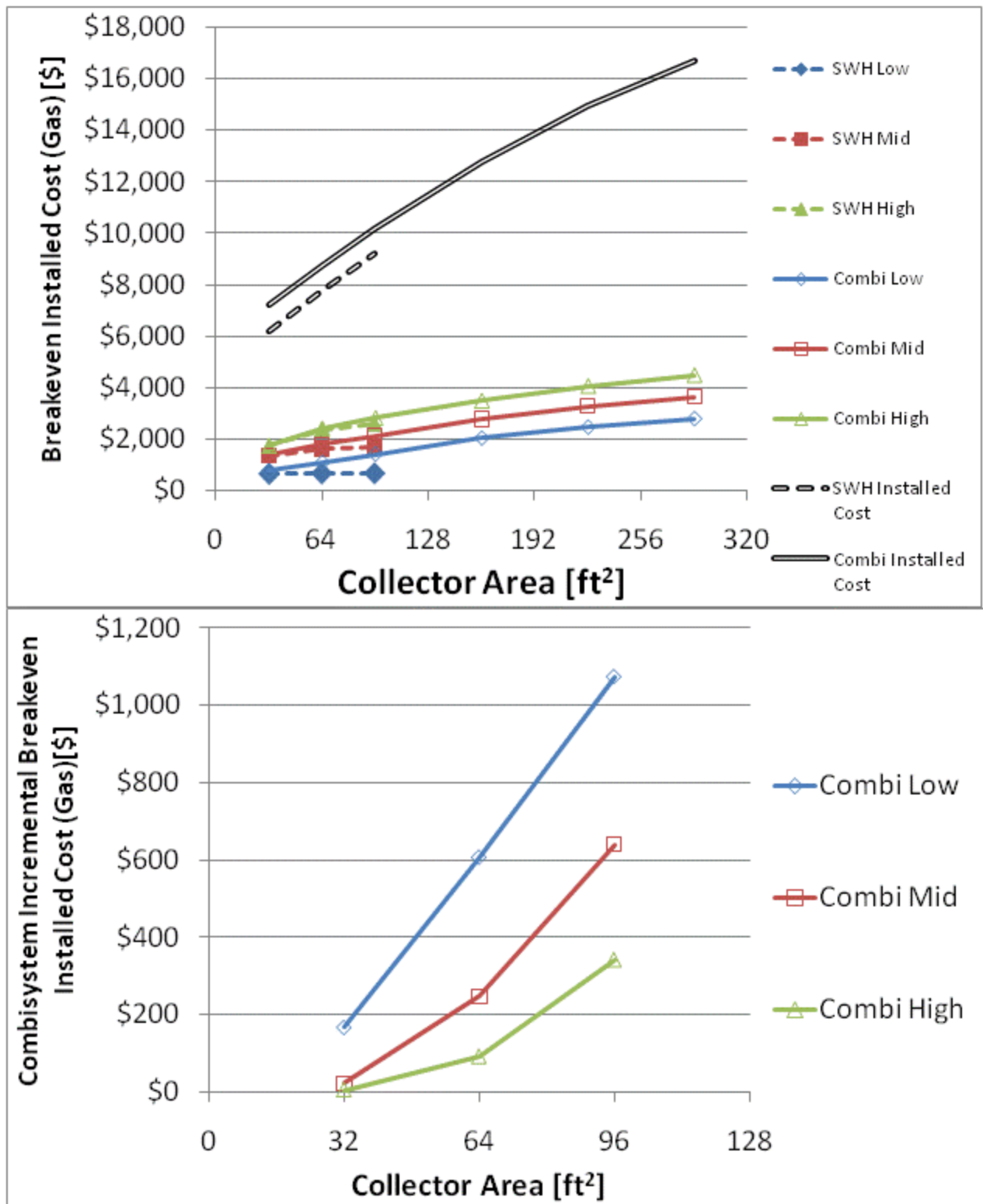


Figure F.6: Breakeven installed cost and combisystem incremental breakeven cost for gas systems for a 1960s Retrofit House(Phoenix)

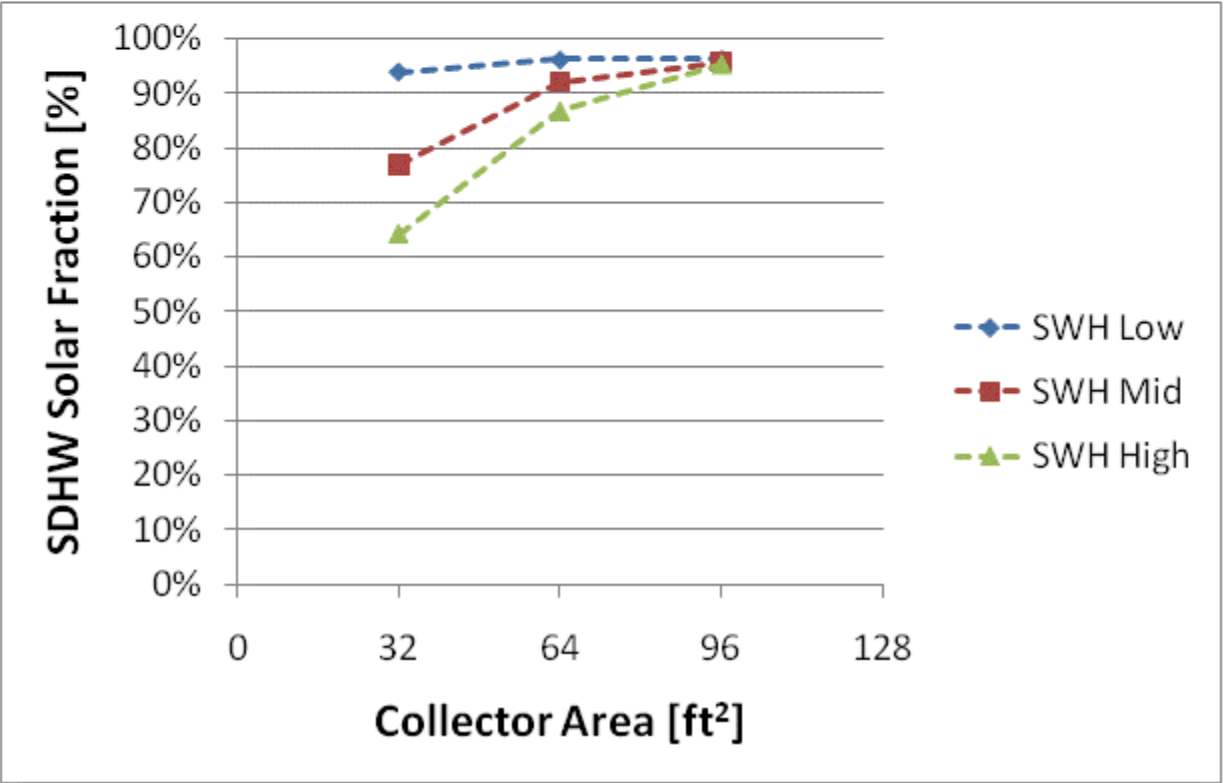
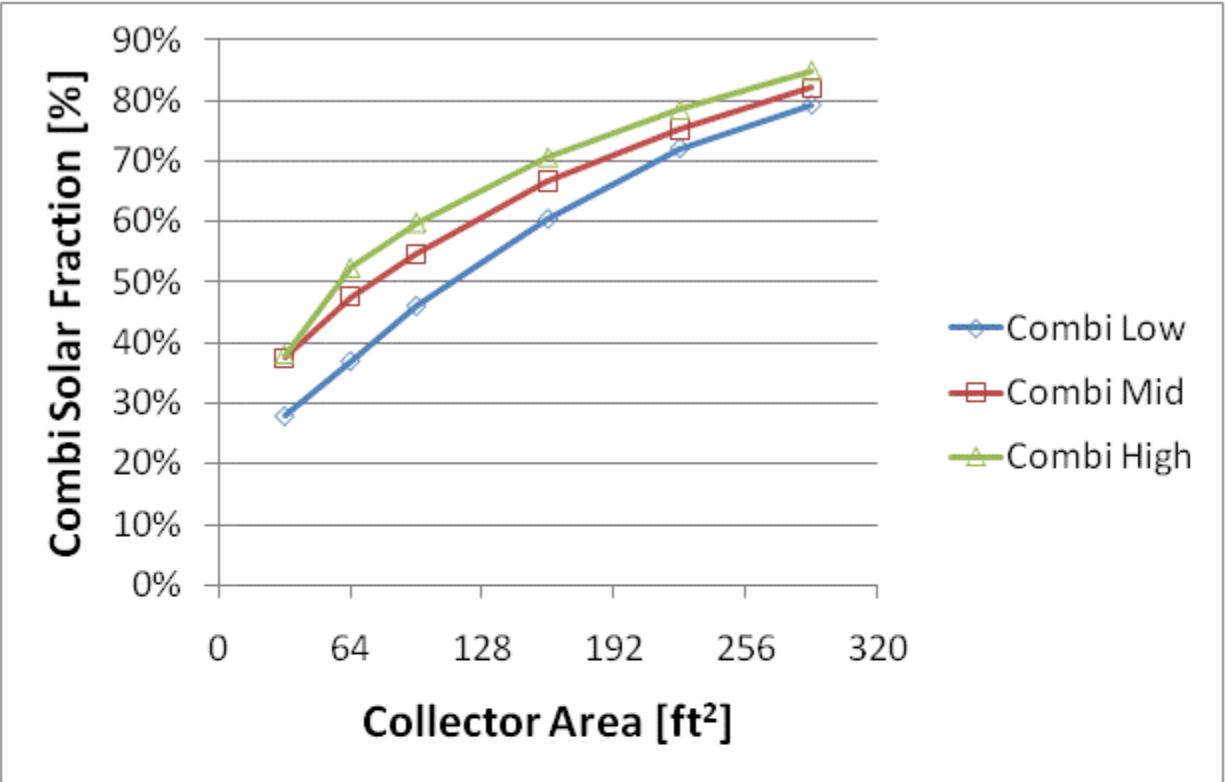


Figure F.7: Combisystem and SWH solar fraction for a IECC 2009 House(Phoenix)

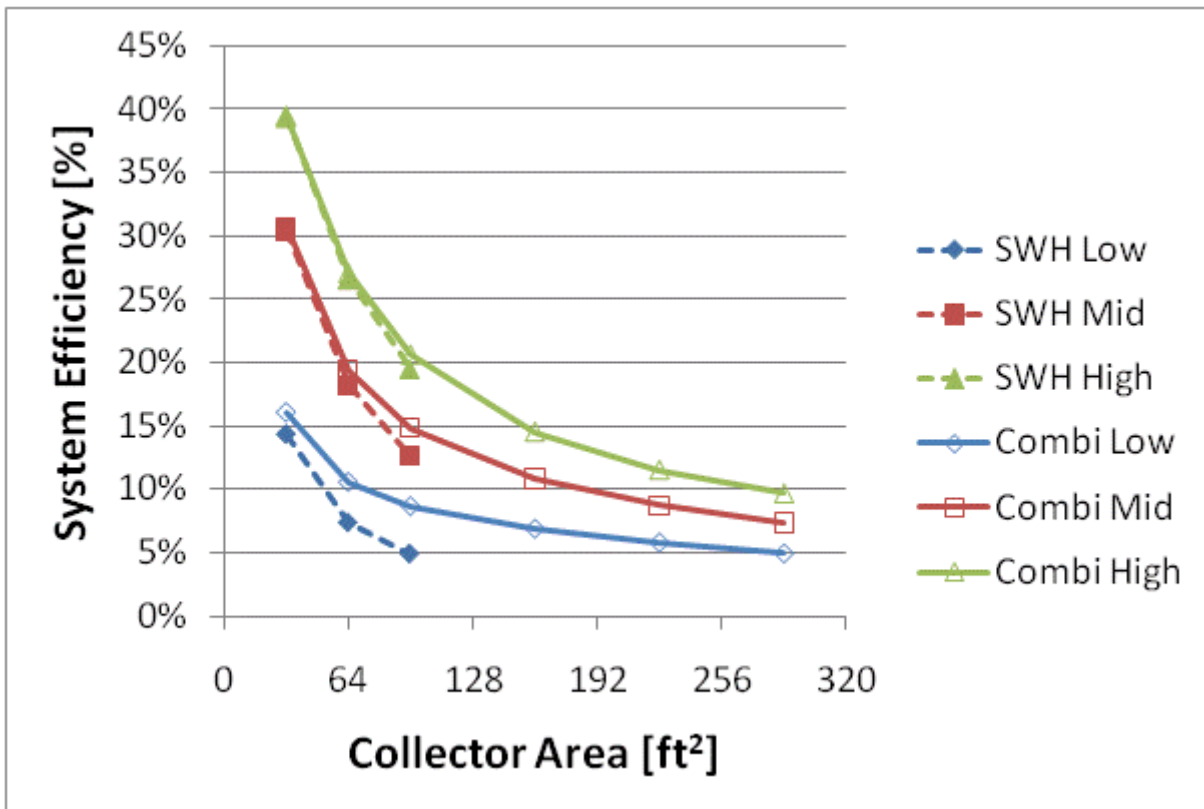
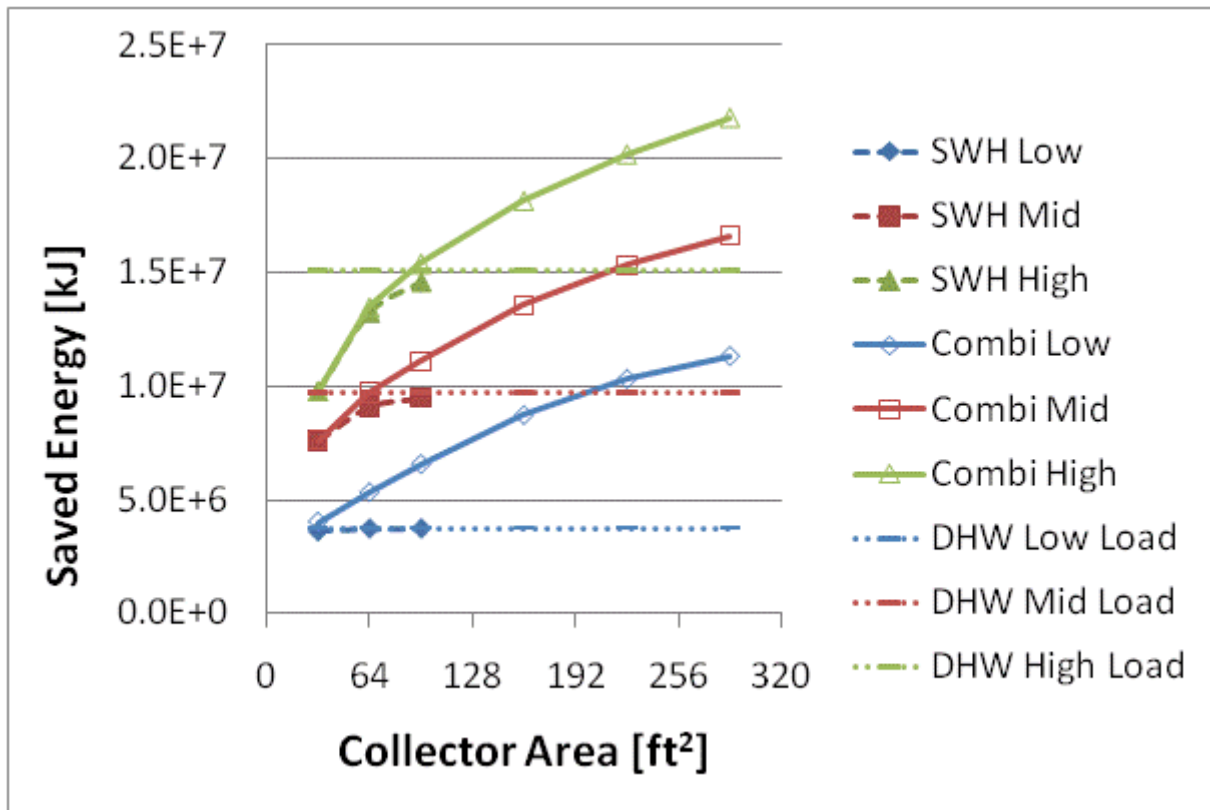


Figure F.8: Annual saved energy and system efficiency for a IECC 2009 House(Phoenix)

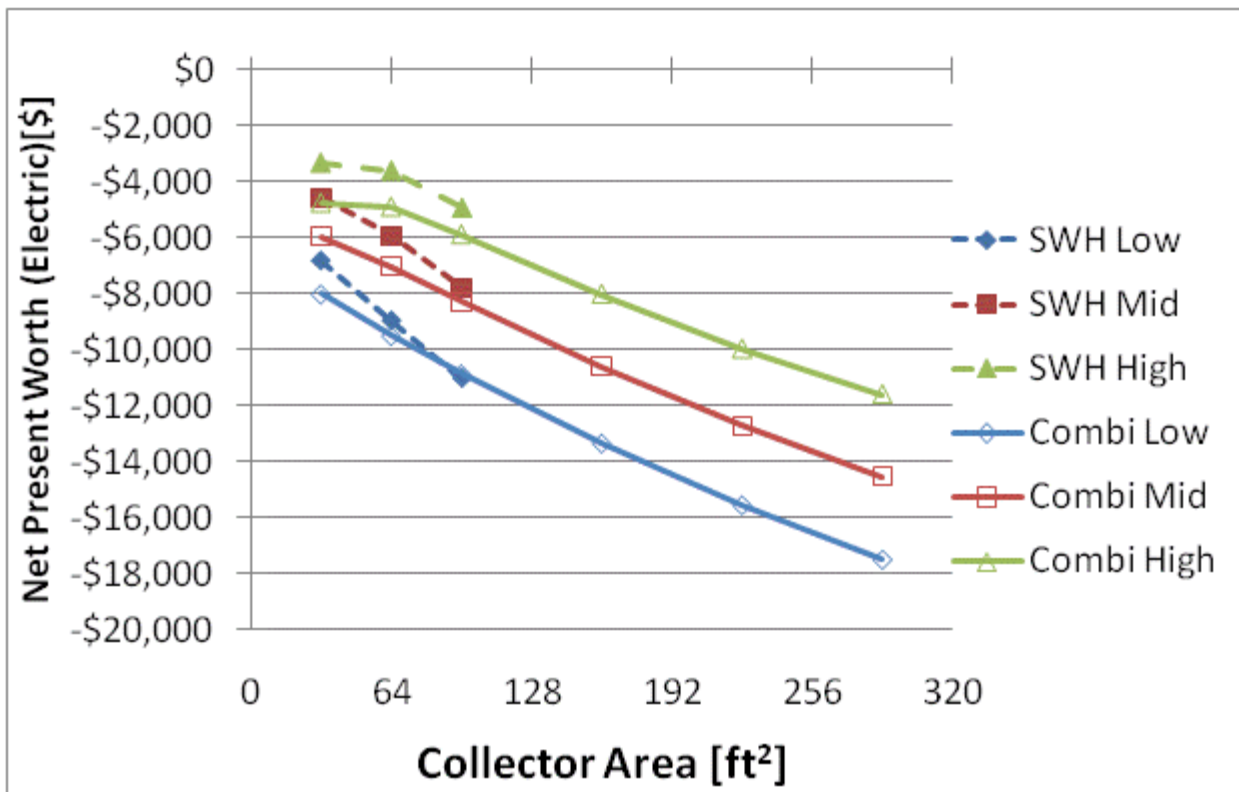
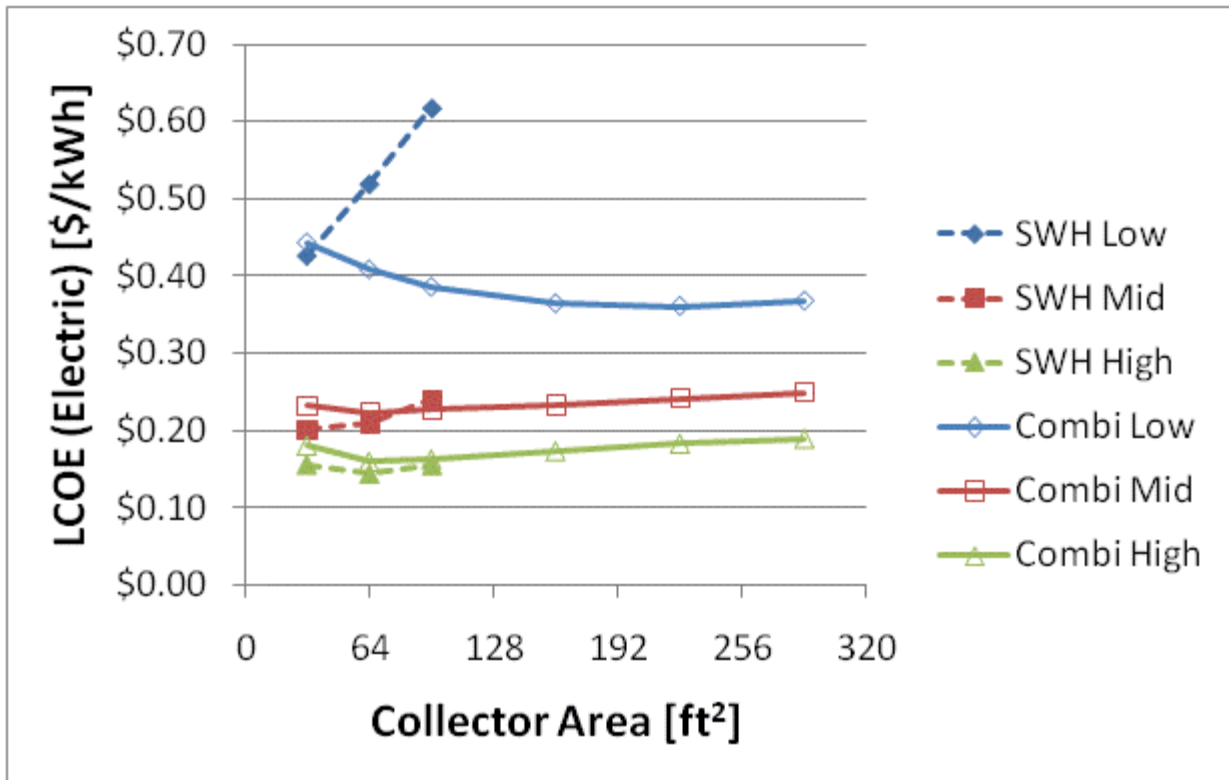


Figure F.9: LCOE and NPW for electric systems for a IECC 2009 House(Phoenix)

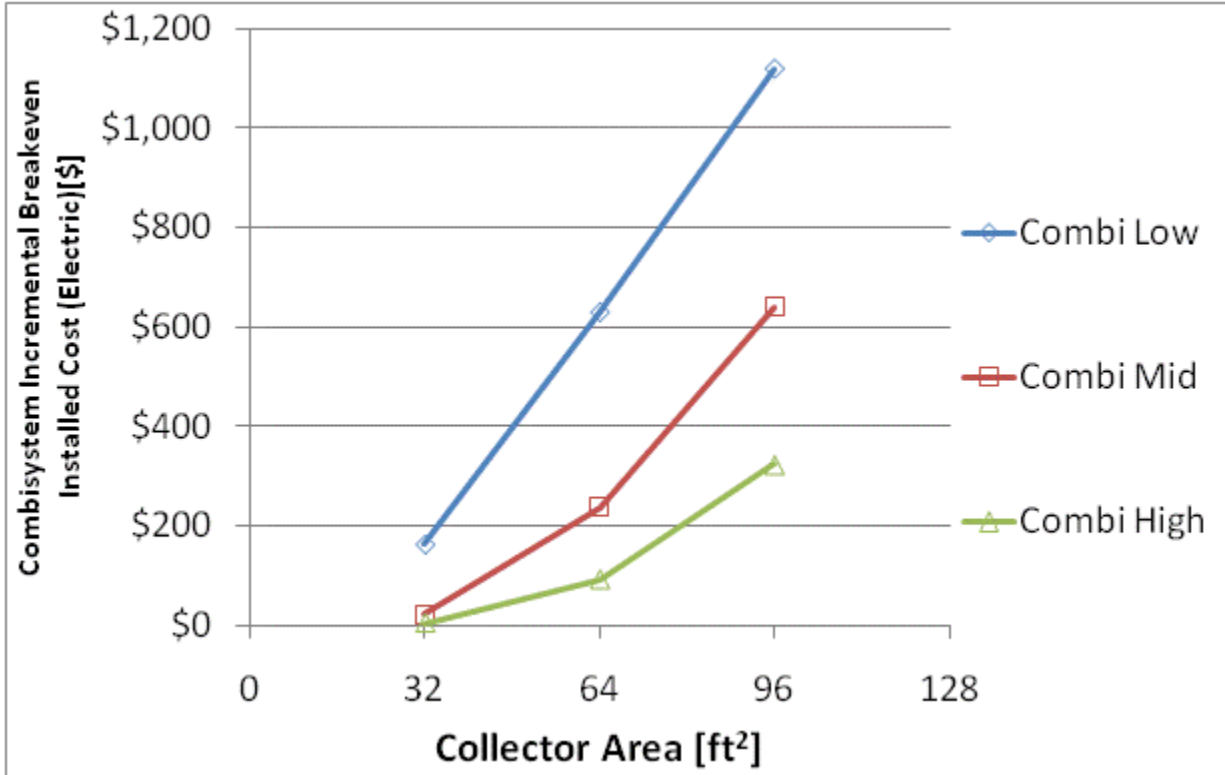
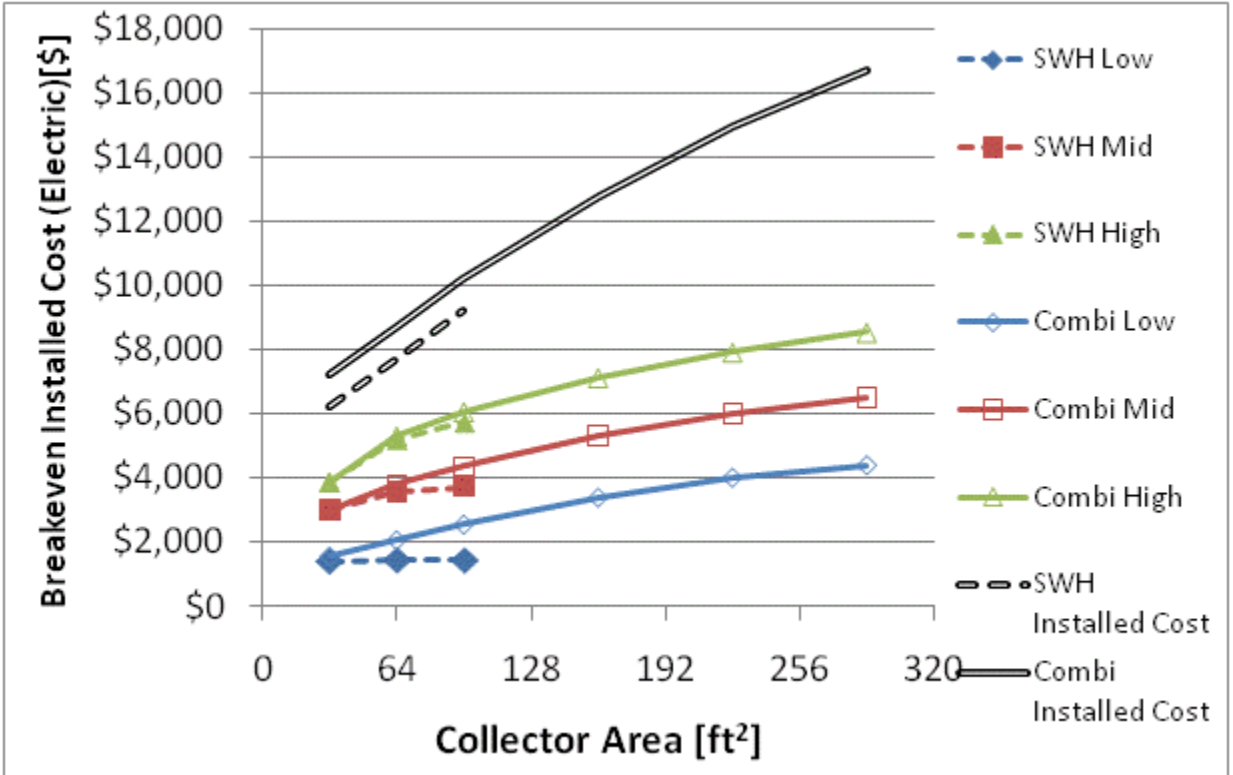


Figure F.10: Breakeven installed cost and combisystem incremental breakeven cost for electric system for a IECC 2009 House(Phoenix)

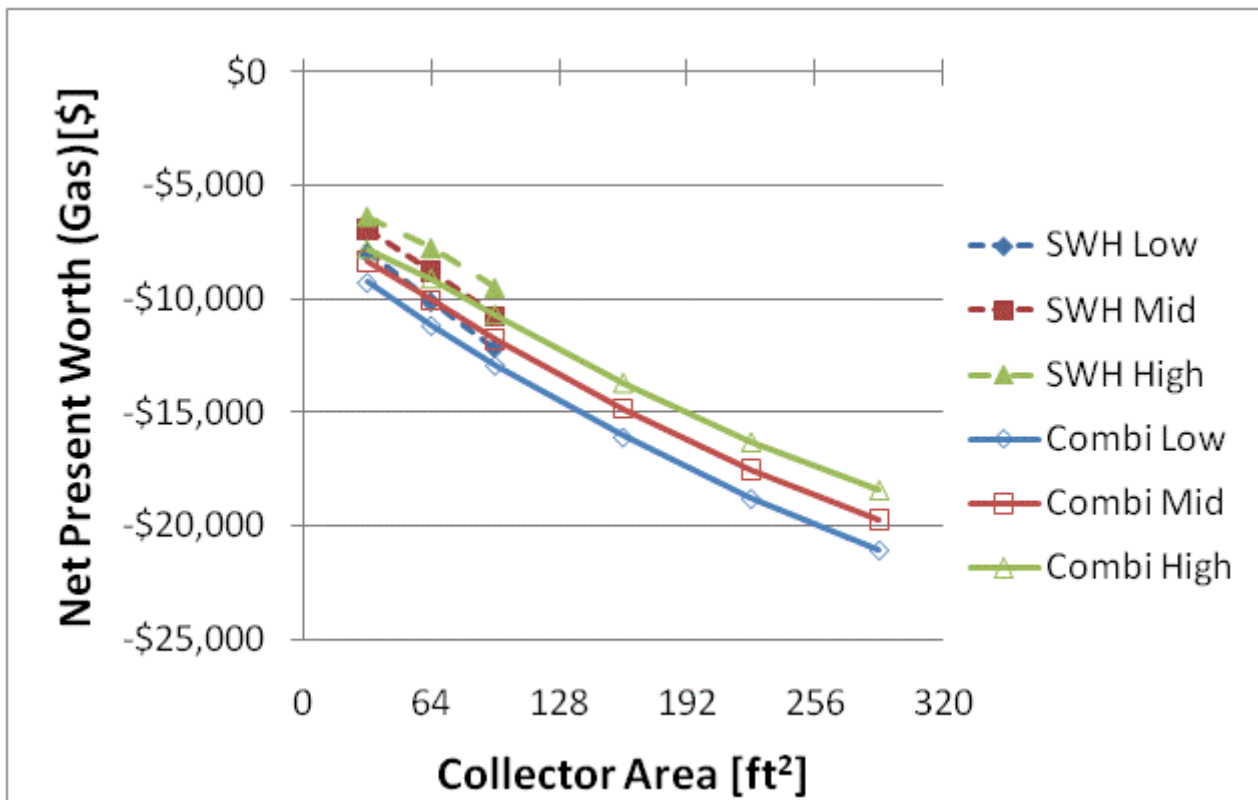
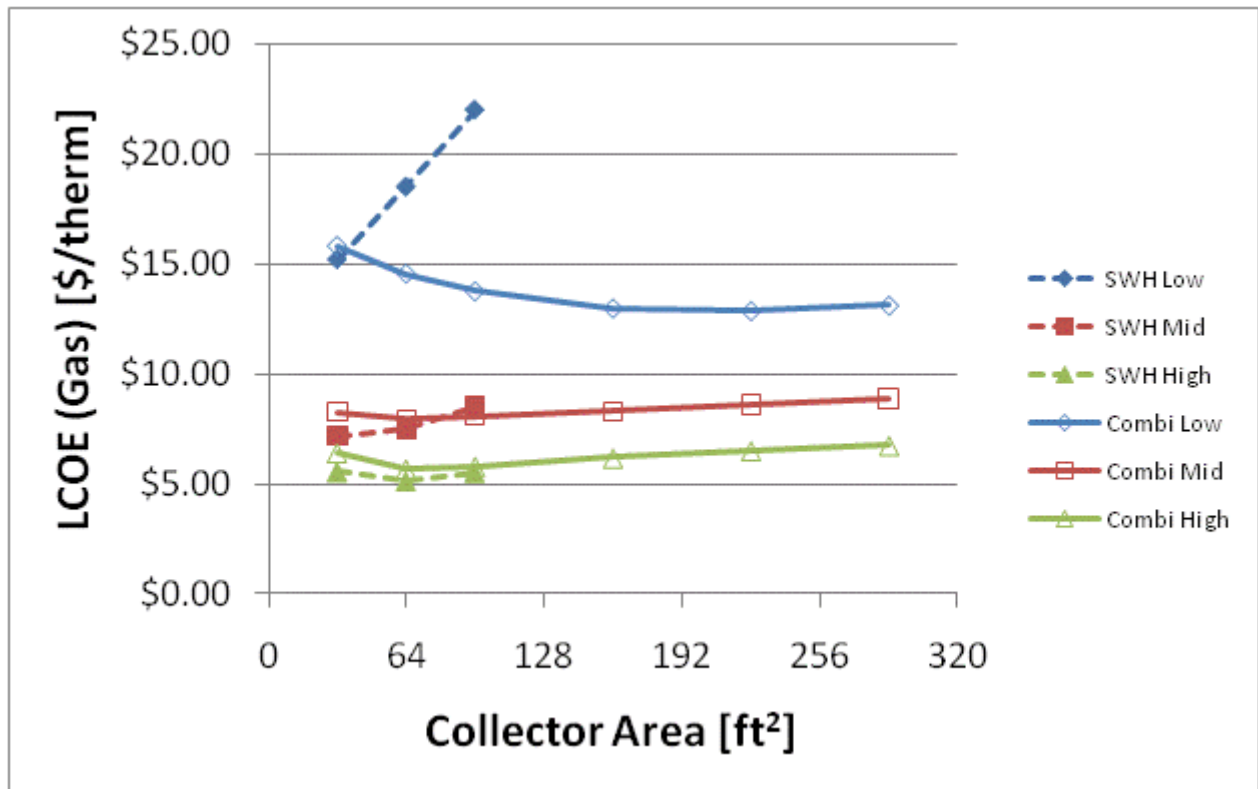


Figure F.11: LCOE and NPW for gas systems for a IECC 2009 House(Phoenix)

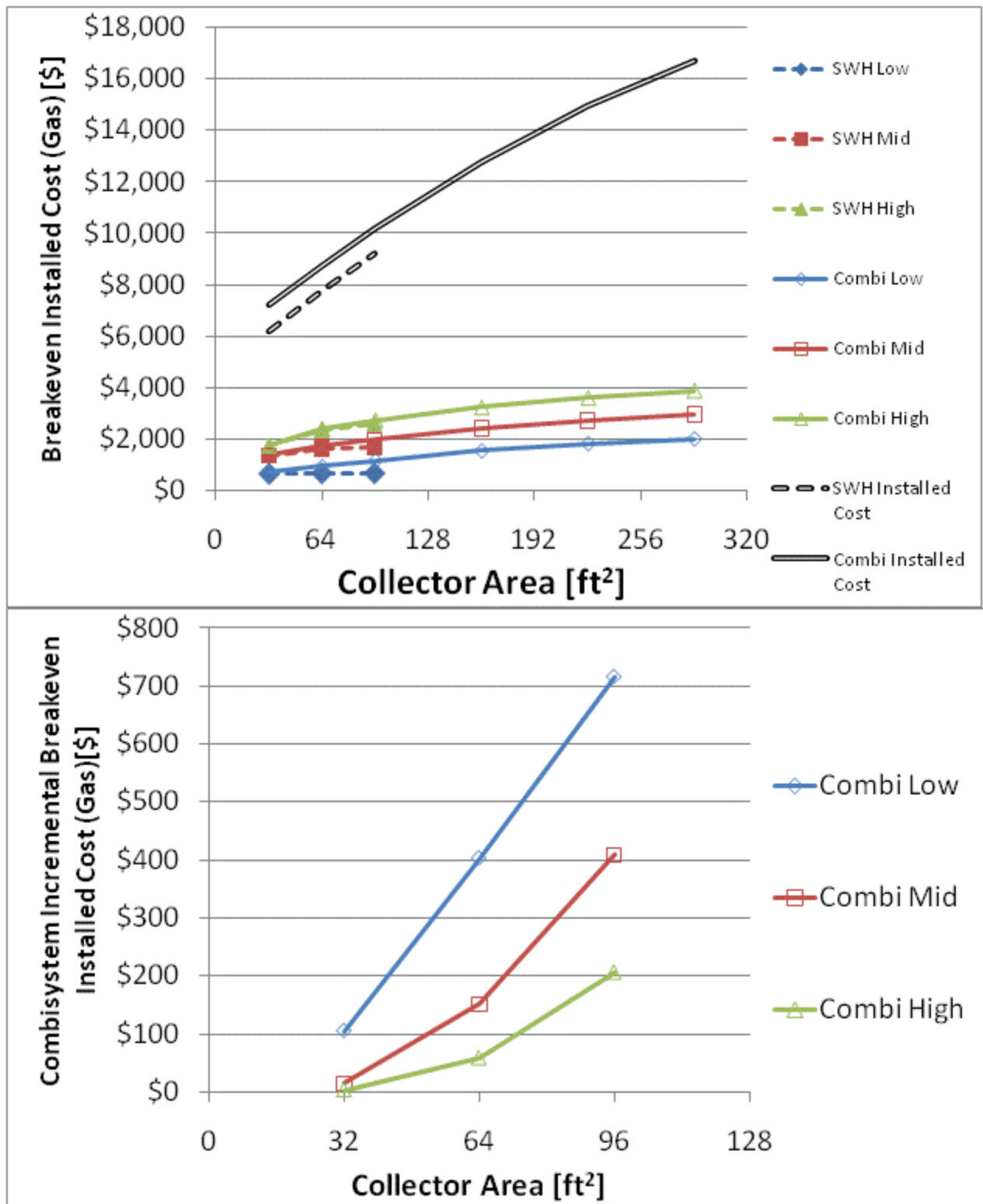


Figure F.12: Breakeven installed cost and combisystem incremental breakeven cost for gas systems for a

IECC 2009 House(Phoenix)

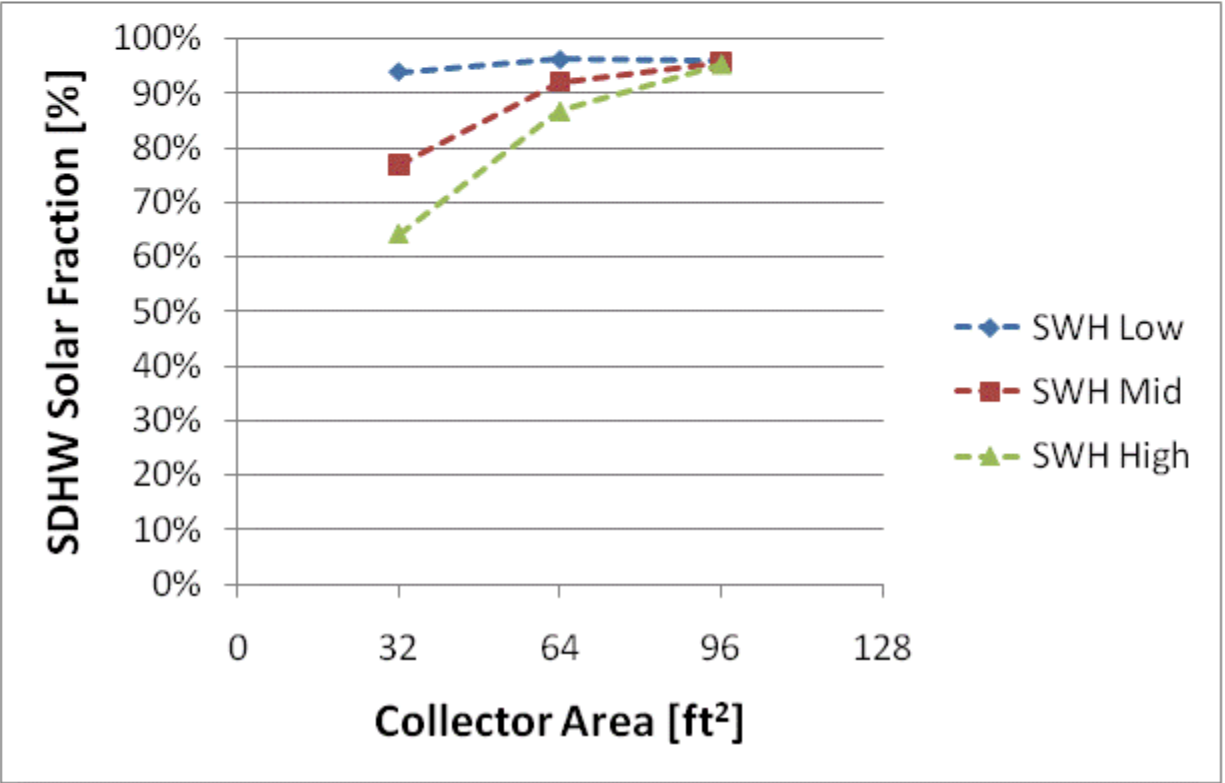
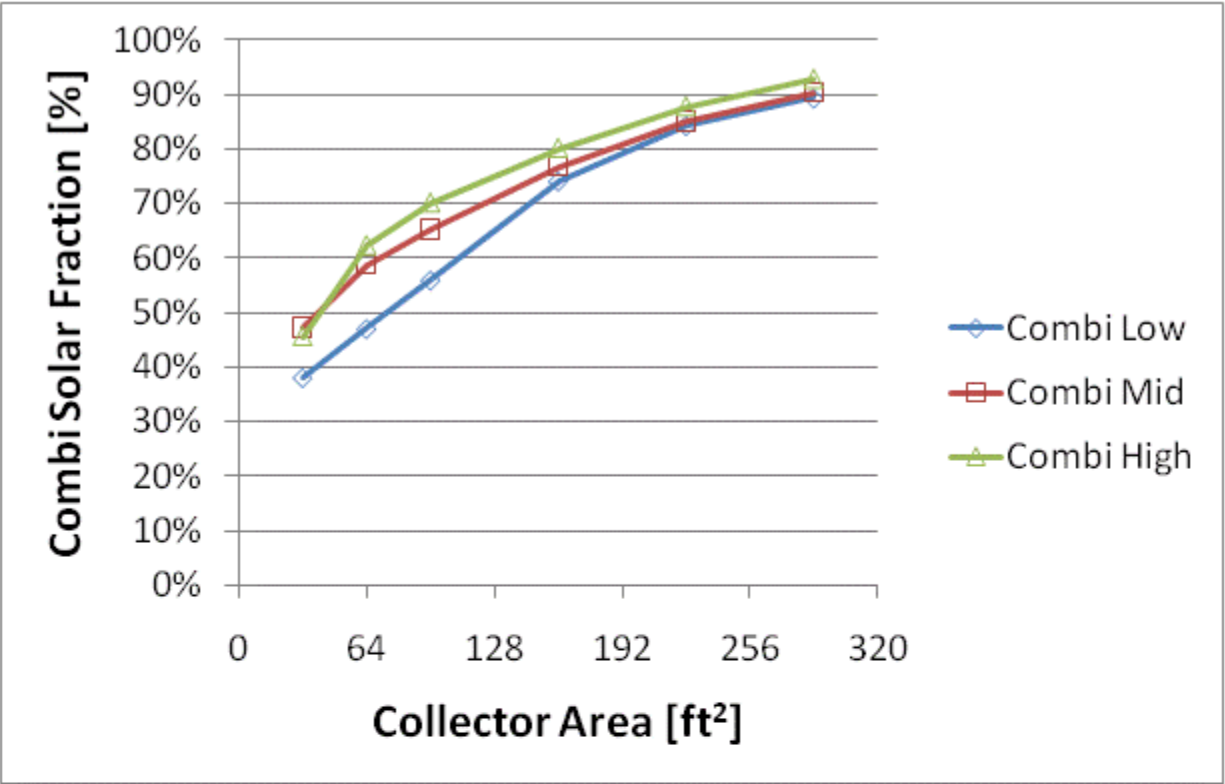


Figure F.13: Combi system and SWH solar fraction for a BA 50% House(Phoenix)

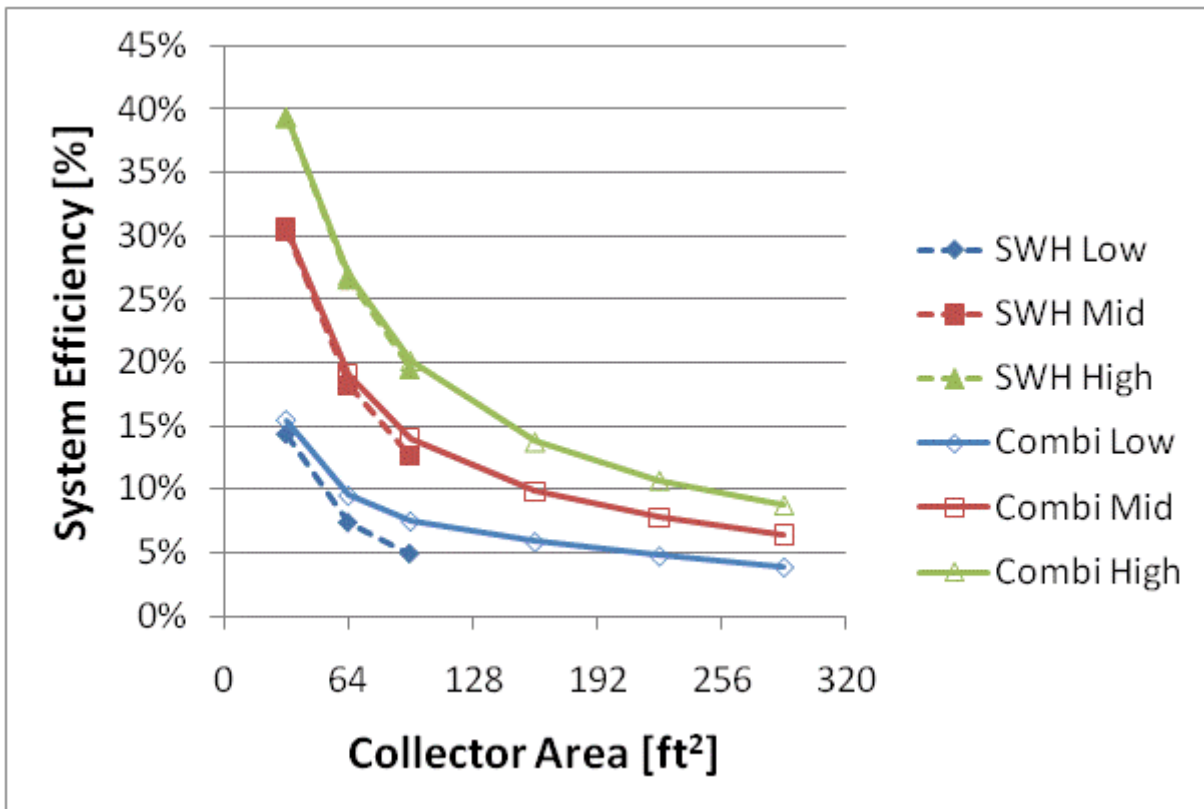
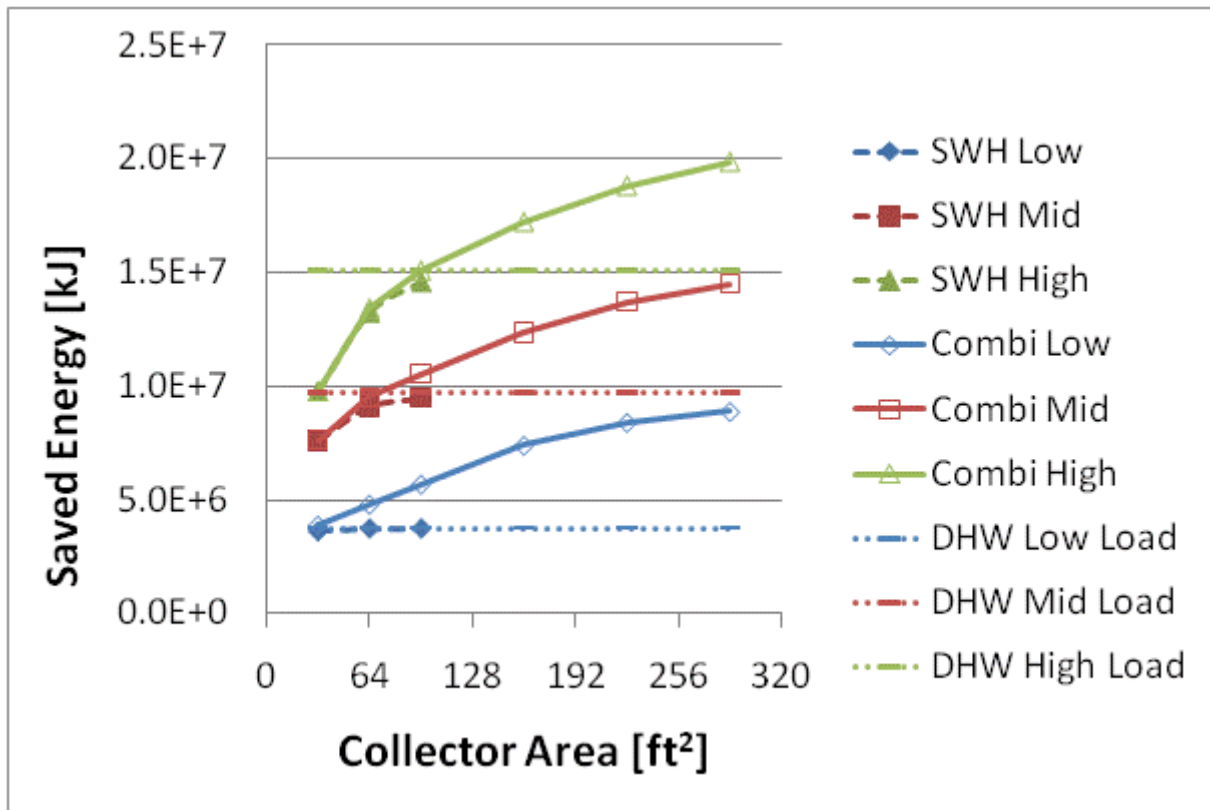


Figure F.14: Annual saved energy and system efficiency for a BA 50% House(Phoenix)

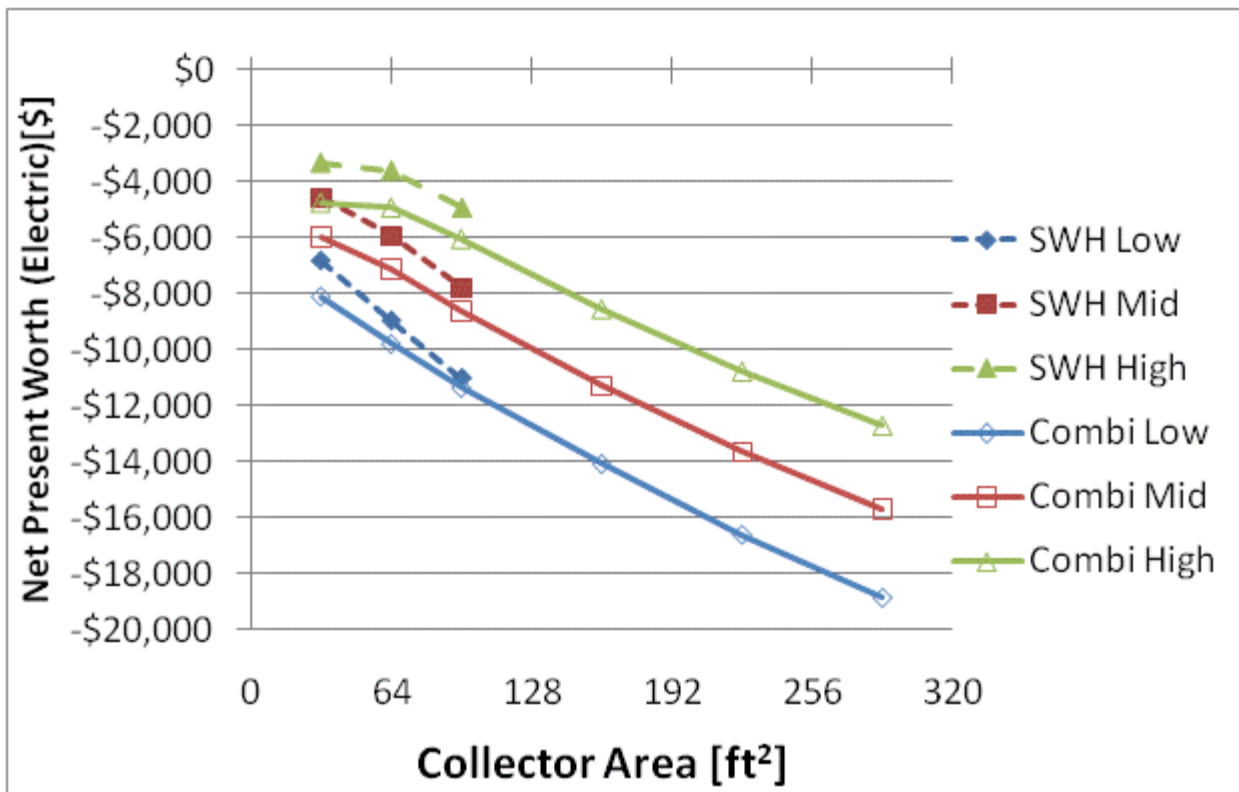
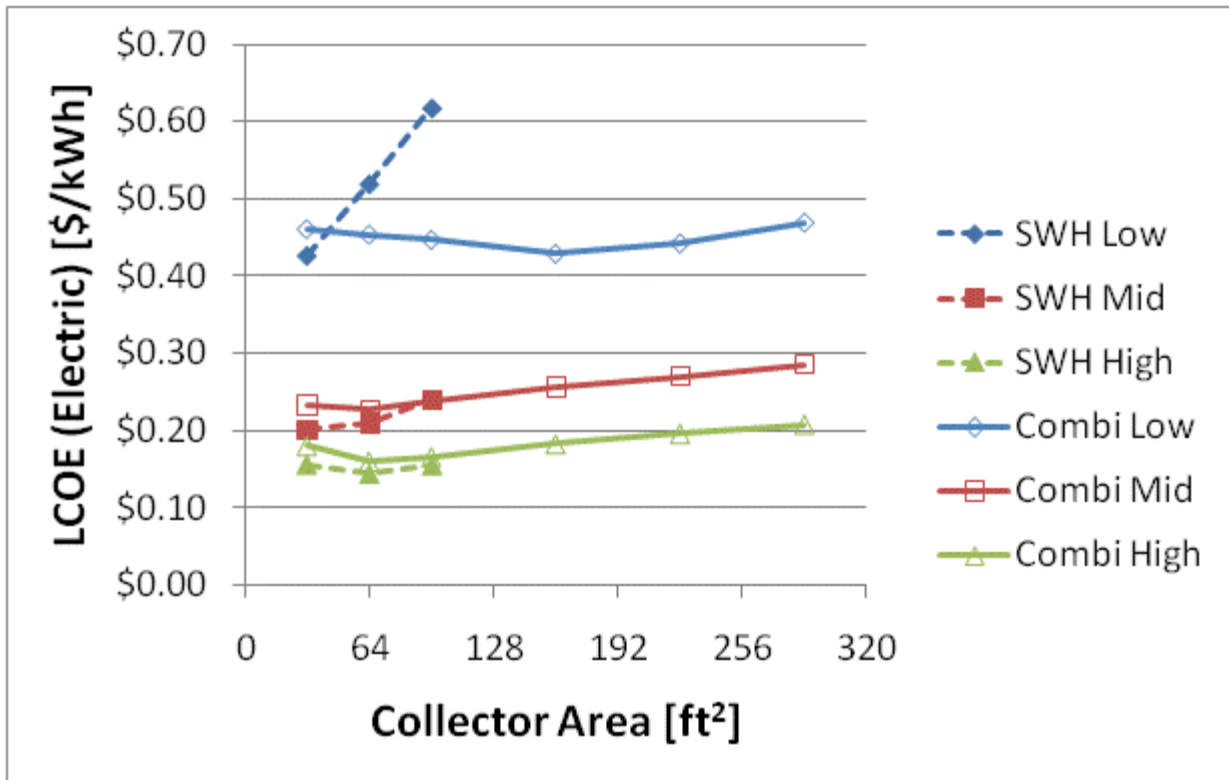


Figure F.15: LCOE and NPW for electric systems for a BA 50% House(Phoenix)

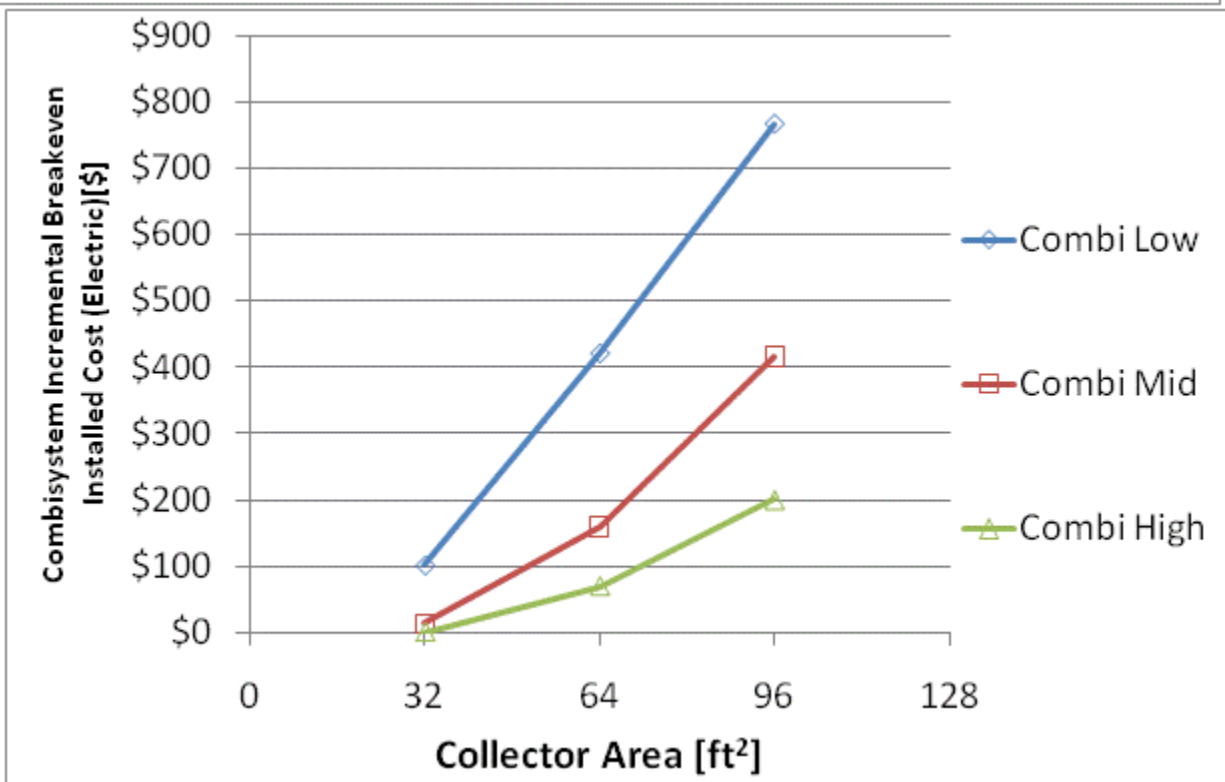
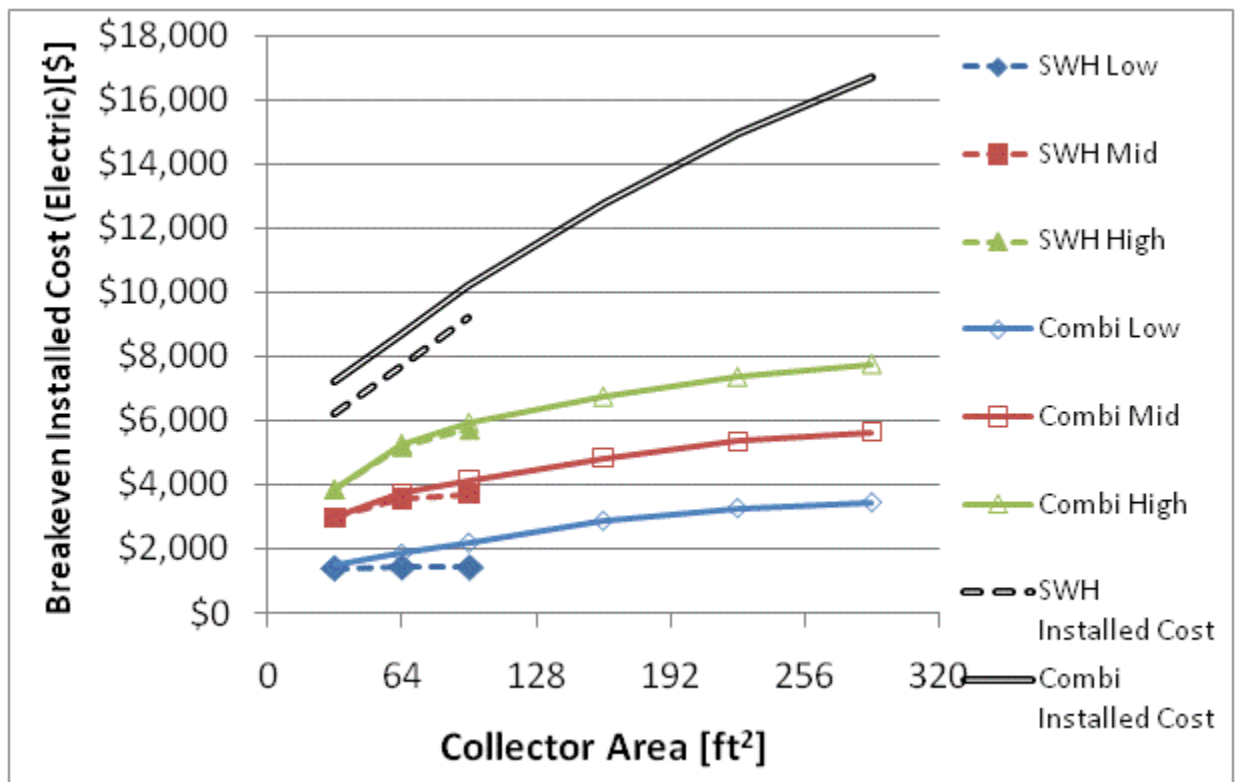


Figure F.16: Breakeven installed cost and combisystem incremental breakeven cost for electric system for a BA 50% House(Phoenix)

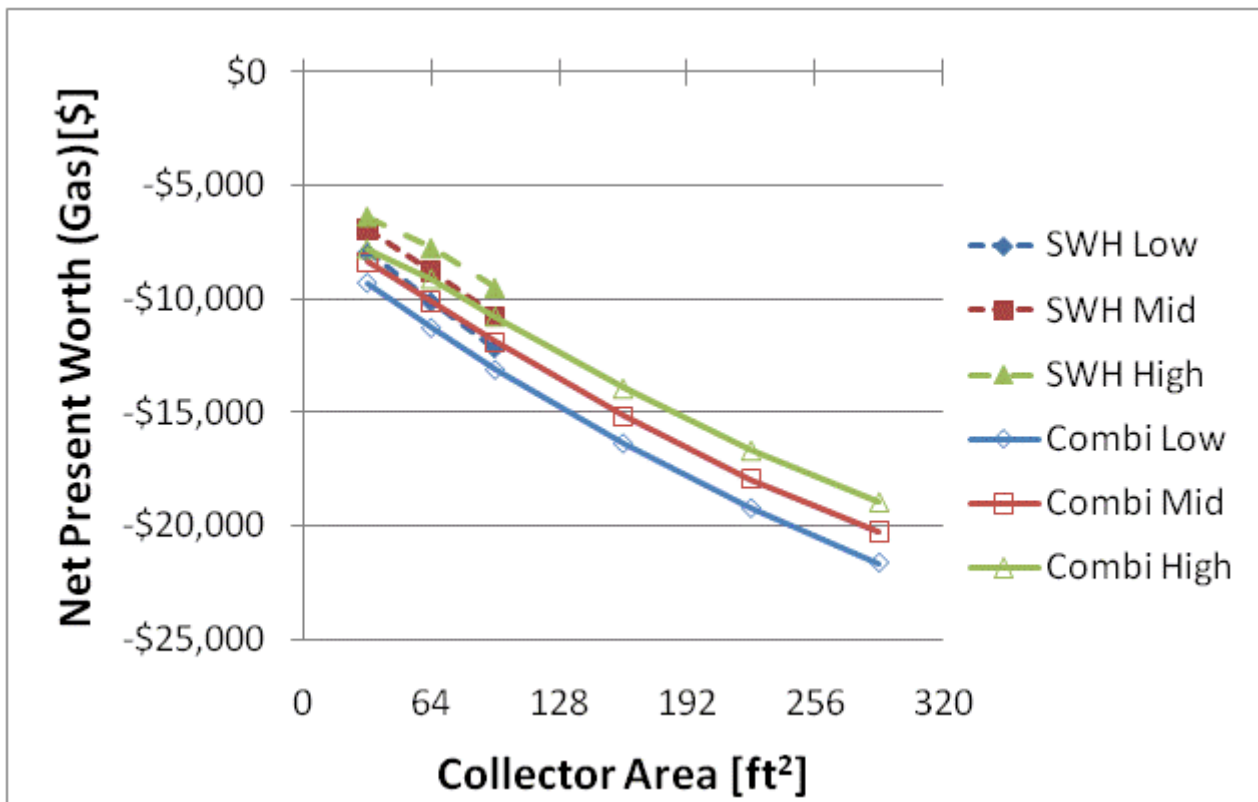
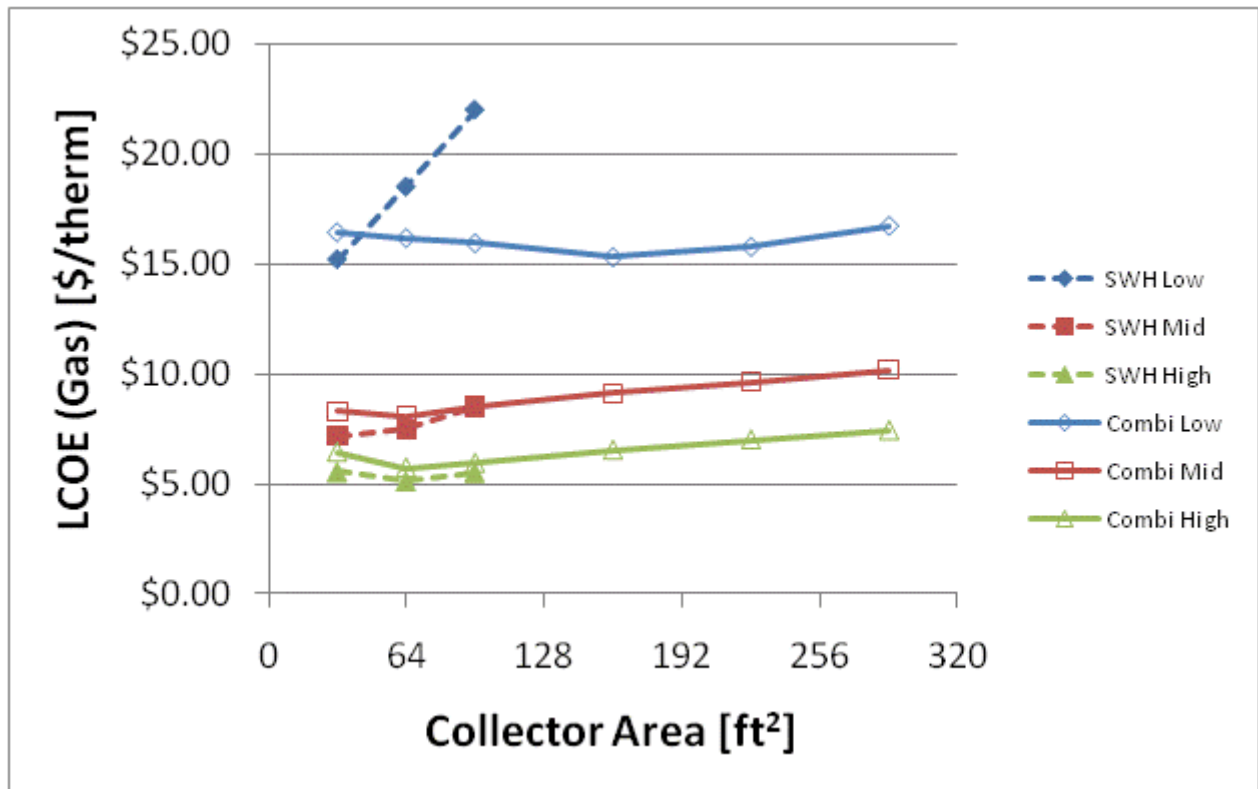


Figure F.17: LCOE and NPW for gas systems for a BA 50% House(Phoenix)

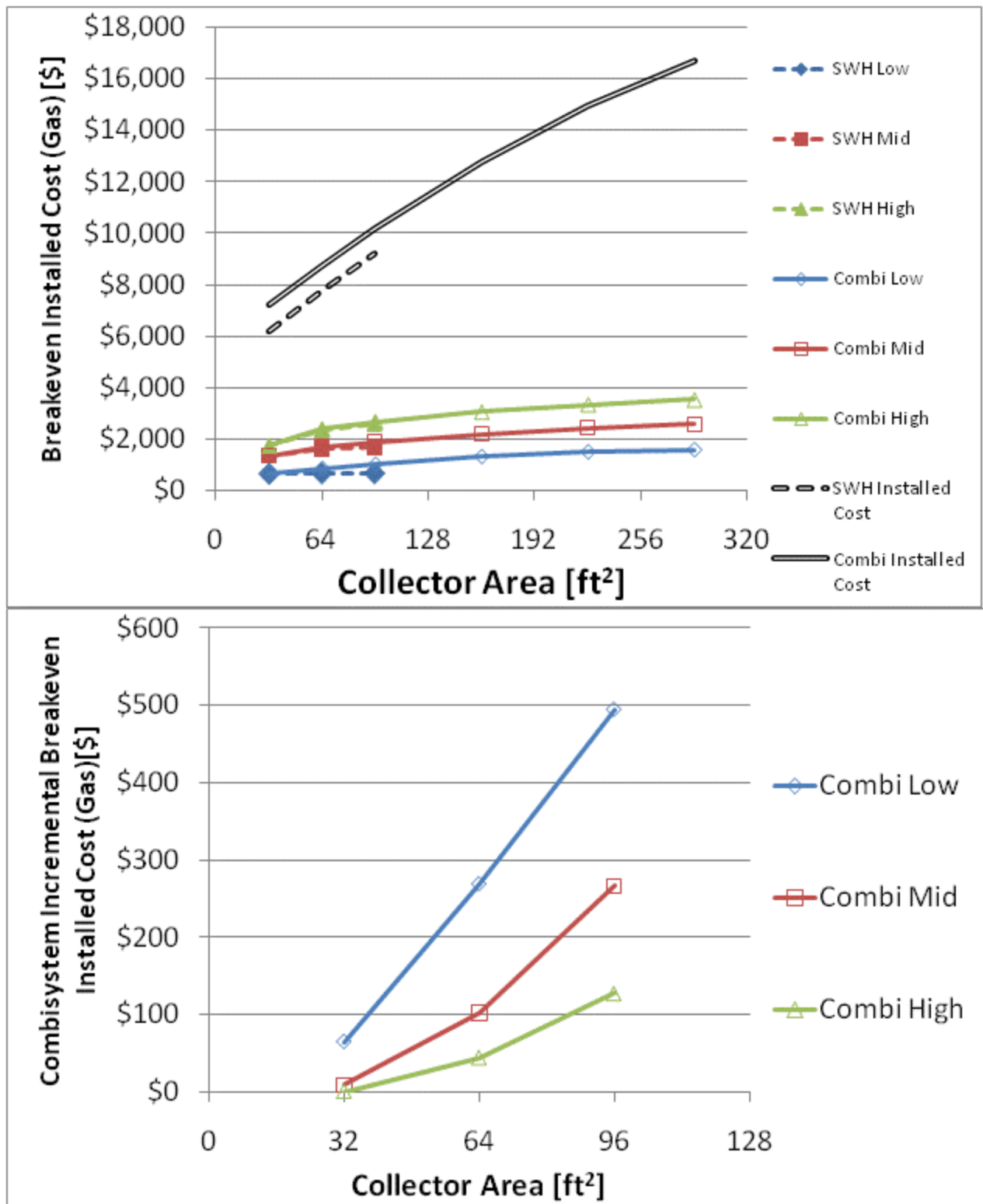


Figure F.18: Breakeven installed cost and combisystem incremental breakeven cost for gas systems for a

BA 50% House(Phoenix)

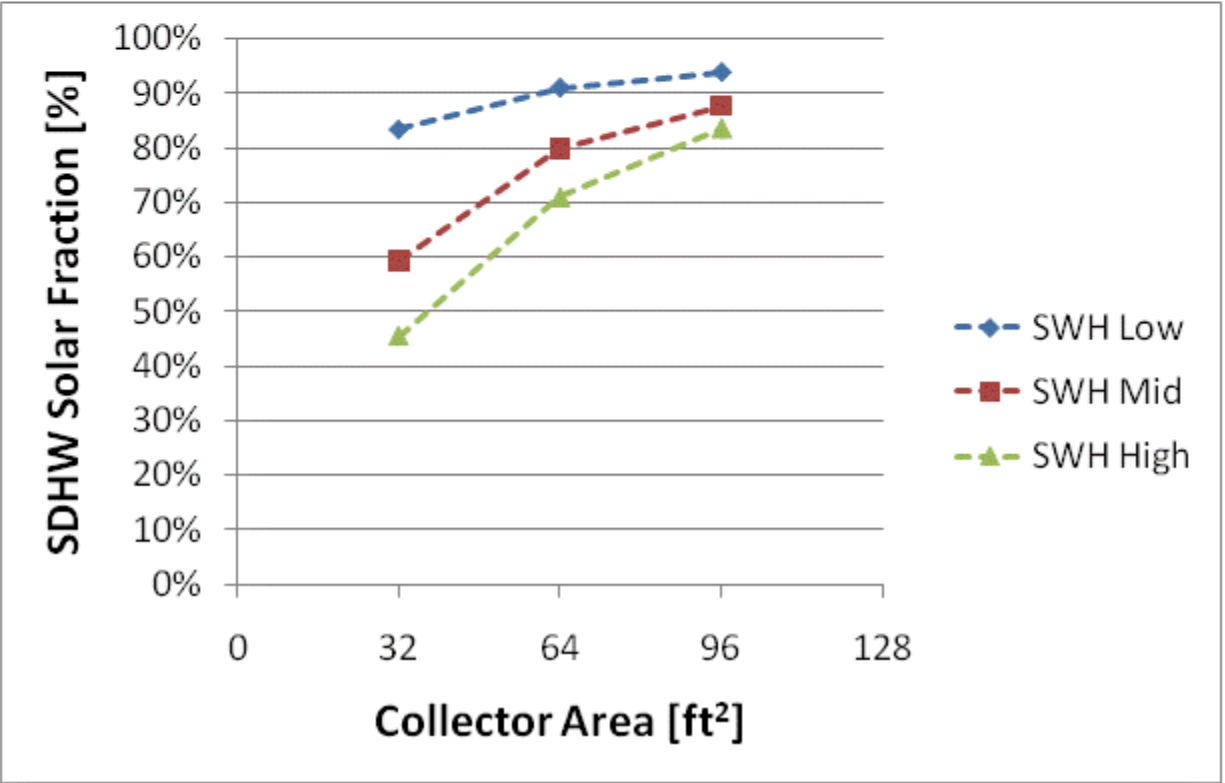
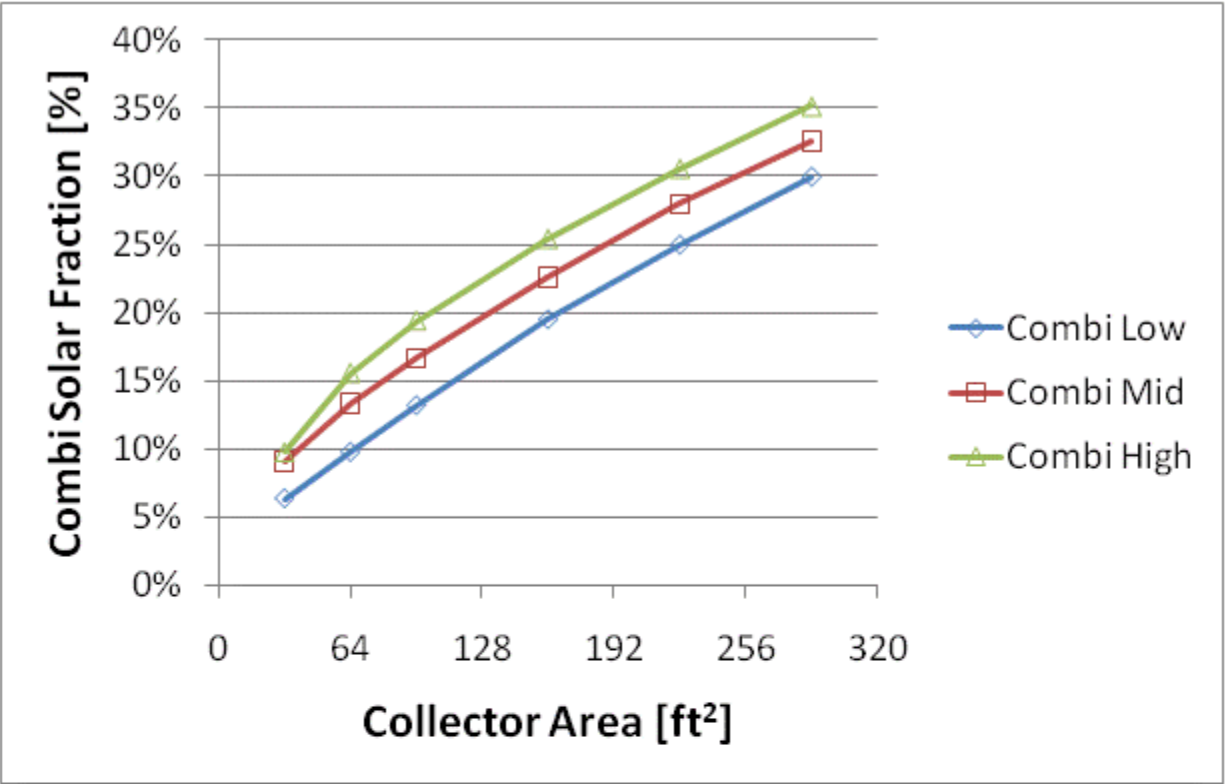


Figure F.19: Combisystem and SWH solar fraction for a 1960s Retrofit House(Atlanta)

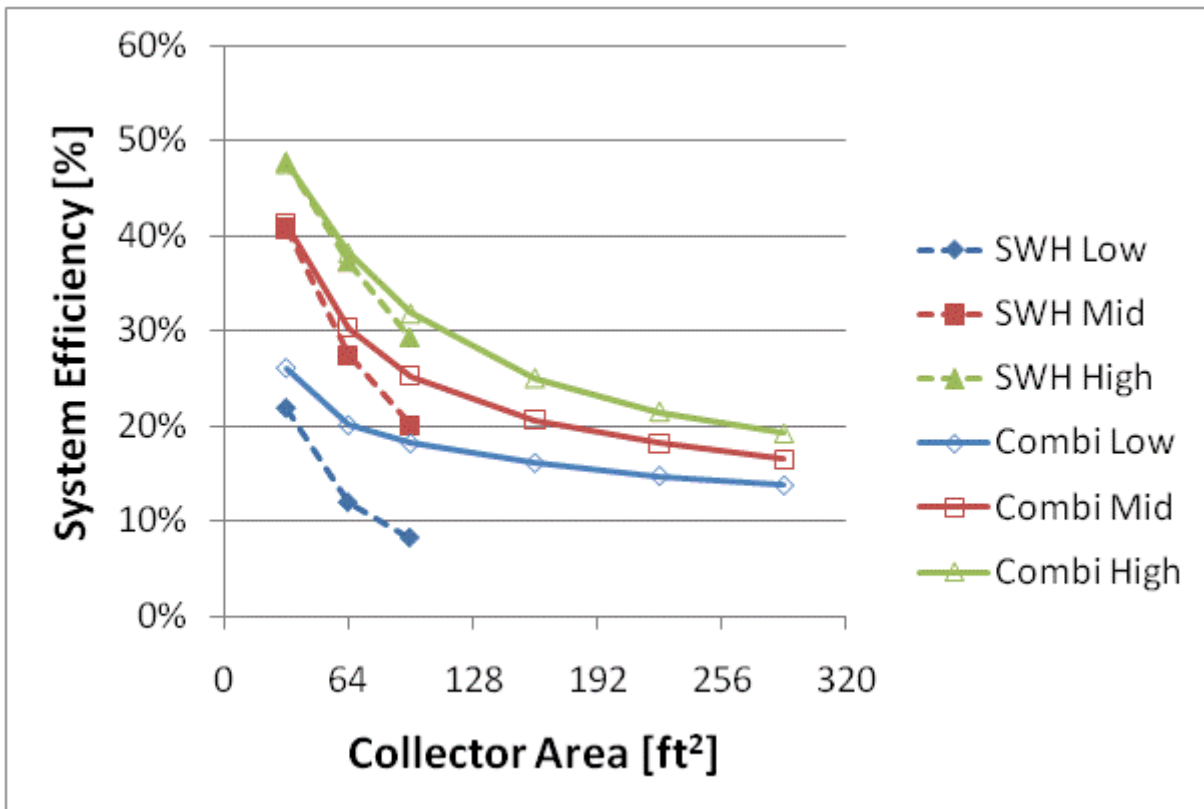
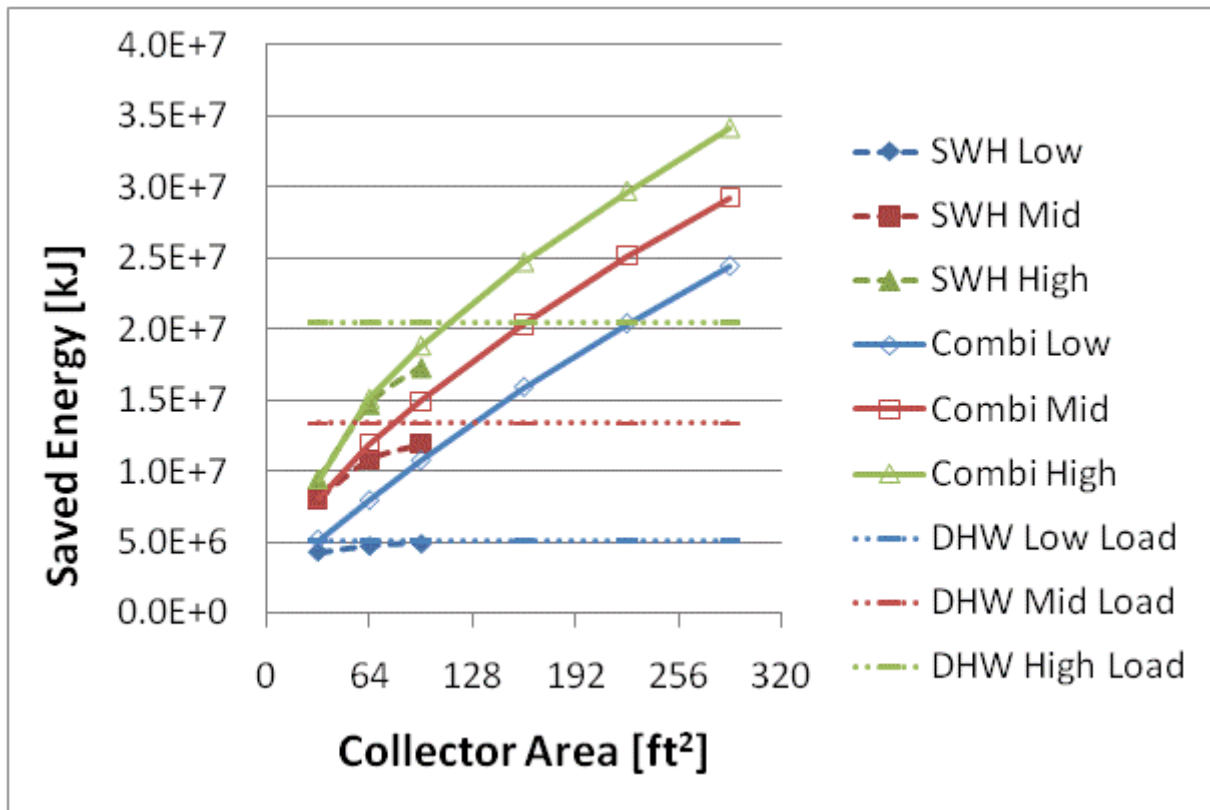


Figure F.20: Annual saved energy and system efficiency for a 1960s Retrofit House(Atlanta)

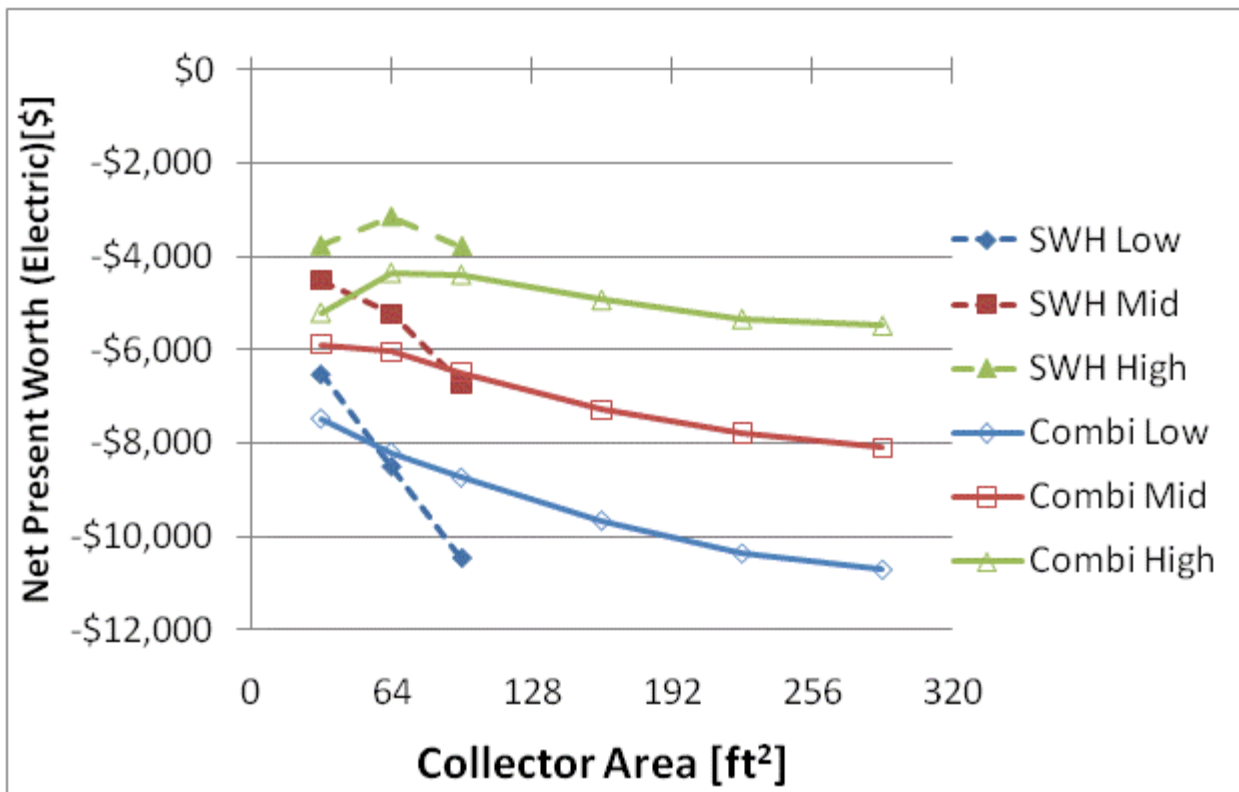
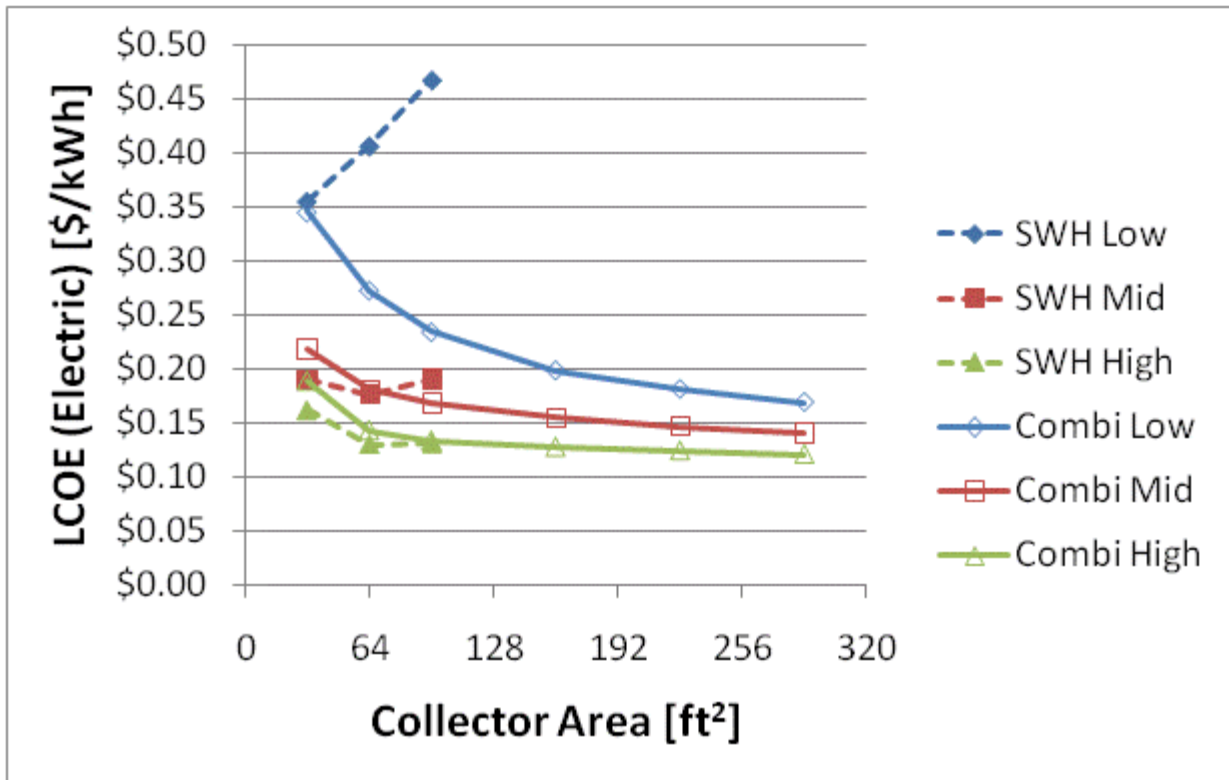


Figure F.21: LCOE and NPW for electric systems for a 1960s Retrofit House (Atlanta)

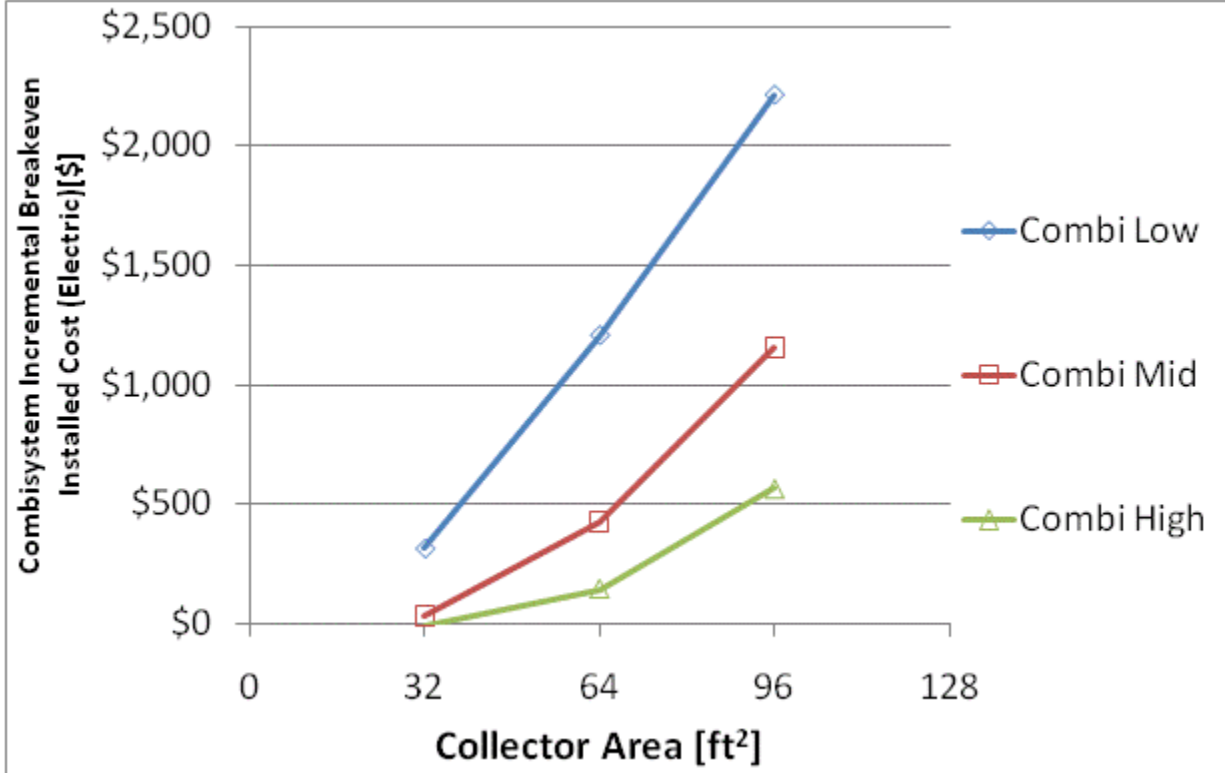
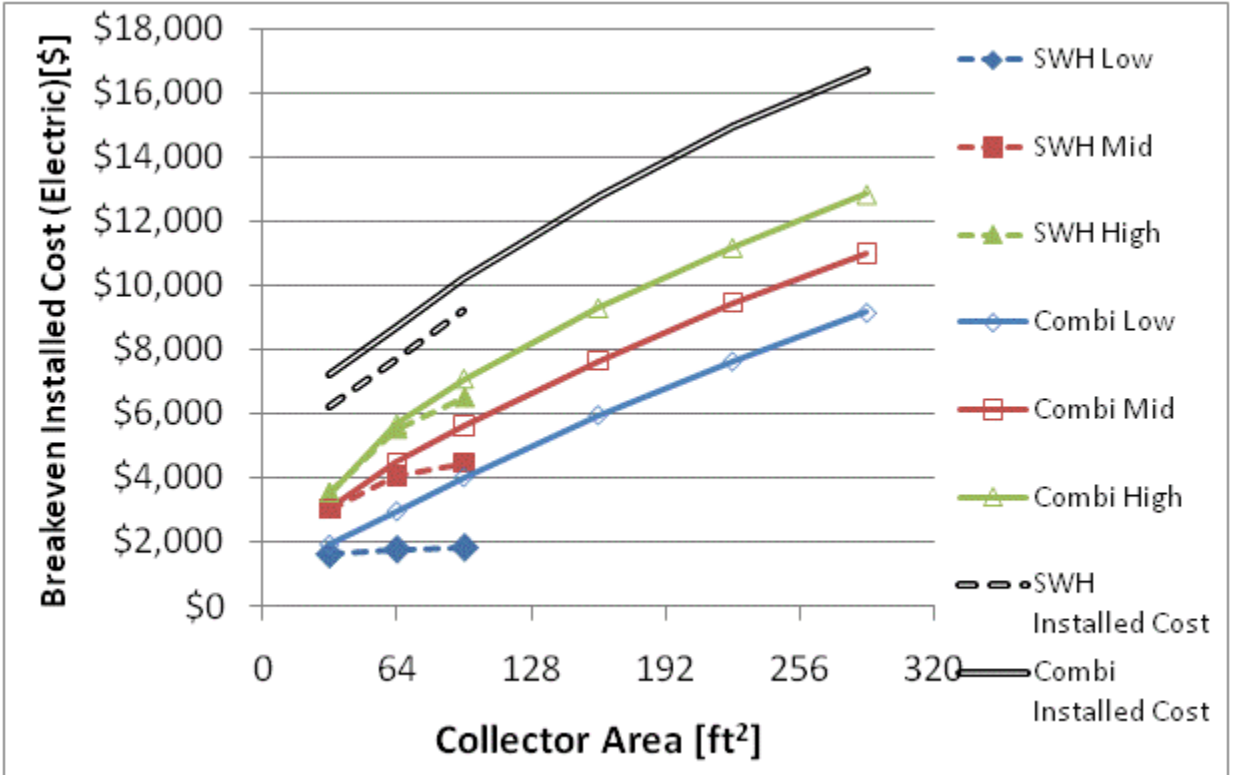


Figure F.22: Breakeven installed cost and combisystem incremental breakeven cost for electric system for a 1960s Retrofit House(Atlanta)

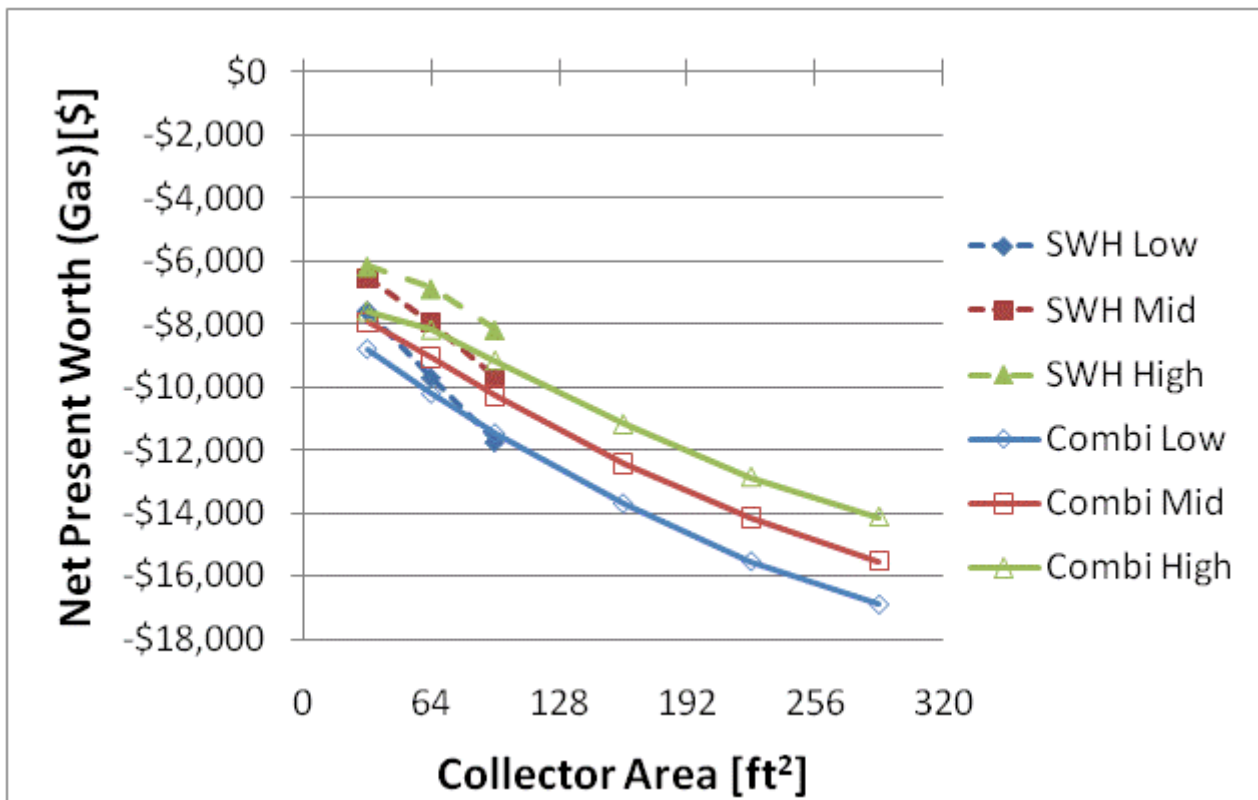
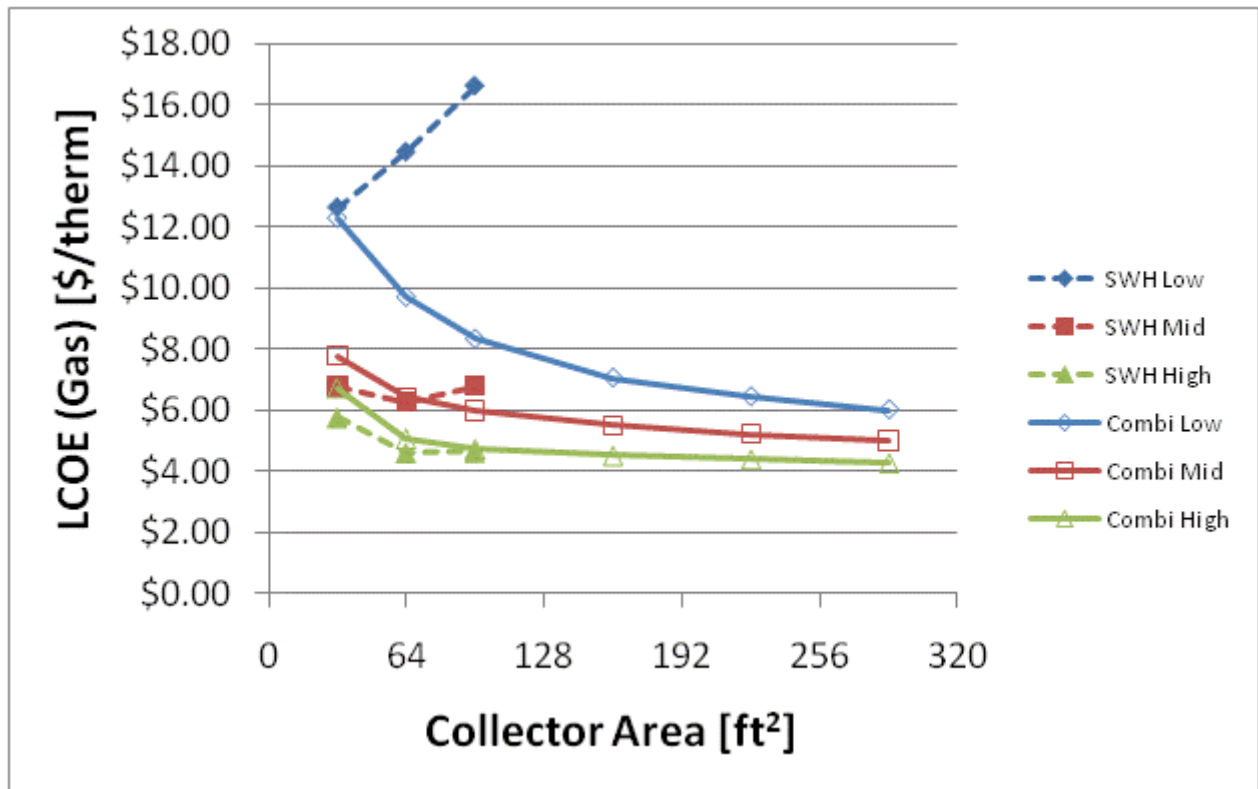


Figure F.23: LCOE and NPW for gas systems for a 1960s Retrofit House(Atlanta)

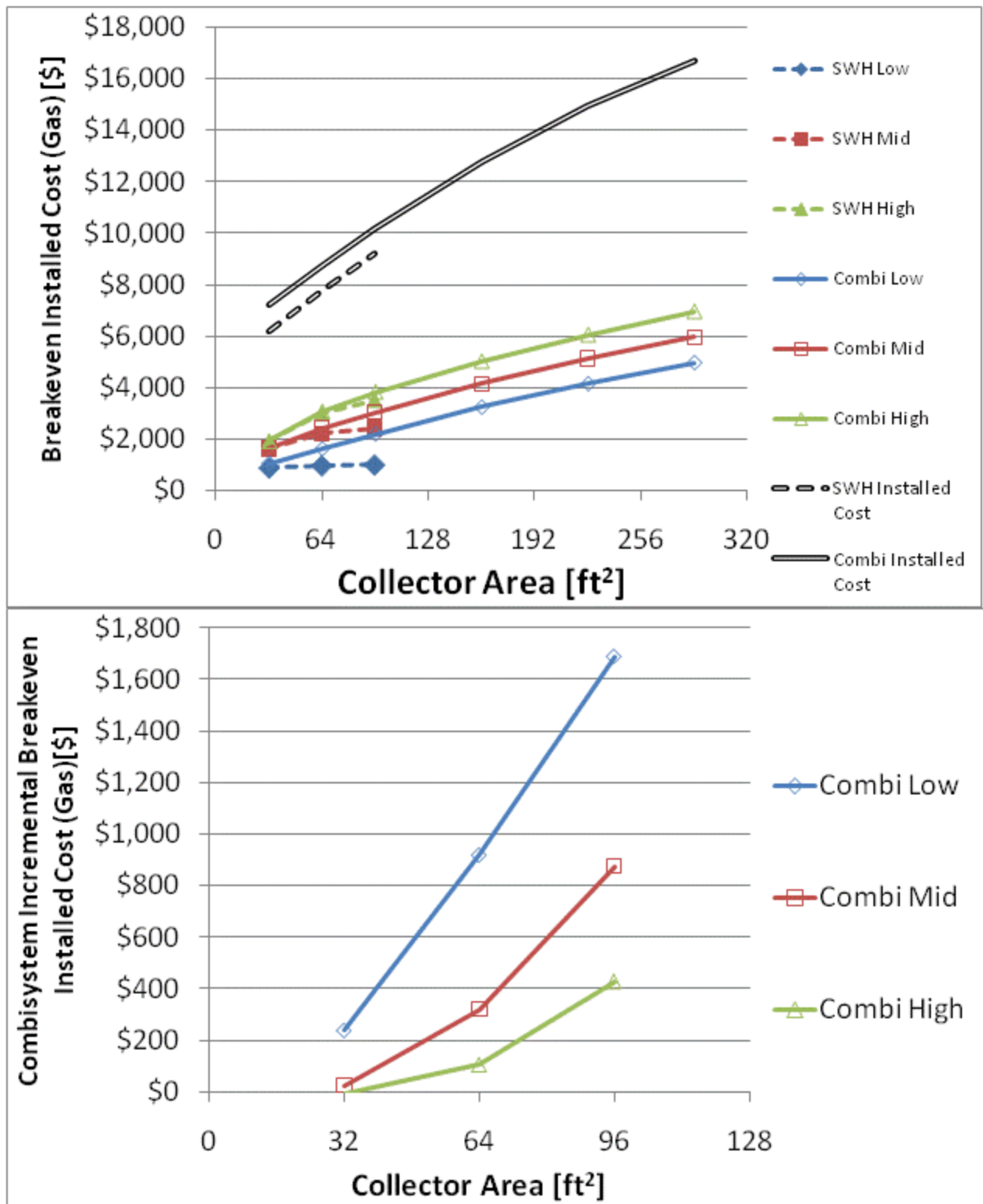


Figure F.24: Breakeven installed cost and combisystem incremental breakeven cost for gas systems for a

1960s Retrofit House(Atlanta)

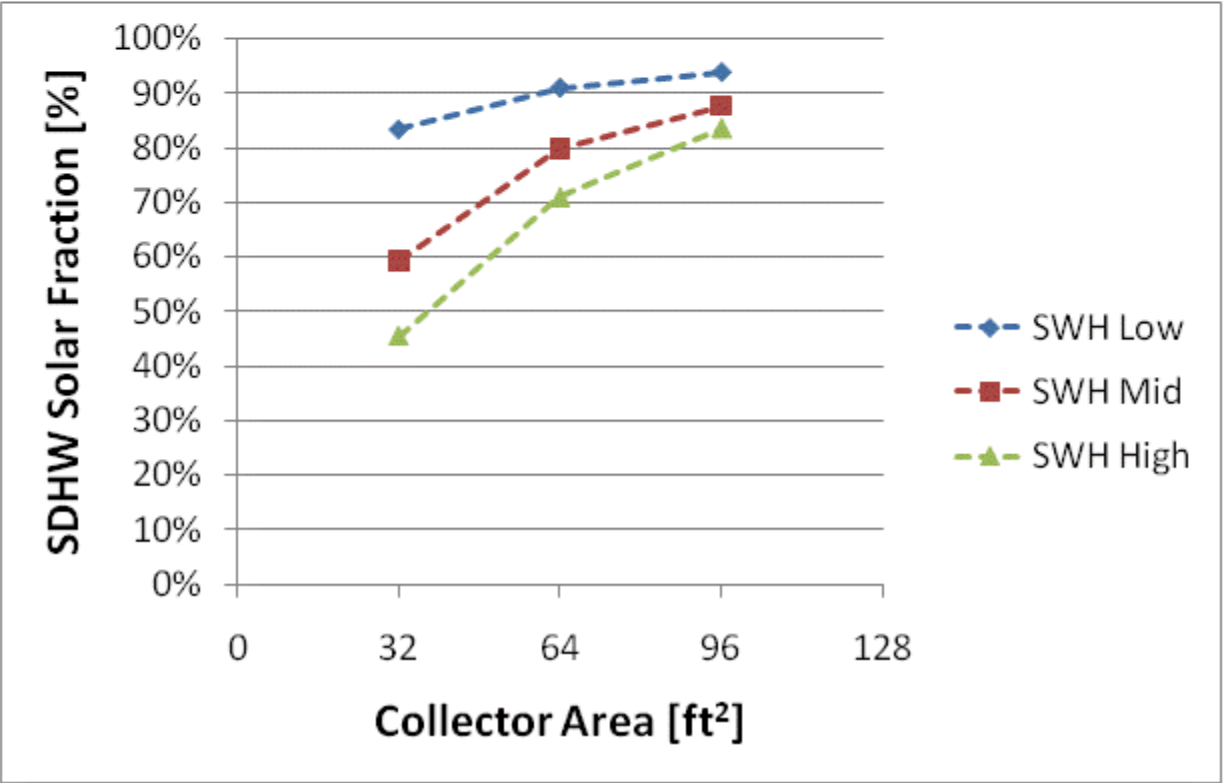
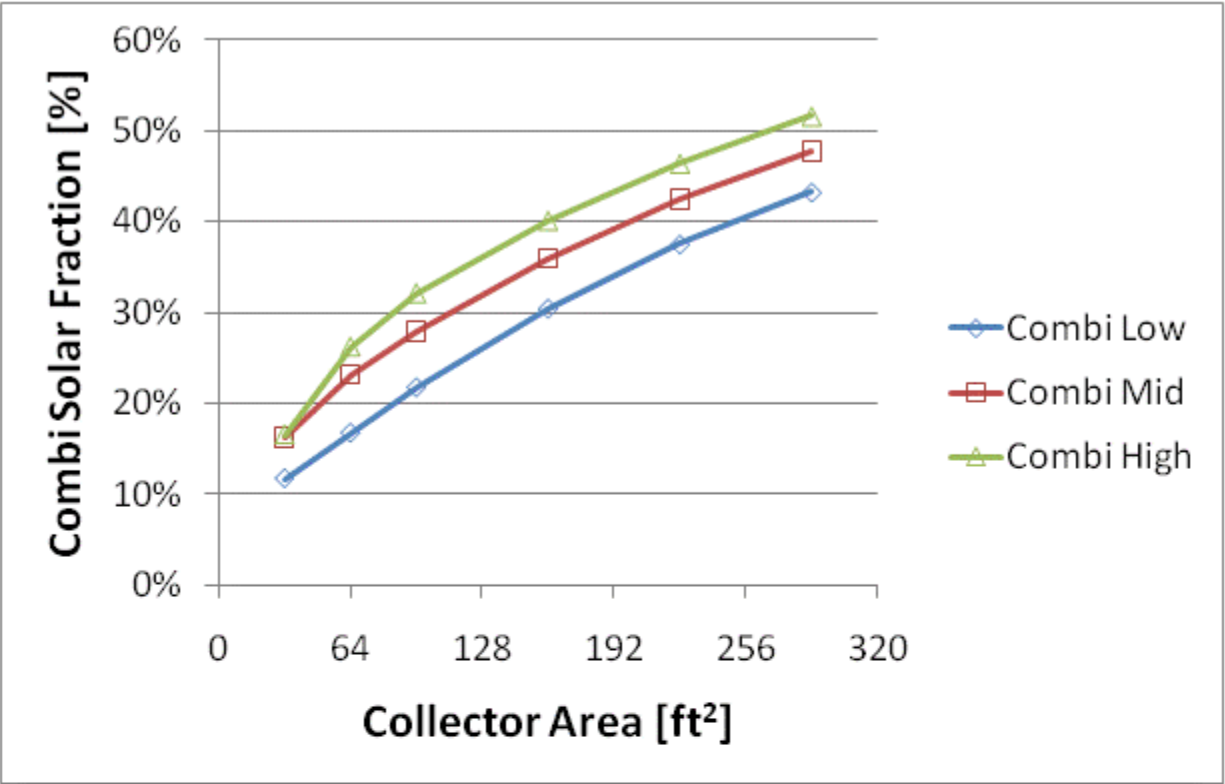


Figure F.25: Combisystem and SWH solar fraction for a IECC 2009 House(Atlanta)

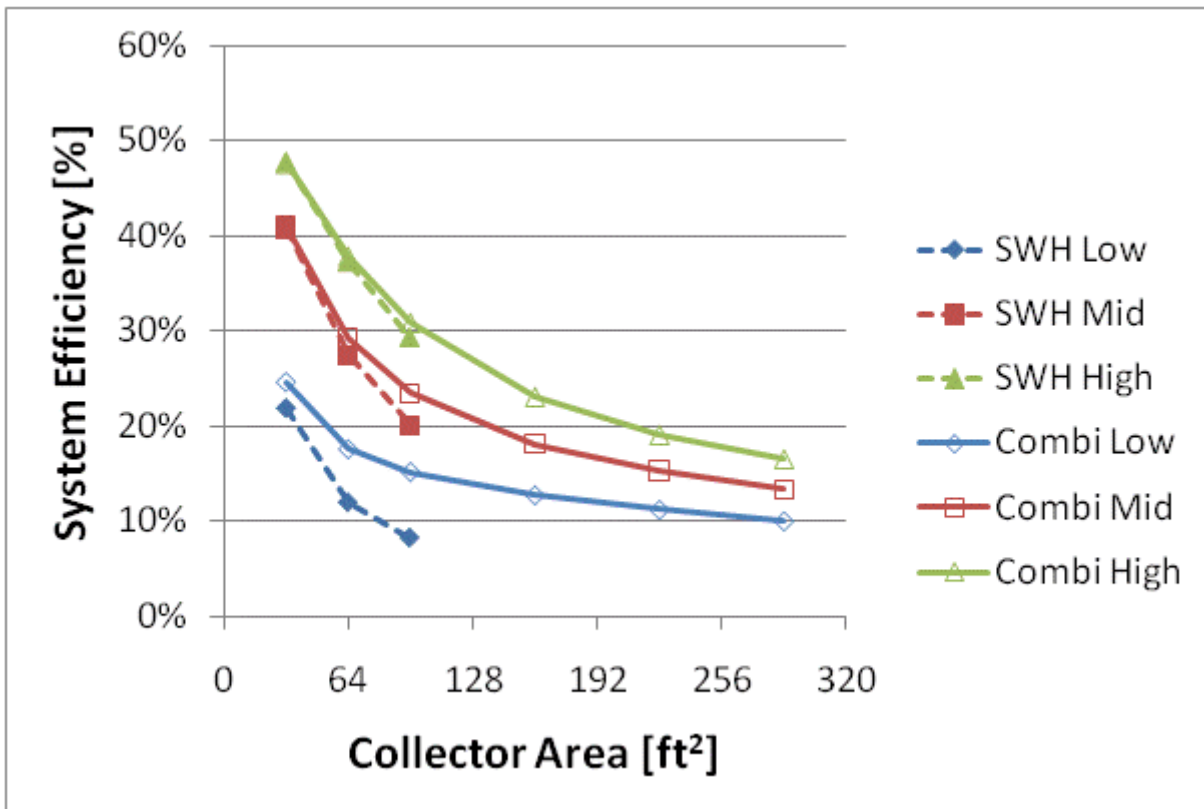
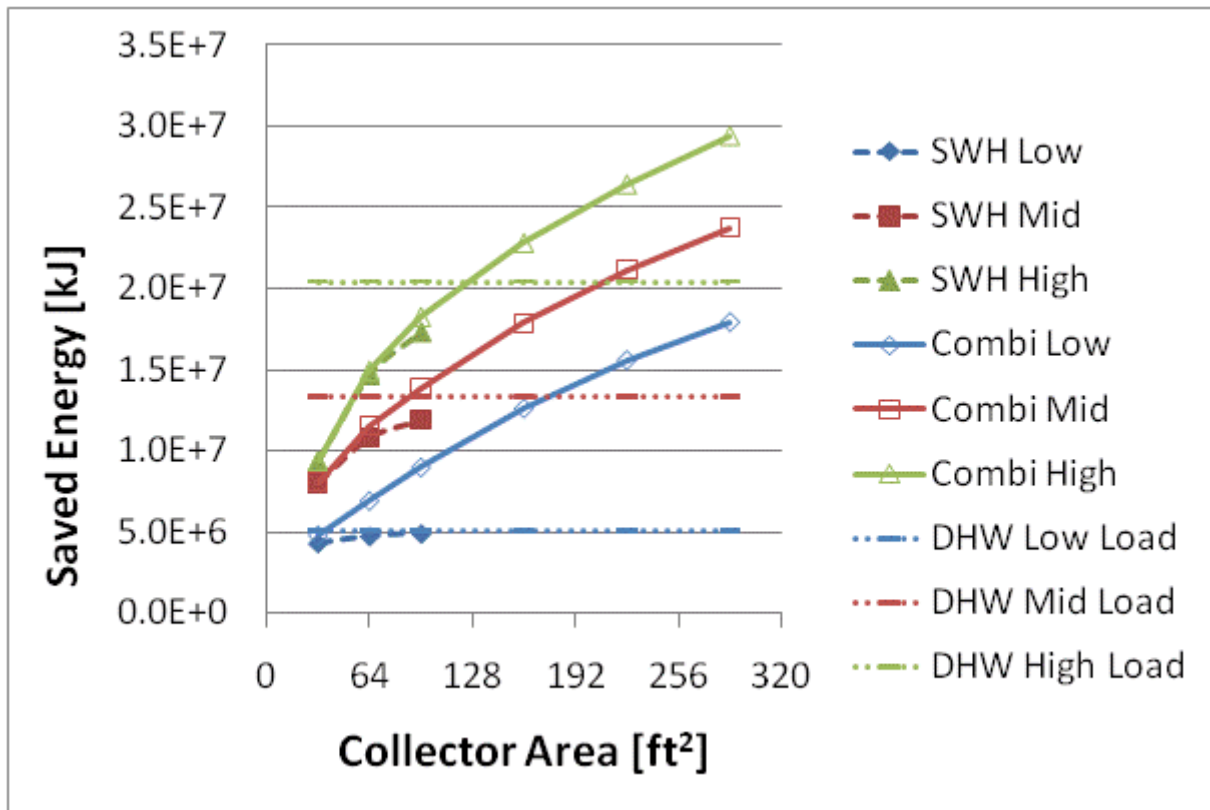


Figure F.26: Annual saved energy and system efficiency for a IECC 2009 House(Atlanta)

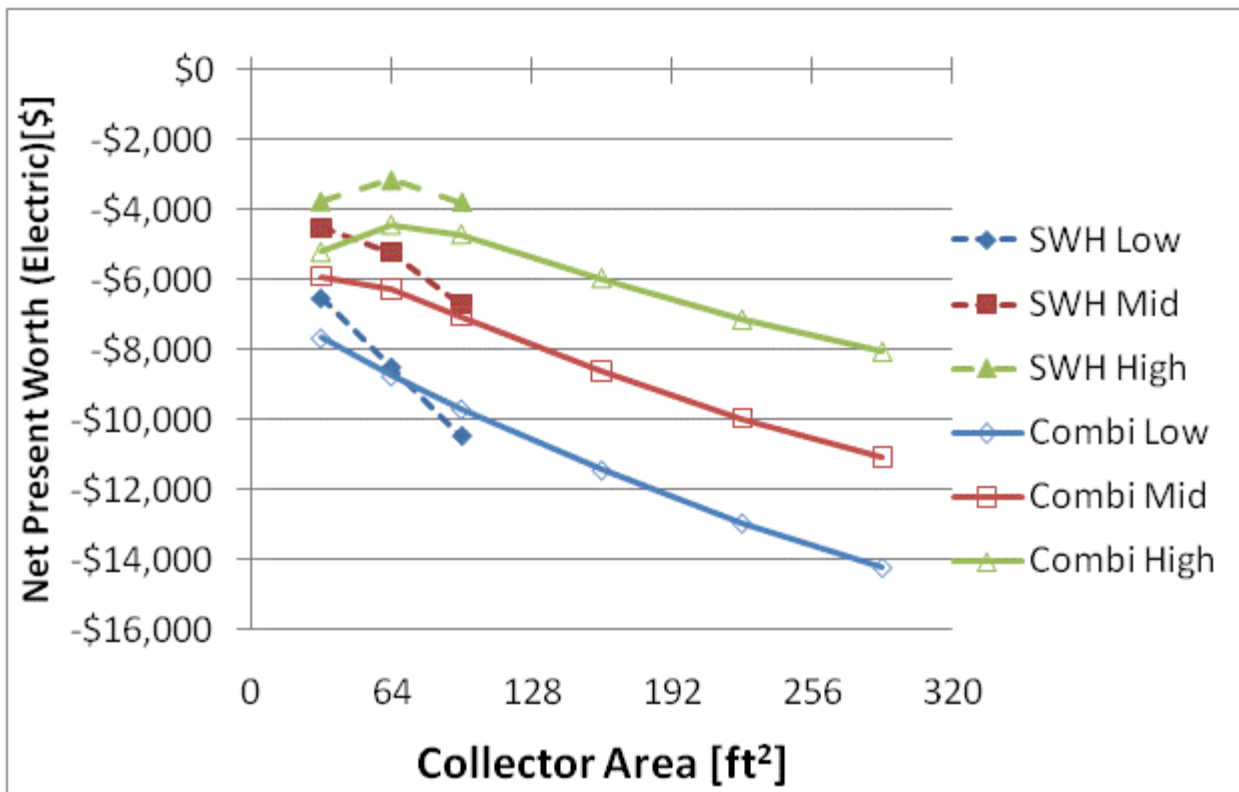
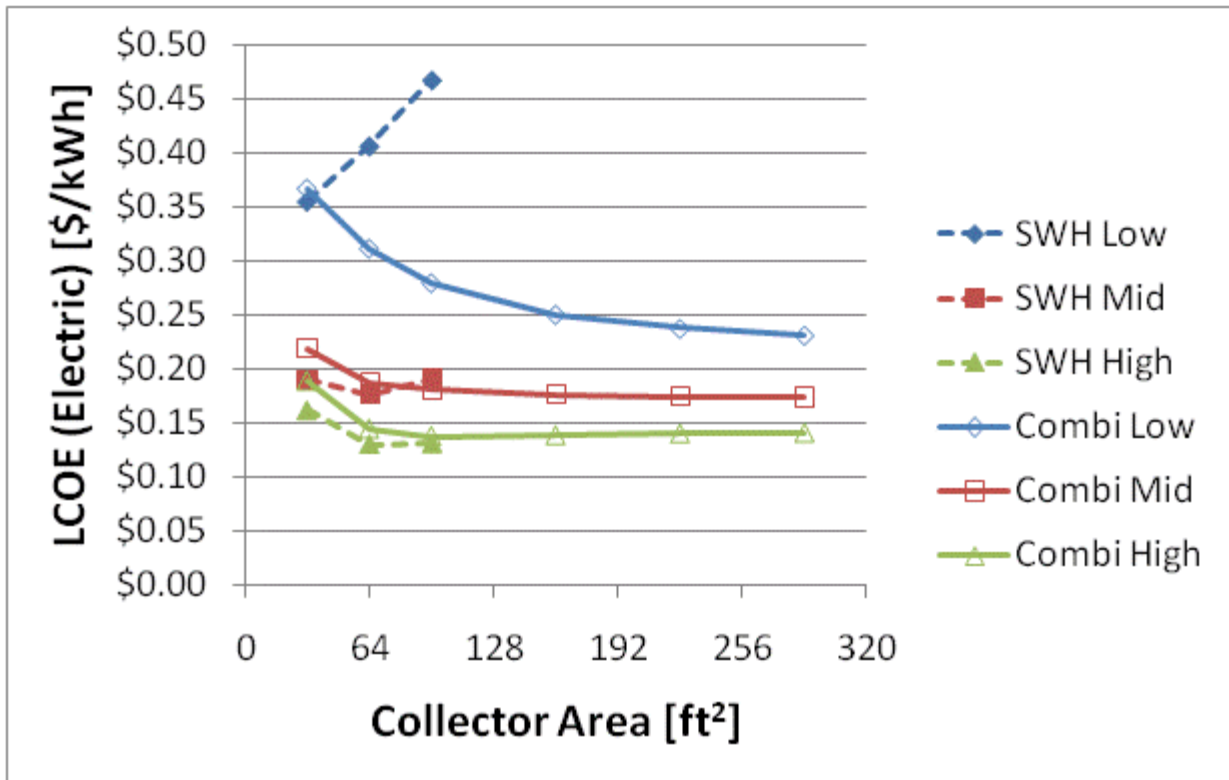


Figure F.27: LCOE and NPW for electric systems for a IECC 2009 House(Atlanta)

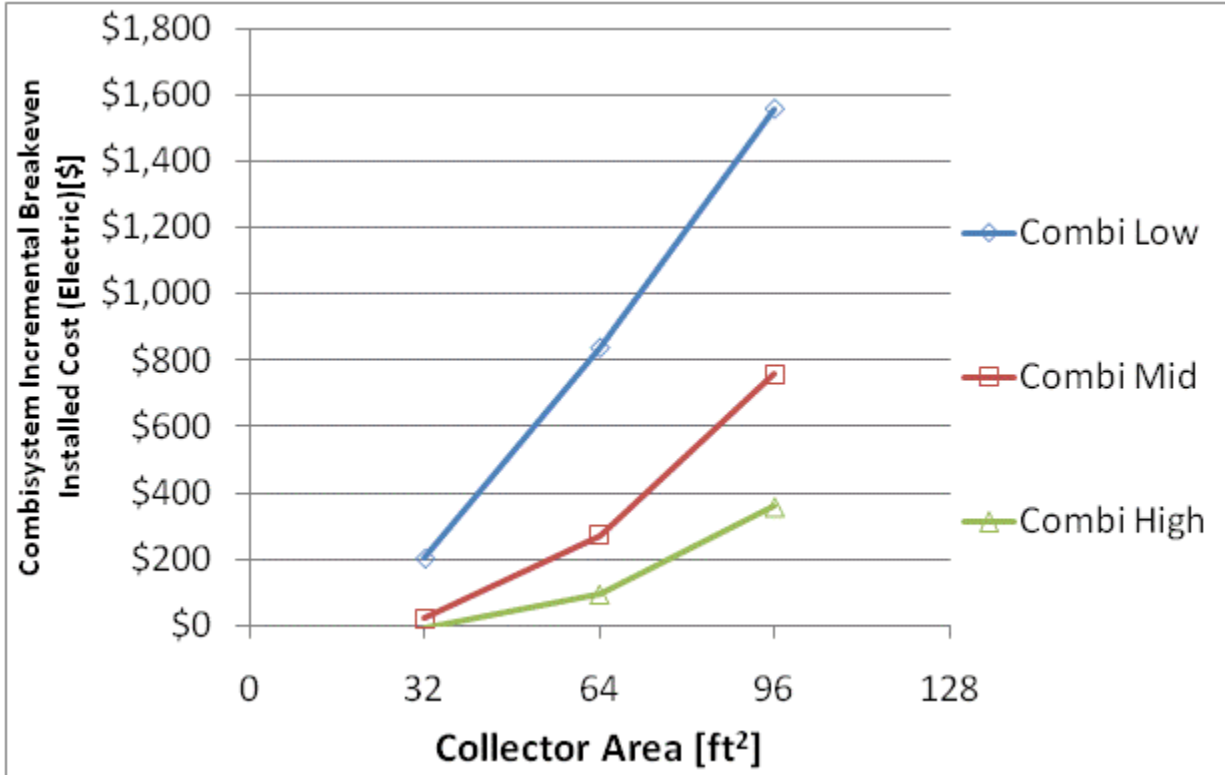
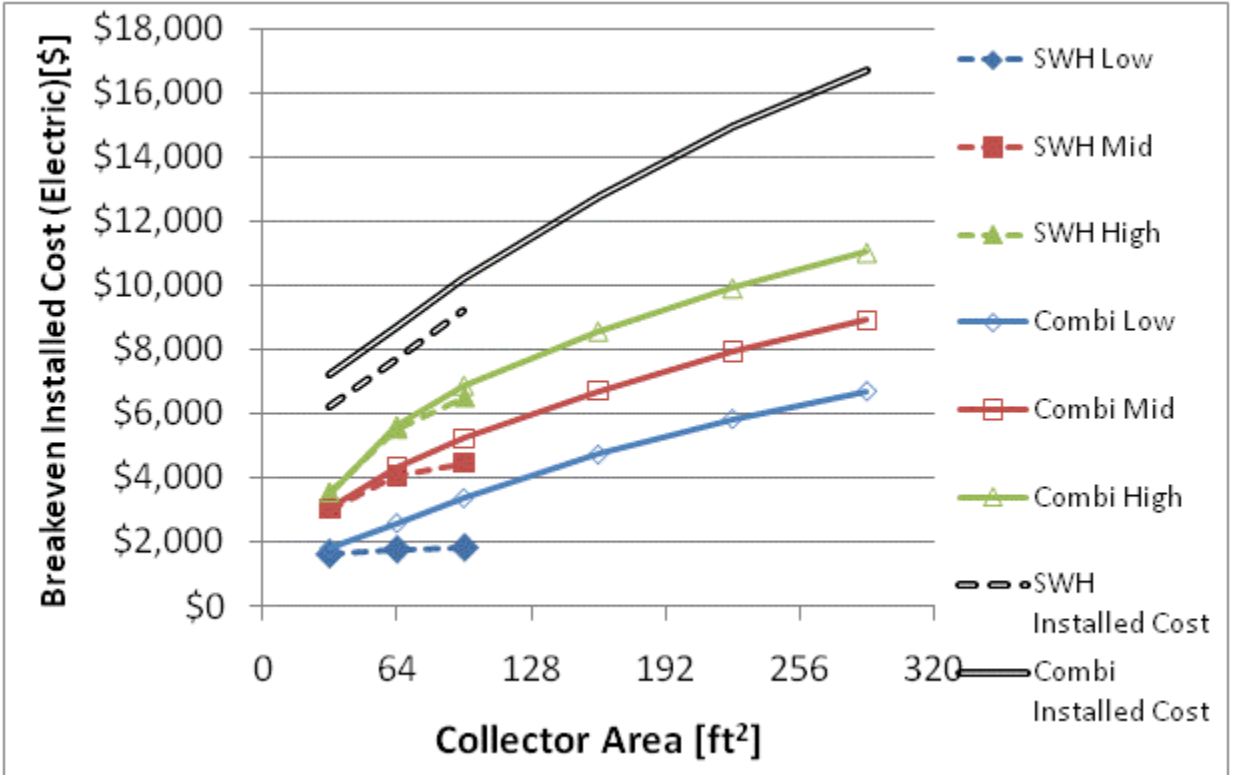


Figure F.28: Breakeven installed cost and combisystem incremental breakeven cost for electric system for a IECC 2009 House(Atlanta)

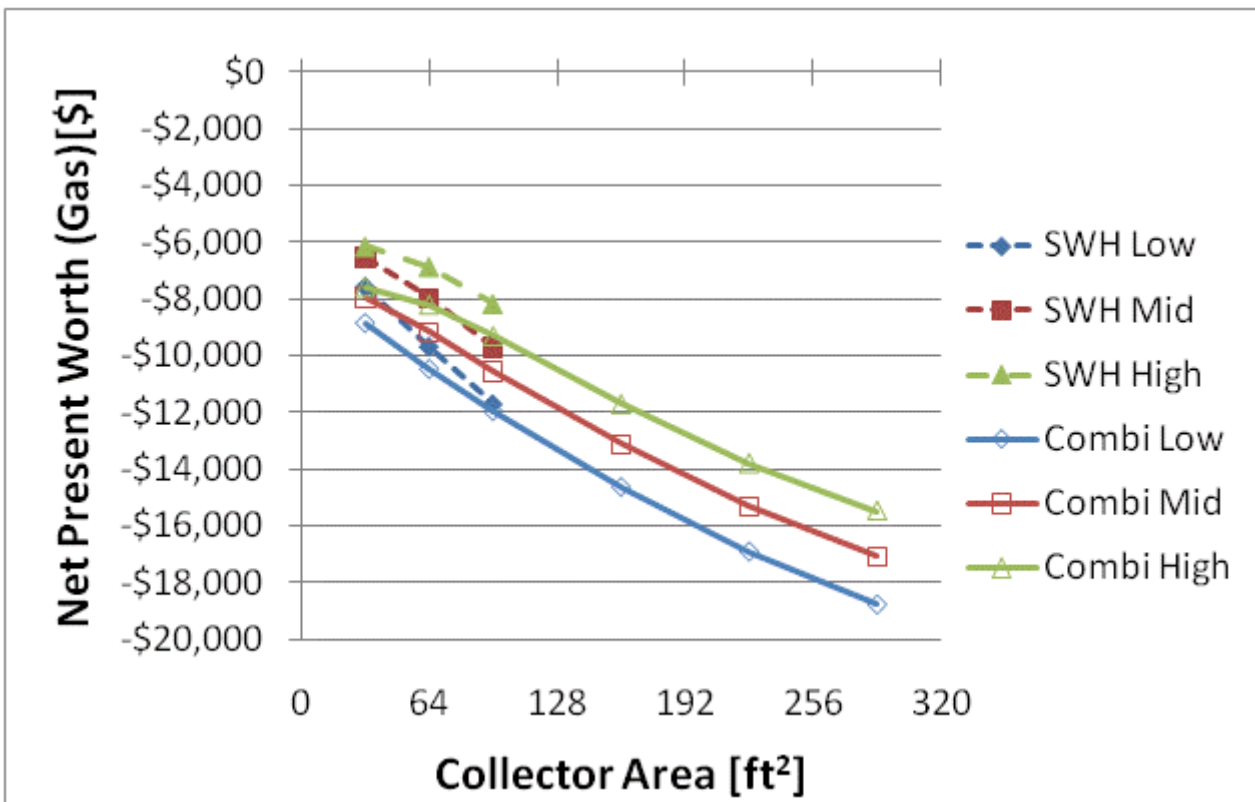
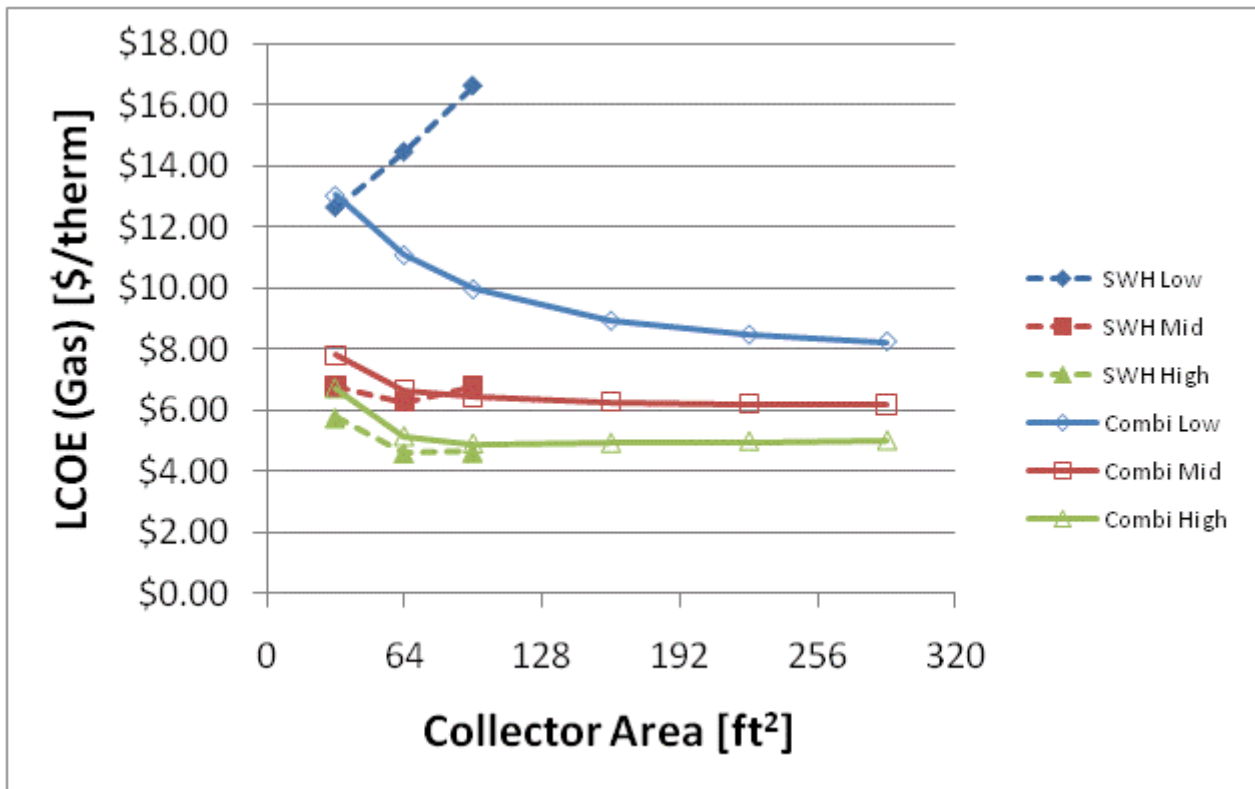


Figure F.29: LCOE and NPW for gas systems for a IECC 2009 House(Atlanta)

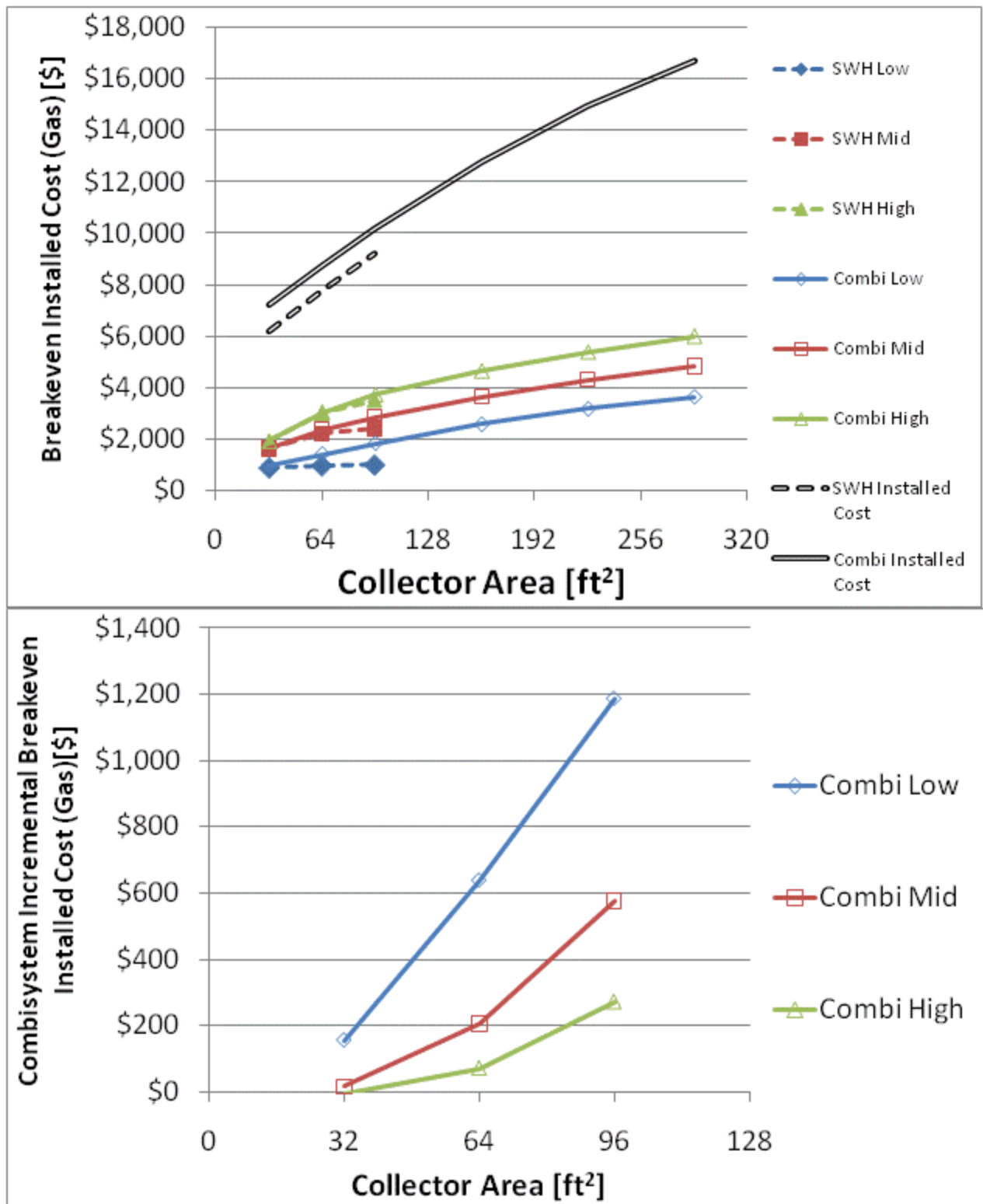


Figure F.30: Breakeven installed cost and combisystem incremental breakeven cost for gas systems for a

IECC 2009 House(Atlanta)

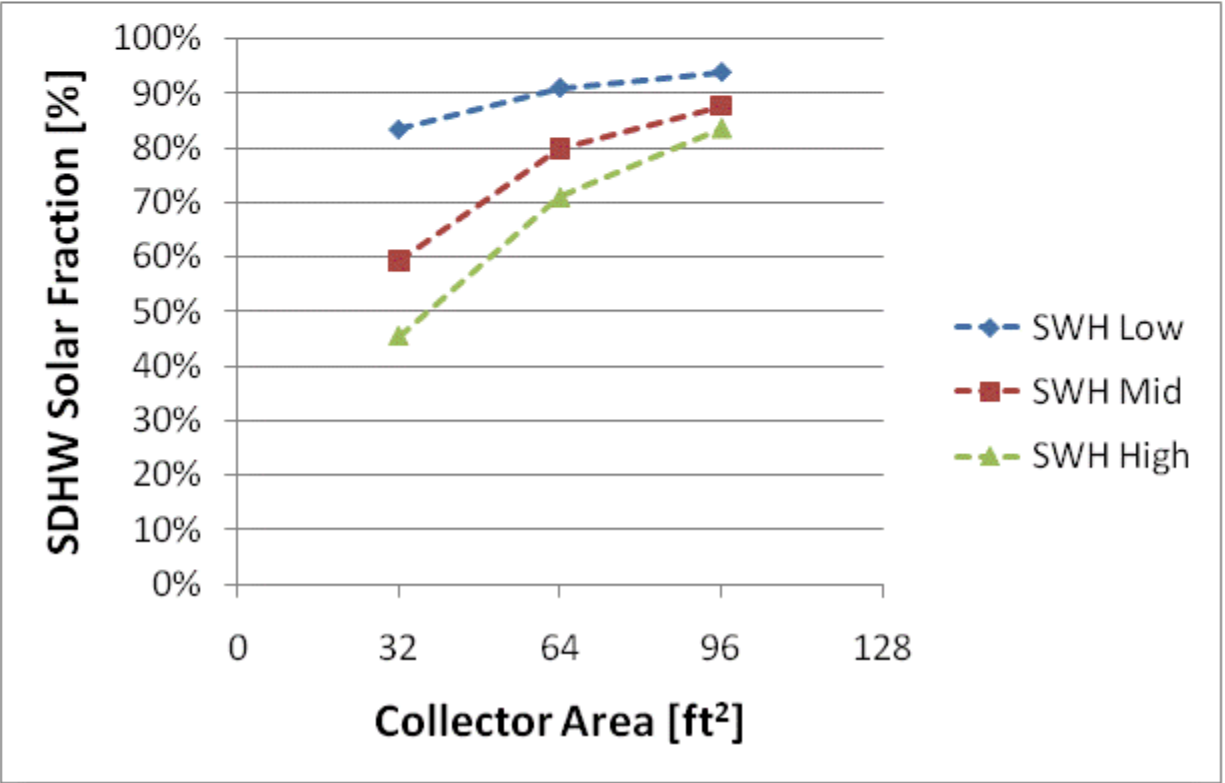
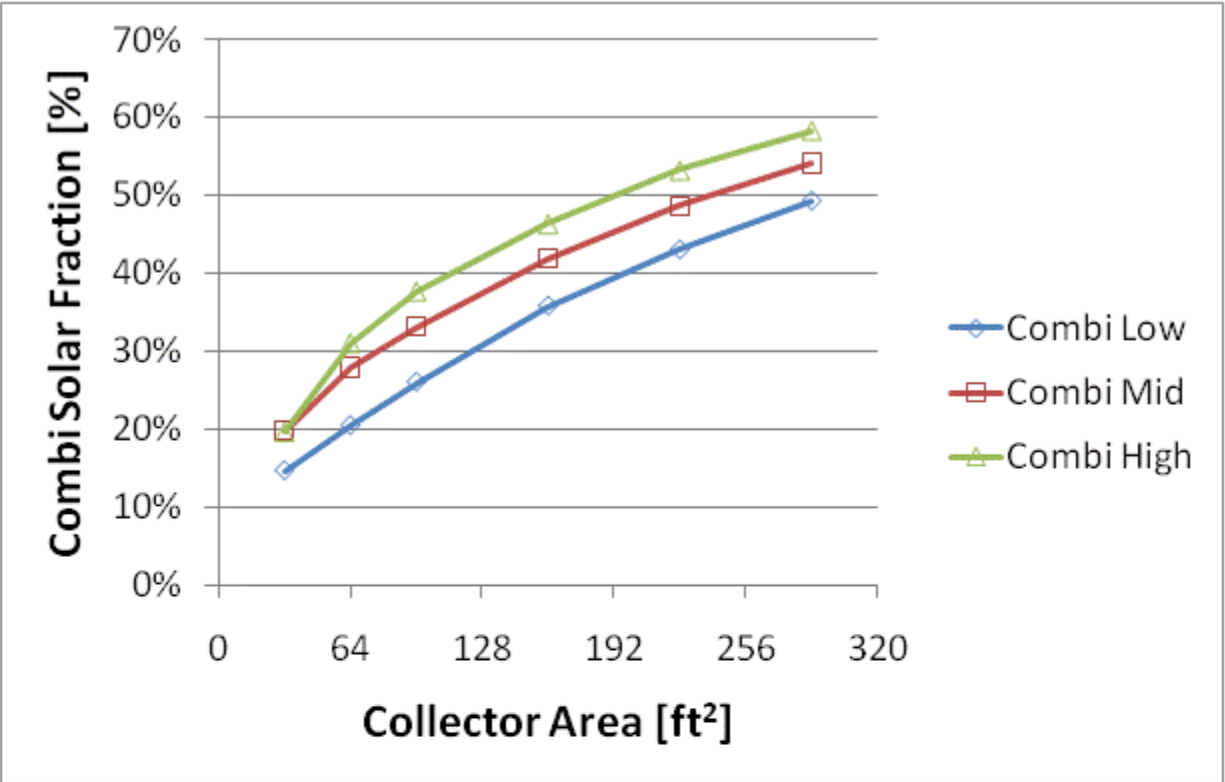


Figure F.31: Combisystem and SWH solar fraction for a BA 50% House(Atlanta)

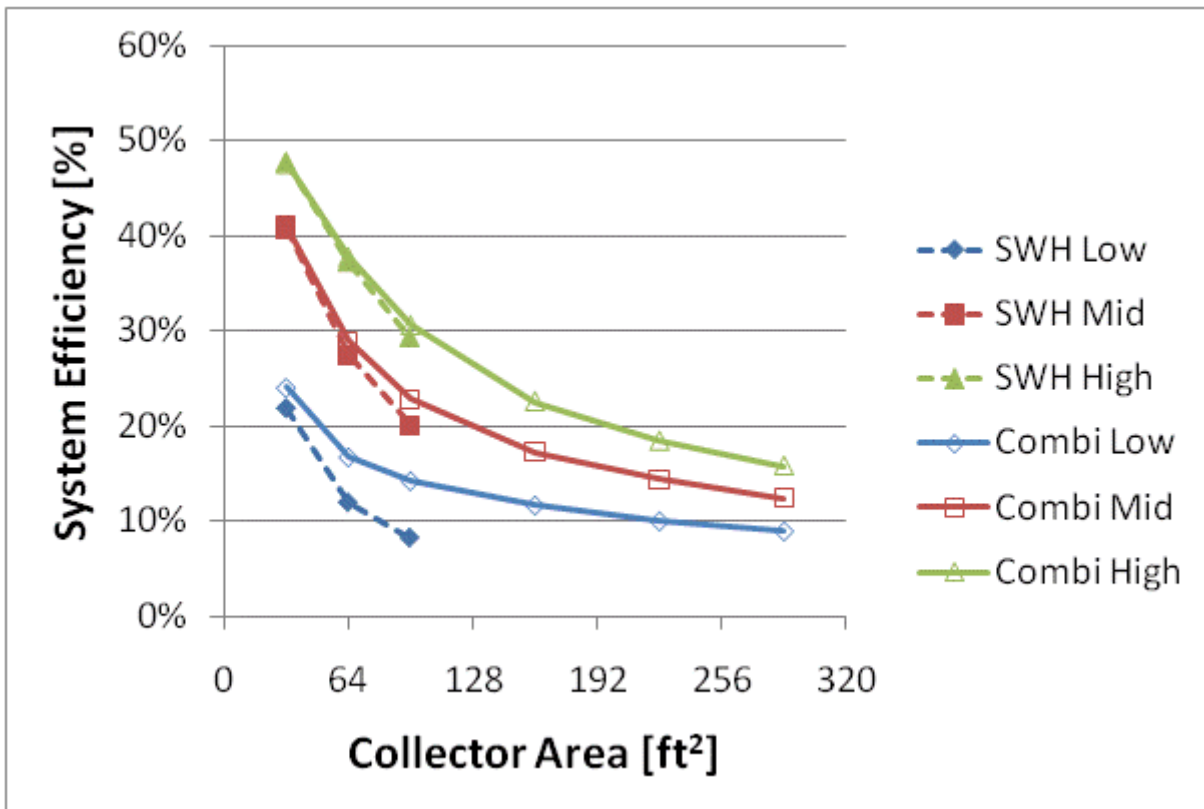
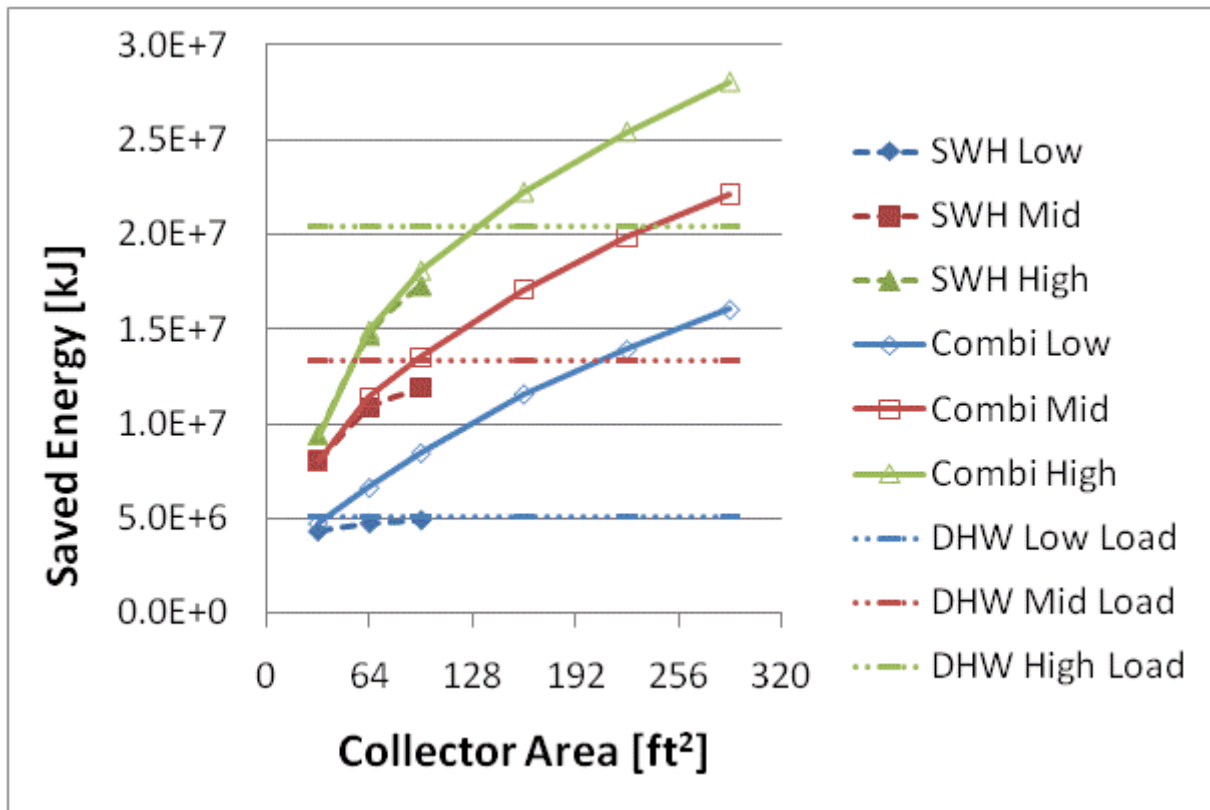


Figure F.32: Annual saved energy and system efficiency for a BA 50% House(Atlanta)

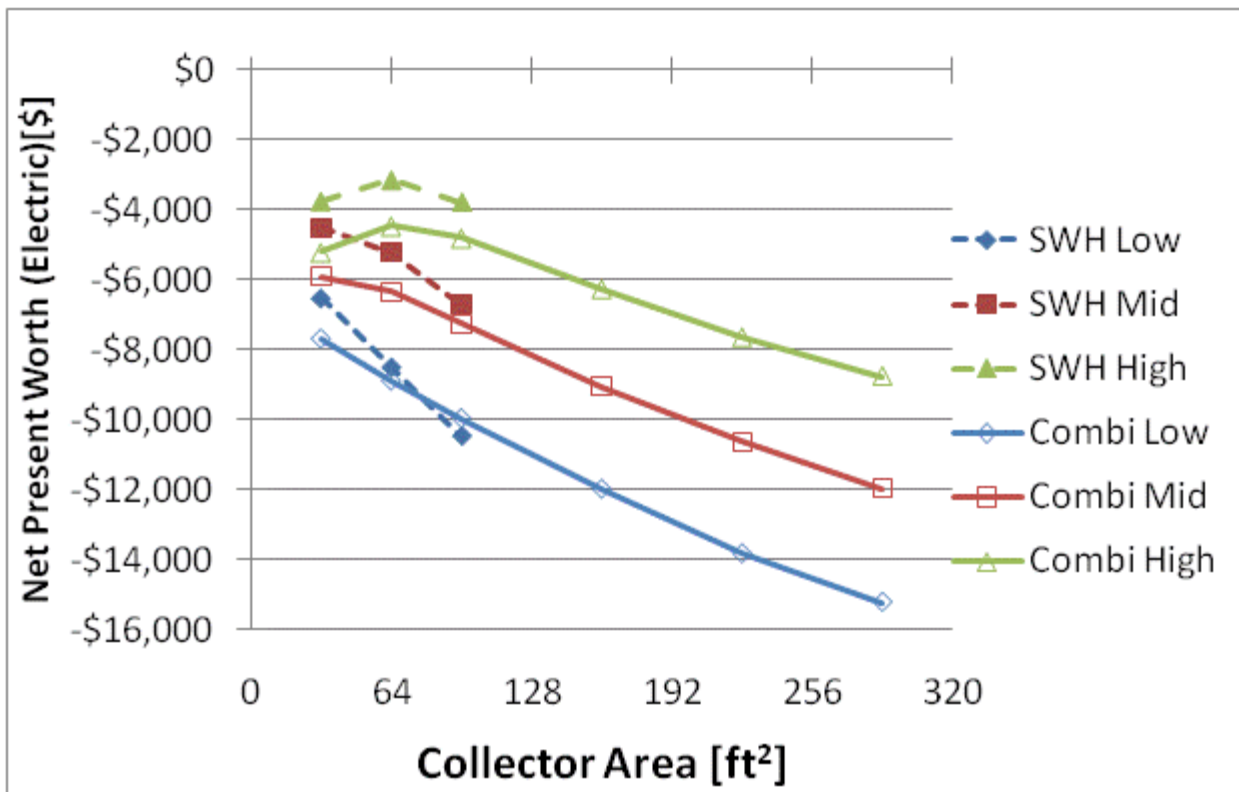
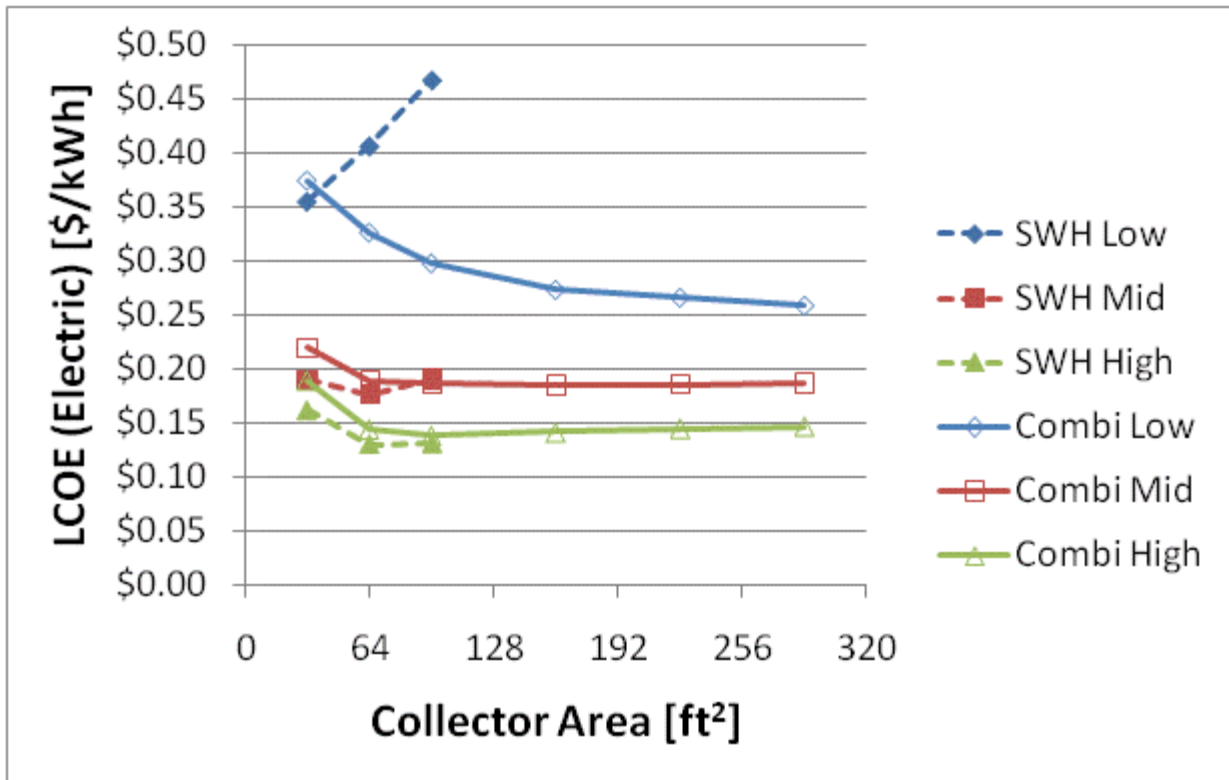


Figure F.33: LCOE and NPW for electric systems for a BA 50% House(Atlanta)

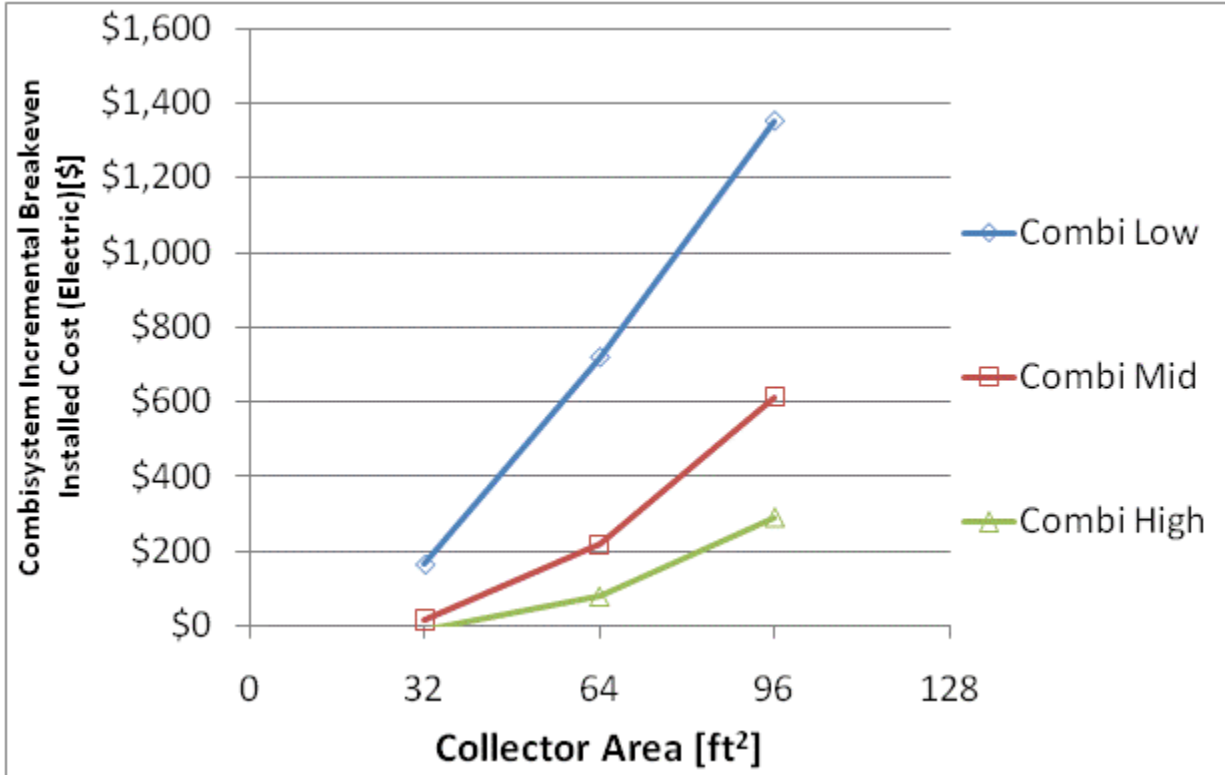
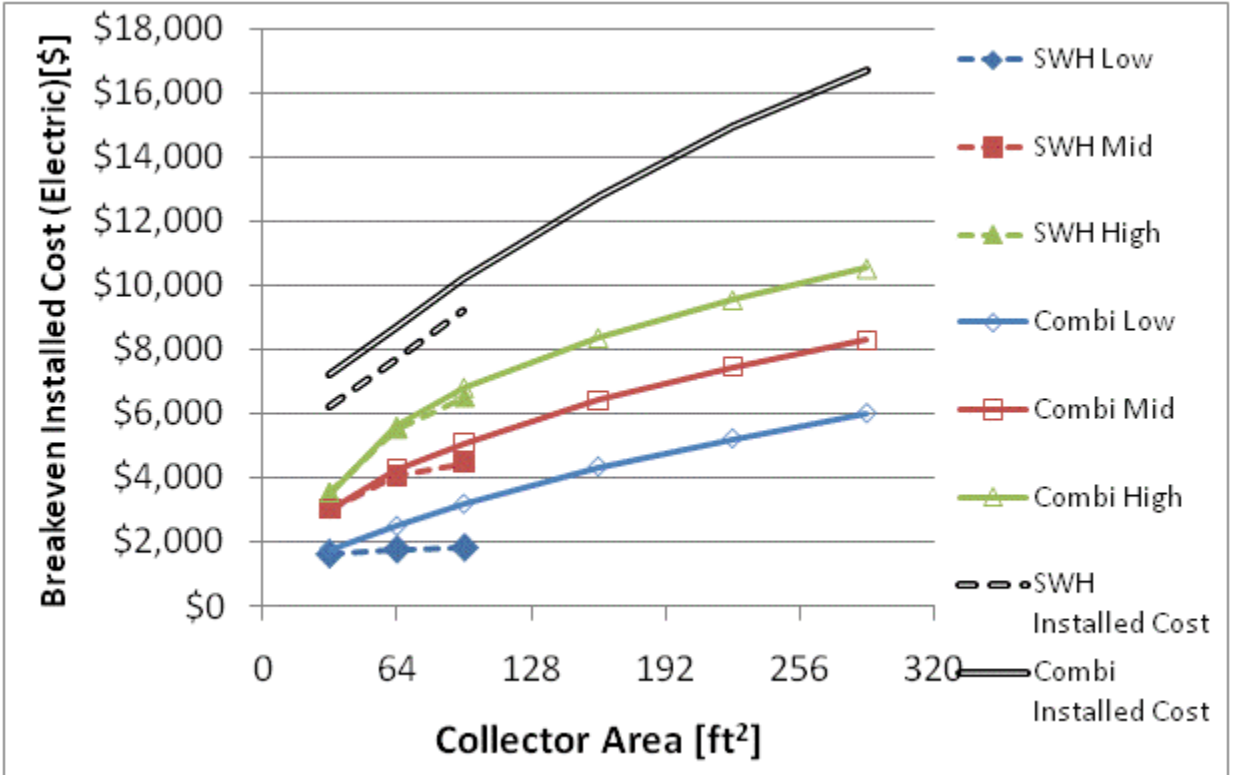


Figure F.34: Breakeven installed cost and combisystem incremental breakeven cost for electric system for a BA 50% House(Atlanta)

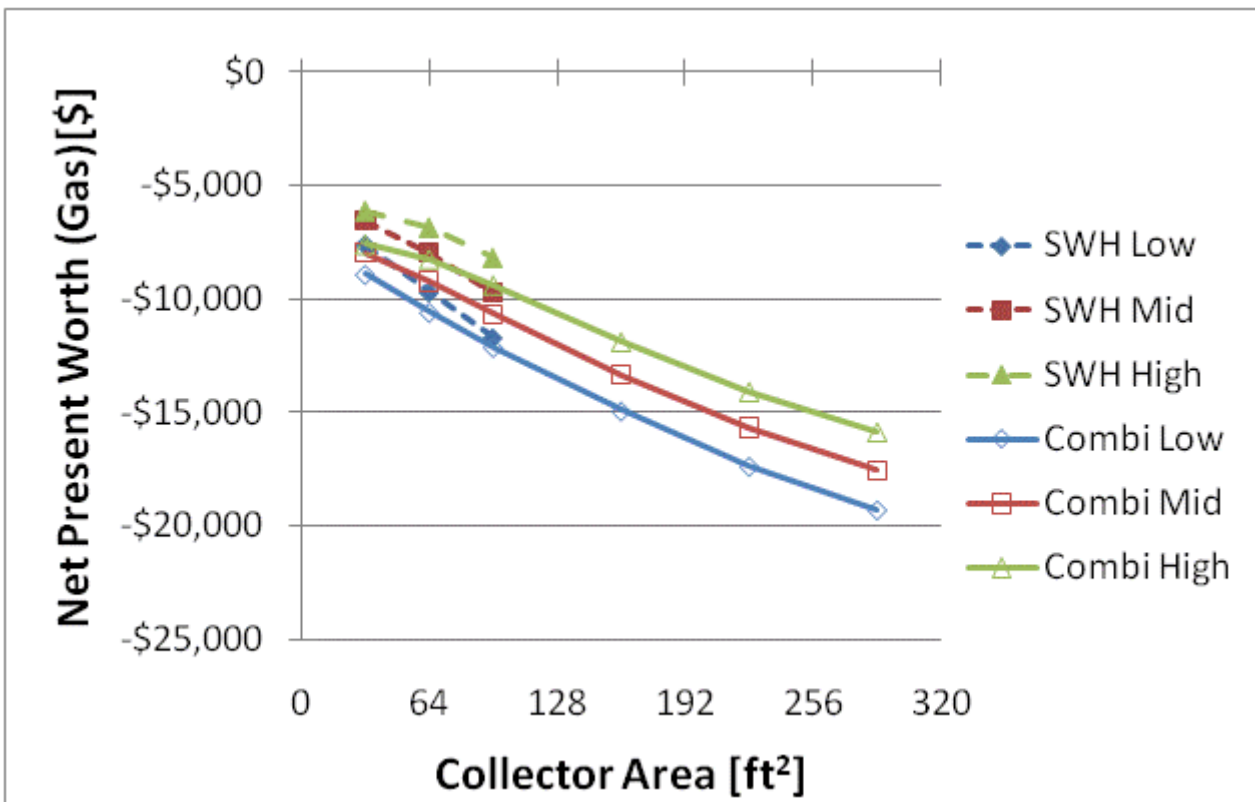
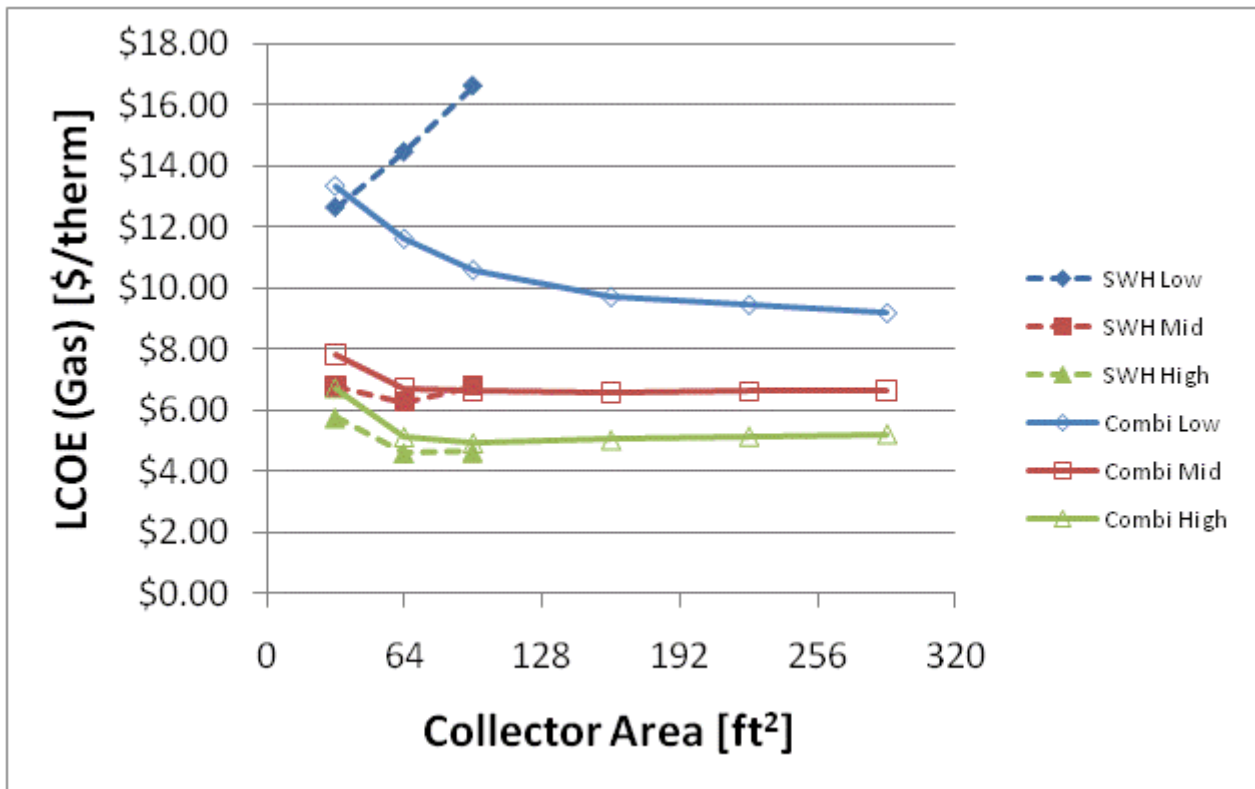


Figure F.35: LCOE and NPW for gas systems for a BA 50% House(Atlanta)

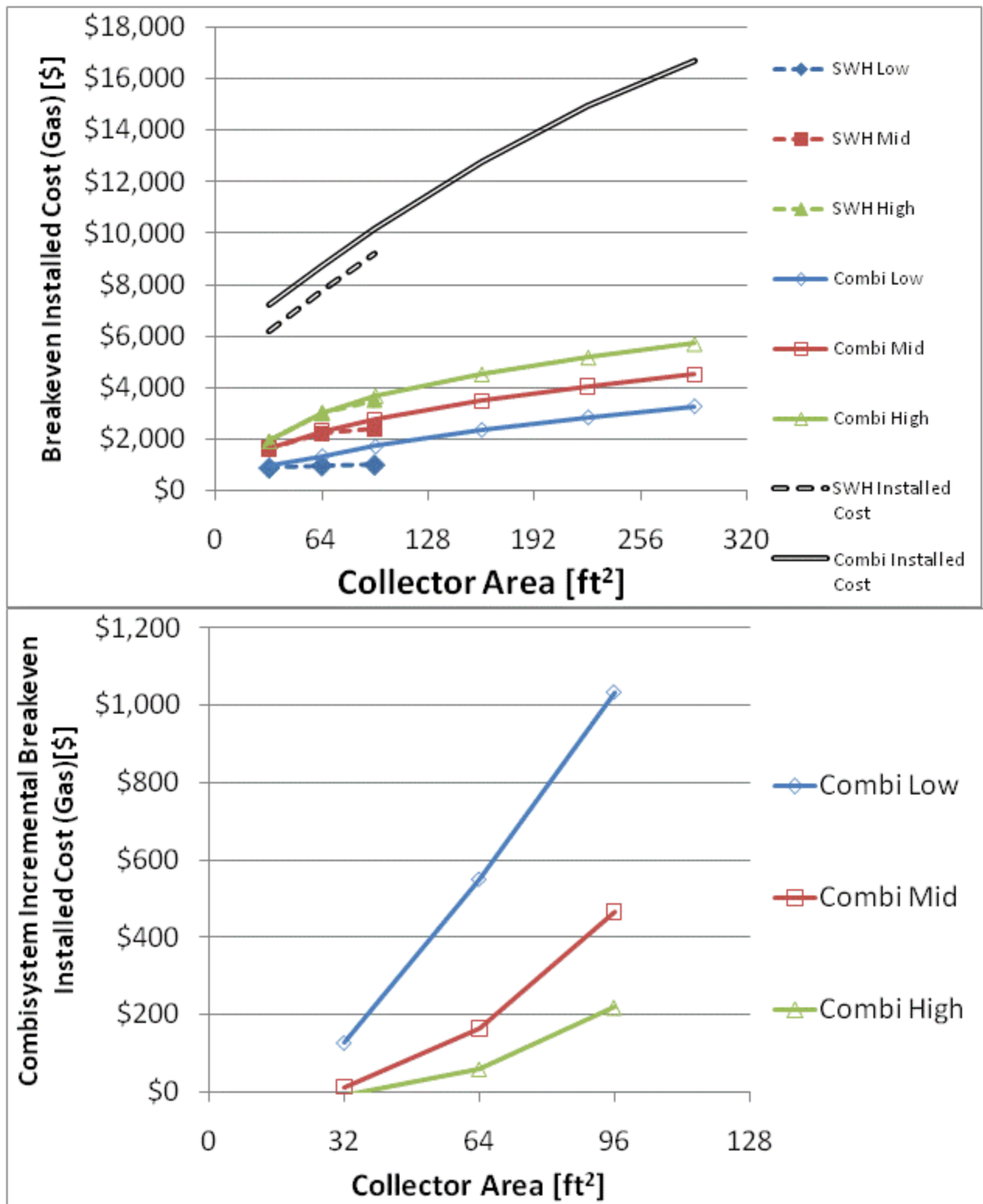


Figure F.36: Breakeven installed cost and combisystem incremental breakeven cost for gas systems for a

BA 50% House(Atlanta)

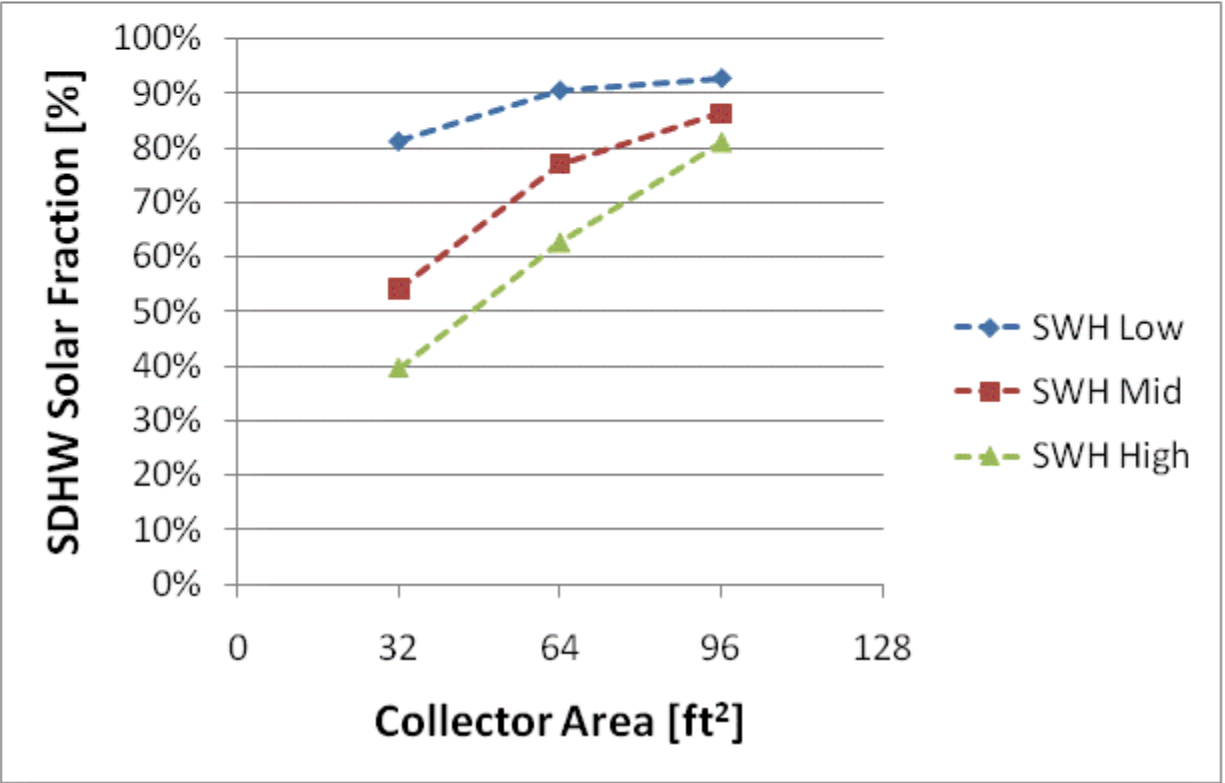
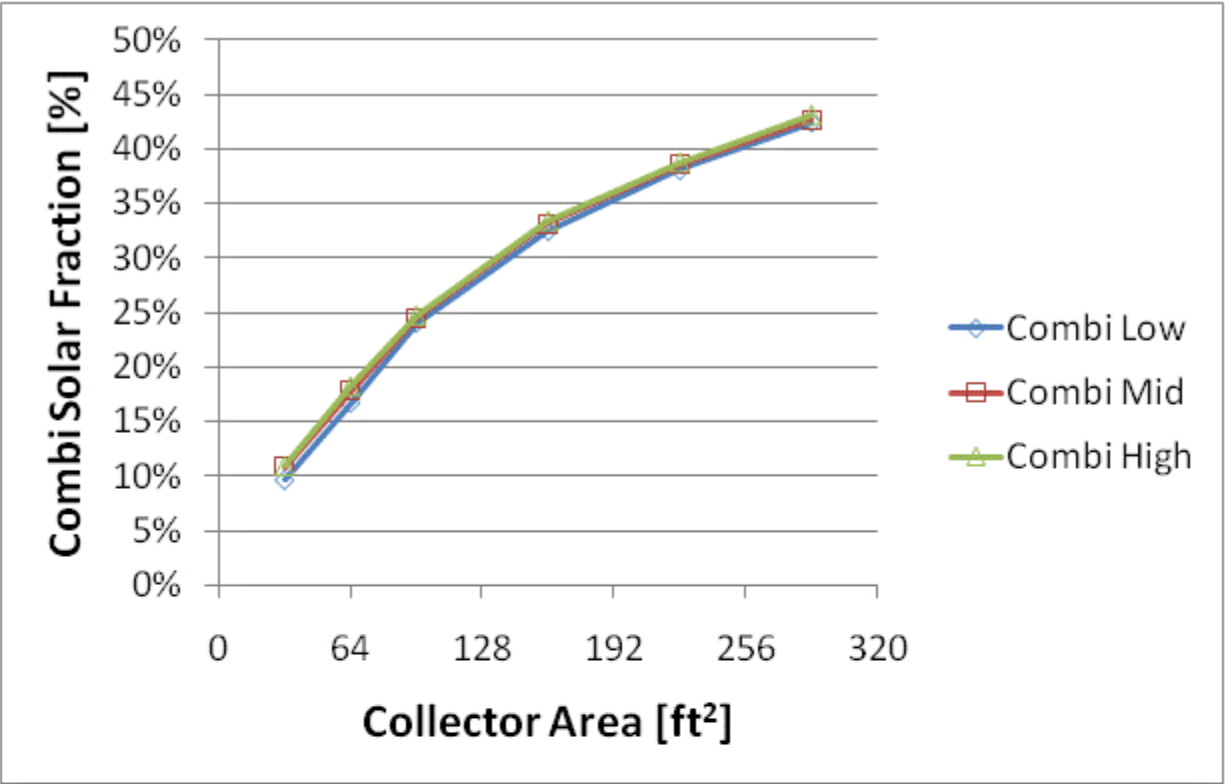


Figure F.37: Combisystem and SWH solar fraction for a 1960s Retrofit House(San Francisco)

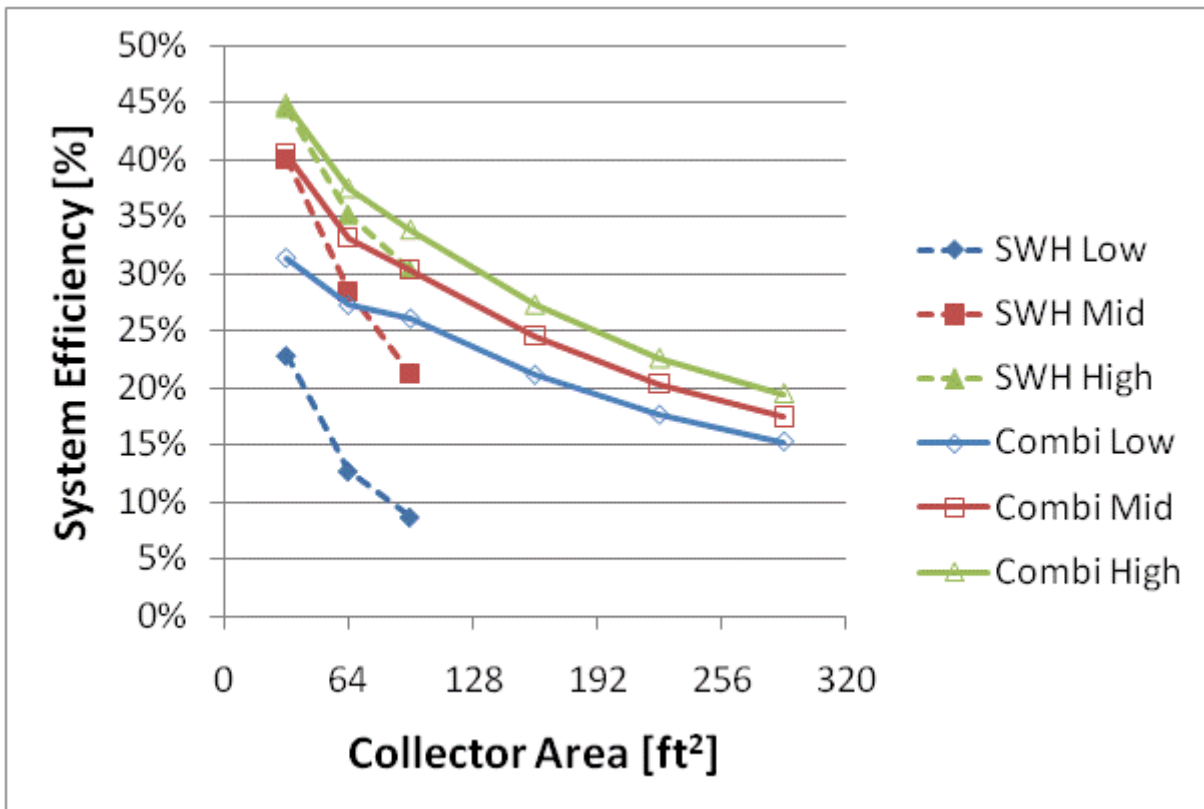
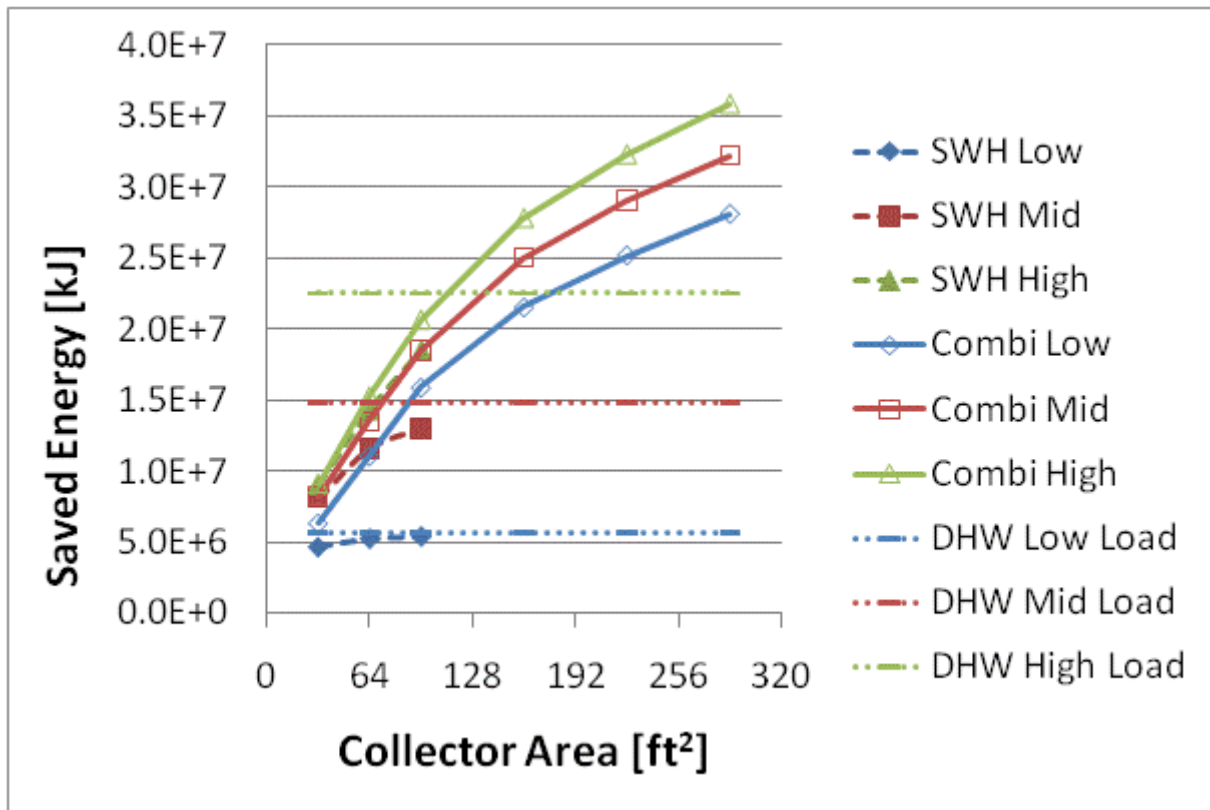


Figure F.38: Annual saved energy and system efficiency for a 1960s Retrofit House(San Francisco)

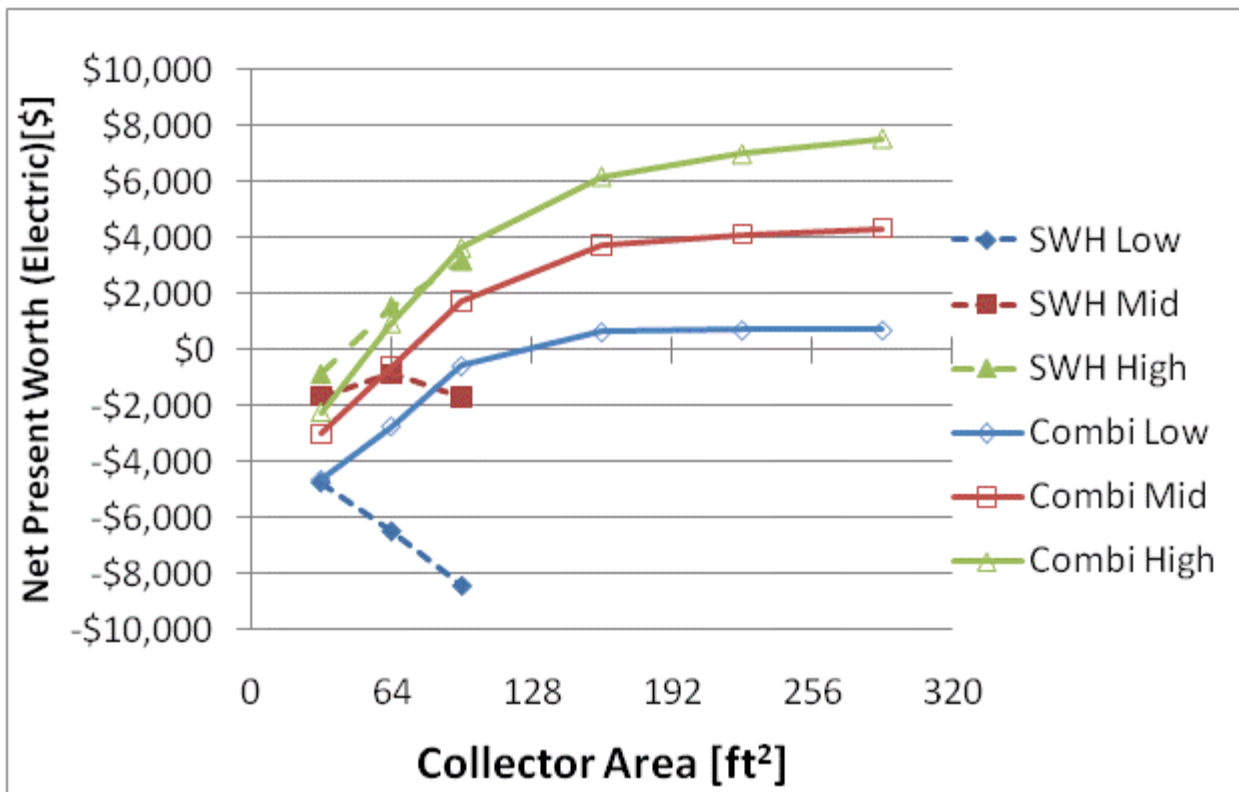
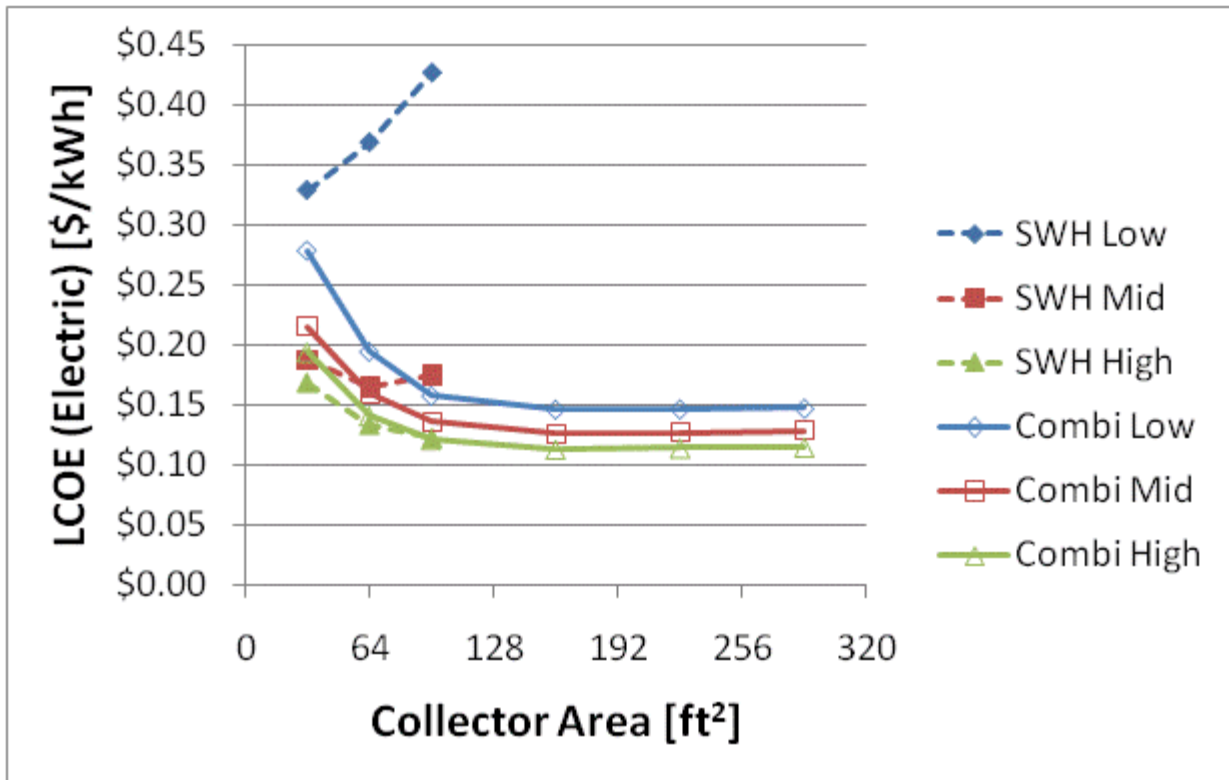


Figure F.39: LCOE and NPW for electric systems for a 1960s Retrofit House(San Francisco)

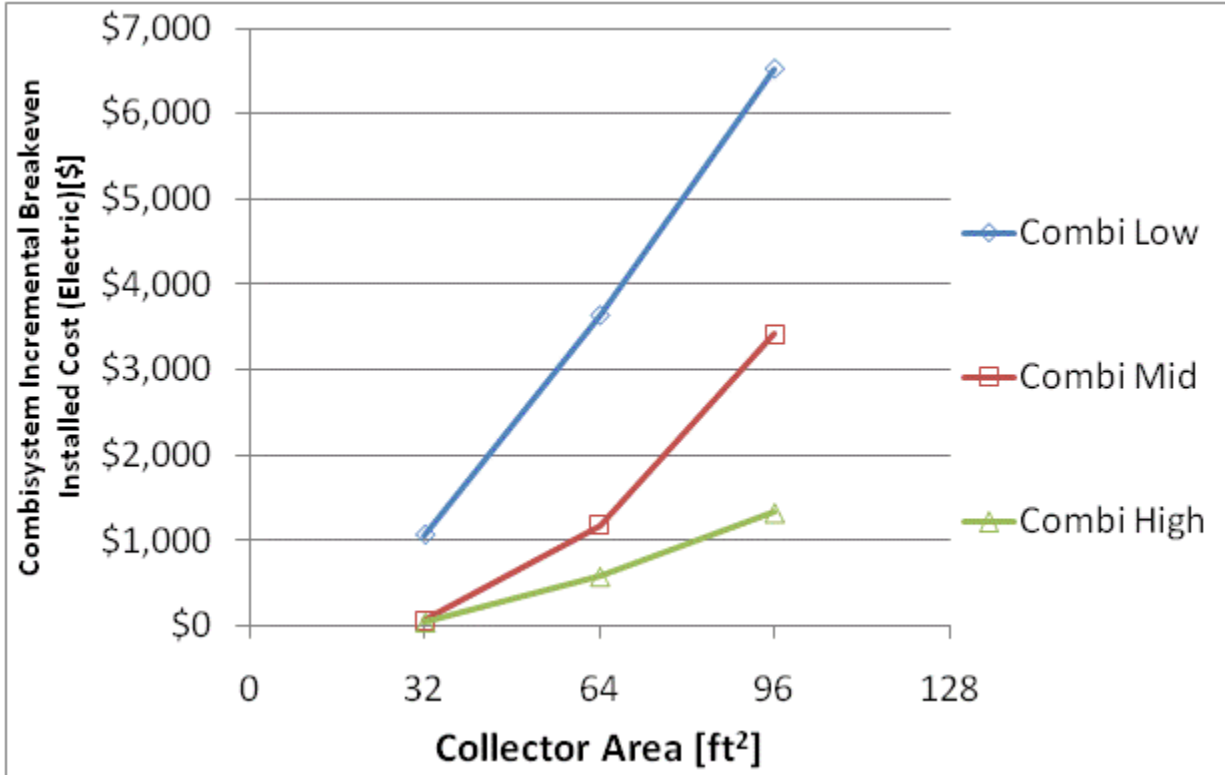
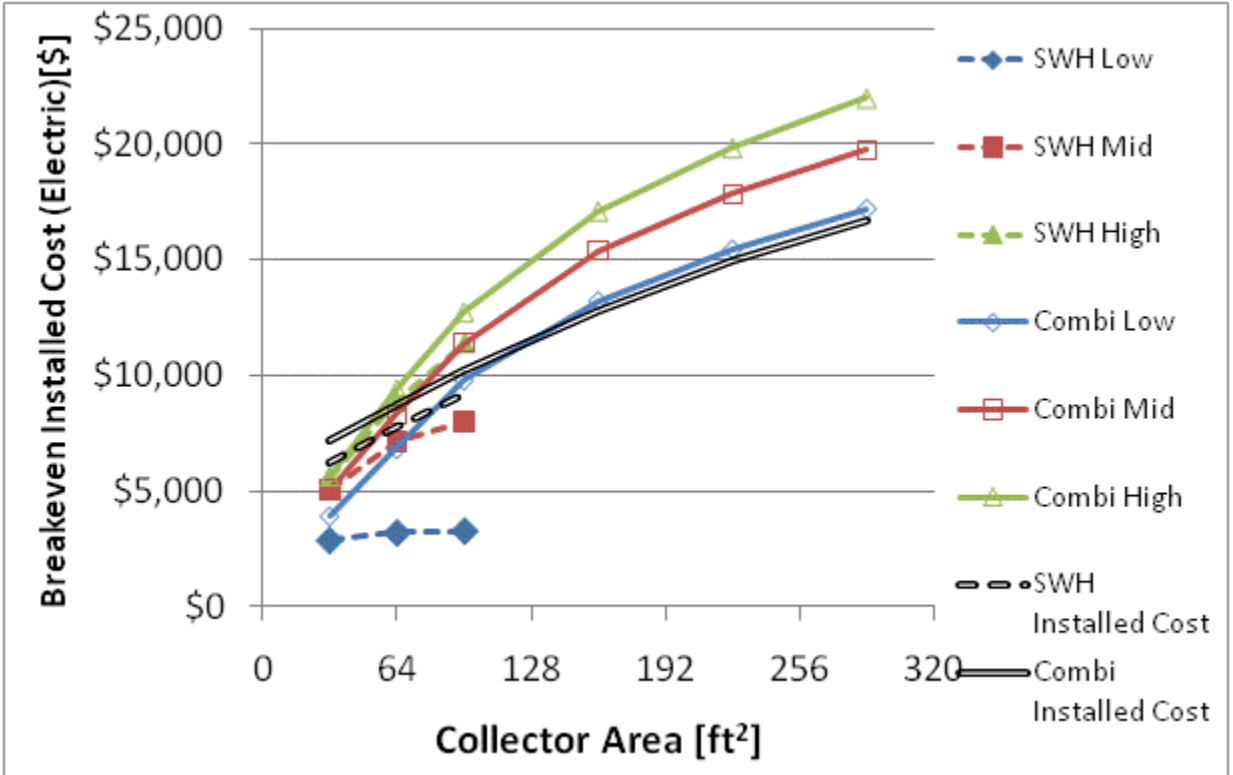


Figure F.40: Breakeven installed cost and combisystem incremental breakeven cost for electric system for a 1960s Retrofit House(San Francisco)

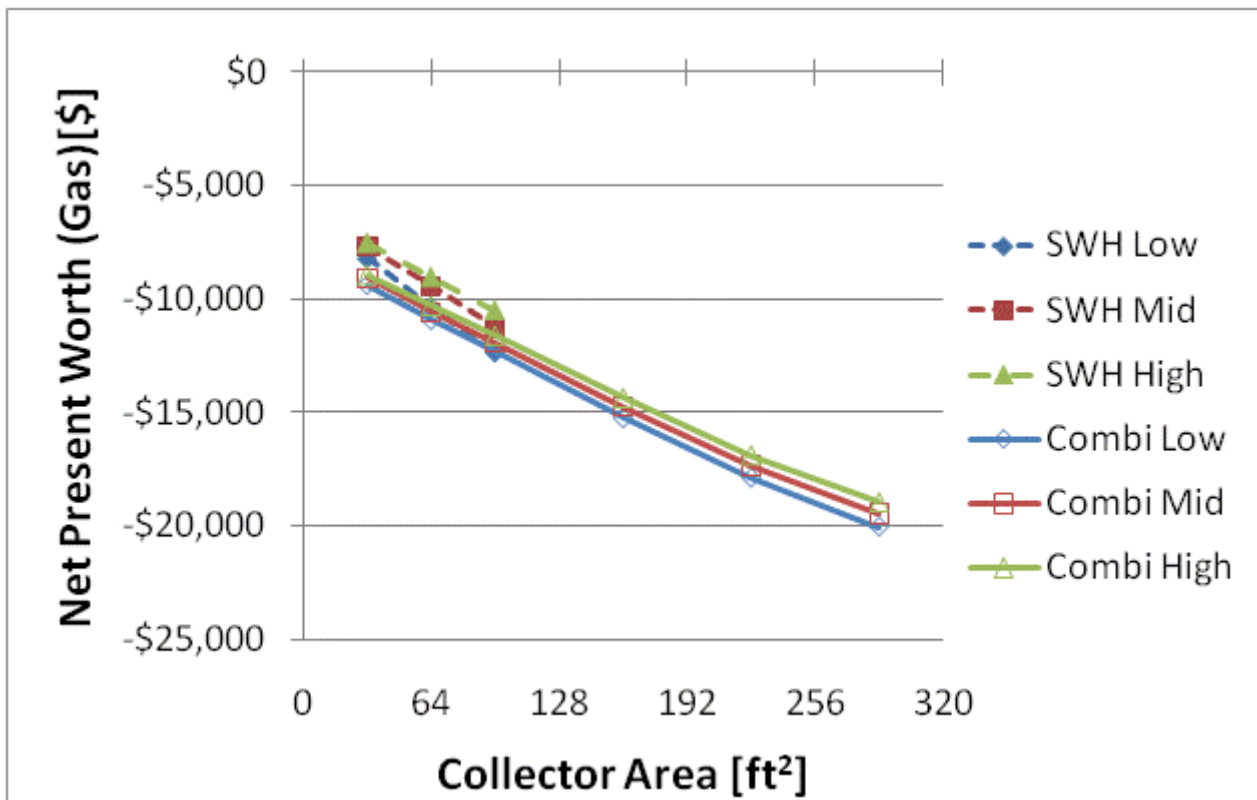
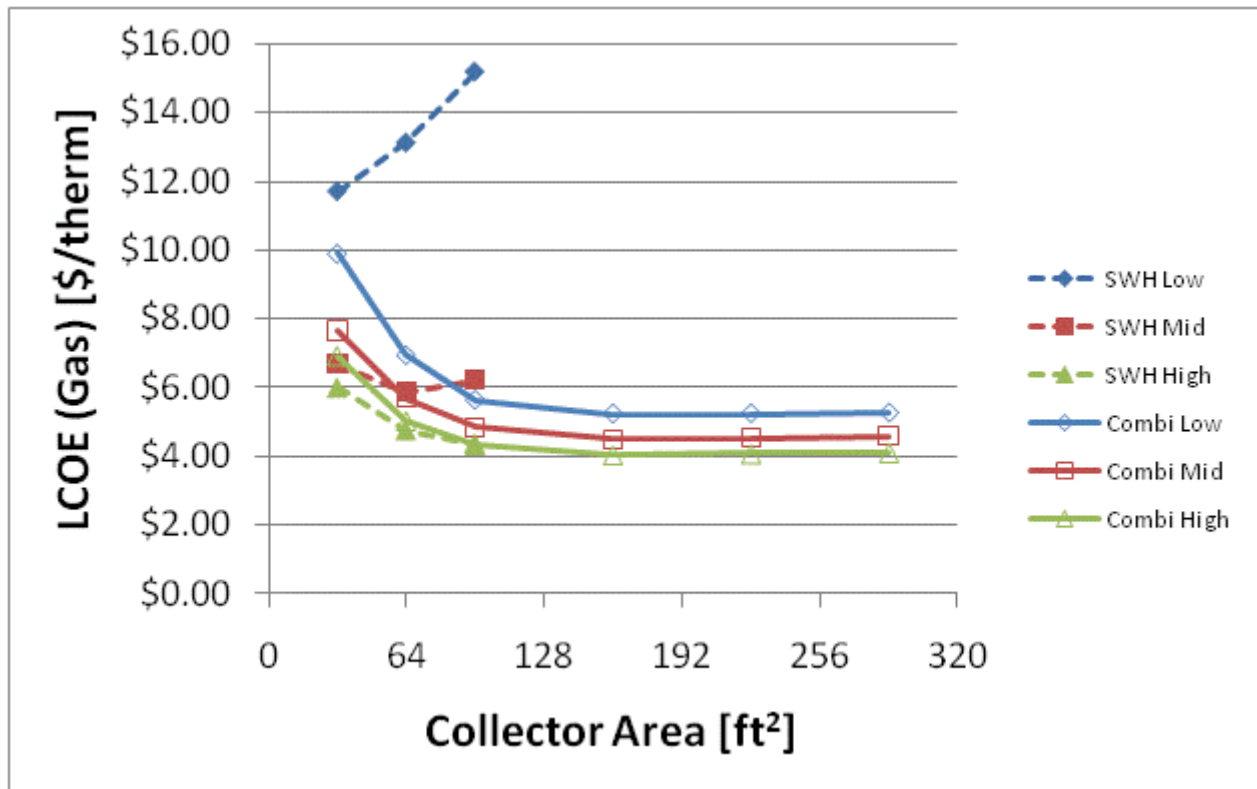


Figure F.41: LCOE and NPW for gas systems for a 1960s Retrofit House(San Francisco)

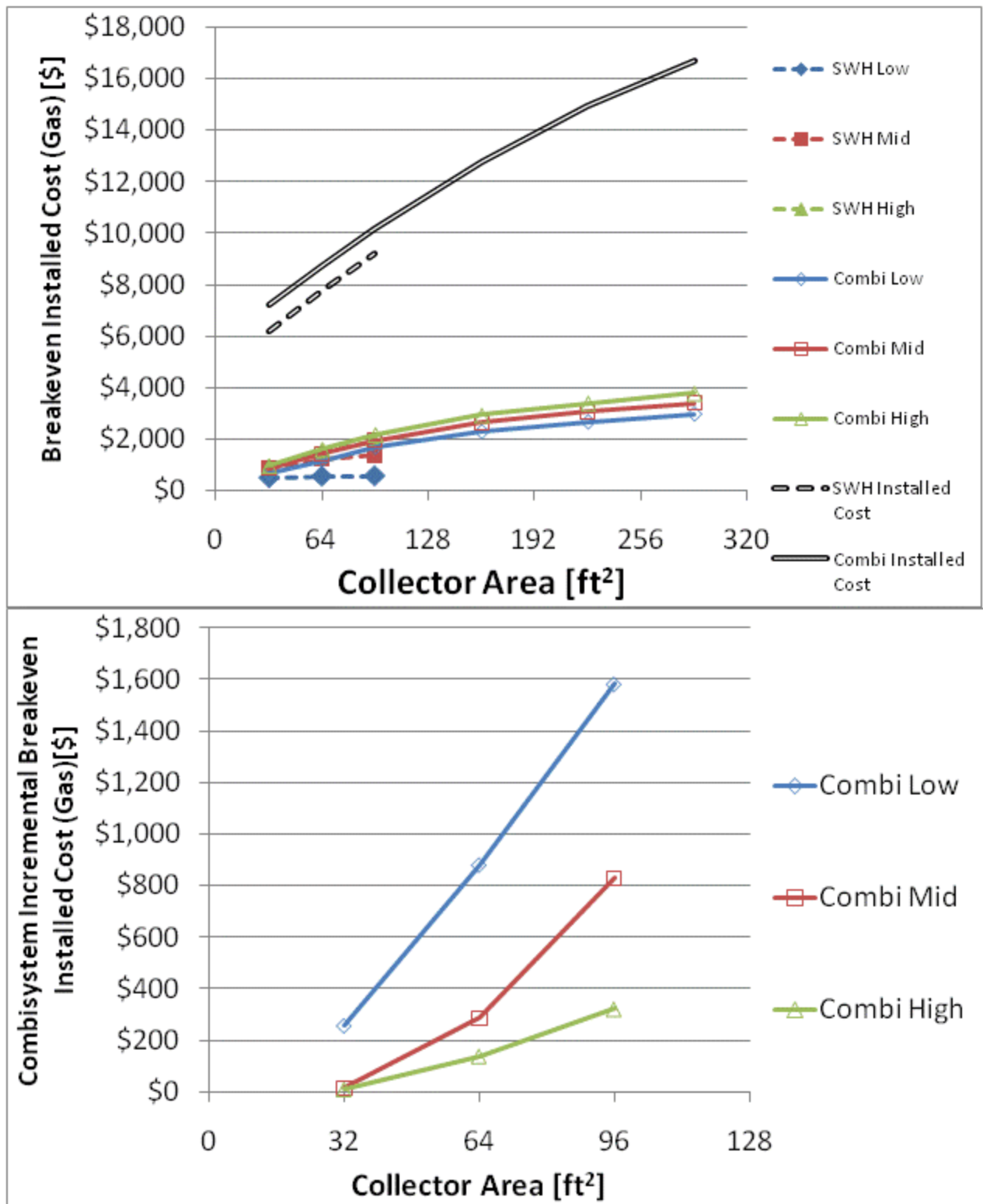


Figure F.42: Breakeven installed cost and combisystem incremental breakeven cost for gas systems for a

1960s Retrofit House(San Francisco)

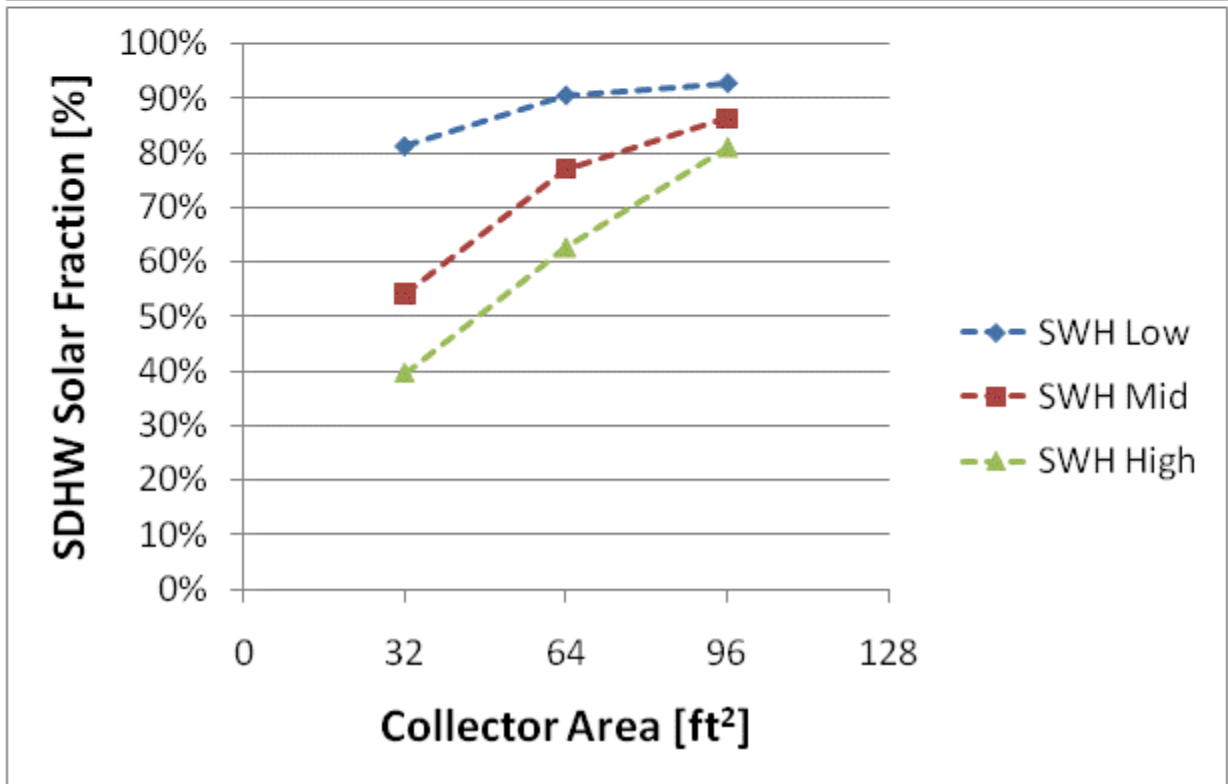
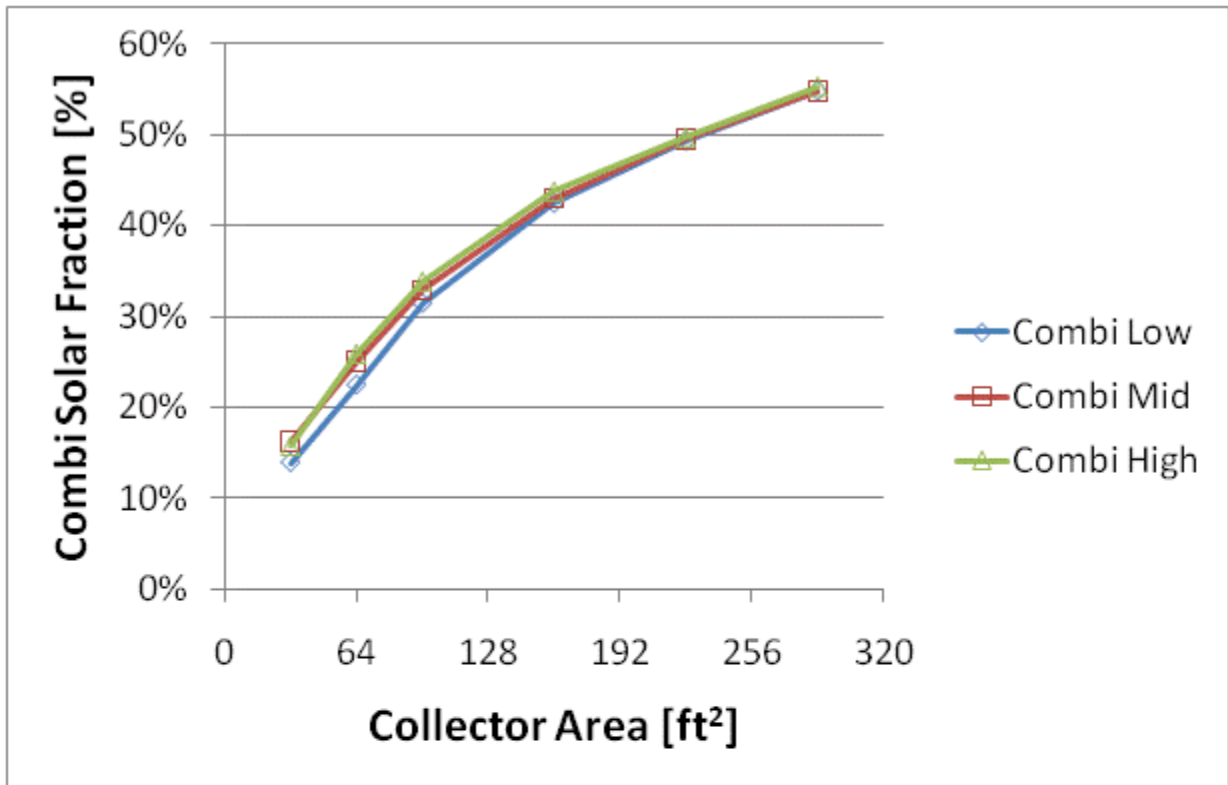


Figure F.43: Combi system and SWH solar fraction for a IECC 2009 House (San Francisco)

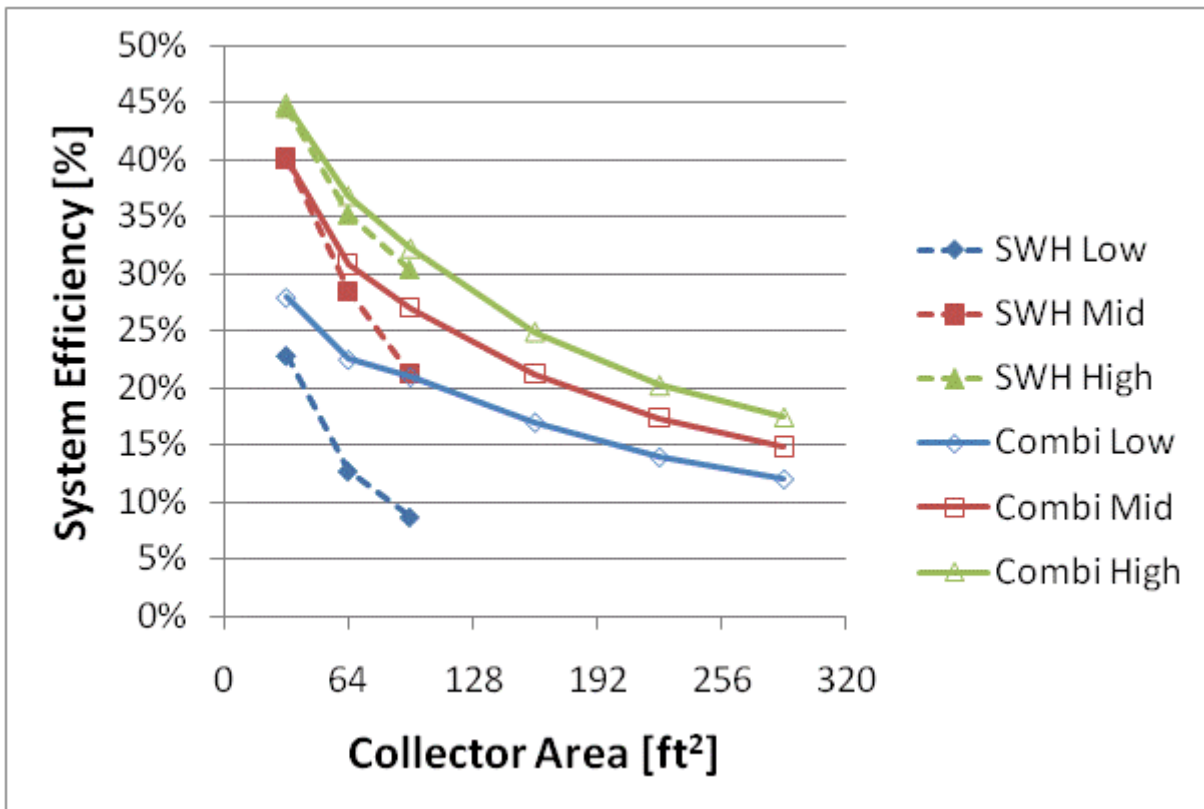
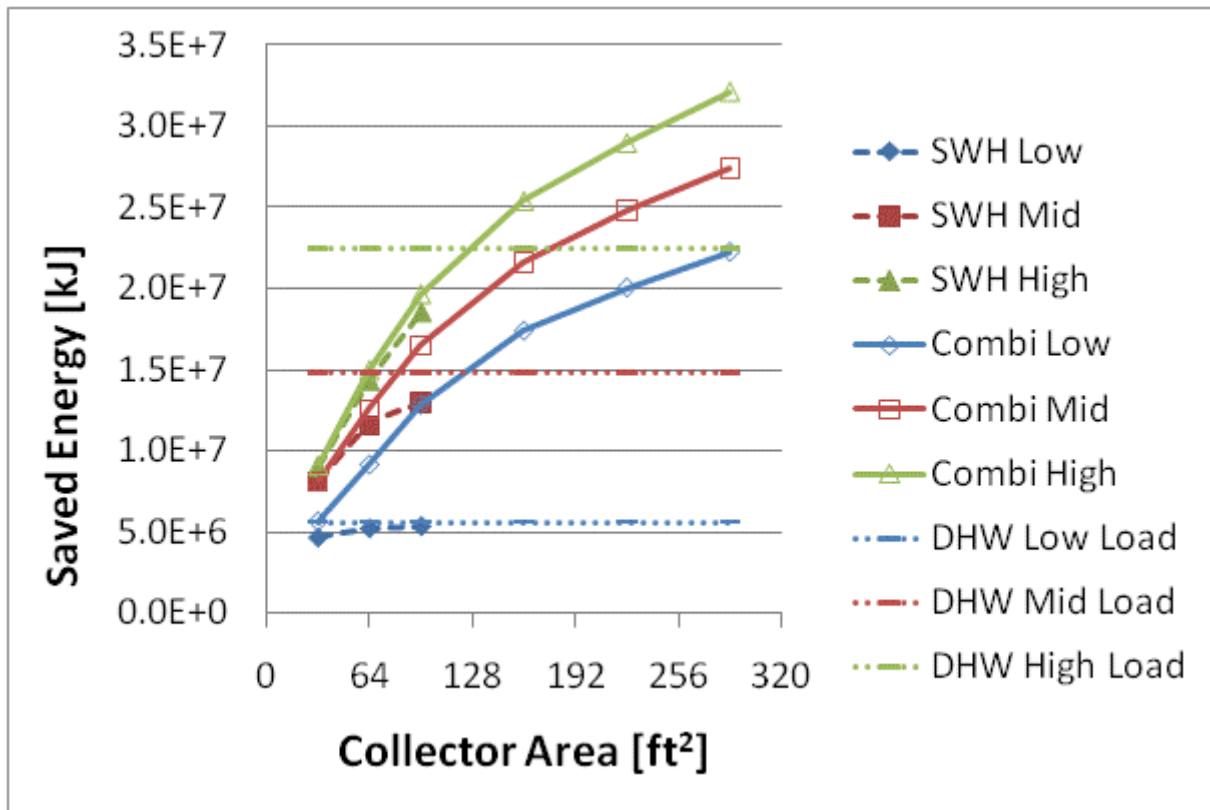


Figure F.44: Annual saved energy and system efficiency for a IECC 2009 House(San Francisco)

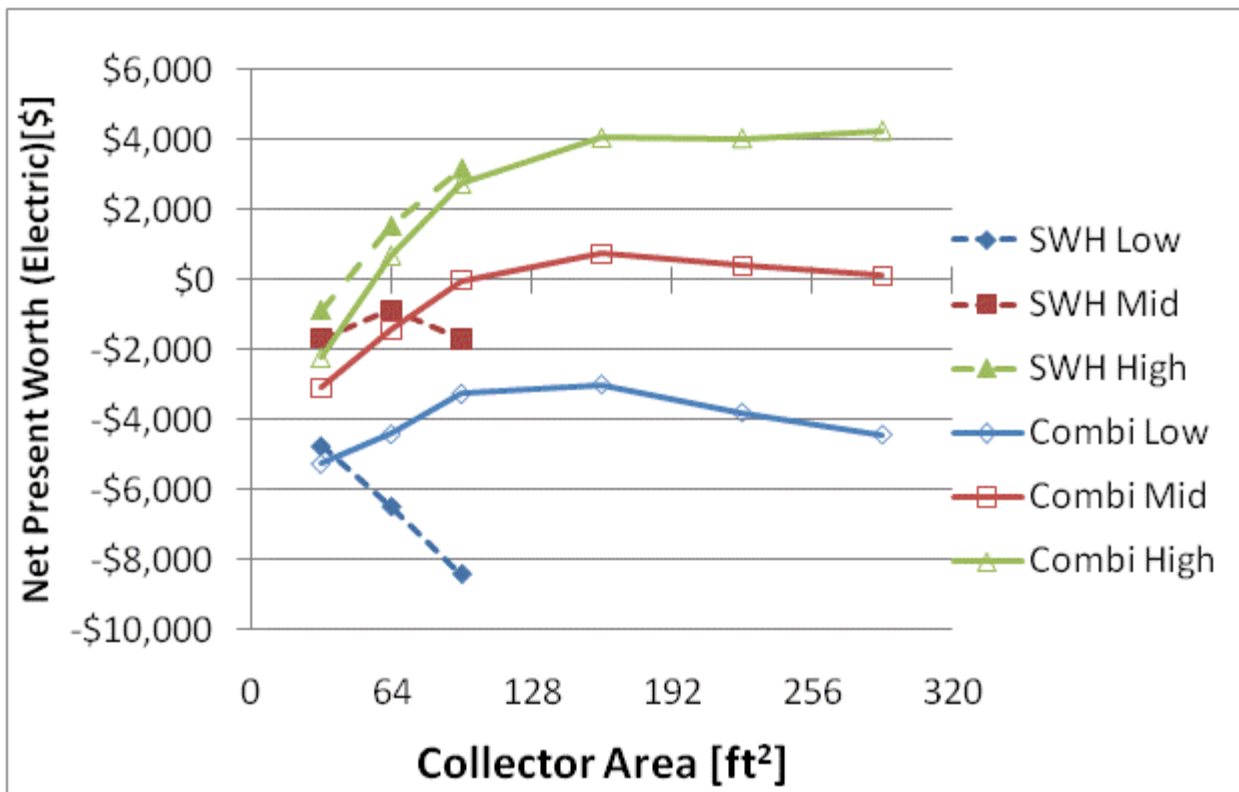
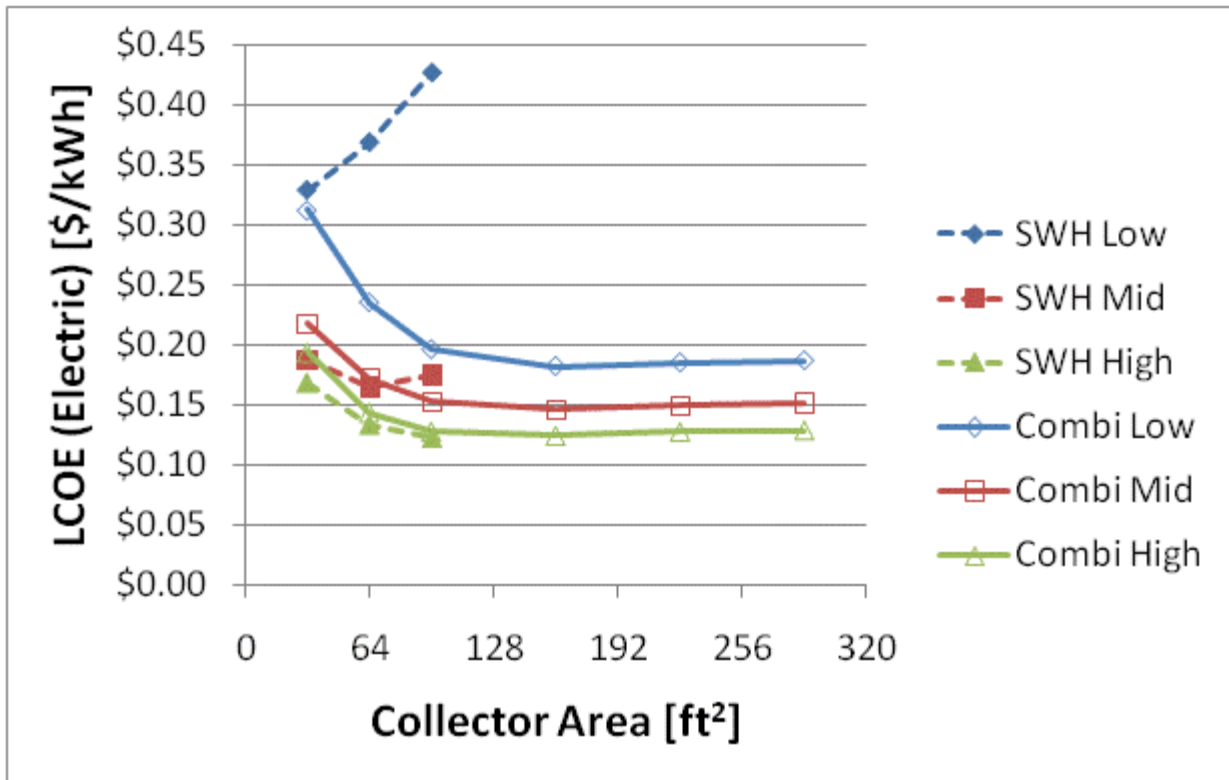


Figure F.45: LCOE and NPW for electric systems for a IECC 2009 House(San Francisco)

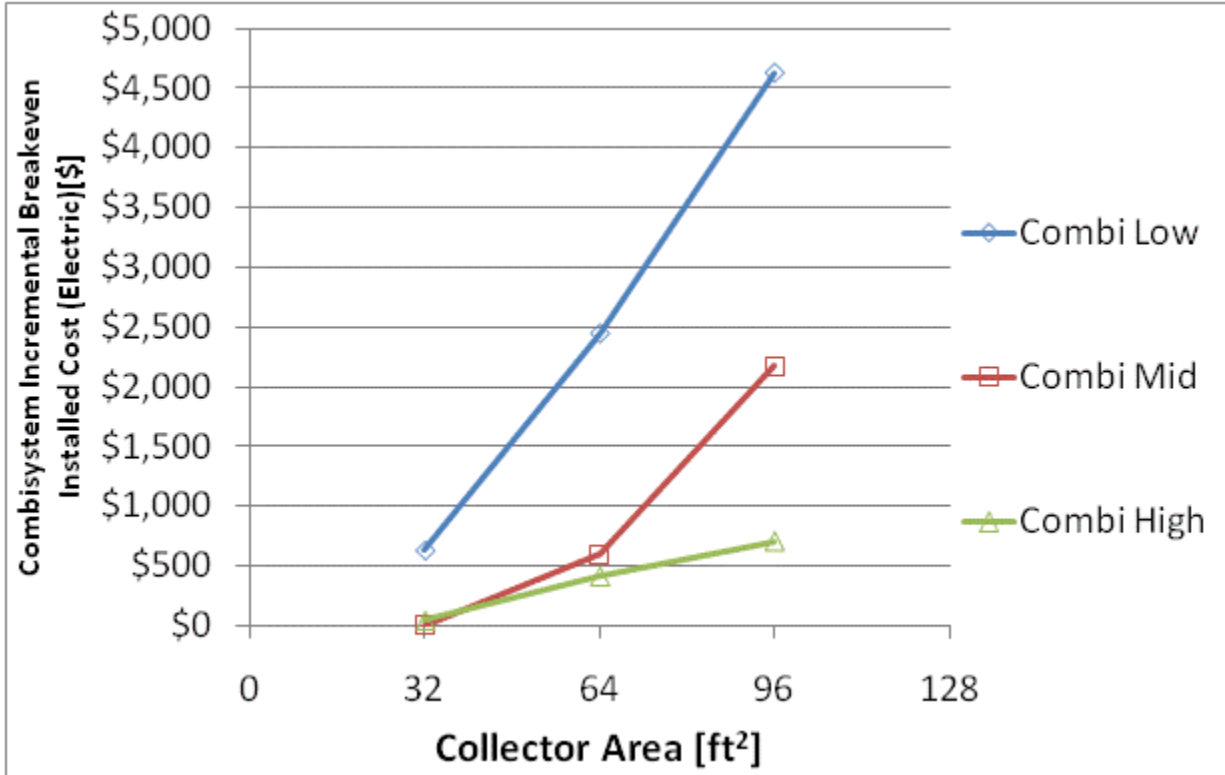
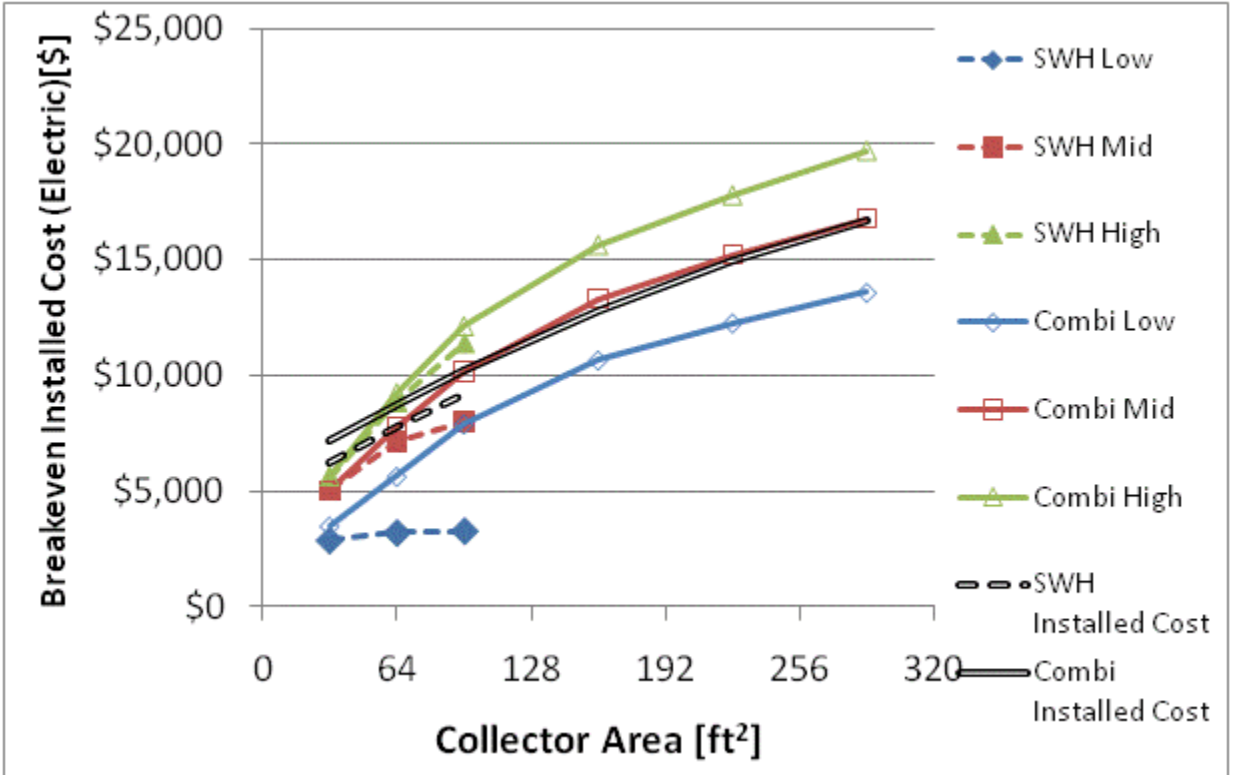


Figure F.46: Breakeven installed cost and combisystem incremental breakeven cost for electric system for a IECC 2009 House(San Francisco)

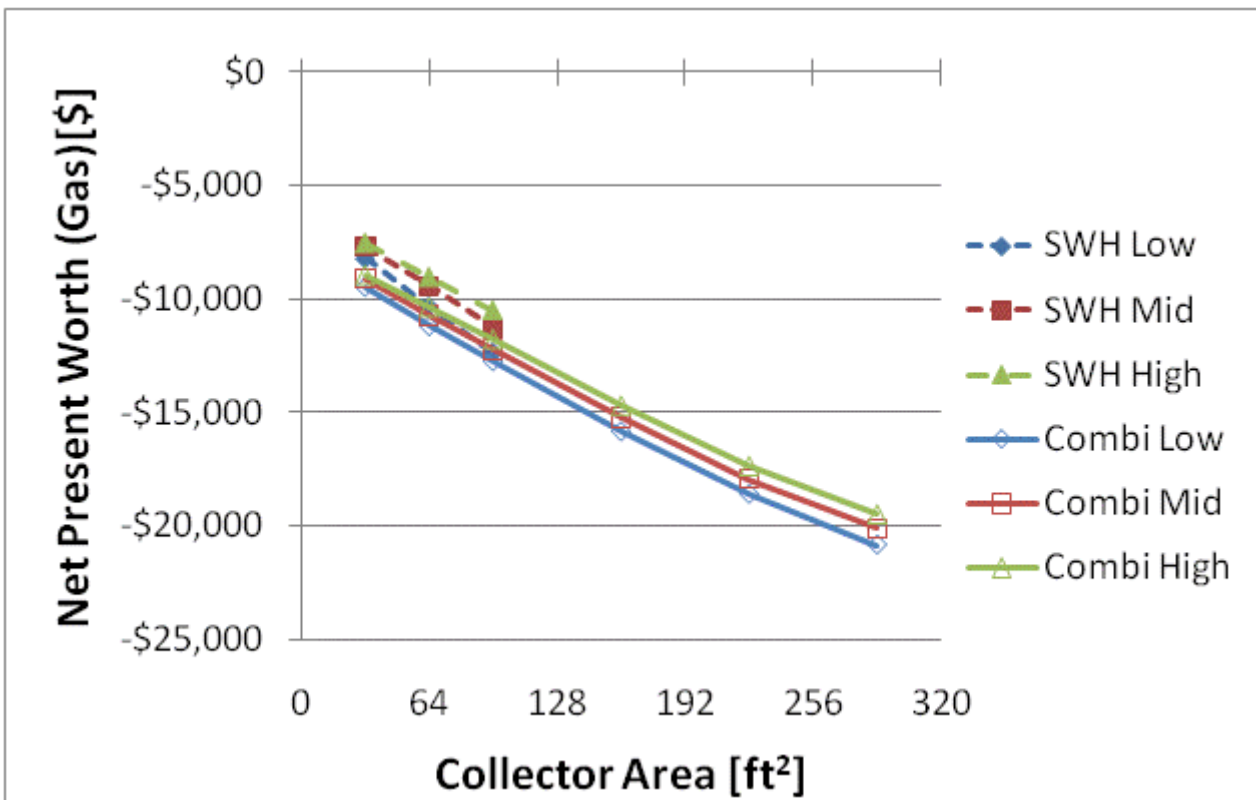
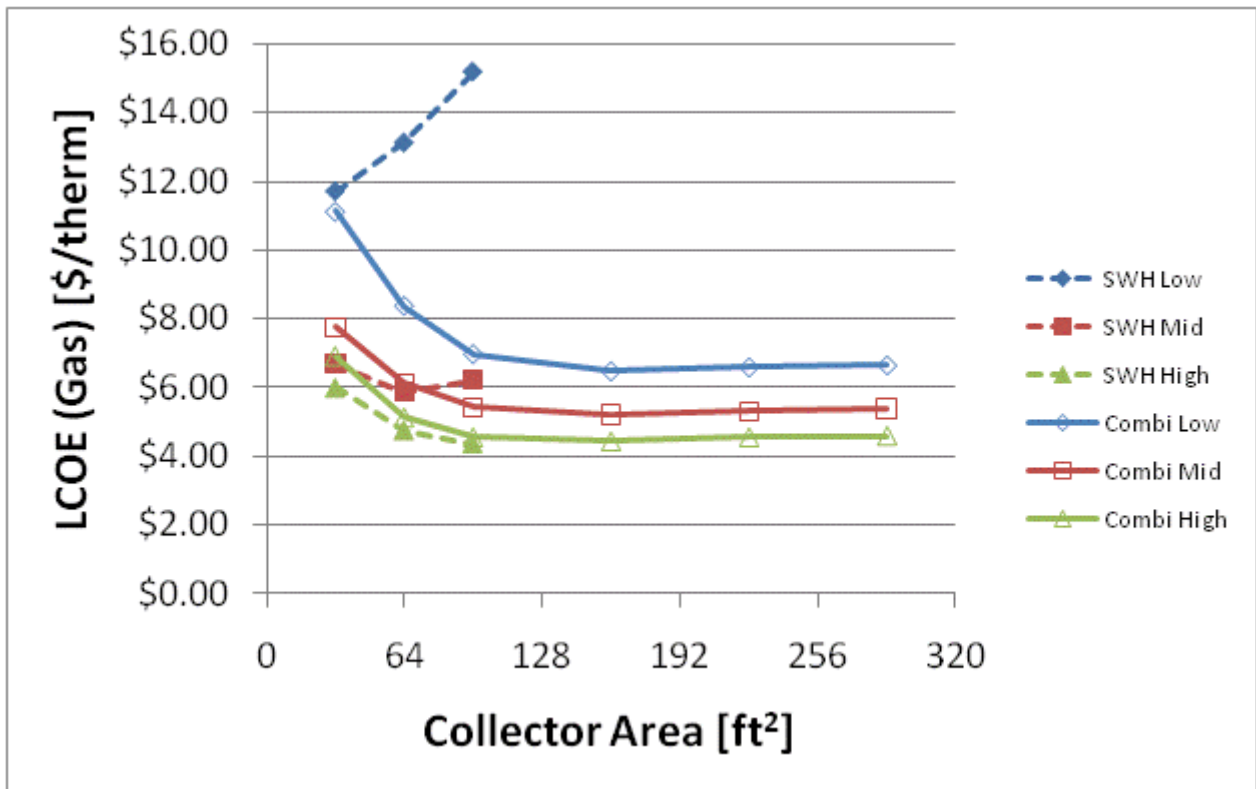


Figure F.47: LCOE and NPW for gas systems for a IECC 2009 House(San Francisco)

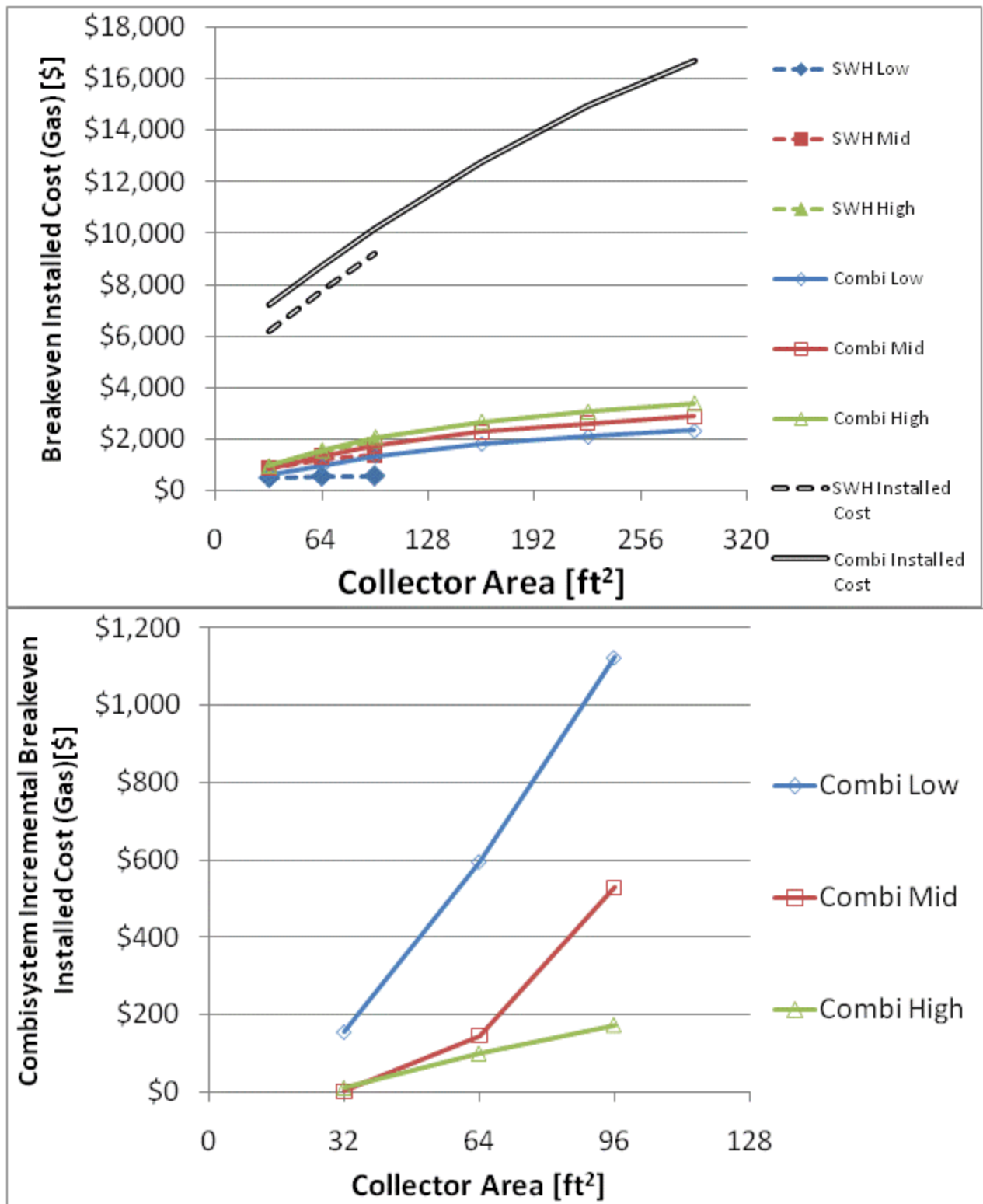


Figure F.48: Breakeven installed cost and combisystem incremental breakeven cost for gas systems for a

IECC 2009 House(San Francisco)

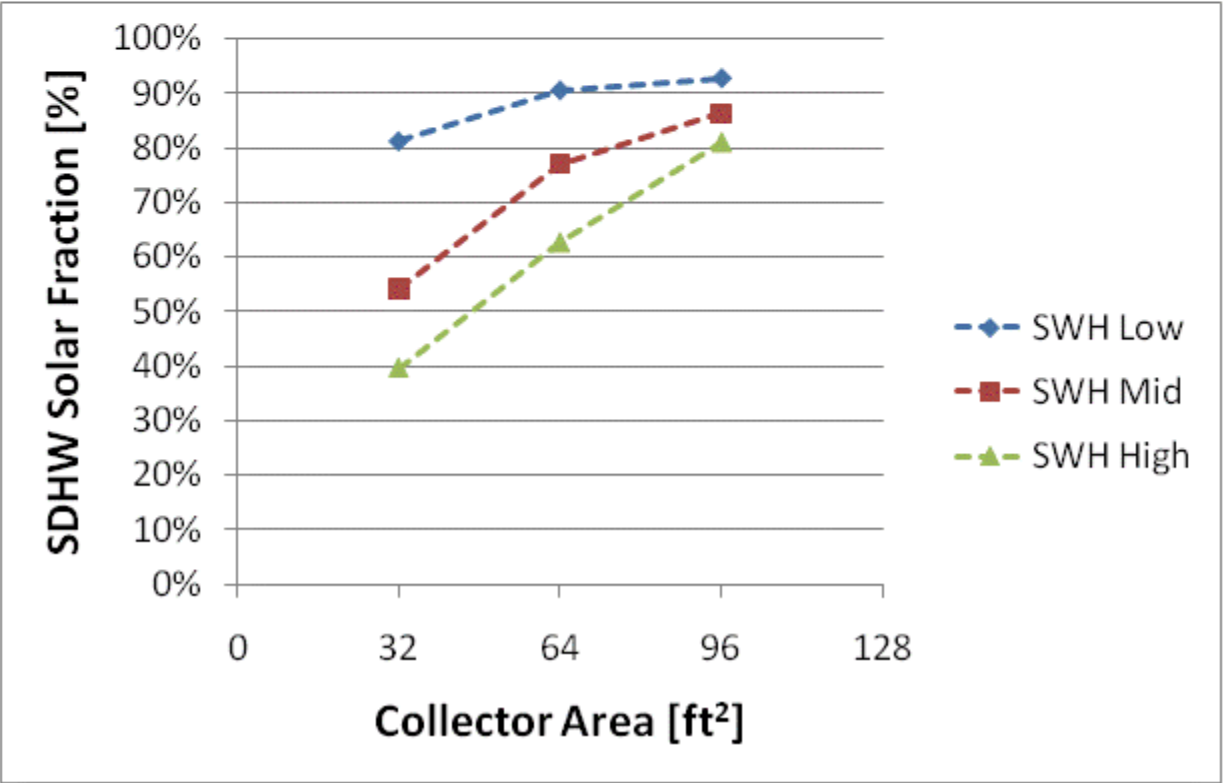
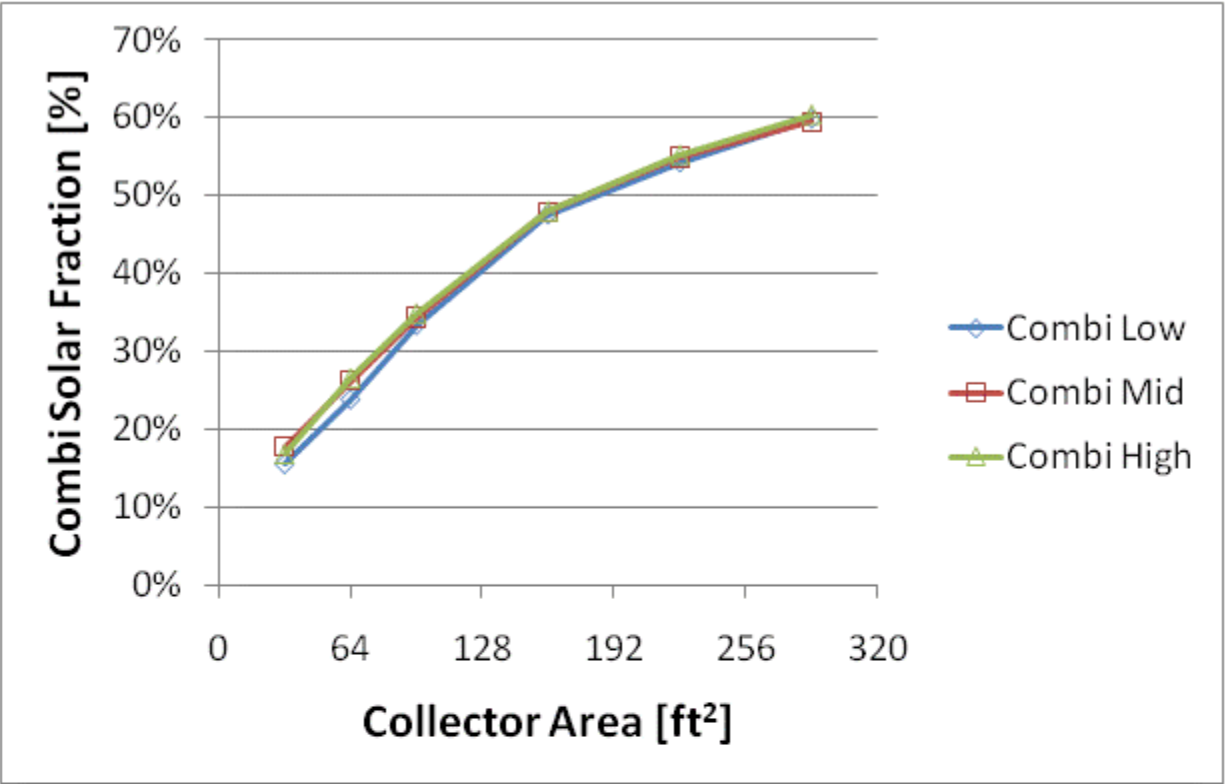


Figure F.49: Combisystem and SWH solar fraction for a BA 50% House(San Francisco)

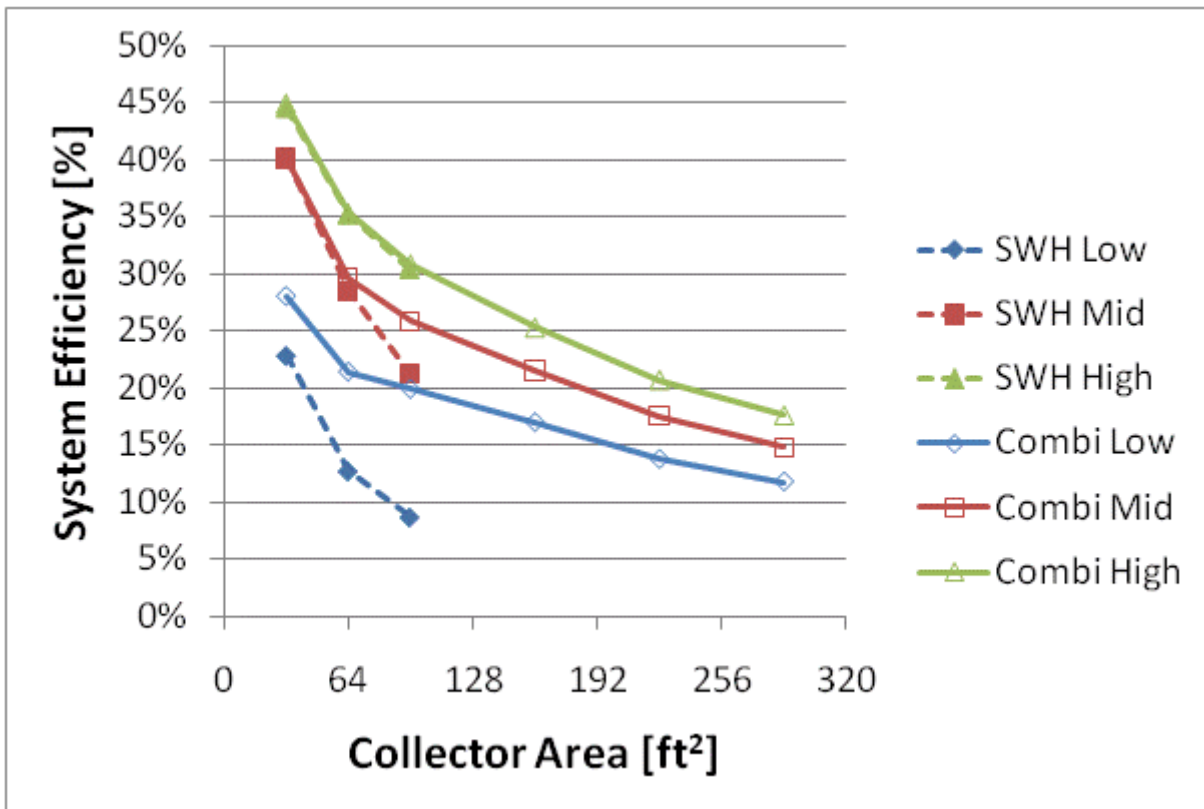
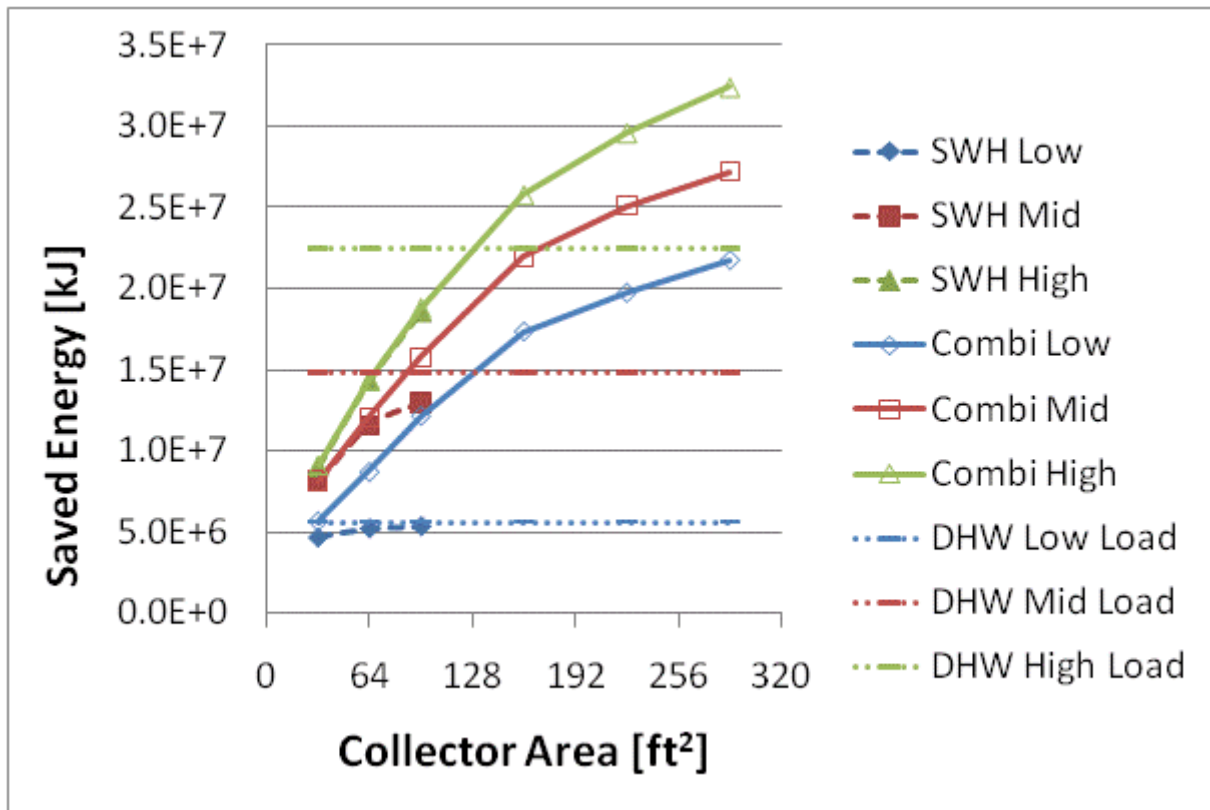


Figure F.50: Annual saved energy and system efficiency for a BA 50% House(San Francisco)

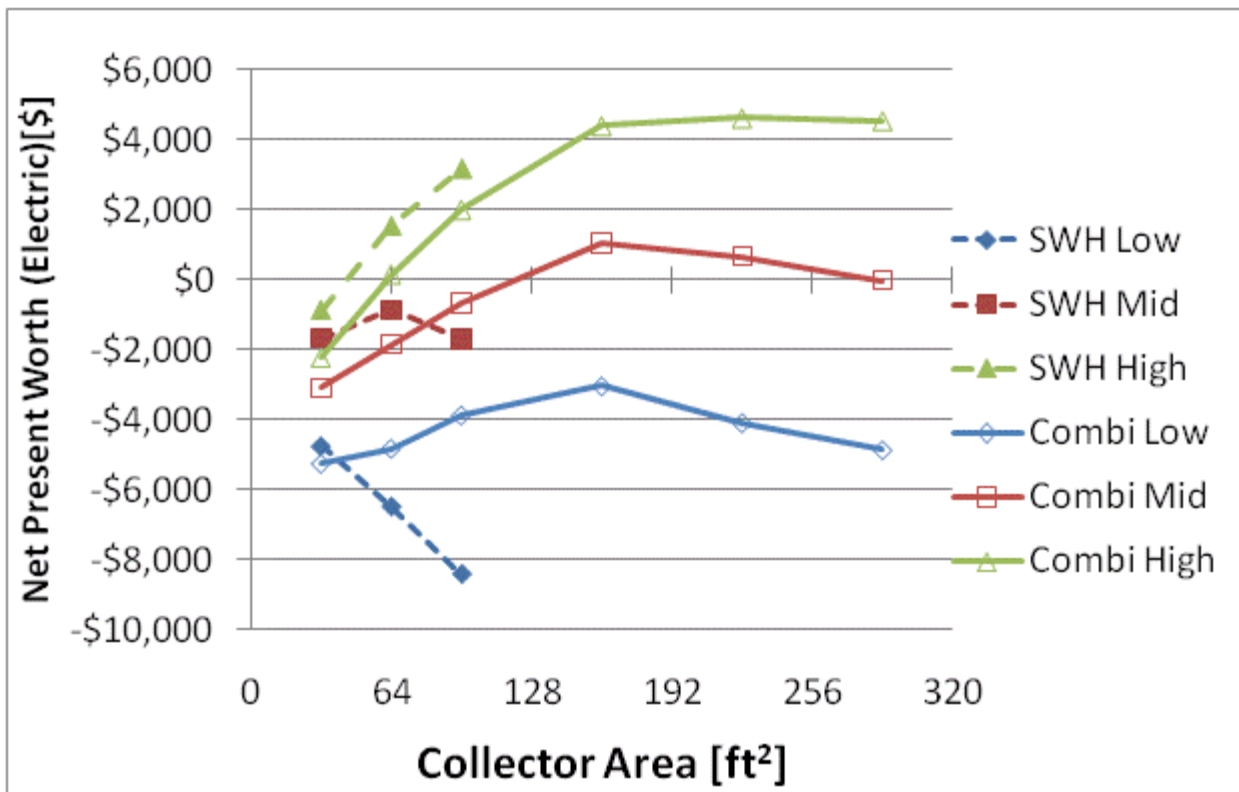
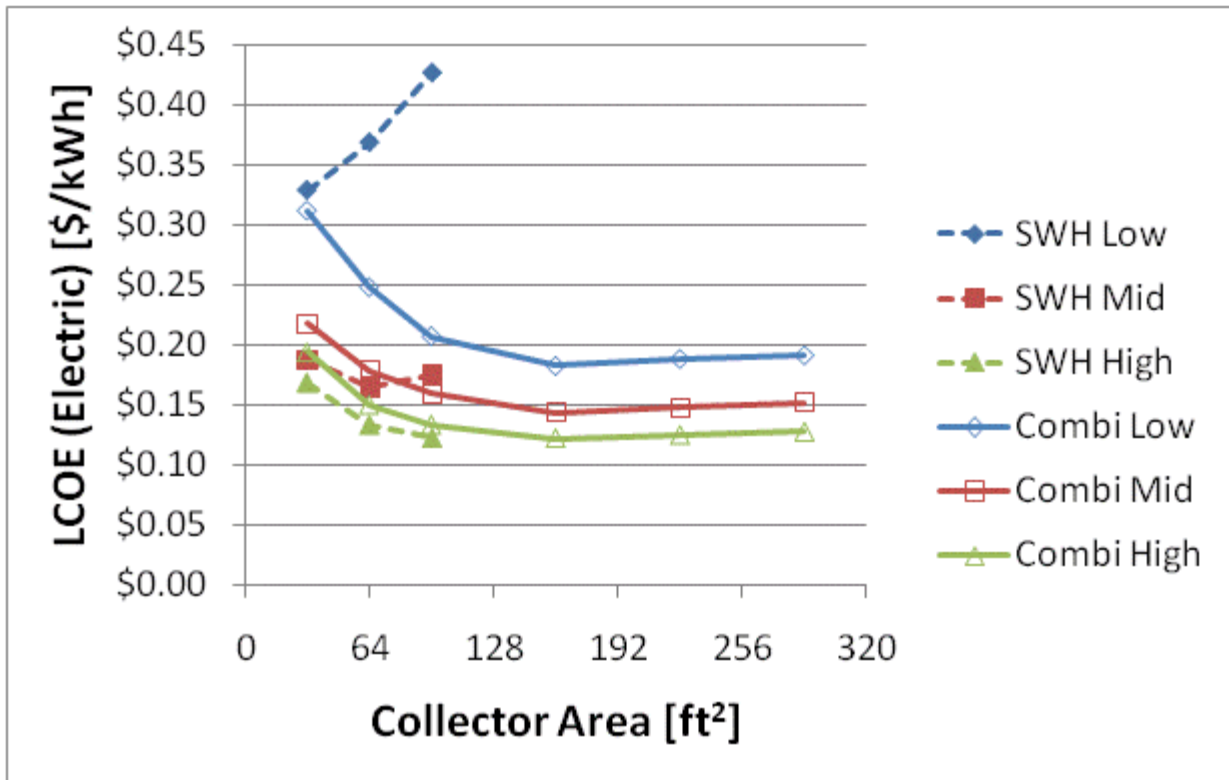


Figure F.51: LCOE and NPW for electric systems for a BA 50% House(San Francisco)

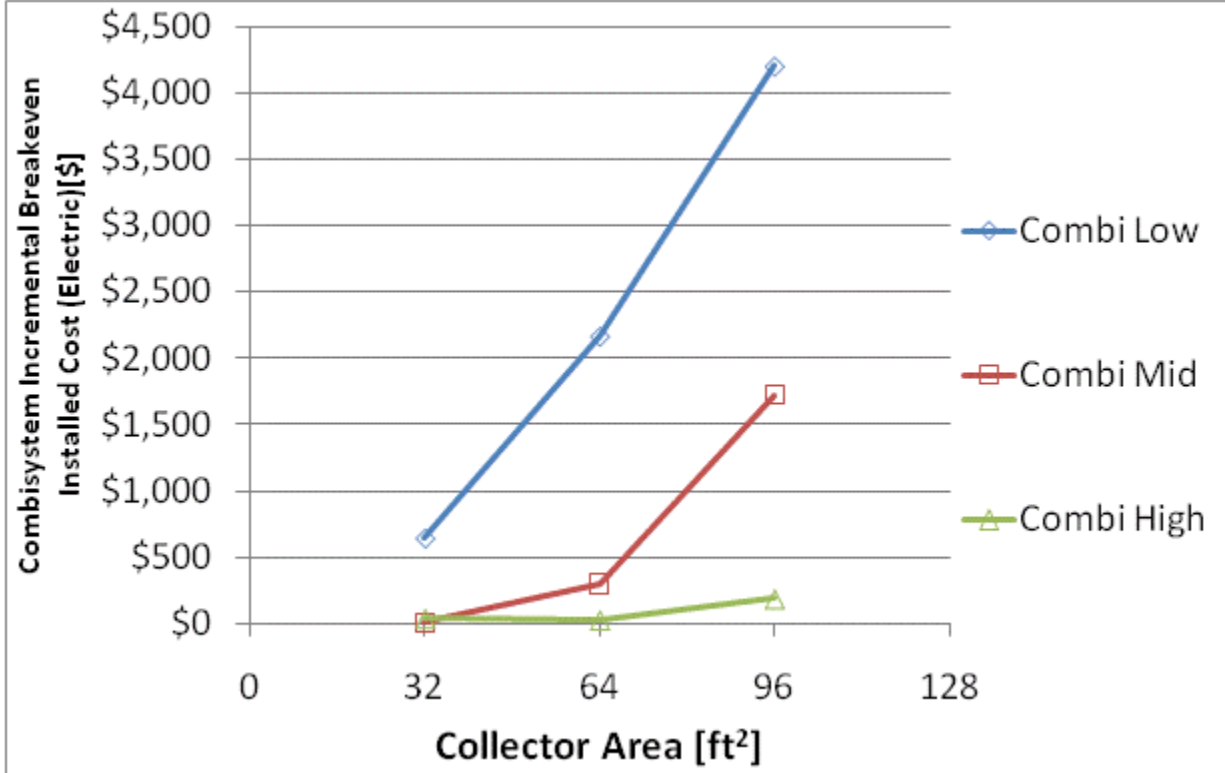
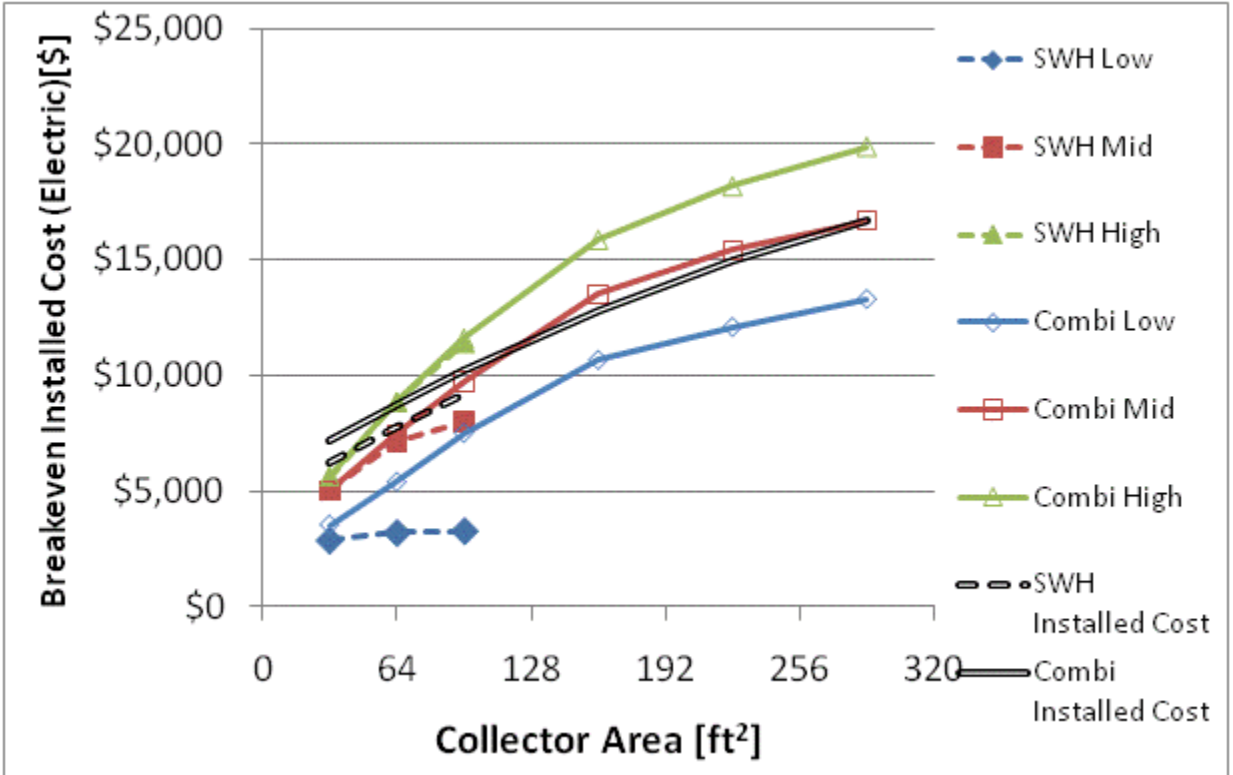


Figure F.52: Breakeven installed cost and combisystem incremental breakeven cost for electric system for a BA 50% House(San Francisco)

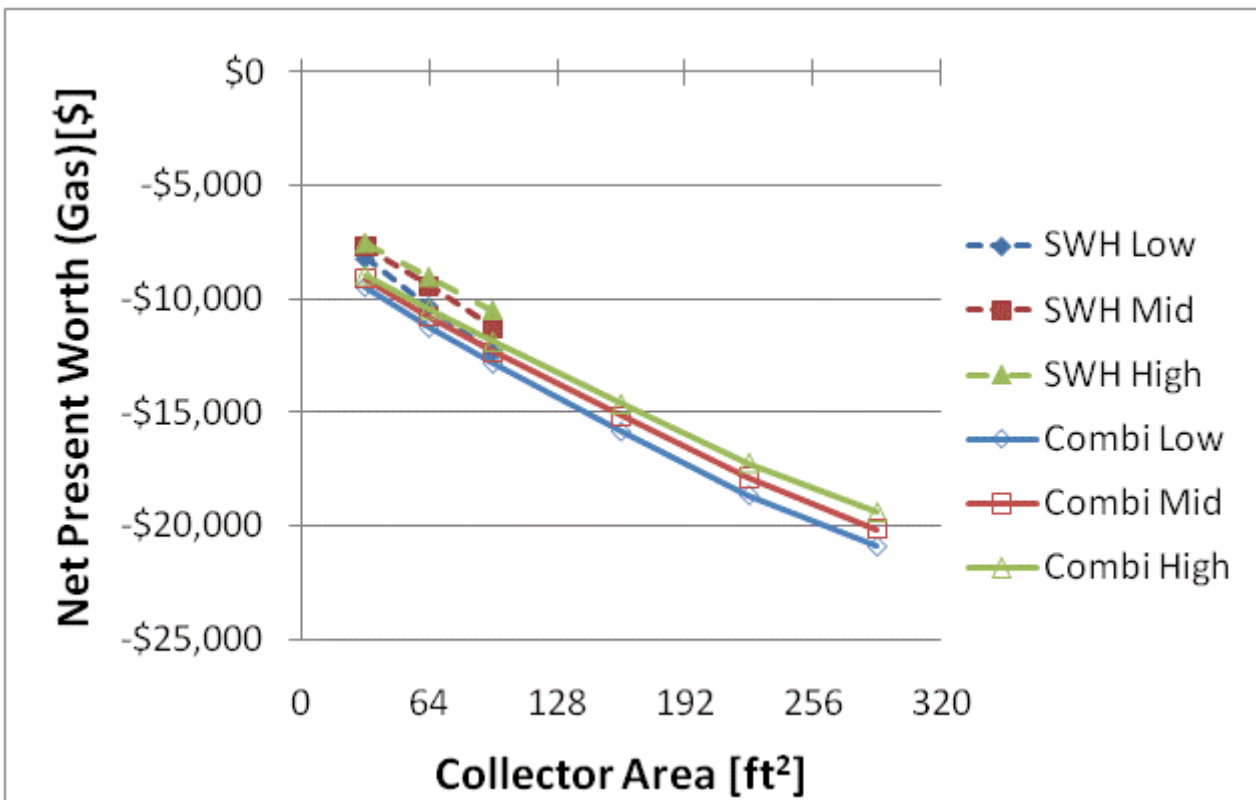
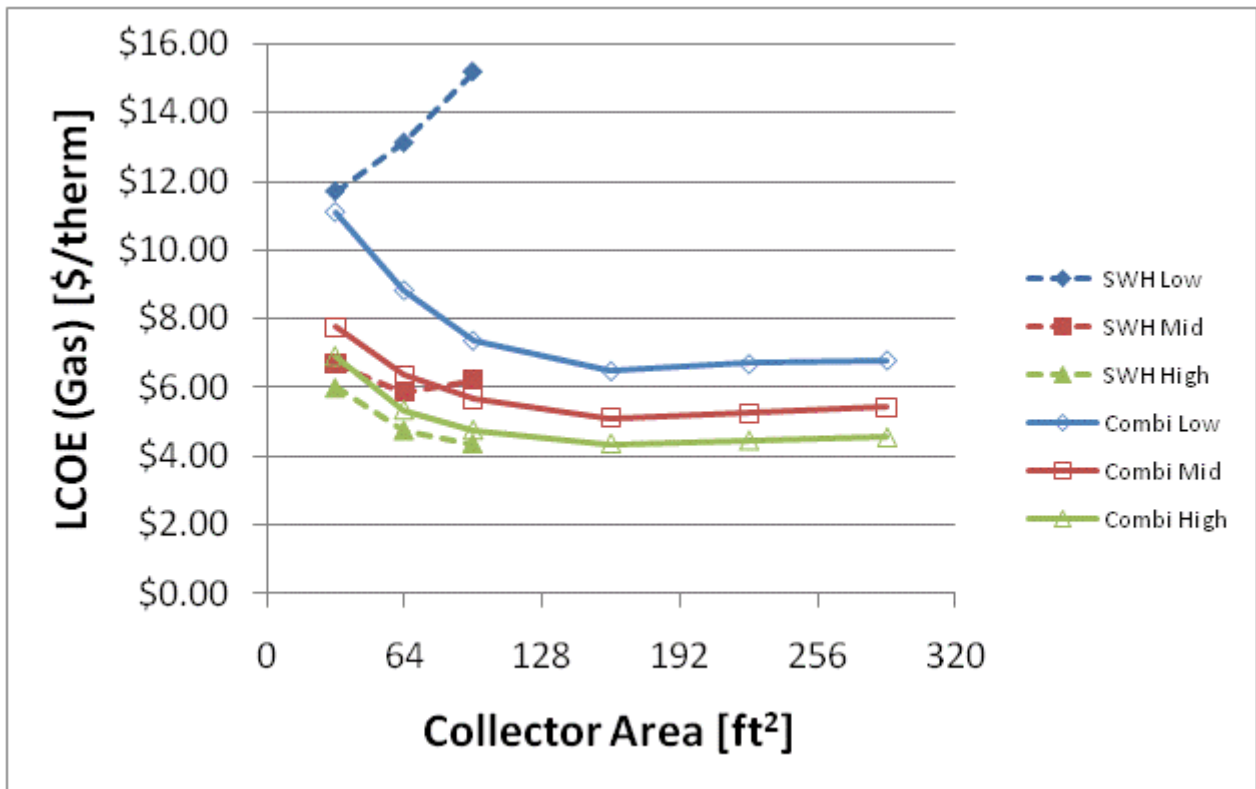


Figure F.53: LCOE and NPW for gas systems for a BA 50% House(San Francisco)

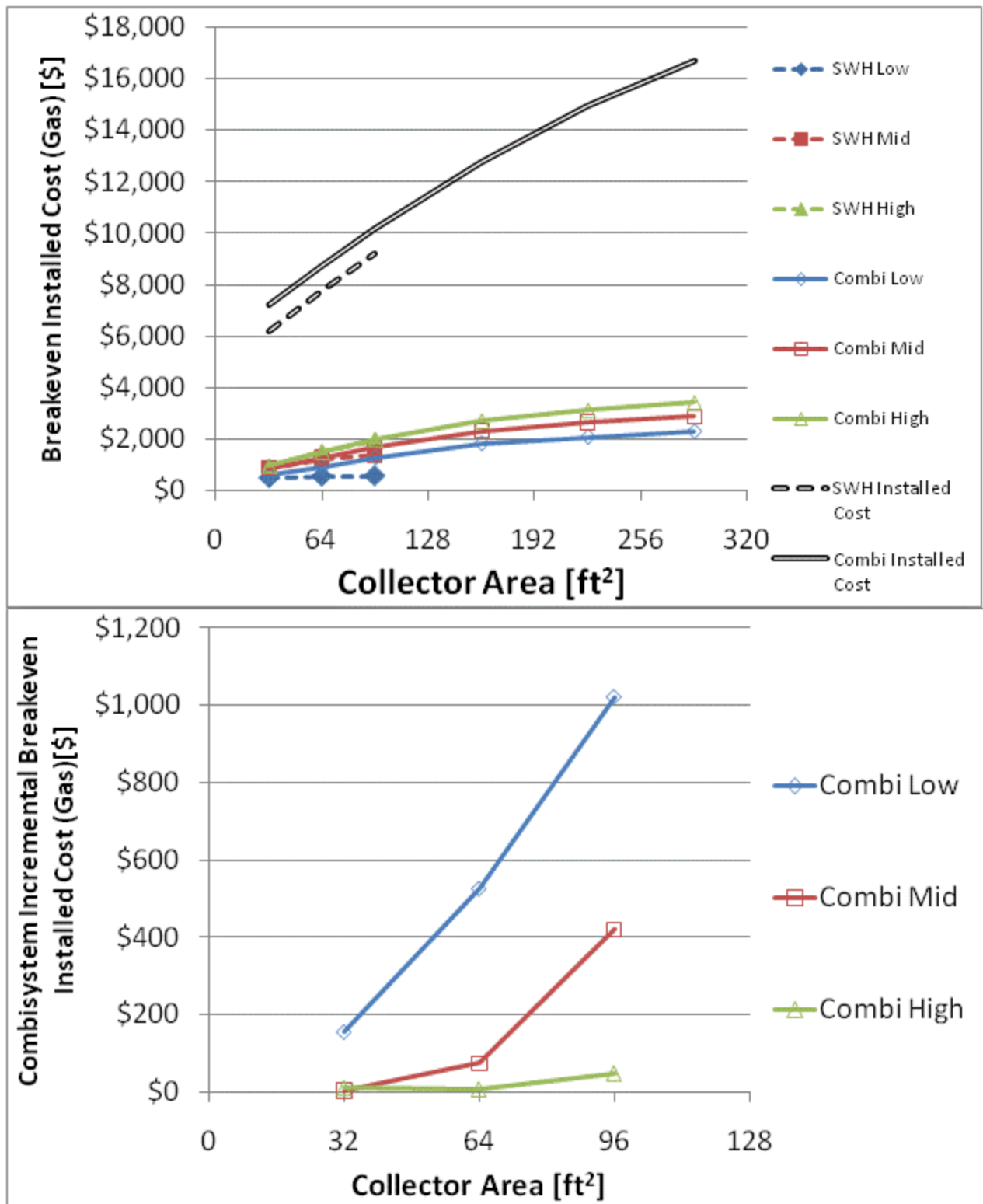


Figure F.54: Breakeven installed cost and combisystem incremental breakeven cost for gas systems for a

BA 50% House(San Francisco)

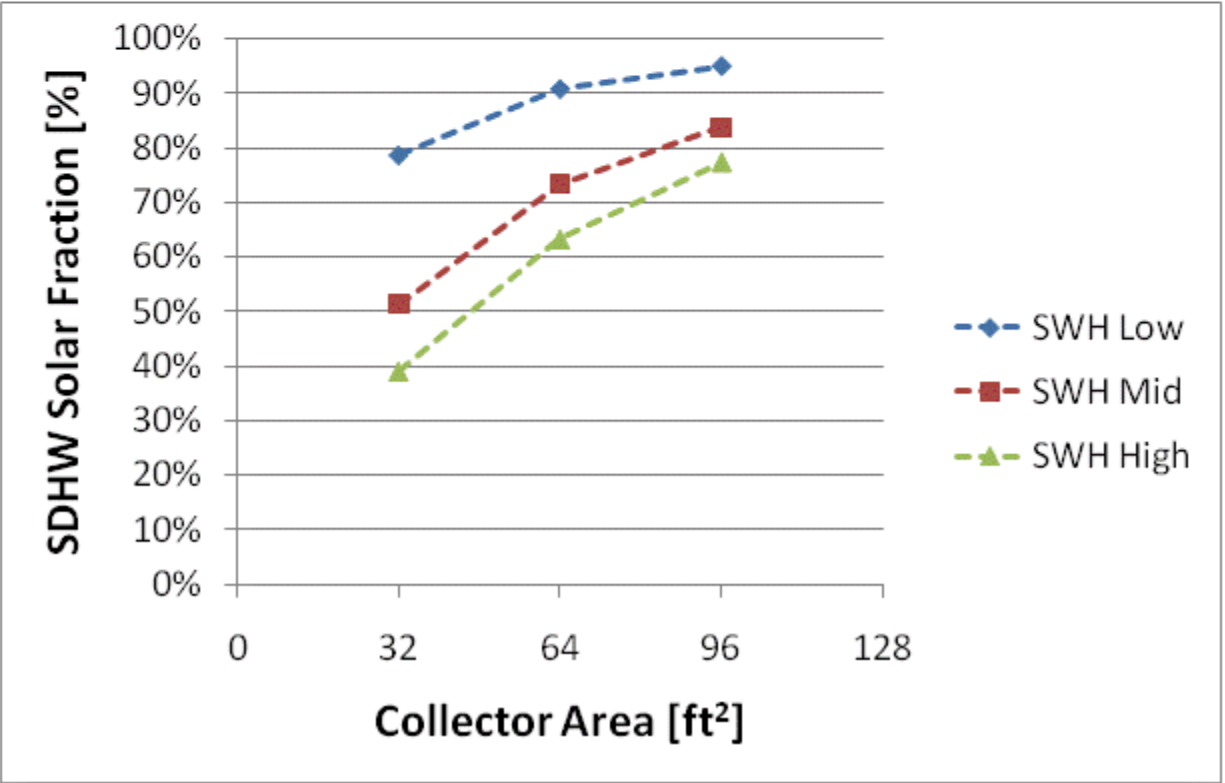
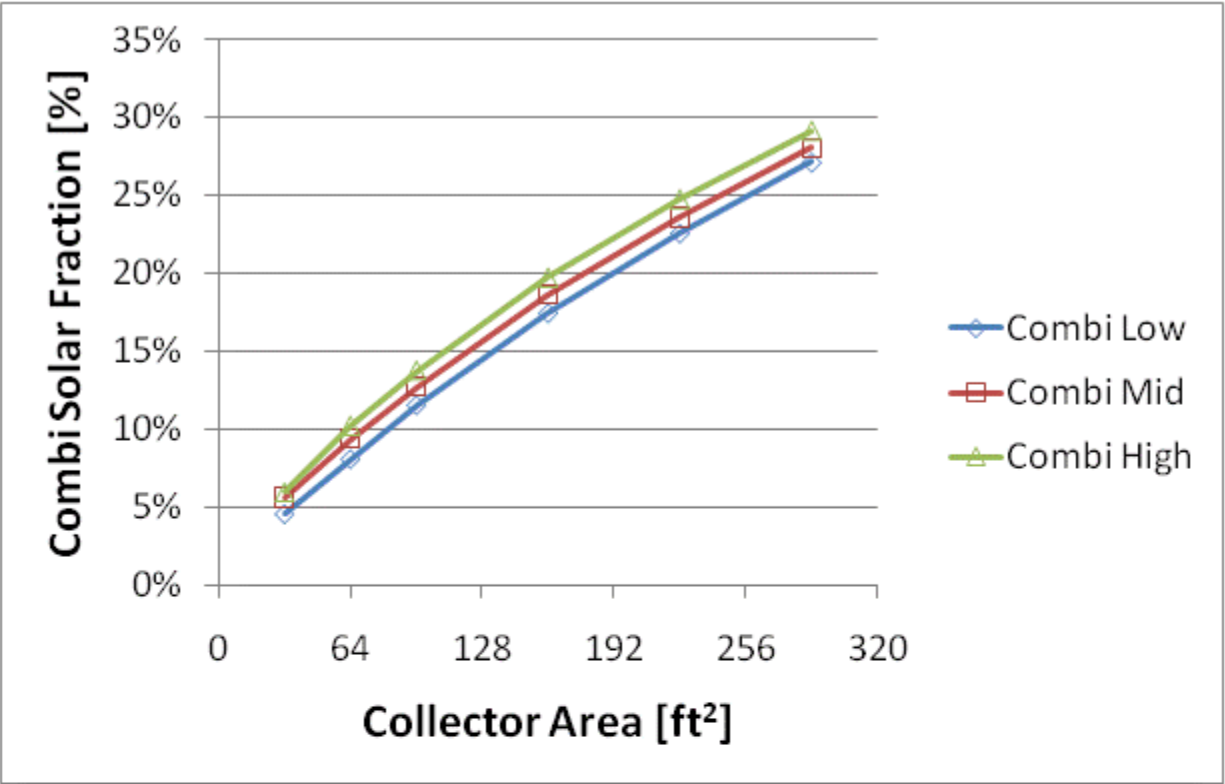


Figure F.55: Combisystem and SWH solar fraction for a 1960s Retrofit House(Denver)

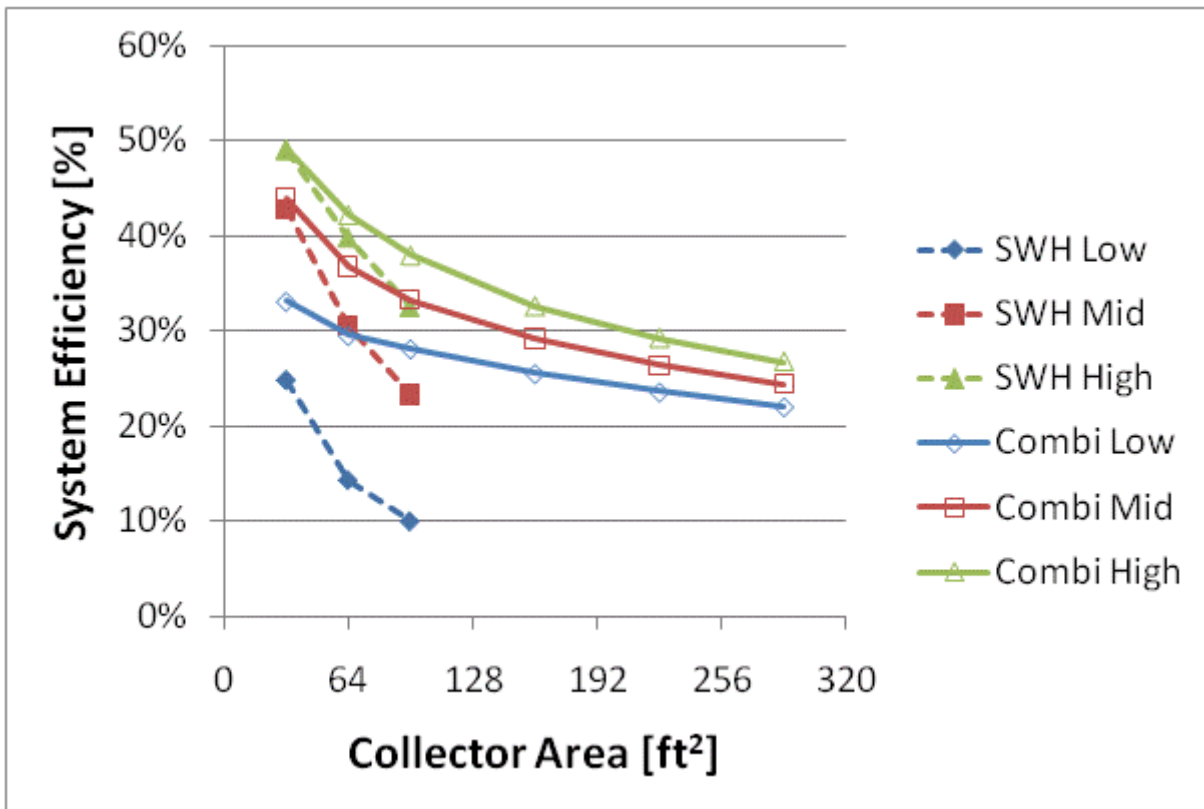
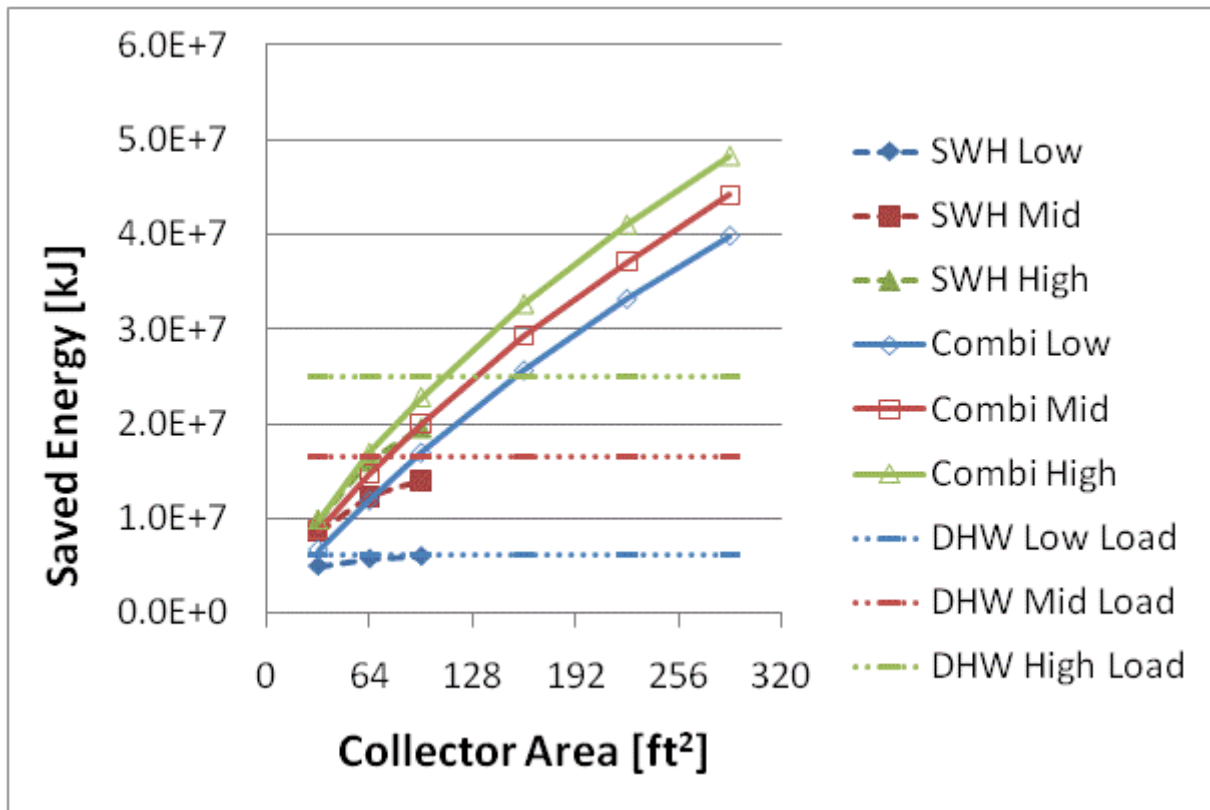


Figure F.56: Annual saved energy and system efficiency for a 1960s Retrofit House(Denver)

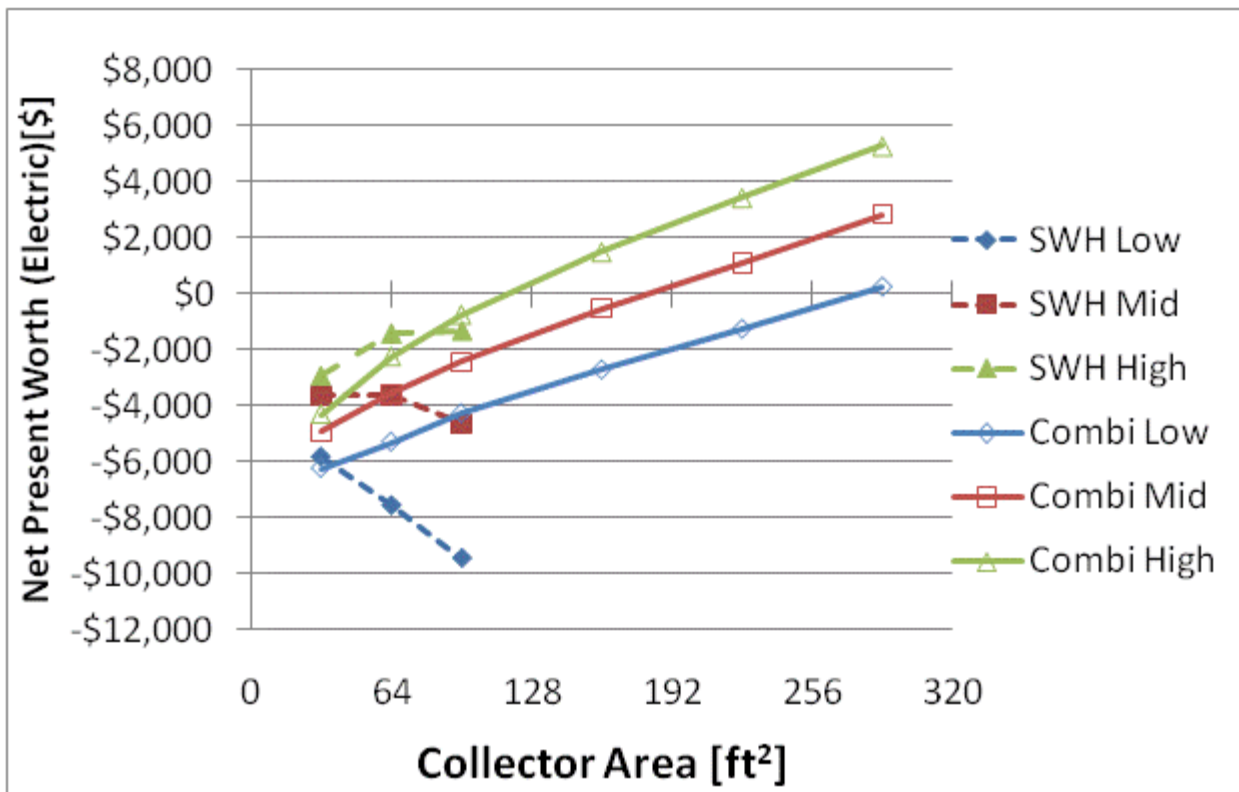
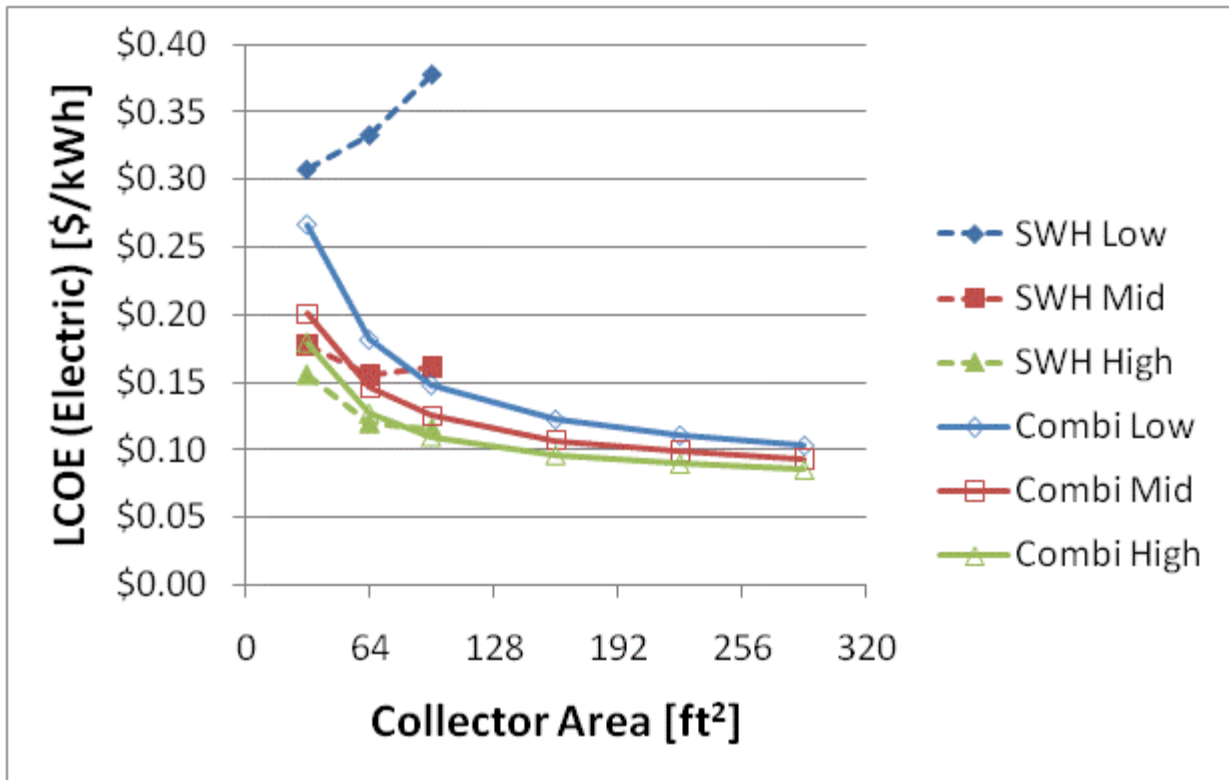


Figure F.57: LCOE and NPW for electric systems for a 1960s Retrofit House(Denver)

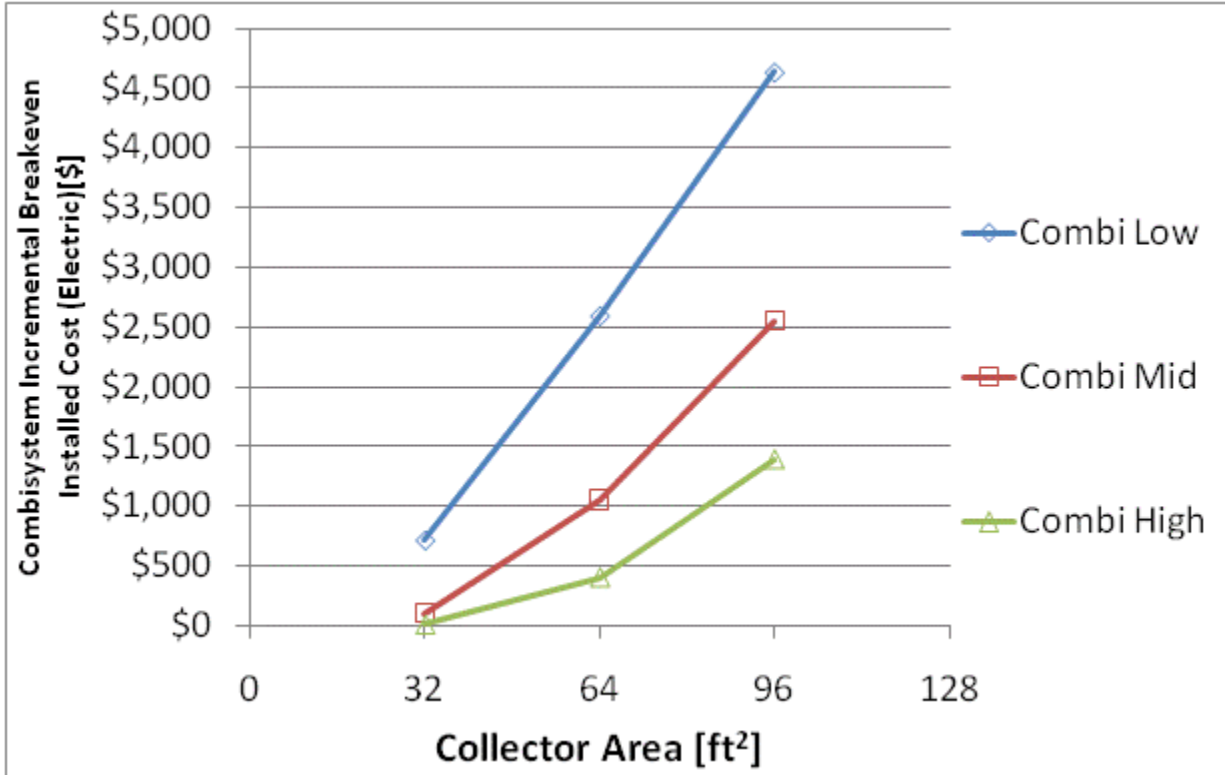
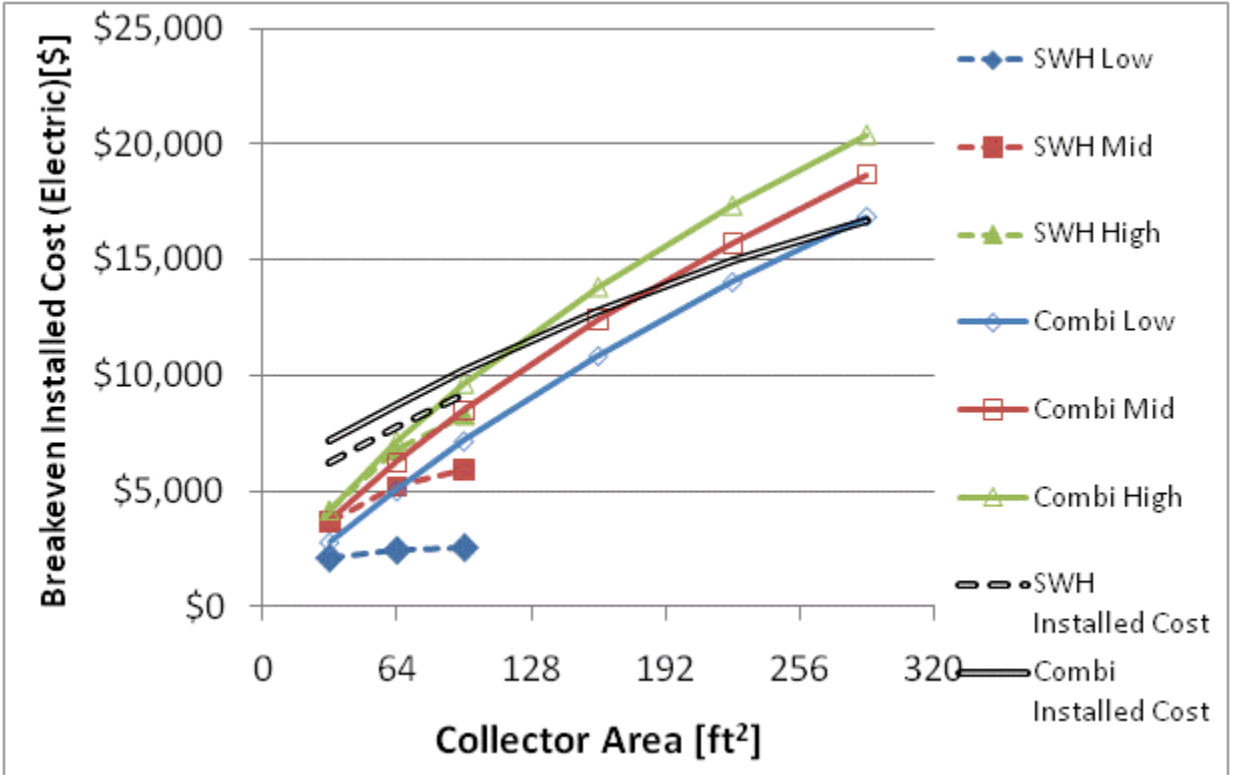


Figure F.58: Breakeven installed cost and combisystem incremental breakeven cost for electric system for a 1960s Retrofit House(Denver)

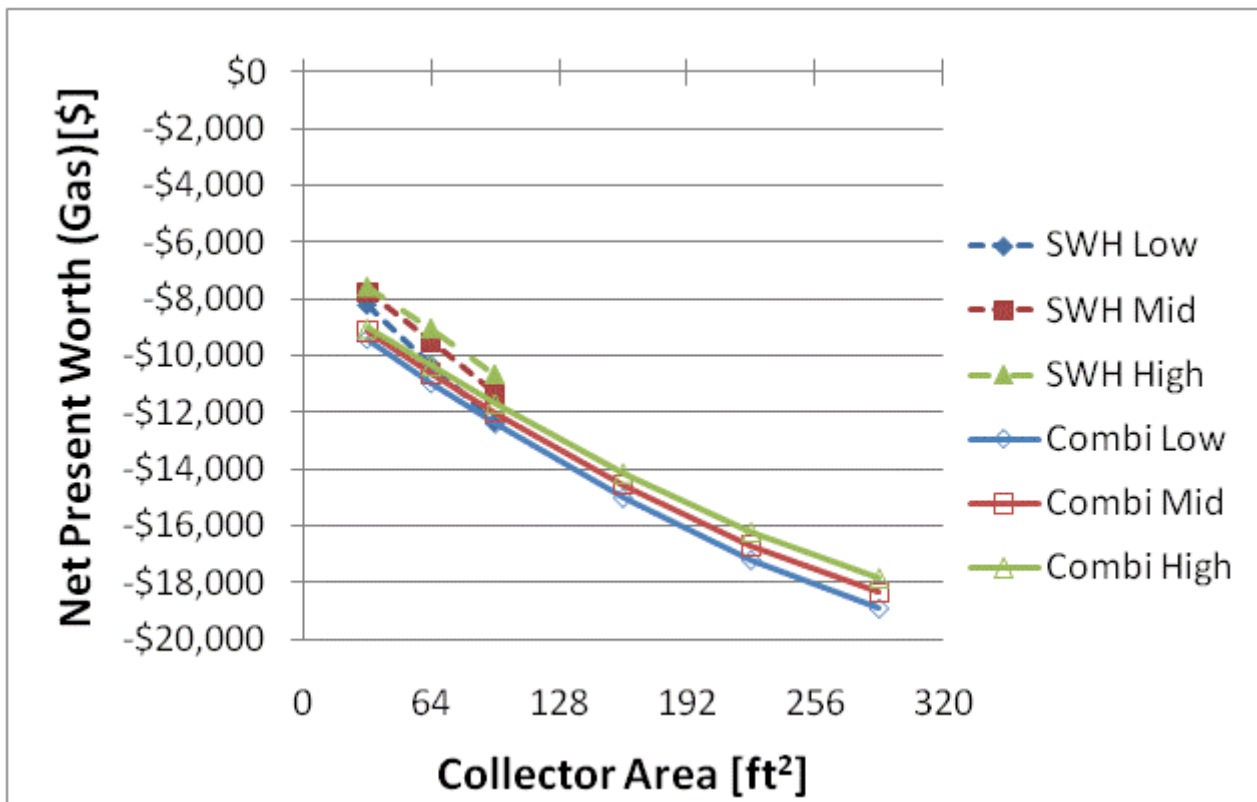
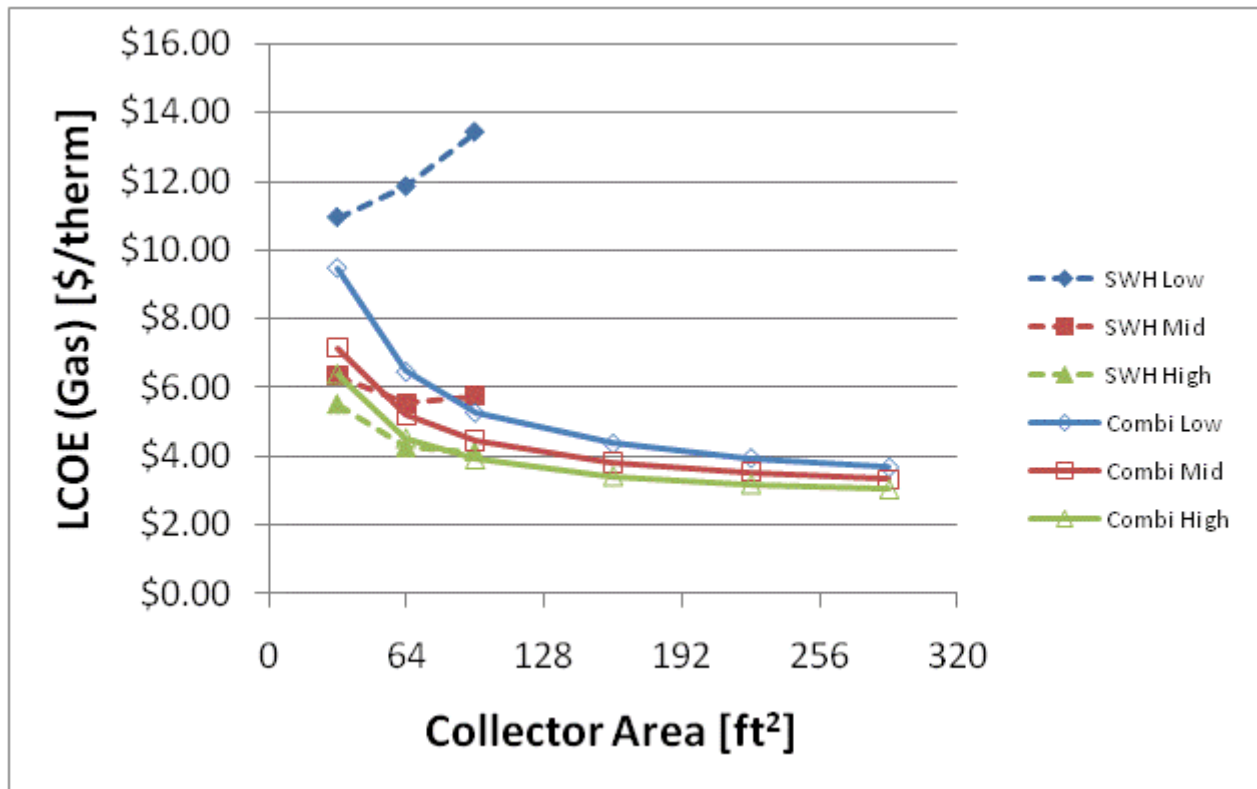


Figure F.59: LCOE and NPW for gas systems for a 1960s Retrofit House(Denver)

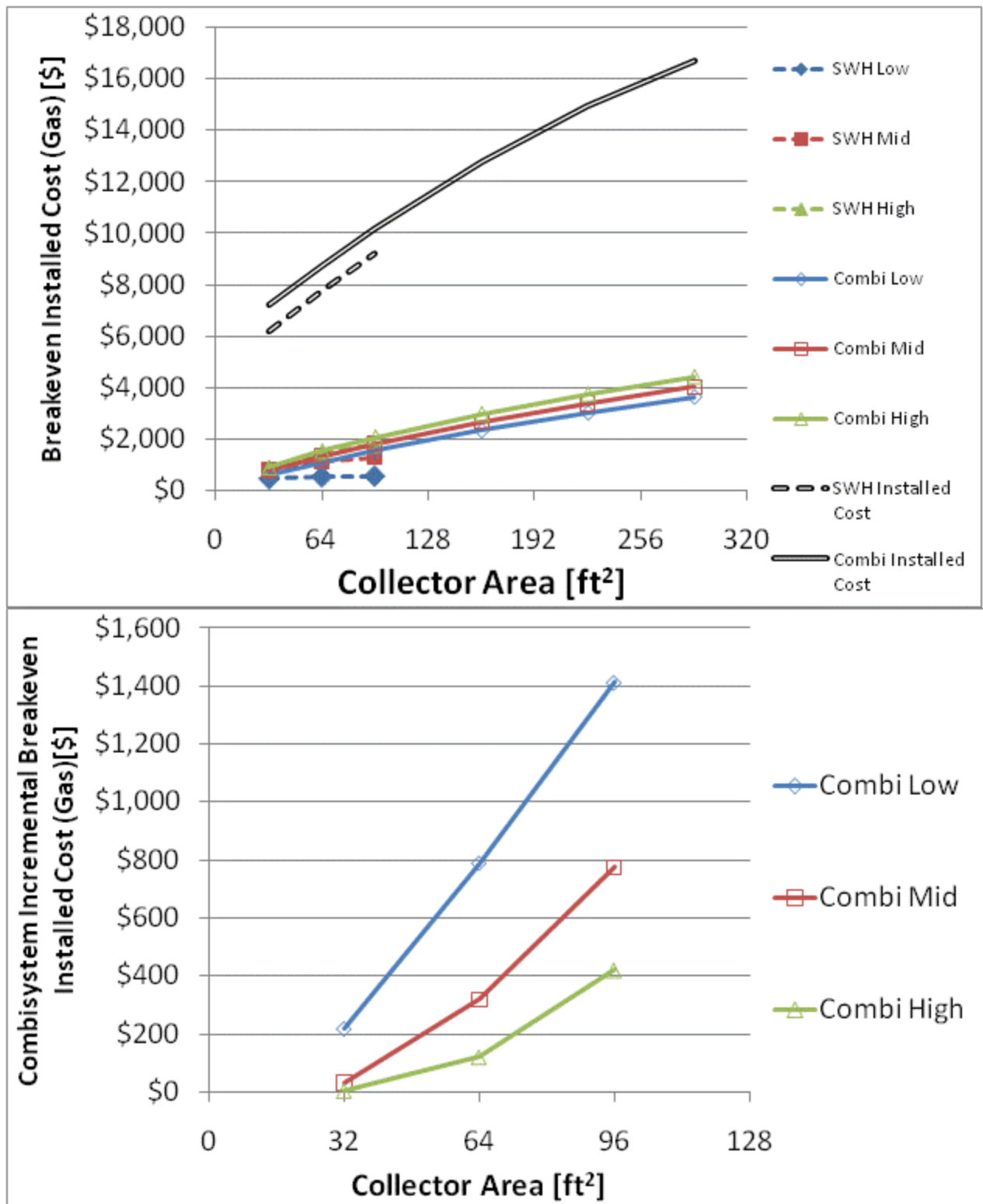


Figure F.60: Breakeven installed cost and combisystem incremental breakeven cost for gas systems for a 1960s Retrofit House(Denver)

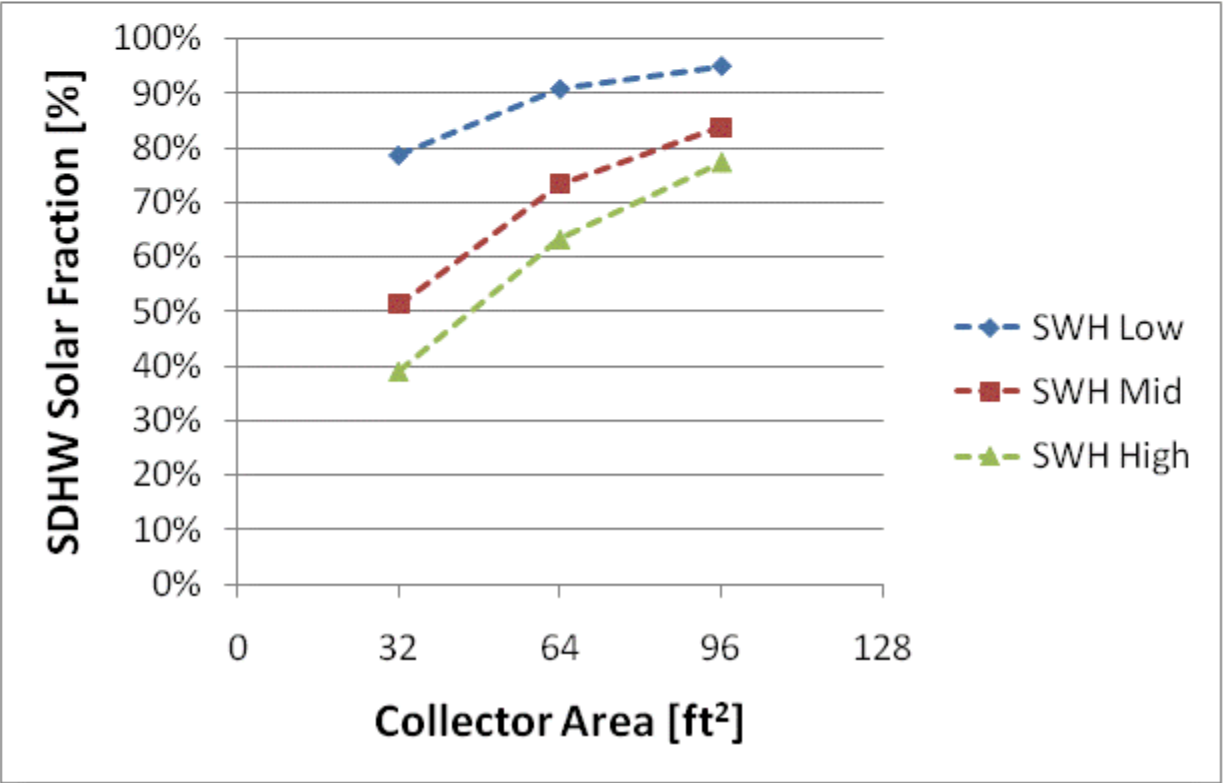
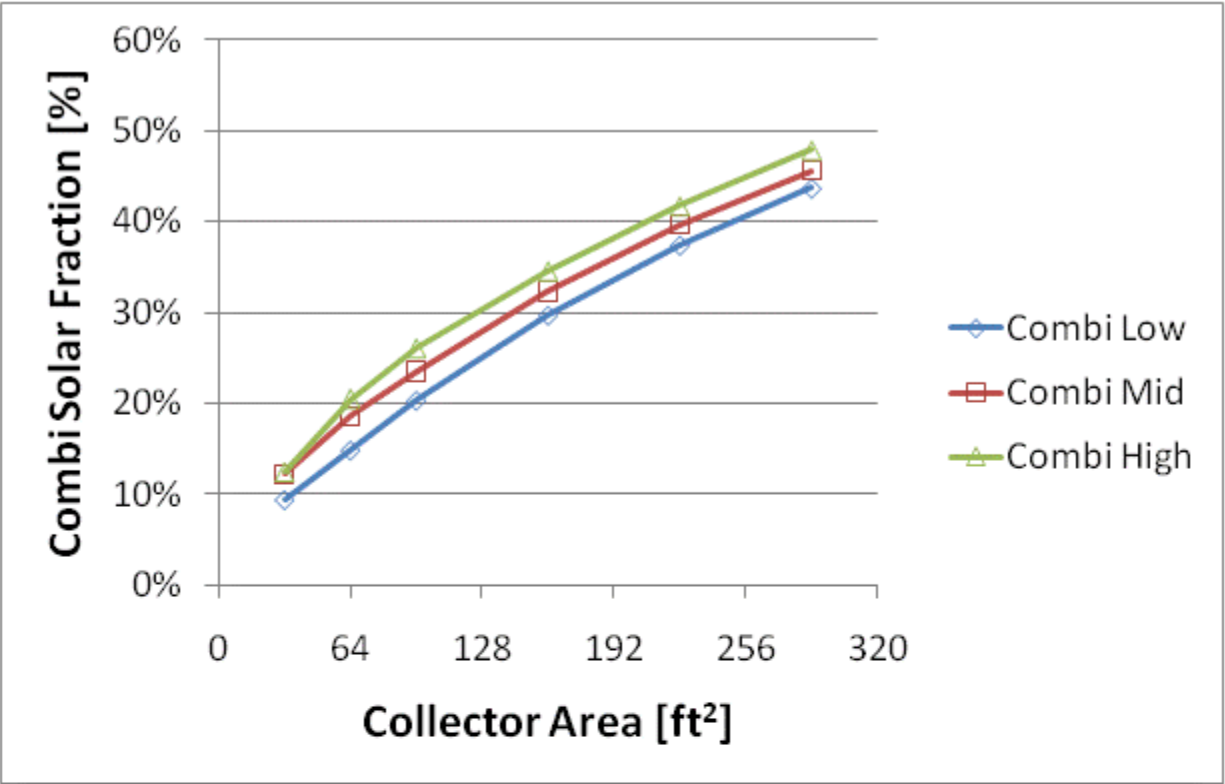


Figure F.61: Combisystem and SWH solar fraction for a IECC 2009 House(Denver)

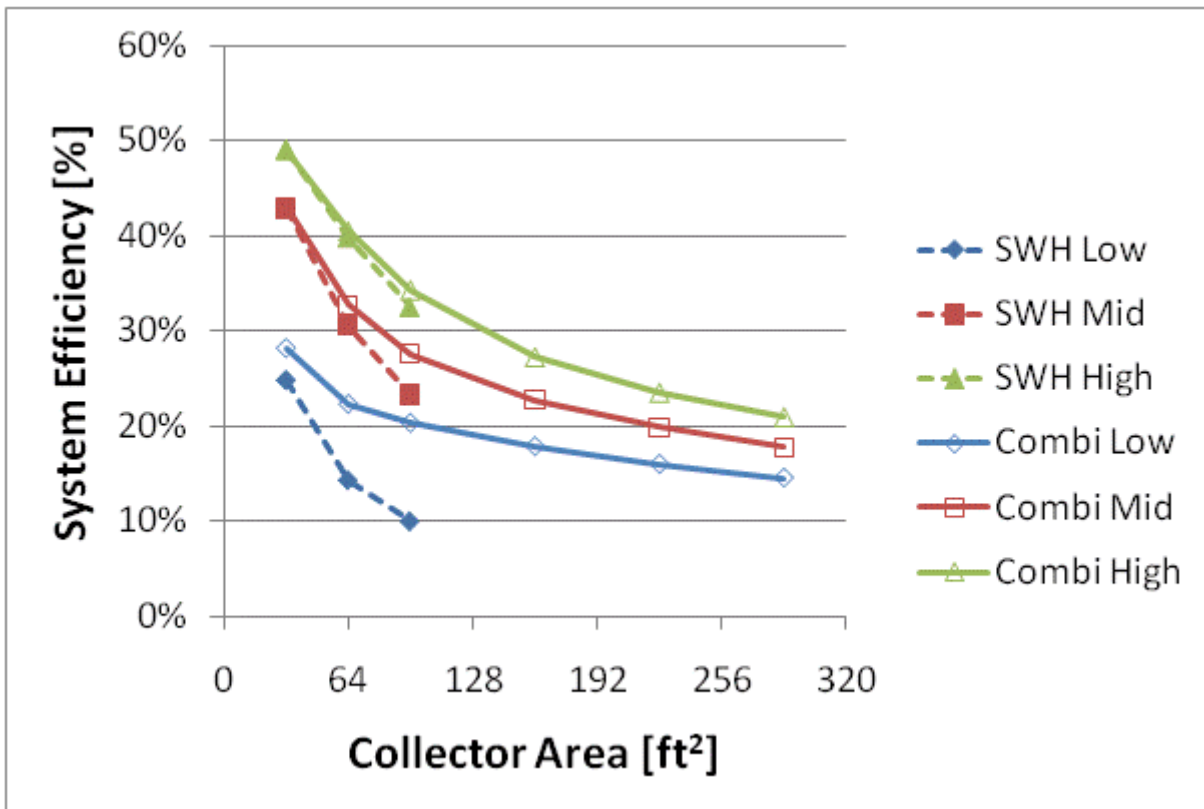
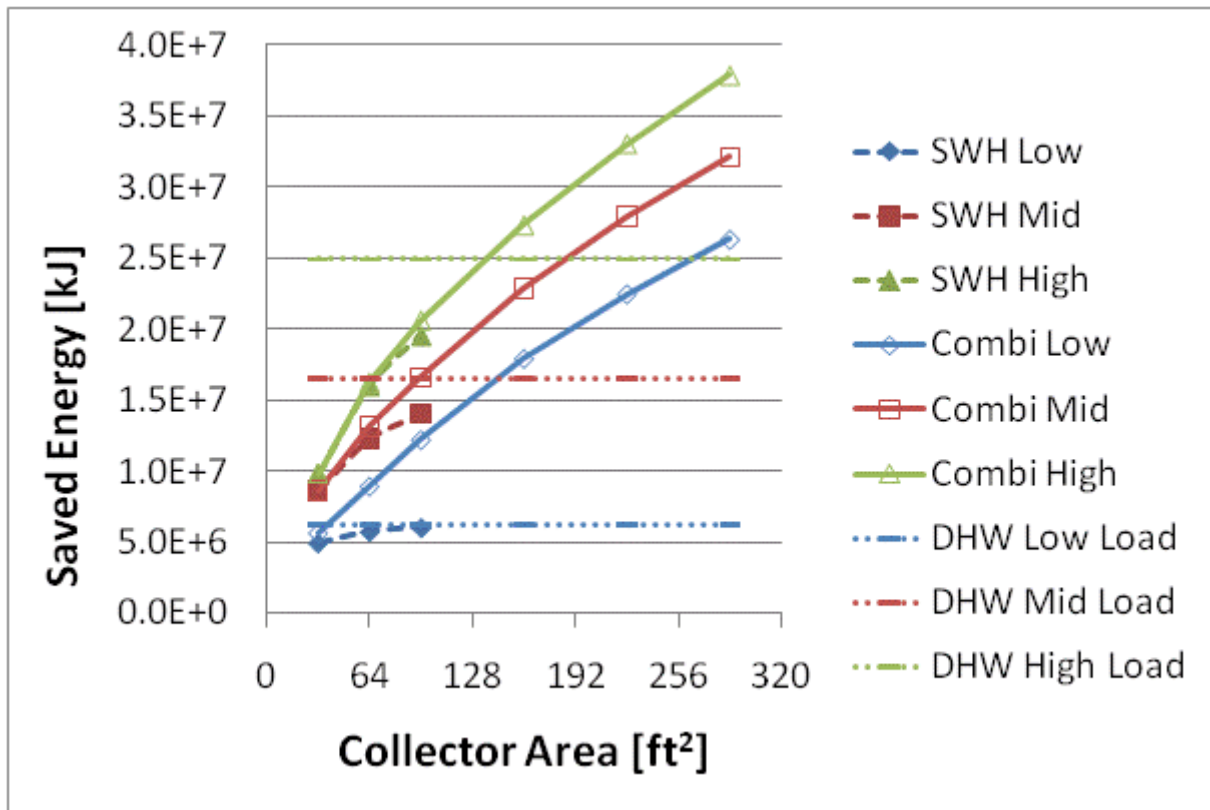


Figure F.62: Annual saved energy and system efficiency for a IECC 2009 House(Denver)

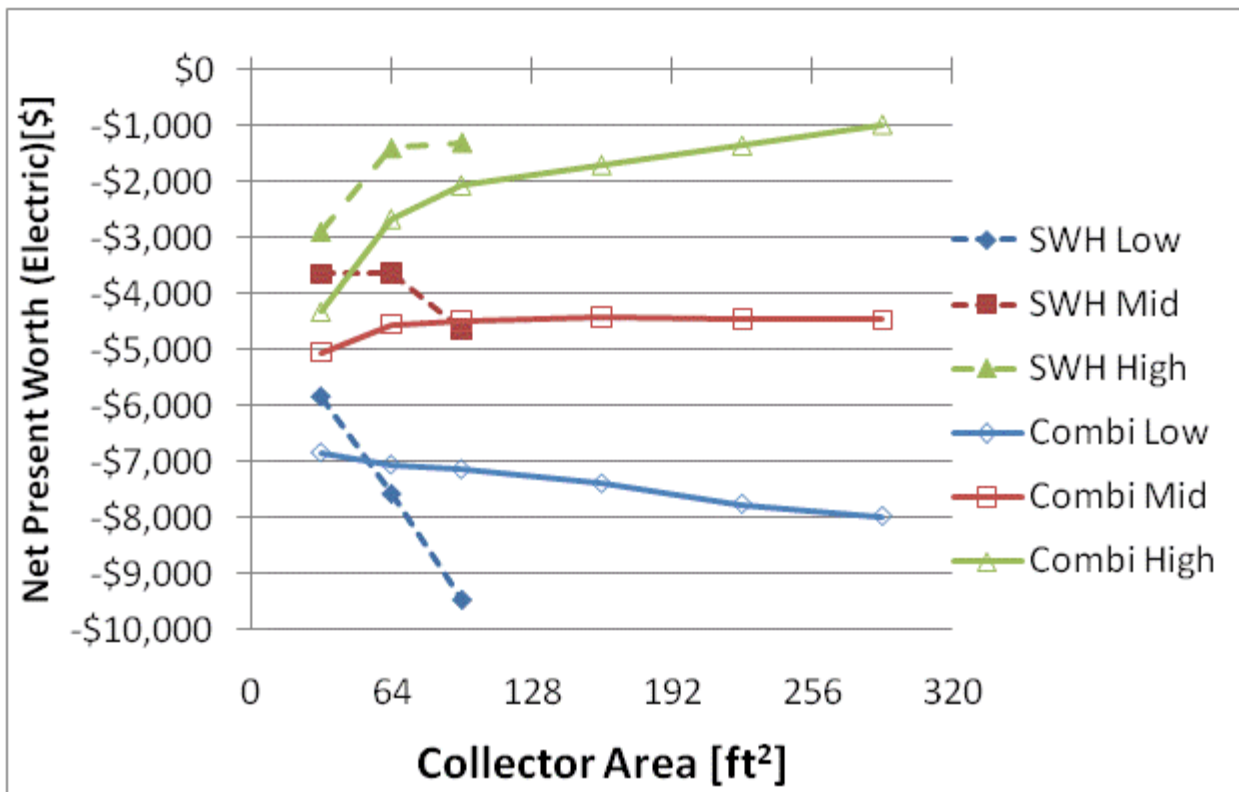
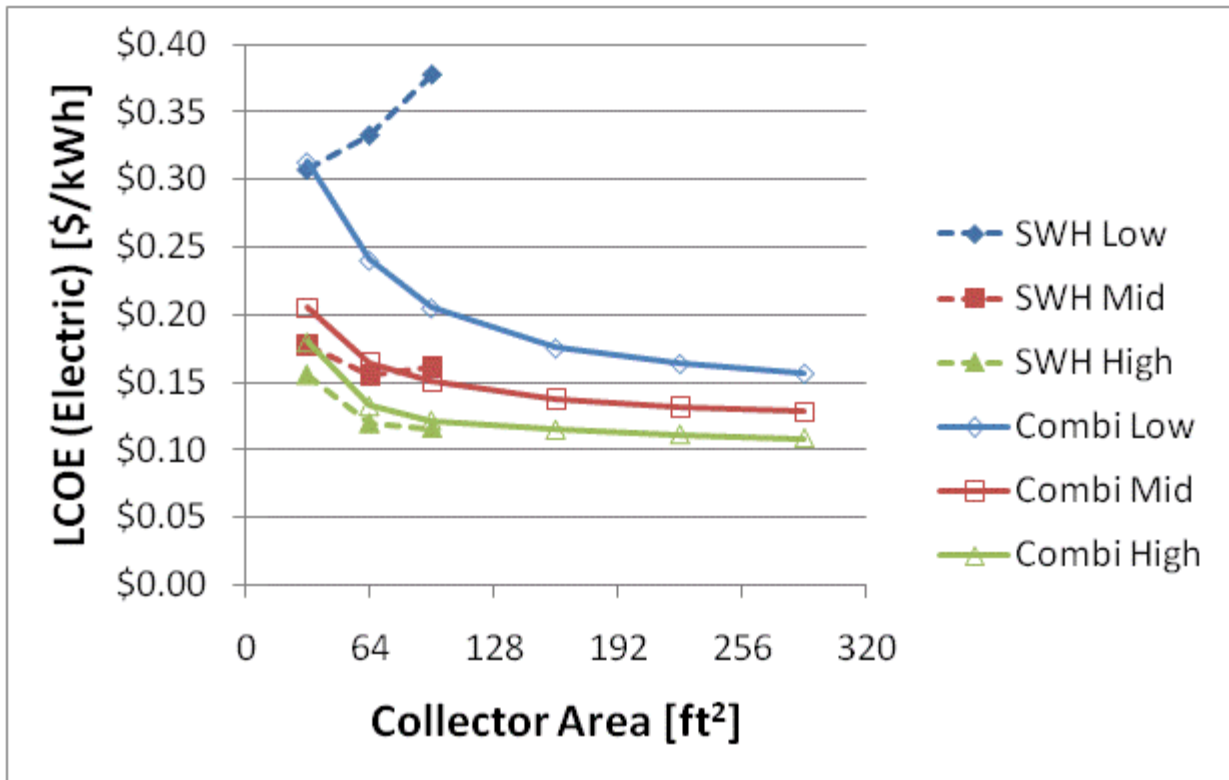


Figure F.63: LCOE and NPW for electric systems for a IECC 2009 House(Denver)

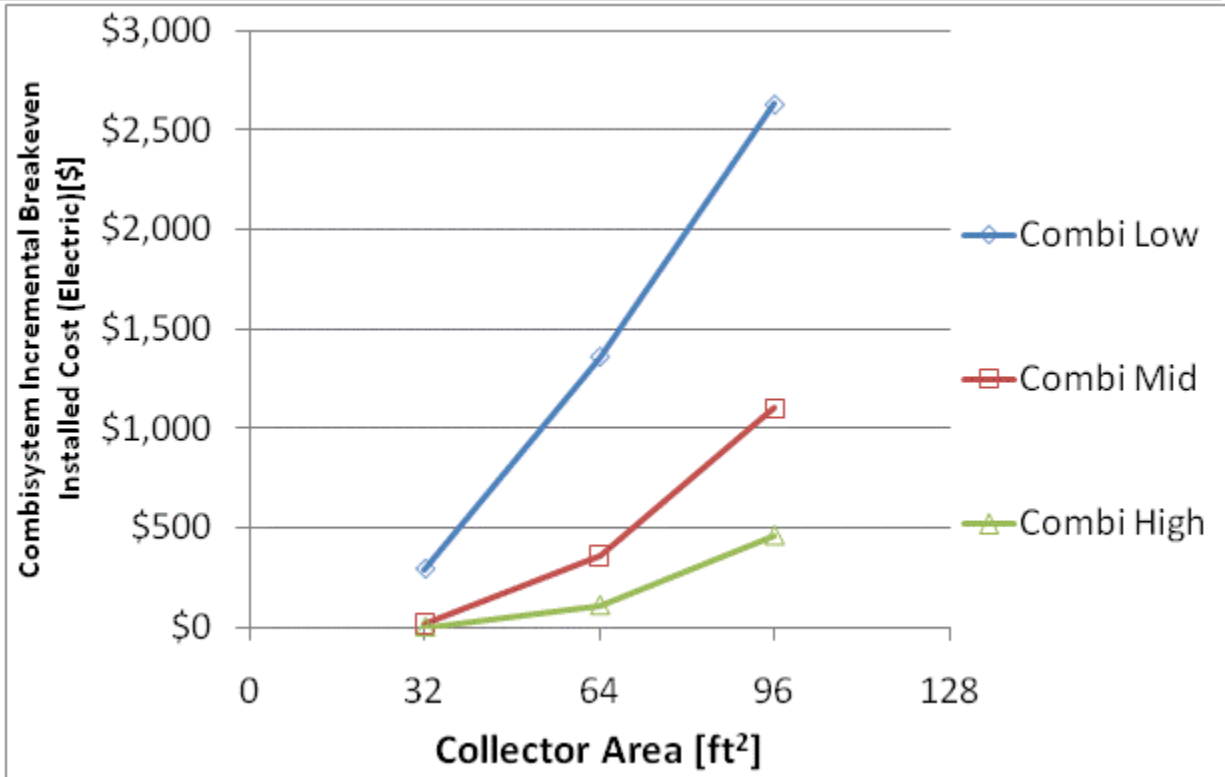
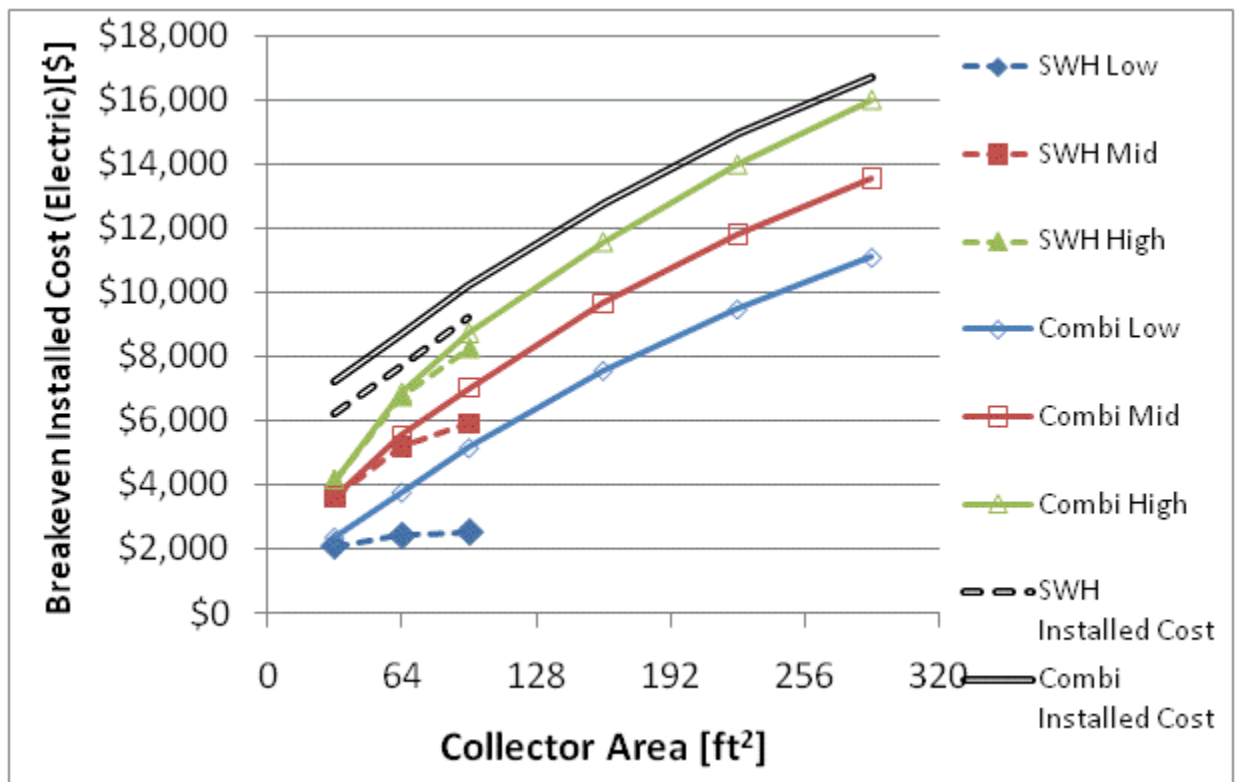


Figure F.64: Breakeven installed cost and combisystem incremental breakeven cost for electric system for a IECC 2009 House(Denver)

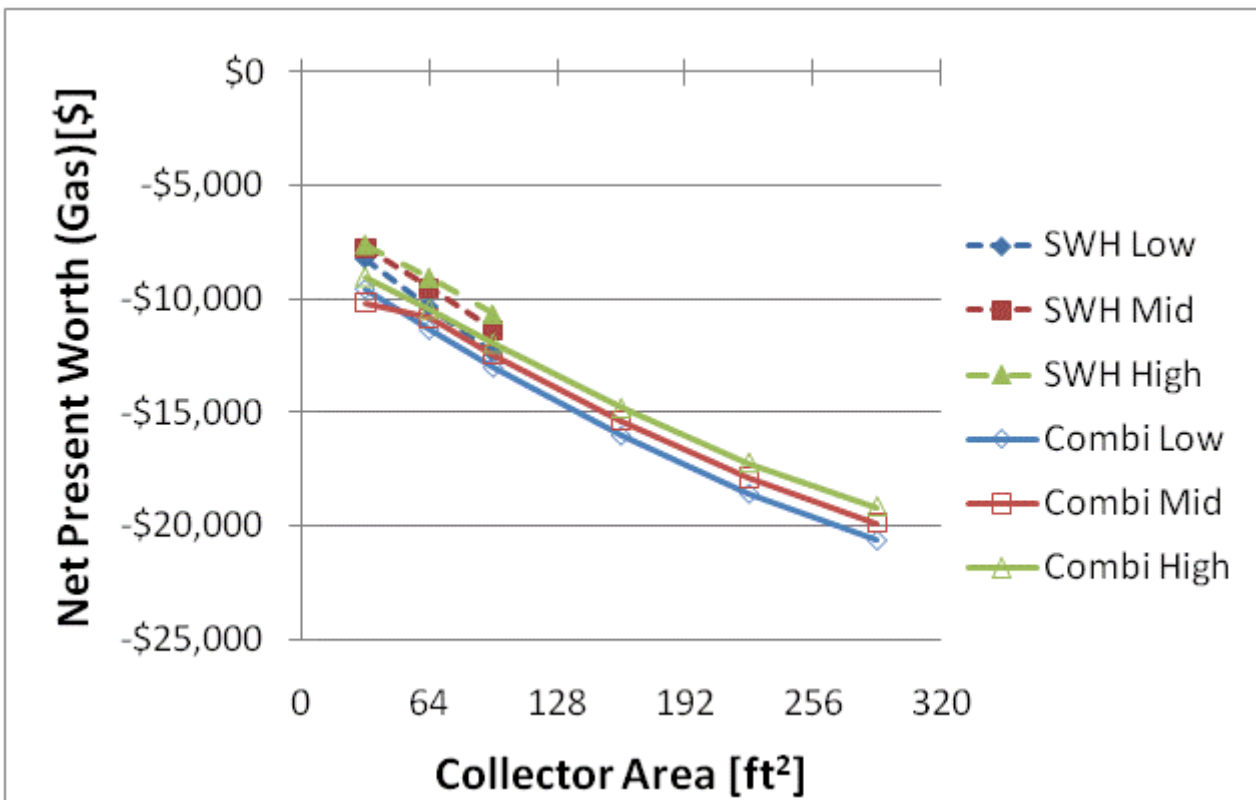
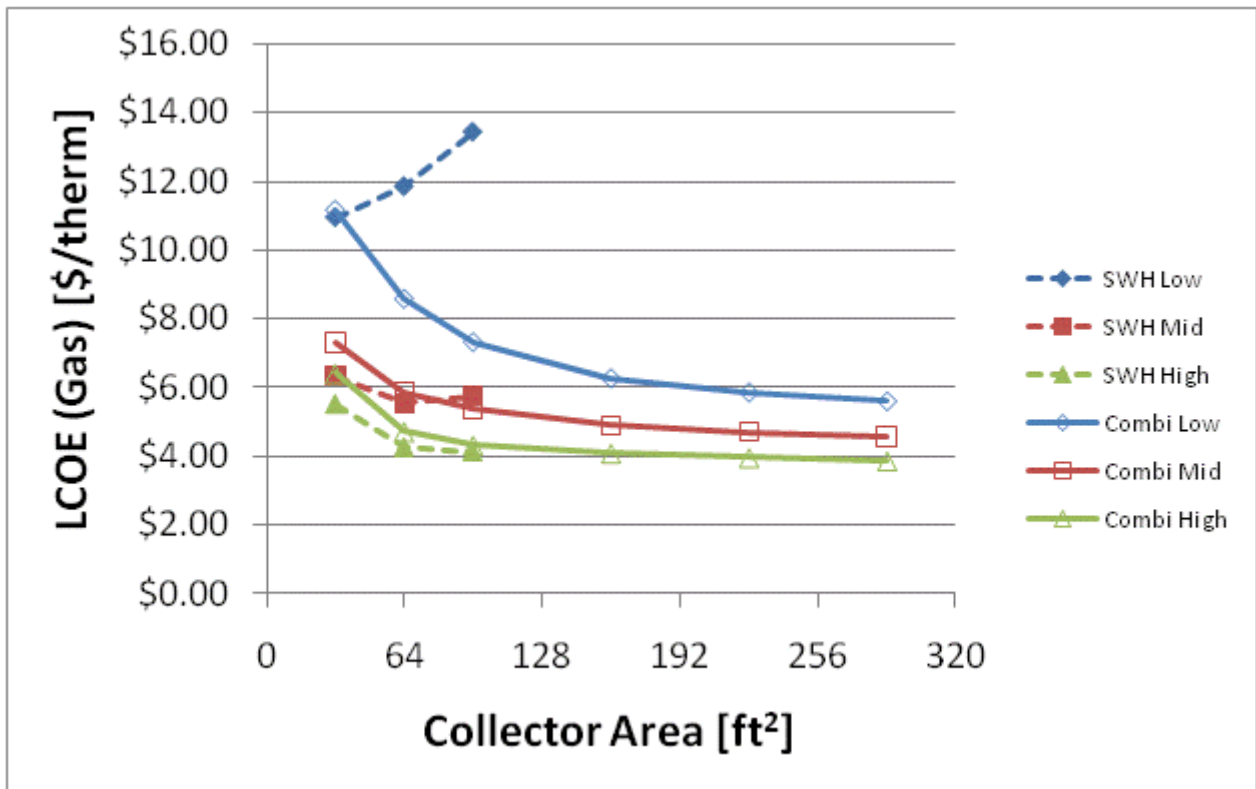


Figure F.65: LCOE and NPW for gas systems for a IECC 2009 House(Denver)

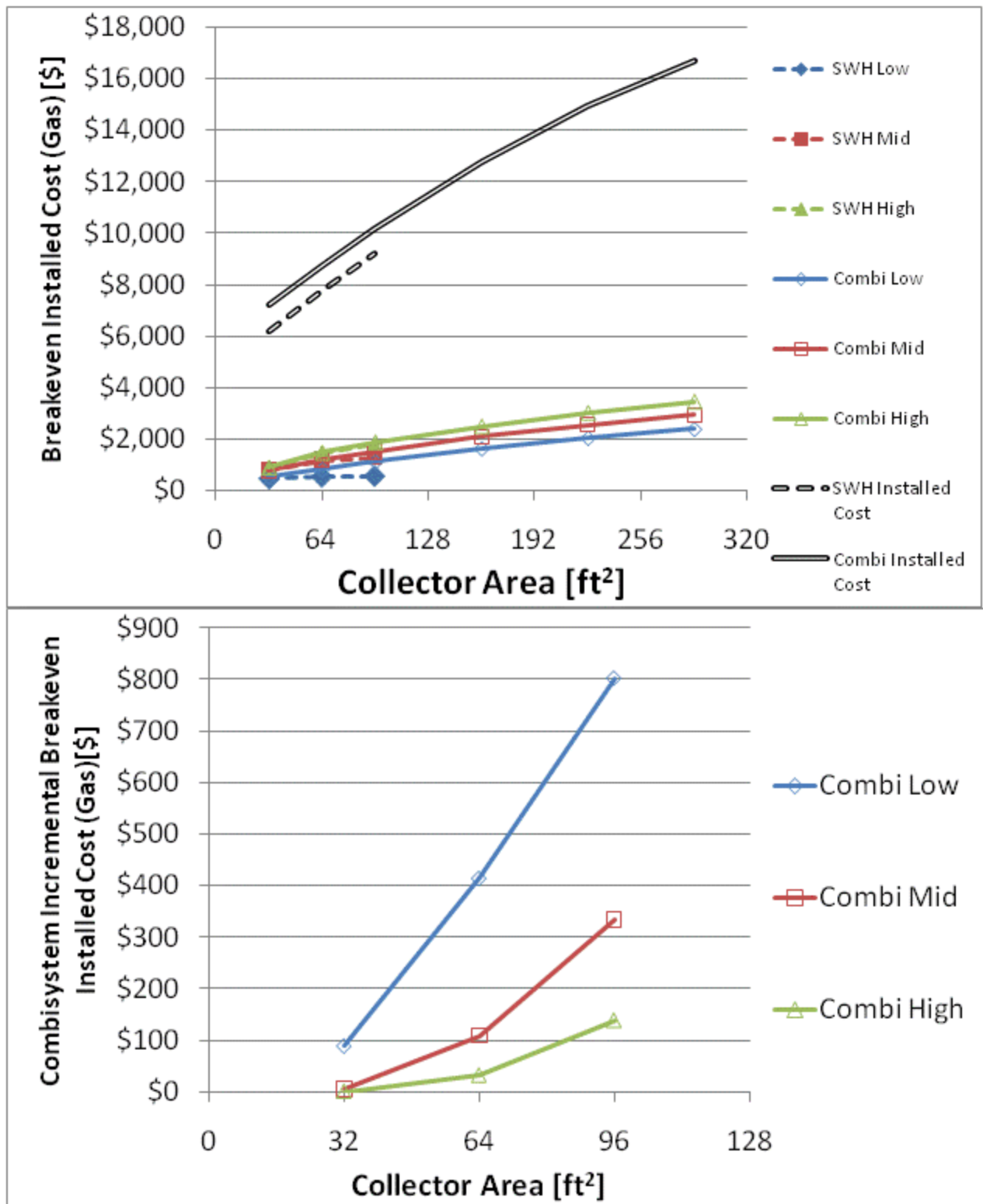


Figure F.66: Breakeven installed cost and combisystem incremental breakeven cost for gas systems for a

IECC 2009 House(Denver)

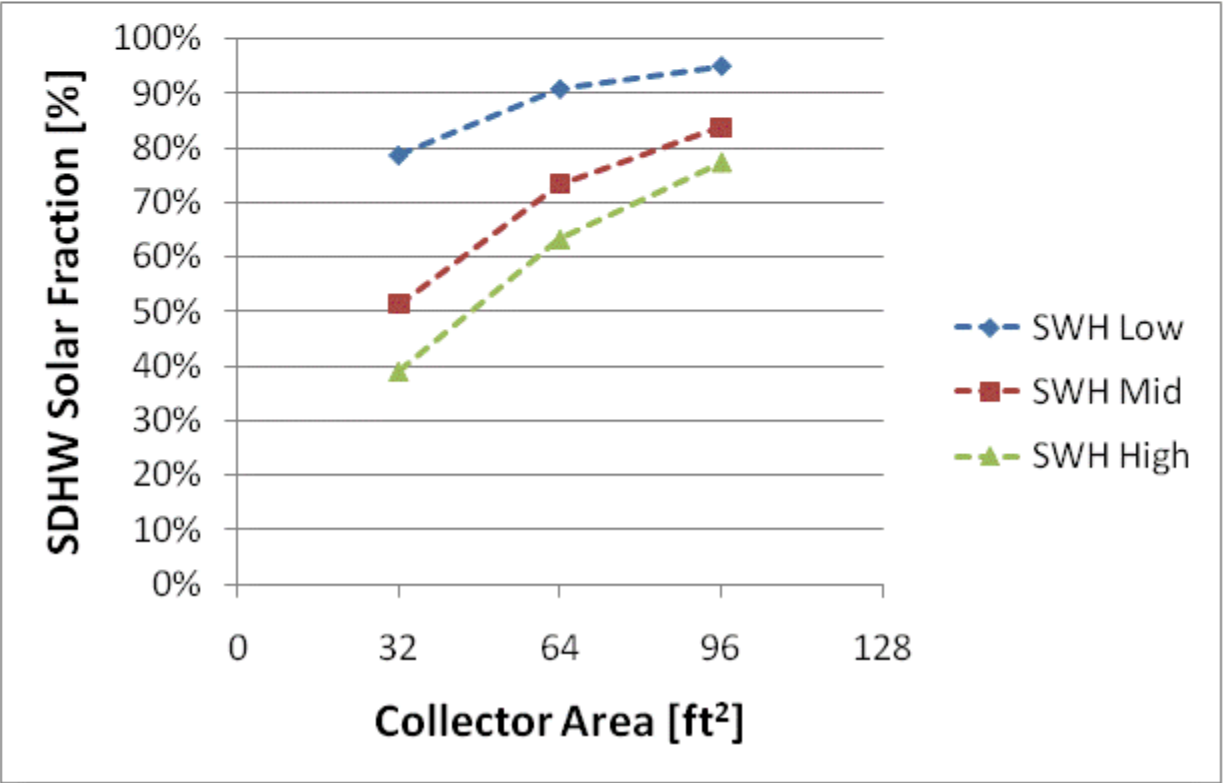
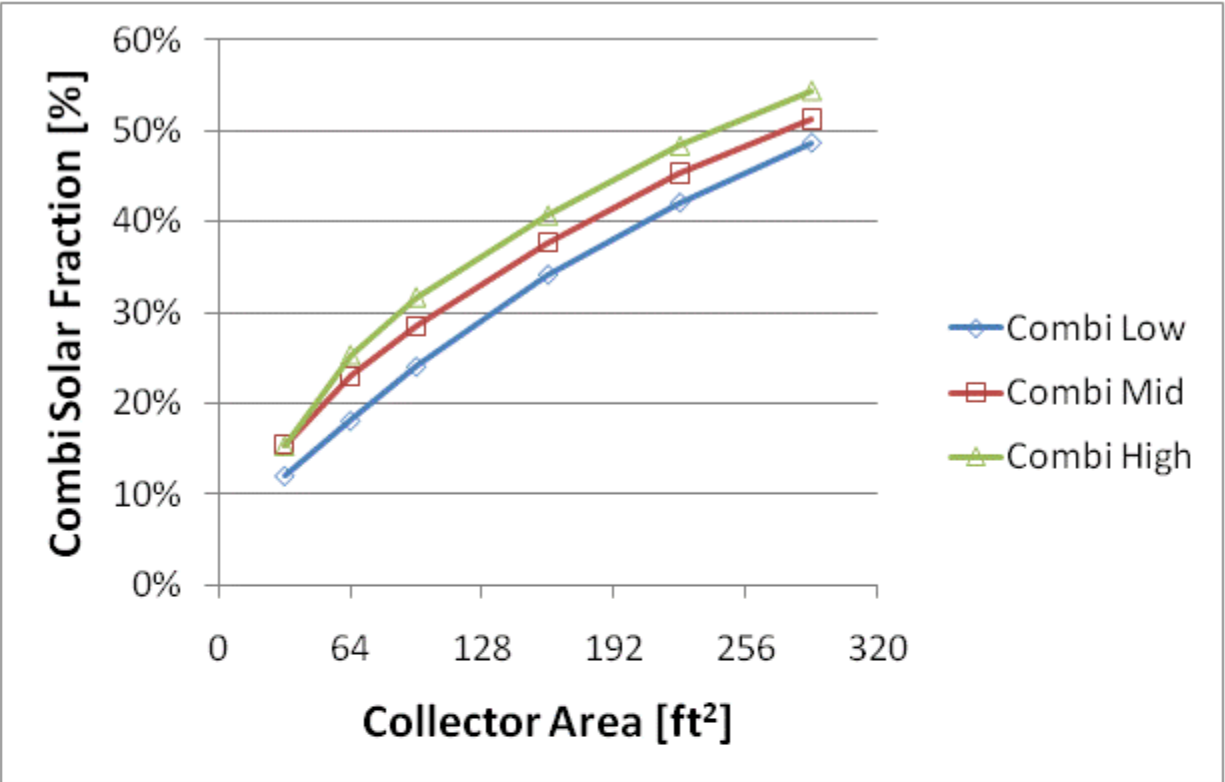


Figure F.67: Combisystem and SWH solar fraction for a BA 50% House(Denver)

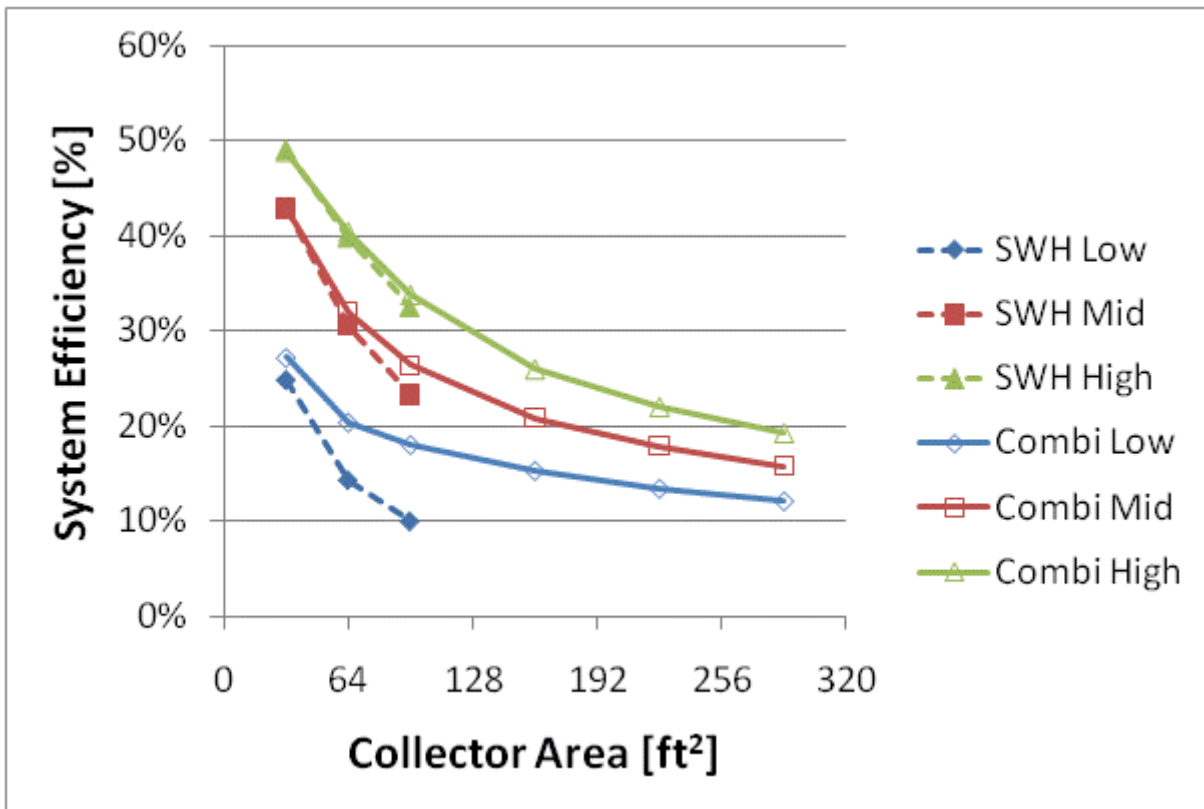
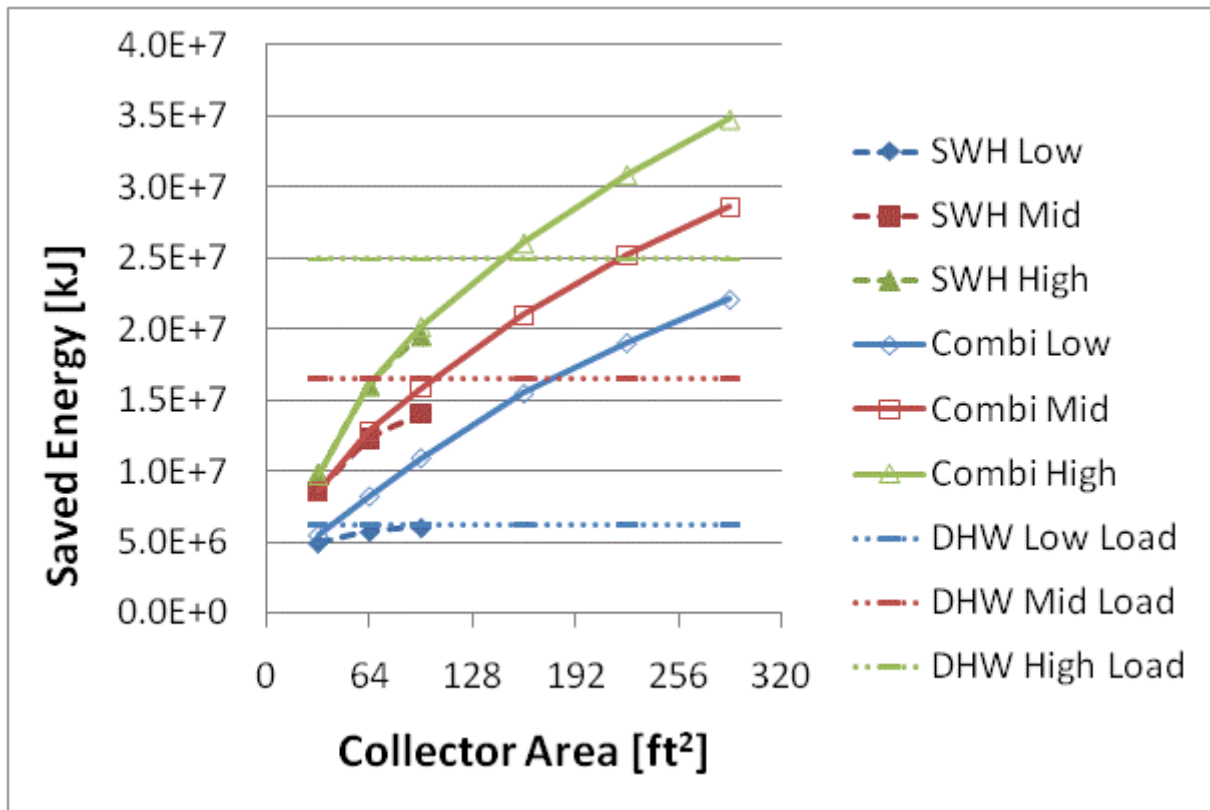


Figure F.68: Annual saved energy and system efficiency for a BA 50% House(Denver)

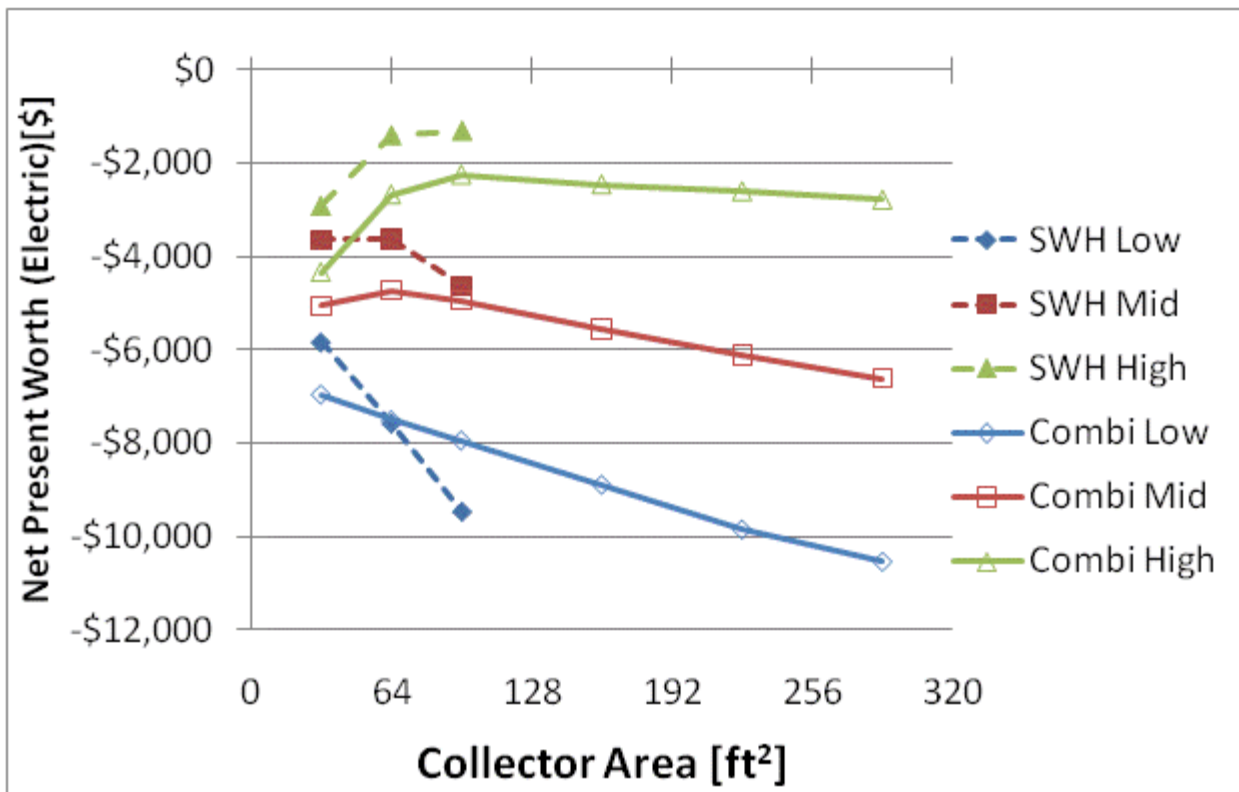
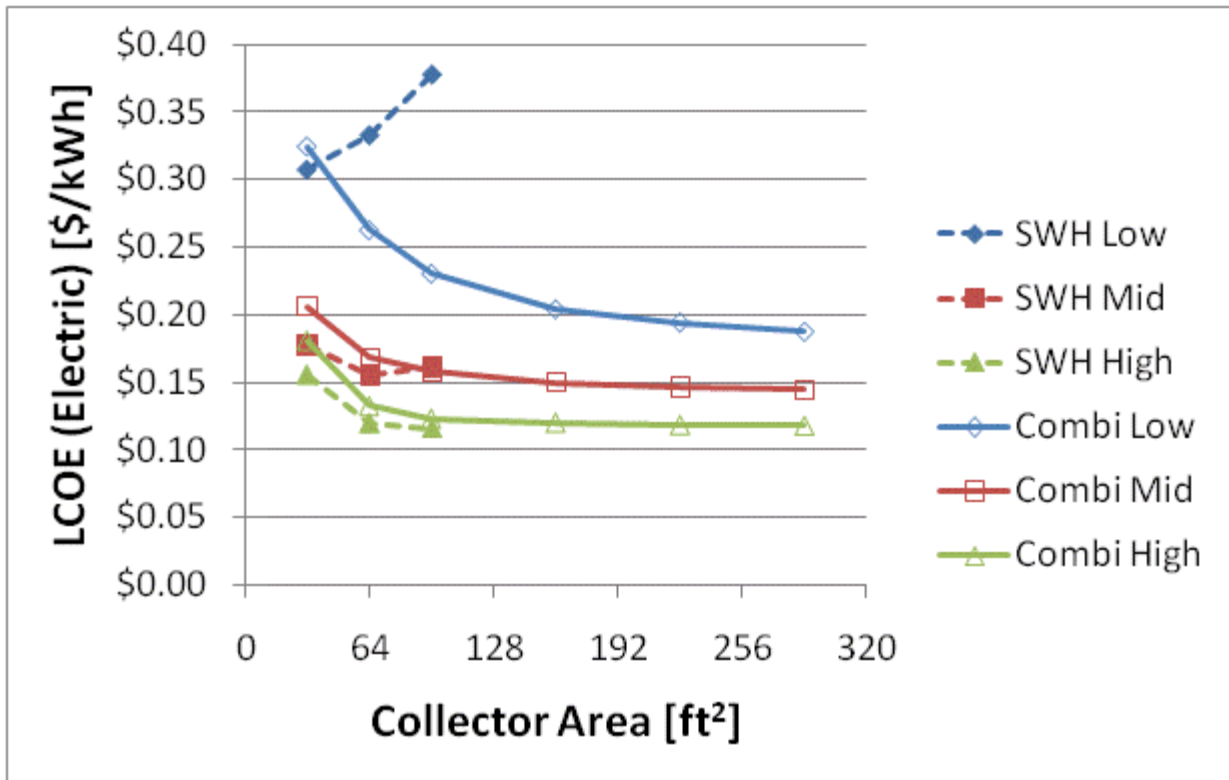


Figure F.69: LCOE and NPW for electric systems for a BA 50% House(Denver)

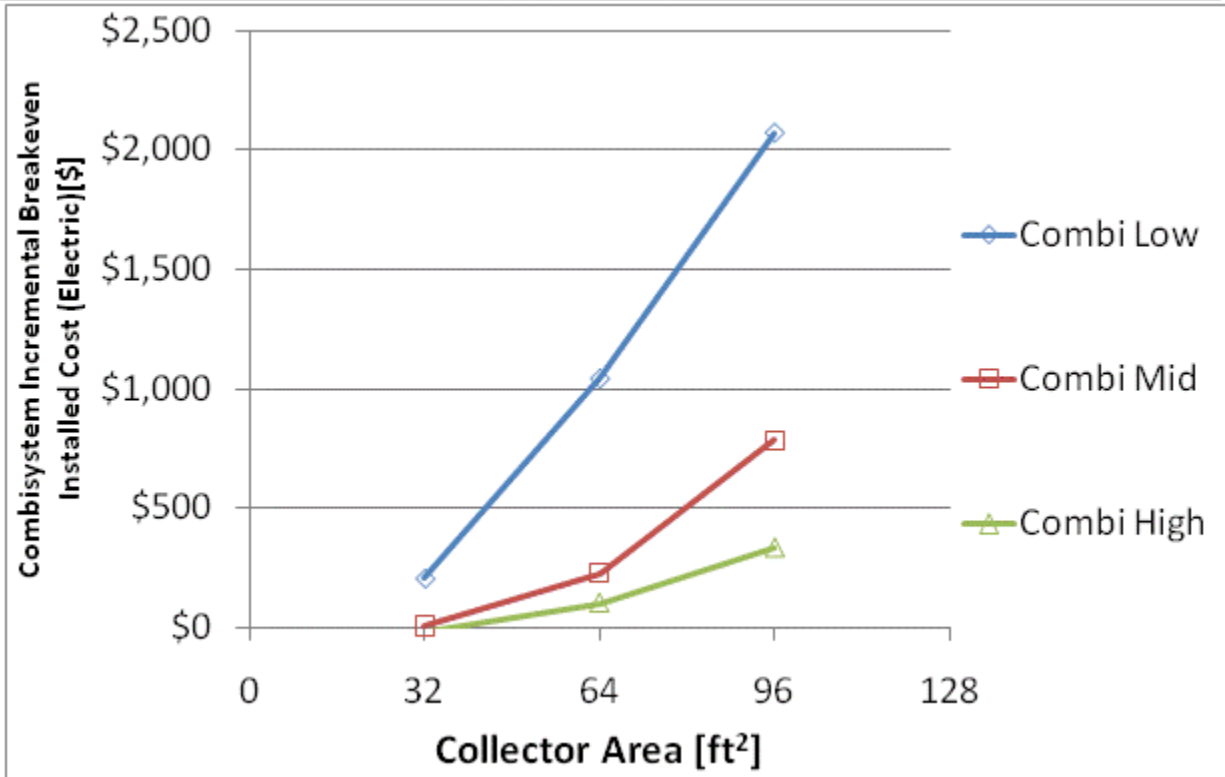
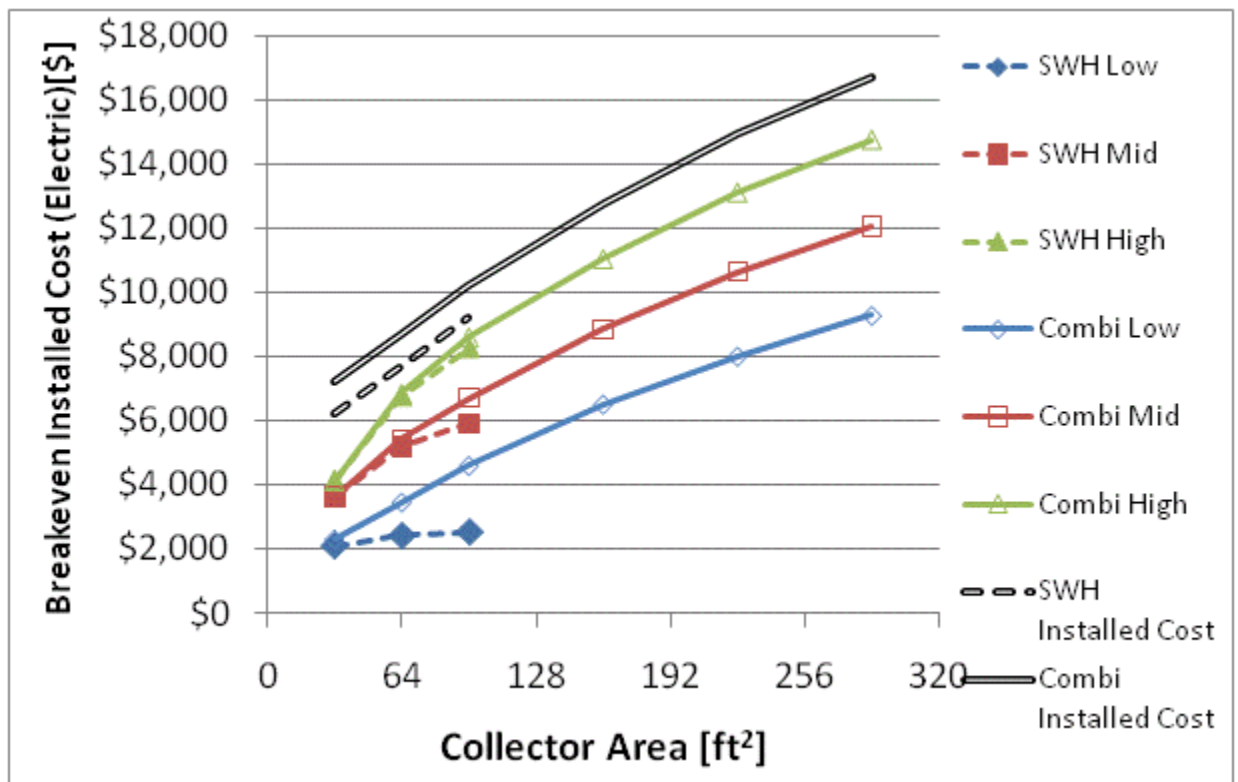


Figure F.70: Breakeven installed cost and combisystem incremental breakeven cost for electric system for a BA 50% House(Denver)

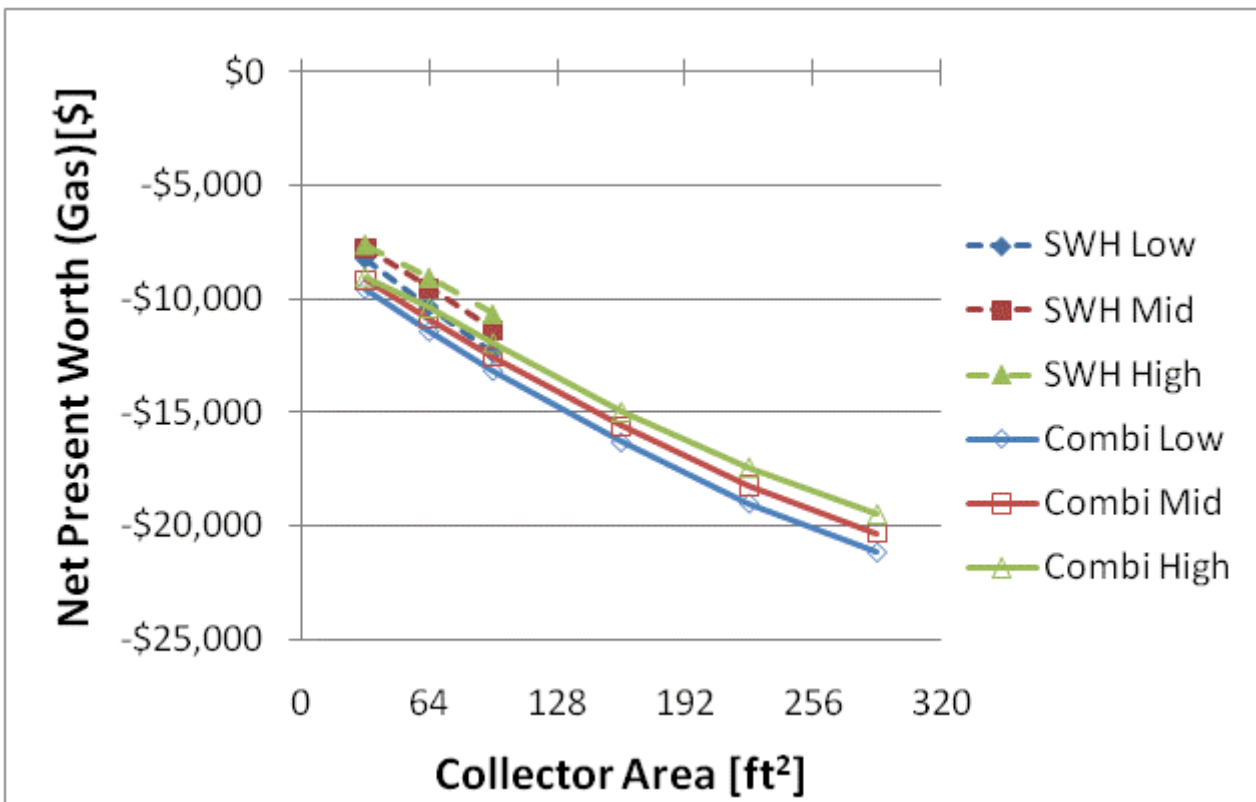
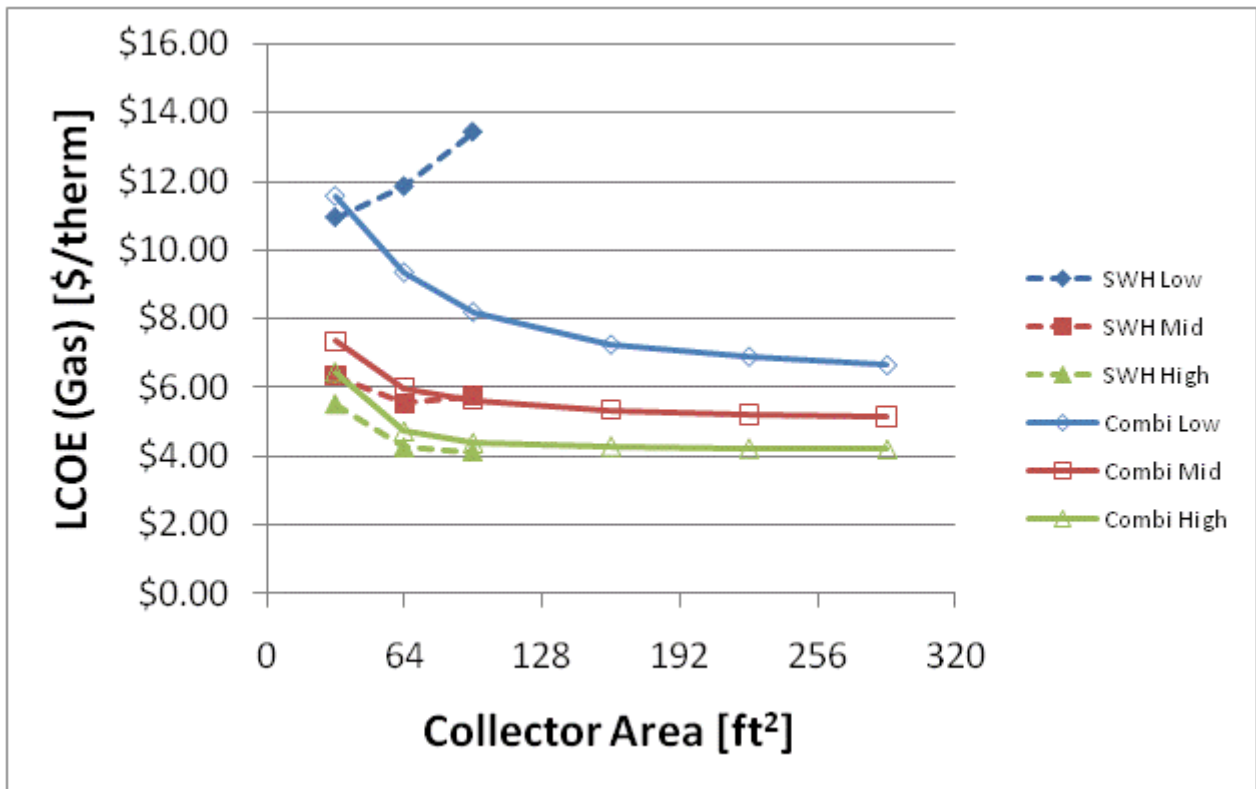


Figure F.71: LCOE and NPW for gas systems for a BA 50% House(Denver)

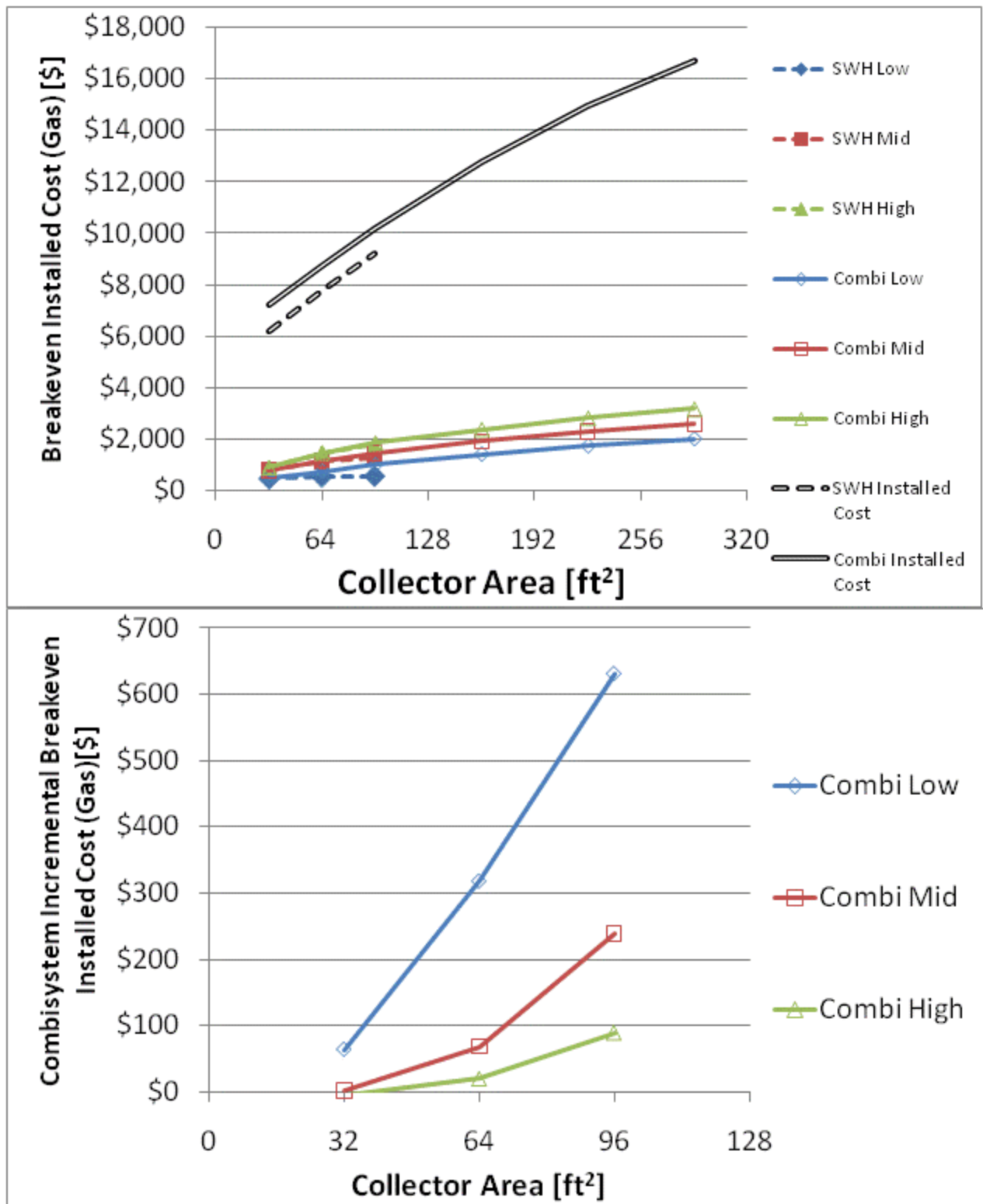


Figure F.72: Breakeven installed cost and combisystem incremental breakeven cost for gas systems for a

BA 50% House(Denver)

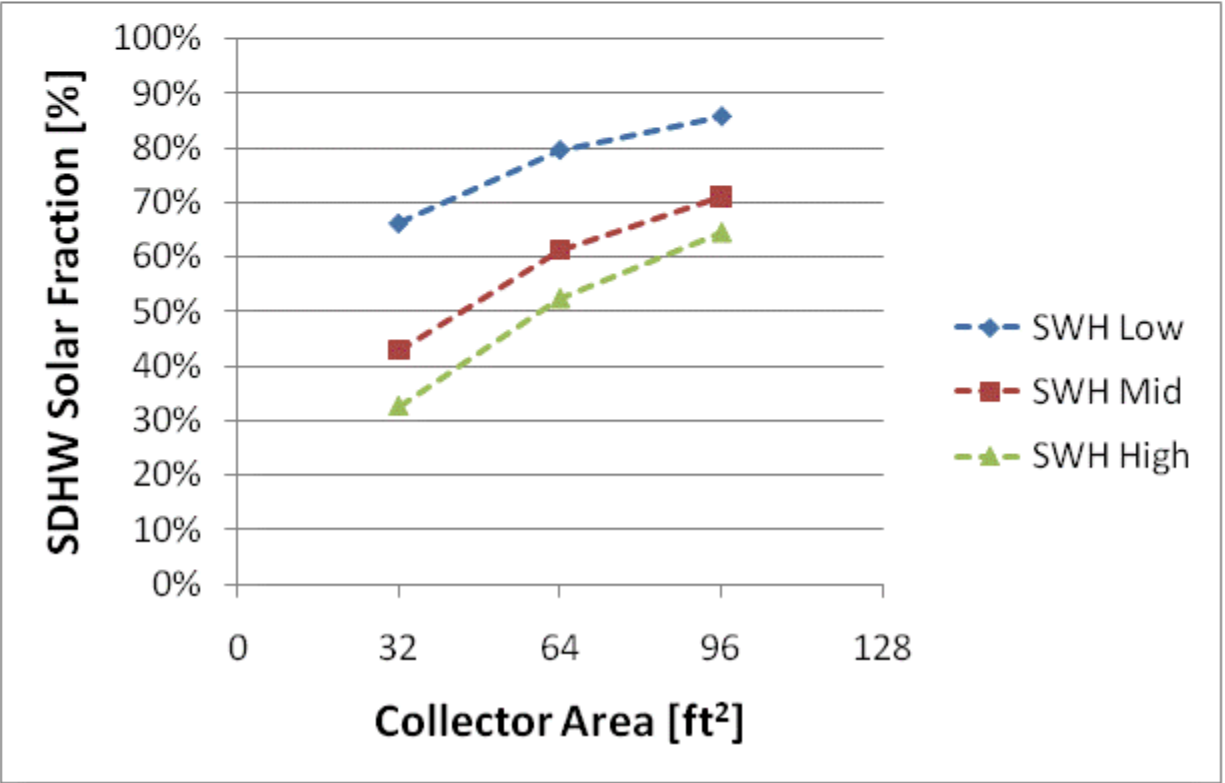
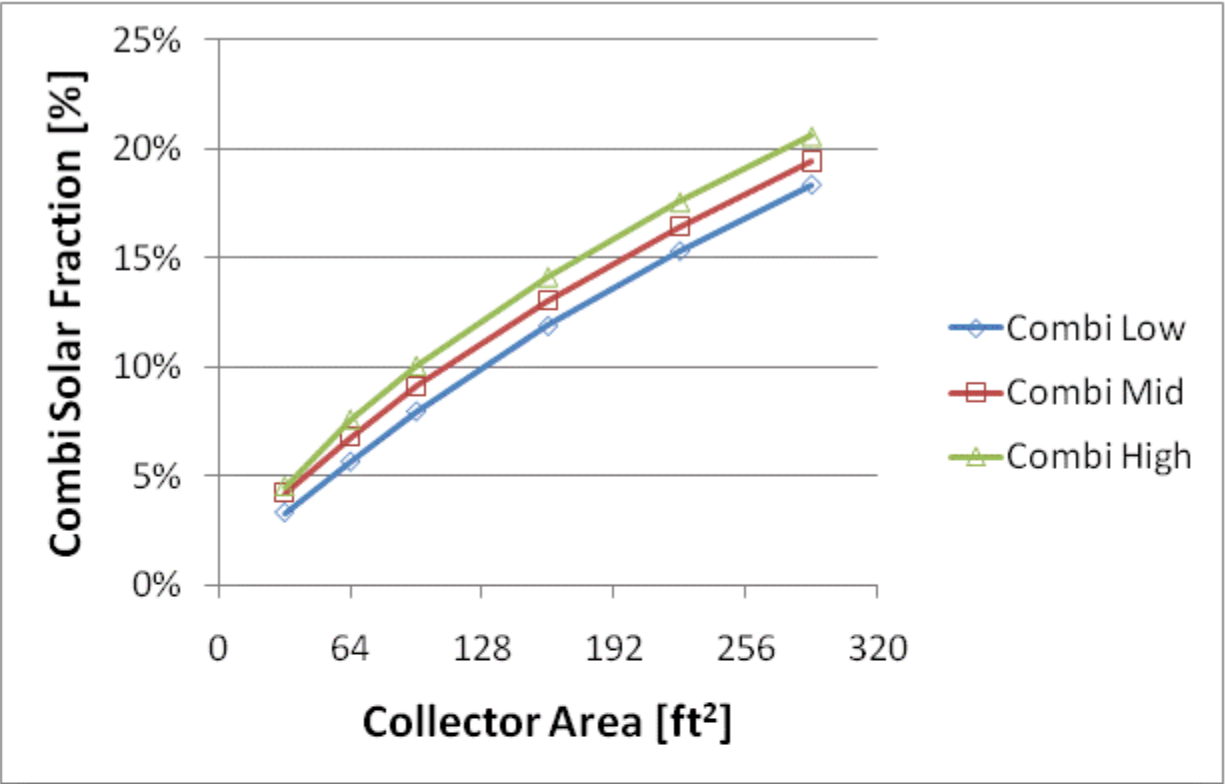


Figure F.73: Combisystem and SWH solar fraction for a 1960s Retrofit House(Boston)

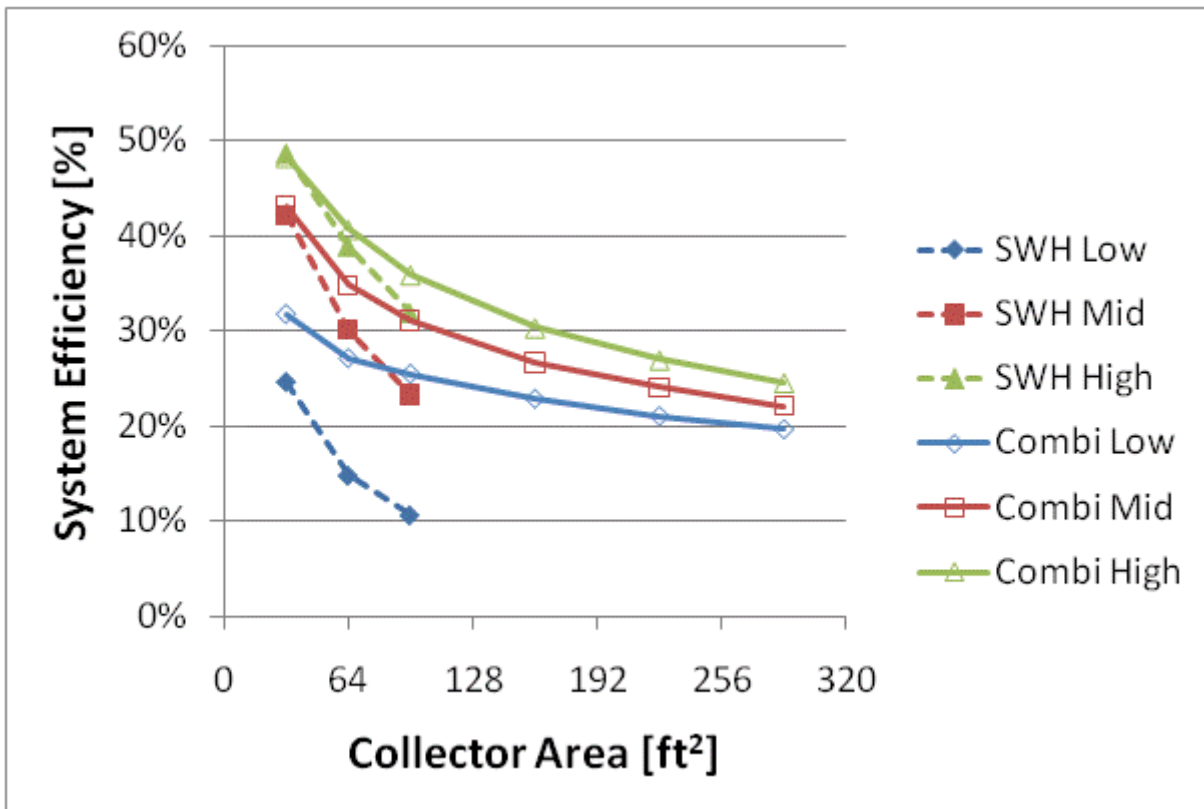
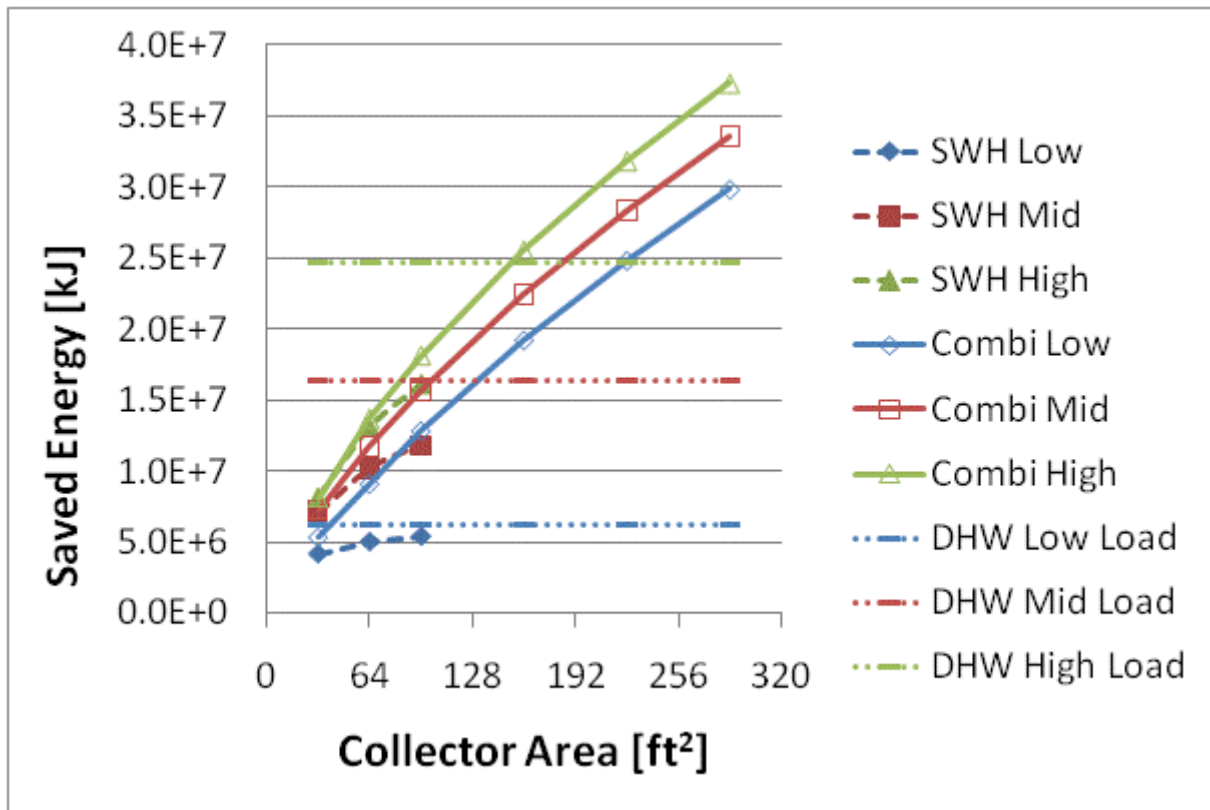


Figure F.74: Annual saved energy and system efficiency for a 1960s Retrofit House (Boston)

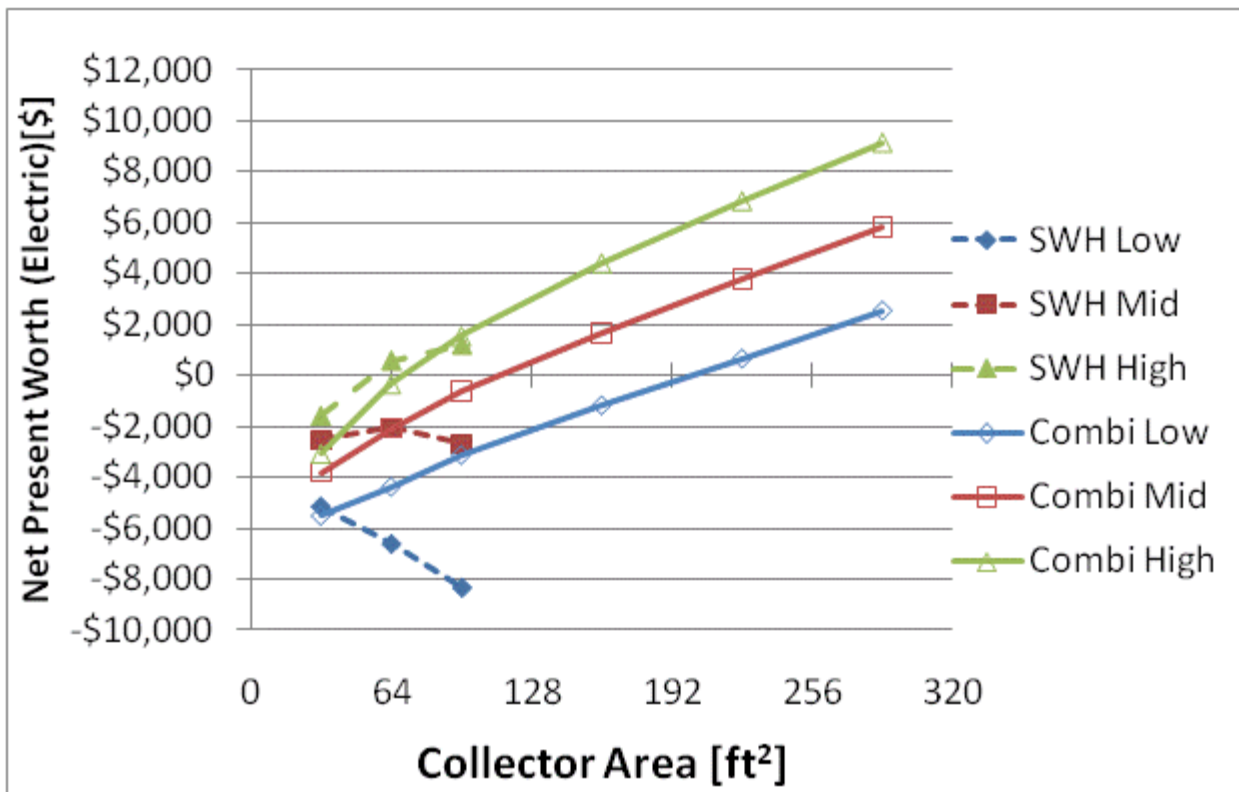
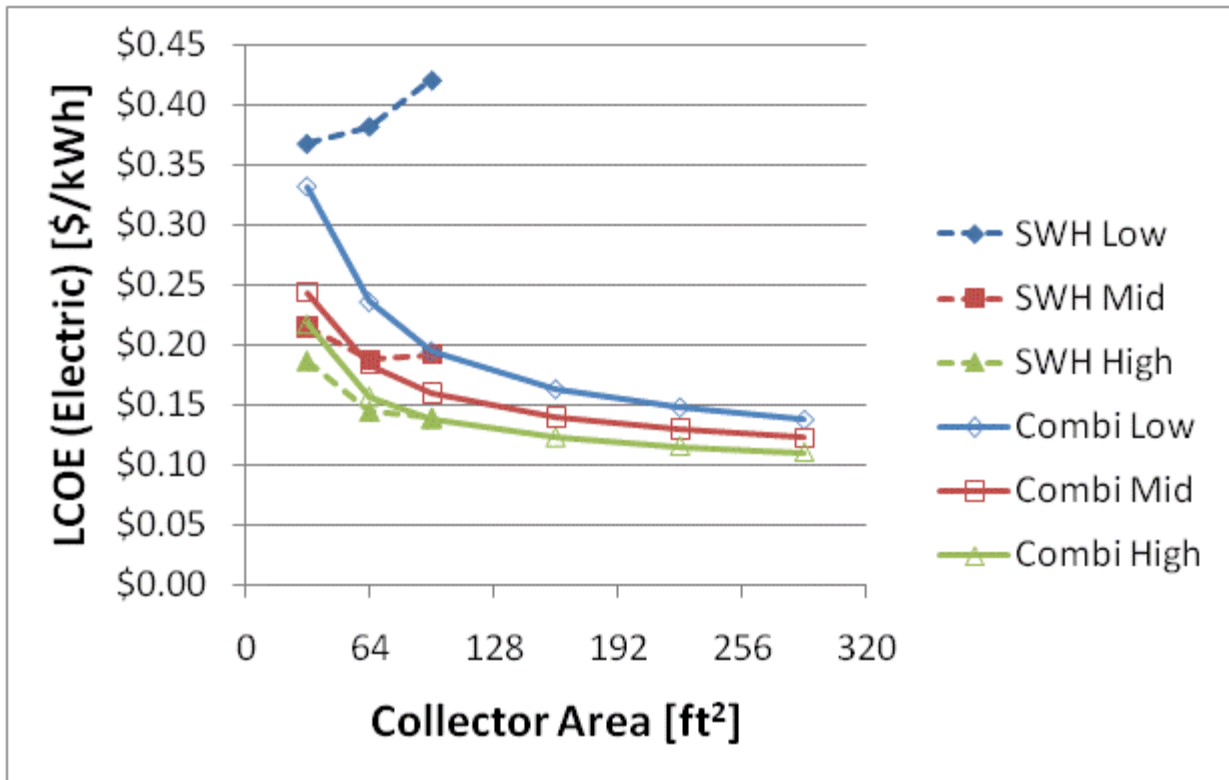


Figure F.75: LCOE and NPW for electric systems for a 1960s Retrofit House(Boston)

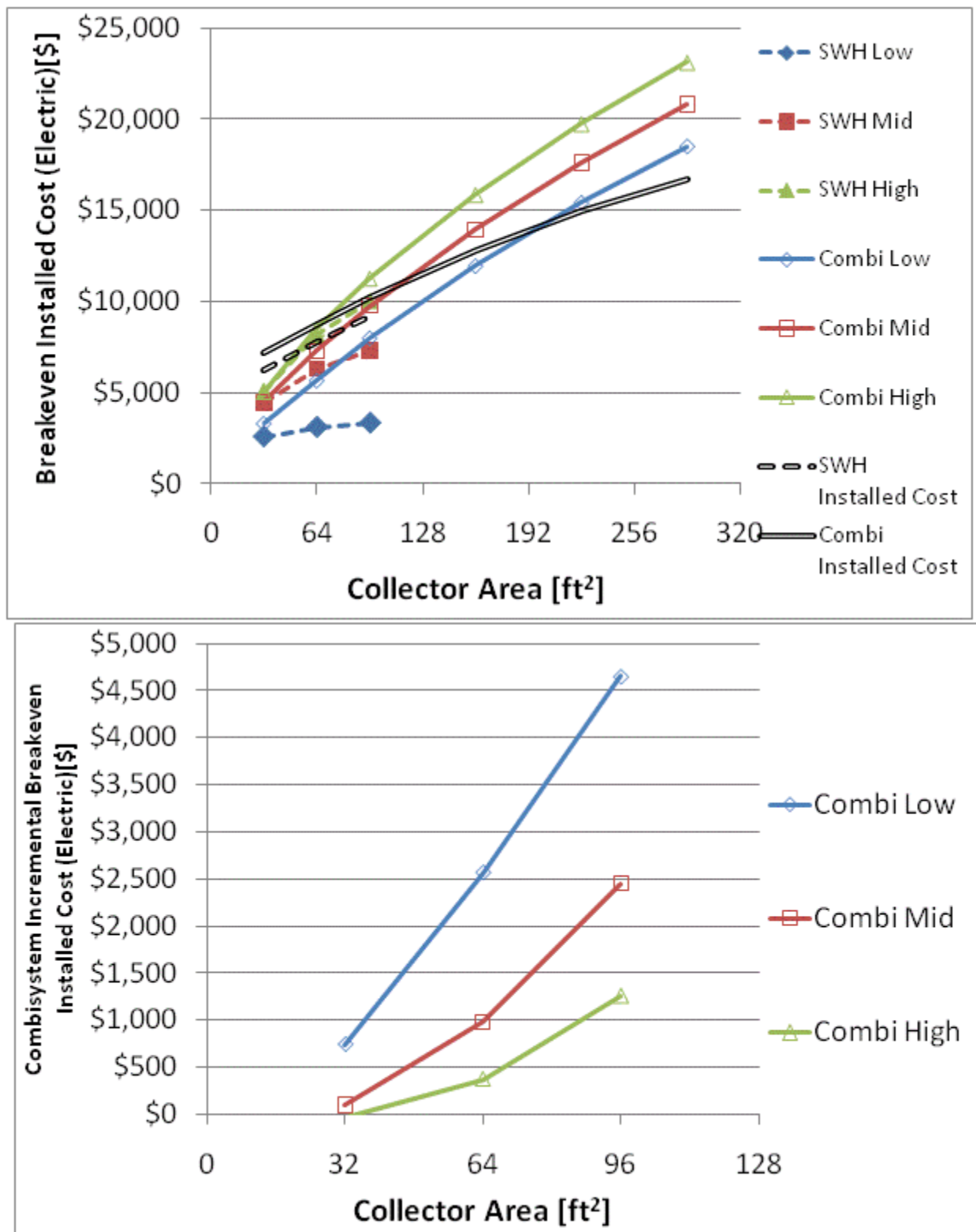


Figure F.76: Breakeven installed cost and combisystem incremental breakeven cost for electric system for a 1960s Retrofit House (Boston)

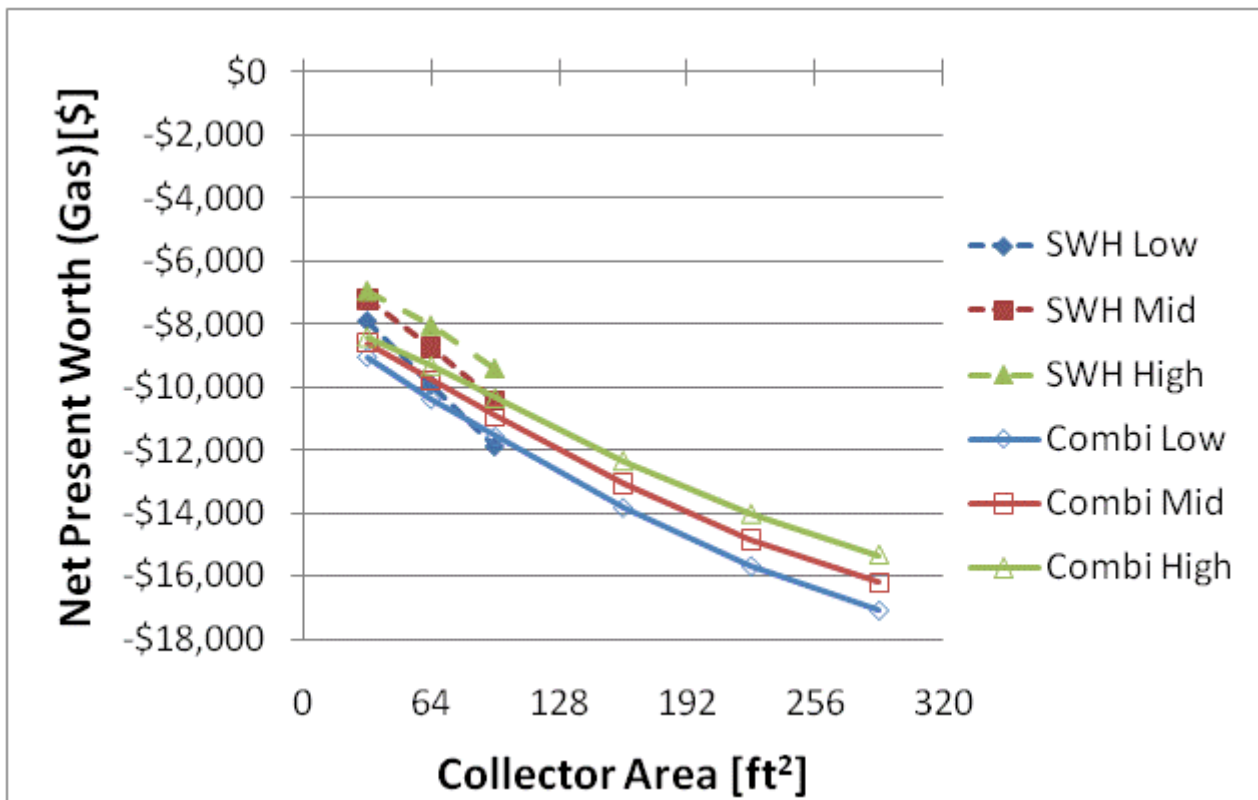
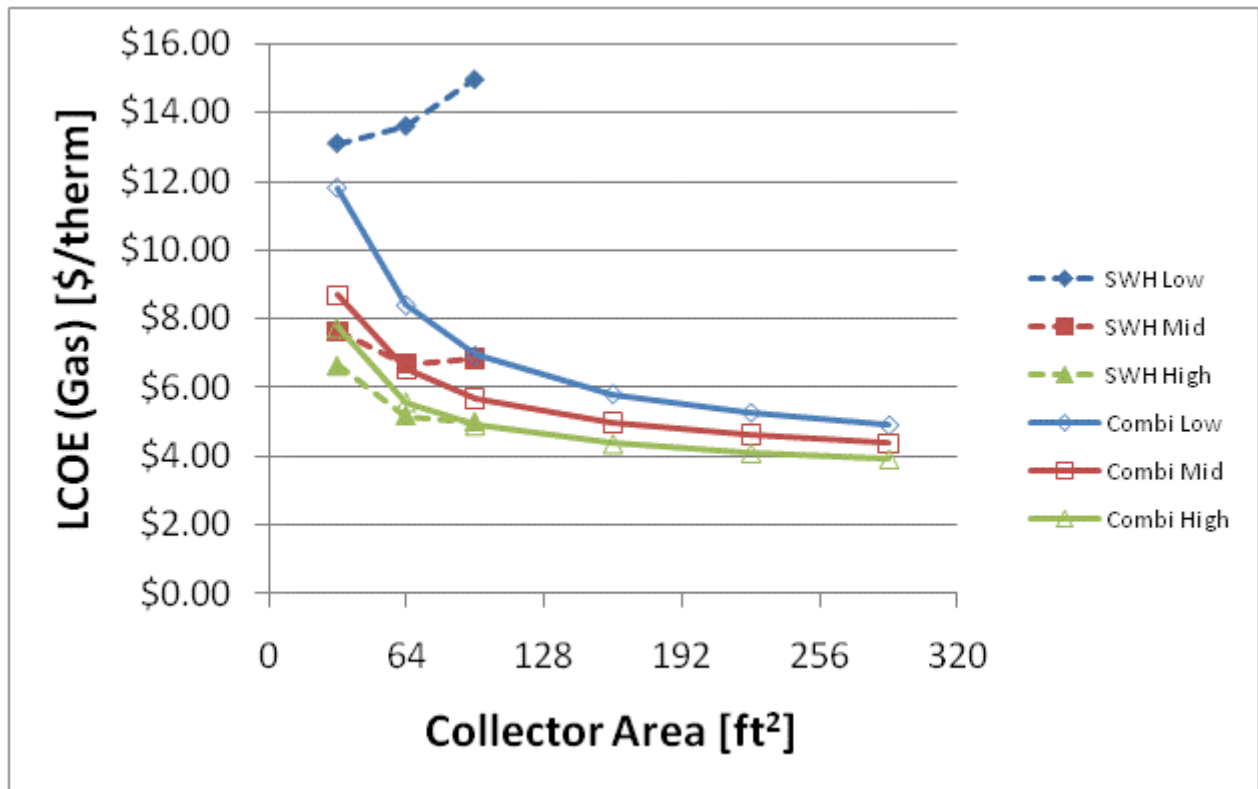


Figure F.77: LCOE and NPW for gas systems for a 1960s Retrofit House(Boston)

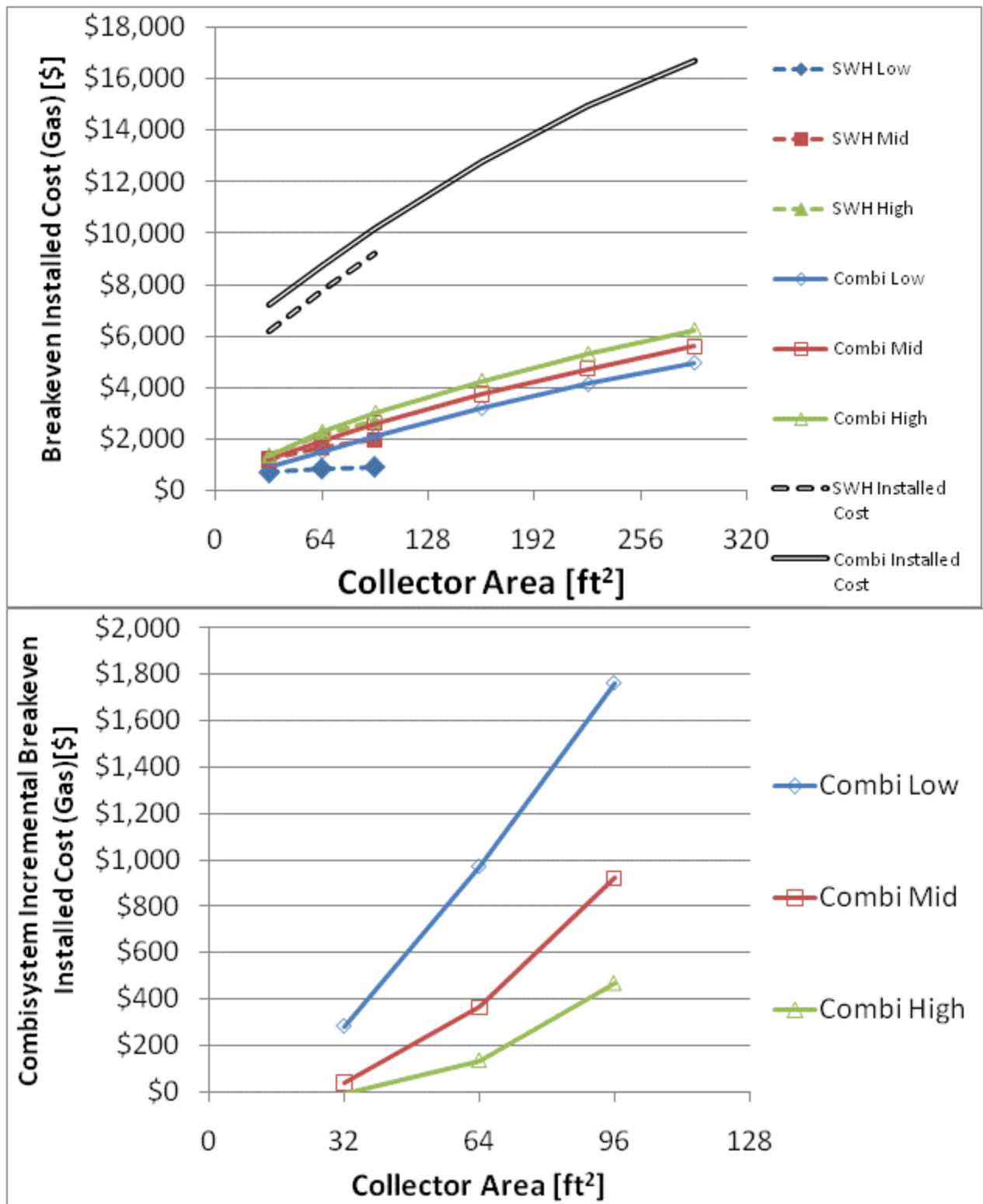


Figure F.78: Breakeven installed cost and combisystem incremental breakeven cost for gas systems for a

1960s Retrofit House(Boston)

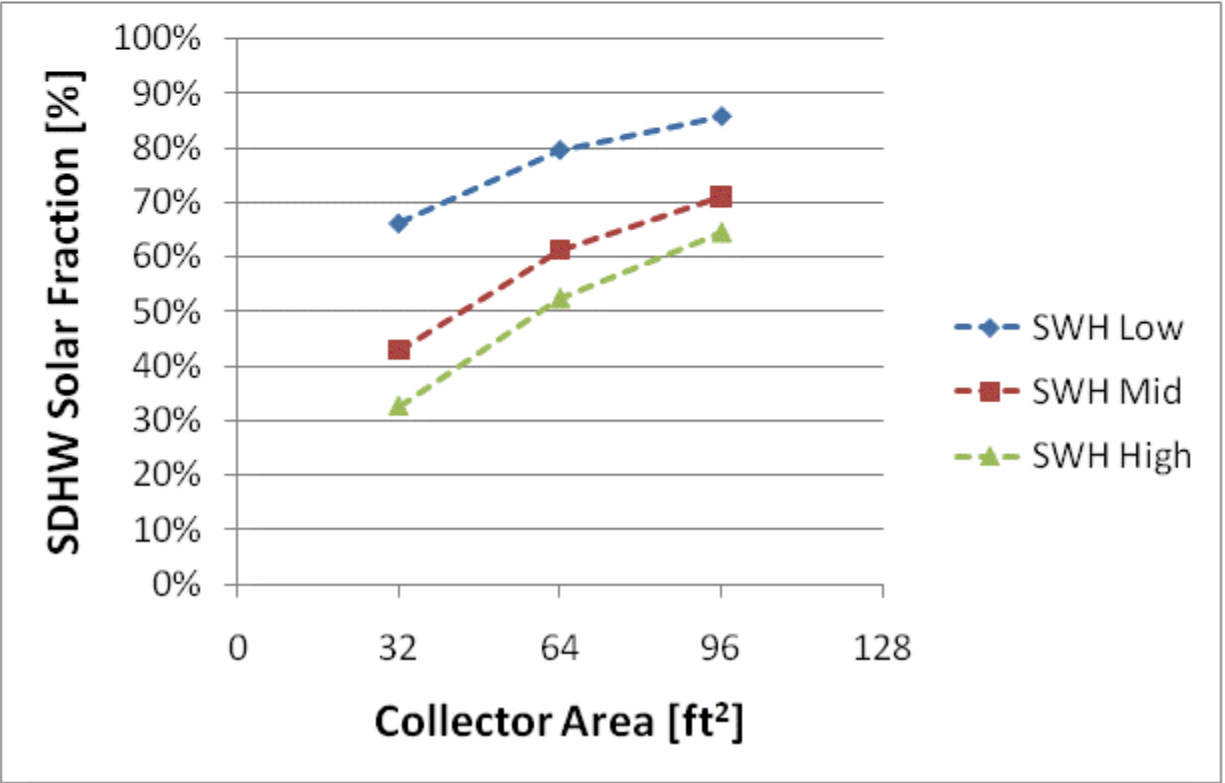
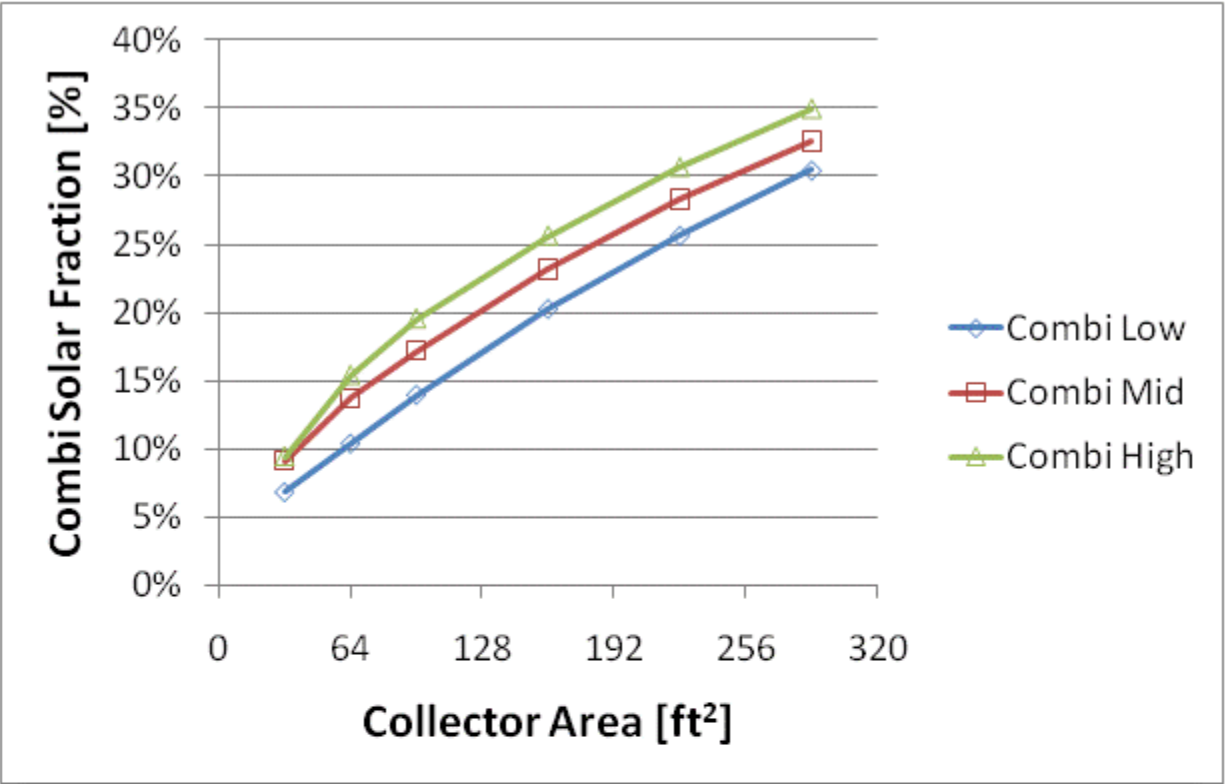


Figure F.79: Combisystem and SWH solar fraction for a IECC 2009 House(Boston)

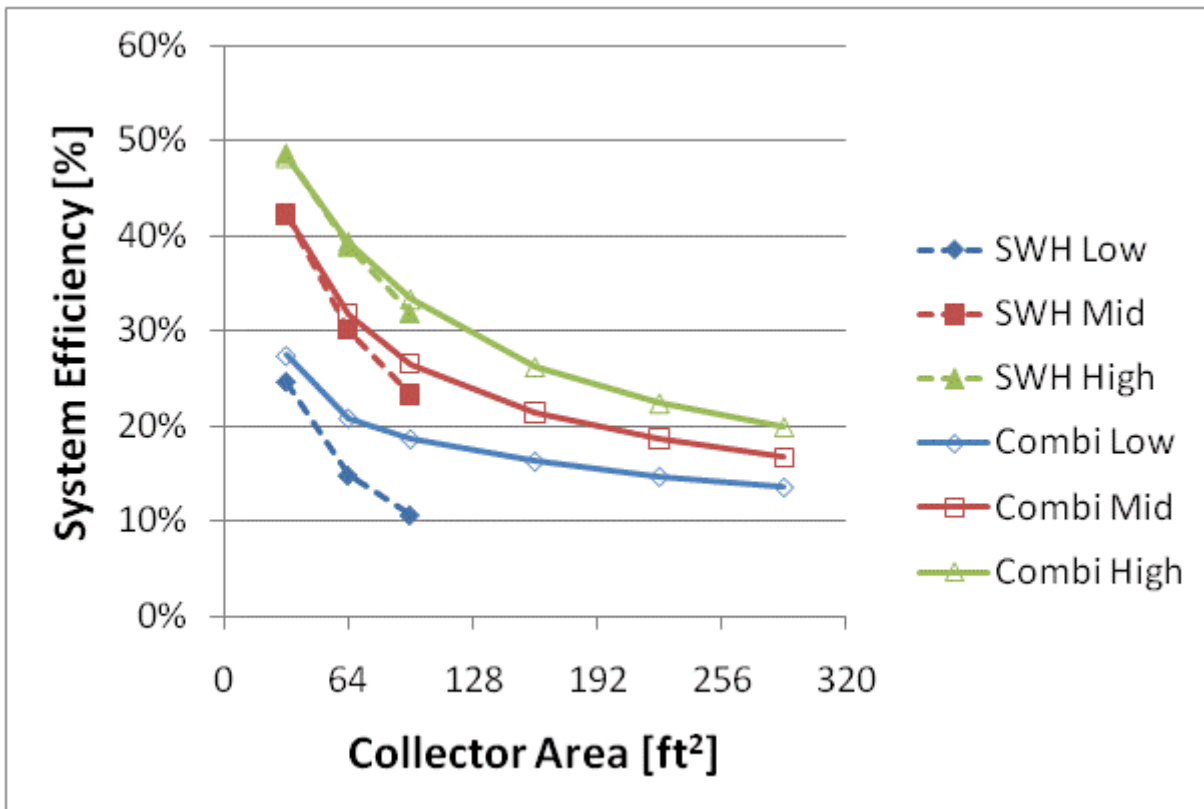
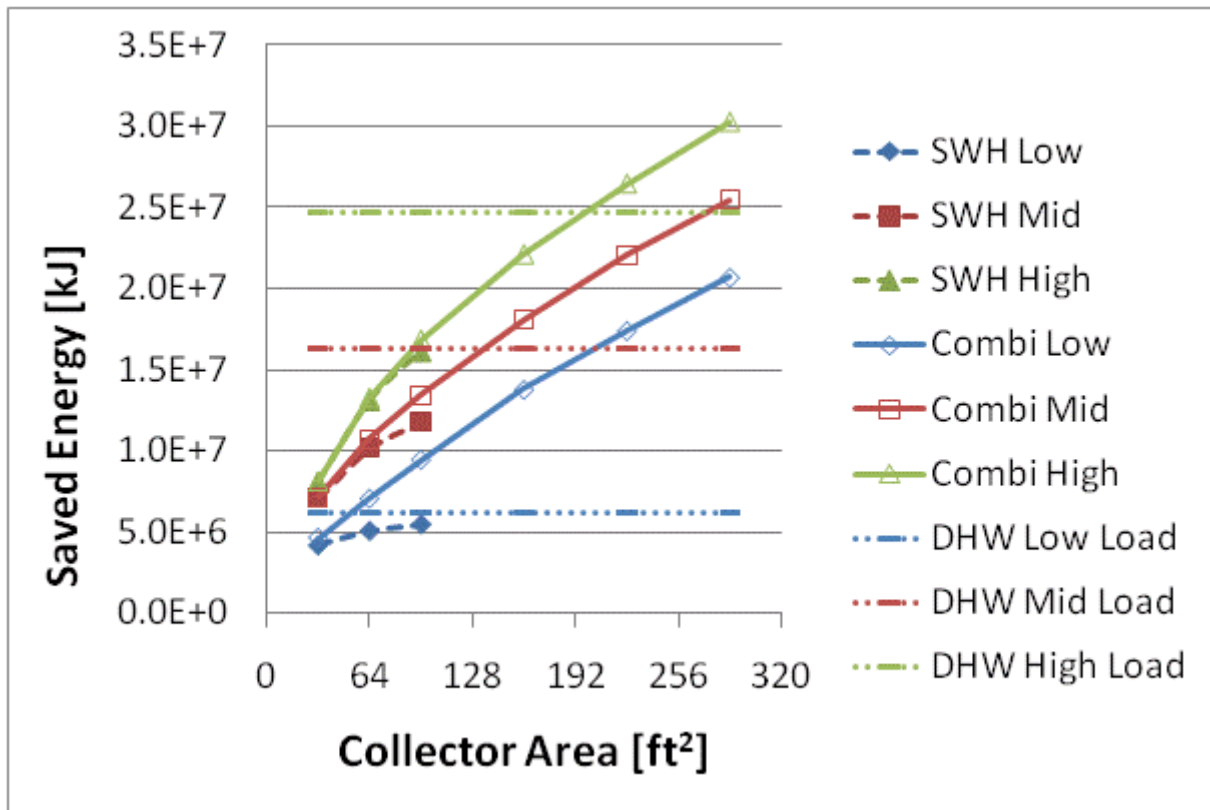


Figure F.80: Annual saved energy and system efficiency for a IECC 2009 House(Boston)

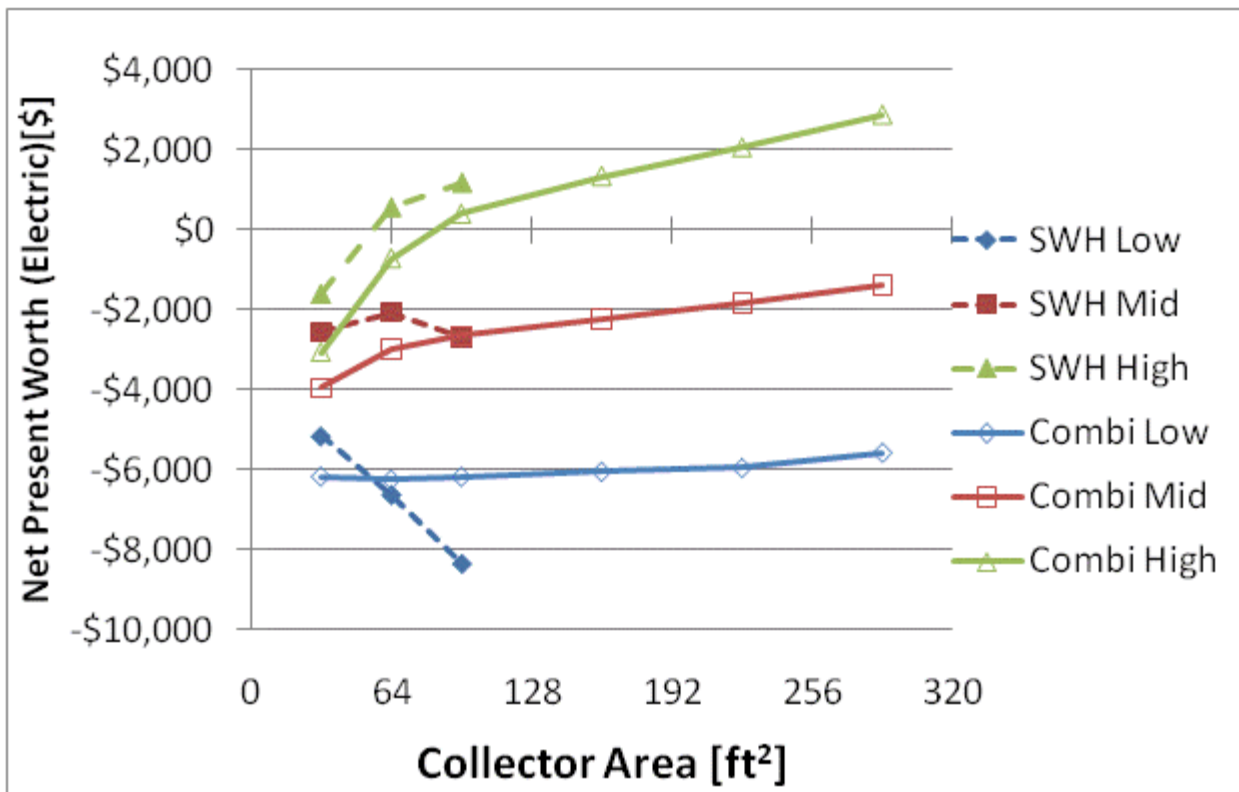
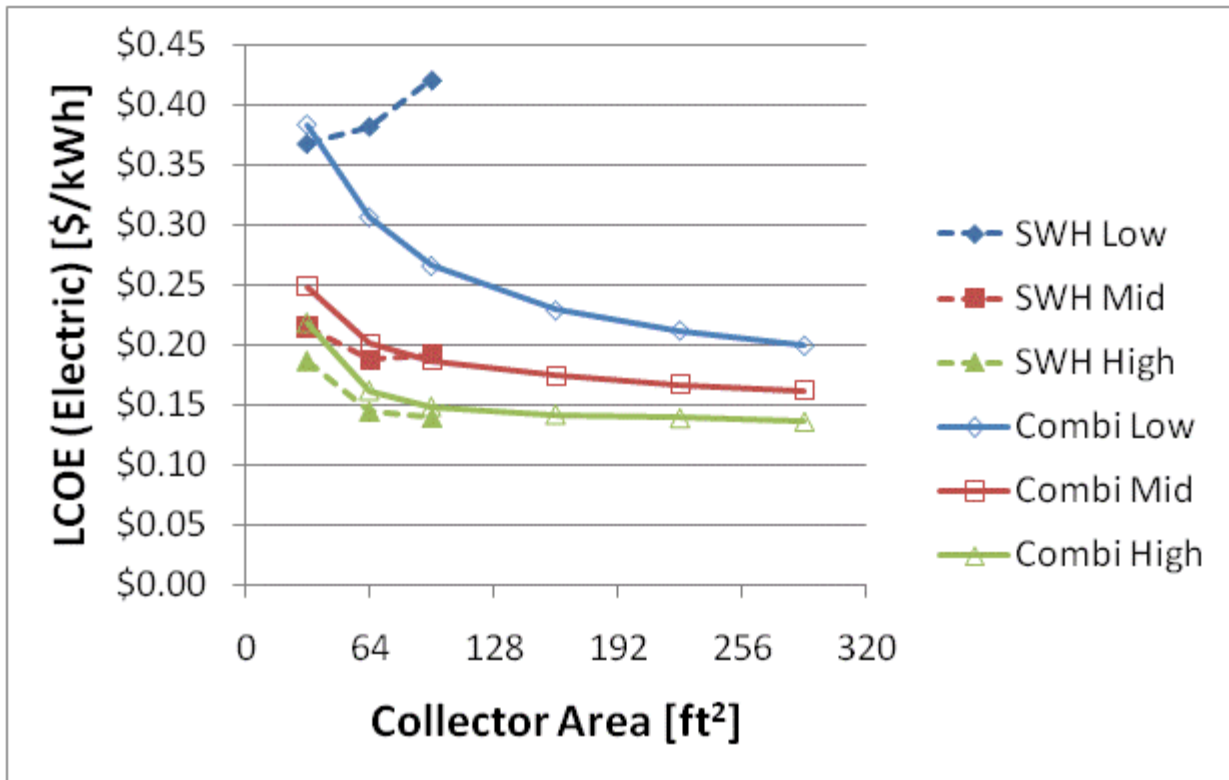


Figure F.81: LCOE and NPW for electric systems for a IECC 2009 House(Boston)

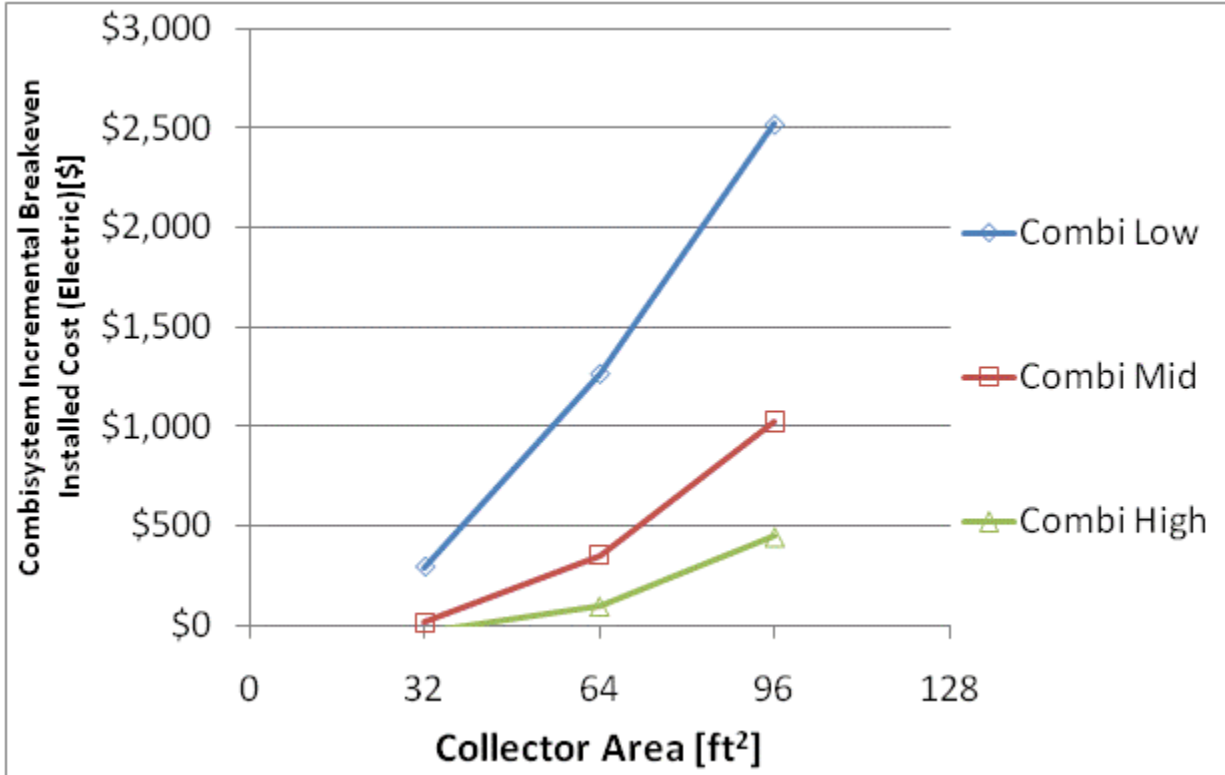
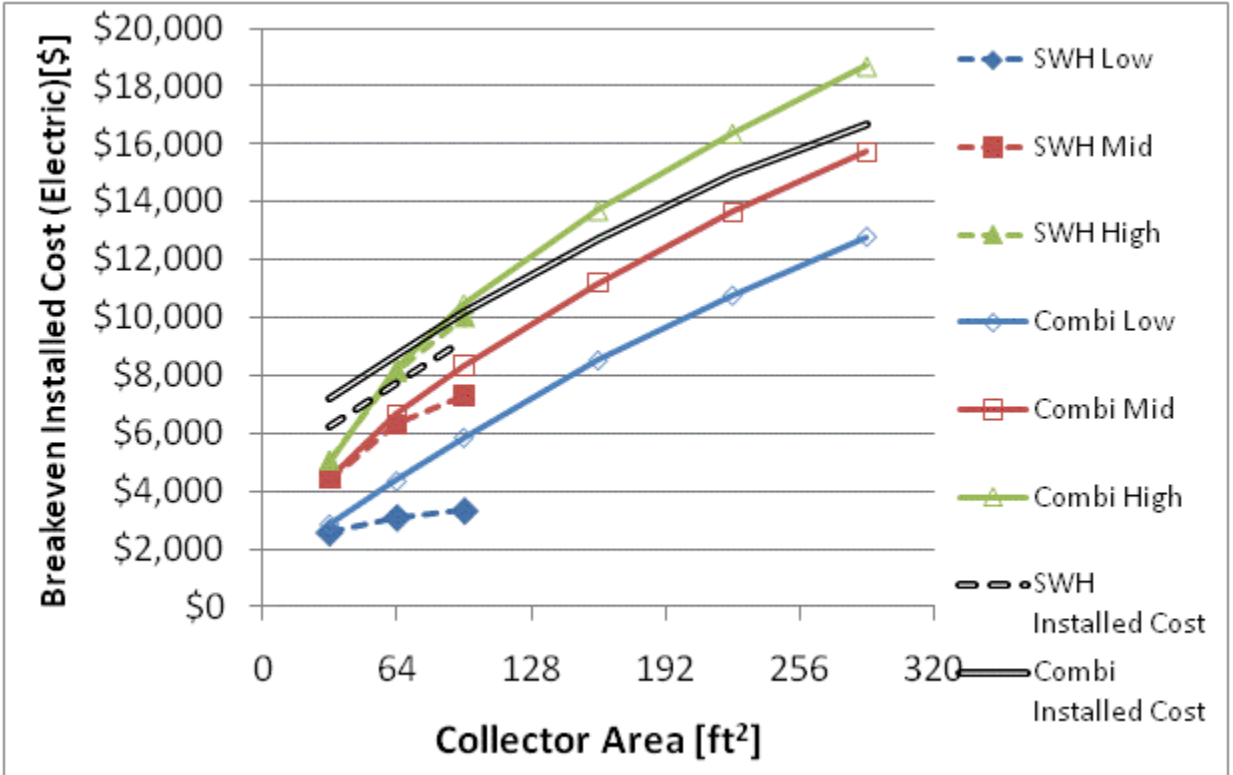


Figure F.82: Breakeven installed cost and combisystem incremental breakeven cost for electric system for a IECC 2009 House(Boston)

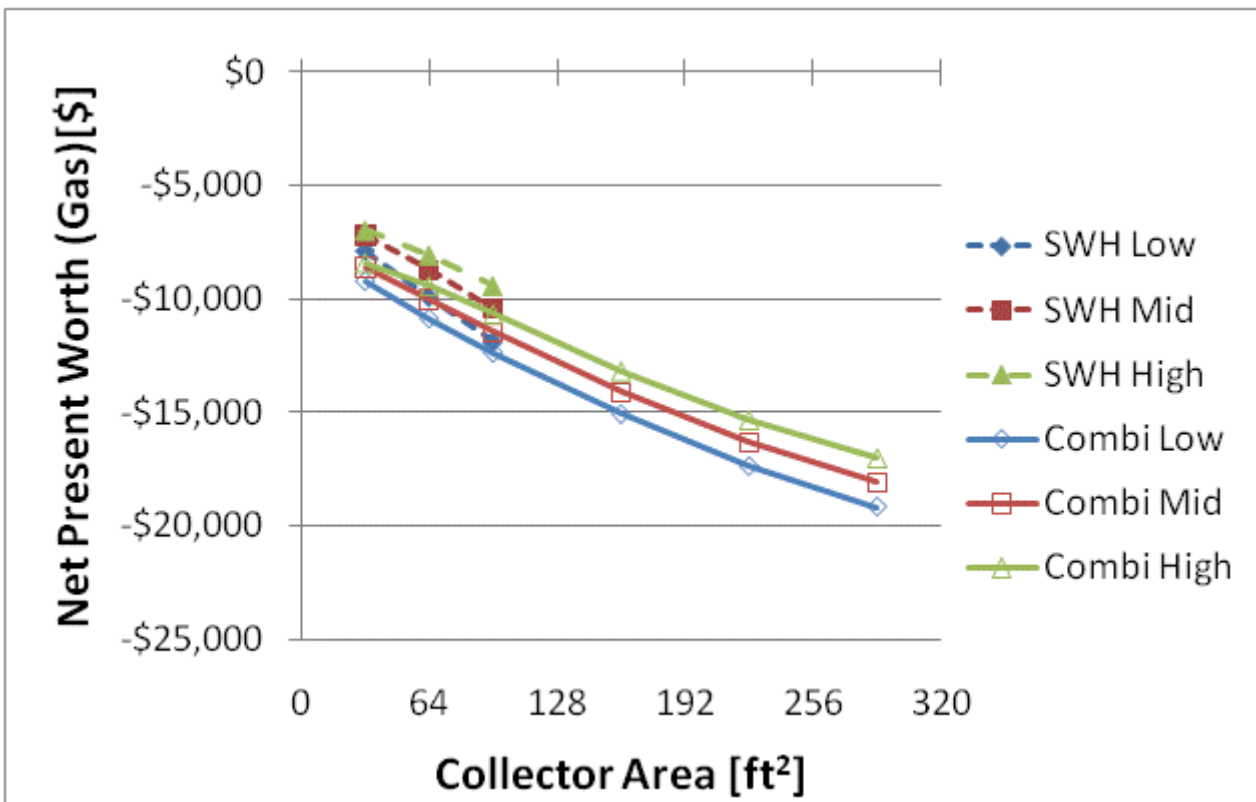
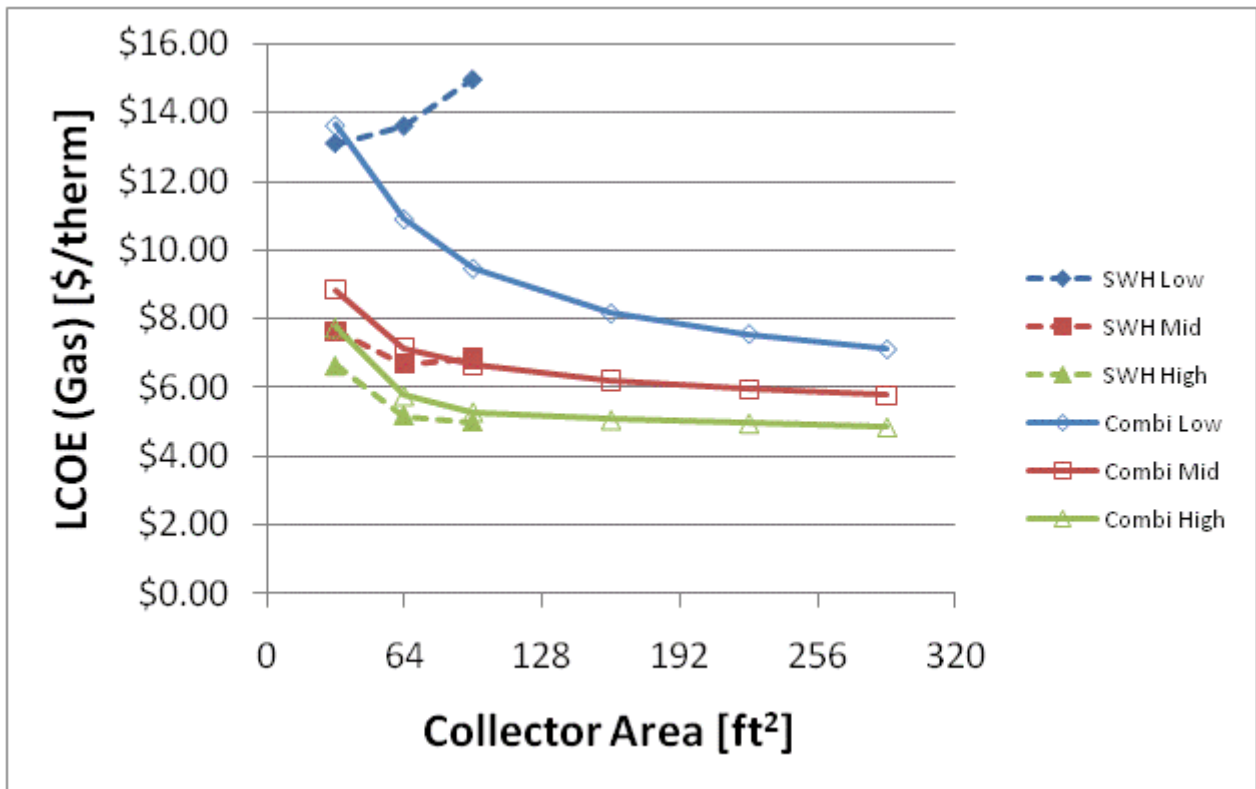


Figure F.83: LCOE and NPW for gas systems for a IECC 2009 House(Boston)

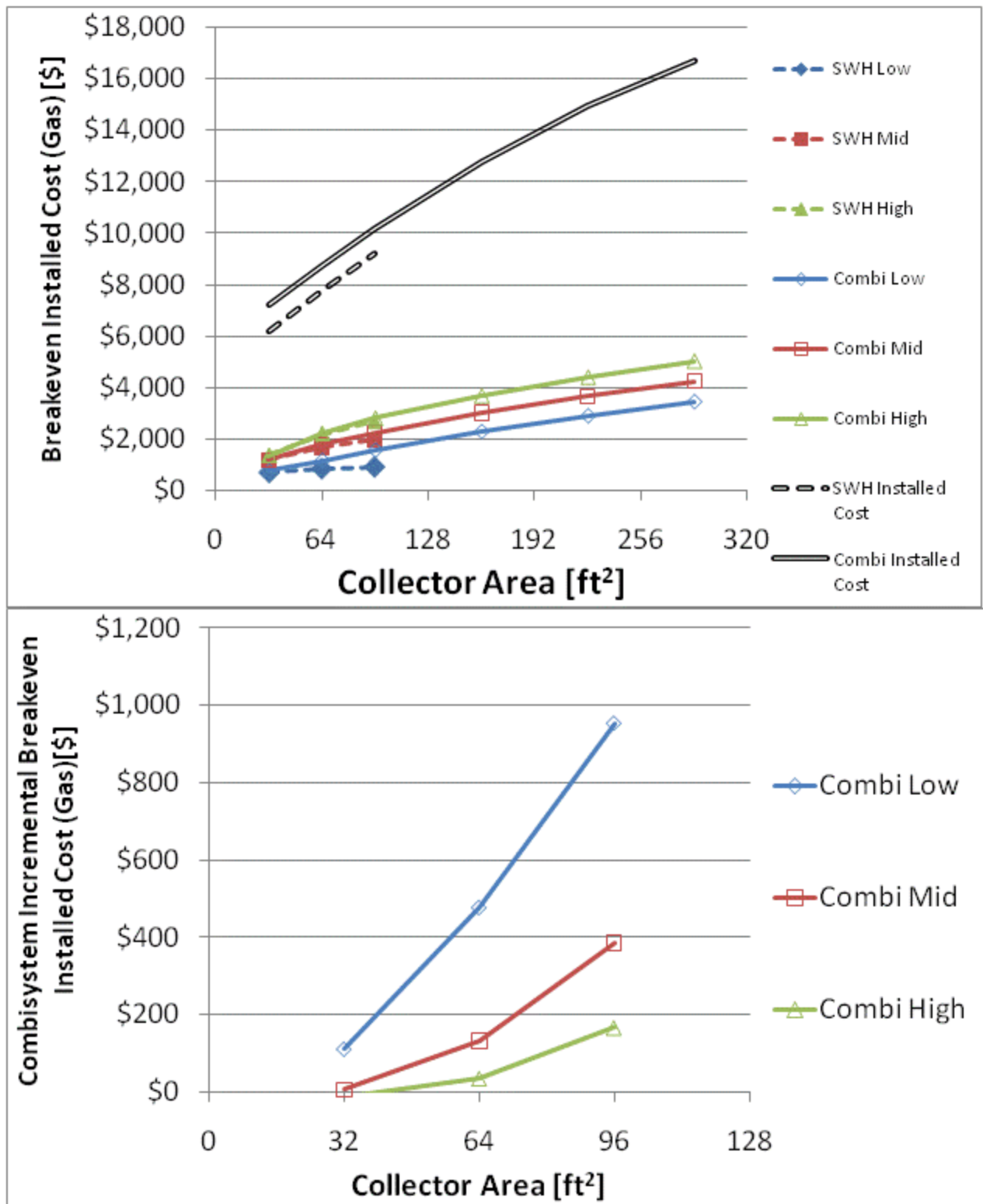


Figure F.84: Breakeven installed cost and combisystem incremental breakeven cost for gas systems for a

IECC 2009 House(Boston)

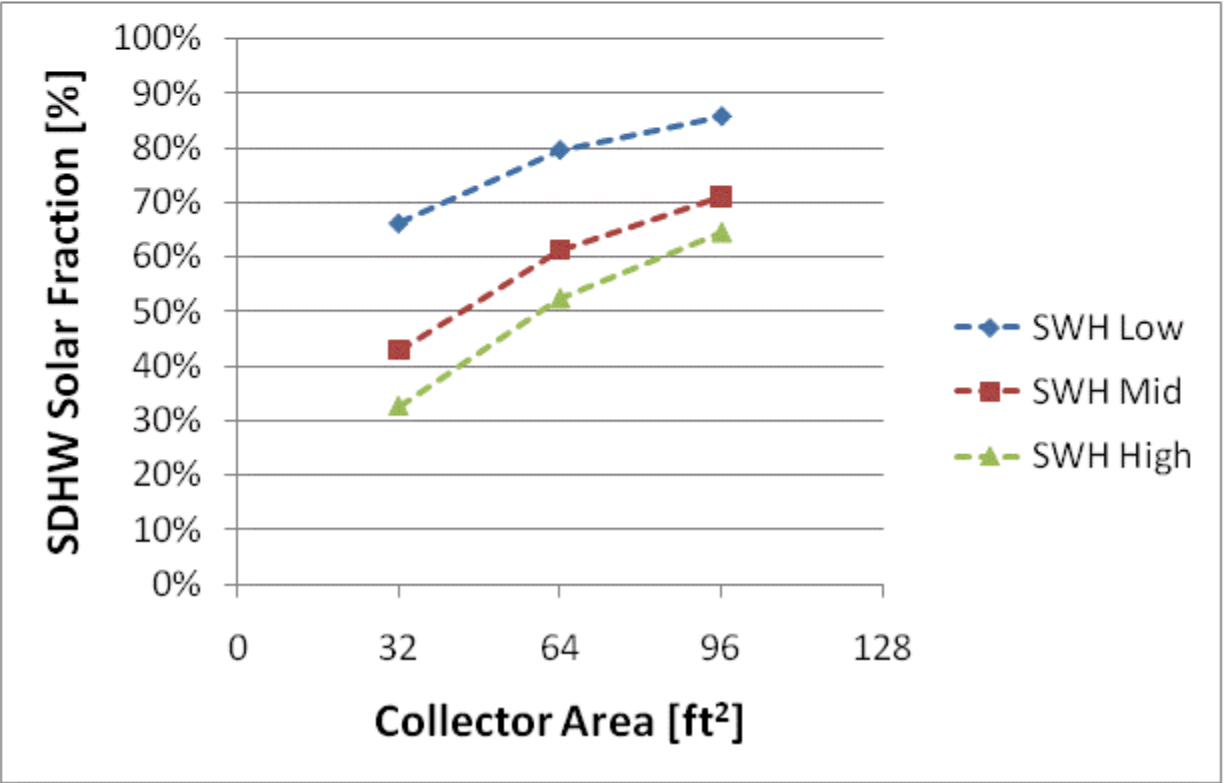
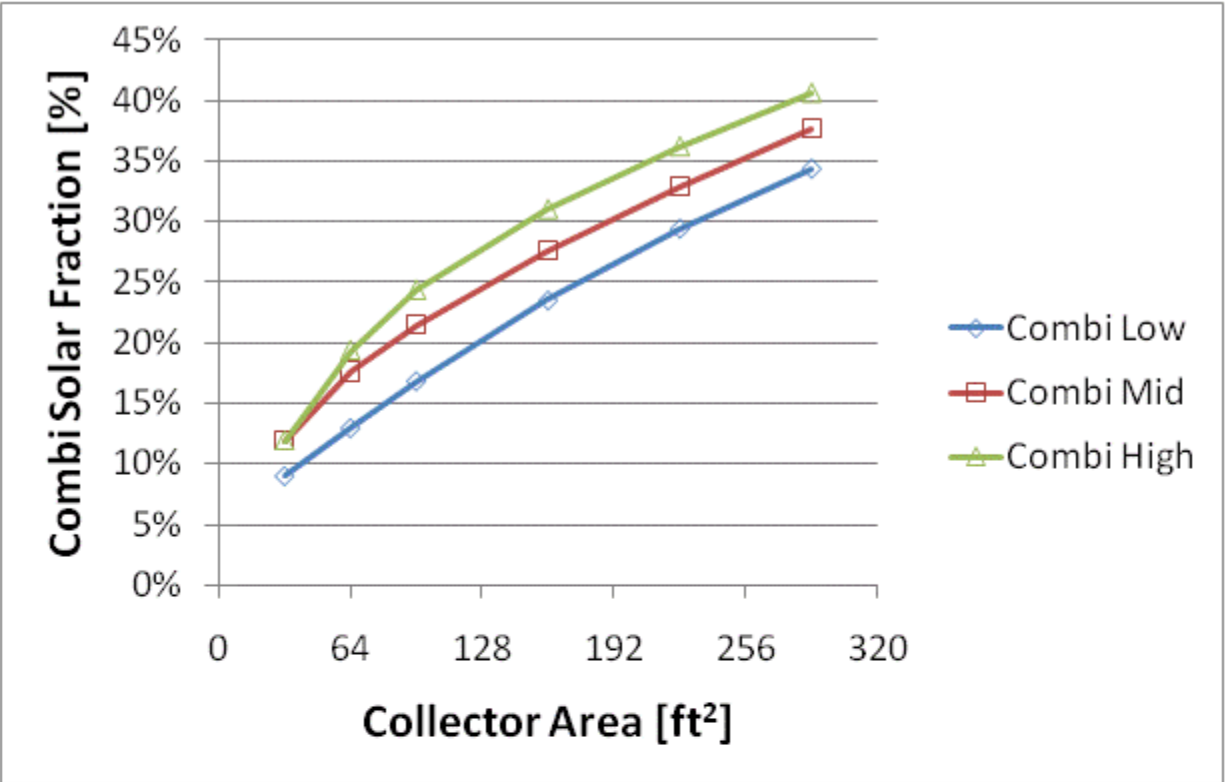


Figure F.85: Combisystem and SWH solar fraction for a BA 50% House(Boston)

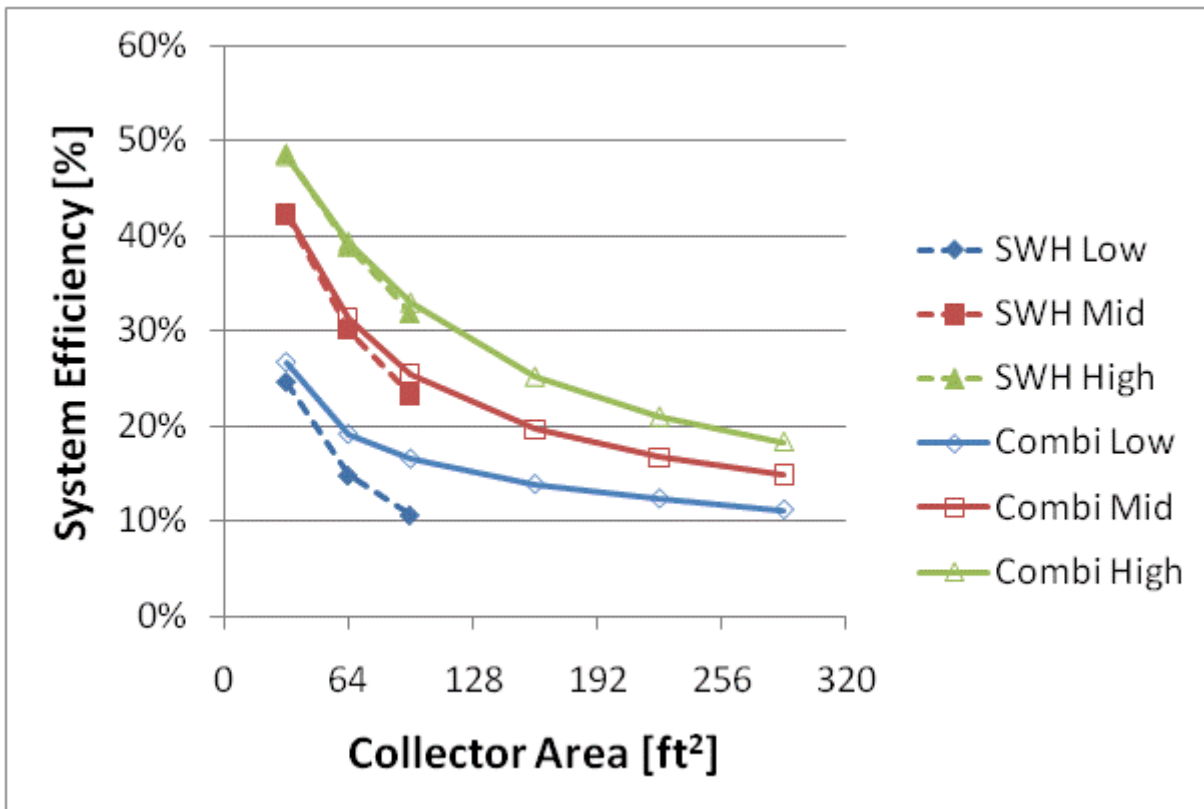
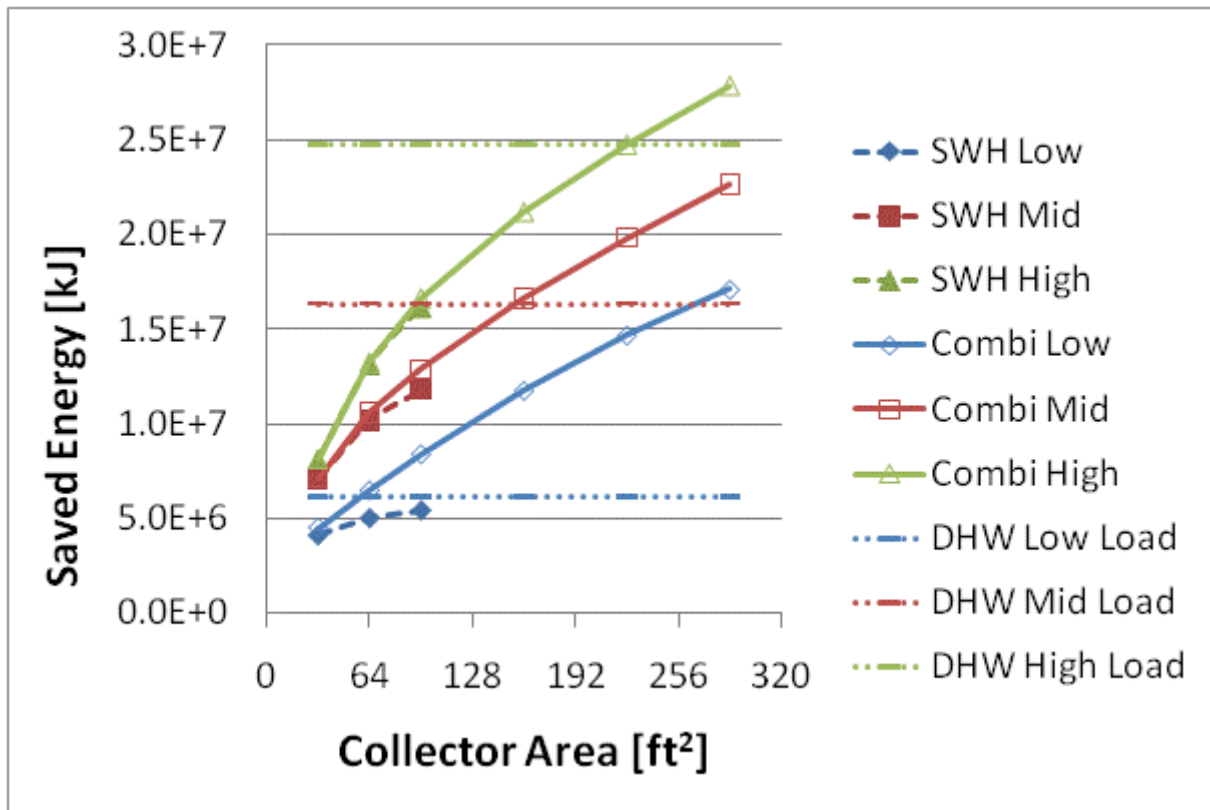


Figure F.86: Annual saved energy and system efficiency for a BA 50% House (Boston)

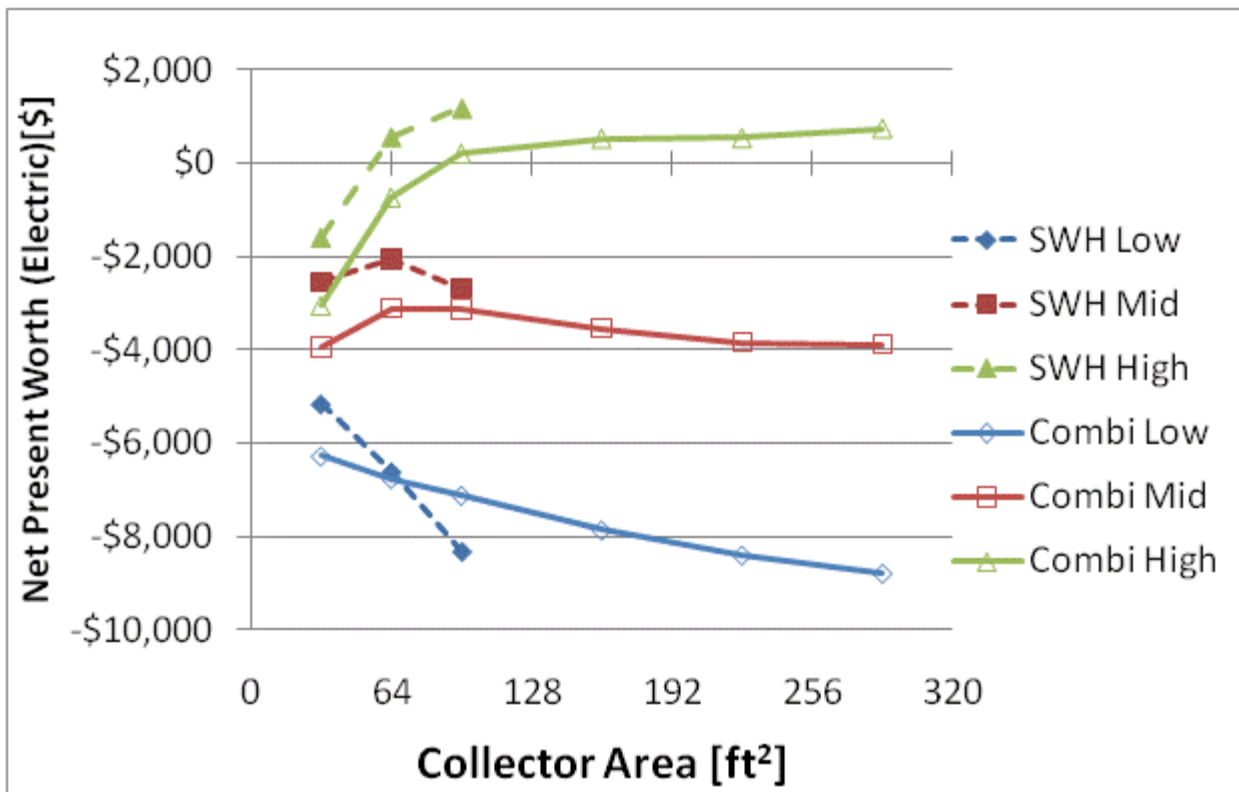
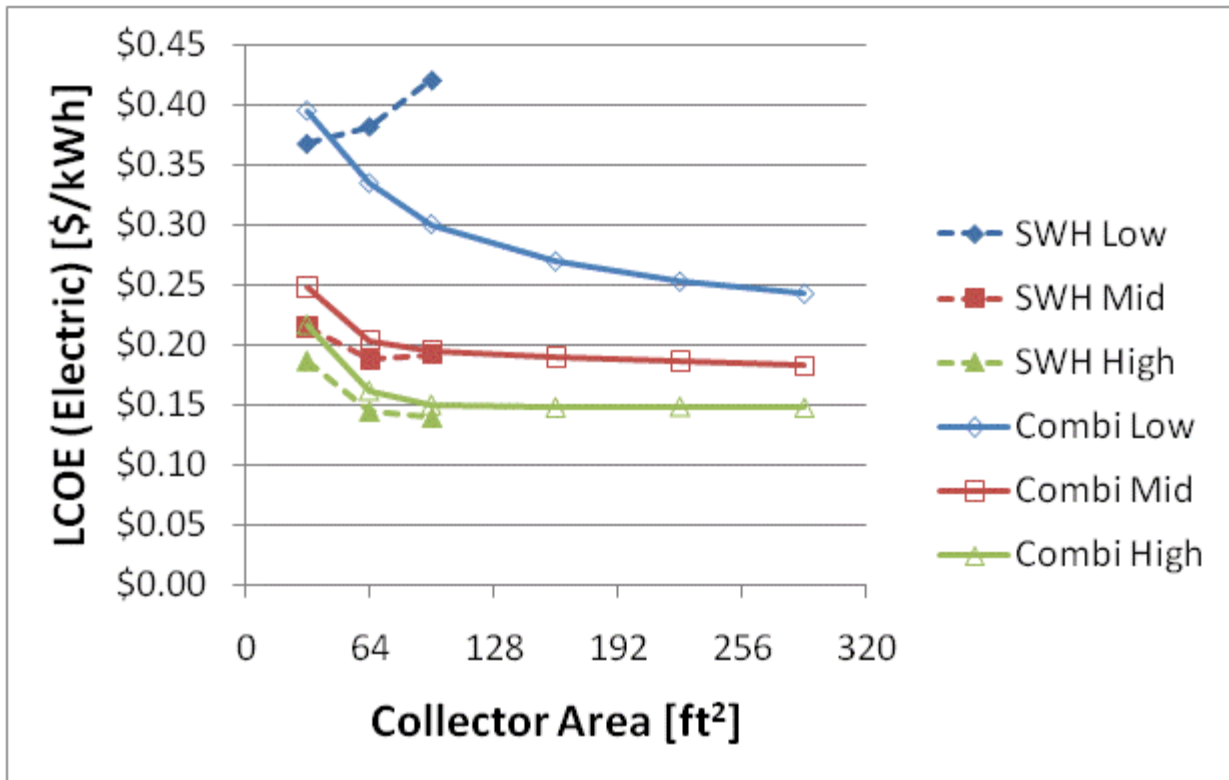


Figure F.87: LCOE and NPW for electric systems for a BA 50% House(Boston)

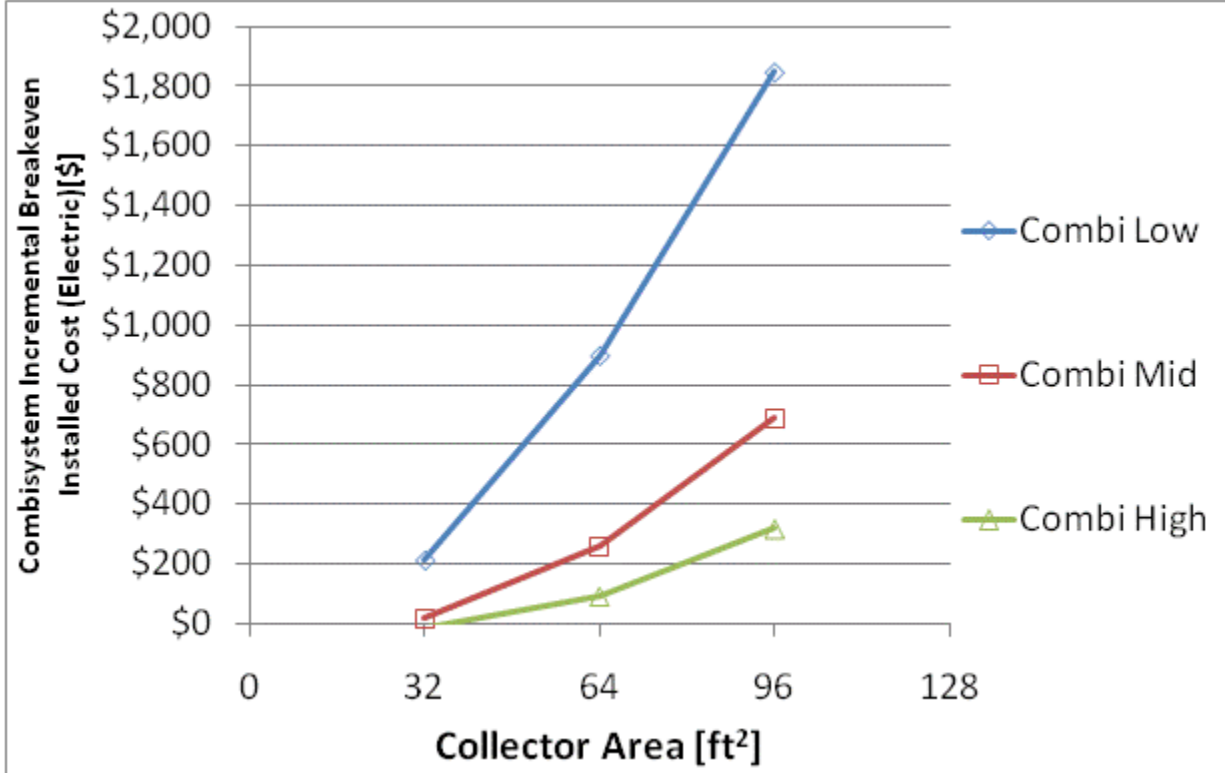
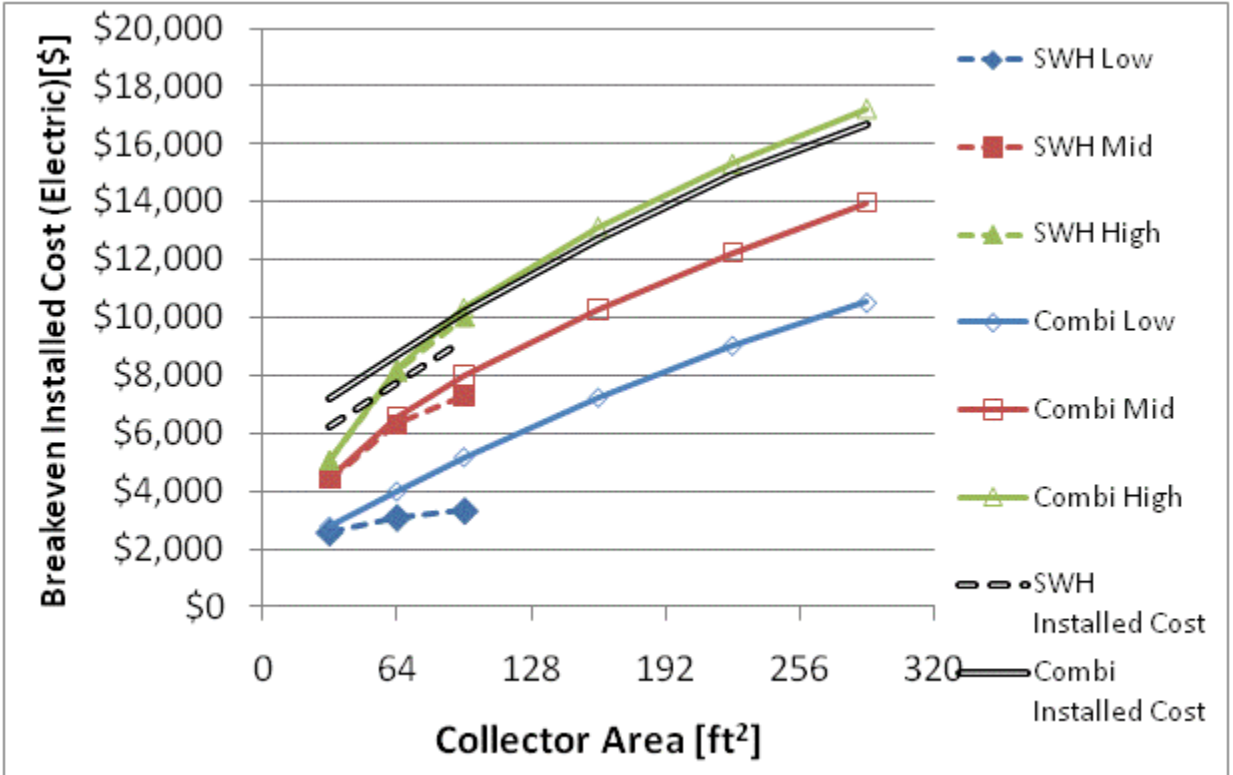


Figure F.88: Breakeven installed cost and combisystem incremental breakeven cost for electric system for a BA 50% House(Boston)

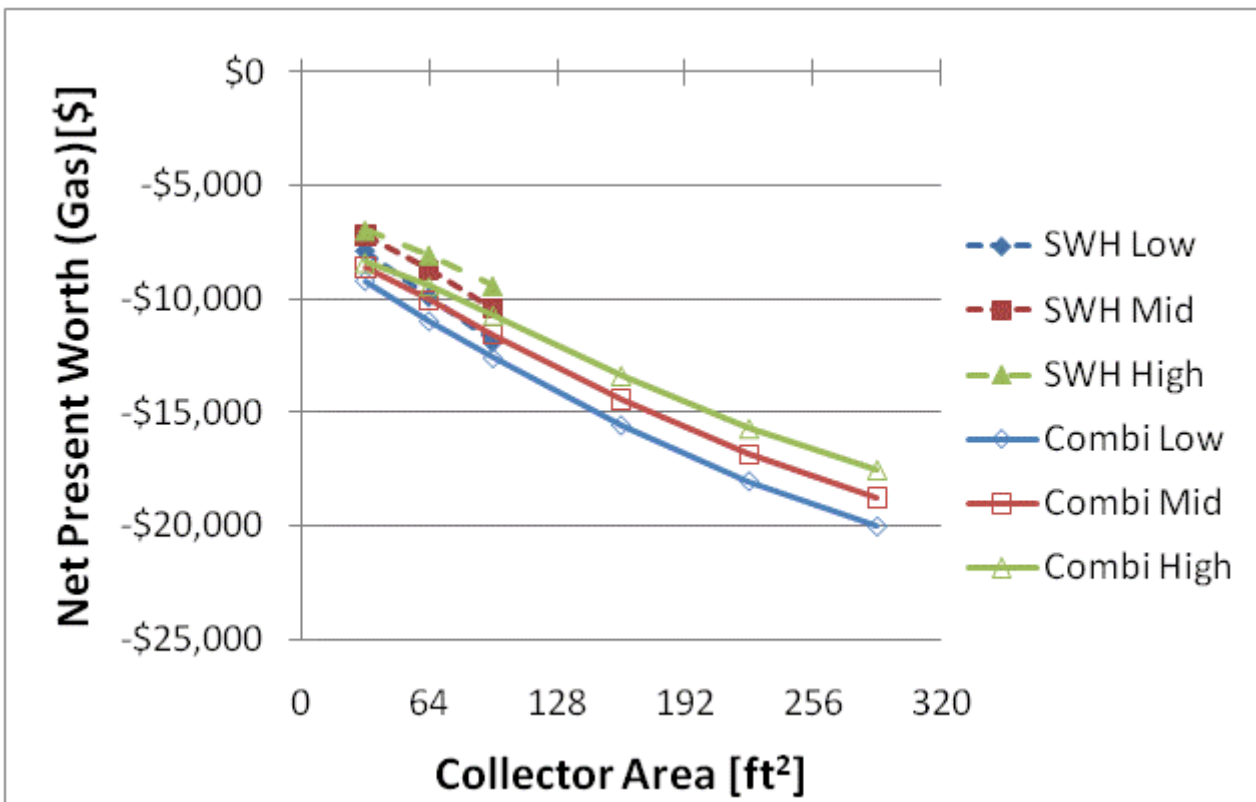
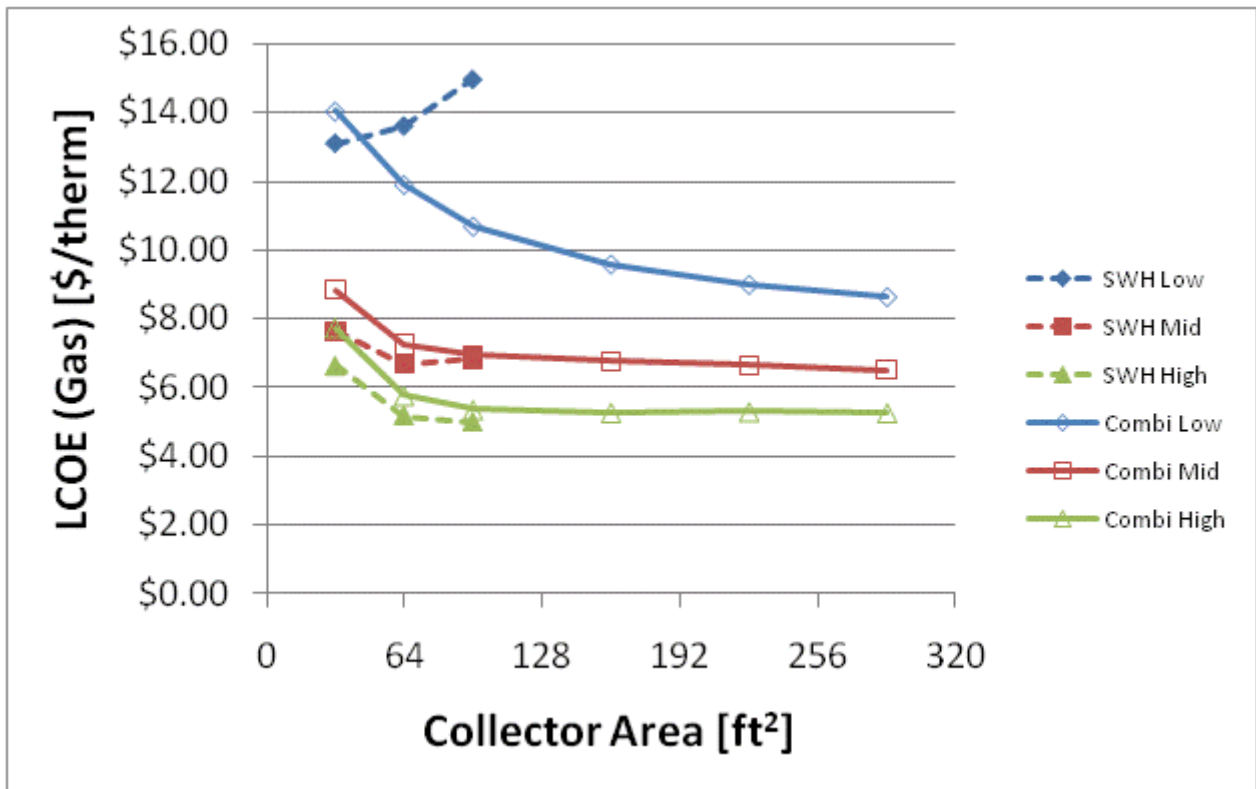


Figure F.89: LCOE and NPW for gas systems for a BA 50% House(Boston)

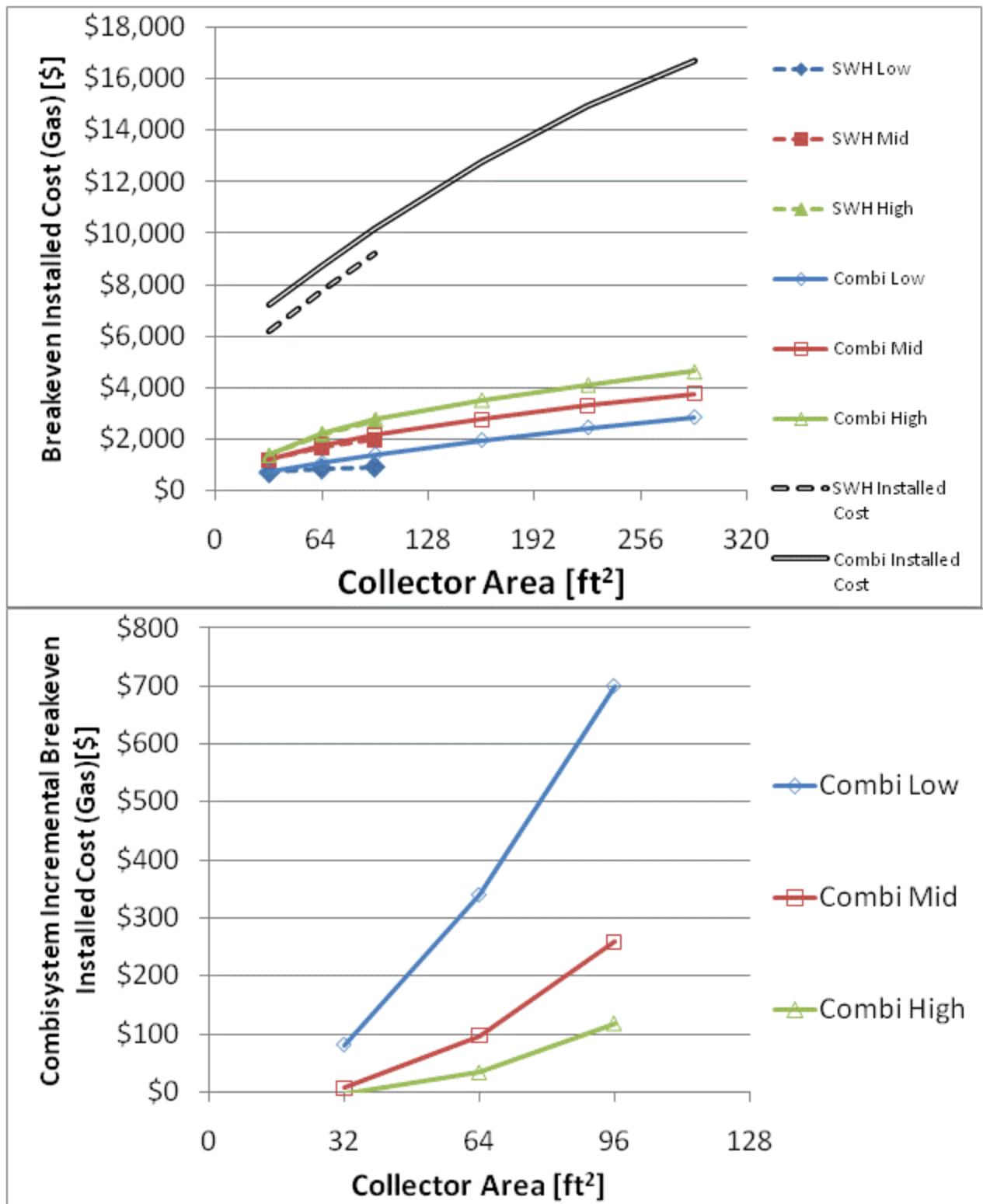


Figure F.90: Breakeven installed cost and combisystem incremental breakeven cost for gas systems for a

BA 50% House(Boston)

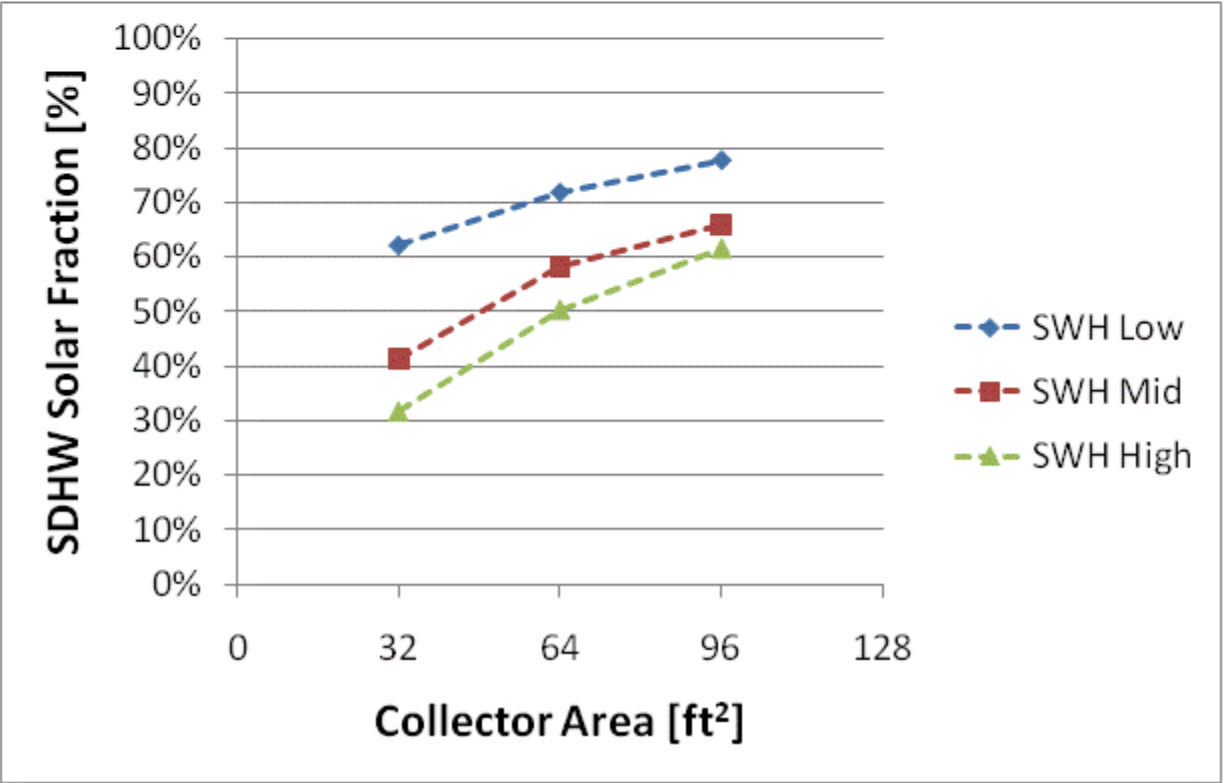
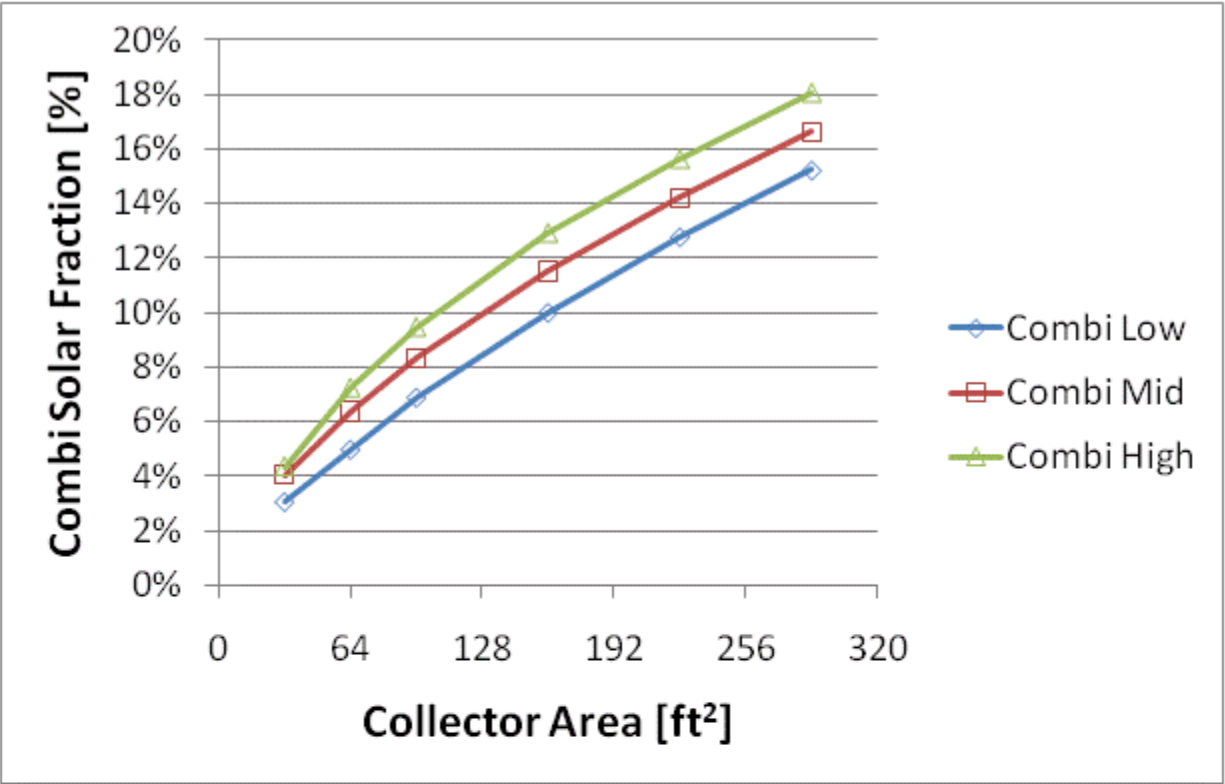


Figure F.91: Combisystem and SWH solar fraction for a 1960s Retrofit House(Chicago)

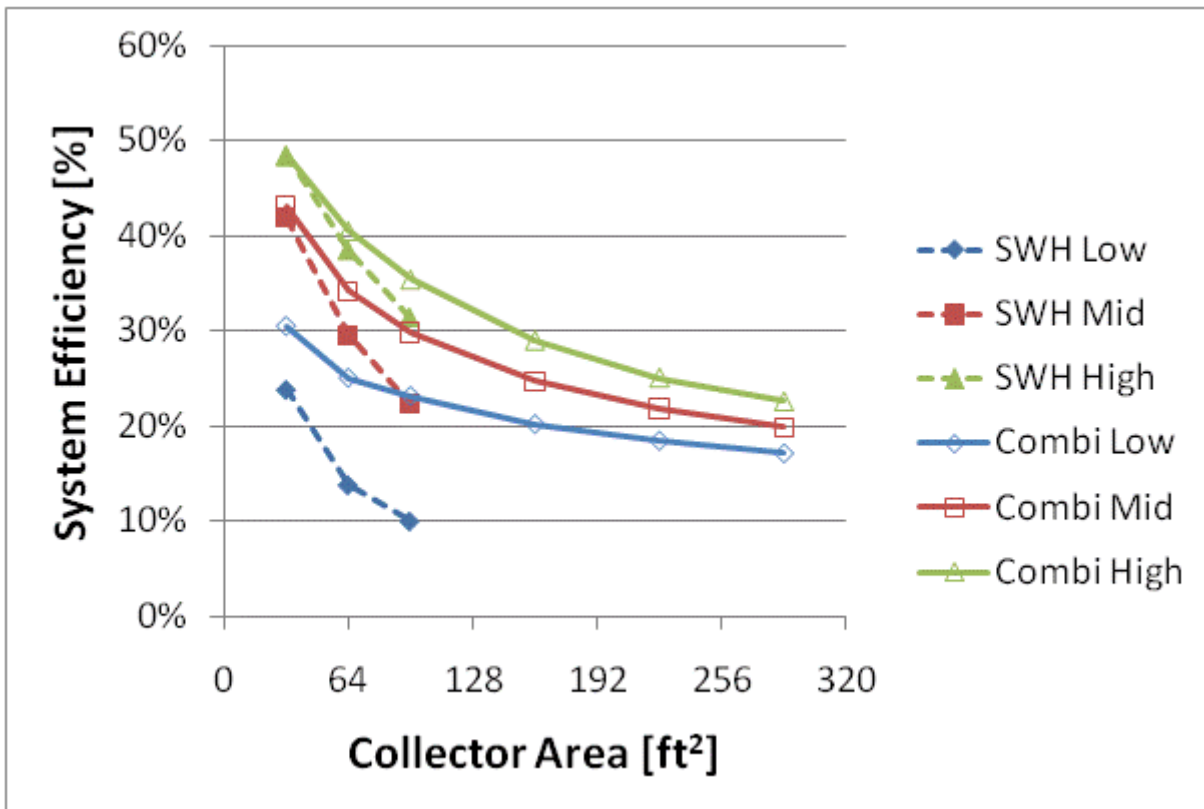
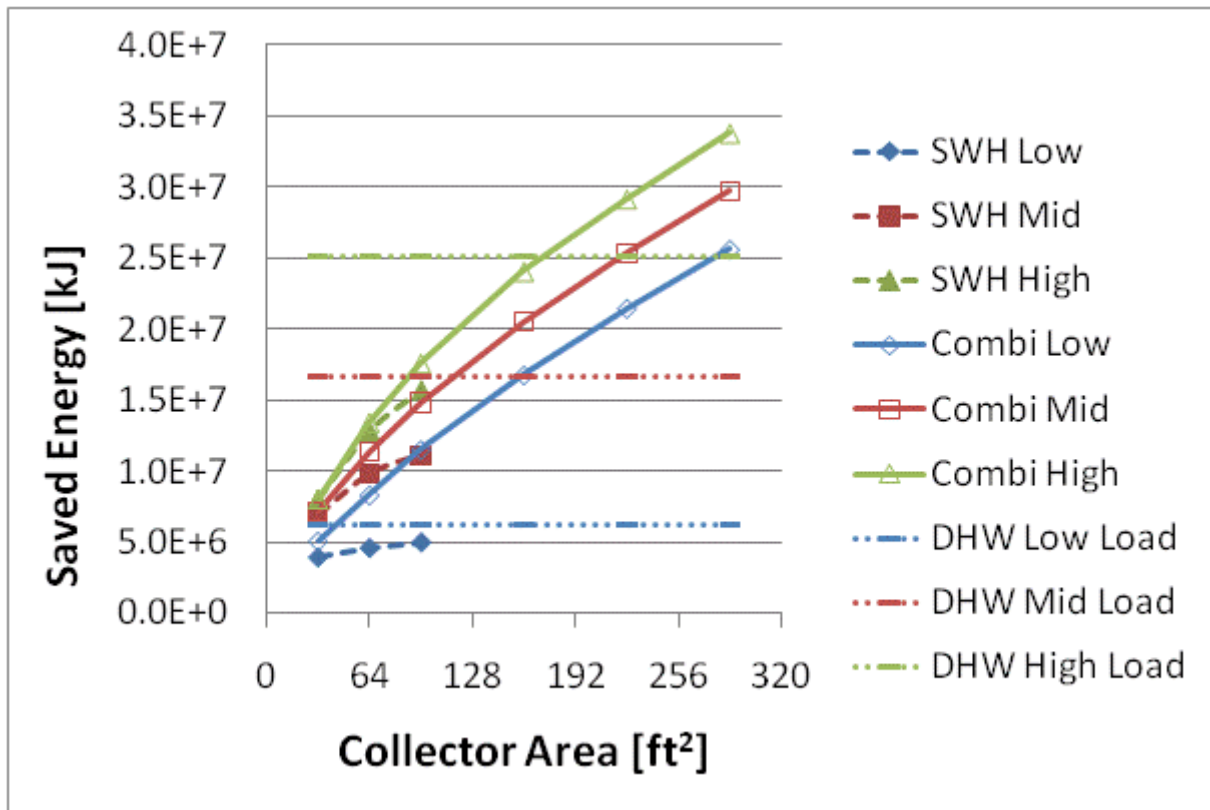


Figure F.92: Annual saved energy and system efficiency for a 1960s Retrofit House(Chicago)

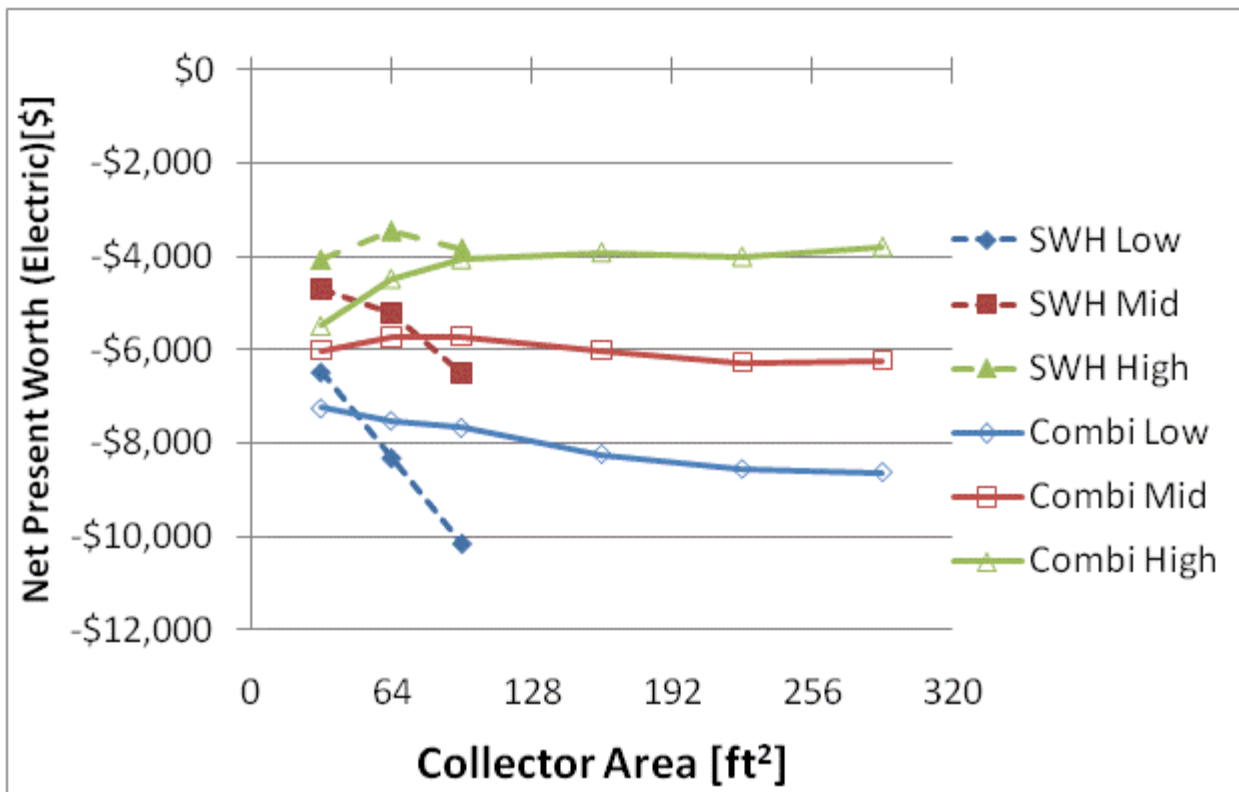
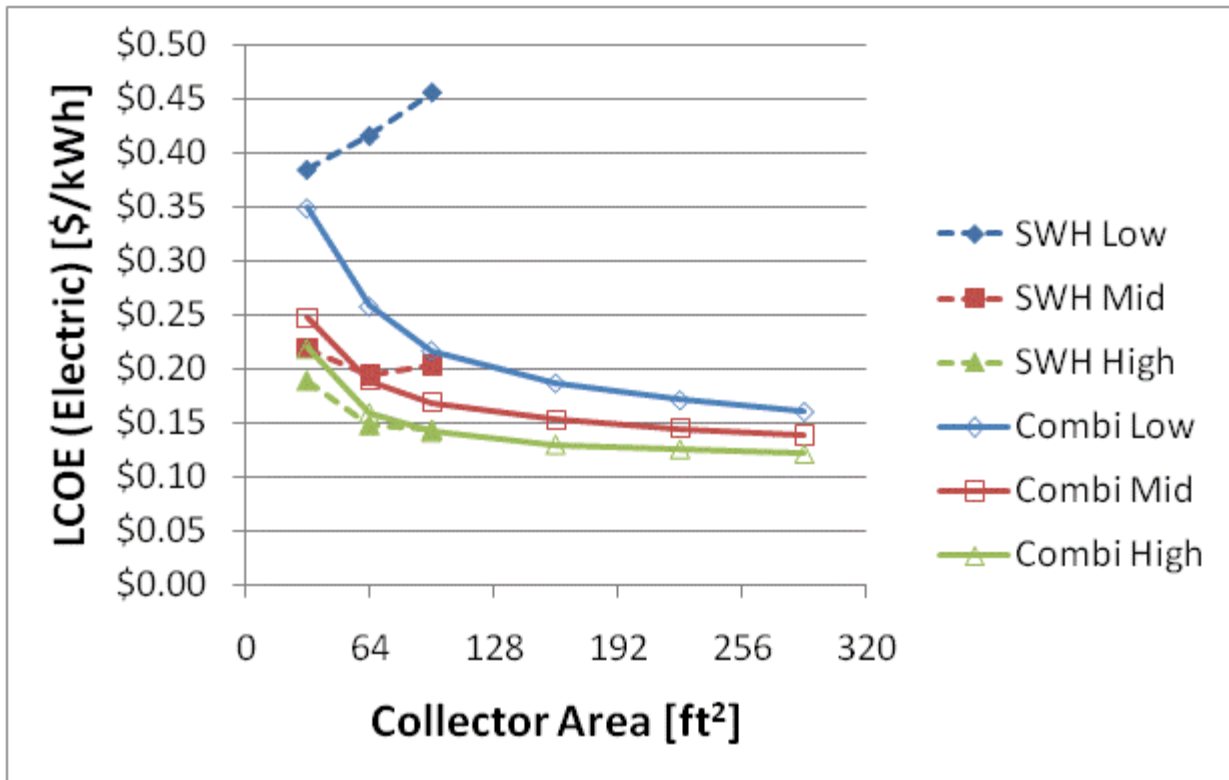


Figure F.93: LCOE and NPW for electric systems for a 1960s Retrofit House(Chicago)

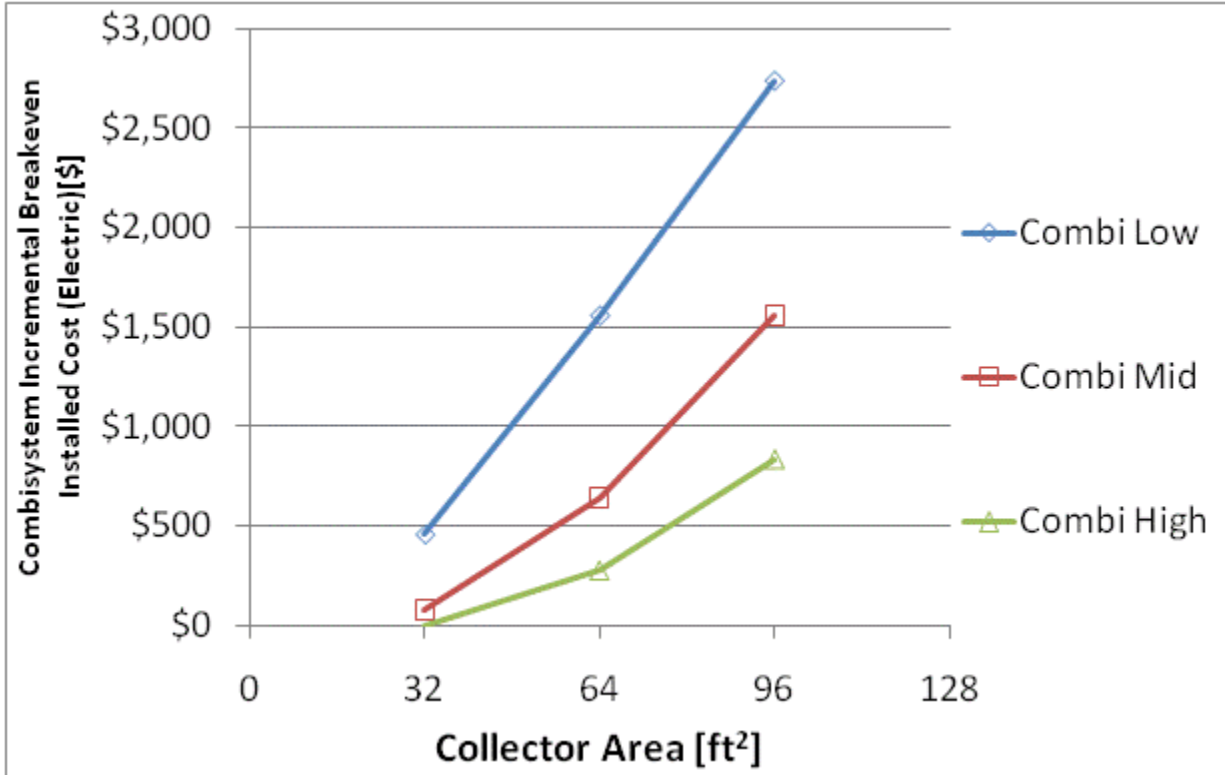
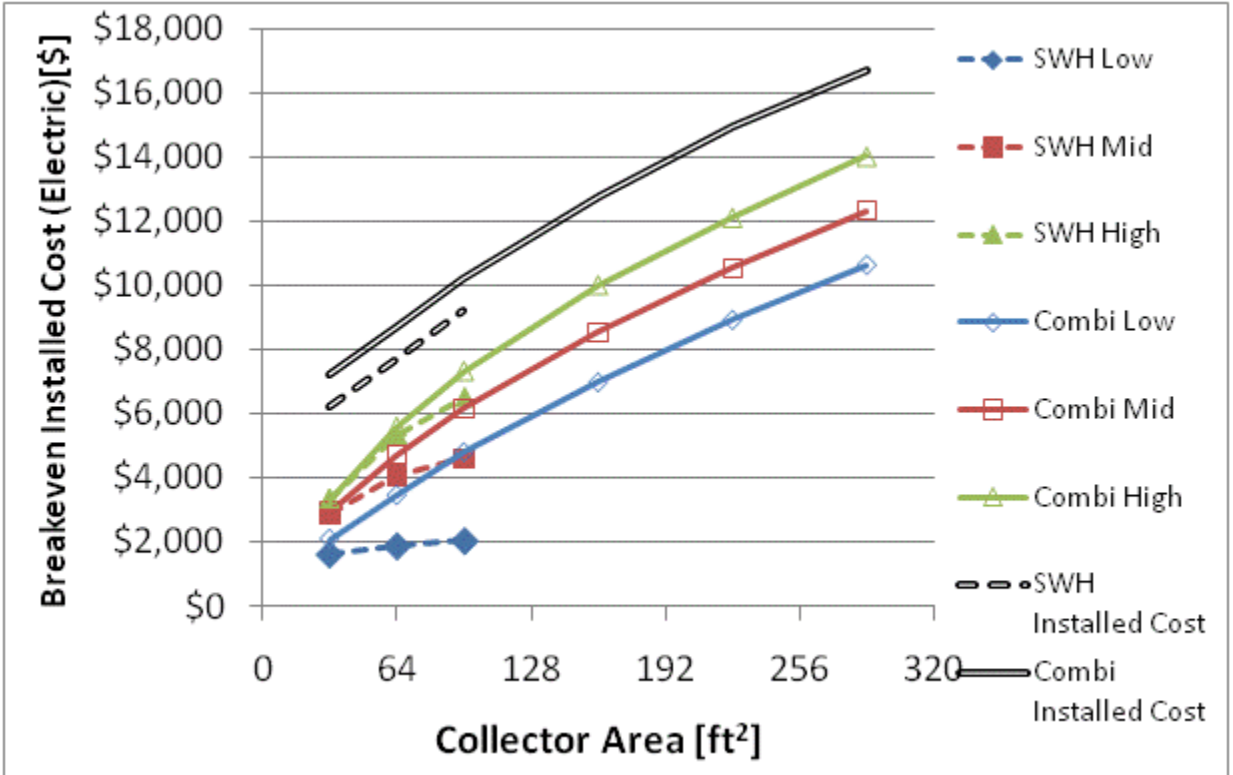


Figure F.94: Breakeven installed cost and combisystem incremental breakeven cost for electric system for a 1960s Retrofit House(Chicago)

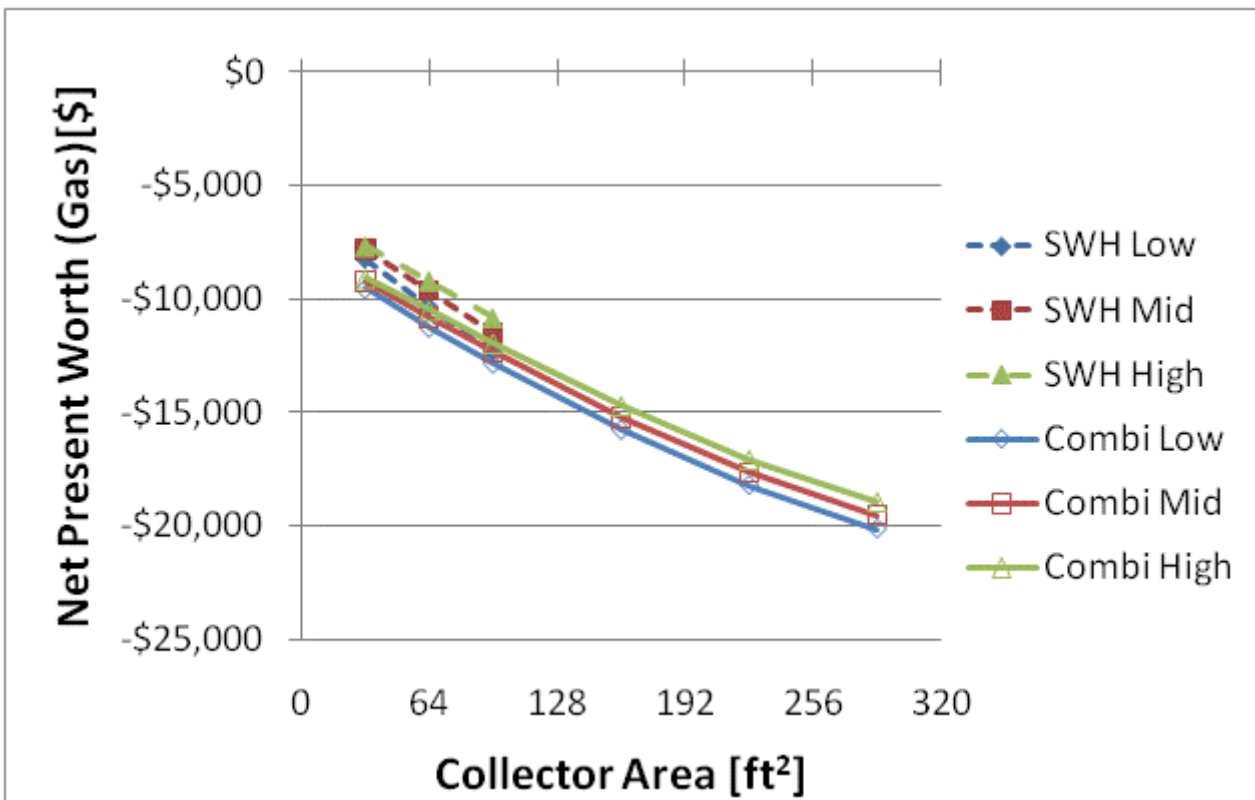
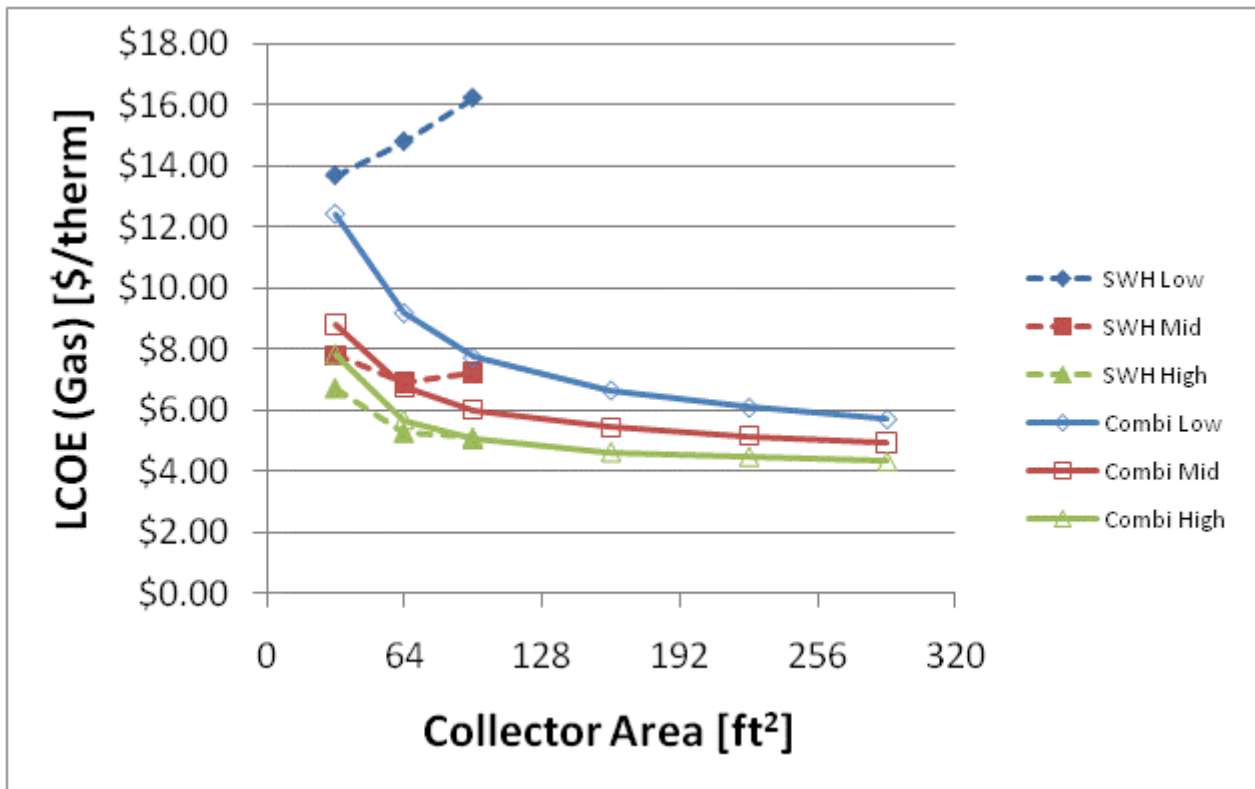


Figure F.95: LCOE and NPW for gas systems for a 1960s Retrofit House(Chicago)

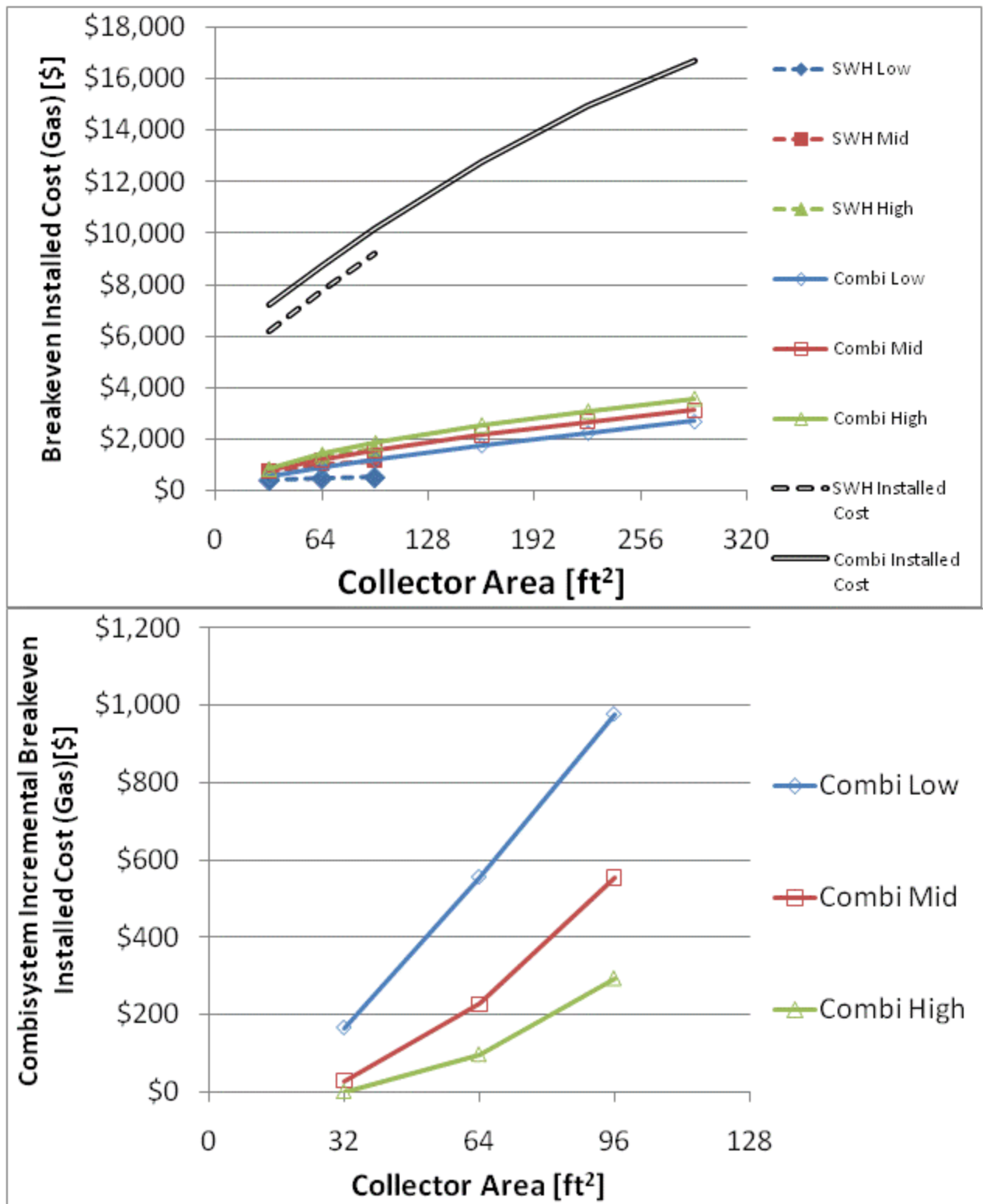


Figure F.96: Breakeven installed cost and combisystem incremental breakeven cost for gas systems for a 1960s Retrofit House(Chicago)

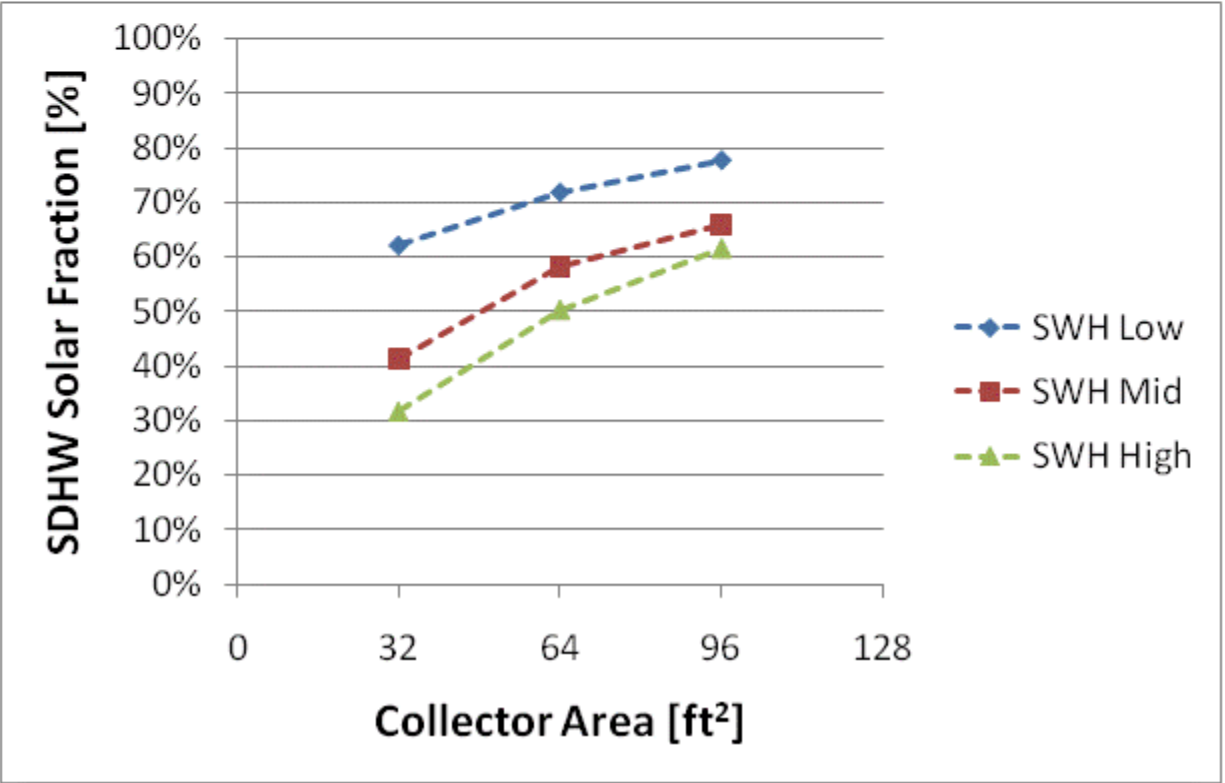
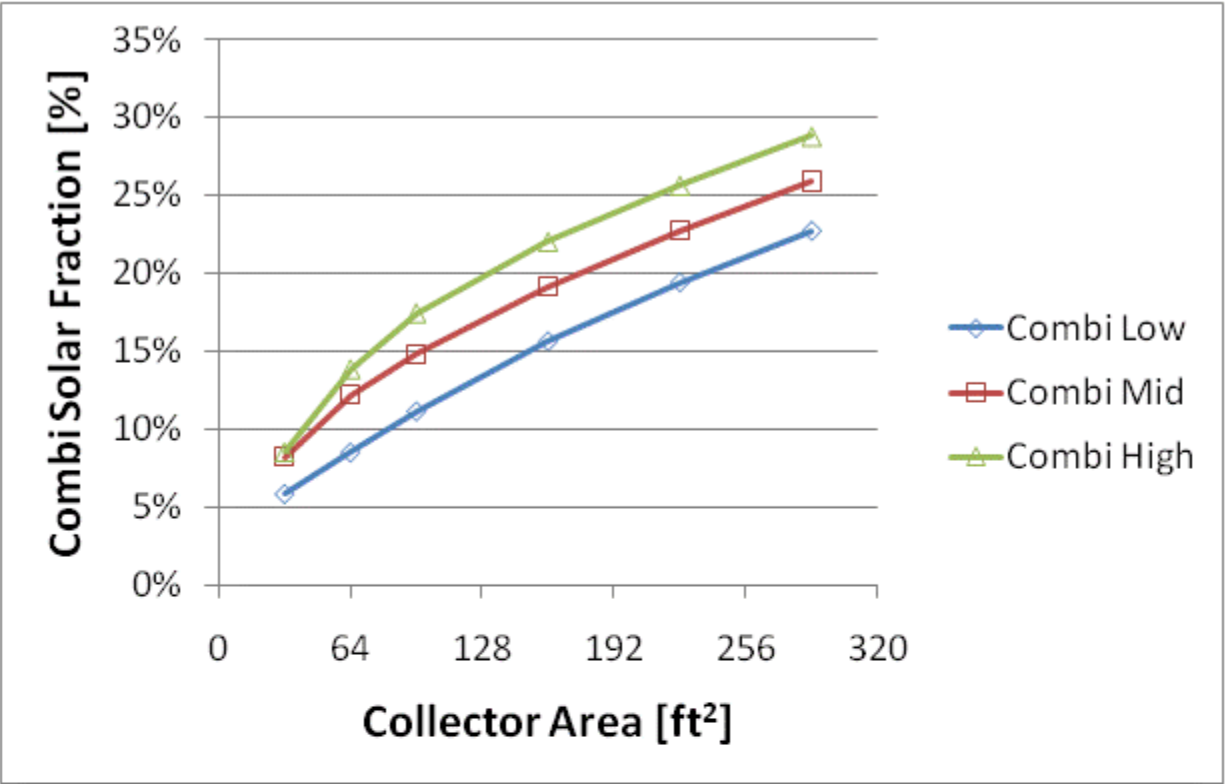


Figure F.97: Combisystem and SWH solar fraction for a IECC 2009 House(Chicago)

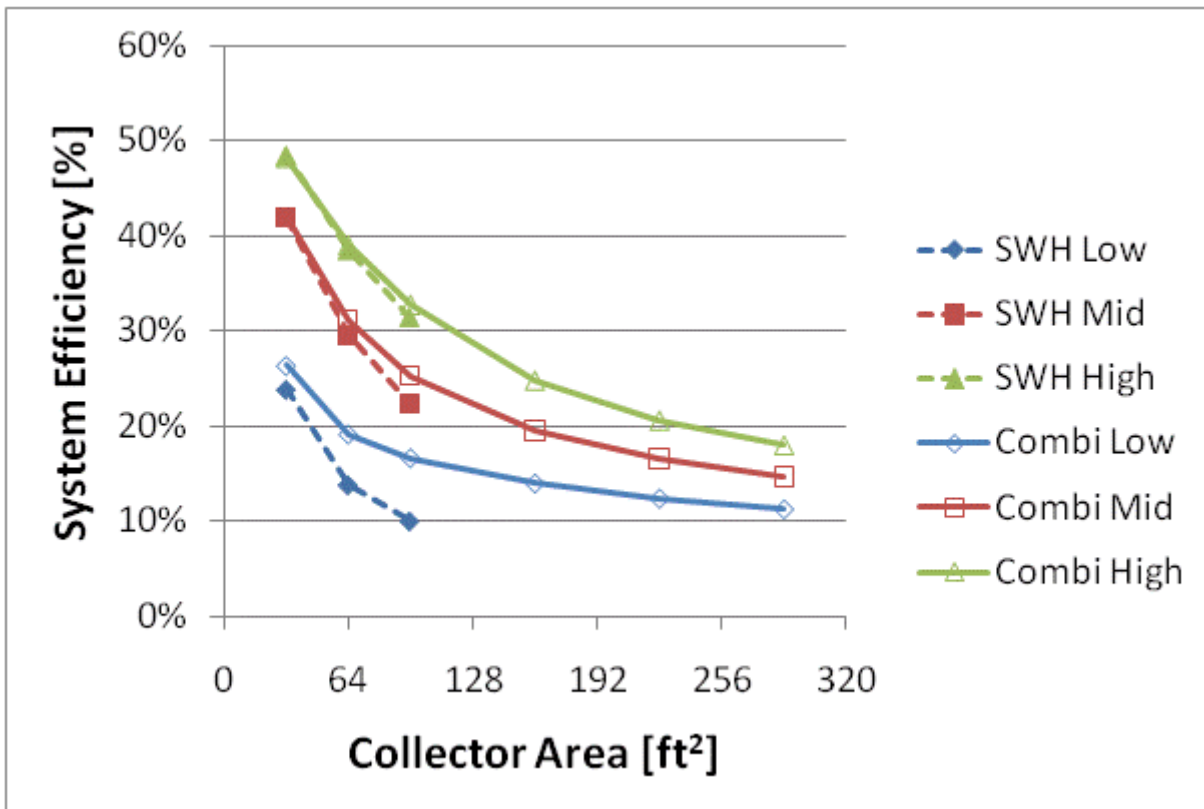
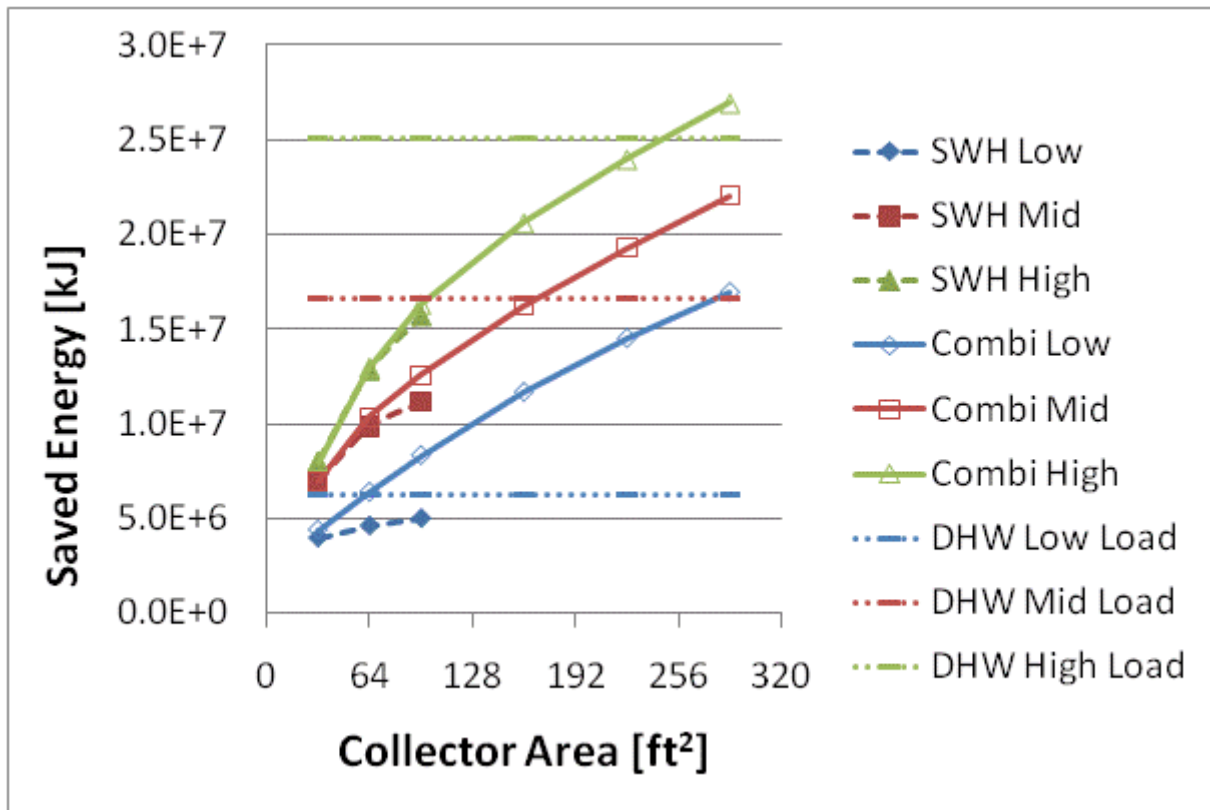


Figure F.98: Annual saved energy and system efficiency for a IECC 2009 House(Chicago)

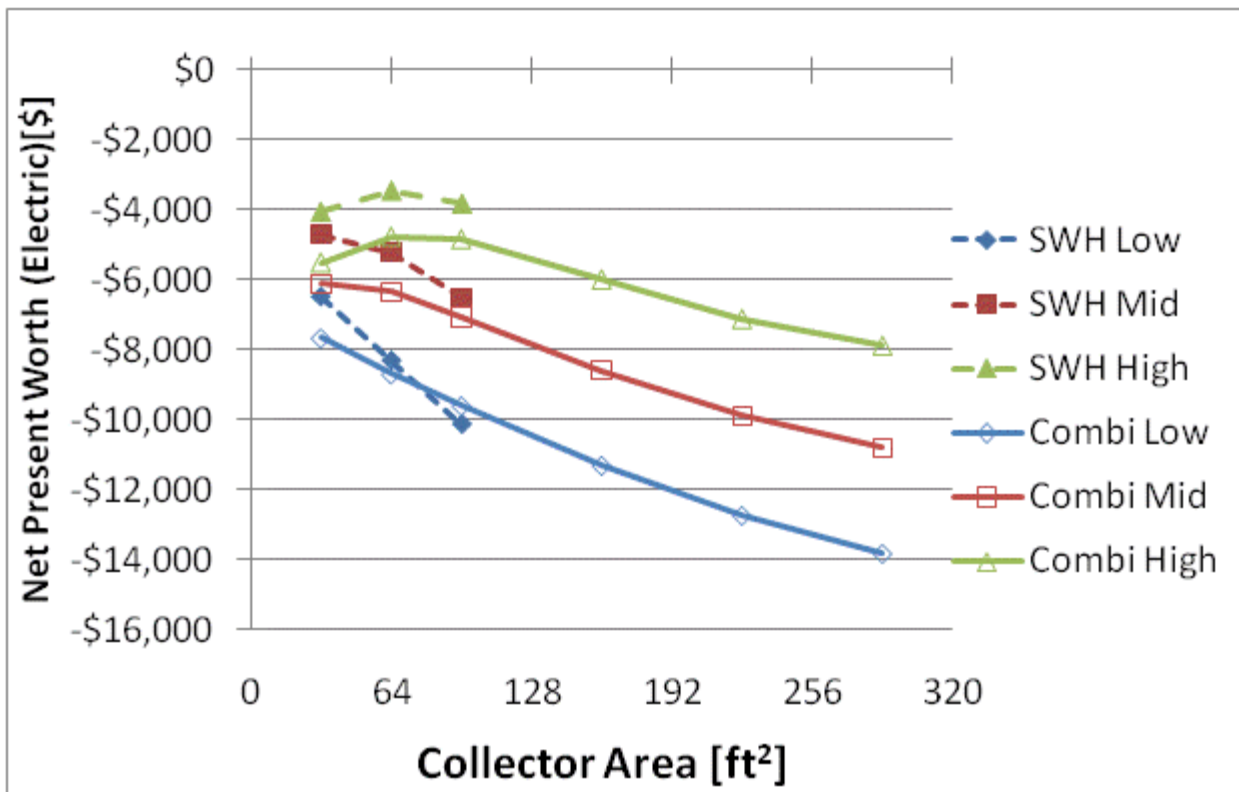
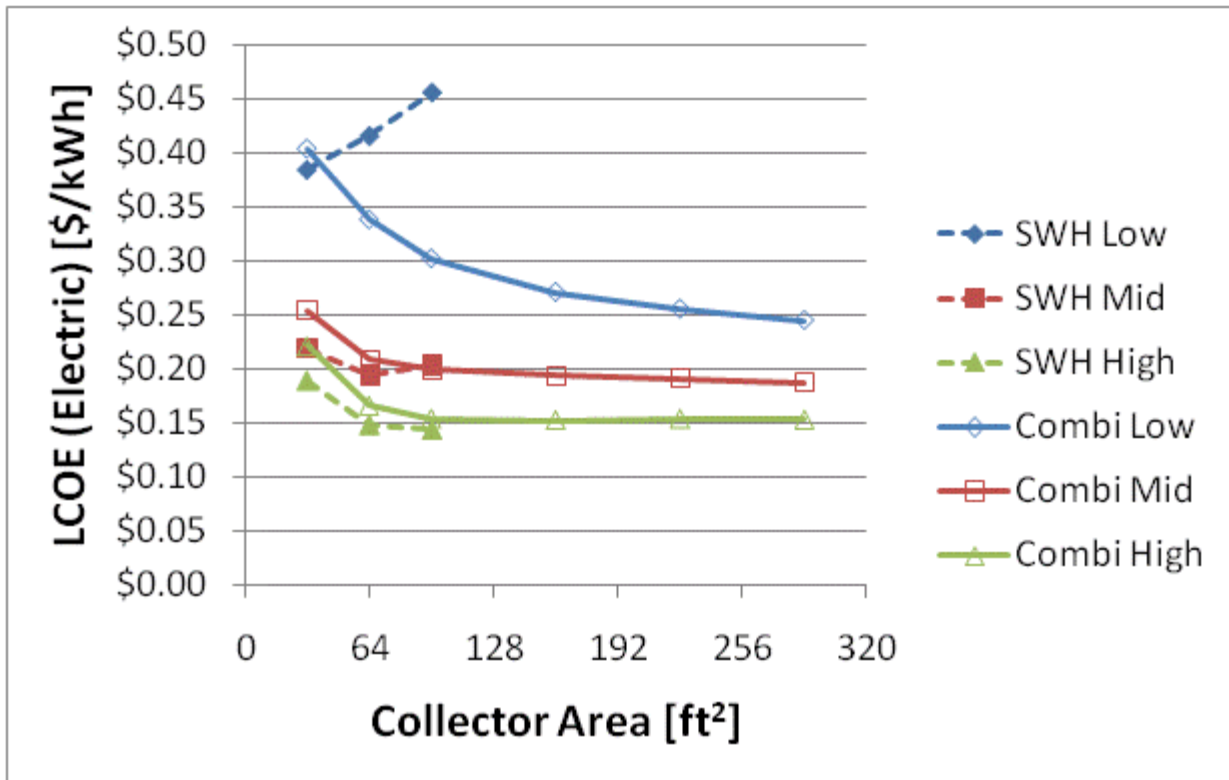


Figure F.99: LCOE and NPW for electric systems for a IECC 2009 House(Chicago)

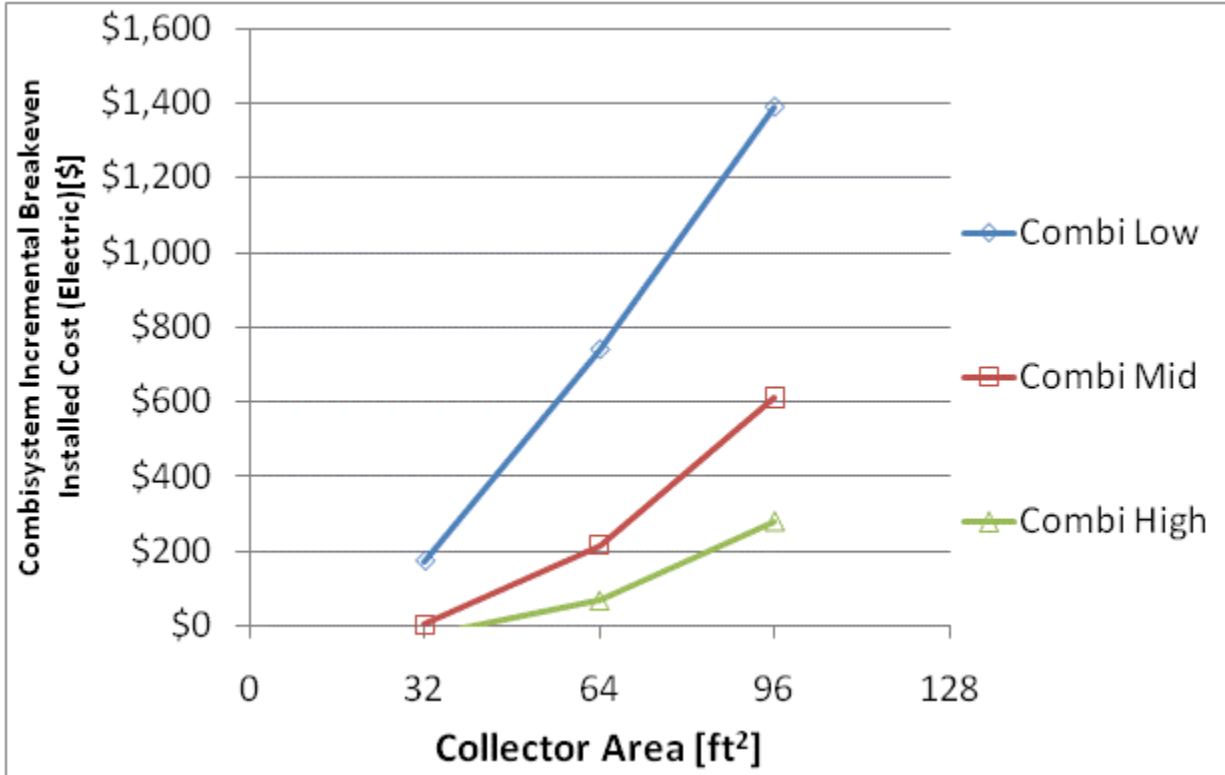
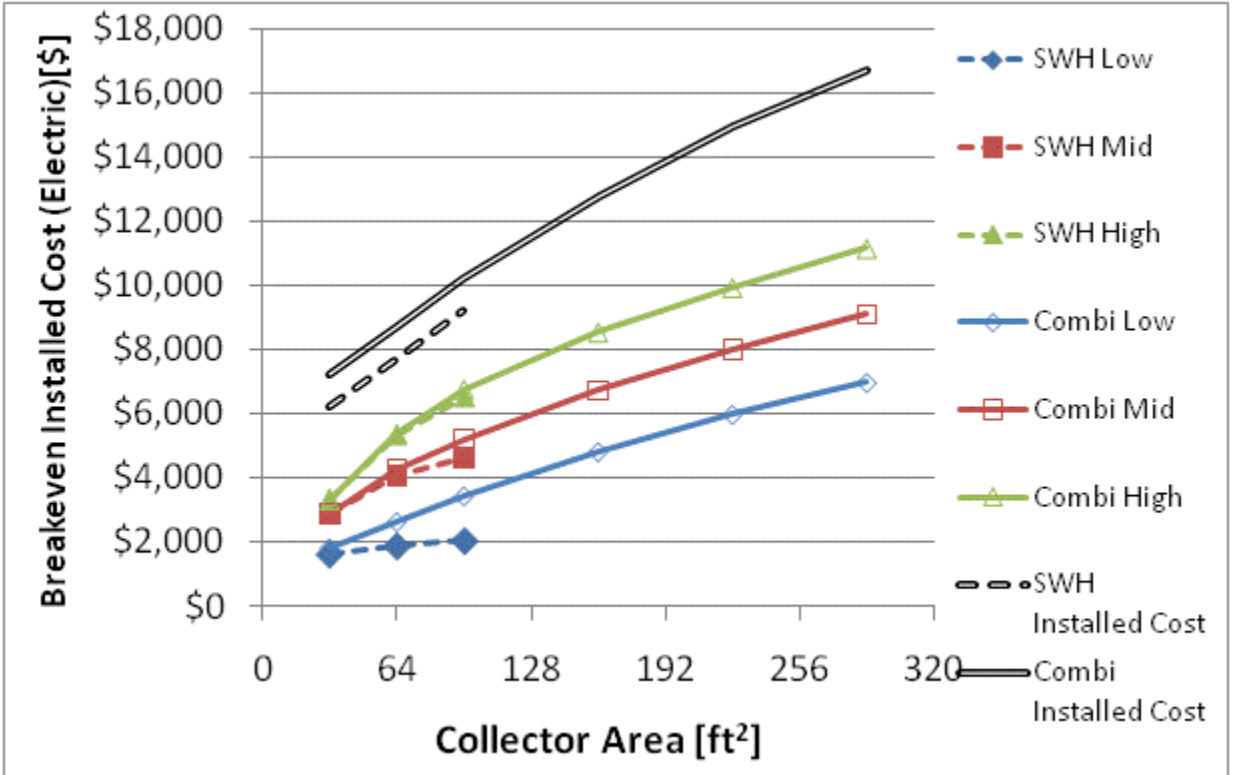


Figure F.100: Breakeven installed cost and combisystem incremental breakeven cost for electric system for a IECC 2009 House(Chicago)

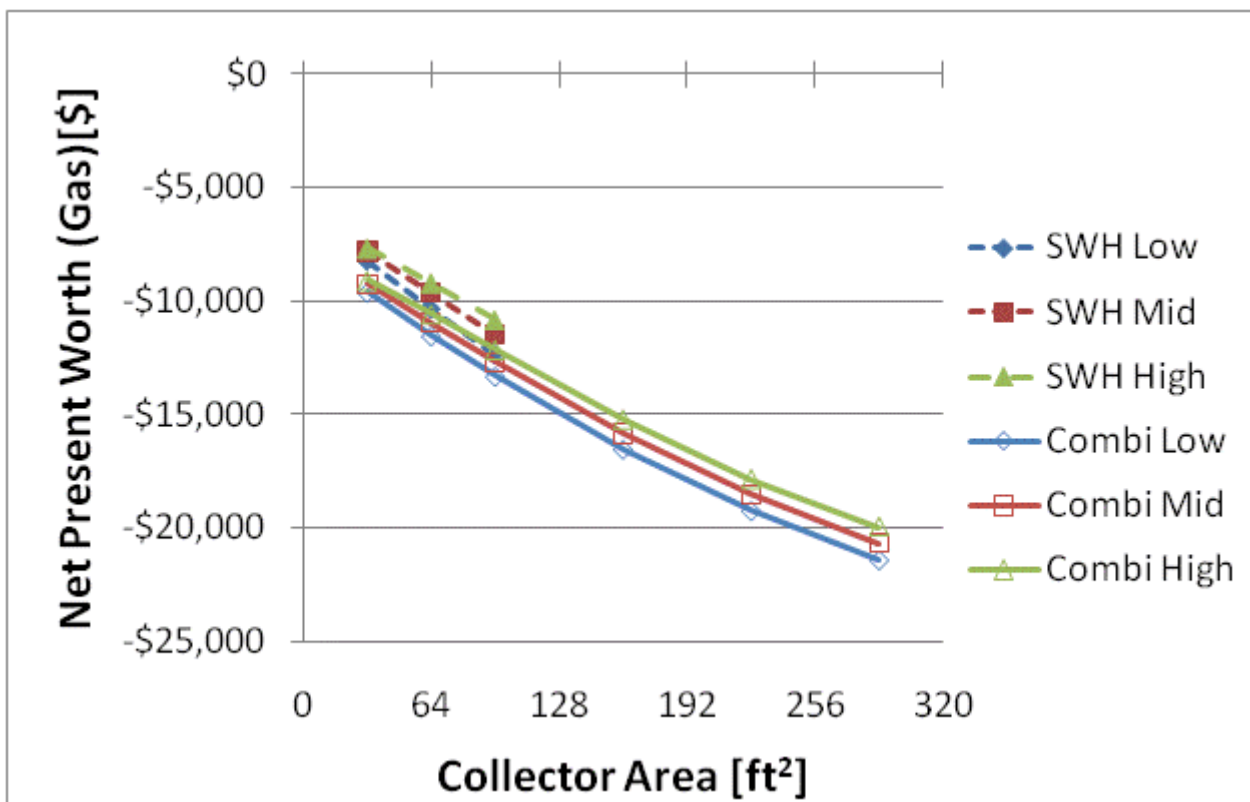
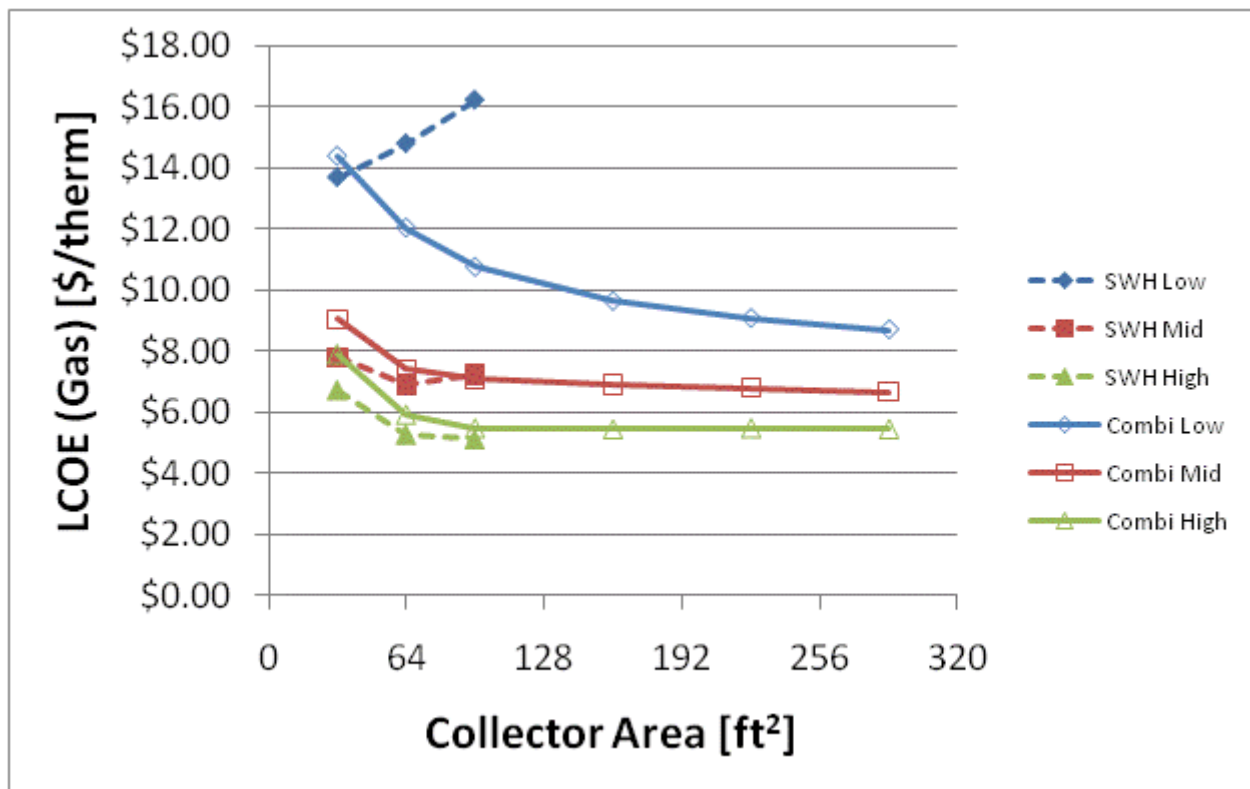


Figure F.101: LCOE and NPW for gas systems for a IECC 2009 House(Chicago)

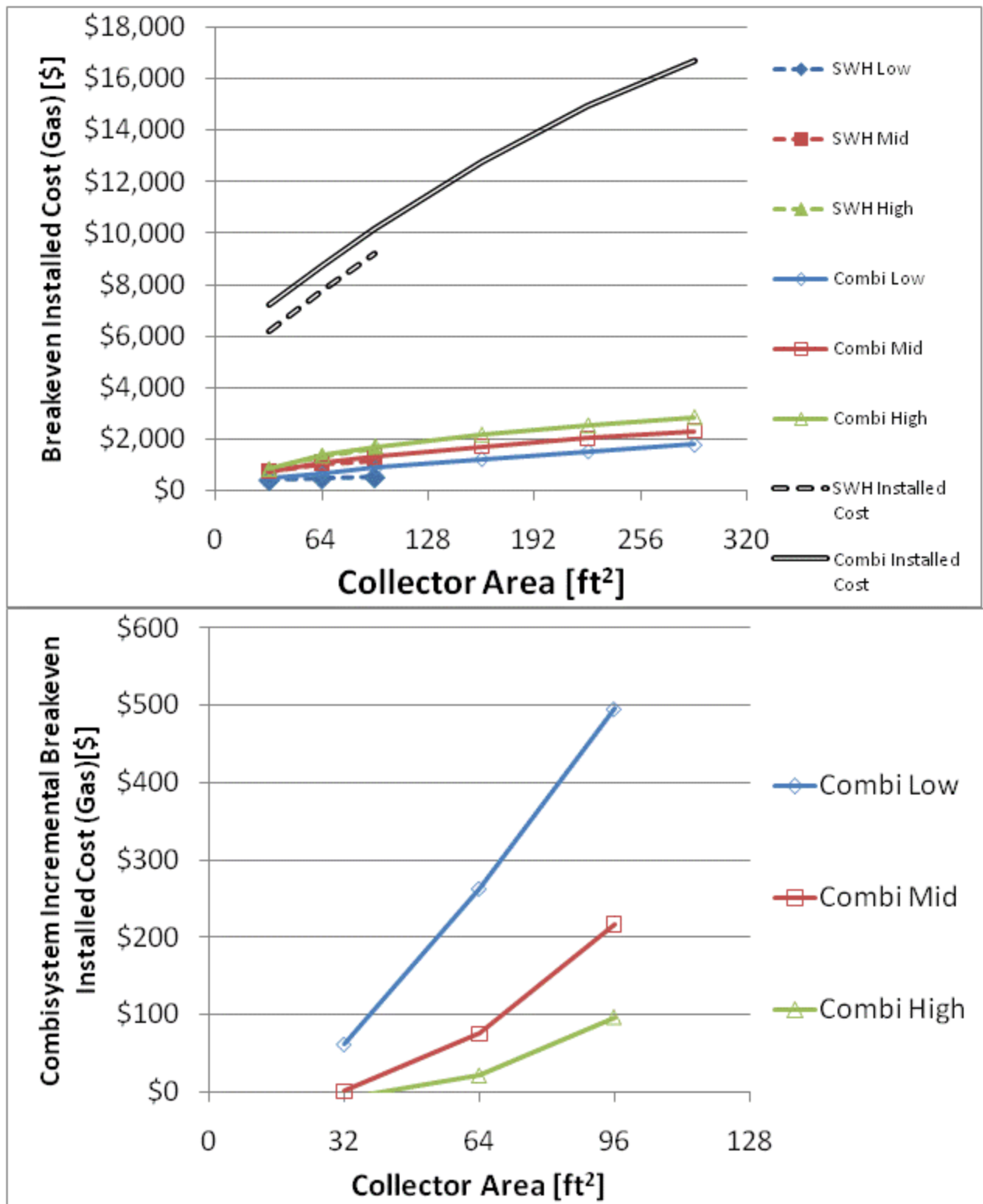


Figure F.102: Breakeven installed cost and combisystem incremental breakeven cost for gas systems for a

IECC 2009 House(Chicago)

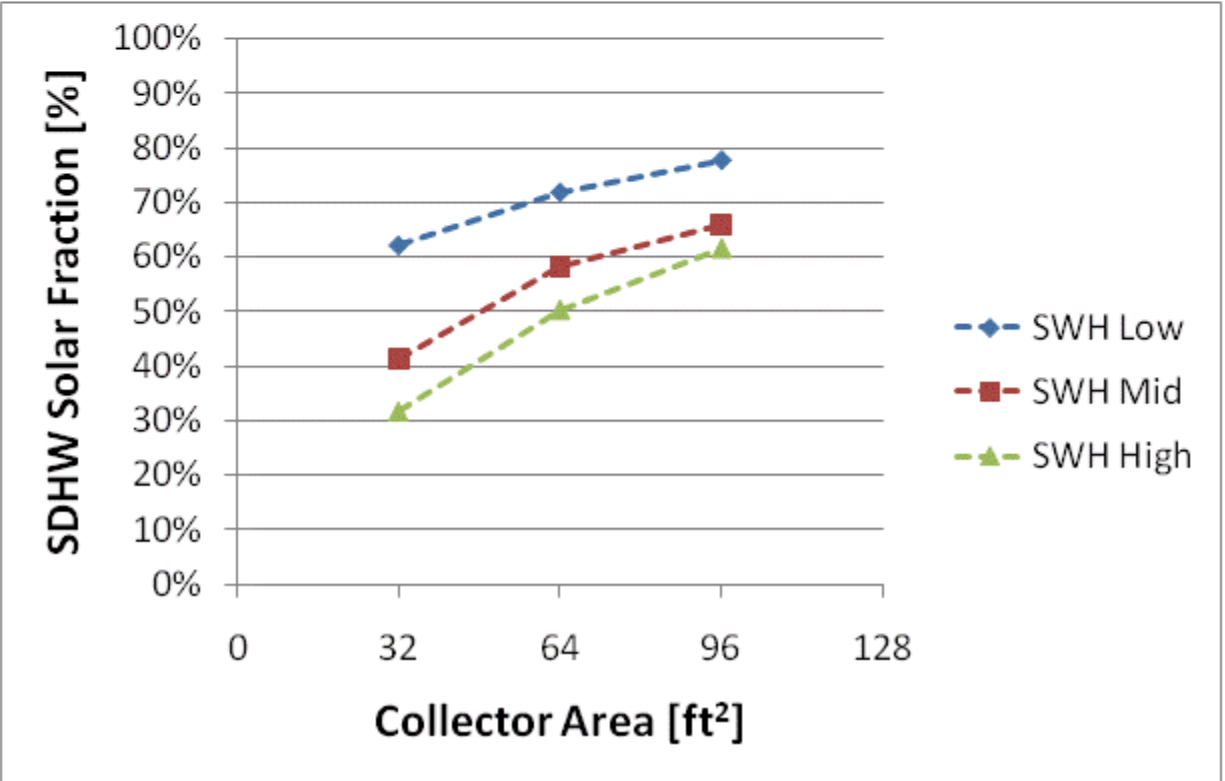
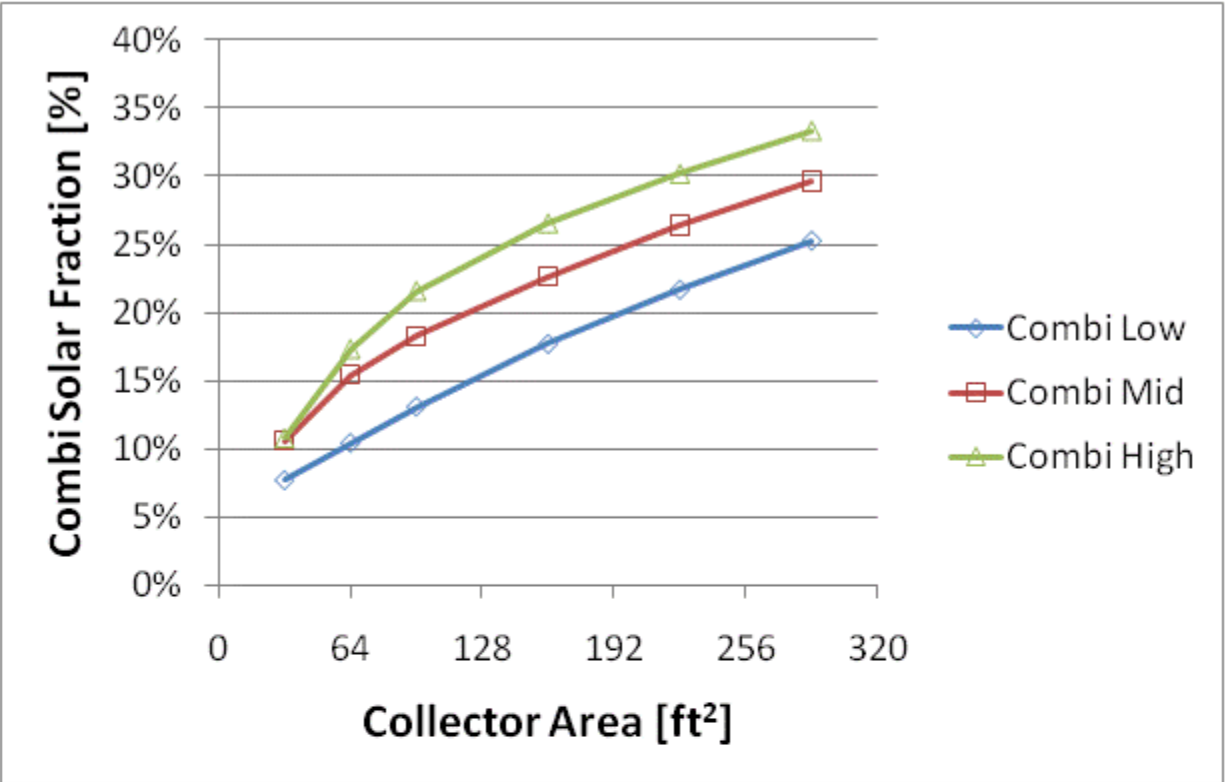


Figure F.103: Combisystem and SWH solar fraction for a BA 50% House(Chicago)

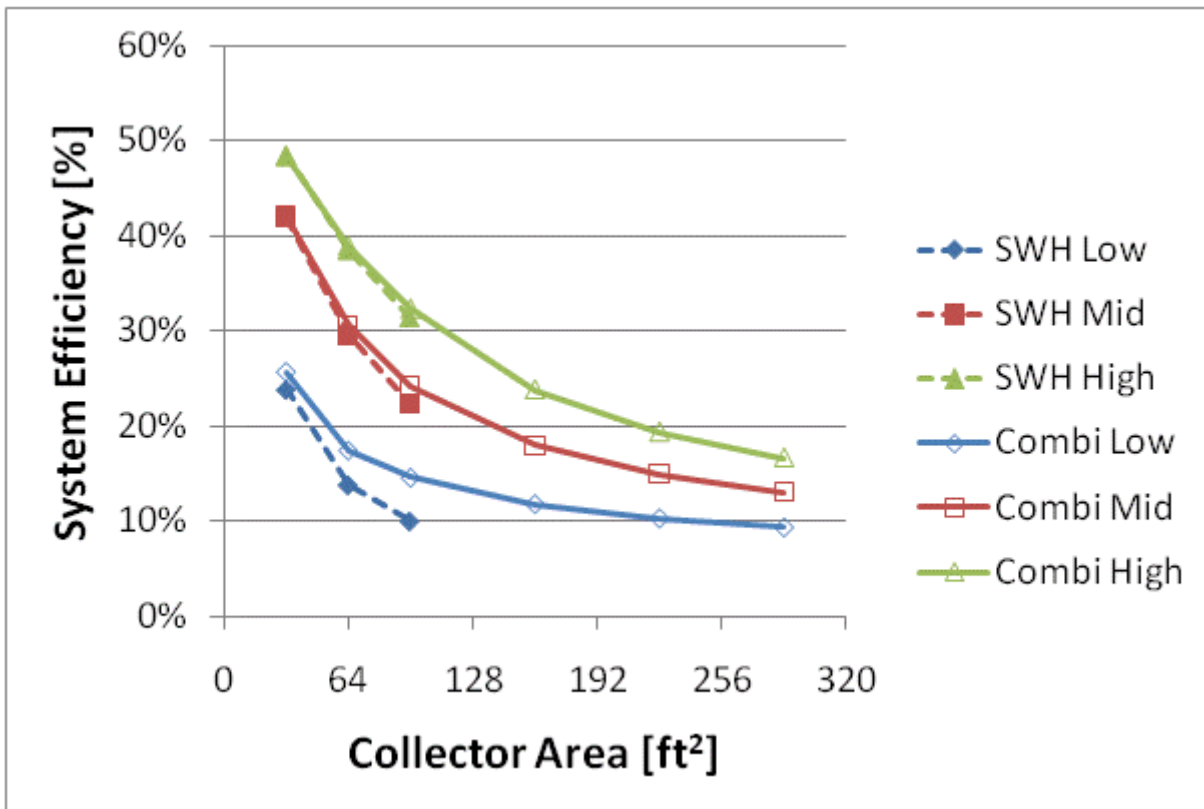
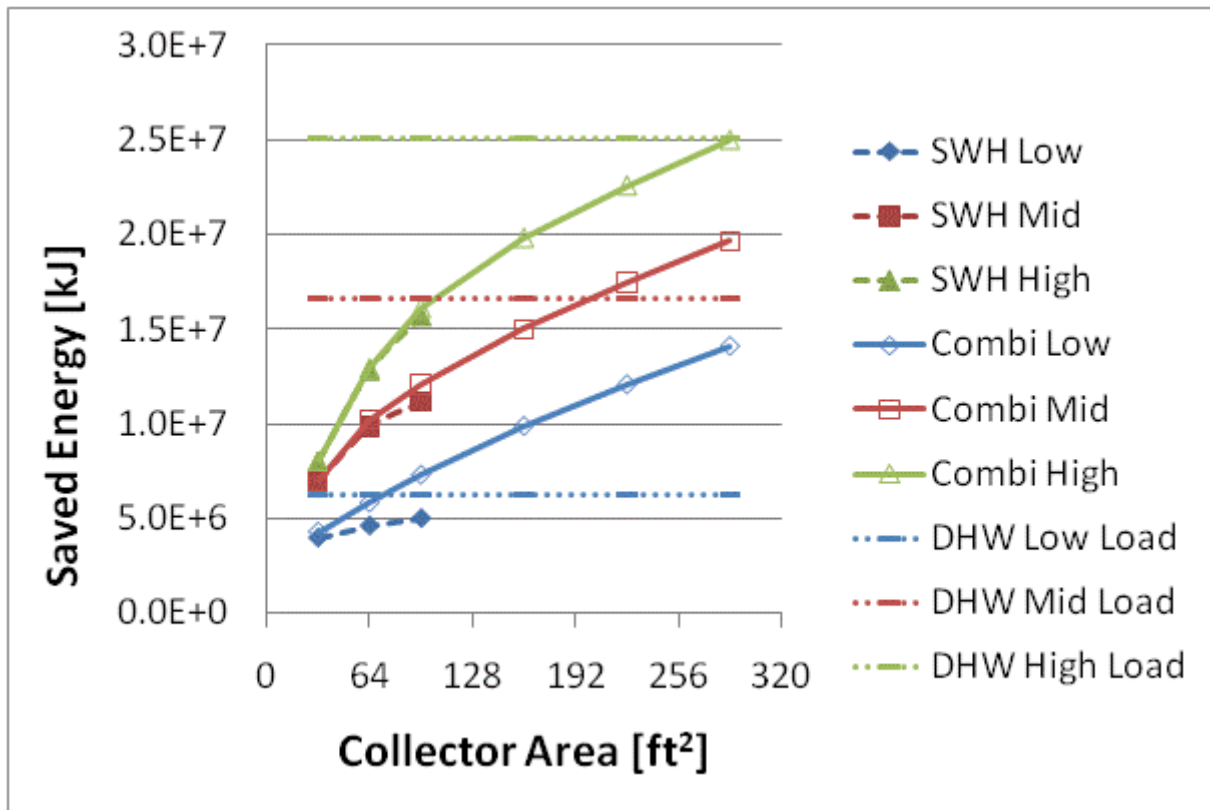


Figure F.104: Annual saved energy and system efficiency for a BA 50% House(Chicago)

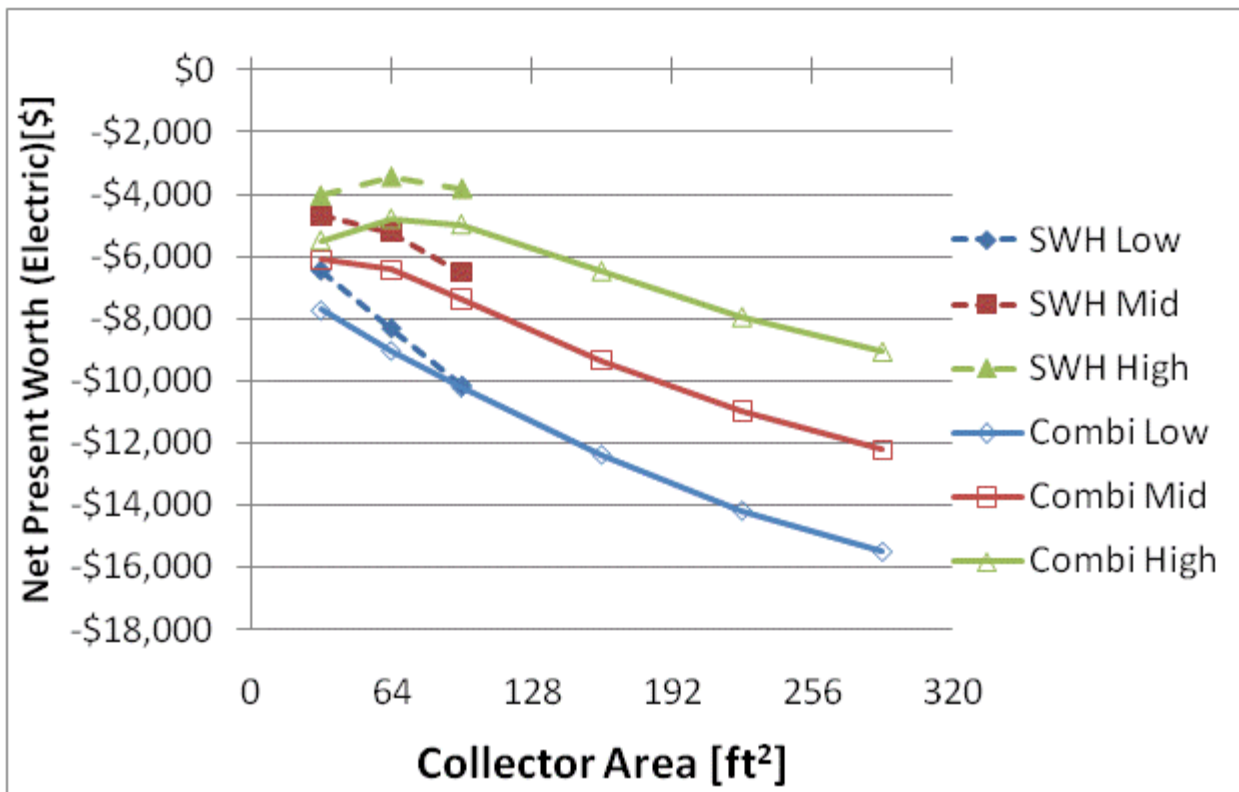
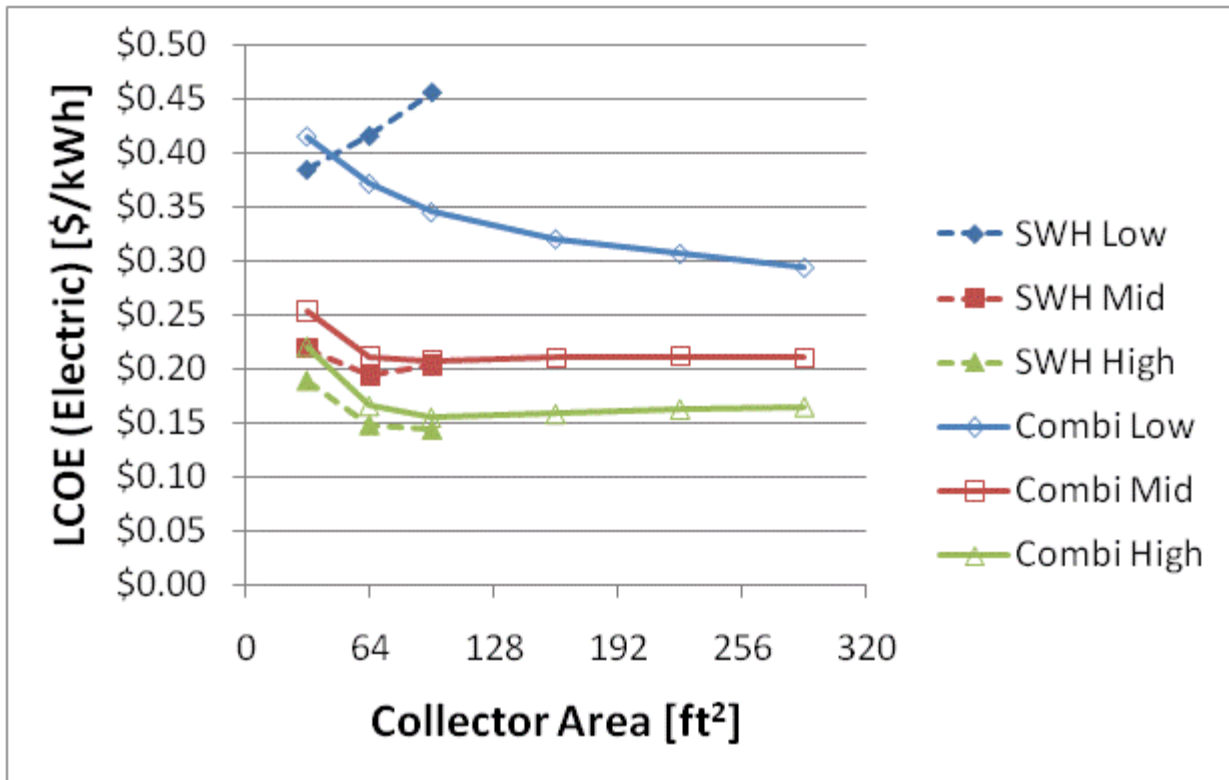


Figure F.105: LCOE and NPW for electric systems for a BA 50% House(Chicago)

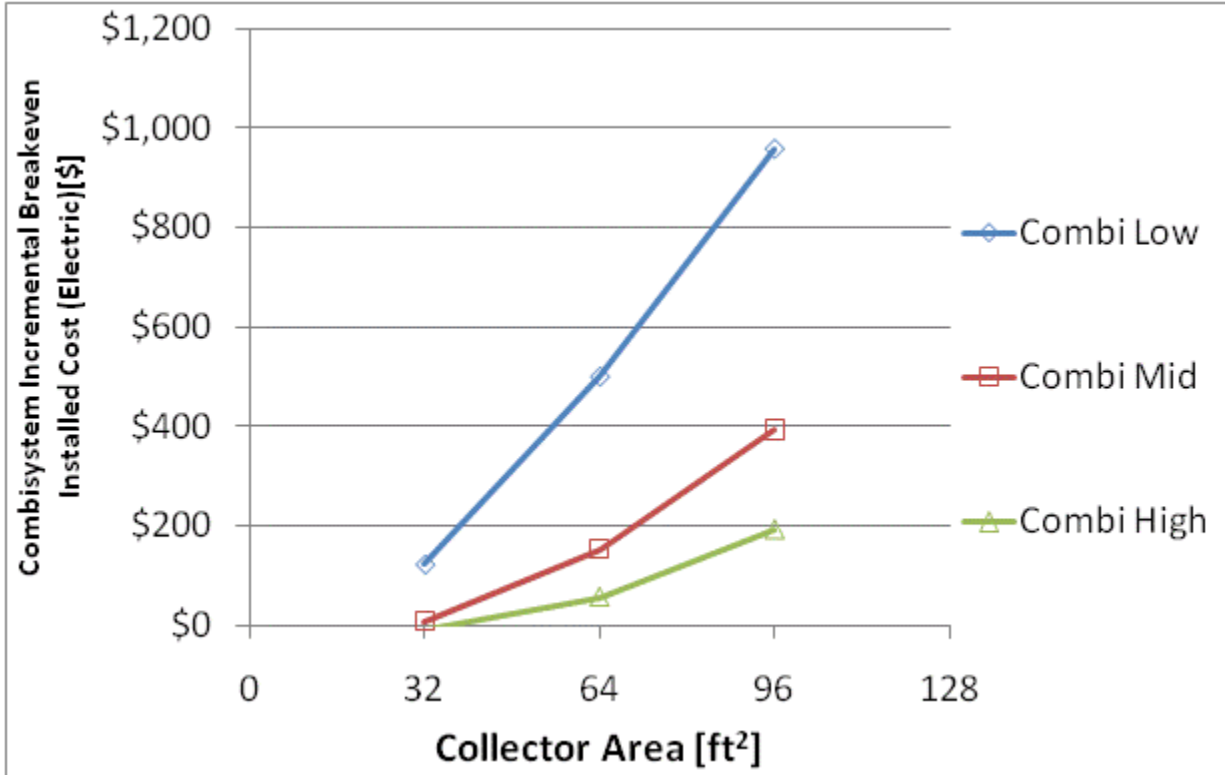
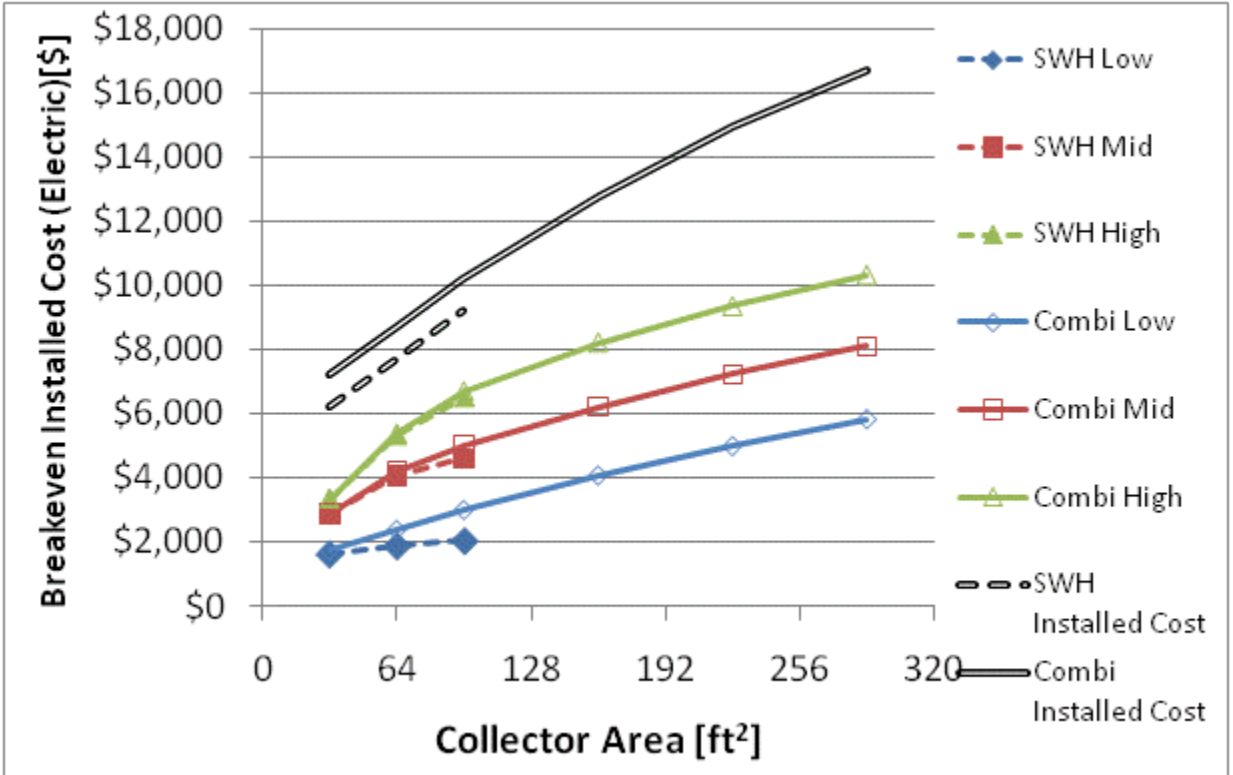


Figure F.106: Breakeven installed cost and combisystem incremental breakeven cost for electric system for a BA 50% House(Chicago)

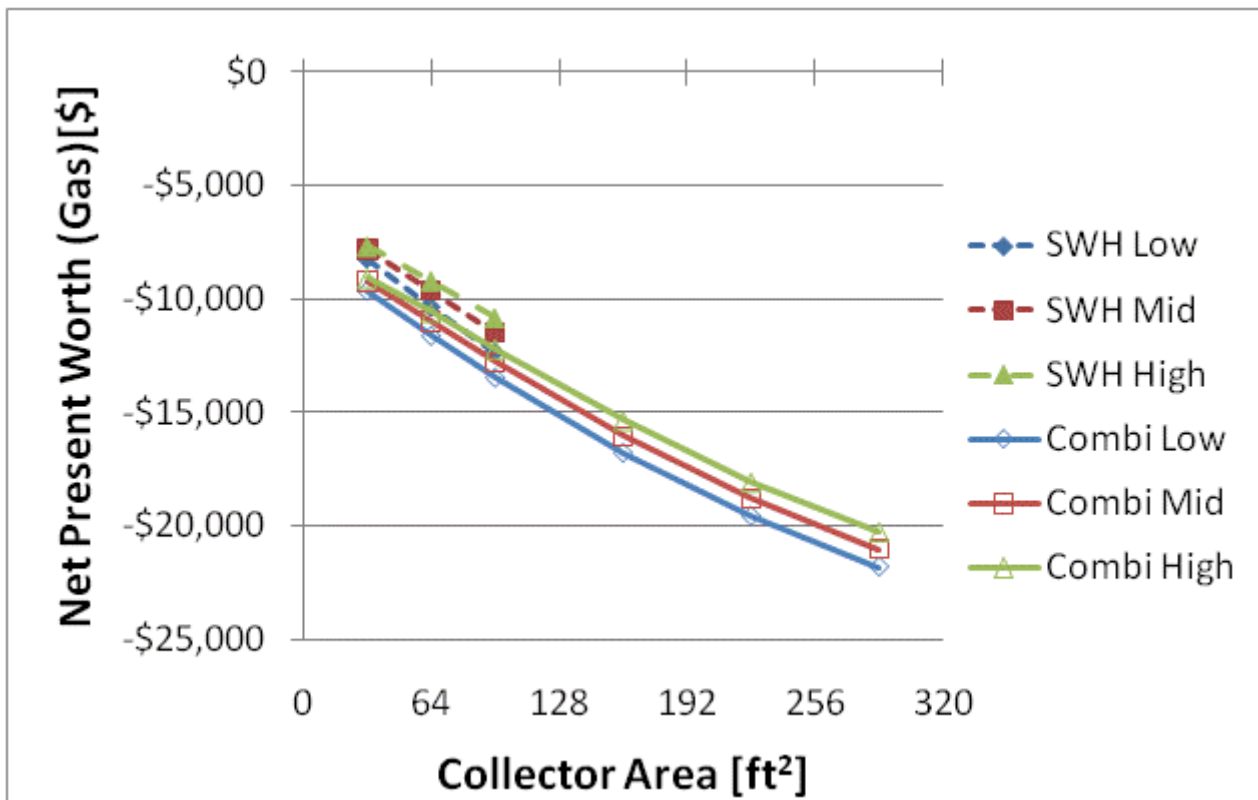
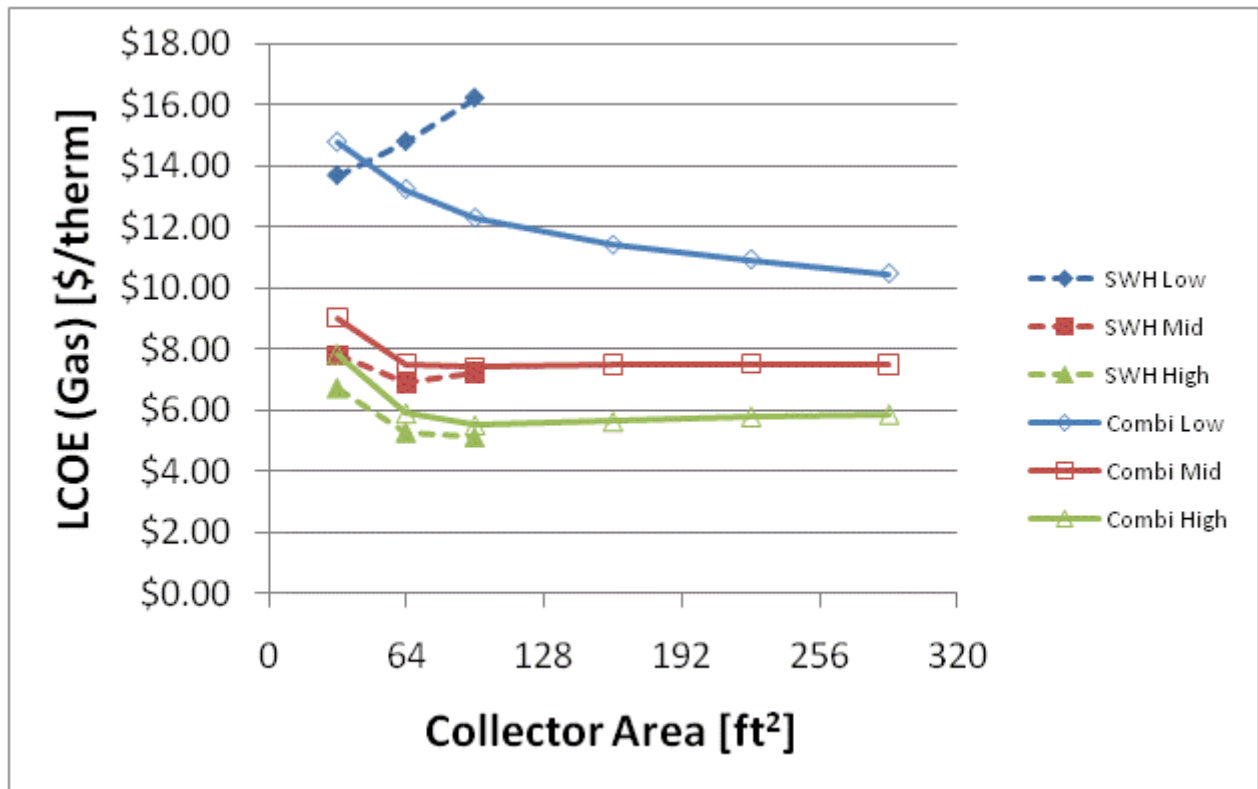


Figure F.107: LCOE and NPW for gas systems for a BA 50% House(Chicago)

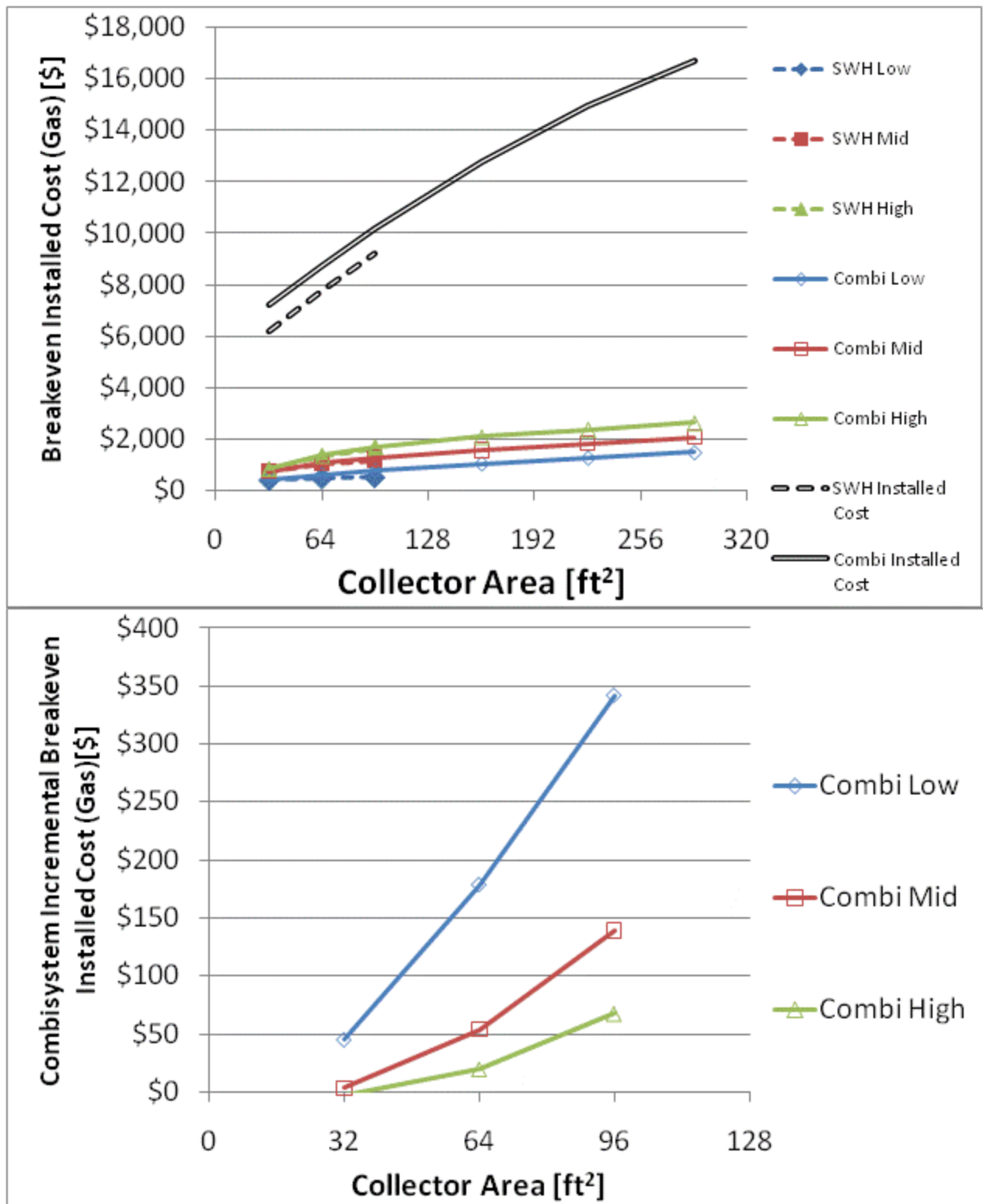


Figure F.108: Breakeven installed cost and combisystem incremental breakeven cost for gas systems for a

BA 50% House(Chicago)